Optimising Recombinant Protein Production in *E. coli*

by

ALEXANDER DAVID OSGERBY

A thesis submitted to the University of Birmingham for the degree of

DOCTOR OF PHILOSOPHY

Biochemical Engineering

School of Chemical Engineering

College of Engineering and Physical Sciences

University of Birmingham

April 2024

UNIVERSITY OF
BIRMINGHAM

University of Birmingham Research Archive

e-theses repository

This unpublished thesis/dissertation is copyright of the author and/or third parties. The intellectual property rights of the author or third parties in respect of this work are as defined by The Copyright Designs and Patents Act 1988 or as modified by any successor legislation.

Any use made of information contained in this thesis/dissertation must be in accordance with that legislation and must be properly acknowledged. Further distribution or reproduction in any format is prohibited without the permission of the copyright holder.

Abstract

Recombinant protein production (RPP), the heterologous overexpression of high-value proteins in more amenable host organisms, is essential for synthesising proteins used in research and with commercial or clinical applications. The use of *Escherichia coli*, exploited as a host in RPP for over 40 years, is not without caveats; this work has addressed several. Firstly, green fluorescent protein (GFP) was overexpressed from the urea-inducible *Proteus mirabilis* urease promoter P_{uti101} as a cost-effective alternative to established systems. Optimisation from flask to bioreactor scale indicated that basal GFP expression from P_{uti101} was low, typically around 2.5-fold higher than that of untransformed cells. Adding urea resulted in an up to 75-fold increase in GFP expression; even concentrations up to 500 mM were shown to have little effect on biomass accumulation. Secondly, many valuable proteins require disulphide bonding for bioactivity, necessitating periplasmic expression in *E. coli*. Oxidation-resistant GFP derivatives sfGFP and cfSGFP2 were evaluated under RPP-centric conditions to understand their application in improving screening throughput. While the export of GFP to the periplasm was detrimental to host physiology, super-resolution microscopy supported prior indications that periplasmic sfGFP fluoresces. Finally, as periplasmic expression was problematic, our focus shifted to detecting host stress via GFP fusion to the P_{spy} promoter from the periplasmic chaperone spheroplast protein Y (Spy). P_{spy} responded to both overexpression of periplasmic recombinant proteins and direct inhibition of translocation machinery. Then, combined with novel repressors, P_{spy} was exploited as a trigger for negative feedback to greatly improve host physiology during overexpression of poorly tolerated periplasmic recombinant proteins.

Acknowledgements

I thank my supervisor, Dr Tim Overton, for his continual guidance, patience, and support throughout this project. Secondly, to all members of the Overton lab and Biochemical Engineering, it was great working alongside you, and you made the duration a thoroughly enjoyable experience. I would like to thank the Browning lab, with whom part of this project was a collaboration. I would also like to thank MIBTP and the BBSRC, who funded this work. Finally, my family, you kept me sane through this, and I can never thank you enough.

Summary of work completed

My PhD research broadly covered optimising recombinant protein production in *Escherichia coli.* However, during this MIBTP studentship, other relevant work was completed, supplementary to the primary PhD project, but which will not be covered in the main body of this thesis. A timeline of work completed during the studentship is provided below.

- **JAN 2020 – APR 2020:** Mini Project 1 at The University of Warwick
- **APR 2020 – JUL 2020:** Mini Project 2 at The University of Birmingham
- **JUL 2020 – OCT 2020:** Professional Internship for PhD Students (PIPS)
- **NOV 2020 – APR 2023:** Main PhD project
- **APR 2020 – JAN 2021:** Cloning work for lab member
- **NOV 2021 – APR 2022:** MSci research project supervision
- **JUN 2022 – AUG 2022:** MSc research project supervision
- **NOV 2022 – APR 2023:** MSci research project supervision
- **JAN 2023 – APR 2023:** MIBTP mini project supervision
- **APR 2023 – JUL 2023:** BBSRC funded IGI-IAS Project
- **JUL 2023 – NOV 2023:** Main PhD Project
- **NOV 2023 – FEB 2023:** BBSRC funded IAA Project
- **FEB 2023 – APR 2023:** Main PhD Project

Mini Projects

Following training modules in year 1 (SEP 2019 – JAN 2020), I undertook two mini-projects, first at an MIBTP partner university and then a second at our home institution. My first mini project at The University of Warwick with Professor Alfonso Jaramillo applied synthetic biology techniques to engineer bacteriophage. This project resulted in two publications, the first a novel method to produce pure transducing particles exploiting the relationship between P2 and P4 phage (Tridgett et al., 2021); the second a method for scarless recombineering of lysogenic phage, using a λRed derived system (Ababi et al., 2022). My second mini-project at The University of Birmingham with Dr Tim Overton was literature-based due to the COVID-19 pandemic. This project resulted in a publication, a review of current methods for high-throughput quantification of recombinant protein exported to the *E. coli* periplasm (Osgerby and Overton, 2023).This paper also served as an initial basis for my PhD research.

PhD Project

My main PhD project focused on optimisation of recombinant protein production in *E. coli* and focused on three main areas. Firstly, with collaborators in the School of Biosciences, we looked at overexpression of recombinant proteins in the cytoplasm using a novel urea inducible promoter hooked up to a GFP reporter. Initial flask scale work from the first part of this project has already resulted in a publication (Hothersall et al., 2022b). Subsequent optimisation of the urea inducible system during scale up and application to more industrially relevant conditions will serve as the basis for a second paper.

Another area of research built on work published through my second mini project (Osgerby and Overton, 2023); namely how can we use GFP to quantify recombinant protein localised to the *E. coli* periplasmic space, and can it be used for process optimisation. We assessed different GFP derivatives using various expression systems and results from this will form the basis for a paper explaining caveats in utilising such a method.

The final area of research looked at ways to detect stress in *E. coli* arising from overexpression of recombinant proteins, and how we can exploit this using synthetic biology to improve host strain performance. To detect stress, we identified promoters which should be switched on during exposure to appropriate stressors and fused them to GFP reporters. Work from this formed the basis for a MSci project and an MIBTP mini project discussed below. Data generated by myself and project students will be used for a publication. The second part looked at manipulating this system to create a negative feedback loop which regulates expression of a recombinant protein in response to stress sensed by the host. This required creation of novel repressors which were then developed further during a BBSRC funded IAA project (discussed below) to generate proof of concept data for patent applications. Data from both will be used for a publication.

During my PhD research I also helped a fellow lab member with cloning work. Using a λRed recombineering method, we tried to create a clean deletion of the *motAB* operon in *E. coli*, while simultaneously knocking in the *motAB* promoter downstream of the deletion site, to prevent polar effects to downstream genes *cheAW.* Unfortunately, we

could not isolate any recombinants but provided knowledge that the knockout and knock in should be done sequentially in future attempts.

Project Student Supervision

I supervised several undergraduate and postgraduate students in the lab during my PhD. During NOV 2021 – APR 2022 I supervised two MSci students working on novel stress response promoters provided by a collaborator in Biosciences. In JUN 2022 – AUG 2022 I supervised an MSc student working on a novel nitrate inducible promoter. Between NOV 2022 – APR 2023 I supervised two MSci students working on a system which detects stress in *E. coli;* developed during my PhD research. This will be combined with my own data for publication. Finally in Jan 2023 – APR 2023 I supervised an MIBTP student in the lab completing their mini project, working on another system to detect stress in *E. coli*; also developed during my PhD research.

IGI-IAS Project

I took a leave of absence from my PhD between APR 2023 – JUL 2023 to work on a BBSRC funded IGI-IAS in *Salmonella*. We looked at how the RND efflux pump *acrAB* mediates membrane potential in addition to removing noxious substances from the cell. Data generated from this work was used for a paper (Whittle et al., 2024) and a grant application.

IAA Project

I took a second leave of absence from my PhD between NOV 2023 – FEB 2023 to complete a BBSRC funded IAA project; building on work from my PhD where I created

novel repressors for use in a negative feedback loop. We wanted to exploit these repressors for regulation of expression systems currently used industrially for RPP and develop proof of concept data for patent applications. Data generated from this project will be used in applications for a follow-on fund.

Abstract 2

Acknowledgements 3

Summary of work completed 4

Abbreviations 12

Chapter 1: Literature Review 13

1.1 Introduction 13

1.2 Recombinant protein production 14

1.3 Host cell selection 16

1.4 Recombinant protein production in *E. coli* 24

1.5 Recombinant protein expression in the periplasm 33

1.6 Export of recombinant proteins 42

1.7 Aims and objectives 48

Chapter 2: Materials and Methods 52

2.1 Media and Reagents 52

2.2 Bacterial Strains and Plasmids 59

2.3 Bacterial Culture 69

2.4 Cloning Techniques 74

2.5 Construct Assembly 87

2.6 Analytical Techniques 107

Chapter 3: Optimising a novel urea inducible promoter 115

3.1 Introduction 115

3.2 Effect of urea on the host 121

3.3 Small-scale expression 141

3.4 Scale-up into baffled flasks 162

3.5 Scale-up into bioreactors 195

3.6 Discussion 218

3.7 Conclusions 230

Chapter 4: Periplasmic GFP Reporters 233

4.1 Introduction 233

4.2 Periplasmic msfGFP reporters using a T7*lac* system 236

4.3 Periplasmic msfGFP reporters using a P_{araBAD} system 248

4.4 Periplasmic cfSGFP2 reporters using a P_{araBAD} system 266

4.5 Microscopy Analysis 273

4.6 Discussion 281

4.7 Conclusions 288

Chapter 5: Biosensors and Feedback Loops 290

5.1 Introduction 290

5.2 SecM as a Periplasmic Biosensor 294

5.3 P_{spy} as a Periplasmic Biosensor..... 303

5.4 P_{spy} response to recombinant proteins and export stressors..... 316

5.5 Designing a negative feedback system..... 329

5.6 Ligand Unresponsive LacI..... 332

5.8 Negative Feedback system 347

5.9 Discussion 353

5.10 Conclusion..... 363

Chapter 6: General conclusions and future work 366

6.1 Urea inducible promoter..... 367

6.2 Periplasmic screening tools 371

6.1 Biosensors and negative feedback loops..... 374

Chapter 7: References 380

Chapter 8: Appendix..... 450

Abbreviations

CHO – Chinese hamster ovary cells

DTT – Dithiothreitol

FCM – Flow cytometry

GFP – Green fluorescent protein

IM – Inner membrane

IPTG – Isopropyl β-D-1-thiogalactopyranoside

LB – Lysogeny broth

LBA – Lysogeny broth agar

OD – Optical density

OM – Outer membrane

PBS – Phosphate Buffered Saline

PI – Propidium Iodide

PMBN – Polymyxin B nonapeptide

PPG – Polypropylene glycol

RB – Rose bengal

RPP – Recombinant protein production

SDS PAGE – Sodium dodecyl sulphate polyacrylamide gel electrophoresis

SIM – Structured illumination microscopy

SP – Signal peptide

TB – Terrific broth

Chapter 1: Literature Review

1.1 Introduction

Across all biological entities, proteins are one of the key driving forces behind cellular functions. Their role and importance mean isolating suitable quantities of individual proteins has become essential for biomedical and pharmaceutical research, industry and clinically. Proteins of interest must be synthesised in a functional state, and in appropriate amounts, dependent on application; bioactivity and correct folding are critical for research, so are the foremost concerns; but in industry, where commercial viability is the driving factor, additional emphasis is placed upon product titre.

Historically a protein of interest would be isolated at their source, often animal tissues, or purified from microbial hosts endogenously expressing them. Insulin, considered the archetypical recombinant protein, was extracted from the pancreas of cows and pigs, though required as much as 8000 kg animal pancreases per 1 kg of insulin (Flier and Kahn, 2021), and elicited immunogenic effects in patients (Quianzon and Cheikh, 2012). Growth hormone was extracted from the pituitary glands of human cadavers with great difficulty and serious issues around the transfer of infectious agents (Tidblad, 2022). Chymosin, the protease constituent of rennet secreted into the stomachs of juvenile ruminants and essential in cheese production had to be isolated from calves or latterly microorganisms naturally synthesising analogous coagulants (Kumar et al., 2010). Incorporating biocatalysts into consumer products, like washing detergents formulated with hydrolytic enzymes amylases, lipases or proteases significantly improved effectiveness, but required purification from the natural microbial host (Falch, 1991).

Native expression of a protein is often too low to purify the necessary amounts, or the host or source is not well adapted to process intensification. Recombinant overexpression in a foreign organism circumvents this, providing access to more amenable physiologies, maximising final product yield. For these reasons, academia and industry alike turn to recombinant protein production (RPP), the heterologous overexpression of a protein of interest.

1.2 Recombinant protein production

The origins of recombinant protein production lie in the advent recombinant DNA technology during the 1970s, reviewed by Berg and Mertz (2010), which itself was dependent on several breakthroughs. First, Jackson et al. (1972) used a restriction endonuclease linearise DNA fragments and a terminal deoxynucleotidyl transferase to add complimentary polynucleotide ends; allowing splicing of λ phage genes and the *Escherichia coli* galactose operon into the SV40 viral genome, creating the first recombinant DNA molecule.

It became apparent that certain restriction enzymes in fact create complimentary cohesive ends, as opposed to blunt ends, which could be more efficiently ligated together (Mertz and Davis, 1972). It was also shown *E. coli* could be chemically induced via calcium chloride treatment to uptake purified foreign DNA such as plasmids for replication, without the assistance of a bacteriophage for delivery (Cohen et al., 1972). Developing both further, Cohen et al. (1973) demonstrated that DNA fragments resulting from restriction digest of two separate plasmids could be spliced together *in vitro* and the recombinant plasmid transformed into *E. coli* for replication.

Finally, this culminated with production of the first recombinant protein; the gene encoding the mammalian hormone somatostatin was chemically synthesised, restriction cloning used to splice the fragment into a plasmid vector and transformation into *E. coli* for replication and synthesis (Itakura et al., 1977). Since then, RPP has developed into an industry worth billions (Walsh and Walsh, 2022), responsible for synthesis of proteins essential across a multitude of sectors, reviewed thoroughly by Demain and Vaishnav (2009).

Many proteins present potentially novel therapeutic targets, making them essential in drug discovery. First in target validation, then via high-throughput and focused compound screening, or systematic design of efficacious treatments against them (Hughes et al., 2011, Assenberg et al., 2013). Recombinant proteins may be exploited for diagnostics, notably in colloidal gold immunochromatography assays using recombinantly expressed SARS CoV 2 spike proteins for antibody detection (Zhang et al., 2021).

Many recombinant proteins are industrially relevant; amylases (Tagomori et al., 2021), lipases (Ghasemian and Moradpour, 2019) and proteases (Niehaus et al., 2011) are widely used in detergents. Cellulases have additional application in industries from ranging from biofuel production to textile manufacture (Ejaz et al., 2021); ligninases and xylanases are employed in the paper industries (Giovannoni et al., 2020).

RPP is required for production of proteins analysed via biophysical techniques like X-ray crystallography (Maveyraud and Mourey, 2020), NMR (Hu et al., 2021) and cryo-

EM (Yip et al., 2020), which are used to determine three dimensional structure; while mass spectrometry (Tamara et al., 2022) and circular dichroism (Greenfield, 2006) can be used for probing and characterisation. Functional and biochemical studies are critical to elucidate mechanistic properties of a specific protein, better understand a complex or define distinct pathways (Pollard, 2010, Bisswanger, 2014, Nguyen et al., 2015). Further, vital research enzymes including DNA polymerase, reverse transcriptase, ligases, kinases, and restriction enzymes are produced recombinantly.

1.3 Host cell selection

1.3.1 Post-translational modifications

Complexity primarily determines choice of host cell; many proteins, particularly in eukaryotes, are exposed to several forms of processing after translation, reviewed by (Zhong et al., 2023), via addition of chemical groups or moieties inside organelles such as the rough endoplasmic reticulum (ER) or Golgi apparatus. While such alterations are often termed post-translational modifications (PTMs), this is partially misleading as some occur co-translationally (Shrimal et al., 2015, Aksnes et al., 2019). Regardless, *in vivo*, PTMs vastly extend the diversity and functionality of available proteins expressed by the cell. Several hundred PTMs are presently known (Ramazi and Zahiri, 2021). Many are of consequence to recombinant proteins, being required for bioactivity (Jenkins et al., 2008), to avoid immunogenicity (Kuriakose et al., 2016) or aid product stability (Lee et al., 2023). Such modifications can be critical in the manufacture of biotherapeutics (Walsh, 2010); so crucially, synthesis of such proteins means hosts must have the necessary intracellular machinery available.

Phosphorylation is universally conserved and the most frequently occurring PTM (Ramazi and Zahiri, 2021) and reviewed thoroughly by (Johnson, 2009). Phosphorylation is mediated by kinases (Peterson and Schreiber, 1999) resulting in the reversible transfer of a phosphate, supplied by ATP, to specific amino acids. In eukaryotes, targeted residues are predominantly serine, but also threonine and tyrosine (Olsen et al., 2006). In bacteria this is similar, but phosphorylation of histidine residues also occurs (Potel et al., 2018). Phosphorylation is implicated in a diverse set of cellular functions ranging from signalling to protein-protein interaction (Nishi et al., 2011, Ardito et al., 2017).

Behind phosphorylation, acetylation is the second most frequently occurring PTM (Ramazi and Zahiri, 2021) and a thorough review is provided by Drazic et al. (2016). In acetylation, which usually occurs in the cytoplasm, an acetyl group, mediated by acetyltransferases, is donated by acetyl coenzyme A predominantly to the α-amino of the N-terminal amino acid (Arnesen, 2011) or the ε-amino of lysine residues (Yang and Seto, 2008). While acetylation is primarily associated with eukaryotes, bacteria including *E. coli* acetylate proteins although capacity is somewhat limited by comparison (Vandrisse and Escalante-Semerena, 2019). Appendage of a negative acetyl group neutralises any positive charge on the acetylated amino acid and in turn modulating protein function, folding, half-life or localisation (Narita et al., 2019).

N- and O-linked glycosylation (Chen et al., 2022, Thompson and Wakarchuk, 2022) involves addition of oligosaccharide chains in various conformations to asparagine and serine or threonine residues respectively. N-linked glycosylation is often critical to

monoclonal antibodies, in particular variants with an Fc region, where proximal glycan chains support mediation with the host immune system to elicit a response (Zlatina and Galuska, 2021). Glycosylation is complex and epitopes are species specific (Brooks, 2004). While mammalian hosts such as CHO cells can synthesise human-like glycoforms (Butler and Spearman, 2014), there are still notable differences (Croset et al., 2012). Such modifications should also be consistent to avoid heterogeneity and thus differences in pharmacokinetics or dynamics between batches. Glycoforms can be somewhat controlled via processing conditions such as growth media composition; although genetic or metabolic engineering are more effective in determining specificity (Gupta and Shukla, 2018). Regardless, any such modification must be paired with an appropriate technique to characterise which glycoforms are present (Mao et al., 2022). Bacteria are not usually associated with glycosylation but *Campylobacter jejuni* is capable of N-linked glycosylation (Linton et al., 2002).

Disulphide bond formation involves covalent linkage between thiol groups of two cysteine residues. Disulphide bridges are relatively common in human proteins at around 20 %; in less complex eukaryotes like yeasts and bacteria this is around 10-fold lower (Wiedemann et al., 2020). Disulphide formation requires an oxidising environment hence occurs upon co-translational export to the endoplasmic reticulum in eukaryotes (Robinson and Bulleid, 2020). Bacteria like *E. coli* catalyse synthesis of disulphide bonds owing to the presence of a disulphide bonding (Dsb) system (Manta et al., 2019). Disulphide bond formation protein A (DsbA) (Bardwell et al., 1991) is the donor for disulphide formation in substrates; reduced DsbA is regenerated by the IM bound Disulphide bond formation protein B (DsbB) (Bardwell et al., 1993), itself

oxidised by quinones from cellular respiration (Kobayashi, 1999, Takahashi et al., 2004). Analogous proteins with opposing function and redox states, Disulphide bond formation protein C (DsbC) and Disulphide bond formation protein D (DsbD), provide quality control through isomerisation of aberrant disulphide bonds (Shevchik et al., 1994, Rietsch et al., 1997).

1.3.2 Which host is optimal

Several hosts are presently used for RPP, and the protein-host dynamic must be carefully considered during development to ensure the characteristics of both are compatible. Very large proteins or those requiring complex PTMs must be produced in hosts with the capacity to synthesise them; as cell complexity increases however, caveats arise in process optimisation. Simpler proteins are then often overexpressed in simpler hosts, reinforcing the notion that the recombinant protein and host properties should be aligned. A thorough review of potential hosts is provided by (Demain and Vaishnav, 2009).

Compatibility with PTMs means mammalian hosts are preferred for overexpressing human proteins; particularly those with clinical value including antibodies, clotting factors, hormones, growth factors, cytokines and enzymes (Walsh and Walsh, 2022). Chinese Hamster Ovary (CHO) cells (Kim et al., 2012) are used for synthesis of over 40% of approved biotherapeutics (Figure 1.1A), typically providing better yields and being more amenable to growth in defined media. Other mammalian hosts in use include Mouse myeloma cell lines (NS0 and Sp2/0) (Dhara et al., 2018, Demirhan et al., 2022) and Baby Hamster Kidney (BHK) cells (Johnson et al., 2014). Where PTMs

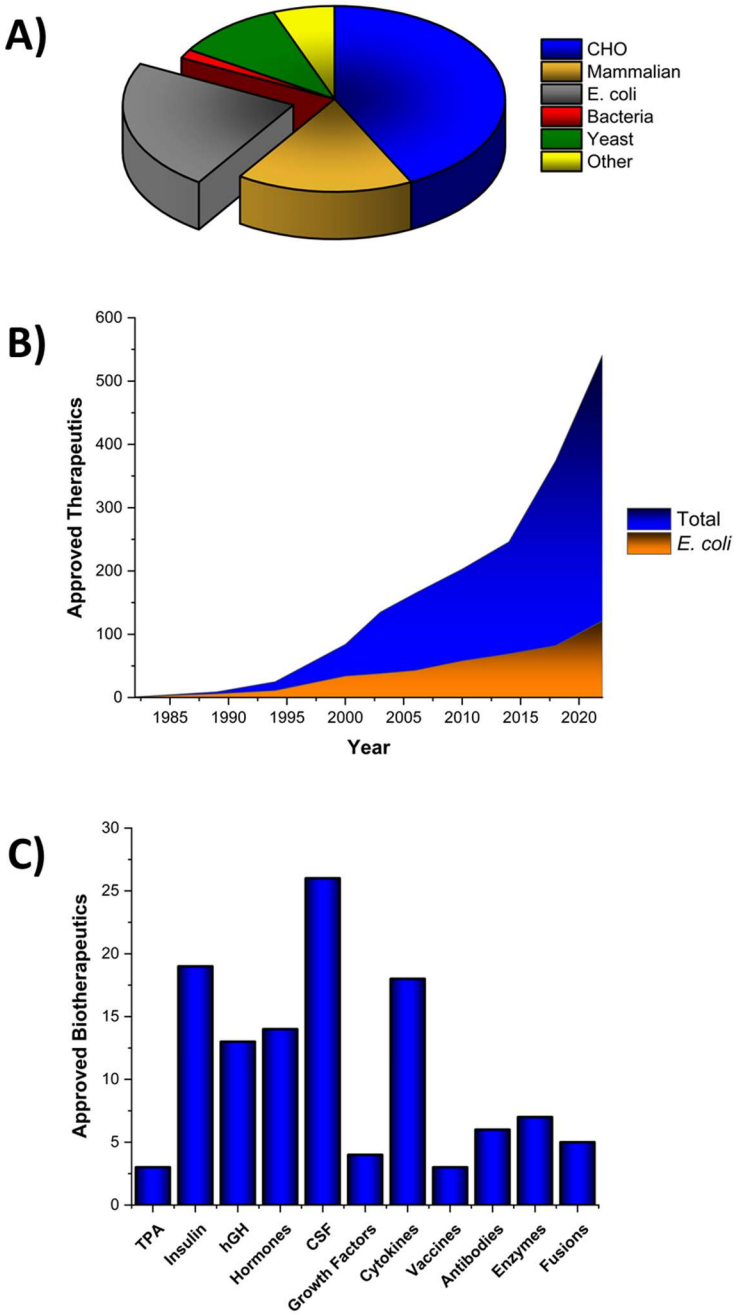


Figure 1.1: Biotherapeutic development and production is an industry worth billions of pounds, and except for emergent technologies like chemically synthesised vaccines, gene therapy and engineered cell treatments, the majority are recombinant proteins.

(A) Mammalian and in particular CHO cells are preferred hosts due to their cellular machinery but are difficult to work with compared to microbial hosts, so yeasts with their eukaryotic physiology also see use. For less complex proteins, *E. coli is* the predominant choice, due to its simplicity and propensity to accumulate large quantities of product.

(B) Following Humulin approval in 1982, the number of biotherapeutics brought to market has increased substantially over the last 40 years, reaching over 500 products. Correlating with the massive increase in number of approved biotherapeutics over the last 40 years, 118 are manufactured in *E. coli*.

(C) *E. coli* is the host for production of a wide variety of biotherapeutics such as recombinant insulin and other hormones like (hGH); colony stimulating factors (CSF); cytokines such as interferon, interleukin, TNF-α; and monoclonal antibodies.

of human origin are essential to function, Human Embryonic Kidney (HEK) cells (Tan et al., 2021) are used.

Limitations do exist in application of mammalian cell lines for RPP, compared with simpler eukaryotes or prokaryotes; they are more difficult to handle, and their fragility means lower resistance to bioprocessing conditions (Schütz et al., 2023). Accumulation of recombinant protein is lower in mammalian cells; coupled with slower growth rates this and requirement for complex, expensive growth media equates to a significant impact on overhead costs (Yin et al., 2007). Generation of cell lines with stable, rather than transient expression, also requires a sizeable time and monetary investment (Hacker and Balasubramanian, 2016) and viral contamination poses a significant risk, managed through preventative means and detection methods during production (Barone et al., 2020).

Yeasts provide a compromise between the complexity of higher eukaryotes and processing advantages of prokaryotes (Çelik and Çalık, 2012). *Saccharomyces cerevisiae* usage is widespread in the food and beverage industries (Parapouli et al., 2020); more recently it has been exploited by pharmaceutical companies for production of hormones, anticoagulants, growth factors and antigens used for vaccines (Huang et al., 2014). *Pichia pastoris* is another yeast used for recombinant protein production, reviewed by Karbalaei et al. (2020); used for production of several biotherapeutics (Walsh and Walsh, 2022); biocatalysts (Spohner et al., 2015); and in antigen production for diagnostics (Ottone et al., 2007). *P. pastoris* is methylotrophic, able to metabolise single carbon compounds like methanol providing inexpensive growth

media; this also facilitates high level inducible expression via the AOX1 promoter, although the system is repressed by glucose and glycerol (Türkanoğlu Özçelik et al., 2019). Unlike *S. cerevisiae*, *P. pastoris* does not accumulate ethanol as a byproduct during aerobic growth, so cell density and yield of recombinant protein is higher (Vieira Gomes et al., 2018). Desirable features of yeast-based systems include the overlapping physiology with mammalian cells while retaining the simplicity and convenience of microbial hosts. Yeasts, like other eukaryotes, possess organelles required for complex processing of proteins, analogous to pathways found in human cells although these do not mimic the resultant modifications exactly (Li et al., 2022)

If the protein is small or requires minimal PTMs, it is often produced in bacteria, attractive hosts due to their simplicity and economic viability. Nutritional requirements are simple and cheap compared with mammalian cell lines (Schütz et al., 2023). Bacteria will readily grow in complex or defined media and some species accumulate large quantities of recombinant protein, potentially upwards of 50% of the total protein content of the cell (Francis and Page, 2010). Under optimal growth conditions, cells divide rapidly meaning biomass formation and in turn final yield of recombinant protein is high. Both Gram positive and negative bacteria see use, reviewed by Chen (2012). *Bacillus* and *Streptomyces* species are notable for their ability to secrete protein directly into the medium, aiding downstream purification (Vary et al., 2007, Wang et al., 2019, Berini et al., 2020, Yang et al., 2021). Pseudomonas species are currently used for production of biotherapeutics (Fabia et al., 2021). *E. coli* is often the preferred choice and thoroughly reviewed by Overton (2014), Rosano et al. (2019) and a generalised workflow is provided (Figure 1.2).

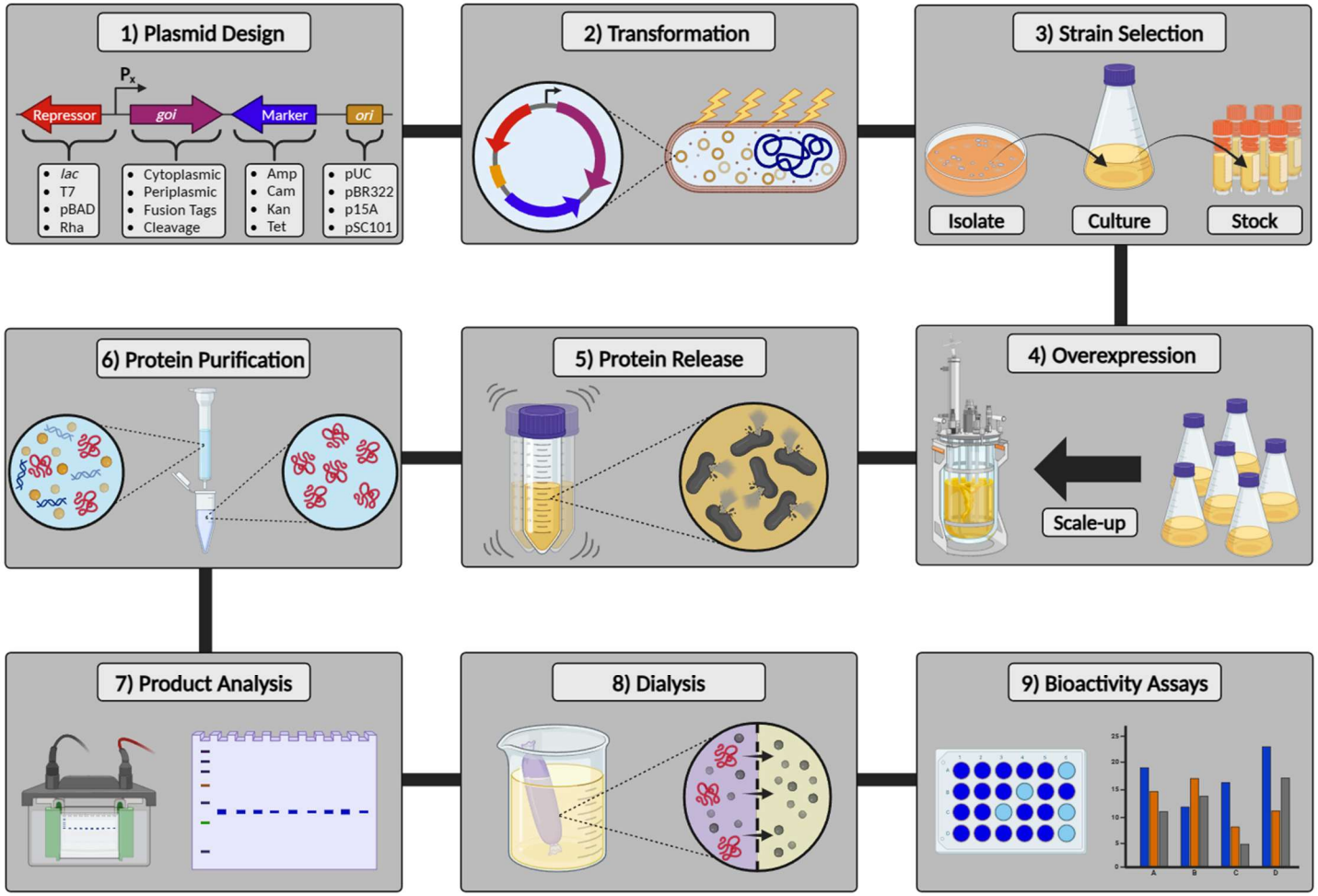


Figure 1.2 Bioprocesses to synthesise recombinant proteins in *E. coli* follow generalised workflows. Plasmid design determines the strength of expression. Plasmids are transformed into optimal expression hosts, isolates cultured and working stocks prepared. Optimising overexpression is generally done in shake flasks prior to scale-up into bioreactors. Raw lysate is extracted from cells through various methods before chromatographic purification to remove bulk contaminants and cell debris. Initial analysis of proteins via SDS PAGE can confirm a desired product is present; dialysis techniques can then be used to further purify the product, removing smaller compounds, and facilitating buffer exchange for downstream functional assays. Created with Biorender.com

In addition to previously discussed benefits of RPP in bacteria, *E. coli* has the distinct advantage of countless genetics tools for modification. Many proteins including hormones, cytokines, growth factors and antibody variants are manufactured in *E. coli* (Baeshen et al., 2015). Behind mammalian CHO cells, *E. coli* is the predominant host for the manufacture of biotherapeutics (Walsh and Walsh, 2022) (Figure 1.1B-C). Expression in *E. coli* is often done using plasmids containing an inducible promoter (Marschall et al., 2017) to control expression, an origin of replication to determine the gene dosage (Shao et al., 2021) and an antibiotic resistance cassette for maintenance during growth.

1.4 Recombinant protein production in *E. coli*

1.4.1 Inducible systems

Inducible promoters are ubiquitous in RPP due to their ability to elicit control over a bioprocess. Overexpressing recombinant proteins has several caveats, and the behaviour of one may be wildly different from the next. Precise control over the timing of initiating expression is desirable to maximise the final yield and quality of recombinant protein. Several reasons exist; cells overexpressing a heterologous protein divert metabolic activity from conventional cellular processes, causing physiological shifts and unnecessarily wasting resources (Wittmann et al., 2008, García-Calvo et al., 2023). Expressing particularly toxic recombinant proteins, which are poorly tolerated by the host and may lead to cell death, should be kept to basal levels until an optimum point for synthesis is reached (Giacalone et al., 2006). It may also be desirable to begin expression once cells reach the logarithmic stage of their growth, facilitating protein production and biomass accumulation concurrently.

Alternatively, de-coupling expression from growth and induction at high cell densities is viable if the promoter is active during the stationary phase (Zhao et al., 2021).

Inducible promoters, reviewed by (Marschall et al., 2017), work under similar principles; triggers for activation or de-repression of a system are restricted from the culture until an optimal point during the bioprocess. Without an inducer present, promoter activity is minimal, but following addition, RNA polymerase more readily binds core promoter elements, initiating transcription of a downstream gene. Such triggers vary; for some promoters, supply of an exogenous inducer molecule is required; often, these are sugars such as lactose or its analogue isopropyl B-D-1 thiogalactopyranoside (IPTG) (Hothersall et al., 2021), L-arabinose (Zulkifly et al., 2023) or L-rhamnose (Wagner et al., 2008). Other compounds such as tetracycline (Skerra, 1994), nitrate (Hothersall et al., 2022a) and propionate (Lee and Keasling, 2005) have been used. Some promoters are induced via shifts in physical conditions such as temperature (Valdez-Cruz et al., 2010) or pH (Chou et al., 1995). Alternatively, auto-inducible systems using specific media have been developed which require no addition of an inducer (Studier, 2005). Due to its long history as a model organism and the scope of genetic and biochemical study, several inducible systems, some native and others exogenous, are presently available in *E. coli*, and are a central reason for its attraction as a manufacturing host. During process optimisation, promoter selection is vital as caveats exist with each.

1.4.2 *lac* promoter systems

The *lac* promoter was the first inducible promoter identified (Jacob and Monod, 1961) and has been regularly applied for RPP. Several variants of the *lac* promoter have been identified which built upon the wild type. Examples include *lacUV5* which has a point mutation in the -10 hexamer (Pribnow box) of the core promoter to match the consensus sequence, improving expression (Arditti et al., 1968). Hybrids like the tac promoter, a fusion of an upstream portion of the endogenous trp promoter with downstream segments from *lacUV5* increased expression further (De Boer et al., 1983). A stronger variant still is the trc promoter, a tac derivative with a 1 bp insertion between the -10 and -35 elements to better match consensus (Brosius et al., 1985). PAR promoters are a series of *lac* promoter derivatives incorporating some of the aforementioned variants, providing a suite of promoter strengths for optimising expression of a recombinant protein (Browning et al., 2019, Hothersall et al., 2021).

Final titre of recombinant protein is obviously critical during RPP and one way to increase this is by application of stronger promoters which direct greater transcription. Hence, perhaps the most widely used inducible systems in *E. coli* are those found on pET vectors (Rosenberg et al., 1987), which utilise an IPTG inducible *lac* promoter to regulate T7 RNA polymerase (Figure 1.3), exploiting its rate of transcription and high affinity for the T7 promoter (Chamberlin et al., 1970, Chamberlin and Ring, 1973) to maximise expression of a downstream gene of interest (Tabor and Richardson, 1985, Studier and Moffatt, 1986). Use of pET vectors requires expression in the strain BL21(DE3), a lysogen which contains a non-excisable λDE3 prophage harbouring an

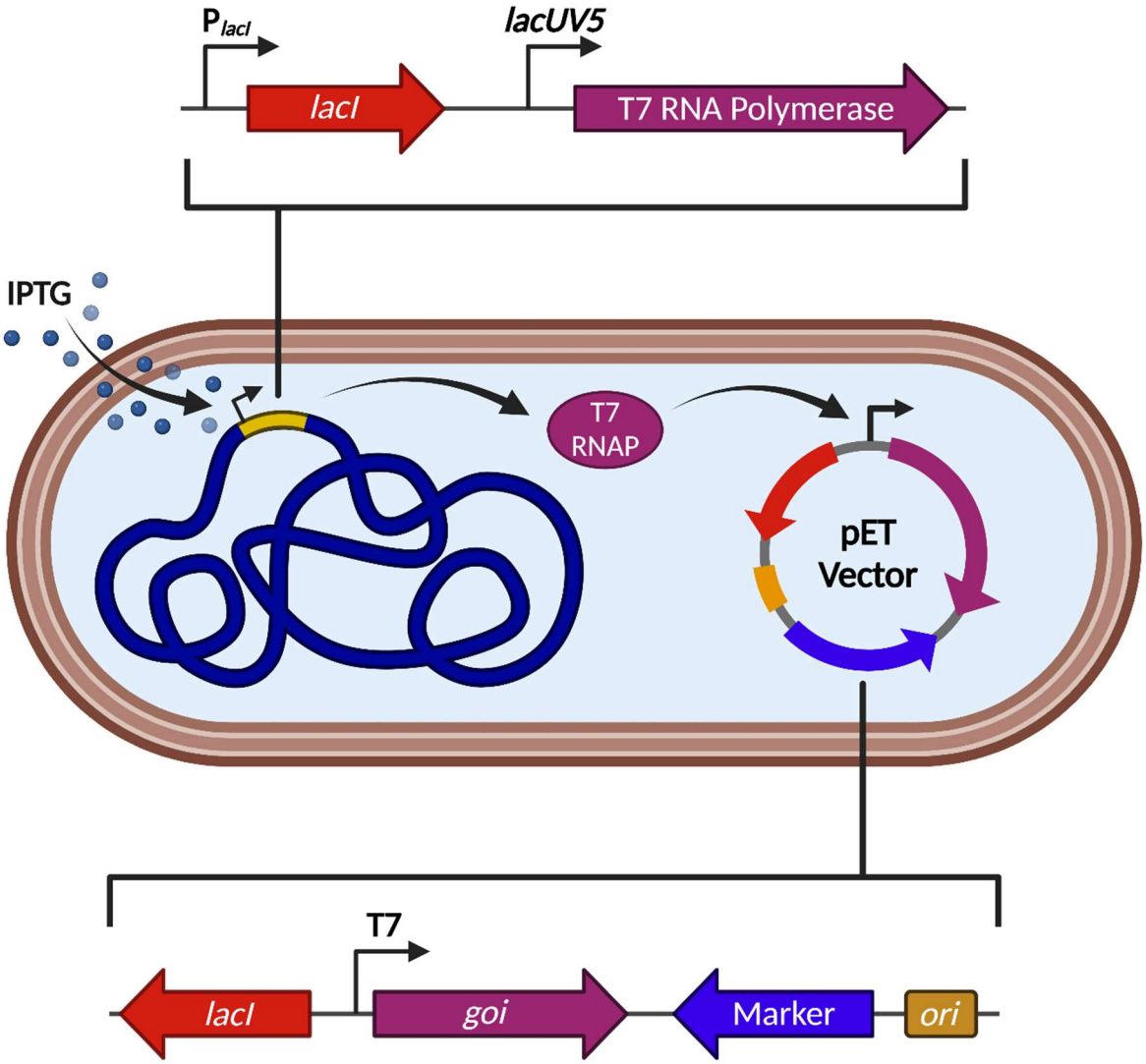


Figure 1.3: pET vectors require use with strains like BL21(DE3), which contains a λDE3 prophage harbouring a copy of *lacI*, and T7 RNA polymerase driven by the *lacUV5* promoter. A small *lacZα* fragment from cloning *lacUV5* is present upstream of T7 RNA polymerase, but each is translated independently. The expression cassette was cloned into the *int* gene of the phage λ genome; stable integration required a helper and conveniently prevents excision of the λDE3 prophage. For expression, a gene encoding the protein of interest is cloned downstream of the T7 promoter and the pET vector transformed into BL21(DE3). Genomic *lacI* and a variant provided *in trans* on the multicopy pET vector prevent initiation of transcription from *lacUV5*. Addition of IPTG causes de-repression, RNA polymerase initiates transcription from *lacUV5* leading to synthesis of T7 RNA polymerase, which initiates transcription of the gene encoding the protein of interest from the T7 promoter. Created with Biorender.com.

expression cassette with the *lacUV5* promoter driving T7 gene 1, encoding T7 RNA polymerase (Studier and Moffatt, 1986), translated from its own RBS (Studier, 1991a).

In the most basic pET systems, two points of regulation exist in the absence of IPTG; LacI repression of *lacUV5*, preventing expression of T7 RNA polymerase; and the near exclusive requirement of T7 RNA polymerase to transcribe from T7 promoters (Chamberlin et al., 1970). To overexpress a protein, IPTG is added to cells de-repressing *lacUV5* controlling the chromosomal copy of T7 RNA polymerase, leading to its synthesis. T7 RNA polymerase initiates transcription from the T7 promoter contained on a pET vector, which drives expression of the gene encoding the protein of interest. Owing to polymerase activity, T7 based pET systems can generate tremendous amounts of mRNA transcripts (Sastry and Ross, 1997); often to the detriment of host physiology (Hoffmann and Rinas, 2004, Guleria et al., 2020, Sharma et al., 2020).

It is well known *lac* regulated expression systems are notoriously leaky (Spehr et al., 2000), meaning basal gene expression in the absence of an inducer is high. In nature such activity is advantageous; low-level read-through allows some synthesis of lactose permease (LacY), responsible for mediating lactose uptake (Abramson et al., 2003), poising the cell for if it becomes metabolically favourable to utilise. For RPP, this is undesirable; loss of process control wastes cellular resources before reaching an optimal point to initiate protein synthesis; use of high-copy expression vectors or combinations with the extremely active T7 promoter compound this further. If the

protein of interest is toxic, high-cell-density fermentation becomes unobtainable, compromising the final yield.

Lac-regulated systems used for RPP often lack a full complement of operator sites; native *lac* promoters have three, O1, O2 and O3 (Oehler et al., 1994). O1, proximal to the core promoter, is the primary operator with the highest binding affinity for LacI (Winter et al., 1981); O2 is downstream of O1 within *lacZ* (Reznikoff et al., 1974), O3 is upstream at the 3' end of *lacI* (Gilbert et al., 1976). While O2 and O3 are weaker auxiliary operators, all three are required for efficient repression; two subunits of tetrameric LacI bind O1, the other two contacting O2 or O3, forming a loop which impairs transcription (Krämer et al., 1987). Deletion of either O2 or O3 results in a 2-3 fold loss of repression, while deletion of both results in a 70-fold reduction (Oehler et al., 1990). Variants like *tac* (De Boer et al., 1983) or *trc* promoters (Brosius et al., 1985) utilised for RPP discard O2 due to its position within *lacZ*. Many *lac* regulated T7 promoter constructs have no operator sequences, while T7*lac* variants have one.

Some solutions to leaky expression from *lac* regulated systems exist. LacI is typically provided *in trans* on the expression vector to counteract the gene dosage from high copy plasmids. This can be improved further through use of *lacIq* (Calos, 1978); a single point mutation in the -35 hexamer of the *lacI* promoter increasing its expression and making more repressor available. Catabolite repression is used extensively by *E. coli* and other bacteria to enforce a hierarchical preference for various carbon sources; expression of genes mediating catabolism of less favourable compounds is repressed. Glucose may be used for repression of lac promoters; intercellular cAMP and glucose

levels are negatively correlated, low cAMP levels mean CRP cannot recruit RNA polymerase to the promoter and activate expression (Stülke and Hillen, 1999). In *lac* systems combined with T7 promoters, leaky expression of T7 RNA polymerase from a *lac* promoter can be somewhat reduced using its natural inhibitor T7 lysozyme. In these systems co-expression of pLysE or pLysS plasmids (Studier, 1991a) curtails background expression of T7 RNA polymerase after expression from *lacUV5*. The pLysE and pLysS plasmids differ by whether T7 lysozyme is in the sense or antisense orientation relative to a constitutive *tet* promoter (Studier, 1991a). Two plasmid systems are not ideal though as they add further burden to the host.

1.4.3 Arabinose inducible systems

Systems utilising other inducers include the endogenous arabinose inducible promoter P_{araBAD} (Guzman et al., 1995); notable for its extremely tight regulation. The system is based on the *araBAD* operon, reviewed by (Schleif, 2021); AraB, AraA and AraD being responsible for catalysing the initial reactions for metabolism of L-arabinose (Englesberg, 1961). The system regulator is the transcription factor AraC (Schleif, 2010), the first member identified in the family of AraC-like transcriptional activators (Martin and Rosner, 2001). In the operon, *araC* and *araBAD* are transcribed from divergent promoters (Miyada et al., 1984), and basal expression of AraC poises the system for activation. In the off state, dimeric AraC binds to two distant operators I_1 and O_2 via DNA looping (Hahn et al., 1984); this obscures sites required for the CRP-cAMP complex and RNA polymerase to bind (Ogden et al., 1980).

Two routes are available for uptake of L-arabinose by the cell (Brown and Hogg, 1972); these are via a low affinity high capacity symporter (AraE) (Novotny and Englesberg, 1966); or a high affinity low capacity ATP-binding cassette (ABC) transporter (AraFGH) (Hogg and Englesberg, 1969, Schleif, 1969, Kolodrubetz and Schleif, 1981a, Scripture et al., 1987). L-arabinose binding to AraC causes conformational changes leading to dissolution of the loop, with dimeric AraC now able bind to I_1 and I_2 operators (Schleif, 2000). CRP-cAMP is now able to access sites upstream of the P_{araBAD} promoter and RNA polymerase is recruited to initiate transcription.

A major issue with the P_{araBAD} is its all-or-nothing induction at sub-saturating inducer concentrations, resulting in limited tunability (Carrier and Keasling, 1999). At the culture level adding lower dosages of L-arabinose gives the illusion of titratable expression. More granular analysis of single cells reveals heterogeneity; split populations of high and low expressing individuals (Siegele and Hu, 1997). At low L-arabinose concentrations, the high affinity low capacity AraFGH transporter is the primary route of entry into cells (Schleif, 2010). It was proposed by Siegele and Hu (1997) that due to the nature of basal expression, distribution of uptake systems is not homogenous throughout a population. Some individuals will have expressed greater amounts of AraFGH at the point of induction and thus uptake more L-arabinose.

The P_{araBAD} system is autocatalytic and so creates positive feedback, AraC expression increases in cells having taken up more L-arabinose; AraC in turn activates greater expression of uptake systems, including the low affinity high capacity AraE transporter (Kolodrubetz and Schleif, 1981b). Hence, further imbalances in the culture are created

with sub-populations of cells with even greater capacity for L-arabinose uptake and thus expression of P_{araBAD} controlled genes. It was noted this process is analogous to that described for *lac* promoter systems (Novick and Weiner, 1957, Siegele and Hu, 1997); although this is less of an issue when using inducers like IPTG which also passively diffuses into cells, circumventing the symporter lactose permease (LacY) (Khlebnikov and Keasling, 2002, Striedner et al., 2003). Work-arounds exist; increasing basal expression of *araE* by replacing its constitutive promoter on the chromosome with a stronger variant, or expressing *araE* from a constitutive promoter on a plasmid, results in better homogeneity when inducing with lower concentrations of L-arabinose (Khlebnikov et al., 2001).

1.4.4 Stress during RPP

An important feature of an expression system is its tunability; a linear relationship between inducer concentration and expression level allows precise control over expression (Marschall et al., 2017). Depending on the nature of the recombinant protein, *E. coli* can be placed under a little or considerable stress during RPP. With highly soluble cytoplasmic proteins, higher expression levels are advantageous but many proteins are difficult to express without serious consequences to the host; for example integral membrane proteins (IMPs) in particular are often recalcitrant to overexpression (Gubellini et al., 2011).

Cytoplasmic stress responses have been well studied in association with recombinant protein production (Hoffmann and Rinas, 2004, Guleria et al., 2020, Sharma et al., 2020). High level expression is well known to upregulate the general stress response,

mediated by the alternative sigma factor RpoS; it is typically upregulated during stationary phase and under nutrient limitation (Battesti et al., 2011). The heat shock response is mediated by the alternative sigma factor RpoH and is induced by elevated temperature (Nagai et al., 1991) but also misfolding of proteins in the cytoplasm (Arsène et al., 2000). The stringent response is induced by depletion of available amino acids leading to accumulation of uncharged tRNA; this induces formation of ppGpp (Haseltine and Block, 1973), which alters gene expression shutting down transcription and translation (Irving et al., 2021). Managing such stress responses has become a valid strategy for optimising a bioprocess; 'low and slow' often results in better yields of bioactive product, as opposed to faster more intense expression using strong promoters and high growth temperatures (Sevastsyanovich et al., 2009, Wyre and Overton, 2014, Selas Castiñeiras et al., 2018a, Chen et al., 2021, Zulkifly et al., 2023).

1.5 Recombinant protein expression in the periplasm

1.5.1 An overview of the periplasm

Research has also focused on expression of recombinant proteins in compartments besides the cytoplasm. Like other Gram negative organisms, *E. coli* possess an extra-cytoplasmic region termed the periplasm, which constitutes one part of the cell envelope (Silhavy et al., 2010). Gram positive organisms contain an analogous area, between the plasma membrane and thick peptidoglycan layer, but it is less substantial than in Gram negatives (Matias and Beveridge, 2005, Matias and Beveridge, 2006).

In Gram negatives, the periplasm is situated between the inner membrane (IM) and outer membrane (OM), and at around 30 % of the total cellular volume (Stock et al., 1977), comparatively little is known about it compared with the cytoplasm. Physically it is a gel-like fluid, with consistency now believed to approach that of the cytoplasm (Sochacki et al., 2011); though, proximity to the more porous OM means the environment is quite different and the periplasm is completely devoid of ATP (Okuda et al., 2012). This second cellular compartment offers several benefits, with many unique functions.

A layer of peptidoglycan runs through the periplasm (Vollmer and Bertsche, 2008), covalently appended to the inner leaflet of the OM by the abundant lipoprotein Lpp, providing skeletal rigidity and protection from internal and external forces (Hantke and Braun, 1973, Braun, 1975). Cell wall assembly and maintenance are mediated by periplasmic proteins which polymerise alternating glycan subunits and crosslink peptide chains (Van Heijenoort, 2011). Nutrient acquisition is facilitated via the periplasm, containing proteins responsible for engaging a variety of ligands including sugars, amino acids, phosphate, and metal ions (Coleman, 1992, Boos and Shuman, 1998, Krewulak et al., 2004, Chu et al., 2013).

While the cytoplasm is a reducing environment (Prinz et al., 1997), the periplasm is oxidising, owing to the presence of a disulphide bond formation (Dsb) system (Manta et al., 2019). Disulphide bond formation protein A (DsbA) is the donor for disulphide formation in substrates (Bardwell et al., 1991); reduced DsbA is regenerated by the IM bound disulphide bond formation protein B (DsbB) (Bardwell et al., 1993), itself

oxidised by quinones from cellular respiration (Kobayashi, 1999, Takahashi et al., 2004). Analogous proteins with opposing function and redox states, disulphide bond formation protein C (DsbC) and disulphide bond formation protein D (DsbD), provide quality control through isomerisation of aberrant disulphide bonds (Shevchik et al., 1994, Rietsch et al., 1997).

1.5.2 Periplasmic stress responses

E. coli has several stress response networks which serve to maintain homeostasis in response to changes to the hosts internal and external environments. Some are responsible for responding to perturbations within the cell envelope (Mitchell and Silhavy, 2019). In general, these are centred around inner membrane (IM) assemblies which detect stress on the periplasmic side and transduce this signal into the cytoplasm, activating transcription factors or alternative sigma factors which regulate gene expression accordingly. There is often overlap between stress responses, with multiple systems being induced to coordinate an effective response to protect the envelope (Bury-Moné et al., 2009).

Of the periplasmic stress responses, the σ^E pathway is one of two which are centred on protein folding (Mecsas et al., 1993). The σ^E pathway is not a phosphorelay, but a IM localised proteolysis cascade (Ades et al., 1999). RseA is the transmebrane protein though which sequential degradation occurs, de-repressing the sysyem; the cytoplasmic domain of RseA acts as an anti-sigma factor (De Las Peñas et al., 1997), for the alternative sigma factor RpoE (σ^E) (Erickson and Gross, 1989). RseA is bound on the periplasmic side of the membrane by RseB, its dissociation mediated by

unfolded proteins (Chaba et al., 2011). A second regulatory component, the IM associated protease DegS transitions to a proteolytic conformation upon exposure to peptide sequences indicative of protein misfolding (Sohn and Sauer, 2009). Active DegS cleaves the periplasmic domain of RseA, exposing transmembrane regions to further cleavage by a second protease RseP, releasing the cytoplasmic domain (Alba et al., 2002). Truncated RseA released into the cytoplasm is finally degraded by the protease ClpXP (Flynn et al., 2004) releasing σ^E, its binding to RNA polymerase allowing initiation of transcription from target promoters (Mecsas et al., 1993). σ^E target genes include those for the protease DegP, chaperone FkpA (Mutalik et al., 2009).

The second periplasmic stress response which responds to protein stressors is CpxAR, a phosphorelay composed of the inner membrane bound sensor CpxA and the cytoplasmic transcription factor CpxR (Raivio, 2014). Like RseB in the σ^E pathway, CpxA responds to periplasmic cues resulting in phosphotransfer to CpxR, which upregulates target genes. Multiple cues activate CpxAR, the shared effect being misfolding of periplasmic proteins (Raivio and Silhavy, 2001). An accessory component CpxP, negatively regulates the system on the periplasmic side, binding CpxA and preventing autocatalytic activity (Raivio et al., 1999); sensing of misfolded substrates by CpxP causes release of CpxA, derepressing the system (Digiuseppe and Silhavy, 2003). The CpxR regulon is composed of around 50 target genes (Price and Raivio, 2009). Like σ^E, CpxR upregulates the gene encoding the periplasmic protease DegP (Pogliano et al., 1997). Other target genes include those for periplasmic chaperones like spheroplast protein Y (Spy), the disulphide bond protein DsbA,

peptidylprolyl isomerases PpiA and PpiD (Pogliano et al., 1997, Dartigalongue and Raina, 1998, Raivio et al., 2013).

Other periplasmic stress responses include BaeSR, a classic two component system formed of the IM sensor histidine kinase BaeS, which auto phosphorylates upon activation by stressors and transfers this to the response regulator BaeR (Raffa and Raivio, 2002). Phosphorylated BaeR is able to bind target DNA sequences (Nagasawa et al., 1993). Several compounds are detected by the periplasmic sensing domain of BaeS, and the system is believed to respond to noxious substances by upregulating efflux pump synthesis (Leblanc et al., 2011). The phage shock protein (Psp) response (Flores-Kim and Darwin, 2016) is induced by generalised perturbations to IM integrity (Joly et al., 2010). PspF is the response regulator for the system and a transcriptional enhancer for RNA polymerase holoenzyme containing the alternative sigma factor σ^{54} (Weiner et al., 1991). A final system, the regulator of capsule synthesis (Rcs) response is upregulated in response to damage of lipopolysaccharide within the OM or the peptidoglycan cell wall (Callewaert et al., 2009, Konovalova et al., 2016). The response regulator of the system is RcsB (Meng et al., 2021).

1.5.3 Benefits and caveats of periplasmic expression

Access to the Dsb system is a prime reason for localisation of recombinant proteins to the periplasm. Biotherapeutics now constitute a large portion of the recombinant protein market (Walsh and Walsh, 2022); many including antibody fragments or growth factors are of mammalian origin, hence disulphide bonding is required for folding into an active conformation *in vivo* (Berkmen, 2012, Rathore and Batra, 2016). Other

advantages include an overall lower protein content with fewer proteases to aid product stability (Talmadge and Gilbert, 1982). Downstream purification is also simplified; periplasmic contents can be released by disrupting the OM and cell wall, leaving spheroplasts intact (Schimek et al., 2020).

Additional complexity is created when forcing the cell to export the recombinant protein though, specifically the act of translocating it across the IM. Localisation of recombinant proteins to the periplasm compounds many difficulties already observed during cytoplasmic production (covered in section 1.4.2). Regardless of the chosen compartment, overexpression places metabolic burden on the host, in addition to saturating cellular machinery required for native proteins; overlapping stress responses are upregulated, compromising yield (Hoffmann and Rinas, 2004). Translocation of a recombinant protein additionally overloads the hosts export machinery. Preventing synthesis of native envelope proteins has been suggested as a primary reason for poor tolerance to high level protein expression in the periplasm (Schlegel et al., 2013, Baumgarten et al., 2018).

1.5.4 Methods for periplasmic screening during RPP

No universally applicable and optimal solution to periplasmic expression has been found; hence, screening of the expression vector, choice of N-terminal signal peptide, media composition and physical parameters which make up the production system is necessary (Selas Castiñeiras et al., 2018a, Karyolaimos et al., 2019b, Mirzadeh et al., 2020, Karyolaimos and de Gier, 2021). Crucial to screening is quantifying how much recombinant protein has been localised to the periplasm. Traditionally this has been

done by liberating the periplasmic contents via chemical or physical means from spheroplasts and resolving the resulting fractions by SDS PAGE or immunoblotting (Lall et al., 1989, Davidson and Sun, 2002); this is time-consuming and not conducive to a high throughput approach though. We have recently reviewed several methods for more rapid quantification of proteins localised to the periplasm (Osgerby and Overton, 2023). Due to export requiring N-terminal signal peptides, most methods involve fusion of a C-terminal tag which can be subsequently detected.

Some systems permit detection of fluorescence, allowing access to powerful cytometric techniques. Halo tags (HT7) exploit the binding of haloalkanes by the 34 kDa haloalkane dehalogenase (DhaA) from *Rhodococcus rhodochorus*. Endogenously, DhaA hydrolyses haloalkanes displacing the halide and releasing the alkane. To engineer a tag which irreversibly binds it target, a H272F mutation was used to prevent recycling of the DhaA after halide displacement and formation of a DhaA-alkane intermediate, locking the ligand in place. In *E. coli*, HT7 was combined with a carboxytetramethylrhodamine (TMR) labelled haloalkane to detect periplasmic proteins exported via fusion to $DsbA^{SP}$ (Ke et al., 2016). Another system, tetracysteine (Tc) tags, use short peptides with the consensus CCXXCC; the system exploiting binding between thiol groups on cysteine residues and arsenic compounds (Adams et al., 2002). The ligand is composed of two trivalent arsenic substituents bound to a fluorescein dye and capped with 1,2-Ethanedithiol (EDT) moieties for quenching in the absence of the tag. Tc tags combined with the bi-arsenical dye fluorescein arsenical hairpin binder-ethanedithiol (FlAsH-EDT_2) and cell sorting was used in *E. coli* to screen for novel mutations which improve export via the co-translational branch of Sec (Lee

et al., 2016) and CRISPR/Cas9 knockout of genes which improved export (Gao et al., 2018).

Other systems utilise enzymatic reactions to detect the presence of periplasmic proteins. β-lactamases are a group of enzymes synthesised by bacteria, which attack the core β-lactam ring, central to the activity of many antibiotic families. Endogenously β-lactamases are active in the periplasm, their target being β-lactam antibiotics; as analogues of peptides within the cell wall, β-lactams irreversibly bind transpeptidases mediating cross-linkage, locking them in a non-functional state (Tooke et al., 2019). TEM-1 β-lactamase has been used for several screens in the *E. coli* periplasm, firstly to detect successful folding of fusion partners, with resistance to ampicillin correlating with efficacy (Mansell et al., 2010). Similarly, signal peptides and translation initiation were optimised by fusion directly to TEM-1 β-lactamase, again monitored by ampicillin resistance (Heggeset et al., 2013, Mirzadeh et al., 2020). A final screen using a library of signal peptides fused TEM-1 β-lactamase downstream of an scFv; detection of export was via ampicillin or the chromogenic substrate nitrocefin (Selas Castiñeiras et al., 2018a). Another periplasmic enzyme alkaline phosphatase (PhoA), which liberates phosphate from containing compounds for transfer to the cytoplasm (Coleman, 1992), has been utilised for detecting export to the periplasm, via another chromogenic substrate 5-Bromo-4-chloro-3-indolyl phosphate which is cleaved by PhoA (Hoffman and Wright, 1985).

Fluorescent proteins, most commonly green fluorescent protein GFP (Shimomura et al., 1962), are excellent tools for screening during production of cytoplasmic

recombinant proteins (DeLisa et al., 2000, Lissemore et al., 2000, Omoya et al., 2004, Su, 2005, Hothersall et al., 2021, Hothersall et al., 2022a, Hothersall et al., 2022b). Through fusion to a protein of interest, GFP can be used to quantify, infer localisation and report on the folding state of its partner and has been regularly employed in optimising RPP (DeLisa et al., 2000, Lissemore et al., 2000, Omoya et al., 2004, Su, 2005, Hothersall et al., 2021, Hothersall et al., 2022a, Hothersall et al., 2022b). Most GFP derivatives do not fluoresce in oxidising environments like the *E. coli* periplasm when exported via the primary Sec translocation pathway, due to misfolding (Jain et al., 2001, Dammeyer and Tinnefeld, 2012). One derivative, superfolder GFP (sfGFP) has been indicated to fluoresce in the periplasm, even when exported via Sec (Aronson et al., 2011, Dinh and Bernhardt, 2011). Application of sfGFP as a periplasmic screening tool formed the basis for Chapter 4 of this work; further details of sfGFP and alternative periplasmic screening methods are covered in section 4.1.

1.5.5 Recombinant proteins manufactured in the periplasm

In spite of the potential caveats, some recombinant proteins are currently synthesised in *E. coli* via export to the periplasm, most notably some biotherapeutics (Walsh and Walsh, 2022). Fab (fragment antigen-binding region) antibodies are monoclonal IgG variants, composed of the variable regions of the light (V_L) and heavy chains (V_H) and constant regions of the light (C_L) and heavy chains (C_H1) (Bates and Power, 2019). Though Fab antibodies require disulphide bonding for bioactivity, production in *E. coli* is possible due to lacking the remaining heavy chain constant domains (C_H2 and C_H3), termed the Fc (fragment crystallizable) region, hence no requirement for glycosylation (Patil et al., 2022).

Examples include ranibizumab (Lucentis® and Susvimo™) and its biosimilar ranibizumab-nuna (Byooviz™) (Tungekar et al., 2024); humanised fab fragments which inhibit vascular endothelial growth factor A (VEGF-A) and are used to treat conditions including age-related wet macular degeneration (Rowe and Ciulla, 2024). Certolizumab pegol (Cimzia®) is another humanised Fab fragment produced in the *E. coli* periplasm (Rashid, 2022); a pegylated tumour necrosis factor (TNF) inhibitor indicated for treating inflammatory autoimmune conditions like Crohn's disease and rheumatoid arthritis (Deeks, 2016).

Other antibody biotherapeutics synthesised in the *E. coli* periplasm include single domain (V_{HH}) nanobodies, consisting of the variable region of a heavy chain from camelid species (Jin et al., 2023). One such example is caplacizumab-yhdp (Cablivi®), a humanised bivalent nanobody with two identical V_{HH} domains connected by a short amino acid linker (Xi et al., 2021). Caplacizumab-yhdp inhibits Von Willebrand factor (VWF) and primarily used to treat acquired thrombotic thrombocytopenic purpura (aTTP) (Scully et al., 2019).

1.6 Export of recombinant proteins

1.6.1 Translocation pathways

In *E. coli*, two routes are available for the translocation of proteins across the inner membrane to the periplasm (Figure 1.4), the the general secretory (Sec) machinery (Oswald et al., 2021) or Twin Arginine Translocation (Tat) system (Frain et al., 2019). Each pathway discriminates substrate proteins in different ways; Sec is only capable

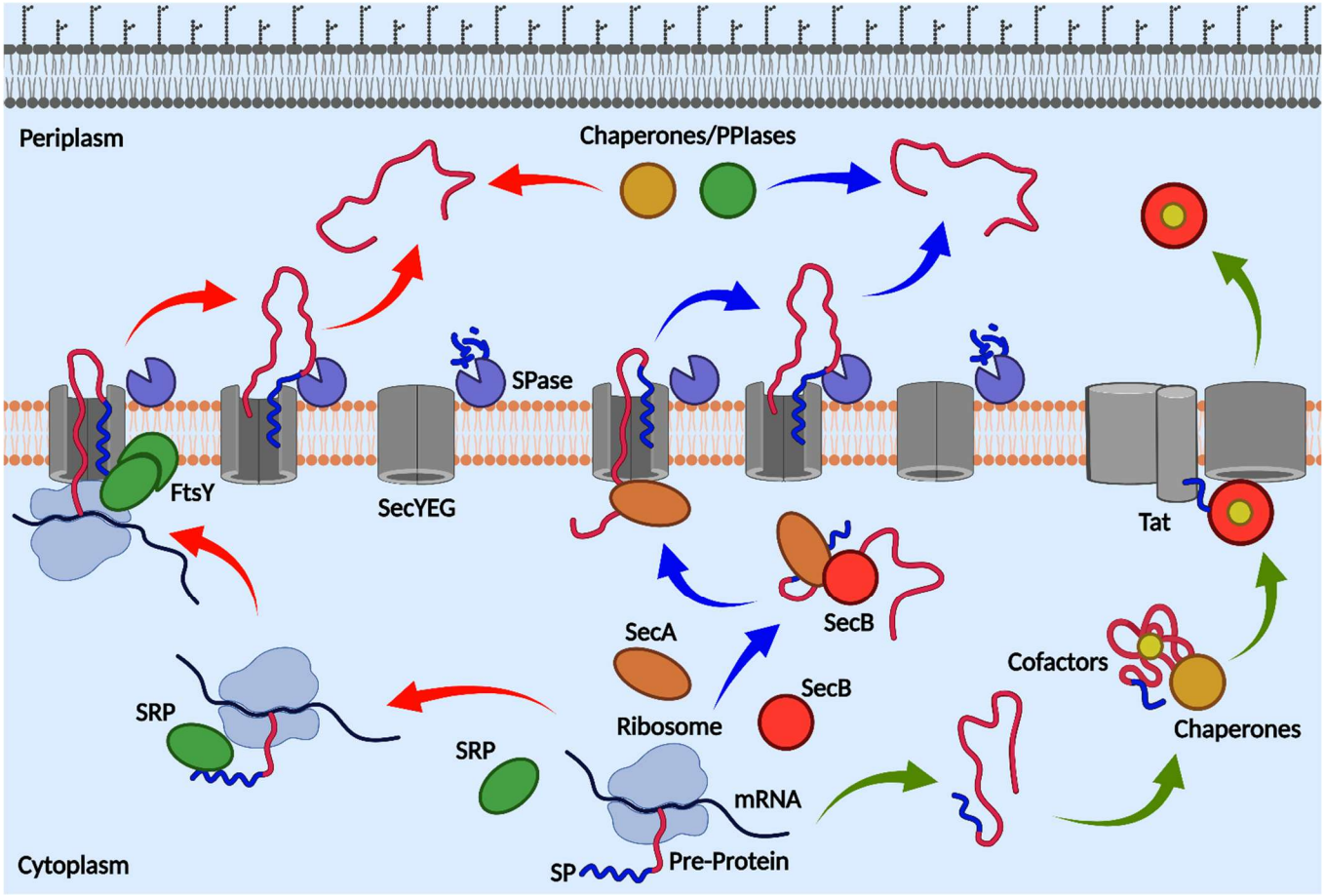


Figure 1.4: Proteins are translocated across the IM into the periplasm by one of three pathways; the route determined by the properties of a N-terminal signal peptide. Two pathways utilise the membrane channel SecYEG and are split into the post-translational (blue arrows) or co-translational (red arrows) branches. The third pathway is via Tat (green arrows). During translation, various export factors interact with the ribosome and signal peptide to determine the route of export. In the post-translational branch, SecA and chaperone SecB shuttle translated but unfolded polypeptides to SecYEG at the IM; ATPase activity of SecA is used to drive proteins through the channel, the signal peptide is cleaved by SPase and the protein falls into periplasmic folding pathways. In the co-translational branch, SRP delivers the entire RNC complex to SecYEG, docking with its receptor FtsY; translation proceeds through the channel, the signal peptide is cleaved by SPase and and the protein falls into periplasmic folding pathways. Tat-dependent export is unique in that proteins are fully synthesised and fold prior to export. Often these proteins require cytoplasmic co-factors for maturation; once folded the signal peptide engages Tat membrane components where it is transferred across the IM in a fully folded state. Created with Biorender.com.

of exporting unfolded proteins; Tat is unusual in that it is somehow able to translocate fully folded proteins across the IM and a quality control system which can identify incorrectly folded substrates and prevent their export (Taw et al., 2020). While the ability of Tat to export fully folded proteins is certainly impressive, its application to RPP is limited compared to Sec. A main advantage to periplasmic expression is Dsb mediated oxidative folding (Berkmen, 2012) and without disulphide bond formation, the protein will likely fold poorly in the cytoplasm which is not appear compatible with Tat mediated translocation (Delisa et al., 2003, Matos et al., 2014). Further, only 32 Tat-dependent proteins have been identified thus far in *E. coli* (Orfanoudaki and Economou, 2014). Estimations have placed the number of proteins in *E. coli* exported to the cell envelope at around 25 % of the proteome (Beckwith, 2013). Of these, around 98 % are Sec dependent highlighting the fact that Sec is the predominant export machinery in *E. coli* (Orfanoudaki and Economou, 2014).

1.6.2 The Sec machinery

The ubiquitous Sec machinery is universally conserved (Bolhuis, 2004, Denks et al., 2014, Oswald et al., 2021). The pathway is split into two branches (Figure 1.4), differentiated by whether translation is coupled to translocation, like in co-translational export (Steinberg et al., 2018), or uncoupled from it as with post-translational export (Crane and Randall, 2017). The two pathways differ in initiation and the driving force behind export, but share the same membrane bound translocon. In *E. coli*, this core element of is the heterotrimeric complex of the IMPs SecY, SecE and SecG, SecYEG (Ito et al., 1983, Riggs et al., 1988, Nishiyama et al., 1994). Around 500 copies of the translocon are proposed to exist within the cell at a given time (Matsuyama et al., 1992)

and the oligomeric state of the complex is apparently variable (Mao et al., 2013, Zheng et al., 2016). The channel proper is formed by SecY, large transmembrane with a distinctive hourglass conformation, the tapered central region combined with an α-helical plug block entry from either side of the IM when translocation is not commencing (Li et al., 2016). SecY has 10 transmembrane domains arranged into two groups of 5; the design of this clamshell conformation creates a lateral gate which supposedly permits release of the central constriction via signal peptide insert, activation of export (Du Plessis et al., 2009) and additionally allows for transfer of IMPs into the membrane (Mercier et al., 2021). Both SecE and SecG have discrete interactions with SecY (Homma et al., 1997). SecE is essential and its deletion will swiftly result in SecY degradation by the protease FtsH (Kihara et al., 1995); its physical contacts with SecY seem to indicate it provides structural support (Veenendaal et al., 2001). SecG is not essential but apparently interacts with another export factor SecA enhancing its activity through inversion (Nagamori et al., 2002).

1.6.3 Post-translational export via Sec

The post-translational branch of Sec involves export of proteins after they have been synthesised by the ribosome (Crane and Randall, 2017) (Figure 1.4). Most periplasmic proteins are delivered across the IM via the post-translational branch (Tsirigotaki et al., 2017). While export occurs post-translationally, actual targeting apparently occurs early during translation (Cranford-Smith and Huber, 2018). The central protein in post-translational export is the ATPase SecA and it has been shown to interact with both the ribosome at L23 and the nascent polypeptide (Huber et al., 2011, Huber et al., 2017). Identification of substrates early is presumably advantageous, ensuring they do

not fall into incorrect pathways or begin folding prior to export. SecA apparently exists in both cytoplasmic and membrane associated forms with the latter actually apparently being favoured (Seinen et al., 2021). Another component SecB is a chaperone, it interacts with SecA (Randall et al., 2004) and is active as a tetramer (Dekker et al., 2003). Interestingly, SecB also appears to act on substrates not exported via Sec (Ullers et al., 2004). SecA-SecB interaction and SecA interaction with the nascent preprotein act to deliver it to SecYEG, facilitated by SecA interaction with SecY (Cranford-Smith and Huber, 2018). Once coupled to SecYEG, ATP hydrolysis by SecA moves the preprotein though the channel via a pushing motion with a clamp preventing backtracking (Catipovic et al., 2019).

1.6.4 Co-translational export via Sec

The second branch of Sec directly coupled protein translation to translocation (Steinberg et al., 2018) (Figure 1.4). Most co-translational proteins are IMPs or those periplasmic proteins that fold quickly to be exported post-translationally (Tsirigotaki et al., 2017). Like the post-translational branch, co-translational export is initiated early on in translation via the signal recognition particle (SRP) (Bernstein et al., 1989), a ribonucleoprotein composed of the fifty-four homologue (Ffh) protein and 4.5S RNA (Akopian et al., 2013). To facilitate identification, SRP interacts with ribosomal proteins L23 and L29 (Schaffitzel et al., 2006) before the preprotein even emerges from the exit tunnel (Mercier et al., 2017). Upon substrate identification, the entire ribosome nascent chain (RNC) complex is transferred to SecYEG. At the membrane, SRP docks with its receptor FtsY; both are GTPases and stimulate one another via alternating hydrolysis

to transfer the RNC onto SecYEG (Zhang et al., 2009). After loading of the RNC, translation occurs directly through SecYEG into the periplasm.

1.6.5 Additional Sec components

YidC is involved in biogenesis of IMPs as part of the holo-translocon, a large complex consisting of SecYEG-SecDFYajC-YidC (Schulze et al., 2014); it also apparently operates as an inserted independent of Sec (Kumazaki et al., 2014). Function of other components of the Sec machinery are less clear. A second heterotrimeric complex SecDFYajC. SecDF are proposed to pull translocating proteins through SecYEG from the periplasmic side of the membrane, the energetic requirements for this filled by the proton motive force(Tsukazaki, 2018). While YajC function is unknown, it is expressed with SecDF so potentially assists in there translocating activities (Fang and Wei, 2011). An essential component toward the end of translocation, SPase I cleaves the N-terminal signal peptides responsible for targeting proteins to either branch of Sec, releasing the preprotein into the periplasm (Auclair et al., 2012).

1.6.6 Signal peptides

Targeting to either branch of Sec, or Tat for that matter, is via the presence of N-terminal signal peptides (SP) (Freudl, 2018). Signal peptides are short sequences, around 15 – 30 amino acids long, encoded at the start of exported proteins and what is recognised by targeting factors like Sec A and SRP (Huber et al., 2017, Mercier et al., 2017). Amino acid sequence of the signal peptide determines physical characteristics and which pathway the protein is targeted to. Each signal peptide is composed of three sections. The first, the N-region is positively charged (Guo et al.,

2018). The H-region is the longest section and is defined by a higher proportion of hydrophobic residues (Chou and Kendall, 1990); in general more hydrophobic signal peptides are directed to the co-translational pathway (Zopf et al., 1990). In support of this the normally post-translational signal peptide for maltose binding protein was swapped to the co-translational pathway by introducing more hydrophobic residues (Lee and Bernstein, 2001). The final C-region contains the SPase cleavage site with a consensus AXA motif (Perlman and Halvorson, 1983). Optimisation of signal peptides to improve expression in the periplasm has been attempted (Low et al., 2013), although there is little consistency in beyond the 3 defined regions in what makes an optimal signal peptide, further the relationship between a signal peptide and recombinant protein varies (Selas Castiñeiras et al., 2018a).

1.7 Aims and objectives

E. coli has a long history use in bioprocessing; even with competition from mammalian hosts capable of synthesising more complex proteins, it is still hugely relevant for producing recombinant proteins for research and industry (Walsh and Walsh, 2022). Nevertheless, several areas are worthy of investigation to further optimise the use of *E. coli* for RPP, and we have focused our attention on three distinct projects.

Inducible systems are central to a bioprocess, providing control over expression of the recombinant protein. Inducible systems should drive strong expression of the gene of interest, tuneable by altering the concentration of the inducer. Basal expression from the promoter in the absence of any inducer should be low, preventing synthesis until a desirable point. Finally, the inducer should have minimal interaction with host cell

physiology. As covered in section 1.4, while existing inducible promoters meet some of the criteria for an optimal system, each has caveats. Expression systems incorporating *lac* promoters, including the popular T7 promoter, suffer from high basal expression and the available solutions are not always optimal (Spehr et al., 2000). Comparatively L-arabinose inducible systems are tightly regulated, but subject to all-or-nothing induction limiting tunability (Siegele and Hu, 1997). Thus, there is a clear opportunity for expansion of the existing genetic toolbox available in *E. coli* for RPP. Hence, the first aim of this work and covered in Chapter 3, was to investigate the applicability of a novel urea inducible promoter for RPP. Our objectives for this centred around a series of metrics gauging promoter performance in relation to RPP, these were:

- Does the urea inducible promoter drive strong and tuneable expression?
- Is basal expression low in the absence of urea?
- How does urea interact with the host cell and its physiology?
- Can we scale the urea inducible system for use in bioreactors?

In section 1.5.3, we discussed how expression of recombinant proteins within the *E. coli* periplasm is an attractive option, most notably for synthesis recombinant proteins requiring disulphide bonding for bioactivity. For *E. coli* to better compete with mammalian hosts for production of more complex proteins, the unique challenges associated with periplasmic expression must be addressed. One such issue is how to rapidly detect recombinant proteins localised here; classical methods relying on sub-cellular fractionation to isolate periplasmic proteins, which are subsequently resolved by SDS PAGE limit throughput. In section 1.5.4, we covered several higher throughput

methods which can be applied for periplasmic screening, although in general these still require multiple processing steps after sampling to detect recombinant proteins (Osgerby and Overton, 2023). GFP reporter fusions to a protein of interest combined with cytometric analysis offers more real-time detection. While sfGFP, unlike other GFP derivatives, was previously indicated to fluoresce in the *E. coli* periplasm (Aronson et al., 2011, Dinh and Bernhardt, 2011), we found little information describing its application for screening during RPP. We theorised sfGFP, fused C-terminally to a recombinant protein and combined with flow cytometry, could provide a useful approach to optimise various parts of an expression system for periplasmic localisation. Thus, the second aim of this work, covered in Chapter 4, was to investigate whether GFP derivatives like sfGFP could be utilised as a periplasmic screening system. Our objectives for this were:

- Is sfGFP localised to the periplasm during high level expression?
- How is overexpression of periplasmic sfGFP tolerated by the host?
- Does sfGFP fluoresce in the periplasm during high level expression?
- What other GFP derivatives could fluoresce in the periplasm?

Through prior indications in the literature, covered in section 1.5.3, and observations during this work (Chapter 4), we also understood that localising recombinant proteins to the periplasm often significantly impacts host viability and final protein titre, likely due to saturating export machinery (Schlegel et al., 2013, Baumgarten et al., 2018). For *E. coli* to present a more attractive alternative to mammalian cells for production of complex recombinant proteins, its capacity and tolerance to periplasmic overexpression must be improved. We wondered whether application of synthetic

biology could be used to engineer a system which lowers such burdens on the host; first by detecting target stressors, namely overloading export systems, then responding through negative feedback; repressing expression of the recombinant protein which initially induced the stress. For example, as covered in section 1.5.2, several stress response networks exist within the periplasm which respond to envelope stress (Bury-Moné et al., 2009, Mitchell and Silhavy, 2019), which could be utilised to sense stressors imposed on the host by overexpression of periplasmic recombinant proteins. Thus, the final aim of this work, covered in Chapter 5, was to develop a system able to detect stress arising during periplasmic overexpression and then exploiting this sensing capability as a trigger to tune expression to a tolerable level. Our objectives for this work were:

- What system can we develop to detect and report on target stressors?
- What tools are available to shut off overexpression following induction?
- Can we engineer turnover into the system, cycling it between on and off states?
- Can such a system improve host tolerance to periplasmic expression?

Chapter 2: Materials and Methods

2.1 Media and Reagents

2.1.1 Antibiotics

2.1.1.1 Ampicillin

Ampicillin (Amp) stocks were prepared at 100 mg mL^{-1} in diH_2O using Ampicillin, Sodium Salt (Merck), 0.2 µm filter sterilised (Fisher) and stored as 2 mL aliquots at -20˚C for up to 3 months. For selection of resistant cells in liquid or solid growth media, Amp thawed on ice was added at 100 µg mL^{-1} immediately prior to use.

2.1.1.2 Kanamycin

Kanamycin (Kan) stocks were prepared at 50 mg mL^{-1} in diH_2O using Kanamycin Sulphate (Sigma), 0.2 µm filter sterilised (Fisher) and stored as 2 mL aliquots at -20˚C for up to 3 months. For selection of resistant cells in liquid or solid growth media, Kan thawed on ice was added at 50 µg mL^{-1} immediately prior to use.

2.1.1.3 Polymyxin B Nonapeptide

Polymyxin B Nonapeptide (PMBN) stocks were prepared at 5 mg mL^{-1} in diH_2O using Polymyxin B Nonapeptide Hydrochloride (Sigma), 0.2 µm filter sterilised (Fisher) and stored as 2 mL aliquots at -20˚C for up to 3 months. To permeabilise the *E. coli* OM, 25 µg mL^{-1} PMBN was added to cultures.

2.1.1.4 Tetracycline

Tetracycline (Tet) stocks were prepared at 20 mg mL^{-1} in diH_2O using Tetracycline Hydrochloride (Sigma), 0.2 µm filter sterilised (Fisher) and stored as 2 mL aliquots,

wrapped in aluminium foil to protect from light, at -20˚C for up to 3 months. For selection of resistant cells in liquid or solid growth media, Tet thawed on ice was added at 20 µg mL^{-1} immediately prior to use.

2.1.2 Growth Media

2.1.2.1 Lysogeny Broth

Lysogeny Broth (LB) was prepared using the Lennox or Miller formulations. LB Lennox was used for all work with cells containing the urea inducible promoter construct pET-15b_P_{uti101}-*6xhis*::*egfp*. LB Miller was used for everything else. LB Lennox was prepared using 10 g L^{-1} Tryptone (OXOID), 5 g L^{-1} Yeast Extract (OXOID) and 5 g L^{-1} Sodium Chloride (Sigma) in diH_2O, pH was adjusted to 7.0 using 2M Hydrochloric acid (HCl) (Fisher) or 2M Sodium Hydroxide (NaOH) (Sigma). LB Miller was prepared using a pre-mixed formulation (Sigma) at 25 g L^{-1} in diH_2O. LB Lennox and LB Miller were sterilised by autoclave at 121˚C for 15 min and stored at room temperature (RT) for up to 3 months. To prepare LB agar (LBA), Agar powder (Sigma) was added to LB at 15 g L^{-1} immediately prior to sterilisation. Approximately 20-25 mL molten LBA was poured into sterile 90 mm triple vented plastic petri dishes, dried under laminar flow for 30 min and LBA plates stored at RT for up to 3 months. Antibiotics and sterile additions were added to LB at RT immediately before use, or LBA cooled to 50-60˚C, which was immediately poured. LBA plates containing such compounds were stored at 2-8˚C for up to 1 month.

2.1.2.2 Terrific Broth

Terrific Broth (TB) was prepared as TB pre-mix containing 20 g L^{-1} Tryptone (OXOID), 24 g L^{-1} Yeast Extract (OXOID) and 0.4% (v/v) glycerol (Fisher) in diH_2O, with pH adjusted to 7.0 using 2 M HCl (Fisher) or 2 M NaOH (Sigma). A 10X phosphate buffer solution containing 0.17 M KH_2PO_4 (Scientific Laboratory Supplies) and 0.72 M K_2HPO_4 (Sigma) was prepared in diH_2O. TB pre-mix and phosphate buffer were sterilised by autoclave at 121˚C for 15 min and stored at RT, for up to 3 months. Before use, phosphate buffer was added to TB pre-mix to a concentration of 1X. Antibiotics and sterile additions were added to TB at RT immediately before use.

2.1.2.3 Semi-defined Growth Medium

Semi-defined growth medium was prepared according to Wyre and Overton (2014). Basal media was prepared as 35 g L^{-1} glycerol (Fisher), 14 g L^{-1} $(NH_4)_2SO_4$ (Sigma), 20 g L^{-1} yeast extract (Fisher), 2 g L^{-1} KH_2PO_4 (SLS), 16.5 g L^{-1} K_2HPO_4 (Sigma), 7.5 g L^{-1} citric acid (Fisher), 1.5 mL L^{-1} 85% (w/v) H_3PO_4 (Fisher), and 0.66 mL L^{-1} Polypropylene Glycol (Sigma) in diH_2O, and sterilised in bioreactors by autoclaving at 121 ˚C for 20 min. Basal media was supplemented post-autoclaving with sterile additions of 10 mM $MgSO_4 \cdot 7H_2O$ (Fisher) and 2 mM $CaCl_2 \cdot 2H_2O$ (Merck), 100 µg mL^{-1} ampicillin or carbenicillin for plasmid selection, and 34 mL L^{-1} trace elements solution. Trace elements solution contained 3.36 g L^{-1} $FeSO_4 \cdot 7H_2O$ (Merck), 0.84 g L^{-1} $ZnSO_4 \cdot 7H_2O$ (Merck), 0.15 g L^{-1} $MnSO_4 \cdot H_2O$ (Sigma), 0.25 g L^{-1} $Na_2MoO_4 \cdot 2H_2O$ (Fluka), 0.12 g L^{-1} $CuSO_4 \cdot 5H_2O$ (Sigma), 0.36 g L^{-1} H_3BO_3 (Sigma), and 48 mL L^{-1} 85% (w/v) H_3PO_4 (Fisher), was prepared in diH_2O, 0.2 µm filter sterilised (Fisher) and stored at 2-8 ˚C for up to 1 month. A supplementary 500 mL feed consisting of 714 g

L^{-1} glycerol (Fisher) and 7.4 g L^{-1} $MgSO_4 \cdot 7H_2O$ (Fisher) sterilised by autoclave at 121 ˚C for 20 min was added at specific time-points during fed-batch fermentations.

2.1.3 Reagents

2.1.3.1 Agarose

Agarose for gel-electrophoresis was prepared by adding 1-2% (w/v) agarose powder (Sigma) in 1X TAE buffer and boiling. Solidified agarose was stored at RT for up to 1 month and melted when needed. Low-melt agarose (VWR) for microscopy was prepared just prior to use as a 1% (w/v) solution in diH_2O and heated to dissolve.

2.1.3.2 Arabinose

Arabinose stocks were prepared at 20% (w/v) using L-(+)-Arabinose (Thermo) dissolved in diH_2O, 0.2 µm filter sterilised (Fisher) and stored at 2-8˚C for up to 1 month.

2.1.3.3 Calcium Chloride

Calcium chloride was prepared as a 1 M stock using $CaCl_2 \cdot 2H_2O$ (Merck) dissolved in diH_2O, 0.2 µm filter sterilised (Fisher) and stored at RT for up to 3 months. For chemical transformation, 1 M $CaCl_2 \cdot 2H_2O$ was diluted to 100 mM in diH_2O, 0.2 µm filter sterilised (Fisher) and stored at RT for up to 3 months. Similarly, 100 mM $CaCl_2 \cdot 2H_2O$ + 10% (w/v) glycerol was prepared using 1 M $CaCl_2 \cdot 2H_2O$ and 50% (w/v) glycerol diluted in diH_2O, 0.2 µm filter sterilised (Fisher) and stored at RT for up to 3 months.

2.1.3.4 DTT

DTT was prepared as a 1 M stock using Dithiothreitol (Sigma) dissolved in diH_2O. DTT was prepared on the day of use and then discarded.

2.1.3.5 Glucose

Glucose stocks were prepared at 20% (w/v) using D-(+)-Glucose (Fisher) dissolved in diH_2O, 0.2 µm filter sterilised (Fisher) and stored at 2-8˚C for up to 1 month.

2.1.3.6 Glycerol

Glycerol (Fisher) was prepared as a 50% (w/v) stock in diH_2O, sterilised by autoclave at 121˚C for 15 min and stored at RT for up to 3 months.

2.1.3.7 Isopropyl β-D-1-thiogalactopyranoside

Isopropyl β-D-1-thiogalactopyranoside (IPTG) was prepared at 100 mM using dioxane free IPTG (Anatrace) dissolved in diH_2O, 0.2 µm filter sterilised (Fisher) and stored in 1 mL aliquots at -20˚C for up to 3 months.

2.1.3.8 Lysozyme

Lysozyme (Sigma) was prepared as a 50 mg mL^{-1} stock in diH_2O and stored at -20 °C for up to 1 month.

2.1.3.9 Magnesium Sulphate

Magnesium Sulphate was prepared as a 1 M stock using $MgSO_4 \cdot 7H_2O$ (Fisher) dissolved in diH_2O, sterilised by autoclave at 121 ˚C for 15 min and stored at RT for up to 3 months.

2.1.3.10 Nile Red

Nile red (Merck) was prepared as a 1 mM stock in DMSO (Fisher) and stored at -20 °C protected from light for up to 1 month.

2.1.3.11 Phosphate Buffered Saline

Phosphate buffered saline (PBS) was prepared using PBS tablets (OXOID) following manufacturer instructions. After autoclaving, PBS was 0.2 µm filtered and stored at RT for up to 3 months.

2.1.3.12 Polypropylene Glycol

Polypropylene glycol 2000 (PPG) (VWR) was prepared as a 10% (v/v) solution in diH_2O, sterilised by autoclave at 121 ˚C for 15 min and stored at RT for up to 6 months.

2.1.3.13 Propidium Iodide

Propidium iodide (PI) (Sigma) was prepared as a 200 µg mL^{-1} stock in diH_2O, 0.2 µm filter sterilised (Fisher) wrapped in aluminium foil to protect from light and stored at -20°C for up to 1 month.

2.1.3.14 Rose Bengal

Rose Bengal (Thermo) was prepared the day prior to use as a 1 mM stock dissolved in diH_2O, 0.2 µm filter sterilised (Fisher), wrapped in aluminium foil to protect from light and stored at RT overnight.

2.1.3.15 SDS PAGE Sample Buffer

SDS PAGE sample buffer was prepared as a 2X stock containing 65.8 mM Tris-HCl pH 6.8, 0.01 % (w/v) bromophenol blue (Electran), 26.3 % (w/v) glycerol (Fisher), 2.1 % (w/v) SDS (Merck) and stored at RT for up to 3 months. DTT was added just prior to mixing with samples.

2.1.3.16 Spheroplast Buffer

Spheroplast buffer was prepared using 100 mM tris-HCl (Fisher), 500 mM sucrose (Fisher), 5 mM EDTA (Fisher) with pH adjusted to 8.2 using HCl (Fisher).

2.1.3.17 TAE Buffer

1X TAE buffer was prepared by mixing 50X TAE Buffer (Thermo) with diH_2O and stored at RT for up to 6 months.

2.1.3.18 Tris-HCl

Tris-HCl was prepared at 100 mM using tris (Fisher). For fractionation pH was adjusted to 6.8 using HCl (Fisher); for SDS PAGE 2x sample buffer, pH was adjusted to 8.0 using HCl (Fisher). Tris-HCl was stored at RT for up to 6 months.

2.1.3.19 Urea

Urea (Scientific Laboratory Supplies) was prepared the day prior to use as a 5 M or 8 M stock dissolved in diH_2O, 0.2 µm filter sterilised (Fisher) and stored at RT overnight.

2.2 Bacterial Strains and Plasmids

2.2.1 Strains

A complete list of strains, their genotype and source is provided in Table 2.1. Genetic manipulation and storage of cloned constructs in bacterial strains at -80 ˚C was done in the *E. coli* K-12 derivative DH5α *fhuA2* (NEB 5-alpha competent cells) (Anton and Raleigh, 2016). *E. coli* K-12 MG1655 was used as a wild-type strain to clone regions of genomic DNA (Blattner et al., 1997), kindly provided by Dr Tim Overton (The University of Birmingham). For expression of msfGFP in pET-26b(+) constructs, *E. coli* BL21(DE3) (Novagen) (Studier and Moffatt, 1986) was used and kindly provided by Dr Douglas Browning (Aston University). To express msfGFP or cfSGFP2 in pBAD30-*kanR* constructs, *E. coli* BL21 (Novagen) (Studier and Moffatt, 1986) was used, kindly provided by Dr Douglas Browning (Aston University). For urea inducible expression of 6xHis::GFP, *E. coli* BL21 (Studier and Moffatt, 1986) and the *E. coli* K-12 derivative JCB387 (Page et al., 1990) were used and kindly provided by Dr Douglas Browning (Aston University). Work with P_{spy} or L-arabinose inducible *lacI* constructs was done in *E. coli* BL21 or BL21(DE3) (Novagen) (Studier and Moffatt, 1986), kindly provided by Dr Douglas Browning (Aston University). P_{spy} was also used to assay a series of efflux mutants, MG1655Δ*acrA*, MG1655Δ*acrB* (Ciusa et al., 2022), MG1655-*acrB*^{D408A} (Wang-Kan et al., 2021) and MG1655Δ*tolC*, kindly provided by Dr Jessica Blair (The University of Birmingham) .

Table 2.1: List of *E. coli* strains used. Genotype and source are provided.

Strain	Genotype	Source
DH5α *fhuA2*	*fhuA*2Δ(*argF-lacZ*)U169 *phoA glnV44* Φ80Δ(*lacZ*)M15 *gyrA96 recA1 relA1 endA1 thi-1 hsdR17*	NEB (Anton and Raleigh, 2016).
JCB387	F^- λ^- Δ*nir* Δ*lac*	Dr Douglas Browning (Aston University) (Page et al., 1990).
BL21	F^- *ompT gal dcm lon* $hsdS_B(r_B^- m_B^-)$ $[malB^+]_{K\text{-}12}(\lambda^S)$	Novagen Dr Douglas Browning (Aston University) (Studier and Moffatt, 1986).
BL21(λDE3)	F^- *ompT gal dcm lon* $hsdS_B(r_B^- m_B^-)$ λ(DE3 [*lacI lacUV5-T7p07 ind1 sam7 nin5*]) $[malB^+]_{K\text{-}12}(\lambda^S)$	Novagen Dr Douglas Browning (Aston University) (Studier and Moffatt, 1986).
MG1655	F- λ- *ilvG- rfb*-50 *rph*-1	Dr Tim Overton (The University of Birmingham) (Blattner et al., 1997).
MG1655Δ*acrA*	MG1655 Δ*acrA*	Dr Jessica Blair (The University of Birmingham)
MG1655Δ*acrB*	MG1655 Δ*acrB*	Dr Jessica Blair (The University of Birmingham) (Ciusa et al., 2022)
MG16655-$acrB^{D408A}$	MG1655 $acrB^{D408A}$	Dr Jessica Blair (The University of Birmingham) (Wang-Kan et al., 2021)
MG16655Δ*tolC*	MG1655 Δ*tolC*	Dr Jessica Blair (The University of Birmingham)

2.2.2 Plasmids

A list of plasmids is available in Table 2.2. For chemical transformations, pUC19 (NEB) (Figure 2.1A) was used as a positive control. pET-26b(+) (Novagen) (Figure 2.1B) and pET GFP LIC (Addgene plasmid #29772) (Figure 2.1C) were used to assemble pET msfGFP constructs. pBAD30 (Guzman et al., 1995) (Figure 2.1D) was used for assembly of a P_{Spy} biosensor construct, in developing a negative feedback loop and to assemble pBAD-*kanR* (Figure 2.1E) for pBAD msfGFP and cfSGFP2 constructs. pRW50 (Lodge et al., 1992) (Figure 2.1F) was used to assemble a SecM biosensor construct.

To evaluate the urea inducible promoter P_{uti101}, 6xHis::EGFP was expressed from pET-15b_P_{uti101}-*6xhis::egfp* (Hothersall et al., 2022b) (Figure 2.2A). A PAR promoter construct driving expression of 6xHis::GFP was expressed using pET-22b-PAR4-*gfp* (Browning et al., 2019, Hothersall et al., 2021) (Figure 2.2B) and used for pulse chase experiments alongside the urea inducible promoter construct. Constructs containing PAR promoters driving expression of anti-IL-1β-6xHis scFv, pET-26b(+)-PAR1-*pelB^{SP}::anti-IL-1β-6xhis* scFv, pET-26b(+)-PAR4-*pelB^{SP}::anti-IL-1β-6xhis* scFv and pET-26b(+)-PAR7-*pelB^{SP}::anti-IL-1β-6xhis* scFv (Browning et al., 2019) (Figure 2.2C), were used as stressors for biosensor constructs pRW50Δ-*secM*::*msfGFP* (Figure 2.2D) and pBAD30Δ-P_{Spy}-*6xhis*::*gfp* (Figure 2.2E).

For development of a stress mediated negative feedback loop, LacI and ligand unresponsive (LU) derivatives $LacI^{R197G}$ or $LacI^{T276F}$ were expressed from pBAD30-*lacI,* pBAD30-*lacI^{R197G}* and pBAD30-*lacI^{T276F}* respectively (Figure 2.2F). A further variant of

Table 2.2: List of plasmids used. Details including antibiotic resistance and source are provided.

Plasmid	Details	Source
pUC19	Positive control plasmid used for all chemical transformations (Amp^R).	NEB (Norrander et al., 1983).
pET-26b(+)	Plasmid containing the T7*lac* promoter, *lacI* and a *pelB*^{SP} (Kan^R).	Novagen Dr Douglas Browning (Aston University)
pET GFP LIC (u-*msfgfp*)	Cloning plasmid containing msfGFP (Amp^R).	Addgene plasmid #29772 Dr Jessica Blair (The University of Birmingham)
pBAD30	Empty expression plasmid expressing AraC and with P_{araBAD} ustream of MCS (Amp^R).	Professor Steve Busby (The University of Birmingham) (Guzman et al., 1995).
pBAD30-*kan*^{R}	Variant of pBAD30 with *amp*^{R} replaced with *kan*^{R} and *rrnB* terminators in the opposing orientation (Kan^R).	This work.
pRW50	Low copy number plasmid expressing LacZ, LacY and LacA (Tet^R).	Dr Douglas Browning (The University of Birmingham) (Lodge, 1992).
pET-15b-P_{uti101}-*6xhis::egfp*	Expresses a 6xHis::EGFP fusion from the urea inducible P_{uti101} promoter (Amp^R).	Dr Douglas Browning (The University of Birmingham) (Hothersall et al., 2022b).
pET-22b-PAR4-*gfp*	Expresses a 6xHis::GFP fusion from the IPTG inducible PAR4 promoter (Amp^R).	Dr Douglas Browning (The University of Birmingham) (Browning et al., 2019).
pET-26b(+)-PAR1-*pelB*^{SP}*::anti-IL-1β-6xhis* scFv	Variant of pET-26b(+) with the T7*lac* promoter replaced with PAR1 expressing PelB^{SP}::anti-IL-1β-6xHis scFv (Kan^R).	Dr Douglas Browning (The University of Birmingham) (Browning et al., 2019).

Plasmid	Details	Source
pET-26b(+)-PAR4-*pelB^{SP}::anti-IL-1β-6xhis* scFv	Variant of pET-26b(+) with the T7*lac* promoter replaced with PAR4 expressing PelB^{SP}::anti-IL-1β-6xHis scFv (Kan^{R}).	Dr Douglas Browning (The University of Birmingham) (Browning et al., 2019).
pET-26b(+)-PAR7-*pelB^{SP}::anti-IL-1β-6xhis* scFv	Variant of pET-26b(+) with the T7*lac* promoter replaced with PAR7 expressing PelB^{SP}::anti-IL-1β-6xHis scFv and LacIq (Kan^{R}).	Dr Douglas Browning (The University of Birmingham) (Browning et al., 2019).
pET-26b(+)-*pelB^{SP}::msfgfp*	Variant of pET-26b(+) with *msfgfp* inserted downstream of *pelB^{SP}* (Kan^{R}).	This work.
pET-26b(+)Δ-*dsbA^{SP}::msfgfp*	Variant of pET-26b(+) with *pelB^{SP}* deleted and replaced with *dsbA^{SP}* and *msfgfp* inserted downstream (Kan^{R}).	This work.
pET-26b(+)Δ-*msfgfp*	Variant of pET-26b(+)Δ-*msfgfp* with the GTG start codon replaced with the canonical ATG (Kan^{R}).	This work.
pBAD30-*kan^{R}-pelB^{SP}::msfgfp*	Variant of pBAD30-*kan^{R}* with *pelB^{SP}::msfgfp* inserted downstream of P_{araBAD} (Kan^{R}).	This work.
pBAD30-*kan^{R}-dsbA^{SP}::msfgfp*	Variant of pBAD30-*kan^{R}* with *dsbA^{SP}::msfgfp* inserted downstream of P_{araBAD} (Kan^{R}).	This work.
pBAD30-*kan^{R}-msfgfp*	Variant of pBAD30-*kan^{R}* with *msfgfp* inserted downstream of P_{araBAD} (Kan^{R}).	This work.
pBAD30-*kan^{R}-cfsgfp2*	Variant of pBAD30-*kan^{R}* with *cfsgfp2* inserted downstream of P_{araBAD} (Kan^{R}).	This work.
pBAD30-kan^{R}-*dsbA^{SP}::cfsgfp2*	Variant of pBAD30-*kan^{R}* with *dsbA^{SP}::cfsgfp2* inserted downstream of P_{araBAD} (Kan^{R}).	This work.
pRW50Δ-*secM::msfgfp*	Variant of pRW50 with LacZ, LacY and LacA deleted expressing a SecM::msfGFP fusion from P_{secM} (Tet^{R}).	This work.

Plasmid	Details	Source
pBAD30Δ-P_{spy}-*6xhis::gfp*	Variant of pBAD30 with *araC* deleted and P_{araBAD} replaced with P_{spy} expressing 6xHis::EGFP (Amp^R).	This work.
pBAD30-*lacI*	Variant of pBAD30 with P_{araBAD} expressing LacI (Amp^R).	This work.
pBAD30-*lacI*^{R197G}	Variant of pBAD30-*lacI* expressing LacI with the R197G mutation (Amp^R).	This work.
pBAD30-*lacI*^{T276F}	Variant of pBAD30-*lacI* expressing LacI with the T276F mutation (Amp^R).	This work.
pBAD30-*lacI*^{R197G}-M	Variant of pBAD30-*lacI*^{R197G} with a medium rate SsrA degradation tag C-terminally fused to $LacI^{R197G}$ (Amp^R).	This work.
pBAD30Δ-P_{spy}-*lacI*^{R197G}	Variant of pBAD30Δ-P_{spy}-*6xhis::egfp* with *6xhis::egfp* deleted and P_{spy} expressing $LacI^{R197G}$-SsrA_M (Amp^R).	This work.

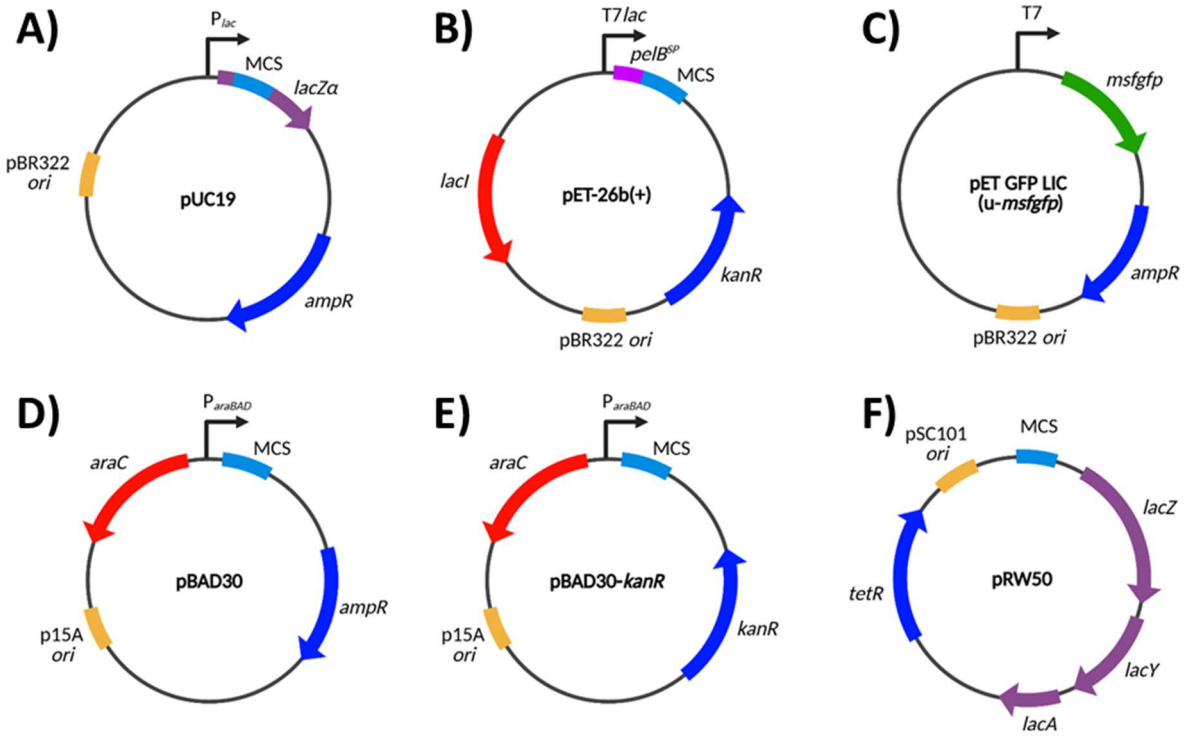


Figure 2.1: Plasmid maps of constructs used in assays and during cloning. Created with BioRender.com. pUC19 **(A)** was used as a positive control for transformations. pET-26b(+) **(B)** and pET GFP LIC (u-*msfgfp*) **(C)** were used in assembly of pET-msfGFP constducts for periplasmic screening studies. pBAD30 **(D)** was used to assemble P_{Spy} and P_{ibpAB} biosensor constructs and pBAD30-*kanR* **(E)**, which was subsequently used to assemble pBAD-msfGFP constructs for periplasmic screening studies. pRW50 **(F)** was used for assembly of a SecM biosensor construct.

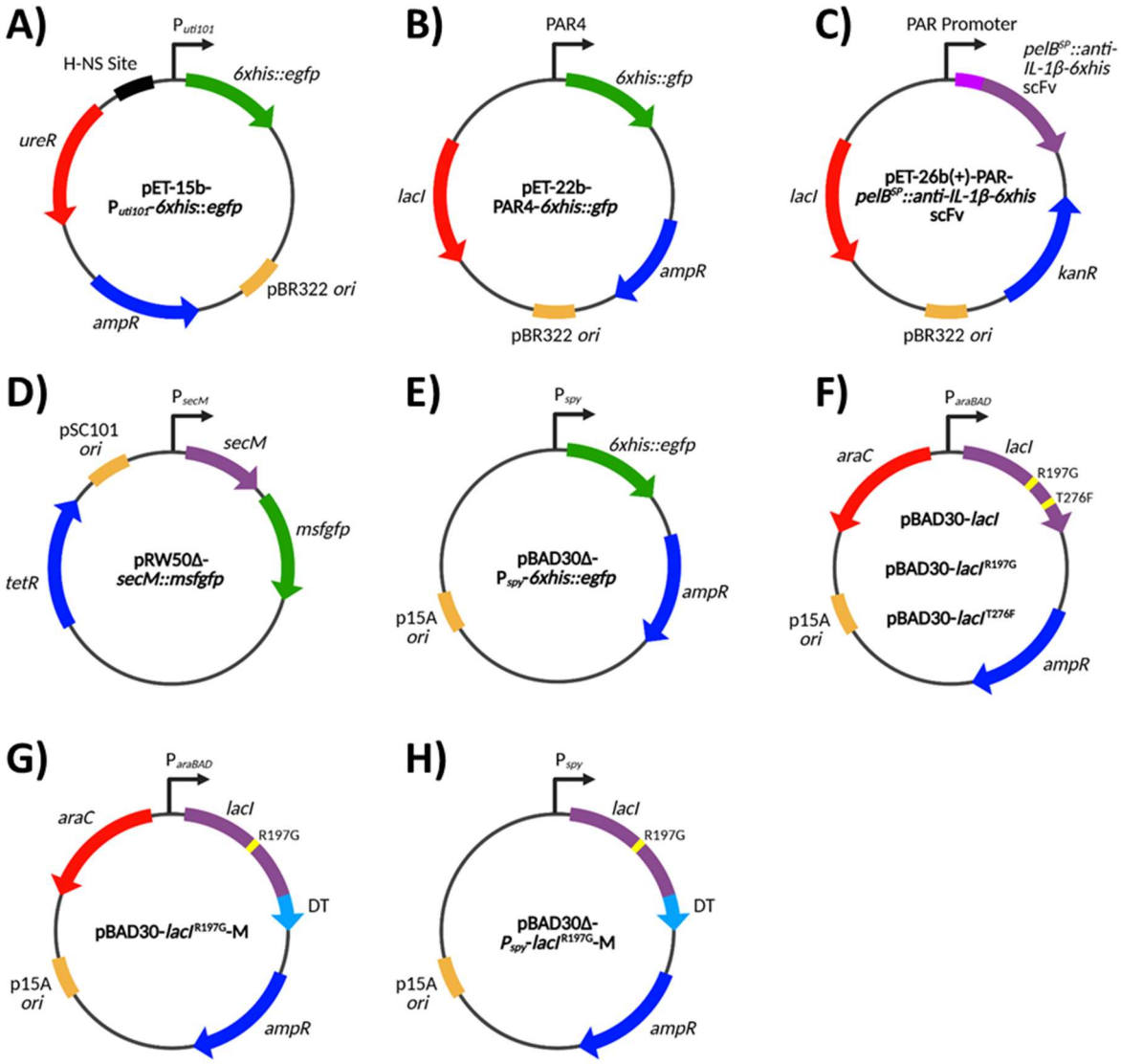


Figure 2.2: Plasmid maps of constructs used for overexpression studies. Created with BioRender.com. pET-15b-P_{uti101}-*6xhis::egfp* **(A)** was expressed in JCB387 and BL21 for urea inducible expression of 6xHis::EGFP. Construct with a PAR4 promoter expressing 6xHis::GFP, pET-22b-PAR4-*6xhis::gfp* **(B)**, was used for pulse chase experiments alongside the urea inducible promoter construct. Constructs with PAR promoters driving expression of anti-IL-1β-6xHis scFv **(C)** pET-26b(+)-PAR1-*pelB^{SP}::anti-IL-1β-6xhis* scFv, pET-26b(+)-PAR4-*pelB^{SP}::anti-IL-1β-6xhis* scFv and pET-26b(+)-PAR7-*pelB^{SP}::anti-IL-1β-6xhis* scFv, were used as stressors for biosensor constructs. pRW50Δ-*secM*::*msfgfp* **(D)** and pBAD30Δ-P_{spy}-*6xhis::egfp* **(E)** were used as biosensor constructs. To develop a repressor for a negative feedback loop, pBAD30-*lacI* was used as a control for constructs containing ligand unresponsive derivatives of LacI, pBAD30-*lacI*^{R197G} and pBAD30-*lacI*^{T276F} **(F)**, with approximate positions for R197G or T276F mutations marked in yellow. LacI^{R197G} construct was used to assemble a variant with a C-terminal ssrA tag attached, pBAD30-*lacI*^{R197G}-**(G)**. pBAD30Δ-P_{spy}-*lacI*^{R197G} was used to create a negative feedback loop **(H)**.

LacI^{R197G} with an SsrA degradation tag fused to the C-terminus was expressed using pBAD30-lacI$^{R197G-M}$ (Figure 2.2G). Stress induced feedback control of cells overexpressing recombinant proteins used pBAD30Δ-P$_{spy}$-lacI^{R197G} (Fig. 2.2H).

In development of GFP-based periplasmic reporters, msfGFP was expressed from an IPTG inducible T7*lac* promoter, periplasmically using constructs pET-26b(+)_*pelB^{SP}::msfGFP* (Figure 2.3A) or pET-26b(+)_*dsbA^{SP}::msfGFP* (Figure 2.3B) and cytoplasmically using the construct pET-26b(+)-*msfgfp* (Figure 2.3C). For arabinose induction of msfGFP, expression was periplasmically from pBAD30-*kanR*-*pelB^{SP}::msfgfp* (Figure 2.3D) or pBAD30-*kanR*-*dsbA^{SP}::msfgfp* (Figure 2.3E) and cytoplasmically from pBAD30-*kanR*-*msfgfp* (Figure 2.3F). Similarly, a cfSGFP2 derivative was expressed by arabinose induction periplasmically from pBAD30-*kanR*-*dsbA^{SP}::cfsgfp2* (Figure 2.3G) and cytoplasmically from pBAD30-*kanR*-*cfsgfp2* (Figure 2.3H).

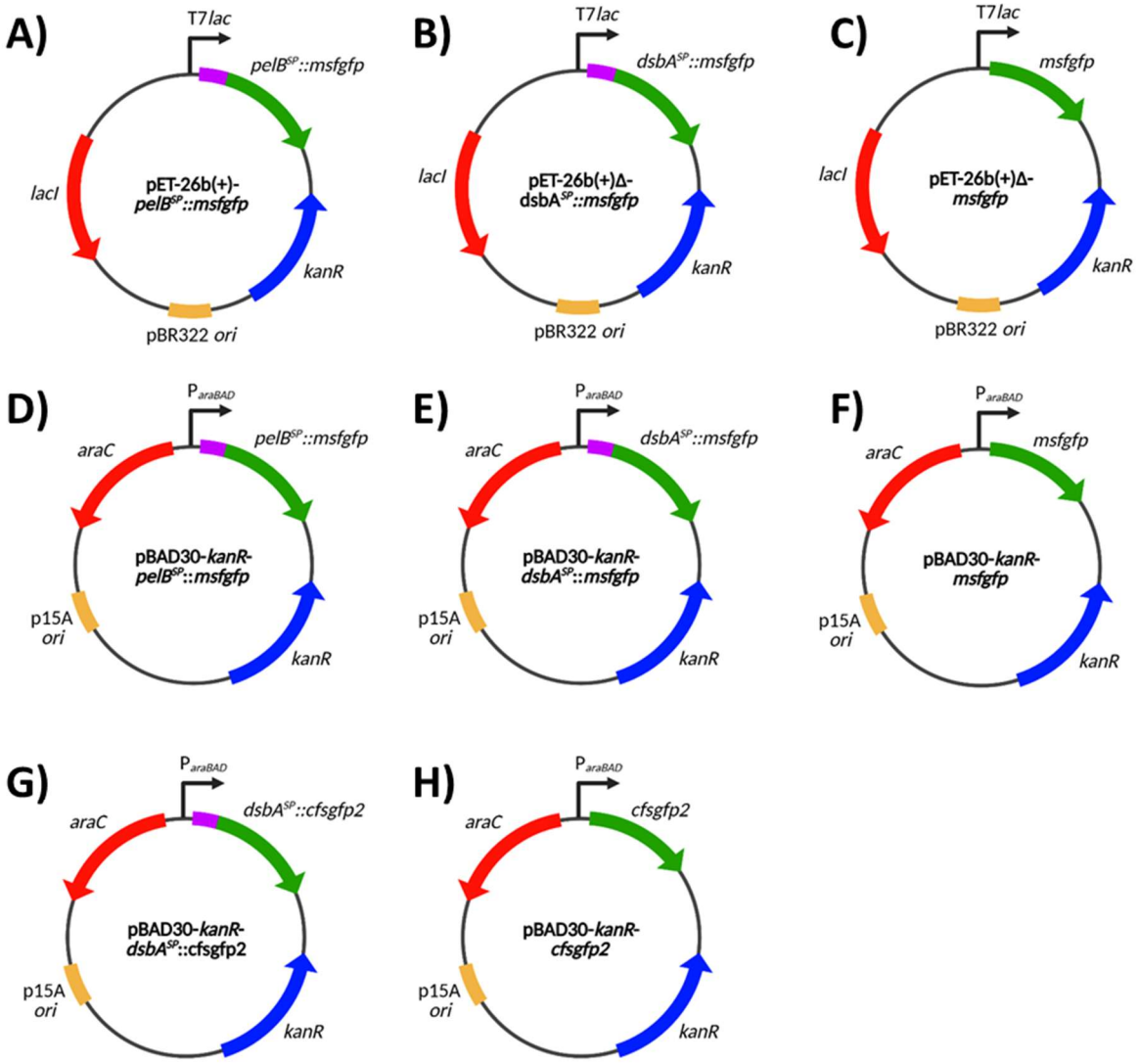


Figure 2.3: Plasmid maps of constructs used for periplasmic screening studies. Created with BioRender.com. pET-26b(+)-*pelB^{SP}::msfgfp* **(A)** and pET-26b(+)Δ-*dsbA^{SP}::msfgfp* **(B)** were used for periplasmic expression of msfGFP driven by the T7 promoter, with pET-26b(+)Δ-*msfgfp* **(C)** used as a cytoplasmic control. pBAD30-*kanR-pelB^{SP}::msfgfp* **(D)** and pBAD30-*kanR-dsbA^{SP}::msfgfp* **(E)** were used for periplasmic expression of msfGFP driven by the P_{araBAD} promoter, with pBAD30-*kanR-msfgfp* **(F)** used as a cytoplasmic control. pBAD30-*kanR-dsbA^{SP}::cfsgfp2* **(G)** was used for periplasmic expression of cfSGFP2 driven by the P_{araBAD} promoter, with pBAD30-*kanR-cfsgfp2* **(H)** used as a cytoplasmic control.

2.3 Bacterial Culture

2.3.1 Overnight Culture

Overnight cultures were grown in a MaxQ 4000 incubator (Thermo Scientific) for 16-18 h, at the same temperature and set in the same growth medium as for protein expression, the experiment or method. Seed cultures for cloning and transformations were inoculated from single colonies re-streaked onto LBA plus appropriate selection from a -80 °C working stock. For all expression work, single transformants were re-streaked onto LBA plus appropriate selection and used to inoculate discrete seed cultures. Overnights for all cloning work, chemical transformation and electroporation were in LB plus appropriate selection at 37 °C, 200 rpm.

Overnights of JCB387 or BL21 containing pET-15b_P_{uti101}-*6xhis*::*egfp* were set in 10 mL LB + Amp, or 10 mL TB + Amp and grown at 37˚C, 200 rpm. Fermentation of BL21 containing pET-15b_P_{uti101}-*6xhis*::*egfp* in semi-defined growth medium used 50 mL TB + Amp for the seed stage, inoculated from a sweep of cells from a single re-streaked transformant.

Overnights of BL21(DE3) containing pET-26b(+) msfGFP constructs were set in 10 mL TB + Kan + 0.4% (w/v) glucose, grown at 30˚C, 200 rpm. BL21 containing pBAD30-kan^R msfGFP or cfSGFP2 constructs were set in 10 mL TB + Kan, grown at 30˚C, 200 rpm.

Overnights of BL21 containing pRW50 *secM::mfsgfp* constructs and co-expressing pET-26b(+) PAR constructs were set in 10 mL TB + Tet, grown at 30˚C, 200 rpm.

Overnights of BL21 containing pBAD30 with P_{spy}-*6xhis::egfp* were set in 10 mL LB + Amp, grown at 37˚C, 200 rpm. For BL21 co-expressing pBAD30 with LacI or its ligand unresponsive derivatives and the cytoplasmic pET-26b(+) msfGFP construct, overnights were set in 10 mL LB + Amp + Kan, grown at 37˚C, 200 rpm. Overnights of BL21 co-expressing pBAD30 P_{spy}-*6xhis::egfp* with pET-26b(+) PAR constructs were set in 10 mL TB + Amp + Kan at 30˚C, 200 rpm. Overnights of BL21 containing pBAD30 P_{spy}-*lacI*^{R197G} constructs and co-expressing pET-26b(+) msfGFP constructs were set in 10 mL TB + Amp + Kan at 30˚C, 200 rpm.

2.3.2 Working Stocks

Working stocks were prepared by adding 750 µL bacterial overnight culture 1:1 with 50% (v/v) glycerol in a 2 mL cryovial, thoroughly mixed by vortex, left at RT for 10 minutes and stored at -80˚C.

2.3.3 Protein Expression

All cultures for protein expression were grown in a MaxQ 4000 incubator (Thermo Scientific). Unless otherwise specified, all cultures were inoculated using overnights to OD_{600} 0.05.

Cultures of JCB387 or BL21 containing pET-15b_P_{uti101}-*6xhis*::*egfp* were grown in 50 mL LB + Amp in 250 mL Erlenmeyer flasks at 37˚C, 200 rpm; or 100 mL TB + Amp in 500 mL baffled Erlenmeyer flasks, grown at 37˚C, 150 rpm. In both instances, cells were aerated until OD_{600} 0.4-0.6, 6xHis::EGFP expression induced by addition of urea, with expression proceeding until 24 h post-induction.

Cultures of BL21(DE3) containing pET-26b(+) msfGFP constructs were grown in 50 mL TB + Kan + 0.4% (w/v) glucose in 250 mL Erlenmeyer flasks at 30˚C, 200 rpm. Cultures of BL21(DE3) containing PelB^{SP}::msfGFP or DsbA^{SP}::msfGFP pET-26b(+) constructs were inoculated to OD_{600} 0.15 and 0.2 respectively. After aeration until OD_{600} 0.4-0.6, msfGFP expression was induced by addition of IPTG, with expression proceeding until 24 h post-induction. Cultures of BL21 containing pBAD30-*kan*^{R} msfGFP or cfSGFP2 constructs were set in 50 mL TB + Kan in 250 mL Erlenmeyer flasks at 30 ˚C, 200 rpm. Cells were aerated until OD_{600} 0.4-0.6 and msfGFP or cfSGFP2 included by addition of L-(+)-arabinose, with expression proceeding until 24 h post-induction.

Cultures of BL21 containing pRW50 *secM::mfsgfp* constructs and co-expressing pET-26b(+) PAR constructs were grown in 50 mL TB + Tet in 250 mL Erlenmeyer flasks at 30 ˚C, 200 rpm. Cells were aerated until OD_{600} 0.4-0.6 when anti-IL-1β-6xHis scFv was induced by addition of IPTG, with expression proceeding until 24 h post-induction.

Cultures of BL21 containing pBAD30 P$_{spy}$-*6xhis::egfp* was grown in 50 mL LB + Amp in 250 mL Erlenmeyer flasks at 37 ˚C, 200 rpm. When co-expressing pBAD30 P$_{spy}$-*6xhis::egfp* with pET-26b(+) PAR constructs, cultures were grown in TB + Amp + Kan at 30 ˚C, 200 rpm and aerated until OD_{600} 0.4-0.6. PelB^{SP}::anti-IL-1β-6xHis scFv was induced by addition of IPTG, with expression proceeding until 24 h post-induction.

Cultures of BL21 containing pBAD30 and *lacI* or its ligand unresponsive derivatives, co-expressing the cytoplasmic pET-26b(+) msfGFP construct were grown in 50 mL LB + Amp + Kan in 250 mL Erlenmeyer flasks at 37 ˚C, 200 rpm. Cultures were aerated until OD_{600} 0.4-0.6, *lacI* or ligand unresponsive derivatives were induced by addition of L-(+)-arabinose; msfGFP was induced by addition of IPTG, with expression proceeding until 24 h post-induction.

Cultures of BL21(DE3) containing pBAD30 P_{spy}-*lacI*^{R197G} and co-expressing pET-26b(+) msfGFP constructs were grown in 50 mL TB + Amp + Kan in 250 mL Erlenmeyer flasks at 30 ˚C, 200 rpm. Cells were aerated till 0.4-0.6 when anti-IL-1β-6xHis scFv or msfGFP were induced by addition of IPTG, with expression proceeding until 24 h post-induction.

2.3.4 Bioreactors

Fermentation in bench-top bioreactors was as described by Wyre and Overton (2014), using a Fermac 310/60 bioreactor (Electrolab). A layout of the vessel showing individual components is provided in Figure 2.4. Agitation was via two six-bladed Rushton impellers with air sparged from below at 3 L min^{-1} through a 0.22 µm filter (Sartorius), assisted by four baffles. Off gas exited the reactor through a condenser, 5 L catch pot and finally a 0.22 µm filter (Sartorius).

Dissolved oxygen was maintained at 30 % by cascade to agitation at 200-800 rpm, controlled by a D140 Oxyprobe (Broadley James) or OxyFerm FDA (Hamilton). DO

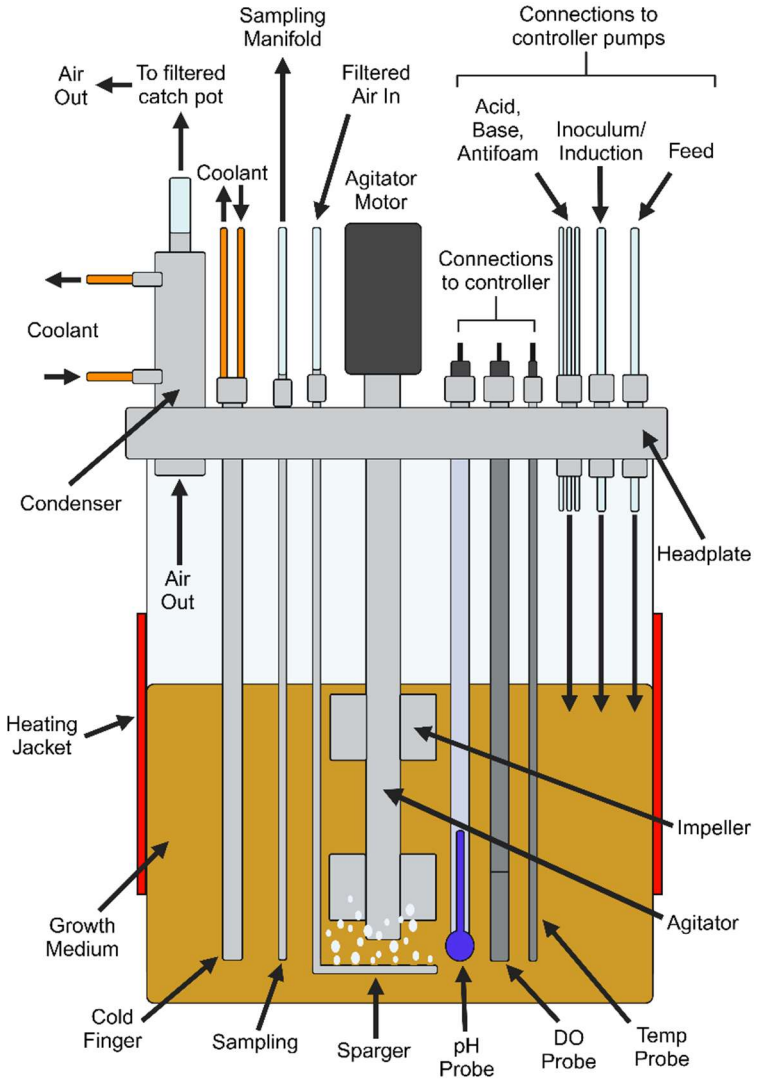


Figure 2.4: An Electrolab Fermac 310/60 bioreactor was used for fermentations. The bioreactor consisted of a glass vessel sealed by a headplate through which components were passed. The agitator powered by a motor had two six-bladed Rushton impellers. Filtered air (0.22 µm) entered the vessel via a sparger underneath the agitator to break up air bubbles. Air exited the vessel through a condenser and then into a 0.22 µm vented catch-pot. The condenser was supplied with cold water from a chiller to remove moisture from warm exhaust air, reducing liquid evaporation and filter blockages.

Dissolved oxygen (DO) was monitored using DO probes D140 Oxyprobe (Broadley James) or OxyFerm FDA (Hamilton). Growth medium pH was monitored using pH probes F695 FermProbe (Broadley James) or EasyFerm Plus (Hamilton). A temperature probe (Electrolab) was used to monitor vessel temperature. An electric heating jacket, and a cold finger supplied by cold water from a chiller, were used to maintain vessel temperature. All probes were connected to the Electrolab Fermac 310/60 control unit to maintain setpoints.

Samples were taken via a sampling line connected to a sampling manifold which used a syringe and sterile universals. Acid (HCl), base (NH_4OH) and antifoam (PPG-2000) were added via vented Duran bottles connected to a triple port on the headplate. Inoculation and induction were via single port on the headplate connected to a vented flask to which inoculum and inducer were aseptically added. Feed was added via a single port on the headplate connected to a vented Duran bottle. Tubing connections were through peristaltic pumps on the Electrolab Fermac 310/60 control unit. Created with BioRender.com.

probes were calibrated using the auto zero function after autoclaving at 121 °C for 20 min and then overnight polarisation of the probe by aerating the vessel before setting the 100 % value. Culture medium pH was maintained at 6.3 +/- 0.1 using 10 % (w/v) NH_4OH (Fisher) or 5 % (w/v) HCl (Fisher), controlled by a F695 FermProbe (Broadley James) or EasyFerm Plus (Hamilton). pH probes were two-point calibrated using pH4 and pH7 buffers; an offline measurement was taken prior inoculation using a FiveEasy FE20 pH probe (Mettler Toledo) to correct drift following autoclaving. Temperature was maintained at 37 °C via an electric heating jacket and cold finger inserted into the head plate. Foaming was controlled by addition of PPG-2000.

Seed cultures were used to inoculate semi-defined growth medium to OD_{600} 0.05. For fed-batch fermentation (1.5 L medium), two strategies were employed. Cells were aerated till ~ OD_{600} 50, induced with 100 mM urea and feeding started at 67.5 mL h^{-1} with aeration proceeding until 24 h post-induction; or cells were aerated till OD_{600} 0.4-0.6 and induced with 100 mM urea, feed was added at 18.5 mL h^{-1} with aeration proceeding until 24 h post-feed. Bioreactor data was logged using Fermentation Management software (Electrolab) and plotted using OriginPro (OriginLab).

2.4 Cloning Techniques

2.4.1 Primers

All primers were designed using SnapGene, secondary structure checked on NetPrimer and purchased lyophilised from Sigma. For primers 35 bp or under purification by desalting was chosen; between 36 and 50 bp, primers were purified by

reverse phase cartridge; and for those over 50 bp, PAGE purification was selected. Lyophilised primers were briefly spun down then resuspended in nuclease free water (NFW) (VWR) to a concentration of 100 µM, thoroughly mixed by vortex and incubated on ice for 5 min. Working stocks were prepared as 50 µL aliquots, diluted in NFW to 10 µM and stored at -20˚C. A list of primers is available in Table 2.3.

Table 2.3: List of primers used. Sequences are provided in the 5’ to 3’ direction.

Primer	Sequence (5'-3')
pRW50_Fwd_GA_3	TGGTCGCCATGATCGATTCCCAGTCAGAAATGAGC
pRW50_Rev_GA_3	CAGATTTGCCAGTCGTCGTTGAACTGAGCCTGA
SecM-SecA_Fwd	CGACTGGCAAATCTGGCAC
SecM-SecA_Rev	AATAAAATCTCAAACGCCCCGC
SecM-SecA_Rev_OE_2	CTCGCCCTTGCTCATAATAAAATCTCAAACGCCCCGC
msfGFP_Fwd_OE_3	GTTTGAGATTTTATTATGAGCAAGGGCGAGGAGC
msfGFP_Rev_OE_3	CGATCATGGCGACCACAC
SecM-msfGFP_Fwd_GA_1	GGCTCAGTTCAACGACGACTGGCAAATCTGGCAC
SecM-msfGFP_Rev_GA_1	TTTCTGACTGGGAATCGATCATGGCGACCACAC
pRW50Δ-Fwd_CP_1	AGAGCCTTGAGTCCACGC
pRW50Δ-Rev_CP_1	CGCTCATTTCTGACTGGG
pBAD30_Fwd_GA_3	GAGCTGTACAAGTAATTGGCGGATGAGAGAAGA
pBAD30_Rev_GA_3	CAGGATTAATCTGTACTTGACGGAGTAGCATAGG
Spy_Fwd_GA_1	TGCTACTCCGTCAAGTACAGATTAATCCTGGTTATTTGC
Spy_Rev_GA_1	TTAAAGTTAAACAAATTATTACGGCTTTCTTAAGTAGC
EGFP_Fwd_GA_1	AGAAAGCCGTAATAATTTGTTTAACTTTAAGAAGGAGATATACC
EGFP_Rev_GA_1	TCTCTCATCCGCCAATTACTTGTACAGCTCGTCC
pBAD30_Fwd	TGTCAAATGGACGAAGCAGG
pBAD30_Rev_CP_2	TCACTTCTGAGTTCGGCAT
pBAD30_Fwd_GA_5	ACTCATTAGGCACCGTTGGCGGATGAGAGAAGA
pBAD30_Rev_GA_5	GAATTGACTCTCTTCGCCCAAAAAAACGGGTATG
lacI_Fwd_GA	CCCGTTTTTTTGGGCGAAGAGAGTCAATTCAGGGTG
lacI_Rev_GA	TCTCTCATCCGCCAACGGTGCCTAATGAGTGAG
pBAD30-lacI_Fwd_1	AACAGTCGTTGCTGATTG
pBAD30-lacI_Fwd_2	TGAATGAGGGCATCGTTC
lacI_R197G_Fwd	GCGTCTGGGCCTGGCTGGCTG
lacI_R197G_Rev	GCCGAGACAGAACTTAATGGGCC

Primer	Sequence (5'-3')
lacI_T276F_Fwd	TACGACGATTTTGAAGACAGCTCATG
lacI_T276F_Rev	TCCCACTACCGAGATATCCG
pBAD30-lacI_Fwd_3	CGGATGAGAGAAGATTTTCAGCCTG
pBAD30-lacI_Rev	CTGCCCGCTTTCCAGTCG
M_SsrA_Fwd_2	TACGCTGACGCTTCTTGACGGATGAGAGAAGATTTTCAGCCTG
M_SsrA_Rev_2	GTTTTCGTCGTTAGCAGCCTGCCCGCTTTCCAGTCG
pBAD-Pspy_Fwd_GA	TCACTCATTAGGCACATACAGATTAAATCAGAACGCA
pBAD-Pspy_Rev_GA	TGGTTTCACATTCACATCTCCTTCTTAAAGTTAAACAAATTAT
lacI-DT_Fwd_GA	CTTTAAGAAGGAGATGTGAATGTGAAACCAGTAACG
lacI-DT_Rev_GA	TGATTTAATCTGTATGTGCCTAATGAGTGAGCTAAC
pET26b_Fwd_GA_1	GACGAGCTGTACAAGTGAGATCCGGCTGCTAACAAAGCCCG
pET26b_Rev_GA_1	CTCCTCGCCCTTGCTGGCCATCGCCGGCTGGG
msfGFP_Fwd_GA_1	CAGCCGGCGATGGCCAGCAAGGGCGAGGAGCTG
msfGFP_Rev_GA_1	AGCAGCCGGATCTCACTTGTACAGCTCGTCCATGCC
pET26b_Fwd_GA_3	TAGTAACCAACTCCATGCTAACAAAGCCCGAAA
pET26b_Rev_GA_3	CCAAATCTTTTTCATATGTATATCTCCTTCTTAAAGTTAAAC
DsbA-msfGFP_Fwd_6	TGAAAAAGATTTGGCTGGCGCTGGCTGGTTTAGTTTTAGCGTTTAGCGCATCGGCGAGCA AGGGCGAGGAGCTG
DsbA-msfGFP_Rev_5	CTTCCTTTCGGGCTTTGTTAGCA
DsbA-msfGFP_Fwd_GA_6	GAAGGAGATATACATATGAAAAAGATTTGGCTGGC
DsbA-msfGFP_Rev_GA_6	CGGGCTTTGTTAGCATGGAGTTGGTTACTACTTGT
pET26b_Fwd_GA_2	CTAACAAAGCCCGAAGCTAACAAAGCCCGAAAG
pET26b_Rev_GA_2	CTCGCCCTTGCTCACATGTATATCTCCTTCTTAAAGTTAAAC
msfGFP_Fwd_GA_4	GAAGGAGATATACATGTGAGCAAGGGCGAGGAG
msfGFP_Rev_GA_4	TCGGGCTTTGTTAGCTTCGGGCTTTGTTAGCAGC
pET-msfGFP_Sub_Fwd	AGATATACATATGAGCAAGGGCG
pET-msfGFP_Sub_Rev	CCTTCTTAAAGTTAAACAAAATTATTTCTAG
pET26b_Fwd_CP_1	GTGATGTCGGCGATATAGG
pET26b_Rev_CP_1	TTCCTTTCGGGCTTTGTTAG
T7 Terminator	GCTAGTTATTGCTCAGCGG

Primer	Sequence (5'-3')
pBAD30_Fwd_GA_1	GATCAAAGGATCTTCCTGTCAGACCAAGTTTACTC
pBAD30_Rev_GA_1	AACGTTGCGAAGCAAAGAGTTTGTAGAAACGCAAA
kan_Fwd_GA_1	AACTTGGTCTGACAGGAAGATCCTTTGATCTTTTCTAC
kan_Rev_GA_1	ACTTCTGAGTTCGGCTTAGAAAAACTCATCGAGCATC
rrnB T1_Fwd	GATGAGTTTTTCTAAGCCGAACTCAGAAGTGAAAC
rrnB T1_Rev	GTTTCTACAAACTCTTTGCTTCGCAACGTTCAAAT
pBAD30_Fwd_CP_1	GGCATCAAATTAAGCAGAAGG
pBAD30_Rev_CP_1	GTAAAGCACTAAATCGGAACC
pBAD30_Fwd_GA_2	TTGAGGGGTTTTTTGAATCAGAACGCAGAAGCG
pBAD30_Rev_GA_2	TTAAACAAAATTATTAAACGGGTATGGAGAAACAG
pET26b-msfGFP_Fwd_GA_1	TCTCCATACCCGTTTAATAATTTTGTTTAACTTTAAGAAGGA
pET26b-msfGFP_Rev_GA_1	TTCTGCGTTCTGATTCAAAAAACCCCTCAAGAC
pBAD30_Fwd_CP_2	CTTTCATTCCCAGCGGTC
pBAD30_Rev_CP_3	CGCCAGGCAAATTCTGTT
pBAD30-Cyto_Fwd	CCAACTCCATAAGGATCC
pBAD30-Cyto_Rev	ATGTATATCTCCTTCTTAAAGTTAAAC
pBAD30-Cyto_Fwd_GA	GAGCTGTACAAGTAACCAACTCCATAAGGATCC
pBAD30-Cyto_Rev_GA	GCCCTTGCTCACCATATGTATATCTCCTTCTTAAAGTTAAAC
cfSGFP2_Fwd_1	TCGTGCTGTGTTAGATGGTG
cfSGFP2_Rev_1	GTTCGTGAGTCGTCAGTTAC
cfGFP_Fwd_GA_1	GAAGGAGATATACATATGGTGAGCAAGGGCGAG
cfGFP_Rev_GA_1	TCCTTATGGAGTTGGTTACTTGTACAGCTCGTCCATGC
pBAD30-cfSGFP2_Fwd	GTGAGCAAGGGCGAGGAG
pBAD30-cfSGFP2_Rev	AAACGGGTATGGAGAAACAGTAGAG
pBAD30-DsbA-cfSGFP2_Fwd	ATGAAAAAGATTTGGCTGGCGCTGGCTGGTTTAGTTTTAGCGTTTAGCGCATCGGCGGTGAGCAAGGGCGAGGAG
pBAD30-cfSGFP2_Rev_2	ATGTATATCTCCTTCTTAAAGTTAAACAAAATTATTAAACGGGTATGGAGAAACAGTAGAG

2.4.2 PCR

2.4.2.1 Two and Three-step PCR

PCR reactions were run following manufacturer instructions and assembled on ice using 0.5 µL Q5 High-Fidelity DNA polymerase (NEB), 10 µL 5X Q5 reaction buffer (NEB), 1 µL 10 mM dNTPs (NEB), 2.5 µL 10 µM forward and reverse primers (Table 2.3), 1 pg – 10 ng template for pDNA or 1 ng – 1 µg for gDNA and NFW (VWR) to a final volume of 50 µL. For primers with GC content over 60%, 10 µL 5X Q5 High GC Enhancer (NEB) was added. In all instances, a negative control using 1 µL NFW (VWR) in place of template DNA was run in parallel. Annealing temperatures were calculated using the NEB Tm Calculator. Thermocycling was done using a Hybaid Px2 thermal cycler (Thermo Scientific) or Alpha Cycler 1 (PCRmax). Thermal cycling parameters were according to manufacturer instructions for Q5 High-Fidelity DNA polymerase.

2.4.2.1 Touchdown PCR

Where specified, a touchdown protocol was used for PCR (TD-PCR). Reaction conditions and thermal cycling conditions were identical to two and three-step reactions; except initial annealing temperatures were set 10 ˚C over the calculated value and decreased by 1 ˚C each cycle for a further 9 cycles.

2.4.2.1 Colony PCR

All colony PCR reactions were run following manufacturer instructions and assembled on ice using 0.25 µL Taq DNA polymerase (NEB), 5 µL 10X ThermoPol Reaction Buffer, 1 µL 10 mM dNTPs (NEB), 1 µL 10 µM forward and reverse primers (Table 2.3), 1 µL of transformant resuspended in 20 µL NFW (VWR) as template DNA and

NFW (VWR) to a final volume of 50 µL. In all instances, a negative control using 1 µL NFW (VWR) in place of template DNA was run in parallel. Annealing temperatures were calculated using the NEB Tm Calculator. Thermocycling was done using a Hybaid Px2 thermal cycler (Thermo Scientific) or Alpha Cycler 1 (PCRmax). Thermal cycling parameters were according to manufacturer instructions for Taq DNA polymerase (NEB) but initial denaturation during stage 1 was set to 95 °C for 5 min.

2.4.3 Gel Electrophoresis

Samples were prepared by mixing 5 µL DNA with 1 µL 6X gel loading dye, no SDS (NEB). Markers were either 100 bp DNA Ladder or 1 kb DNA Ladder (NEB), used according to manufacturer instructions. DNA over 1.5 kb was resolved on 1% (w/v) agarose gels and under 1.5 kb resolved on 2% (w/v) agarose gels. To stain DNA, 1X SYBR Safe (Invitrogen) was added to molten agarose prior to casting. DNA was resolved at 100 V for 60 min using a MP 250V power supply (Cleaver Scientific). Gels were visualised using a Visi-Blue Transilluminator and PhotoDoc-It imaging system (UVP).

2.4.4 Gel Purification

To gel purify PCR products, DNA was resolved on 2 % (w/v) agarose gels and then isolated using QIAquick Gel Extraction Kit (Qiagen) according to manufacturer instructions. In all instances, final elution of DNA was in NFW (VWR) pre-warmed to 65 °C. Spin columns were centrifuged in an Eppendorf 5418 microcentrifuge.

2.4.5 PCR Purification

Purification of PCR products was done using a QIAquick PCR Purification Kit (Qiagen) according to manufacturer instructions. In all instances, final elution of DNA was in NFW (VWR) pre-warmed to 65 °C. Spin columns were centrifuged in an Eppendorf 5418 microcentrifuge.

2.4.6 DpnI Digestion

To digest template DNA, 1 µL DpnI (NEB) was added to PCR reactions and incubated in a Hybaid Px2 thermal cycler (Thermo Scientific) or Alpha Cycler 1 (PCRmax), at 37 °C for 2 h and heat inactivated at 65 °C for 20 min.

2.4.7 Nanodrop

DNA concentration was quantified by absorbance at 260 nm using a NanoDrop 1000 (Thermo Scientific) or NanoPhotometer N50 (Implen) nanodrop. A volume of 1 µL DNA was used and 1 µL NFW (VWR) was used as a blank. Purity was confirmed by checking A_{260}/A_{280} ratio was ~ 1.8.

2.4.8 HiFi DNA Assembly

HiFi DNA assembly was done using NEBuilder HIFI DNA Assembly Master Mix (NEB) according to manufacturer instructions, except primers were designed to create 30 bp overlaps at each junction. Overlapping regions at both ends of backbone and insert were created by using primer pairs for amplification of each fragment which contained 5’ ends with homology to the other primer pair and vice versa. During assembly reactions, a DNA polymerase with 5’ exonuclease activity created 3’ overhangs on

backbone and insert fragments, which annealed due to homology. Remaining gaps were filled in by DNA polymerase and the backbone sealed by DNA ligase. Details of an example reaction are provided in Fig. 2.5. Backbone amount in reactions was always 100 ng with a 1:2 backbone to insert molar ratio. Concentration in pmol of DNA samples was calculated using the NEB mass-moles calculator. Reactions were incubated at 50 °C for 1 h in a Hybaid Px2 thermal cycler (Thermo Scientific) or Alpha Cycler 1 (PCRmax) and immediately transformed by chemical transformation into competent DH5α. Reactions were validated through resolving by gel-electrophoresis using backbone and insert as controls.

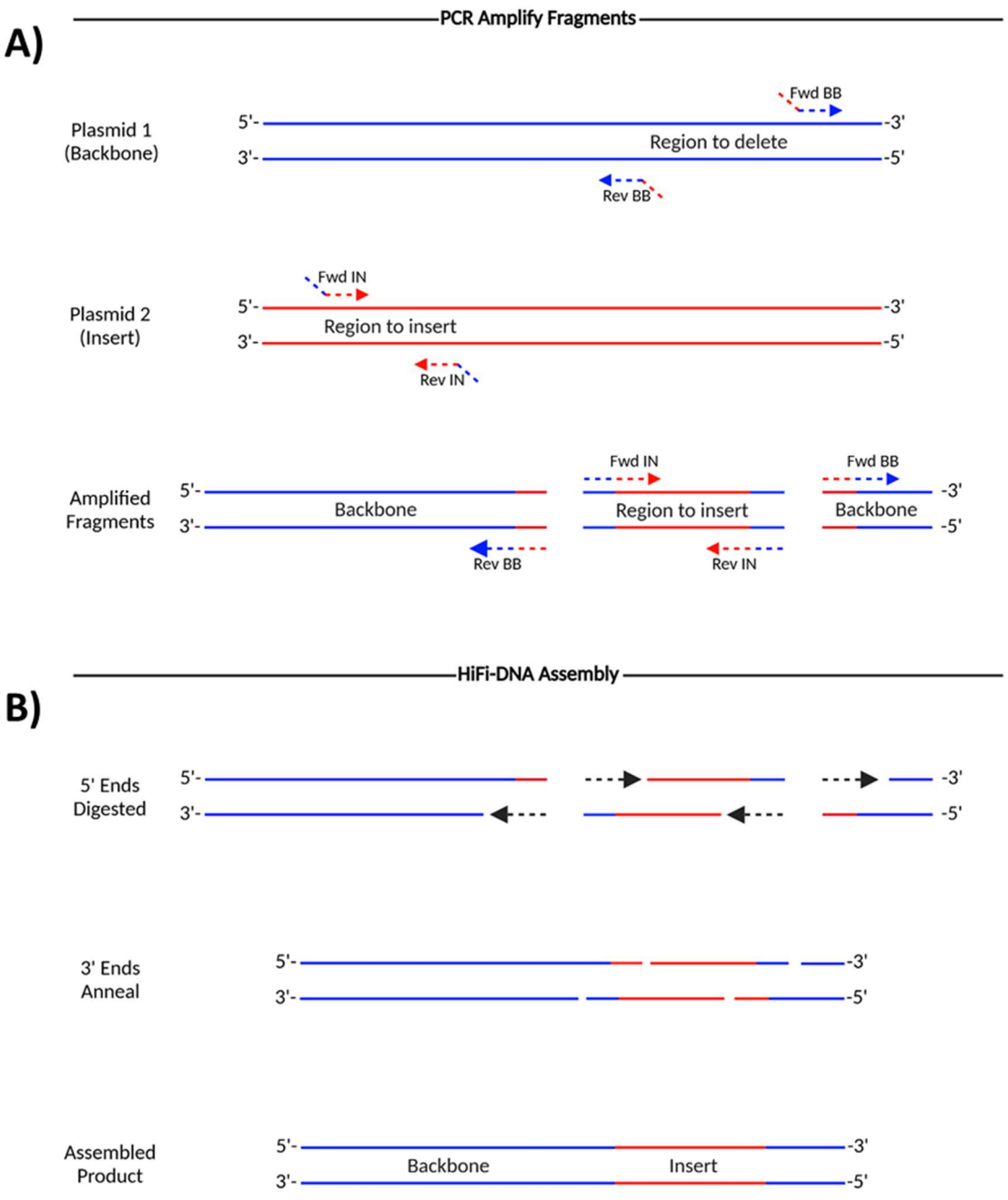


Figure 2.5: HiFi DNA assembly was used for cloning of multiple constructs. An example workflow demonstrates how regions of DNA from one plasmid were inserted seamlessly into a desired backbone. Created with BioRender.com. **(A)** Backbone and insert were amplified from pDNA using primer pairs (indicated by blue or red arrows) with complimentary 5' ends to the primer pair used to amplify the other fragment, resulting in amplicons with homologous ends. **(B)** During HiFi DNA assembly, a 5' exonuclease creates 3' overhangs, which due to homology, allowed fragments to anneal. Remaining gaps were filled in by DNA polymerase and the backbone sealed by DNA ligase.

2.4.9 Ligation

For blunt-end ligation, purified DNA quantified by nanodrop was first phosphorylated using T4 Polynucleotide Kinase (NEB) according to manufacturer instructions, except 10X T4 DNA Ligase Buffer (NEB) was used in place of 10X T4 PNK Reaction Buffer (NEB), due to the former containing ATP. Phosphorylated DNA was ligated using T4 DNA Ligase (NEB) according to manufacturers instructions; 5 ng/µL DNA was used for an overnight reaction at 16 °C. Both phosphorylation and ligation were done using a Hybaid Px2 thermal cycler (Thermo Scientific) or Alpha Cycler 1 (PCRmax).

2.4.10 Plasmid Mini-Prep

Plasmid DNA was purified using a QIAprep Spin Miniprep Kit (Qiagen) according to manufacturer instructions. In all instances, 5 mL of culture was centrifuged at 3200 x g for 10 min in an Eppendorf 5810 centrifuge prior to resuspension in Buffer P1, Buffer P2 was pre-warmed at 37 °C for ~ 30 min prior to use and lysis left to proceed for ~ 4 min 30 s. Final elution of DNA was in NFW (VWR) pre-warmed to 65 °C. Spin columns were centrifuged in an Eppendorf 5418 microcentrifuge.

2.4.11 Genomic Extraction

Genomic DNA was purified from *E. coli* strains using a DNeasy Blood & Tissue Kit (Qiagen) according to manufacturer instructions. The final elution was in NFW (VWR) pre-heated to 65 °C. In all instances, final elution of DNA was in NFW (VWR) pre-warmed to 65 °C. Spin columns were centrifuged in an Eppendorf 5418 microcentrifuge.

2.4.12 Sequencing

Plasmid DNA or PCR products were sequenced via a Sanger sequencing SpeedREAD service (Source Bioscience). Purified DNA quantified by nanodrop was diluted to 100 ng/µL in 5 µL using NFW (VWR). Sequencing primers for each sample were diluted to 3.2 pmol/µL in 5 µL using NFW (VWR). Alternatively, entire plasmids were sequenced via a Nanopore sequencing service (PlasmidsNG). Purified DNA quantified by nanodrop was diluted to 100 ng/µL in 10 µL using NFW (VWR).

2.4.13 Chemical Transformation

To prepare chemically competent cells, overnight cultures of *E. coli* grown in 10 mL LB at 37˚C, 200 rpm were used to inoculate 100 mL LB in a 500 mL Erlenmeyer flask, to OD_{600} 0.05 and aerated at 37˚C, 200 rpm until OD_{600} 0.35-0.45. Cultures were aliquoted into ice cold 50 mL tubes and incubated on ice for 20 min. Cells were pelleted at 3200 x g for 10 min in an Eppendorf 5810 centrifuge. Pellets were gently resuspended in ice cold 100 mM calcium chloride, incubated on ice for 20 min and pelleted at 3400 x g for 10 min. Pellets were gently resuspended in ice cold 100 mM calcium chloride + 10% (v/v) glycerol, incubated on ice for 20 min, then 200 µL aliquoted into ice cold 1.5 mL microcentrifuge tubes and stored at -80˚C.

Chemically competent *E. coli* were thawed on ice and transforming DNA added, 1-2 µL for plasmid DNA or 5 µL for HiFi DNA assembly reactions. A positive control, using 1 µL pUC19 (NEB) and negative control without addition of transforming DNA were run in parallel. After incubation on ice for 30 min, cells were heat shocked at 42˚C for 45 s

and immediately placed on ice for 2 min. Then, 450 µL SOC medium (NEB) (prewarmed to 37˚C) was added, with outgrowth at 37˚C, 200 rpm for 1 h. Cells were pelleted at 775 x g for 5 min in an Eppendorf 5418 microcentrifuge, 550 µL supernatant removed and the pellet resuspended in the remaining volume (~ 100 µL). Transformation reactions were plated onto LBA plus appropriate selection (pre-warmed to 37 °C) for overnight incubation at 37 °C. Positive controls were selected on LBA + Amp. Negative controls were selected on the same growth medium used for transforming DNA.

2.4.14 Electroporation

Preparation of electrocompetent cells was performed according to Tu et al. (2016), except the following. Overnight cultures of *E. coli* grown in 10 mL LB at 37˚C, 200 rpm were diluted to OD_{600} 0.05 in 10 mL LB, aerated at 37˚C, 200 rpm until OD_{600} 0.4-0.6. Initially, 5 mL of culture was pelleted at 3900 x g for 10 min in an Eppendorf 5810 centrifuge and resuspended in 1 mL diH_2O. Cells were pelleted twice more at 5000 x g for 5 min in an Eppendorf 5418 microcentrifuge, with the final resuspension in 30 µL diH_2O. Cells were electroporated using an ECM 399 Electroporation System (BTX), in 1 mm gap width electroporation cuvettes at 1.25 kV. Immediately, 600 mL SOC medium (NEB) (pre-warmed to 37 °C) was added to electroporated cells, with outgrowth at 37 °C, 200 rpm for 1 h. Cells were pelleted at 775 x g for 5 min in an Eppendorf 5418 microcentrifuge, 500 µL supernatant removed. Cells were resuspended in the remaining volume (~ 130 µL) and plated onto LBA plus appropriate selection (pre-warmed to 37 °C) for overnight incubation at 37 °C. A negative control

was run in parallel using the same strain without addition of transforming DNA and plated onto the same growth medium.

2.5 Construct Assembly

2.5.1 pET msfGFP Constructs

pET msfGFP constructs (Figure 2.6) were created via PCR and HiFi DNA assembly or blunt end ligation. Following amplification, PCR products were verified by gel electrophoresis. Template DNA in pET-26b(+) backbone amplicons was DpnI digested. After purification, DNA concentration of backbone and insert were quantified by nanodrop and assembled by HiFi DNA assembly. Reactions were transformed into chemically competent DH5α, plated on LBA + Kan. Transformants were screened by colony PCR. Positive clones were grown overnight in LB + Kan and constructs purified by mini prep. Constructs were verified by sequencing using primer pET26b_Fwd_CP_1.

2.5.1.1 pET msfGFP Construct for Post-Translational Export

pET-26b(+)_*pelB*^{SP}*::msfgfp* (Figure 2.3A and 2.6A) was assembled by PCR amplifying pET-26b(+) (Figure 2.1B) using primers pET26b_Fwd_GA_1 and pET26b_Rev_GA_1, deleting the multiple cloning site (MCS). The msfGFP insert was PCR amplified from pET GFP LIC (Figure 2.1C) using primers msfGFP_Fwd_GA_1 and msfGFP_Rev_GA_1. Backbone and insert were purified by PCR purification and assembled by HiFi DNA assembly, fusing the *msfgfp* insert to the 3' end of *pelB*^{SP}. Transformants were screened by colony PCR using primers pET26b_Fwd_CP_1 and

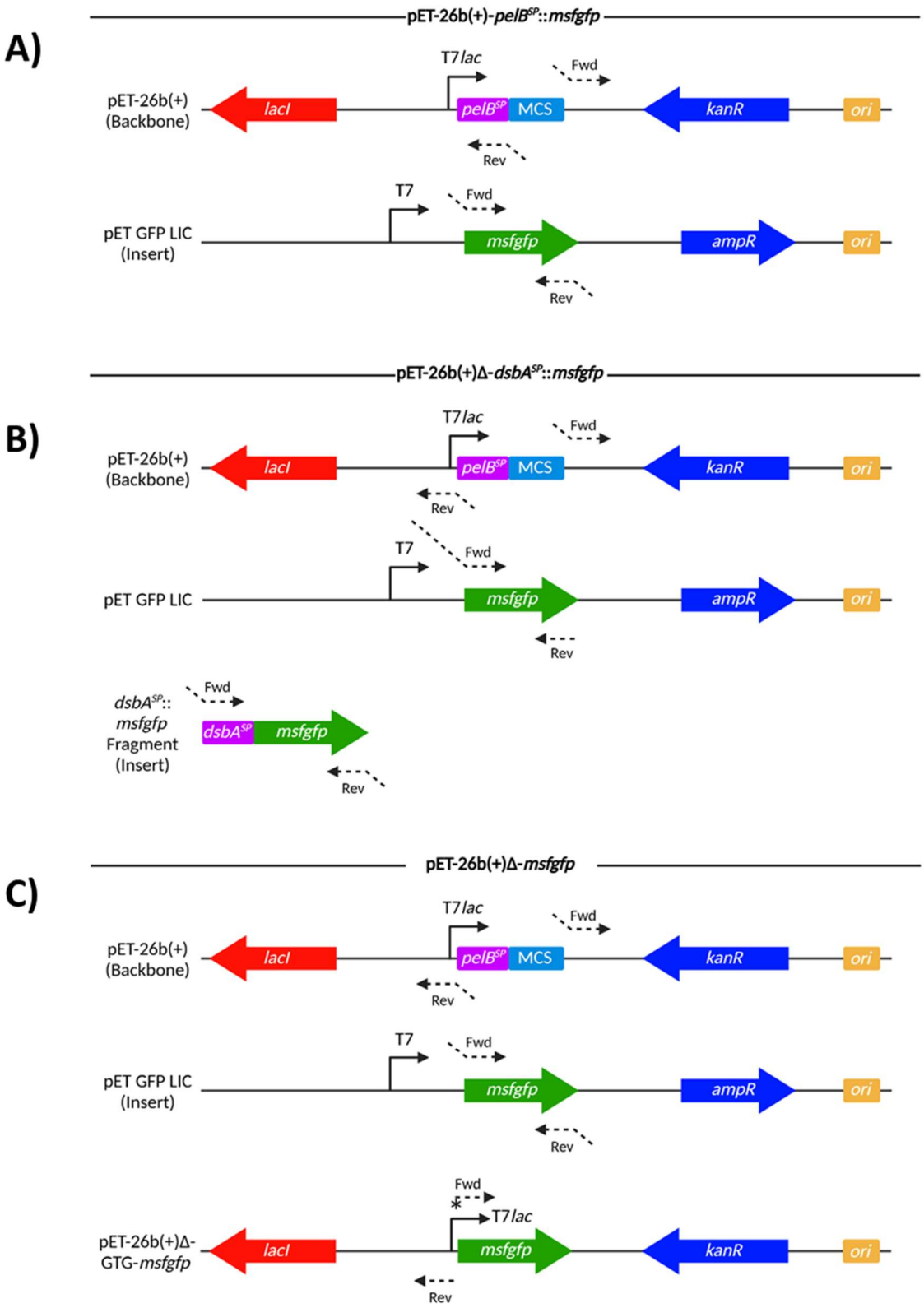

A)
pET-26b(+)-pelB^SP::msfgfp
T7lac
Fwd
pET-26b(+)
(Backbone)
lacI
pelB^SP
MCS
kanR
ori
Rev
T7
Fwd
pET GFP LIC
(Insert)
msfgfp
ampR
ori
Rev
B)
pET-26b(+)Δ-dsbA^SP::msfgfp
T7lac
Fwd
pET-26b(+)
(Backbone)
lacI
pelB^SP
MCS
kanR
ori
Rev
T7
Fwd
pET GFP LIC
msfgfp
ampR
ori
Rev
dsbA^SP::
msfgfp
Fragment
(Insert)
Fwd
dsbA^SP
msfgfp
Rev
C)
pET-26b(+)Δ-msfgfp
T7lac
Fwd
pET-26b(+)
(Backbone)
lacI
pelB^SP
MCS
kanR
ori
Rev
T7
Fwd
pET GFP LIC
(Insert)
msfgfp
ampR
ori
Rev
Fwd
*
T7lac
pET-26b(+)Δ-
GTG-msfgfp
lacI
msfgfp
kanR
ori
Rev

Figure 2.6: pET-msfGFP constructs were created using PCR and HiFi DNA assembly or blunt end ligation. Maps of sequences are provided in the 5'-3' orientation with forward and reverse primer annealing locations marked by arrows. Angled tails at the 5' end of primers indicate regions which do not anneal to the target sequence. Created with BioRender.com. **(A)** To assemble pET-26b(+)_*pelB*^{SP}*::msfgfp*, the backbone was PCR amplified from pET-26b(+) to delete the MCS and add homologous regions. The msfGFP insert was PCR amplified from pET GFP LIC to add homologous regions and HiFi DNA assembly used to insert it into the pET-26b(+) backbone, immediately downstream of *pelB*^{SP}. **(B)** To assemble pET-26b(+)_*dsbA*^{SP}*::msfgfp*, the backbone was PCR amplified from pET-26b(+), deleting *pelB*^{SP}, the MCS and adding homology arms. To create the insert, msfGFP was first PCR amplified from pET GFP LIC using a forward primer containing the entire *dsbA*^{SP} sequence at its 5' end, creating a *dsbA*^{SP}::*msfgfp* fragment. This fusion was PCR amplified again to add homology arms creating the insert. Then *dsbA*^{SP}::*msfgfp* was inserted into the pET-26b(+) backbone via HiFi DNA assembly, in the same position as *pelB*^{SP}.**(C)** To assemble pET-26b(+)-*msfgfp* the backbone was PCR amplified from pET-26b(+)_GTG_*msfgfp* using primers annealing back to back. Forward primer contained a single point mutation (G>A) in the middle of its sequence, mutagenising a GTG start codon to ATG. The linear fragment was re-circularised by blunt end ligation.

pET26b_Rev_CP_1 and positive clones verified by Sanger sequencing using pET26b_Fwd_CP_1.

2.5.1.2 pET msfGFP Construct for Non Post-Translational Export

pET-26b(+)_*dsbA*^{SP}*::msfgfp* (Figure 2.3B and 2.6B) was assembled by PCR amplifying pET-26b(+) (Figure 2.1B) using primers pET26b_Fwd_GA_3 and pET26b_Rev_GA_3, deleting *pelB*^{SP} and the MCS. The pET-26b(+)Δ backbone was gel purified. The msfGFP insert prepared in two steps. First, pET GFP LIC (u-msfGFP) (Figure 2.1C) was PCR amplified using primers DsbA-msfGFP_Fwd_5, which incorporated the entirety of *dsbA*^{SP} at its 5' end, and DsbA-msfGFP_Rev_5. The *dsbA*^{SP}::*msfGFP* fusion was purified by PCR purification. Primers DsbA-msfGFP_Fwd_GA_6 and DsbA-msfGFP_Rev_GA_6 were used to PCR amplify *dsbA*^{SP}::*msfgfp* creating the insert which was gel purified. During HiFi DNA assembly, the *dsbA*^{SP}::*msfgfp* insert was inserted in the same position as *pelB*^{SP} was. Transformants were screened by colony PCR using primers pET26b_Fwd_CP_1 and pET26b_Rev_CP_1 and positive clones verified by Sanger sequencing using pET26b_Fwd_CP_1.

2.5.1.3 pET msfGFP Construct for Cytoplasmic Expression

To assemble pET-26b(+)-*msfgfp*, first a separate plasmid pET-26b(+)_GTG_*msfgfp* (not shown but essentially identical to Figure 2.3C) was assembled by PCR amplifying pET-26b(+) (Figure 2.1B) using primers pET26b_Fwd_GA_2 and pET26b_Rev_GA_2, deleting *pelB*^{SP} and the MCS. The *msfgfp* insert was PCR amplified from pET GFP LIC (u-msfGFP) (Figure 2.1C) using primers msfGFP_Fwd_GA_4 and

msfGFP_Rev_GA_4. The pET-26b(+)Δ backbone and *msfgfp* insert were gel purified and assembled by HiFi-DNA assembly, inserting *msfgfp* into the same position as *pelB*^{SP} was. Transformants were screened by colony PCR using primers pET26b_Fwd_CP_1 and T7_Terminator and positive clones verified by Sanger sequencing using pET26b_Fwd_CP_1.

pET-26b(+)-*msfgfp* (Figure 2.3C and 2.6C) was then PCR amplified from pET-26b(+)_GTG_*msfgfp* (not shown but essentially identical to Figure 2.3C) using primers pET-msfGFP_Sub_Fwd and pET-msfGFP_Sub_Rev, annealing back to back. Forward primer pET-msfGFP_Sub_Fwd contained a single G>A point mutation in the middle of its sequence, mutagenising the msfGFP GTG start codon in pET-26b(+)_GTG_*msfgfp* to ATG. The linear fragment following PCR was gel purified and then re-circularised by blunt-end ligation. Transformants were screened by colony PCR using primers pET26b_Fwd_CP_1 and T7_Terminator and positive clones verified by Sanger sequencing using pET26b_Fwd_CP_1.

2.5.2 pBAD msfGFP Constructs

pBAD msfGFP constructs (Figure 2.7) were created via PCR and HiFi DNA assembly. Following amplification, PCR products were verified by gel electrophoresis. Template DNA in backbone and inserts amplicons was DpnI digested. After purification, DNA concentration of backbone and insert were quantified by nanodrop and assembled by HiFi DNA assembly. Reactions were transformed into chemically competent DH5α, plated on LBA + Kan. Where specified, transformants were screened by colony PCR.

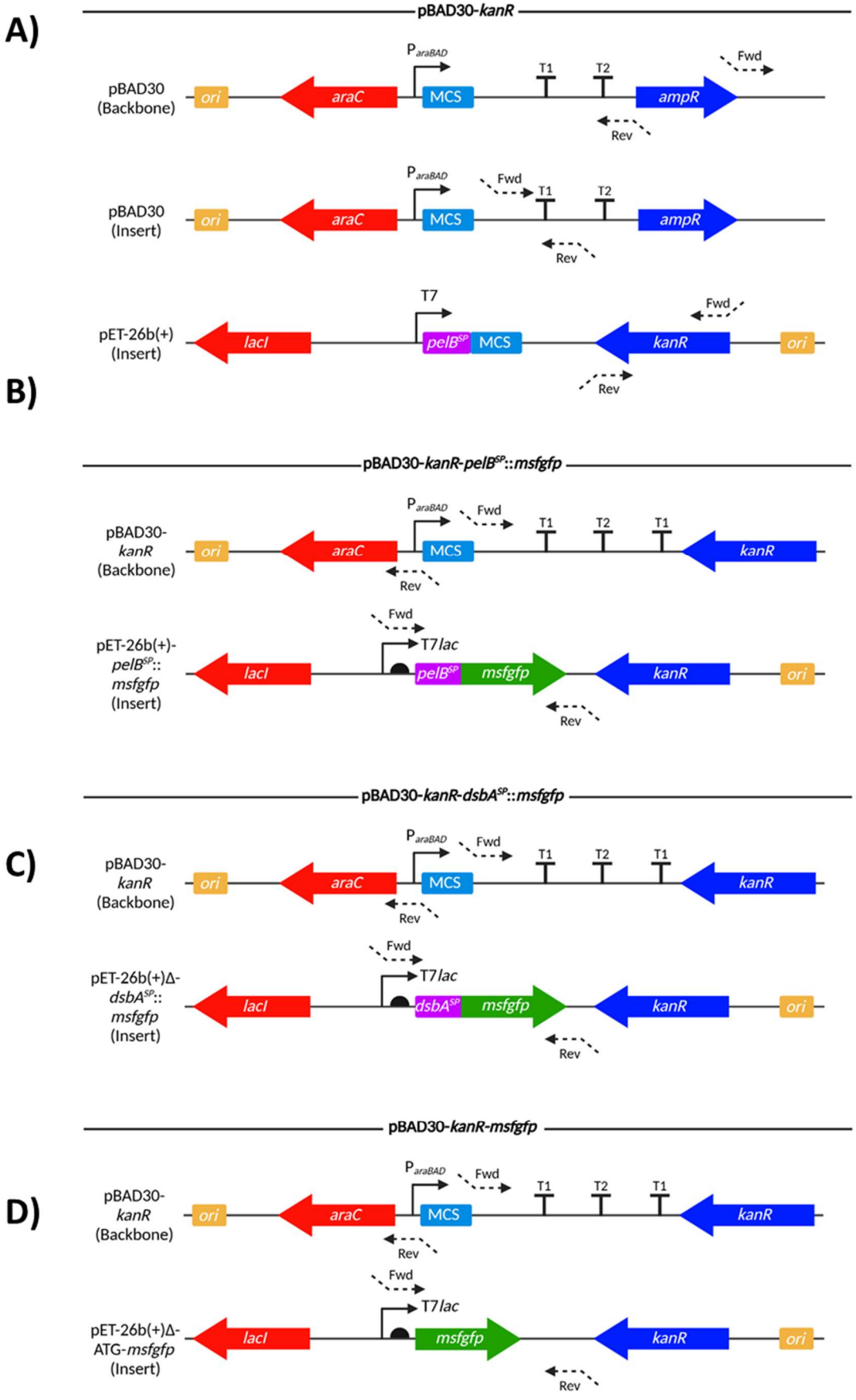

A)
pBAD30-kanR
pBAD30 (Backbone)
ori
araC
P araBAD
MCS
T1
T2
ampR
Fwd
Rev
pBAD30 (Insert)
pET-26b(+) (Insert)
T7
lacI
pelB SP
kanR
B)
pBAD30-kanR-pelB SP::msfgfp
pBAD30-kanR (Backbone)
pET-26b(+)-pelB SP::msfgfp (Insert)
T7lac
msfgfp
C)
pBAD30-kanR-dsbA SP::msfgfp
pET-26b(+)Δ-dsbA SP::msfgfp (Insert)
dsbA SP
D)
pBAD30-kanR-msfgfp
pET-26b(+)Δ-ATG-msfgfp (Insert)

Figure 2.7: pBAD-msfGFP constructs were created using PCR and HiFi DNA assembly. Maps of sequences are provided in the 5'-3' orientation, primer annealing locations are marked by arrows, RBSs by black semi circles and terminators by a T. Angled tails at the 5' end of primers indicate regions which do not anneal to the target sequence. Created with BioRender.com. **(A)** Before assembling pBAD-msfGFP constructs, a pBAD30-*kanR* backbone was prepared by PCR amplifying pBAD30 while deleting *ampR* and adding homologous regions. Two inserts were prepared by PCR to add homologous regions. The first by amplifying *rrnB* T1 terminator from pBAD30 and the second by amplifying *kanR* from pET-26b(+). During HiFi DNA assembly, the *kanR* fragment was inserted into pBAD30 in the same position as *ampR* but in the opposite orientation, with the *rrnB* T1 terminator downstream. **(B)** To assemble pBAD30-*kanR*-*pelB*^{SP}::*msfgfp*, the backbone was PCR amplified deleting the MCS and adding homologous regions. The T7 RBS and *pelB*^{SP}::msfGFP insert was PCR amplified from pET-26b(+)_*pelB*^{SP}*::msfgfp* to add homologous regions and then inserted into the pBAD30-*kanR* backbone via HiFi DNA assembly, in the same position as the MCS. **(C)** To assemble pBAD30-*kanR*-*dsbA*^{SP}::*msfgfp*, the backbone was PCR amplified to delete the MCS and add homologous regions. The T7 RBS and *dsbA*^{SP}::msfGFP insert was PCR amplified from pET-26b(+)_*dsbA*^{SP}*::msfgfp* to add homologous regions and then inserted into the pBAD30-*kanR* backbone via HiFi DNA assembly, in the same position as the MCS. **(D)** To assemble pBAD30-*kanR*-*msfgfp*, the backbone was PCR amplified to delete the MCS and add homologous regions. The T7 RBS and msfGFP insert was PCR amplified from pET-26b(+)-ATG-*msfgfp* to add homologous regions and then inserted into the pBAD30-*kanR* backbone via HiFi DNA assembly, in the same position as the MCS.

Positive clones were grown overnight in LB + Kan, constructs purified by mini prep and verified by sanger sequencing.

2.5.2.1 pBAD with kanamycin resistance

pBAD30-*kanR* (Figure 2.1E and 2.7A) was assembled by PCR amplifying pBAD30 (Figure 2.1D) using primers pBAD30_Fwd_GA_1 and pBAD30_Rev_GA_1 to prepare the backbone, deleting *ampR*. The kanamycin resistance cassette was PCR amplified from pET-26b(+) (Figure 2.1B) using primers kan_Fwd_GA_1 and kan_Rev_GA_1 for the first insert. A second insert containing the *rrnB* T1 terminator was PCR amplified from pBAD30 (Figure 2.1D) using primers rrnB T1_Fwd and rrnB T1_Rev. Backbone and inserts were purified by PCR purification and assembled by HiFi DNA assembly. Primers for both inserts were designed so that *kanR* and *rrnB* T1 were assembled in the reverse orientation to *ampR*. Transformants were verified by sequencing using primers pBAD30_Fwd_CP_1 and pBAD30_Rev_CP_1.

2.5.2.2 pBAD msfGFP Construct for Post-Translational Export

pBAD30-*kan*^{R}-*pelB*^{SP}::*msfgfp* (Figure 2.3D and 2.7B) was assembled by PCR amplifying pBAD30-*kanR* (Figure 2.1E) using primers pBAD30_Fwd_GA_2 and pBAD30_Rev_GA_2 to prepare the backbone, deleting the MCS. For the insert, a region containing the T7 gene 10 RBS and *pelB*^{SP}::*msfgfp* was PCR amplified from pET-26b(+)-*pelB*^{SP}::*msfgfp* (Figure 2.3A) using primers pET26b-msfGFP_Fwd_GA_1 and pET26b-msfGFP_Rev_GA_1. Backbone and insert were purified by PCR purification. During HiFi DNA assembly, the T7 gene 10 RBS and *pelB*^{SP}::*msfgfp* fragment was inserted downstream of P_{araBAD} in the same orientation, and upstream of

the *rrnB* T1 and T2 terminators. Transformants were screened by colony PCR using primers pBAD30_Fwd_CP_2 and pBAD30_Rev_CP_3, then verified by sequencing using primers pBAD30_Fwd_CP_1.

2.5.2.3 pBAD msfGFP Construct for Non Post-Translational Export

pBAD30-*kan*^{R}-*dsbA*^{SP}::*msfgfp* (Figure 2.3E and Figure 2.7C) was assembled by PCR amplifying pBAD30-*kanR* (Figure 2.1E) using primers pBAD30_Fwd_GA_2 and pBAD30_Rev_GA_2 to prepare the backbone, deleting the MCS. For the insert, a region containing the T7 gene 10 RBS and *dsbA*^{SP}::*msfgfp* was PCR amplified from pET-26b(+)Δ-*dsbA*^{SP}::*msfgfp* (Figure 2.3B) using primers pET26b-msfGFP_Fwd_GA_1 and pET26b-msfGFP_Rev_GA_1. Backbone and inserts were purified by PCR purification. During HiFi DNA assembly, the T7 gene 10 RBS and *dsbA*^{SP}::*msfgfp* fragment was inserted downstream of P_{araBAD} in the same orientation, and upstream of the *rrnB* T1 and T2 terminators. Transformants were screened by colony PCR using primers pBAD30_Fwd_CP_2 and pBAD30_Rev_CP_3, then verified by sequencing using primers pBAD30_Fwd_CP_1.

2.5.2.4 pBAD msfGFP Construct for Cytoplasmic Expression

pBAD30-*kanR-msfgfp* (Figure 2.3F and 2.7D) was assembled by PCR amplifying pBAD30-*kanR* (Figure 2.1E) using primers pBAD30_Fwd_GA_2 and pBAD30_Rev_GA_2 to prepare the backbone, deleting the MCS. For the insert, a region containing the T7 gene 10 RBS and *msfgfp* was PCR amplified from pET-26b(+)Δ-ATG-*msfgfp* (Figure 2.3C) using primers pET26b-msfGFP_Fwd_GA_1 and pET26b-msfGFP_Rev_GA_1. Backbone and inserts were purified by PCR purification.

During HiFi DNA assembly, the T7 gene 10 RBS and *msfgfp* fragment was inserted downstream of P_{araBAD} in the same orientation, and upstream of the *rrnB* T1 and T2 terminators. Transformants were screened by colony PCR using primers pBAD30_Fwd_CP_2 and pBAD30_Rev_CP_3, then verified by sequencing using primers pBAD30_Fwd_CP_1.

2.5.3 pBAD cfSGFP2 Constructs

pBAD cfSGFP2 constructs (Figure 2.8) were created via PCR and all amplicons verified by gel electrophoresis. Amplicons of backbones and inserts were DpnI digested to remove template DNA and then purified by PCR or gel purification. DNA concentrations of backbones and inserts were quantified by nanodrop. Assembly was via HiFi DNA assembly or blunt-end ligation. Reactions were transformed into chemically competent DH5α, plated on LBA + Kan. Clones were grown overnight in LB + Kan and constructs purified by mini prep. Constructs were verified by Nanopore sequencing.

2.5.3.1 pBAD cfSGFP2 Construct for Cytoplasmic Expression

Backbone for assembly of pBAD30-*kan*^{R}-*cfsgfp2* (Figure 2.3H and Figure 2.8A) was prepared via PCR in two steps. First, *msfgfp* was deleted from pBAD30-*kanR-msfgfp* (Figure 2.3F) using primers pBAD30_Cyto_Fwd and pBAD30_Cyto_Rev, followed by amplification using primers pBAD30-Cyto_Fwd_GA and pBAD30-Cyto_Rev_GA. Both fragments to prepare the backbone were purified by gel purification. To prepare the insert, a fragment containing *cfsgfp2* flanked by to optimal priming locations was chemically synthesised by GENEWIZ using the FragmentGENE service. First, the

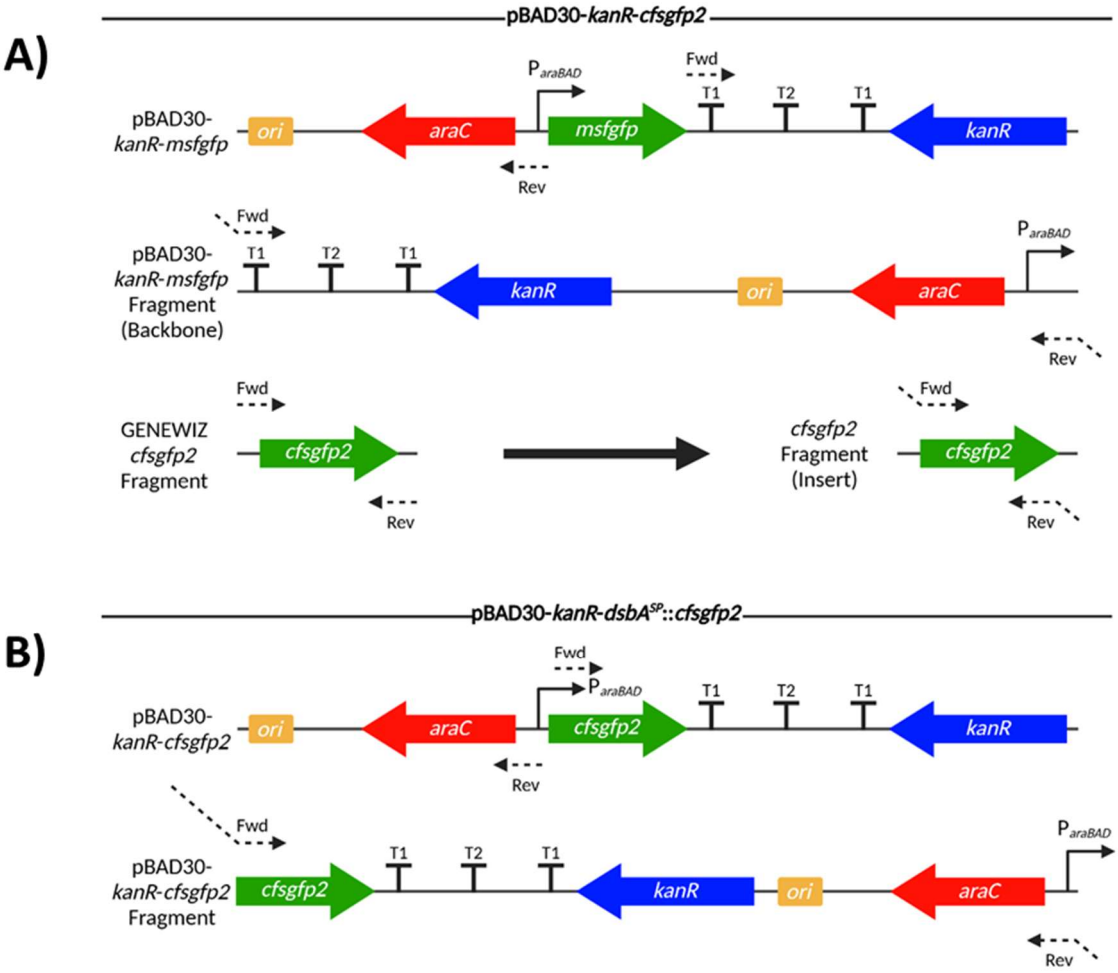


Figure 2.8: pBAD-cfSGFP2 constructs were created using PCR and HiFi DNA assembly or blunt end ligation. Maps of sequences are provided in the 5'-3' orientation with primer annealing locations marked by arrows and terminators by a T. Angled tails at the 5' end of primers indicate regions which do not anneal to the target sequence. Created with BioRender.com. **(A)** To assemble pBAD30-*kanR-cfsgfp2*, the backbone was prepared in two steps by PCR amplifying pBAD30-*kanR-msfgfp* to delete *msfgfp*, with a second round of PCR used to insert homologous regions for HiFi DNA assembly. The *cfsgfp2* gene flanked by two optimal priming sequences was chemically synthesised by GENEWIZ and PCR amplified. Homologous regions were then added, and the priming locations deleted via another round of PCR to create the insert. During HiFi DNA assembly, the *cfsgfp2* was inserted into pBAD30-*kanR* in the same position as *msfgfp*. **(B)** To assemble pBAD30-*kanR-dsbA*^{SP}::*cfsgfp2*, the backbone prepared by PCR amplifying pBAD30-*kanR-cfsgfp2* to delete the *cfsgfp2* ATG start codon. Due to differences in annealing temperatures for priming locations, a small region upstream of *cfsgfp2* including the T7 RBS was also deleted. A second round of PCR on this fragment was used to add *dsbA*^{SP} by incorporating it into the 5' end of the forward primer, while the reverse primer contained the region deleted in the previous step at its 5' end. Backbone was re-assembled by blunt end ligation, inserting *dsbA*^{SP} immediately upstream of *cfsgfp2*.

cfsgfp2 fragment was amplified using primers cfSGFP2_Fwd_1 and cfSGFP2_Rev_1, followed by a second amplification using primers cfSGFP2_Fwd_GA_1 and cfSGFP2_Rev_GA_1. Both fragments to prepare the insert were purified by PCR purification. During HiFi DNA assembly, *cfsgfp2* was inserted into the pBAD30-*kanR* backbone in the same position as *msfgfp* had been. Following transformation, clones were verified by Sanger sequencing using primers pBAD30_Fwd_CP_1.

2.5.3.2 pBAD cfSGFP2 Construct for Non Post-Translational Export

Backbone for pBAD30-kan^R-$dsbA^{SP}$::*cfsgfp2* (Figure 2.3G and 2.8B) was prepared via PCR in two steps. Due to differences in annealing temperatures for necessary priming locations, a small region between P_{araBAD} and the start of *cfsgfp2,* which included the T7 gene 10 RBS, was deleted from pBAD30-*kanR-cfsgfp2* (Figure 2.3H) using primers pBAD30-cfSGFP2_Fwd and pBAD30-cfSGFP2_Rev. This fragment was purified by PCR purification and a second round of amplification fused $dsbA^{SP}$ immediately upstream of *cfsgfp2* and re-inserted the deleted region, using primers pBAD30-DsbA-cfSGFP2_Fwd and pBAD30-cfSGFP2_Rev_2. The forward primer contained the entire $dsbA^{SP}$ coding sequence and reverse primer the previously deleted region at their 5' ends. This fragment was purified by gel purification and blunt-end ligation used to reassemble the construct. Following transformation, clones were verified by Sanger sequencing using primers pBAD30_Fwd_CP_1.

2.5.4 Biosensor Constructs

Biosensor constructs (Figure 2.9) were created via PCR and all amplicons verified by gel electrophoresis. Amplicons of backbones and inserts were DpnI digested to

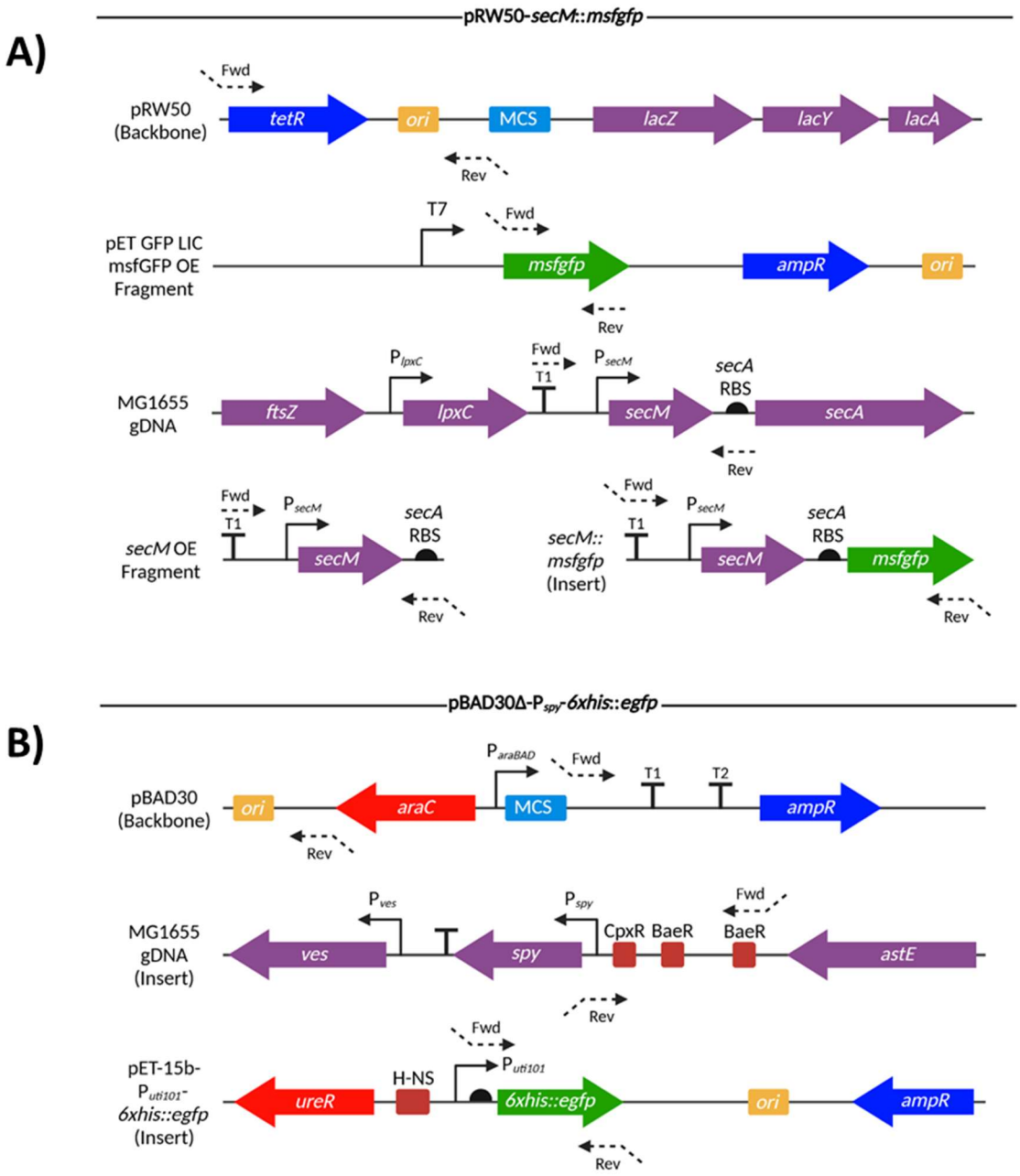

A)
pRW50-secM::msfgfp
Fwd
pRW50
(Backbone)
tetR
ori
MCS
lacZ
lacY
lacA
Rev
T7
Fwd
pET GFP LIC
msfGFP OE
Fragment
msfgfp
ampR
ori
Rev
P lpxC
Fwd
T1
P secM
secA
RBS
MG1655
gDNA
ftsZ
lpxC
secM
secA
Rev
Fwd
P secM
T1
secA
RBS
secM OE
Fragment
secM
Rev
Fwd
P secM
T1
secA
RBS
secM::
msfgfp
(Insert)
secM
msfgfp
Rev
B)
pBAD30Δ-P spy-6xhis::egfp
P araBAD
Fwd
T1
T2
pBAD30
(Backbone)
ori
araC
MCS
ampR
Rev
P ves
P spy
Fwd
MG1655
gDNA
(Insert)
ves
spy
CpxR
BaeR
BaeR
astE
Rev
Fwd
pET-15b-
P uti101-
6xhis::egfp
(Insert)
H-NS
P uti101
ureR
6xhis::egfp
ori
ampR
Rev

Figure 2.9: Biosensor constructs were created using PCR and HiFi DNA assembly. Maps of sequences are provided in the 5'-3' orientation with primer annealing locations marked by arrows, RBSs by black semi circles and terminators by a T. Angled tails at the 5' end of primers indicate regions which do not anneal to the target sequence. Created with BioRender.com. **(A)** To assemble pRW50Δ-*secM*::*msfgfp*, the backbone prepared by PCR amplifying pRW50 to delete *lacZ*, *lacY* and *lacA* while adding homologous regions for HiFi DNA assembly. A *secM*::*msfgfp* insert was prepared in multiple steps via overlap extension PCR. First, *msfgfp* was PCR amplified from pET GFP LIC using a forward primer with homology at its 5' end to the 3' end of *secM*. Next, P_{secM}, *secM* and the *secA* RBS were PCR amplified from MG1655 gDNA. This fragment was PCR amplified again using a reverse primer with homology at its 5' end to the 5' end of *msfgfp*. The *secM* and *msfgfp* fragments were then stitched together via overlap extension PCR. A final PCR amplification was used to add homologous regions to *secM*::*msfgfp* for HiFi DNA assembly, where it was inserted into the pRW50 backbone in the same position as the MCS. **(B)** To assemble pBAD30Δ-P_{spy}-*6xhis*::*egfp*, the backbone was prepared by PCR amplifying pBAD30 to delete *araC*, P_{araBAD} and the MCS while adding homologous regions for HiFi DNA assembly. For inserts, the P_{spy} promoter was PCR amplified from MG1655 gDNA and homology arms added, while *6xhis*::*egfp* was PCR amplified from pET-15b-P_{uti101}-*6xhis*::*egfp*. During assembly, a P_{spy}-*6xhis*::*egfp* fusion was created which was inserted into the pBAD30 backbone in the same position as *araC*.

remove template DNA and then purified by PCR or gel purification. DNA concentrations of backbones and inserts were quantified by nanodrop, followed by HiFi DNA assembly. Reactions were transformed into chemically competent DH5α, plated on LBA + Amp. Clones were grown overnight in LB + Amp and constructs purified by mini prep. Where specified, constructs were screen by colony PCR. Constructs were verified by sanger sequencing.

2.5.4.1 SecM Construct

Backbone for HiFi DNA assembly of pRW50Δ-*secM*::msf*gfp* (Figure 2.2D and Figure 2.9A) was prepared via PCR amplification of pRW50 (Figure 2.1F) using primers pRW50_Fwd_GA_3 and pRW50_Rev_GA_3, deleting *lacZ*, *lacY* and *lacA*. The pRW50Δ backbone was purified by PCR purification. A *secM*::*msfgfp* insert for HiFi DNA Assembly was prepared in multiple steps and fused by overlap extension PCR. First, *msfgfp* was amplified by touchdown PCR from pET GFP LIC using primers msfGFP_Fwd_OE_3, which contained a region at its 5' end with homology to the 3' end of *secM*, and msfGFP_Rev_OE_3. Gel purification was used to purify the *msfgfp* fragment. A fragment including P_{secM} -*secM*, and the downstream *secA* RBS was cloned by PCR from gDNA extracted from MG1655, using primers SecM-SecA_Fwd and SecM-SecA_Rev. PCR purification was used to purify the P_{secM}-*secM-secA* RBS fragment.

A second round of amplification via touchdown PCR was used to prepare the P_{secM}-*secM-secA* RBS fragment for fusion to *msfgfp*, using primers SecM-SecA_Fwd and SecM-SecA_Rev_OE_2, which contained a region at its 5' end with homology to the

5’ end of the *msfgfp* fragment. Fragments of P_{secM}-*secM-secA* RBS and *msfgfp*, with homology at their 3' and 5' ends respectively, were fused by overlap extension touchdown PCR using primers SecM-SecA_Fwd and msfGFP_Rev_OE_3. Gel purification was used to purify the P_{secM}-*secM-secA* RBS::*msfgfp* overlap extension product. Finally, the P_{secM}-*secM-secA* RBS::*msfgfp* insert was amplified by PCR using primers SecM-msfGFP_Fwd_GA_1 and SecM-msfGFP_Rev_GA_1 then gel purified. During HiFi DNA assembly, the P_{secM}-*secM-secA* RBS::*msfgfp* fragment was inserted into the pRW50Δ in the position of the MCS. Following transformation, clones were screened by colony PCR using primers pRW50Δ-Fwd_CP_1 and pRW50Δ-Rev_CP_1 and verified by Sanger sequencing using primers pRW50Δ-Fwd_CP_1 and pRW50Δ-Rev_CP_1.

2.5.4.2 P_{Spy} Construct

Backbone for HiFi DNA assembly of pBAD30Δ-P_{spy}-*6xhis*::*egfp* (Figure 2.2E and Figure 2.9B) was prepared via PCR amplification of pBAD30 (Figure 2.1D) using primers pBAD30_Fwd_GA_3 and pBAD30_Rev_GA_3, deleting *araC* and P_{araBAD}. The pBAD30Δ backbone was purified by PCR purification. A P_{spy} insert containing the P_{spy} core promoter and upstream CpxR and BaeR sites was cloned by PCR amplification of gDNA extracted from MG1655, using primers Spy_Fwd_GA_1 and Spy_Rev_GA_1. The P_{spy} insert was purified by PCR purification. A *6xhis*::*egfp* insert, which included the upstream T7 gene 10 RBS was cloned by PCR amplification of pET-15b-P_{uti101}-*6xhis*::*egfp* using primers EGFP_Fwd_GA_1 and EGFP_Rev_GA_1. The *6xhis*::*egfp* insert was purified by PCR purification. During HiFi DNA assembly, the P_{spy} and *6xhis*::*egfp* inserts were fused and inserted into the pBAD30Δ backbone in the same

position and orientation as P_{araBAD} was. Transformants were verified by Sanger sequencing using primer pBAD30_Fwd.

2.5.5 Negative Feedback Constructs

Constructs to create a negative feedback loop (Figure 2.10) were created via PCR and all amplicons verified by gel electrophoresis. Amplicons of backbones and inserts were DpnI digested to remove template DNA and then purified by PCR or gel purification. DNA concentrations of backbones and inserts were quantified by nanodrop. Assembly was via HiFi DNA assembly or blunt-end ligation. Reactions were transformed into chemically competent DH5α, plated on LBA + Amp. Clones were grown overnight in LB + Amp and constructs purified by mini prep. Constructs were verified by sanger sequencing unless specified.

2.5.5.1 LacI Ligand Unresponsive Constructs

Backbone for HiFi DNA assembly of pBAD30-*lacI* (Figure 2.2F and Figure 2.10A) was prepared via PCR amplification of pBAD30 (Figure 2.1D) using primers pBAD30_Fwd_GA_5 and pBAD30_Rev_GA_5, deleting the MCS. The pBAD30 backbone was purified by PCR purification. The *lacI* insert was cloned by PCR on pET-26b(+) (Figure 2.1B), using primers lacI_Fwd_GA and lacI_Rev_GA, amplifying a region which included the entirety of *lacI* and its RBS. The *lacI* insert was purified by gel purification. During HiFi DNA assembly, the *lacI* fragment was inserted into the pBAD30 backbone just downstream of P_{araBAD} in the same orientation. Transformants were verified by Sanger sequencing using primers pBAD30_Fwd_CP_2, pBAD30-lacI_Fwd_1 and pBAD30-lacI_Fwd_2.

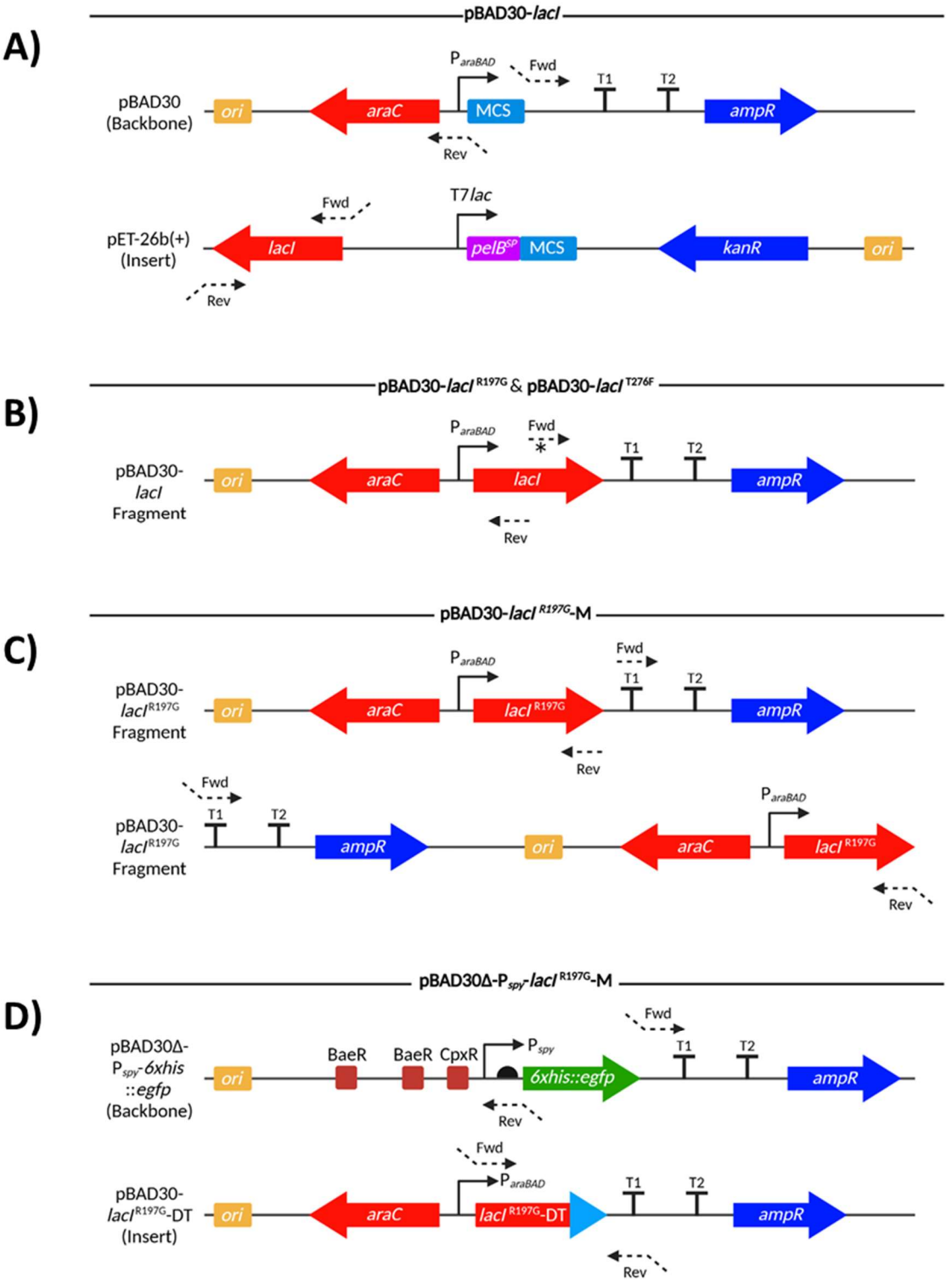

A)
pBAD30-lacI
pBAD30 (Backbone)
ori
araC
P araBAD
Fwd
MCS
T1
T2
ampR
Rev
pET-26b(+) (Insert)
Fwd
T7lac
lacI
pelB SP
MCS
kanR
ori
Rev
B)
pBAD30-lacI R197G & pBAD30-lacI T276F
pBAD30-lacI Fragment
ori
araC
P araBAD
Fwd
lacI
T1
T2
ampR
Rev
C)
pBAD30-lacI R197G-M
pBAD30-lacI R197G Fragment
ori
araC
P araBAD
Fwd
lacI R197G
T1
T2
ampR
Rev
pBAD30-lacI R197G Fragment
Fwd
T1
T2
ampR
ori
araC
P araBAD
lacI R197G
Rev
D)
pBAD30Δ-P spy-lacI R197G-M
pBAD30Δ-P spy-6xhis::egfp (Backbone)
ori
BaeR
BaeR
CpxR
P spy
6xhis::egfp
Fwd
T1
T2
ampR
Rev
pBAD30-lacI R197G-DT (Insert)
ori
araC
Fwd
P araBAD
lacI R197G-DT
T1
T2
ampR
Rev

Figure 2.10: Negative feedback constructs were created using PCR and HiFi DNA assembly or blunt end ligation. Maps of sequences are provided in the 5'-3' orientation with primer annealing locations marked by arrows, mutations by (*), RBS by black semi circles and terminators by a T. Angled tails at the 5' end of primers indicate regions which do not anneal to the target sequence. Created with BioRender.com. **(A)** To assemble pBAD30-*lacI*, the backbone prepared by PCR amplifying pBAD30 to delete the MCS and add homologous regions for HiFi DNA assembly. The *lacI* insert was prepared by PCR amplifying pET-26b(+) and adding homology arms. During HiFi DNA assembly, *lacI* was inserted into the pBAD30 backbone in the same position as the MCS. **(B)** To assemble pBAD30-$lacI^{R197G}$ and pBAD30-$lacI^{T276F}$, the backbone prepared by PCR amplifying pBAD30-*lacI* to create mutations R197G or T276F, using primers annealing back-to-back, with each forward primer containing the mutation in the middle of its sequence. The backbone was re-circularised by blunt end ligation. **(C)** To assemble pBAD30-$lacI^{R197G}$-M, the backbone was prepared in multiple steps. First, pBAD30-$lacI^{R197G}$ was PCR amplified to open the backbone at the insertion site and delete the TGA stop codon. A second round of PCR was then used to add the SsrA degradation tag and stop codon to the 3' end of $lacI^{R197G}$ using forward and reverse primers each containing half the sequence at their 5' ends. The backbone was re-circularised by blunt end ligation. **(D)** To assemble pBAD30Δ-P_{spy}-$lacI^{R197G}$, the backbone was PCR amplified from pBAD30Δ-P_{spy}-*6xhis*::*egfp*, deleting *6xhis*::*egfp* and adding homology arms. For the insert, $lacI^{R197G}$ was PCR amplified from pBAD30-$lacI^{R197G}$. During HiFi DNA assembly, $lacI^{R197G}$-M was inserted into the backbone in the same position as *6xhis*::*egfp*. Created with Biorender.com.

Backbone for pBAD30-*lacI*^{R197G} (Figure 2.2F and Figure 2.10B) was prepared via PCR amplification of pBAD30-*lacI* (Figure 2.2F) using primers lacI_R197G_Fwd and lacI_R197G_Rev, with the forward primer containing 3 point mutations in the middle of its sequence to create the R197G mutation. The pBAD30-*lacI*^{R197G} backbone was purified by gel purification and re-assembled via blunt end ligation. Transformants were verified by Sanger sequencing using primers pBAD30_Fwd_CP_2, pBAD30-lacI_Fwd_1 and pBAD30-lacI_Fwd_2.

Backbone for pBAD30-*lacI*^{T276F} (Figure 2.2F and Figure 2.10B) was prepared via PCR amplification of pBAD30-*lacI* (Figure 2.2F) using primers lacI_T276F_Fwd and lacI_T276F_Rev, with the forward primer containing 3 point mutations in the middle of its sequence to create the T276F mutation. The pBAD30-*lacI*^{T276F} backbone was purified by gel purification and re-assembled via blunt end ligation. Transformants were verified by Sanger sequencing using primers pBAD30_Fwd_CP_2, pBAD30-lacI_Fwd_1 and pBAD30-lacI_Fwd_2.

Backbone for pBAD30-*lacI*^{R197G}-M (Figure 2.2G and Figure 2.10C) was prepared in two steps. First, pBAD30-*lacI*^{R197G} (Figure 2.2F) was amplified by PCR using primers pBAD30-lacI_Fwd_3 and pBAD30-lacI_Rev, deleting 50 bp immediately downstream of *lacI*^{R197G} including its TGA stop codon. This pBAD30-*lacI*^{R197G} fragment was purified by PCR purification and PCR amplified again using primers M_SsrA_Fwd_2 and M_SsrA_Rev_2. Forward and reverse primers each contained half of a moderately fast SsrA degradation tag at their 5' ends (Part: BBa_M0052 in the igem registry of standard biological parts), with the forward primer also incorporating the deleted TGA stop

codon. The pBAD30-*lacI*^{R197G}-M backbone was purified by PCR purification and re-assembled via blunt end ligation, fusing the moderately SsrA degradation tag to the 3' end of *lacI*^{R197G}. Transformants were verified by Sanger sequencing using primers pBAD30_Fwd_CP_2, pBAD30-lacI_Fwd_1 and pBAD30-lacI_Fwd_2.

2.5.5.2 P$_{Spy}$ Negative Feedback Construct

Backbone for pBAD30Δ-P$_{spy}$-*lacI*^{R197G} (Figure 2.2H and Figure 2.10D) was prepared by PCR amplification of pBAD30Δ-P$_{spy}$-*6xhis*::*egfp* (Figure 2.2E) using primers pBAD-Pspy_Fwd_GA and pBAD-Pspy_Rev_GA, deleting *6xhis*::*egfp*. The pBAD30Δ-P$_{spy}$ backbone was purified by PCR purification. The *lacI*^{R197G} insert was cloned by PCR amplification of pBAD30-*lacI*^{R197G} (Figure 2.2F), using primers lacI-DT_Fwd_GA and lacI-DT_Rev_GA, amplifying the entire *lacI*^{R197G}-M sequence and a 41 bp region downstream. The *lacI*^{R197G}-M insert was purified by gel purification. During HiFi DNA assembly, the *lacI*^{R197G}-M fragment was inserted into the pBAD30Δ-P$_{spy}$ backbone in the same position and orientation as *6xhis*::*egfp* had been. Transformants were verified by Sanger sequencing using primers pBAD30_Fwd_CP_2, pBAD30-lacI_Fwd_1 and pBAD30-lacI_Fwd_2.

2.6 Analytical Techniques

2.6.1 Flow Cytometry

Samples were analysed using a BD Accuri C6 flow cytometer or BD Accuri C6 Plus flow cytometer (Becton Dickinson), both of which use a 488 nm laser. Samples were diluted in 0.2 µm filter sterilised (Fisher) Phosphate Buffered Saline (PBS) (OXOID), prepared according to manufacturer instructions and stored at RT for up to 3 months,

so the event rate was below 4000 events s^{-1}. A flow rate of 14 µL min^{-1}, core size of 10 µm and primary threshold of 12,000 on FSC-H were used. Data collection proceeded until 25,000 events within a user defined gated on FSC-A and SSC-A (Fig. 2.11A). Green fluorescence was detected using a 533/30 band pass filter (FL1-A or FL2-A) and red fluorescence using 670 nm long pass filter (FL3-A). Data was analysed using BD Accuri C6 or BD Accuri C6 Plus software (Becton Dickinson).

To evaluate viability, cells were stained with the nucleic acid intercalating and non-membrane permeable dye PI. Upon binding nucleic acids like DNA, PI fluorescence increases, with an emission maximum around 620 nm. As such, PI staining was used to measure membrane integrity as an indicator of live or dead cells. To stain cells, 4 µg mL^{-1} PI was added to samples prepared in in 0.2 µm filter sterilised PBS, incubated for 5 min in the dark at RT, and red fluorescence (FL4-A) measured. To optimise staining for each strain and generate gates (examples provided in Fig. 2.11B), live and dead cells were prepared. Live cells were prepared by diluting cultures in PBS, so the event rate was below 4000 events s^{-1}. For dead cells, 1 mL of culture diluted to OD_{600} 1.0 was pelleted at 5000 rpm for 5 min in an Eppendorf 5418 microcentrifuge, resuspended in 1 mL PBS and pelleted at 5000 rpm for 5 min. Cells were resuspended in 1 mL 0.22 µm filtered 70% (v/v) ethanol (Thermo Fisher) and incubated at RT for 15 min. Cells were pelleted at 5000 rpm for 5 min, resuspended in 1 mL PBS and diluted in PBS so the event rate was below 4000 events s^{-1}. PI was then added to live and dead samples for analysis by flow cytometry.

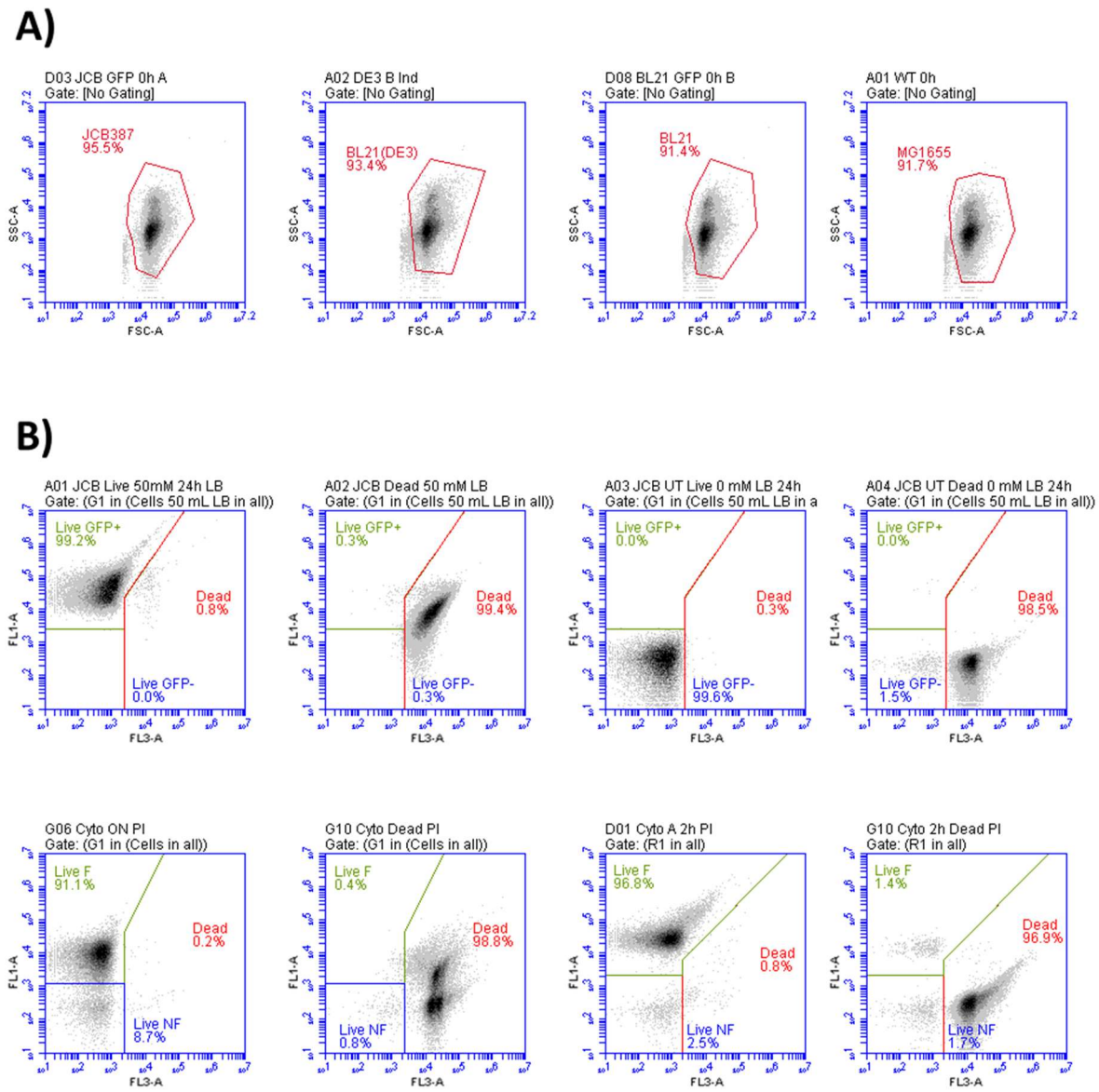


Figure 2.11: During flow cytometric analysis, a threshold of 12,000 on FSC-H was used to remove background noise. **(A)** Additional noise that couldn't be removed by thresholding was removed from analysis by gating cells on FSC-A and SSC-A. Examples are given for strains JCB387, BL21(DE3), BL21 and MG1655. **(B)** Flow cytometry combined with PI staining was used to differentiate between live and dead cells and quantify the amount of each within a culture. PI is non-permeant to live cells but readily stains dead cells, which can be measured as red fluorescence (FL3-A). Combined with untransformed strains, gates were created by analysing live and dead cells and plotting red fluorescence (FL3-A) against green fluorescence (FL1-A). From left to right, examples are given for strains, live JCB387 containing GFP, dead JCB387 containing GFP, live untransformed JCB387, dead untransformed JCB387, live BL21(DE3) containing GFP, dead BL21(DE3) containing GFP, live BL21 containing GFP and dead BL21 containing GFP.

2.6.2 Microscopy

2.6.2.1 Bright-field Microscopy

Untransformed JCB387 and BL21 were imaged by bright-field microscopy using a Zeiss Axiolab microscope which had a halogen lamp and Moticam 10+ camera. Cells were diluted to OD_{600} 0.1-0.2 in sterile diH_2O, transferred to sterile 50 mm petri dish and imaged using a 50x water immersion objective (Zeiss). Images were processed and cell length calculated using ImageJ (Fiji).

2.6.2.2 Fluorescence Microscopy

Cells expressing GFP were imaged using a fluorescence microscopy using a Zeiss Axiolab microscope which had a standard mercury arc lamp, excitation filter, dichroic mirror, emission filter for GFP and Moticam 10+ camera. JCB387 and BL21 expressing pET-15b-P_{uti101}-*6xhis::egfp* were diluted to OD_{600} 0.1-0.2 in sterile diH_2O, transferred to sterile 50 mm petri dish and imaged using a 50x water immersion objective (Zeiss). To image BL21(DE3) expressing pET-26b(+) msfGFP constructs and BL21 expressing pBAD30-*kanR* msfGFP or cfSGFP2 constructs by fluorescence microscopy, cells were diluted to OD_{600} 0.1 in sterile diH_2O, 2 µL transferred to 1 mm glass slides (Fisher) topped with #1.5 glass cover slips (Fisher). Immersion oil (PanScan Xtra) with a refractive index of 1.518 was added just prior to switching to the 100x oil immersion objective (Zeiss). Images were processed and cell length calculated using ImageJ (Fiji).

2.6.2.2 Structured Illumination Microscopy

BL21 expressing pBAD30-*kanR* msfGFP or cfSGFP2 constructs were imaged by structured illumination microscopy (SIM) using a Nikon N-SIM S. Cells were grown according to the protein expression section until 2 h post-induction and diluted to OD_{600} 0.4 in sterile diH_2O. To stain cells, 30 µM nile red was added for 15 min, centrifuged at 5000 x g for 5 min, supernatant removed and resuspended in sterile diH_2O. For imaging, 2 µL cell resuspension was transferred to agarose pads prepared according to Skinner et al. (2013) using 1 % low-melt agarose (VWR) dissolved in diH_2O and topped with #1.5 glass cover slips (Fisher). Immersion oil (Nikon) with a refractive index of 1.518 was added prior to imaging using a 100x oil immersion objective. GFP was excited using a 488 nm laser and emission detected using a Chroma ET525/50m bandpass filter. Nile red was excited with a 561 nm laser and emission detected using a Chroma ET 700/75m bandpass filter. Images were acquired using Nikon NIS Elements 5, analysed using NIS Elements 5 workstation and processed using Fiji.

2.6.3 Optical Density

Optical density was determined using an Evolution 300 UV-Vis spectrophotometer (Thermo Scientific) at 600 nm, in disposable plastic cuvettes. Sterile growth medium was used to blank the instrument and samples diluted above OD_{600} 0.8.

2.6.4 Plate Reader

Plate reader analysis was done using a Fluostar Omega Plate Reader (BMG Labtech) using 96-well black walled plates with a clear top and bottom. Plates were incubated at 37 °C with double orbital shaking for 24 h with OD_{600} and green fluorescence

recorded at 15-minute intervals. Gain for green fluorescence intensity was adjusted prior to start so that the well with the highest fluorescence was under 50000 AU.

2.6.5 SDS-PAGE

Proteins from whole-cell lysates or sub-cellular fractions were separated by SDS-PAGE. Whole-cell lysates were prepared by centrifuging a volume of culture, equal to an OD_{600} of 1.0, at 10000 x g for 5 min in an Eppendorf 5418 microcentrifuge, supernatant removed, and samples stored at -20 °C. Sub-cellular fractionation of samples into cytoplasmic and periplasmic fractions was done according to Selas Castiñeiras et al. (2018a). Briefly, a volume of culture, equal to an OD_{600} of 1.0, was spun down at 12000 x g for 10 min in an Eppendorf 5418 microcentrifuge. Supernatant was discarded, pellets resuspended in 49.2 µL ice cold spheroplast buffer; 0.8 µL lysozyme added, followed by 50 µL ice cold diH_2O. Samples were incubated on ice for 5 min, 19.6 mM $MgSO_4$ added and spun down at 12000 x g for 2 min. Supernatant was transferred to sterile 1.5 mL eppendorfs as the periplasmic fraction and stored at -20 °C. Remaining pellet was resuspended in 100 µL 100 mM Tris-HCl pH 8.0 (Fisher), 0.7 µL benzonase at > 250 U μL^{-1} (Merck) added and samples stored at -20 °C as the cytoplasmic fractions.

Samples were thawed on ice and mixed 1:1 with 15 µL 2X SDS PAGE sample buffer containing; 65.8 mM Tris-HCl pH 6.8 (Fisher), 0.01% bromophenol blue (Electran), 26.3% glycerol (Merck), 2.1% SDS (Merck). To this, 1.5 µL 1 M dithiothreitol (DTT) (Sigma) was added and samples heated at 95˚C for 5 min. Samples were resolved on Novex™ WedgeWell™ 16%, Tris-Glycine, 1.0 mm, 12-well, Mini Protein Gels (Thermo

Scientific) at 140 V for 45 min using a mini gel tank (Life Technologies). 10-20 µL of each sample was loaded and 3 µL Color Prestained Protein Standard, Broad Range (10-250 kDa) (NEB) was run in parallel. Gels were stained using SimplyBlue SafeStain (Invitrogen) according to manufacturer instructions and imaged.

Protein concentration was estimated using ImageJ (Fiji). Individual band intensities for the Color Prestained Protein Standard (NEB) were calculated based on a 2.0 mg mL^{-1} concentration. Intensity and estimated concentration data was plotted in Prism (GraphPad) and a curve fitted with the resulting equation used to estimate the concentration of each band of interest. Analysis of the percentages of proteins between lanes for cytoplasmic and periplasmic fractions was also estimated using ImageJ; bands were measured and the integrated density values for each used to calculate the percentage within each lane.

2.6.5 Statistical Analysis

Statistical analysis of data was done using GraphPad Prism 10. Raw data was inserted so that replicates were in side-by-side sub-columns and processed in Prism to calculate mean values and standard deviation. All significance testing was performed in Prism using recommended settings. For all analysis the assumptions of significance tests were confirmed through normality testing (Shapiro-Wilk) with QQ plots analysed; checking for equal variances (Brown-Forsythe or Spearman's test for heteroscedasticity) with homoscedasticity plots analysed. Residual plots were also analysed to check any problems with the assumptions of a model or test. For comparison of 2 samples, two sample t-tests were performed; to correct for multiple

comparisons the Holm-Šídák was used (alpha = 0.05). For comparison of ≥ 3 samples ANOVA was used via the Prism built in analysis. For analysis of single time-points across conditions, one-way ANOVA was used. For analysis of multiple time-points, two-way ANOVA was used. In both one-way and two-way ANOVA, corrections for multiple comparisons were applied (Tukey). Specific growth rates (μ h^{-1}) were calculated in Prism by log transforming OD_{600} or cell density (cells mL^{-1}) data and determining the linear portion of the growth curve (typically 0 – 2 h post-induction or 0 – 4 h post-induction) was identified and analysed using linear regression. The slope of the resulting fit ($R^2 > 0.95$) was used as the specific growth rate.

Chapter 3: Optimising a novel urea inducible promoter

3.1 Introduction

Universal solutions to bioprocessing are uncommon; how a recombinant protein is expressed varies considerably, so different parts of a production system must be optimised each time. A key component in expression systems is inducible promoters (covered in section 1.4); short regions of DNA upstream of the gene of interest that determine the transcription rate and provide control over when it is initiated. While several promoters for RPP currently exist for use in *E. coli*, caveats exist with each of them.

IPTG inducible *lac* promoter derivatives (Hothersall et al., 2021), particularly those combined with T7 expression systems (Wyre and Overton, 2014, Castiñeiras et al., 2018), are often still the gold standard for RPP in *E. coli* but have several issues. Basal expression in *lac* regulated systems is known to be high, compounded by the strength of the T7 promoter (Spehr et al., 2000). Alternatives with tighter regulation include the *araBAD* promoter (Guzman et al., 1995) although it is weaker than many *lac* promoters (Balzer et al., 2013) and addition of submaximal inducer concentrations results in culture heterogeneity, preventing tuneable ex pression (Siegele and Hu, 1997). The *rhaBAD* promoter is also very tightly regulated and unlike the *araBAD* promoter, highly dose dependent, but its inducer L-rhamnose is metabolised by *E. coli* necessitating modified promoters to utilise orthogonal inducers (Kelly et al., 2016). A further issue with many available inducible promoters is cost. For *lac* promoters, the lactose analogue IPTG is favoured as it is not metabolised by *E. coli*, but pharmaceutical grade costs over £20,000 kg $^{-1}$. L-arabinose and L-rhamnose are cheaper, albeit still

expensive at around £6,000 kg $^{-1}$ for high purity product. Further, all three inducers require an appropriate cold chain for stability. As batch sizes increase during scale-up and transitioning into commercial production, induction can represent a sizable cost.

This has led to recent interest into novel inducible systems which utilise cheap inducers that are stable at ambient temperatures (Hothersall et al., 2022a). Further, expanding the genetic toolbox with novel promoters would be beneficial during process optimisation. With collaborators at The University of Birmingham and Aston University (Douglas Browning), we have explored the use of a novel urea inducible promoter for overexpressing recombinant proteins in *E. coli* (Hothersall et al., 2022b). Urea could prove a useful inducer for several reasons; it is extremely cheap at approximately £20 kg $^{-1}$, reducing costs during process intensification and batch production. Urea is stable at room temperature for extended periods as a solid or in aqueous solution (Welles et al., 1971, Panyachariwat and Steckel, 2014), simplifying storage concerns. Generally *E. coli* K-12 and B strains are unable to metabolise urea, being a pathway typically associated with pathogens (Konieczna et al., 2012); an orthologous system means inducer concentration should remain stable throughout a process, avoiding transient expression.

Metabolism of urea is found among eukaryotes, prokaryotes and archaea (Kappaun et al., 2018), its breakdown to ammonia and carbon dioxide catalysed by urease, a nickel-containing metalloenzyme (Dixon et al., 1975). In bacteria, this capacity has been well studied due to a clinical association with urinary tract infections (UTIs) in humans (Flores-Mireles et al., 2015). Bacterial urease and its accessory proteins are encoded

from a gene cluster localised to the chromosome or in some instances on a plasmid (Mobley and Hausinger, 1989). This work utilised a urea inducible promoter from the genome of *Proteus mirablis*, a Gram negative facultative anaerobe and one of the more prevalent pathogens in UTIs (Schaffer and Pearson, 2017). *P*. *mirablis* will readily metabolise urea during pathogenesis; its urease gene cluster being a major virulence determinant (Mobley et al., 1994). Expressed as an operon, urease synthesis is tightly regulated by an inducible system which is repressed in the absence of urea; a 33 kDa activator UreR (D'Orazio and Collins, 1993, Nicholson et al., 1993) orchestrating the switch from the off to on state. UreR belongs to the family of AraC-like transcriptional activators (D'Orazio and Collins, 1993, Nicholson et al., 1993) which share common features for activity (Martin and Rosner, 2001, Cortés-Avalos et al., 2021). At the UreR N-terminus are domains for binding its cognate ligand urea and for dimerization, as functional UreR is dimeric (Poore et al., 2001, Gendlina et al., 2002). A characteristic HTH motif is present at the C-terminus; such arrangements are well known to facilitate protein-DNA interactions and are ubiquitous among transcription factors (Brennan and Matthews, 1989).

Two divergent promoters drive expression of the urease gene cluster (Island and Mobley, 1995, D'Orazio et al., 1996) (Figure 3.1A); P_{ureR} drives expression of *ureR*, while in the opposing direction, P_{ureD} drives an operon consisting of seven structural genes *ureDABCEFG* (Jones and Mobley, 1989). Between P_{ureR} and P_{ureD} lies binding sites for sites for dimeric UreR, which favours the consensus T(A/G)(T/C)(A/T)(T/G)(C/T)T(A/T)(T/A)ATTG (Thomas and Collins, 1999). Two such sites are localised within this intergenic region (Thomas and Collins, 1999), one for

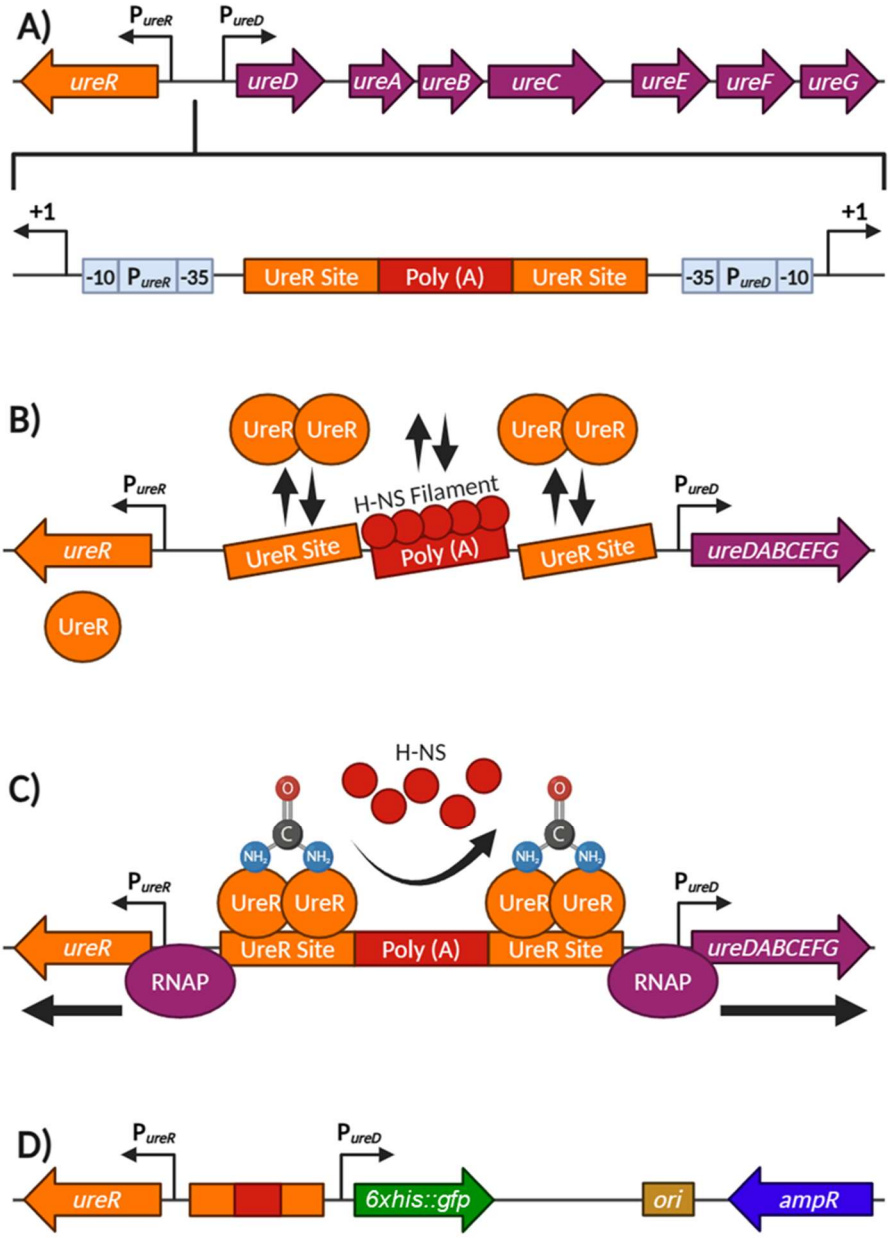


Figure 3.1: The Urease gene cluster in *P. mirabilis* is activated in the presence of urea. Created with Biorender.com.

(A) In *P. mirabilis*, the Urease gene cluster consists of two divergent promoters: P_{ureR}, driving expression of the system's positive regulator UreR, and P_{ureD}, driving expression of the *ureDABCEFG* operon, encoding structural genes.

(B) Low levels of UreR are maintained in the systems off state via basal expression from P_{ureR}. Two mechanisms prevent background expression; UreR binds poorly to sites within the region between P_{ureR} and P_{ureD}, and H-NS represses the system via binding to a proximal poly (A) tract causing DNA bending.

(C) Addition of urea induces conformational changes in UreR allowing it to displace H-NS and bind both sites in the intergenic region, recruiting RNA polymerase to initiate transcription from both P_{ureR} and P_{ureD}.

(D) To evaluate the systems applicability to RPP, an expression cassette containing divergent P_{ureR} and P_{ureD} promoters and *ureR*, the urea inducible P_{uti101} promoter, was cloned into a pET-15b plasmid backbone upstream of *6xhis::gfp*.

each promoter; UreR activates transcription from both (D'Orazio et al., 1996). Activation of transcription in the absence of urea is prevented in two stages (Figure 3.1B). Firstly, dimeric UreR has lower affinity for intergenic DNA binding sites in the absence of urea (Thomas and Collins, 1999), limiting recruitment of RNA polymerase. Parallel to this, both P_{ureR} and P_{ureD} are repressed by the 15.6 kDa hugely abundant histone-like nucleoid-structuring protein (H-NS) (Coker et al., 2000, Poore and Mobley, 2003). As a global negative transcriptional regulator H-NS regulation is complex and gene silencing may occur at the local level, or proliferate to larger scales across multiple sites (Dorman, 2004). HN-S preferentially binds curved A/T-rich tracts along DNA (Yamada et al., 1990, Lang et al., 2007). Such sites encourage nucleation; HN-S oligomers assemble into filament-like structures altering DNA topology and depending on the position relative to a target promoter, blocking recruitment of RNA polymerase sterically, through further bending, or inhibiting the elongation phase via bridged hairpin-like structures (Stoebel et al., 2008, Ricksen et al., 2015).

In the urease gene cluster, a region consistent with H-NS binding is found between the two UreR sites within the intergenic region (Coker et al., 2000, Poore and Mobley, 2003). Fluidity in the occupation of relevant sites within the intergenic region by UreR and H-NS has been apparent, with one displacing the other; higher temperatures favouring UreR binding (Poore and Mobley, 2003). Some basal transcription from P_{ureR} is necessary even in the off state, so that upon exposure to urea, basal levels of UreR are available to activate full expression (Dattelbaum et al., 2003). Upon uptake of urea (Figure 3.1C), binding with dimeric UreR induces conformational changes increasing its affinity for target sites (Thomas and Collins, 1999), H-NS bound to the intergenic

region is displaced and de-repression of the system occurs (Poore and Mobley, 2003). As with other AraC-like family members, recruitment of RNA polymerase by UreR is presumably via direct contact with subunits, enhancing binding to the promoter (Martin and Rosner, 2001, Cortés-Avalos et al., 2021).

In this work, we have looked at exploiting the urea inducible nature of this system for overexpression of recombinant proteins and assessed its applicability for RPP. An expression cassette containing *ureR,* P_{ureR}, the intergenic regulatory region and P_{ureD} (henceforth termed the P_{uti101} promoter), was cloned from *P. mirablis* and a truncated variant inserted into a pET-15b-*6xhis*::*gfp* backbone, upstream of the T7 gene 10 RBS (Figure 3.1D) (Hothersall et al., 2022b). The Browning lab (Aston University) completed initial expression work on the urea inducible P_{uti101} promoter in *E. coli* K12 JCB387, analysed by SDS PAGE and western blotting (Hothersall et al., 2022b). Such methods determine output across an entire culture but lack the resolution to detect potential sub-populations. Overexpression of GFP permits access to powerful single cell analysis using FCM, which proved applicable to RPP previously (Wyre and Overton, 2014, Kasli et al., 2019, Zulkifly et al., 2023, Hothersall et al., 2021, Hothersall et al., 2022a) to observe promoter behaviour throughout process optimisation and scale-up.

By utilising FCM in combination with GFP expression and viability staining, we wanted to observe heterogeneity in GFP expression profiles, or perturbations to host physiology caused by P_{uti101} characteristics and the inducer urea. Using analysis from this, application of the urea inducible P_{uti101} promoter for RPP was optimised from flask through to bioreactor scale.

3.2 Effect of urea on the host

Ideally, inducers used to trigger RPP should be inert and not interact with host-cell physiology. Unlike many sugars used to switch on other inducible promoters, urea is chaotropic and is commonly used to denature proteins at high concentrations (≥ 5 M). While such high concentrations of urea would not be feasible for induction during RPP, there was an obvious need to determine how urea interacted with host cells. The Browning lab completed initial expression work on the urea inducible P_{uti101} promoter in *E. coli* K12 JCB387, originally constructed for studying the regulation of nitrate reduction (Page et al., 1990). Several *E. coli* strains are more commonly used for RPP like BL21 (Studier and Moffatt, 1986) which has several advantages. Like other B strains, BL21 is deficient in Lon and OmpT proteases for improved yields (Jeong et al., 2015), can achieve faster growth rates, has improved sensitivity to high glucose concentrations by way of lower acetate production, and generally better tolerance to high-level overexpression (Phue et al., 2005, Marisch et al., 2013). For consistency with prior work, promoter analysis in JCB387 was continued, with the addition of BL21 for its relevance to RPP.

3.2.1 Uncoupling the effect of urea from 6xHis::GFP expression

To uncouple any physiological effect of urea on JCB387 and BL21 from that of overexpressing 6xHis::GFP, untransformed variants of both were grown under similar conditions in two separate experiments. Cultures were aerated at 37 °C, 200 rpm in 50 mL LB (Lennox) in Erlenmeyer flasks. At OD_{600} 0.4-0.6, 0 mM, 10 mM, 100 mM or 500 mM urea was added to flasks in triplicate, with growth proceeding for a further 24 h. An upper limit of 500 mM urea was selected as a high concentration which could be

conceivably used for induction during RPP. The lower limit of 10 mM was based off prior work by the Browning lab (Aston University) (Hothersall et al., 2022b).

Biomass accumulation was monitored via OD_{600} in untransformed JCB387 and BL21, in response to treatment with urea (Figure 3.2A). Addition of 0 mM – 100 mM urea had little effect on biomass accumulation in untransformed JCB387, with OD_{600} similar throughout all 24 h. Compared with the untreated control (0 mM), untransformed JCB387 cultures treated with 500 mM urea appeared to have some growth arrest between 2 h and 24 h post-induction; this was significant when analysed by two-way ANOVA (adjusted $p < 0.0001$ for all comparisons). Addition of urea to untransformed BL21 had little impact on biomass accumulation between 0 h and 4 h, with OD_{600} virtually the same; at 24 h there were some differences, but these were not significant and there was no clear correlation with urea concentration.

Specific growth rates (μ h^{-1}) for untransformed JCB387 and BL21 cultures were calculated from OD_{600} (Figure 3.2B). In untransformed JCB387 cultures treated with 0 – 100 mM urea, there was little difference in the specific growth rate. However, specific growth rate was significantly lower in untransformed JCB387 cultures treated with 500 mM urea compared with the untreated control (0 mM urea), when analysed by one-way ANOVA (adjusted $p = 0.004$). In BL21, there was little difference in specific growth rate for cultures treated with 0 – 500 mM urea. As with OD_{600}, higher specific growth was observed in JCB387 cultures compared with BL21 cultures.

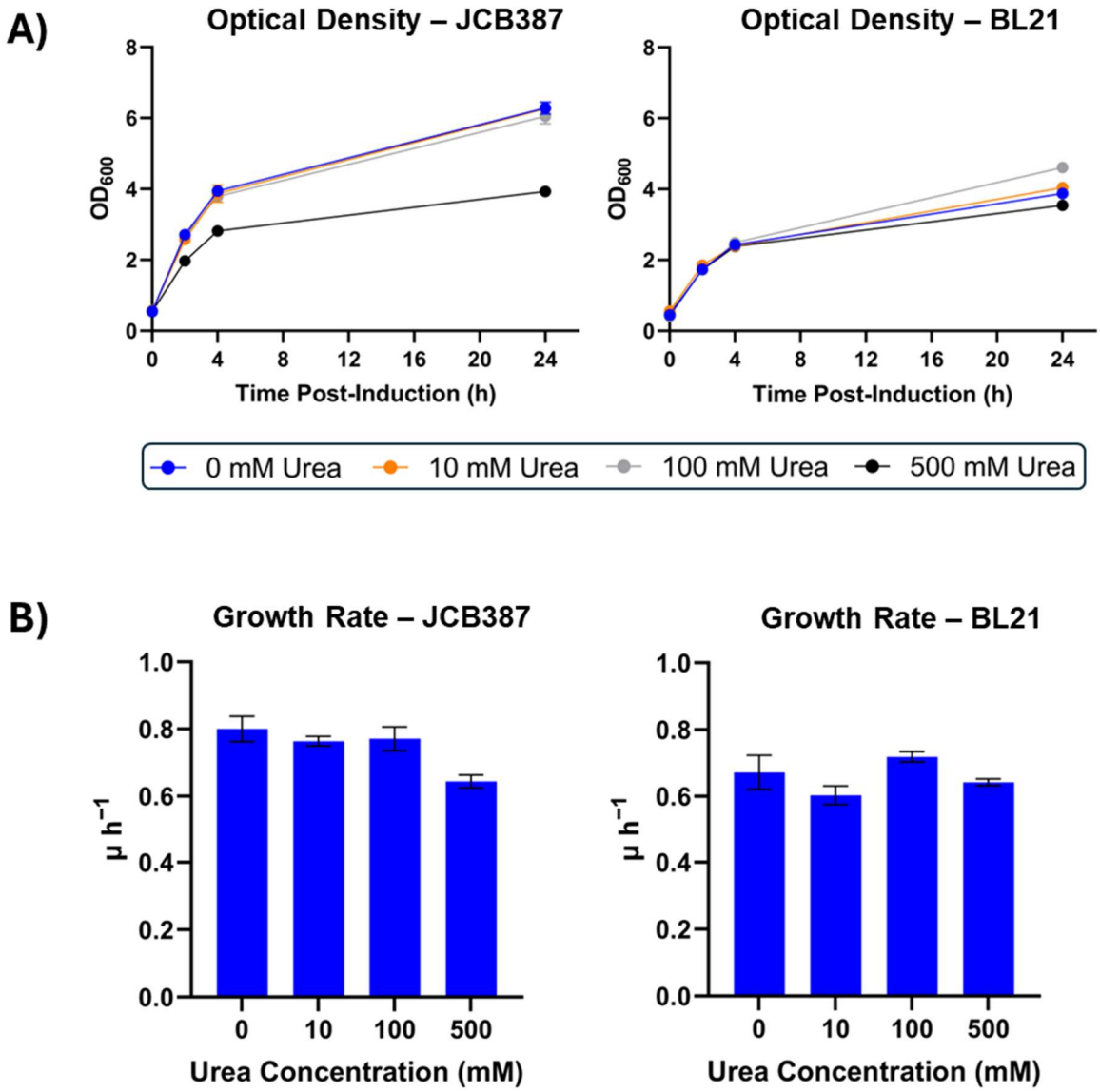


Figure 3.2: Growth data of untransformed *E. coli* JCB387 and BL21 treated with varying concentrations of urea.

To determine the effect of urea on host cells, untransformed variants of JCB387 and BL21 were grown under RPP-like conditions in 50 mL LB at 37 °C, 200 rpm. At OD_{600} 0.4-0.5, 0 – 500 mM urea was added to cultures in biological triplicates. Data provided is from separate experiments for JCB387 and BL21. Error bars represent +/- SD from biological triplicates.

(A) OD_{600} was monitored throughout to observe the effect on urea on biomass accumulation in the absence of 6xHis::GFP expression. In JCB387, addition of 0 – 100 mM urea had little effect on OD_{600}; when adding 500 mM urea, significant growth arrest compared to the 0 mM urea control was observed at 2 h – 24 h post-induction (adjusted $p < 0.0001$ for all comparisons) when analysed by two-way ANOVA. In BL21 little difference in OD_{600} was observed between induction and 4 h post-induction, regardless of the concentration of urea added. At 24 h post-induction, BL21 cultures induced with 500 mM urea were slightly lower, although there was no clear correlation between urea concentration and OD_{600}.

(B) Specific growth rate (μ h^{-1}) was calculated from OD_{600}. In JCB387, there was little difference in specific growth rates between cultures induced with 0 – 100 mM urea, but specific growth rate was significantly lower in cultures treated with 500 mM urea compared with the 0 mM urea control ($p = 0.004$) when analysed by one-way ANOVA. In BL21, there was little difference in specific growth rate for cultures treated with 0 – 500 mM urea.

It was clear that addition of 500 mM urea affected biomass accumulation in JCB387 more so than in BL21 (Figure 3.3). We wondered what other impact the addition of urea had on host physiology, so cultures were analysed using FCM. Firstly, as a measure of viability, cells were stained with the intercalating dye PI, which exhibits increased fluorescence upon binding nucleic acids like DNA. Being non-membrane permeable, PI measures membrane integrity, hence, increased fluorescence is indicative of whether a cell is alive or dead (Stiefel et al., 2015).

It was not possible to stain BL21 with PI in the presence of urea and this is further described in Chapter 3, section 3.3.2. However, given little growth arrest was observed in BL21, even upon addition of 500 mM urea (Figure 3.2A), we did not believe cell viability was massively impacted. In JCB387, some growth arrest was observed upon addition of 500 mM urea (Figure 3.2A) so measuring viability was of interest (Figure 3.3). However, staining JCB387 with PI indicated typically over 98 % of cells were PI- throughout all 24 h following addition of urea. Even upon addition of 500 mM urea, the proportion PI- cells did not drop below 95 %. Thus, while biomass accumulation in JCB387 slowed in response to addition of 500 mM urea (Figure 3.2), it was unlikely cells were non-viable (Figure 3.3).

Forward scatter (FSC) was also measured during FCM analysis as an indicator of cell size; increases in which may indicate stress resulting in division defects leading to filamentation (Karasz et al., 2022). FSC of untransformed cultures was analysed by FCM (Figure 3.4). In untransformed JCB387 (Figure 3.4A), mean FSC decreased between 0 h and 2 h post-induction in cultures treated with 0 mM – 100 mM urea,

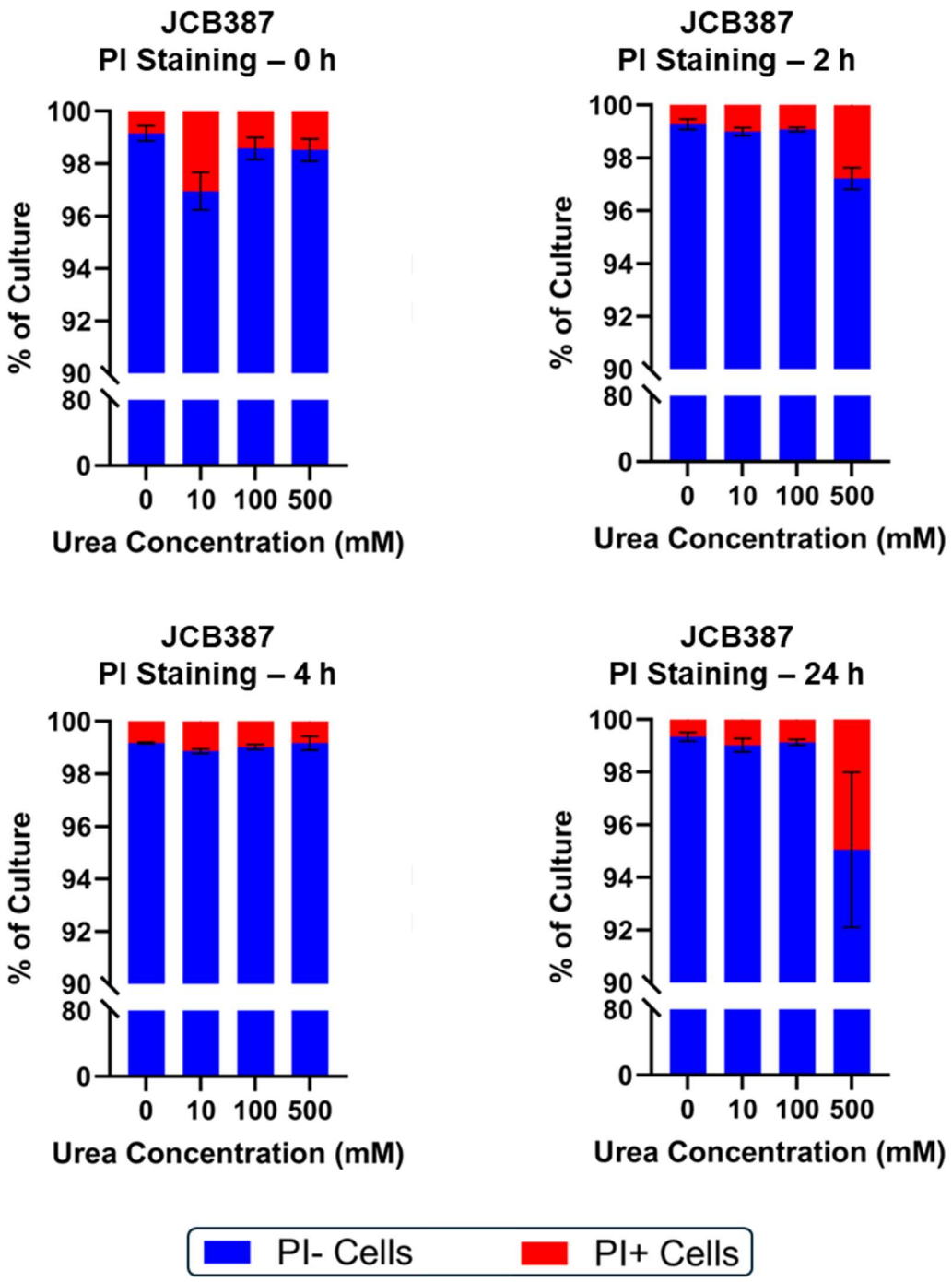


Figure 3.3: JCB387 was stained with PI to monitor cell viability.

To determine the effect of urea on host cells, untransformed JCB387 was grown under RPP-like conditions in 50 mL LB at 37 °C, 200 rpm. At OD_{600} 0.4-0.5, 0 – 500 mM urea was added to cultures. As a measure of viability, cells were stained with 4 µg mL^{-1} PI for 5 min and analysed via FCM. Cells were gated based on red fluorescence to calculate the proportion of cells that were PI- (indicative of viable cells) or PI+ (indicative of non-viable cells). Data is shown for 0 h, 2 h, 4 h and 24 h post-induction. Error bars represent +/- SD from biological triplicates.

Proportion of PI+ cells within JCB387 cultures was low throughout, indicating the majority were viable. Even after addition of 500 mM urea, the proportion of PI- cells did not drop below 95 %.

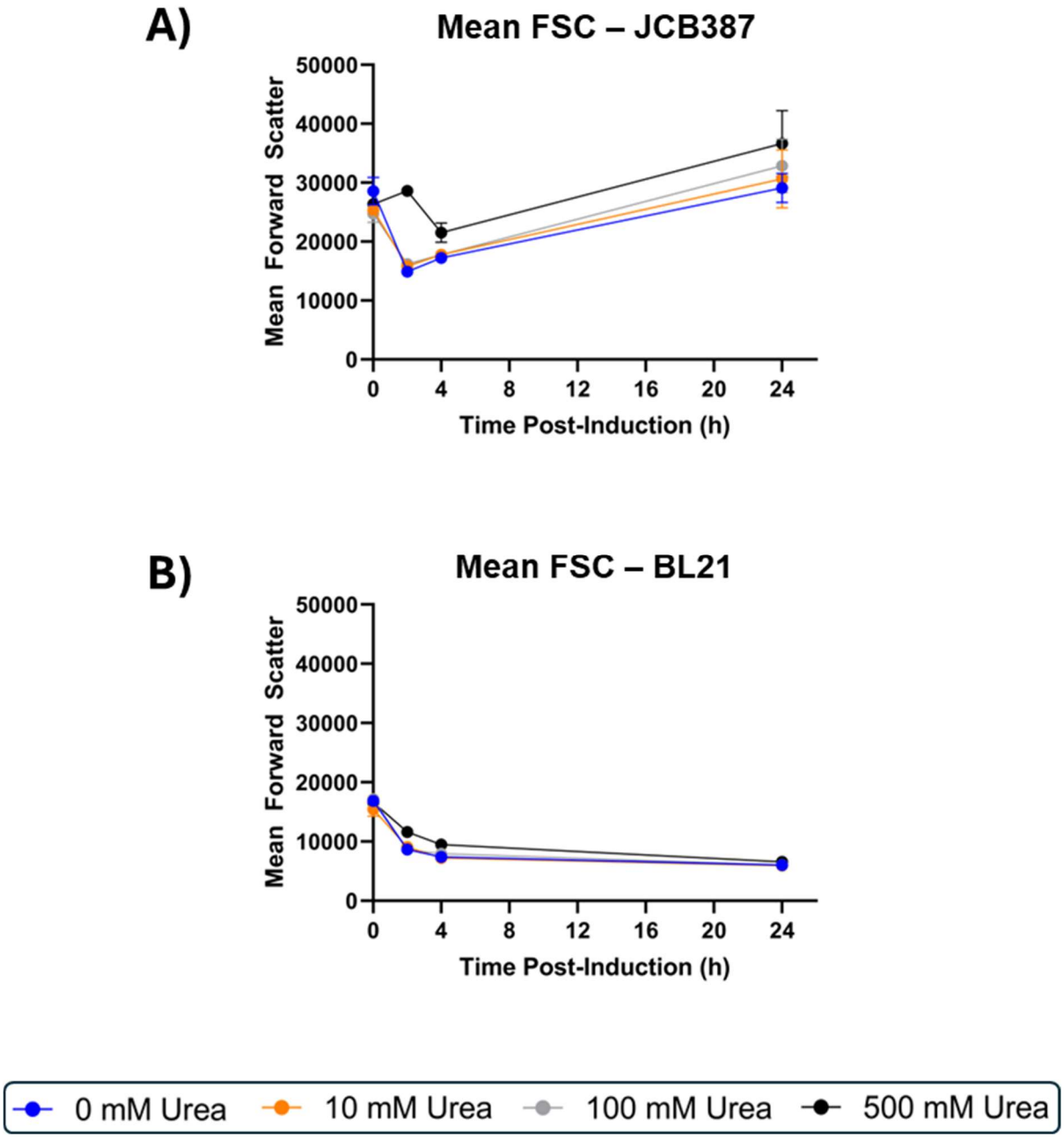


Figure 3.4: Mean FSC data of untransformed *E. coli* JCB387 and BL21 treated with varying concentrations of urea.

To determine the effect of urea on host cells, untransformed variants of JCB387 and BL21 were grown under RPP-like conditions in 50 mL LB at 37 °C, 200 rpm. At OD_{600} 0.4-0.5, 0 – 500 mM urea was added to cultures. FCM was used to monitor FSC and detect potential changes in cell size arising from treatment with urea, with FSC values shown representing the mean from replicate cultures. Data provided is from separate experiments for JCB387 and BL21. Error bars represent +/- SD from biological triplicates.

In untransformed JCB387 **(A)** and BL21 **(B)**, mean forward scatter negatively correlated with the concentration of urea added. Untransformed JCB387 treated with 500 mM urea increased in forward scatter between induction and 2 h post-induction but dropped by 4 h post-induction to levels comparable to cultures induced with 0 mM – 100 mM. Little difference in forward scatter was apparent in untransformed BL21 treated with 0 mM – 500 mM urea.

decreasing to approximately 15000 AU from 25000 AU. Comparatively, in untransformed JCB387 cultures treated with 500 mM urea, mean FSC increased slightly at 2 h by approximately 2000 AU, a 2-fold increase over the untreated 0 mM urea control. Mean FSC of untransformed JCB387 cultures treated with 500 mM urea was higher than the untreated control at 2 h – 24 h post-induction; when analysed by ANOVA this difference was significantly (adjusted $p < 0.025$ for all comparisons), suggesting treatment with 500 mM urea increased cell size. Mean FSC changed little in untransformed BL21 (Figure 3.4B); cultures treated with 0 mM – 100 mM were indistinguishable throughout all 24 h. Untransformed BL21 treated with 500 mM urea had slightly elevated mean FSC at 2 h and 4 h; this was still significant at both time-points compared with the untreated 0 mM control when analysed by ANOVA (adjusted $p < 0.0001$ for both comparisons). In single cells, FSC of untransformed JCB387 was comparable in cultures treated with 0 mM – 100 mM urea at all time-points (Figure 3.5A). Treatment of untransformed JCB387 with 500 mM urea increased forward scatter at all time-points, but cultures were mostly a single population. In untransformed BL21 (Figure 3.5B), there was little difference between cultures treated with 0 mM – 500 mM urea, only a small increase in forward scatter present at 2 h and 4 h post-induction in cultures treated with 500 mM urea. In all conditions, untransformed BL21 remained a single population. Raw data for histograms is provided in Chapter 8 – Appendix, Table 8.1 (untransformed JCB387) and Table 8.2 (untransformed BL21). It was notable that BL21 cultures appeared to have far lower heterogeneity in FSC following addition of urea than for JCB387 cultures. For example, at 2 h post-induction mean CV of peaks were around 44 % in JCB387 (Table 8.1), but around 23% in BL21 (Table 8.2).

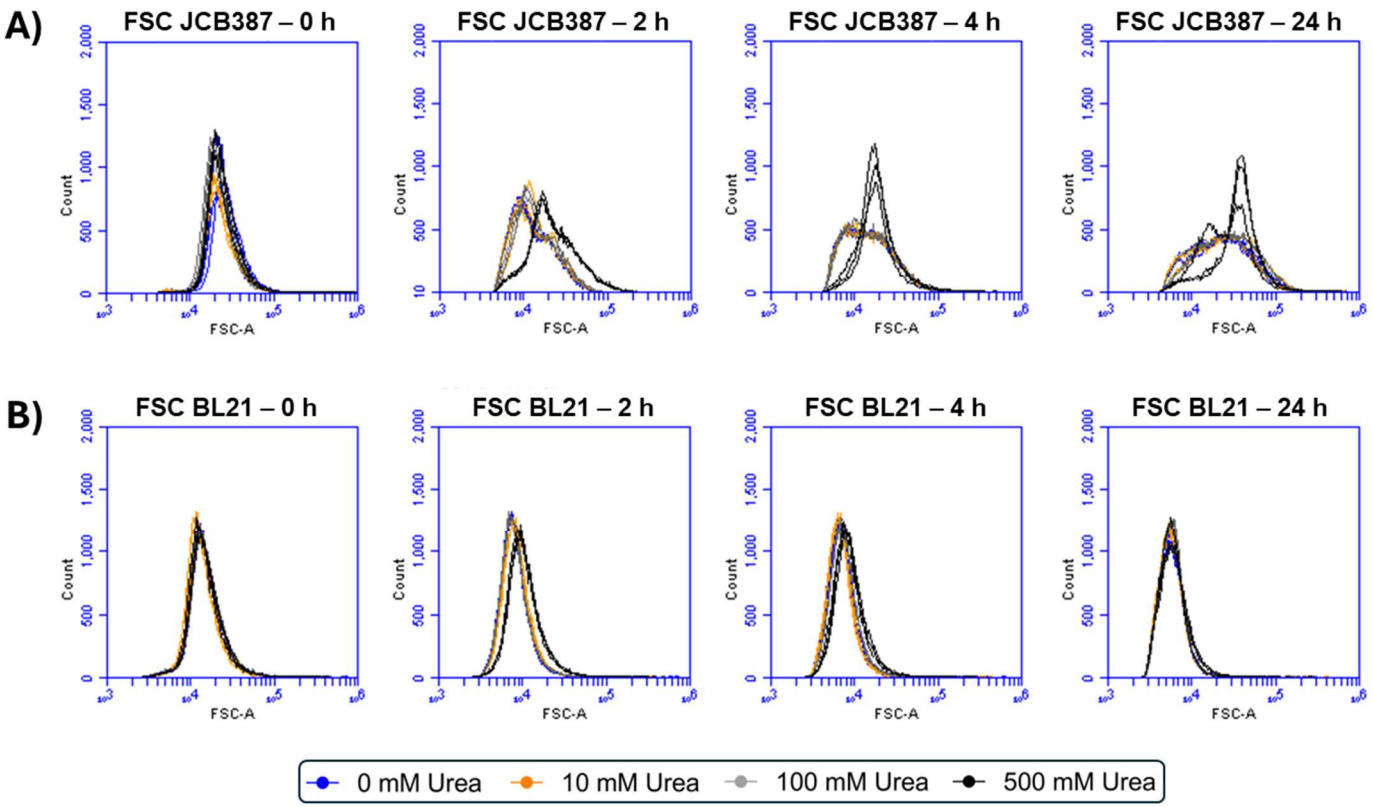


Figure 3.5: Forward scatter (FSC) data at the single cell level for untransformed *E. coli* JCB387 and BL21 treated with varying concentrations of urea.

To determine the effect of urea on host cells, untransformed variants of JCB387 and BL21 were grown under RPP-like conditions in 50 mL LB at 37 °C, 200 rpm. At OD_{600} 0.4-0.5, 0 – 500 mM urea was added to cultures. FCM was used to monitor FSC and detect potential changes in cell size arising from treatment with urea, FSC-A values shown are for individual cultures. Data provided is from separate experiments for JCB387 and BL21. Each condition shown is in biological triplicates.

(A) Forward scatter (FSC-A) of untransformed JCB387 was comparable in cultures treated with 0 mM – 100 mM urea; at 500 mM, forward scatter was elevated at all time-points, but the cultures were mostly a single population.

(B) Forward scatter (FSC-A) of untransformed BL21 showed little difference between cultures treated with 0 mM – 500 mM urea; a small increase in forward scatter was present at 2 h and 4 h post-induction in cultures treated with 500 mM urea. Under all conditions, untransformed BL21 remained a single population with less heterogeneity than JCB387.

3.2.2 Transformed and untransformed cells response to urea

It was clear that treatment of untransformed cells with 500 mM urea, particularly JCB387, had some effect on biomass accumulation (Figure 3.2A) and based on FSC analysis using FCM, potentially increased cell size (Figure 3.4). Some stress arising from treatment with 500 mM urea was not unexpected. Being chaotropic, urea denatures proteins and destabilises the membrane or nucleic acids (Bennion and Daggett, 2003, Lambert and Draper, 2012); high solute concentrations also create osmotic stress for the cell (Record Jr et al., 1998). Increased cell size in untransformed cells following treatment with 500 mM urea could have been filamentation arising from stress; DNA damage can instigate such changes in morphology (Justice et al., 2008). Filamentation is also known to occur in cells undergoing high level overexpression of a recombinant protein (Jeong and Lee, 2003). Hence, we wanted to directly compare JCB387 and BL21 physiology, with and without 6xHis::GFP expression from the urea inducible P_{uti101} promoter. Cultures of JCB387 and BL21, with and without the pET15b-P_{uti101}-*6xhis::gfp* construct were aerated in Erlenmeyer flasks at 37 °C, 200 rpm. Untransformed cells were grown in 50 mL LB (Lennox); transformed cells were grown in 50 mL LB (Lennox) + Amp. At OD_{600} 0.4-0.6, 500 mM urea was added to flasks in duplicate, with growth proceeding for a further 24 h.

Based on OD_{600}, there was little difference in biomass accumulation between transformed JCB387 overexpressing 6xHis::GFP from P_{uti101} and untransformed JCB387 (Figure 3.6A). Comparatively, cultures of transformed BL21 overexpressing 6xHis::GFP from P_{uti101} had a higher OD_{600} than untransformed variants (Figure 3.6A). Cell density (cells mL^{-1}) was monitored via FCM (Figure 3.6B) and appeared to show

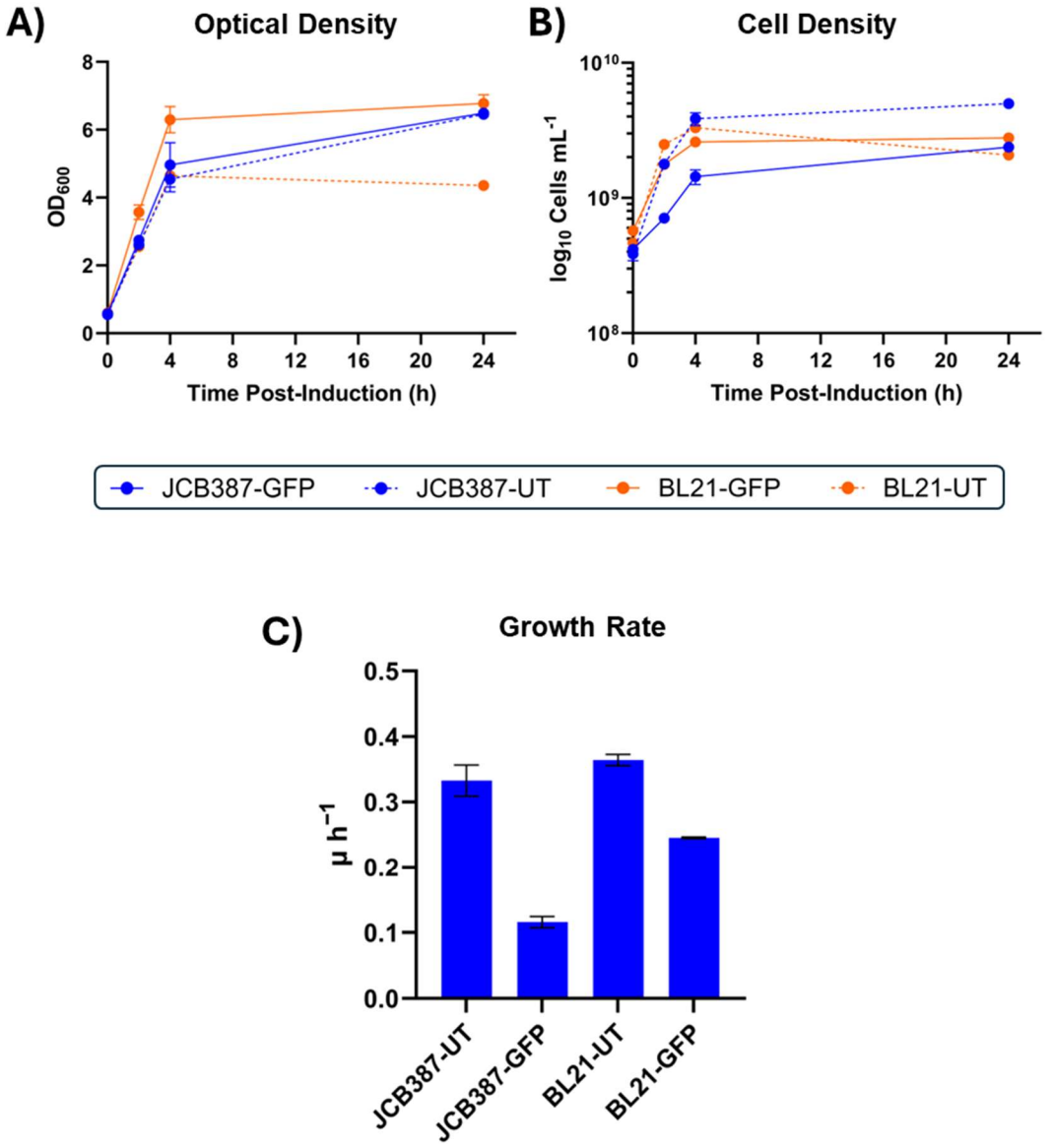


Figure 3.6: Growth data of untransformed and transformed *E. coli* JCB387 and BL21 treated with 500 mM urea.

To further determine the effect of high urea concentrations on host cells, untransformed JCB387 and BL21 (UT) were compared with transformed JCB387 and BL21 (GFP) harbouring the urea inducible promoter construct pET15b-P*uti101*-*6xhis::gfp*. Untransformed strains were grown in 50 mL LB, transformed strains were grown in LB + Amp. Cultures were incubated at 37 °C, 200 rpm. At OD_{600} 0.4-0.5, 500 mM urea was added to cultures. Error bars represent +/- SD from biological triplicates.

(A) OD_{600} was monitored throughout and there was little difference in OD_{600} between untransformed (UT) and transformed (GFP) JCB387 induced with 500 mM urea; interestingly, transformed BL21 (GFP) induced with 500 mM urea had far higher OD_{600} than untransformed (UT) cells.

(B) Cell density (cells mL^{-1}) of cultures was measured using FCM. While transformed (GFP) JCB387 had a similar OD_{600} to untransformed (UT) cells, cell density was far lower at all time-points following addition of 500 mM urea. Conversely, untransformed (UT) and transformed (GFP) BL21 had similar cell densities throughout.

(C) Specific growth rate (μ h^{-1}) was calculated from cell density. In both JCB387 and BL21, growth rate was predictably lower in transformed (GFP) cultures and BL21 cultures appeared to grow quicker than JCB387 variants.

the reverse of what was observed for OD_{600} (Figure 3.6A). This was that cell density in transformed JCB387 cultures was lower than in untransformed JCB387 cultures; conversely, cell density in transformed and untransformed BL21 was similar (Figure 3.6B). However, by 4 h post-induction, all cultures had reached over 10^9 cells mL^{-1}. Cell density was used to calculate specific growth rates (μ h^{-1}); predictably, growth rates were lower in transformed JCB387 and BL21 overexpressing 6xHis::GFP (Figure 3.6C). We wondered whether disparity between what was observed for OD_{600} (Figure 3.6A) and cell density (Figure 3.6B) was due to 6xHis::GFP expression and any effect that had on cell size. To confirm transformed JCB387 and BL21 were overexpressing 6xHis::GFP from P_{uti101}, mean green fluorescence of cultures was monitored using FCM. Predictably, mean green fluorescence of untransformed JCB387 and BL21 was low, at around 200 AU throughout growth (Figure 3.7A). Comparatively, transformed cultures of JCB387 and BL21 reached a maximum mean green fluorescence of 50000 AU and 35000 AU respectively at 24 h post-induction (Figure 3.7A).

Mean FSC was then measured using FCM and was higher in JCB387 and BL21 cultures overexpressing 6xHis::GFP from 2 h to 24 h post-induction (Figure 3.7B). By 4 h post-induction mean FSC in transformed JCB387 cultures had increased to 33000 AU and dropped to 18000 AU in untransformed variants (Figure 3.7B). Similarly, mean FSC of transformed BL21 cultures was 31000 AU at 4 h post-induction, a 3-fold increase over untransformed BL21 cultures (Figure 3.7B). Differences in mean FSC of transformed and untransformed cultures was significant, between 2 h and 24 h post-induction, when analysed using multiple t-tests (adjusted $p < 0.05$ for all comparisons in JCB387; adjusted $p < 0.0006$ for all comparisons in BL21). FSC analysed at the

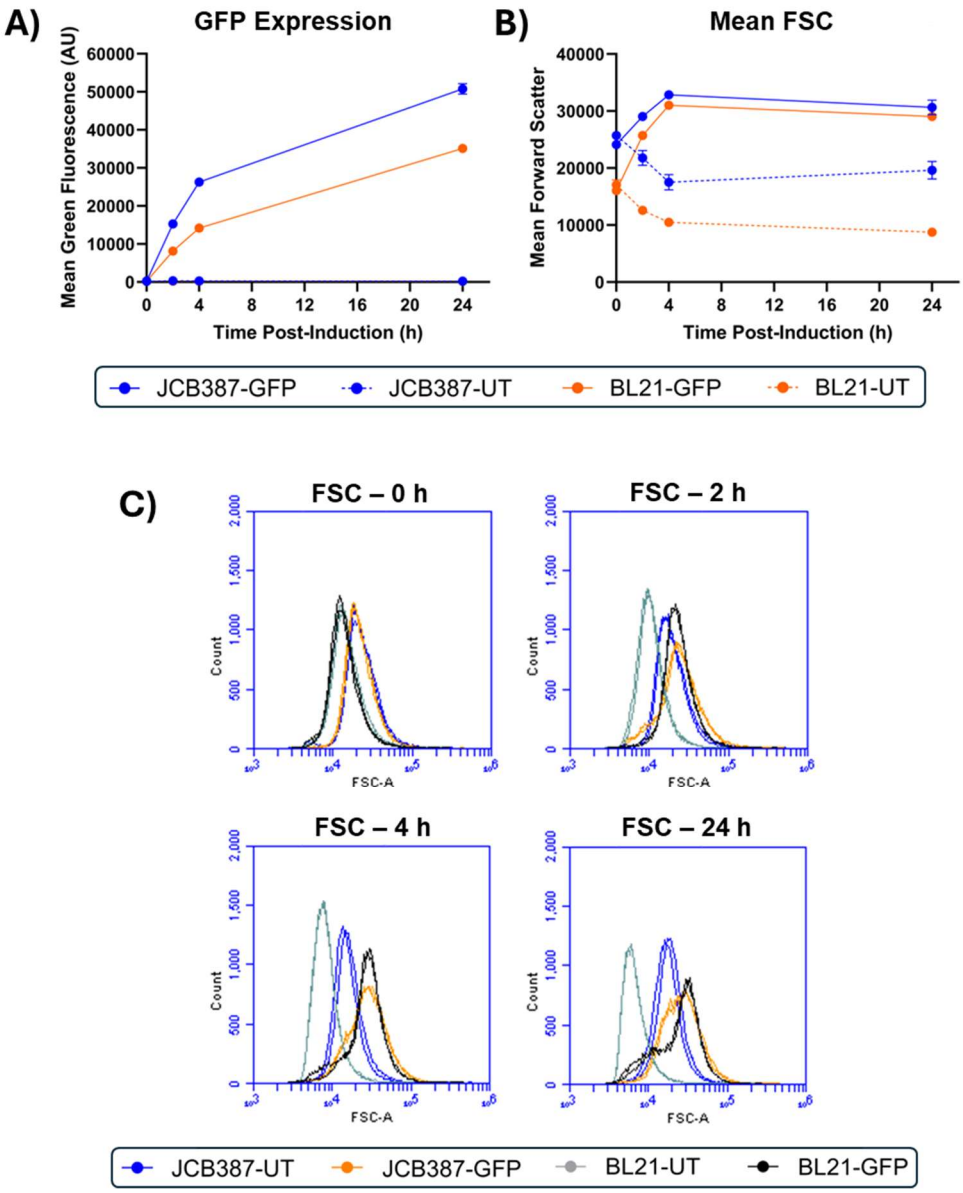


Figure 3.7: 6xHis::GFP overexpression in combination with 500 mM urea increased FSC in *E. coli* JCB387 and BL21.

To further determine the effect of high urea concentrations on host cells, untransformed JCB387 and BL21 (UT) were compared with transformed JCB387 and BL21 (GFP) harbouring the urea inducible promoter construct pET15b-P$_{uti101}$-*6xhis::gfp*. Untransformed strains were grown in 50 mL LB, transformed strains were grown in LB + Amp. Cultures were incubated at 37 °C, 200 rpm. At OD_{600} 0.4-0.5, 500 mM urea was added to cultures. Error bars represent +/- SD from biological triplicates.

(A) Mean green fluorescence of cultures was monitored via FCM. Predictably, mean green fluorescence was low in untransformed (UT) cells due to lacking the expression construct. Interestingly, transformed (GFP) JCB387 had higher mean green fluorescence than transformed BL21 at all time-points following induction with 500 mM urea.

(B) Mean FSC from each culture was measured via FCM. In both JCB387 and BL21, mean forward scatter correlated with the presence of the pET15b-P$_{uti101}$-*6xhis::gfp* and thus overexpression of 6xHis::GFP.

(C) FSC was monitored at the single cell level using FCM, data is shown duplicate cultures for each strain. FSC of untransformed (UT) JCB387 and BL21 was homogenous at all time points. Transformed (GFP) JCB387 and BL21 appeared to have greater heterogeneity at 4 h and 24 h, with populations of higher and lower FSC present.

single cell level using FCM indicated greater heterogeneity in transformed JCB387 and BL21 overexpressing 6xHis::GFP from P_{uti101}; particularly at 4 h (JCB387 mean CV = 39.29 %) and 24 h post-induction (JCB387 mean CV = 39.24%) where there appeared to be populations with lower and higher FSC (Figure. 3.7C). Raw data for histograms is provided in Chapter 8 – Appendix, Table 8.3. Untransformed JCB387 and BL21 cultures displayed single populations regarding FSC at all time points (Figure 3.7C).

As FSC and thus likely cell size appeared correlated with 6xHis::GFP expression, we concluded the previous disparity between OD_{600} and cell density data (Figure 3.6), was because of the effect larger cells would have on scattering light during optical density measurements. To confirm this, cultures were also analysed by fluorescence (transformed cells) or brightfield (untransformed cells) microscopy at each time point following induction and cell length calculated using ImageJ (Figures 3.8 – 3.13). For both JCB387 and BL21, cells expressing 6xHis::GFP appeared much larger and filamented; untransformed cells were generally smaller, around 1 – 2 µm. Regardless of the presence of pET-15b-P_{uti101}-*6xhis::gfp*, JCB387 was generally larger than BL21 (Figure 3.8 – 3.13), supporting mean FSC data (Figure 3.7B). Heterogeneity was noted at 4 h and 24 h post-induction for transformed JCB387 and BL21, with lower and higher FSC populations (Figure 3.7C); this was apparent during microscopy, with some cells around 2 – 3 µm with others as large as 5 – 9 µm. Such heterogeneity was not unexpected in cells overexpressing 6xHis::GFP; during RPP host cells are subjected to various stressors (section 1.4.2), in addition to effects high concentrations of solute like urea (500 mM) may cause (Record Jr et al., 1998, Jeong and Lee, 2003, Justice et al., 2008).

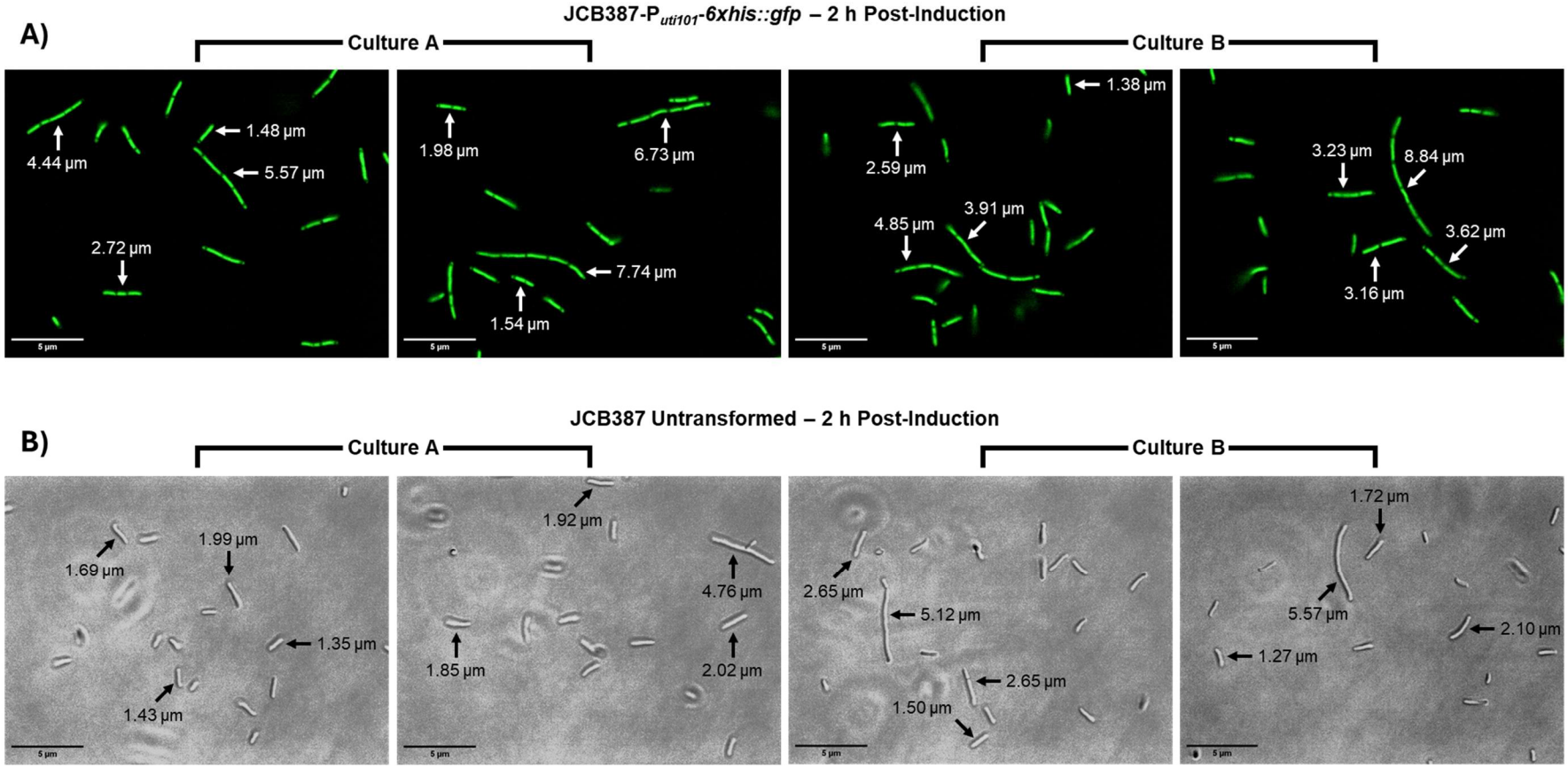


Figure 3.8: Microscopy analysis of JCB387 at 2 h post-induction with 500 mM urea was used to further determine the effect of high urea concentrations on host cells.

Untransformed strains were grown in 50 mL LB, transformed strains harbouring the urea inducible promoter construct pET15b-P$_{uti101}$-*6xhis::gfp* were grown in LB + Amp. Cultures were incubated at 37 °C, 200 rpm. At OD_{600} 0.4-0.5, 500 mM urea was added to cultures. At 2 h post-induction, cells were imaged using fluorescence microscopy for transformed cultures and brightfield microscopy for untransformed cultures. Cell length (µm) was calculated using ImageJ. For each strain, two images are shown for biological duplicates.

Transformed JCB387 **(A)** generally appeared larger than untransformed variants **(B)**. Most transformed JCB387 appeared filamented, some reaching almost 9 µm in length.

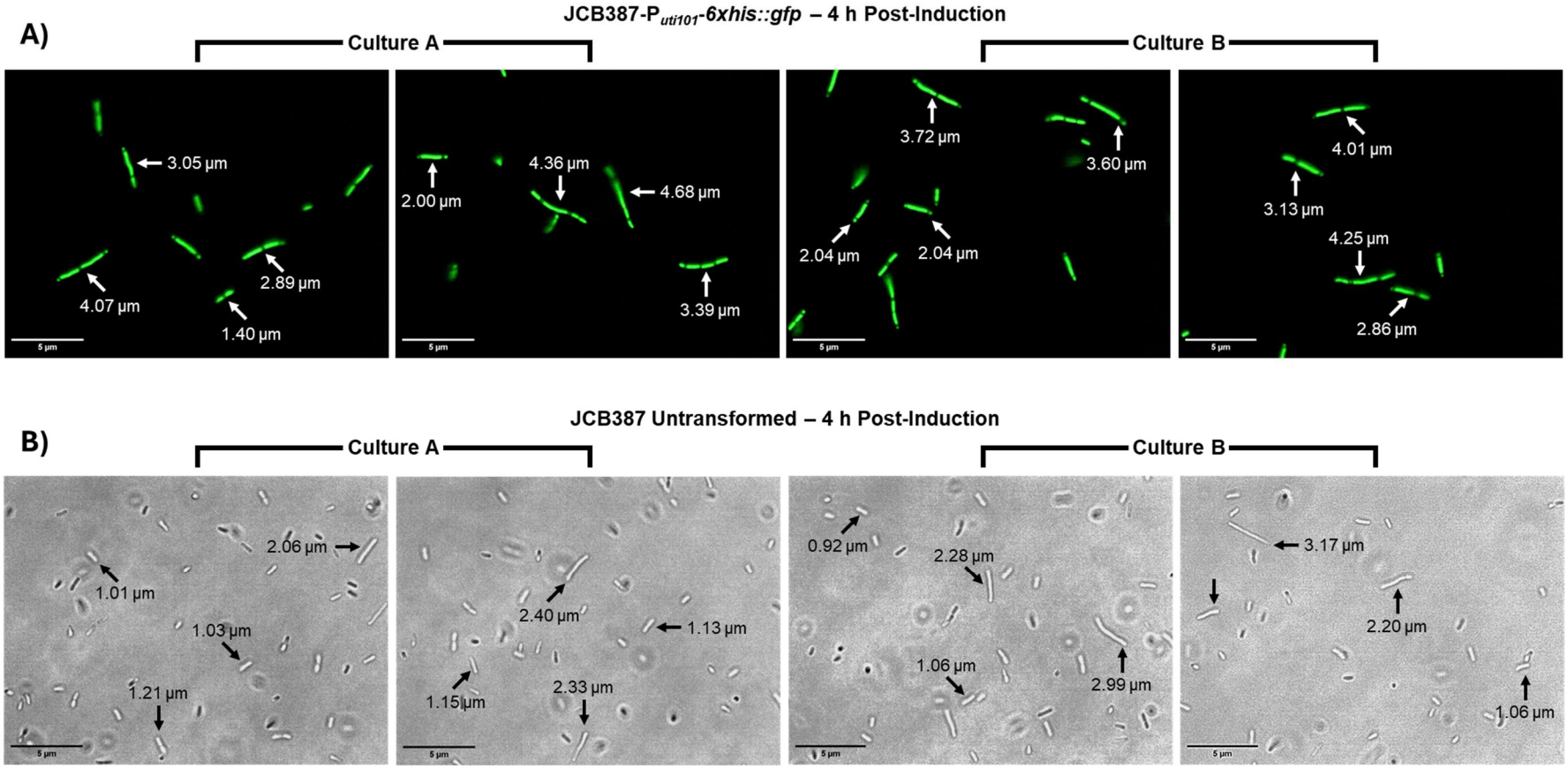


Figure 3.9: Microscopy analysis of JCB387 at 4 h post-induction with 500 mM urea was used to further determine the effect of high urea concentrations on host cells.

Untransformed strains were grown in 50 mL LB, transformed strains harbouring the urea inducible promoter construct pET15b-P$_{uti101}$-*6xhis::gfp* were grown in LB + Amp. Cultures were incubated at 37 °C, 200 rpm. At OD_{600} 0.4-0.5, 500 mM urea was added to cultures. At 4 h post-induction, cells were imaged using fluorescence microscopy for transformed cultures and brightfield microscopy for untransformed cultures. Cell length (µm) was calculated using ImageJ. For each strain, two images are shown for biological duplicates.

Transformed JCB387 **(A)** generally appeared larger than untransformed variants **(B)**. Most transformed JCB387 appeared filamented, some near 5 µm in length.

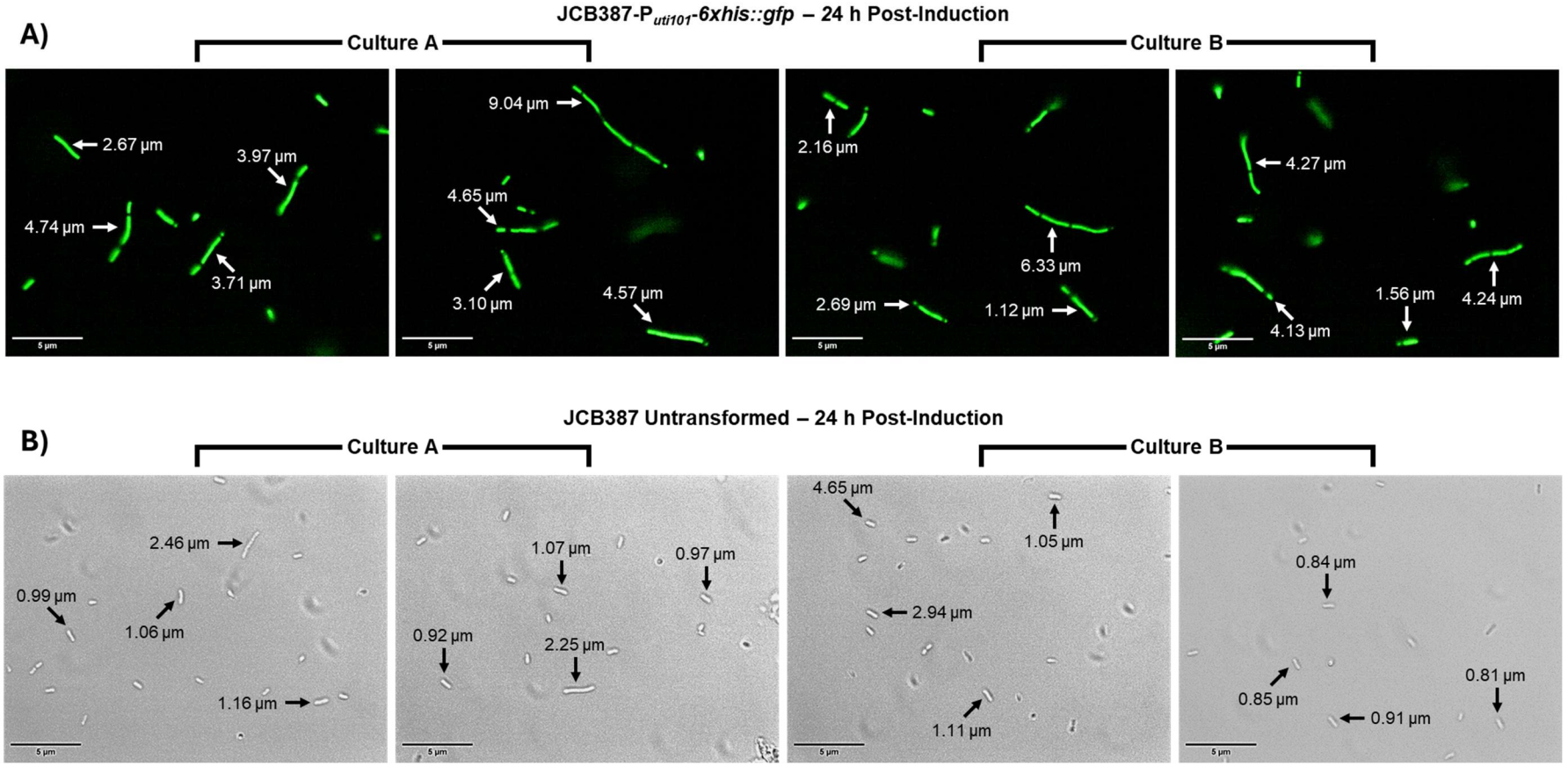


Figure 3.10: Microscopy analysis of JCB387 at 24 h post-induction with 500 mM urea was used to further determine the effect of high urea concentrations on host cells.

Untransformed strains were grown in 50 mL LB, transformed strains harbouring the urea inducible promoter construct pET15b-P$_{uti101}$-*6xhis::gfp* were grown in LB + Amp. Cultures were incubated at 37 °C, 200 rpm. At OD_{600} 0.4-0.5, 500 mM urea was added to cultures. At 24 h post-induction, cells were imaged using fluorescence microscopy for transformed cultures and brightfield microscopy for untransformed cultures. Cell length (µm) was calculated using ImageJ. For each strain, two images are shown for biological duplicates.

Transformed JCB387 **(A)** generally appeared larger than untransformed variants **(B)**. Most transformed JCB387 appeared filamented, some over 9 µm in length.

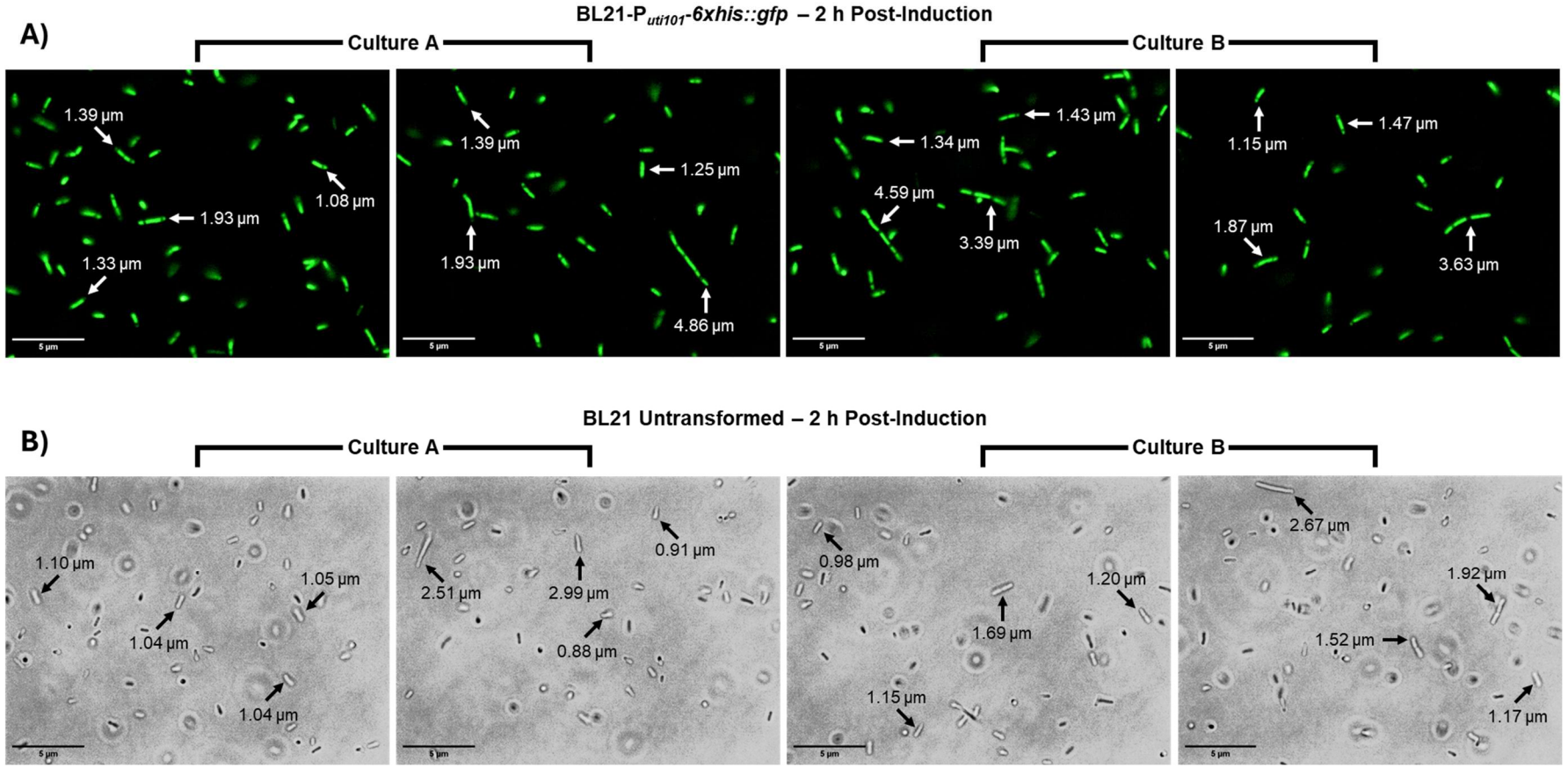


Figure 3.11: Microscopy analysis of BL21 at 2 h post-induction with 500 mM urea was used to further determine the effect of high urea concentrations on host cells.

Untransformed strains were grown in 50 mL LB, transformed strains harbouring the urea inducible promoter construct pET15b-P$_{uti101}$-*6xhis::gfp* were grown in LB + Amp. Cultures were incubated at 37 °C, 200 rpm. At OD_{600} 0.4-0.5, 500 mM urea was added to cultures. At 2 h post-induction, cells were imaged using fluorescence microscopy for transformed cultures and brightfield microscopy for untransformed cultures. Cell length (µm) was calculated using ImageJ. For each strain, two images are shown for biological duplicates.

Transformed BL21 **(A)** generally appeared larger than untransformed variants **(B)**. Most transformed BL21 appeared filamented, some just under 5 µm in length.

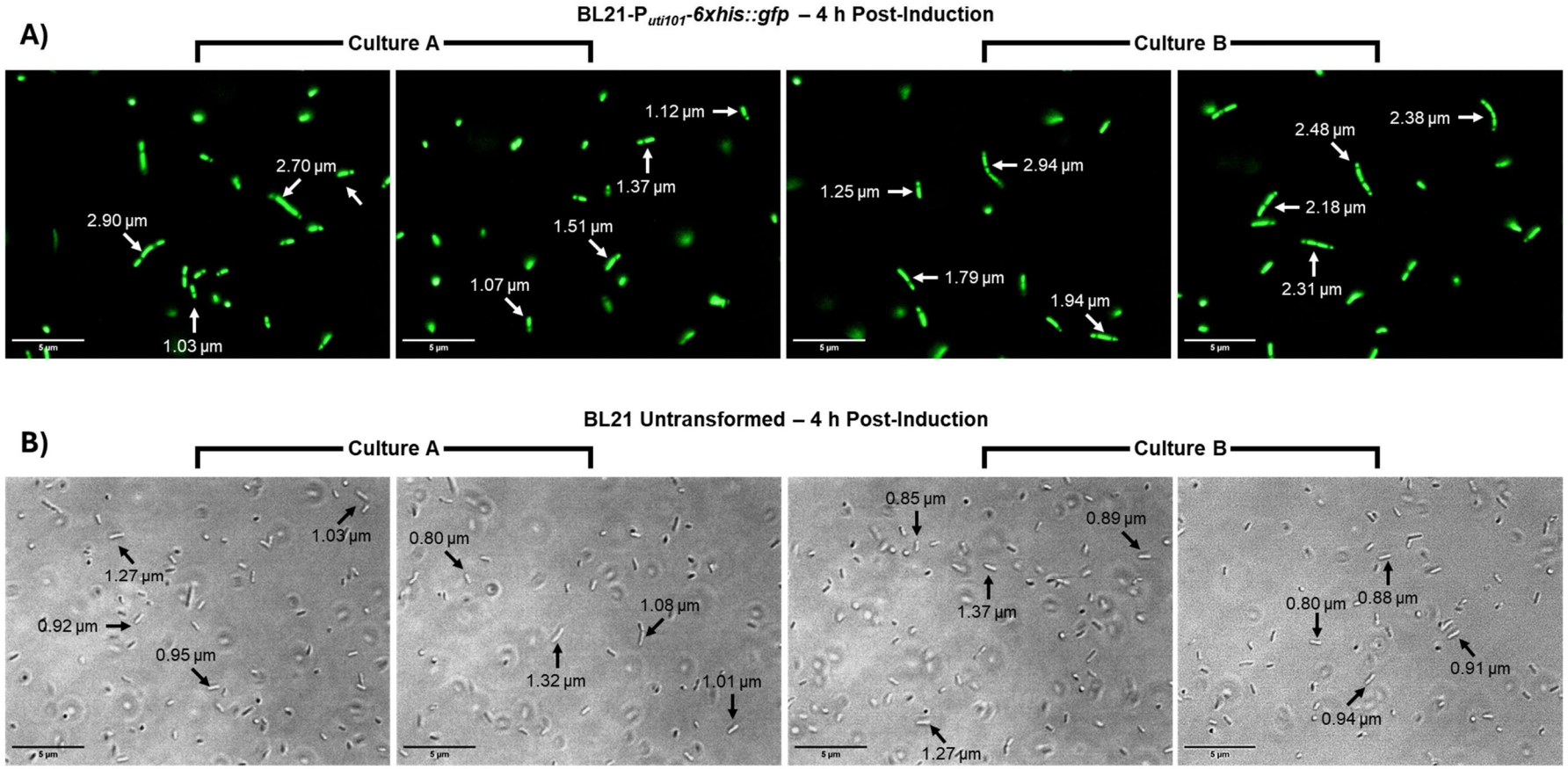


Figure 3.12: Microscopy analysis of BL21 at 4 h post-induction with 500 mM urea was used to further determine the effect of high urea concentrations on host cells.

Untransformed strains were grown in 50 mL LB, transformed strains harbouring the urea inducible promoter construct pET15b-P$_{uti101}$-*6xhis::gfp* were grown in LB + Amp. Cultures were incubated at 37 °C, 200 rpm. At OD_{600} 0.4-0.5, 500 mM urea was added to cultures. At 4 h post-induction, cells were imaged using fluorescence microscopy for transformed cultures and brightfield microscopy for untransformed cultures. Cell length (µm) was calculated using ImageJ. For each strain, two images are shown for biological duplicates.

Transformed BL21 **(A)** generally appeared larger than untransformed variants **(B)**. Many transformed BL21 still appeared filamented.

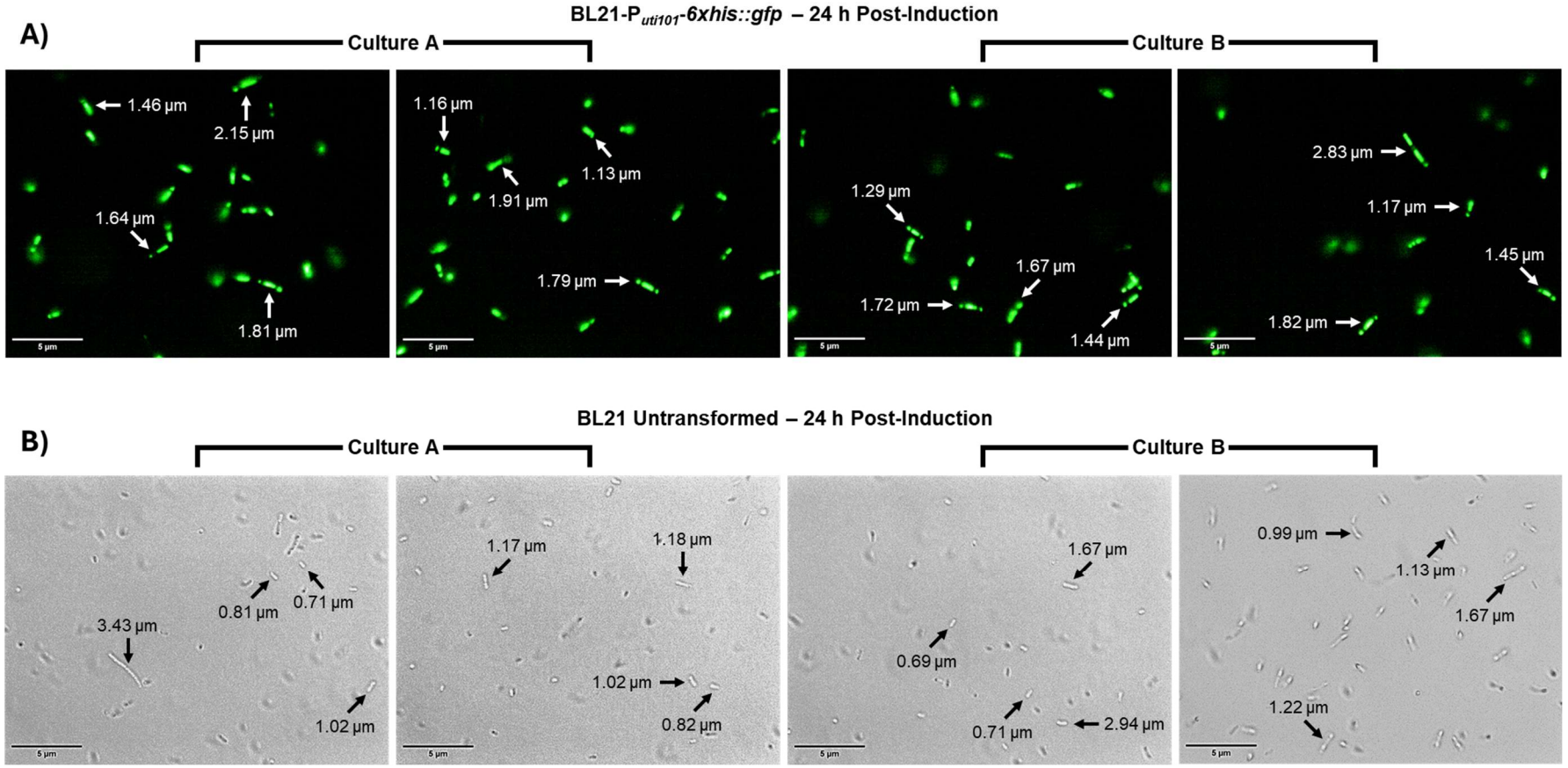


Figure 3.13: Microscopy analysis of BL21 at 24 h post-induction with 500 mM urea was used to further determine the effect of high urea concentrations on host cells.

Untransformed strains were grown in 50 mL LB, transformed strains harbouring the urea inducible promoter construct pET15b-P$_{uti101}$-*6xhis::gfp* were grown in LB + Amp. Cultures were incubated at 37 °C, 200 rpm. At OD_{600} 0.4-0.5, 500 mM urea was added to cultures. At 24 h post-induction, cells were imaged using fluorescence microscopy for transformed cultures and brightfield microscopy for untransformed cultures. Cell length (µm) was calculated using ImageJ. For each strain, two images are shown for biological duplicates.

Transformed BL21 **(A)** generally appeared larger than untransformed variants **(B)**. Some transformed BL21 still appeared filamented.

Through studying the effect of urea on untransformed JCB387 and BL21, we identified that up to 100 mM urea resulted in minimal effects to biomass accumulation (Figure 3.2A), growth rate (Figure 3.2B), JCB387 viability based on PI staining (Figure 3.3) and cell size based on FSC measurements (Figure 3.4). At higher urea concentrations (500 mM), there was some decrease in JCB387 biomass accumulation and growth rate (Figure 3.2), but cell viability appeared to be high (Figure 3.3). We also noted that untransformed JCB387 and BL21 appeared to have higher FSC when treated with 500 mM urea (Figure 3.4) but found that increases in FSC correlated more with overexpression of 6xHis::GFP than the effect of urea, when comparing untransformed and transformed cells (Figure 3.7). JCB387 and BL21 overexpressing 6xHis::GFP were subsequently shown to be larger and filamented than untransformed variants (Figure 3.8 – 3.13). Given this, we were confident that urea, particularly concentrations of 100 mM or less, were well tolerated by JCB387 and BL21.

3.3 Small-scale expression

Following the analysis on the effect of urea on JCB387 and BL21 (section 3.2), we wanted to look at P_{uti101} promoter performance in driving expression of 6xHis::GFP, beginning at small scale. Our main questions were how strong the P_{uti101} promoter was, what was its inducible range, whether it was dose dependent and if basal expression was low in the absence of urea.

3.3.1 Inducible range of P_{uti101} in JCB387

As a continuation of work done by the Browning lab (Aston University) using JCB387, we first assessed the expression characteristics of the P_{uti101} promoter in this strain. JCB387 containing pET-15b-P_{uti101}-*6xhis*::*gfp* was aerated at 37 °C, 200 rpm in 50 mL LB (Lennox) + Amp in Erlenmeyer flasks. In two separate experiments, 6xHis::GFP expression from P_{uti101} was induced at OD_{600} 0.4-0.6, using low (0 mM – 10 mM), or high (50 – 500 mM) concentrations of urea. Induction with each concentration of urea was repeated in triplicate flasks. Overexpression proceeded until 24 h post-induction.

In section 3.2, we had observed that up to 100 mM urea appeared to have little effect on biomass accumulation and growth rates in untransformed JCB387 (Figure 3.2). We wondered if this would change in transformed cells which were also overexpressing 6xHis::GFP. Hence, biomass accumulation was monitored by OD_{600} (Figure 3.14). In experiment 1, little difference was observed between cultures induced with lower (0 mM – 10 mM) urea concentrations (Figure 3.14A). Specific growth rates were calculated using OD_{600} and were similar for all cultures in experiment 1, indicating up to 10 mM urea did not affect JCB387 growth (Figure 3.14A).

In experiment 2 (Figure 3.14B), at higher (50 mM – 500 mM) urea concentrations, OD_{600} appeared to negatively correlate with the concentration of urea used. OD_{600} was lower in

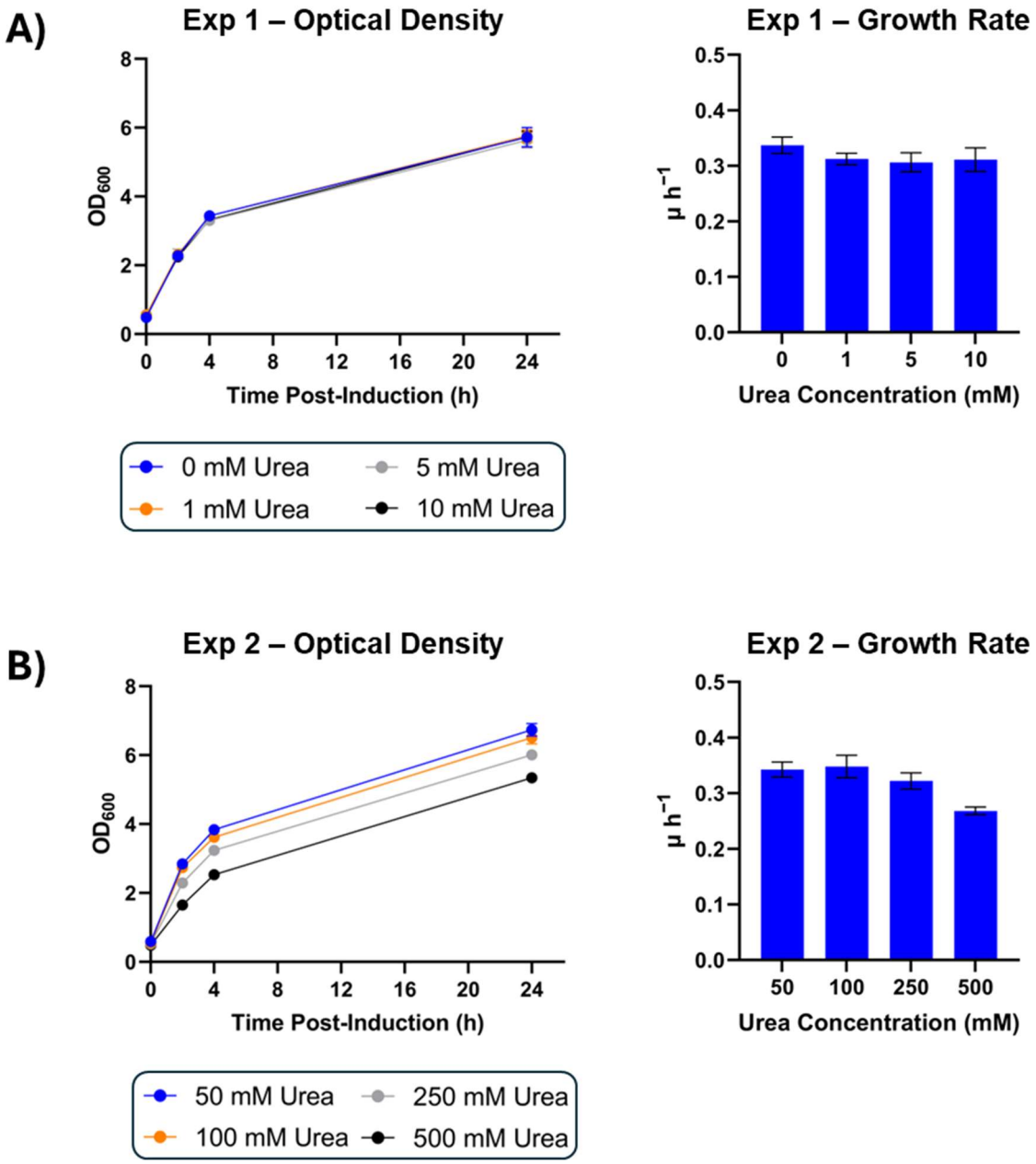


Figure 3.14: Growth data of JCB387 harbouring the pET15b-P_{uti101}-*6xhis::gfp* construct, with 6xHis::GFP expression from P_{uti101} induced with varying concentrations of urea.

JCB387 was cultured in 50 mL LB + Amp and incubated at 37 °C, 200 rpm. At OD_{600} 0.4-0.6, 6xHis::GFP expression was induced by adding urea to cultures in triplicate for each concentration. Data is shown for two separate experiments (Exp 1 and Exp 2). XY plots show optical density, error bars represent +/- SD from biological triplicates. Bar charts specific growth rate (μ h^{-1}), error bars represent +/- SD from biological triplicates.

(A) Exp 1 – OD_{600} was monitored to observe the effect of inducing 6xHis::GFP expression with low concentrations of urea. Biomass accumulation across all conditions was similar; specific growth rate was calculated from OD_{600} and predictably there was little difference.

(B) Exp 2 – OD_{600} was monitored to observe the effect of inducing 6xHis::GFP expression with high concentrations of urea. Biomass accumulation correlated with the concentration of urea used for induction. Specific growth rate was calculated from OD_{600} and was significantly lower for cultures induced with 500 mM urea when analysed by one-way ANOVA (adjusted $p < 0.009$ for all comparisons).

cultures induced with 250 mM – 500 mM urea (Figure 3.14B). Specific growth rates (Figure 3.14B) calculated using OD_{600} indicated that cultures induced with 500 mM urea were significantly lower than in cultures induced with 50 – 250 mM urea when analysed by one-way ANOVA (adjusted $p < 0.009$ for all comparisons). Effects on growth were expected when inducing transformed JCB387 with 500 mM urea, given what was observed for untransformed JCB387 using the same concentration of urea (Figure 3.2). Given the effects to growth for cultures induced with 500 mM urea in experiment 2 (Figure 3.14B), membrane integrity as a measure of viability was only checked in experiment 2 by staining cells with PI. Even in cultures induced with 500 mM urea, there were less than 1 % PI+ cells at all time points after induction (Figure 3.15). We concluded that induction of 6xHis::GFP from P_{uti101} using up to 100 mM urea was well tolerated by the JCB387, and that while 250 mM – 500 mM urea affected growth (Figure 3.14), cells were likely still viable based on PI staining (Figure 3.15).

In section 3.2, higher concentrations of urea were shown to increase JCB387 size as measured by FSC, more so during overexpression of 6xHis::GFP (Figure 3.7B). While we had established impacts on growth were minimal at urea concentrations under 100 mM (Figures 3.14 and 3.15), it was still possible cells were being stressed and so FSC was monitored using FCM. In experiment 1, inducing with low concentrations (0 mM – 10 mM) of urea had little effect on FSC compared with the 0 mM control cultures (Figure 3.16, top panel). At the single cell level, even uninduced cultures displayed two FSC peaks (Figure 3.16, top panel); although overall there was little difference in FSC profiles for cultures induced with 0 mM to 10 mM urea (raw data for histograms is provided in Chapter 8 – Appendix, Table 8.4).

For experiment 2, inducing 6xHis::GFP with 50 mM – 100 mM urea, FSC correlated with the concentration of urea used (Figure 3.16, bottom panel). The largest difference in FSC between cultures induced with 50 mM – 500 mM urea was at 2 h post-induction (Figure 3.16, bottom panel); this correlation between FSC and urea concentration was significant when analysed

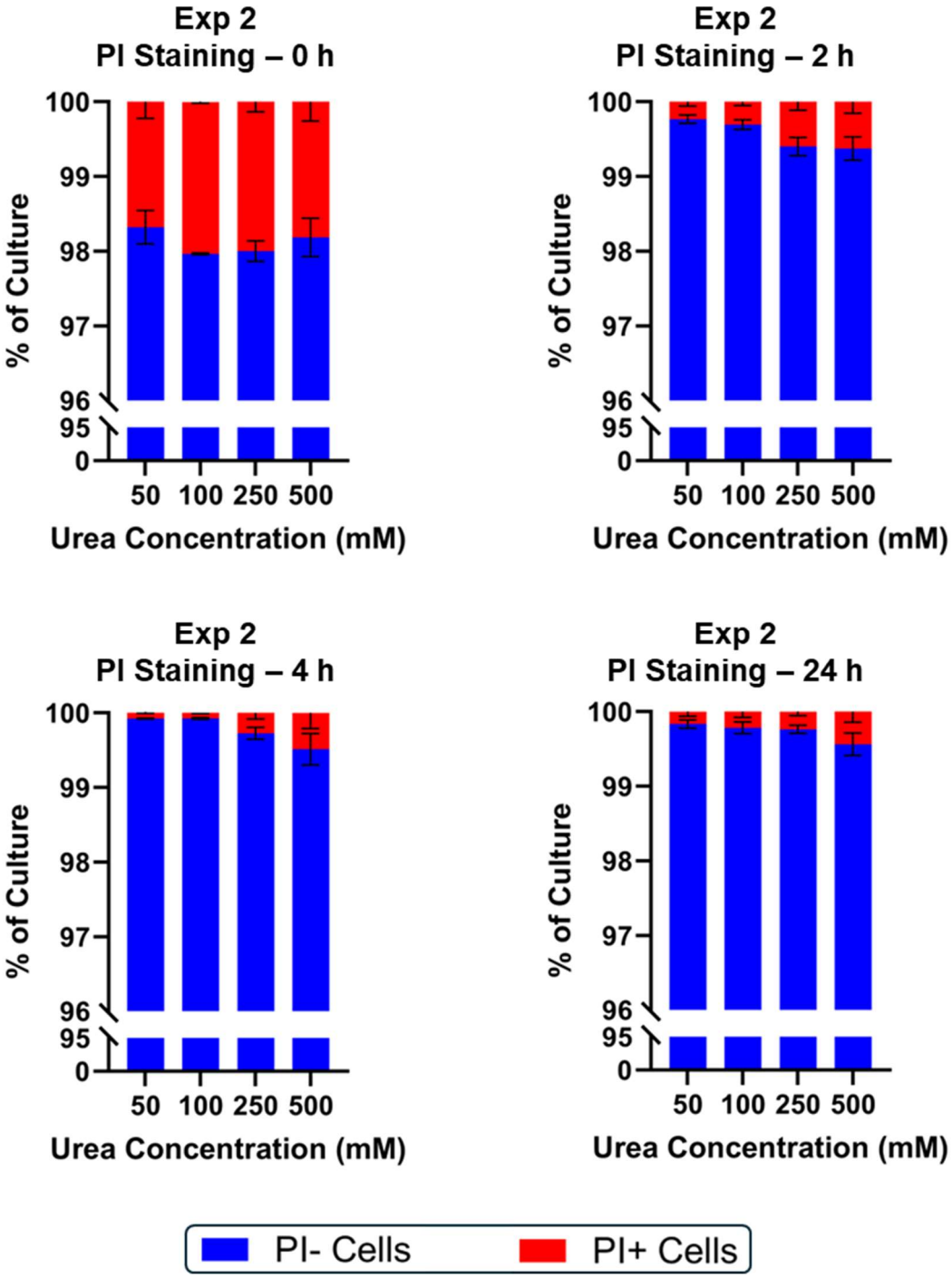


Figure 3.15: PI was used to monitor cell viability in JCB387 overexpressing 6xHis::GFP from P_{uti101}.

JCB387 harbouring the pET15b-P_{uti101}-*6xhis::gfp* construct was cultured in 50 mL LB + Amp and incubated at 37 °C, 200 rpm. At OD_{600} 0.4-0.6, 6xHis::GFP expression was induced by adding urea to cultures in triplicate for each concentration. As a measure of viability, cells were stained with 4 µg mL^{-1} PI for 5 min and analysed via FCM. Cells were gated based on red fluorescence to calculate the proportion of cells that were PI- (indicative of viable cells) or PI+ (indicative of non-viable cells). Data is shown for 0 h, 2 h, 4 h and 24 h post-induction for Exp 2 only (50 mM – 500 mM urea). Error bars represent +/- SD from biological triplicates.

Proportion of PI+ cells within JCB387 cultures was low throughout, indicating the majority were live. Even when inducing with 500 mM urea, the proportion of PI- cells in the cultures did not drop below 98 %.

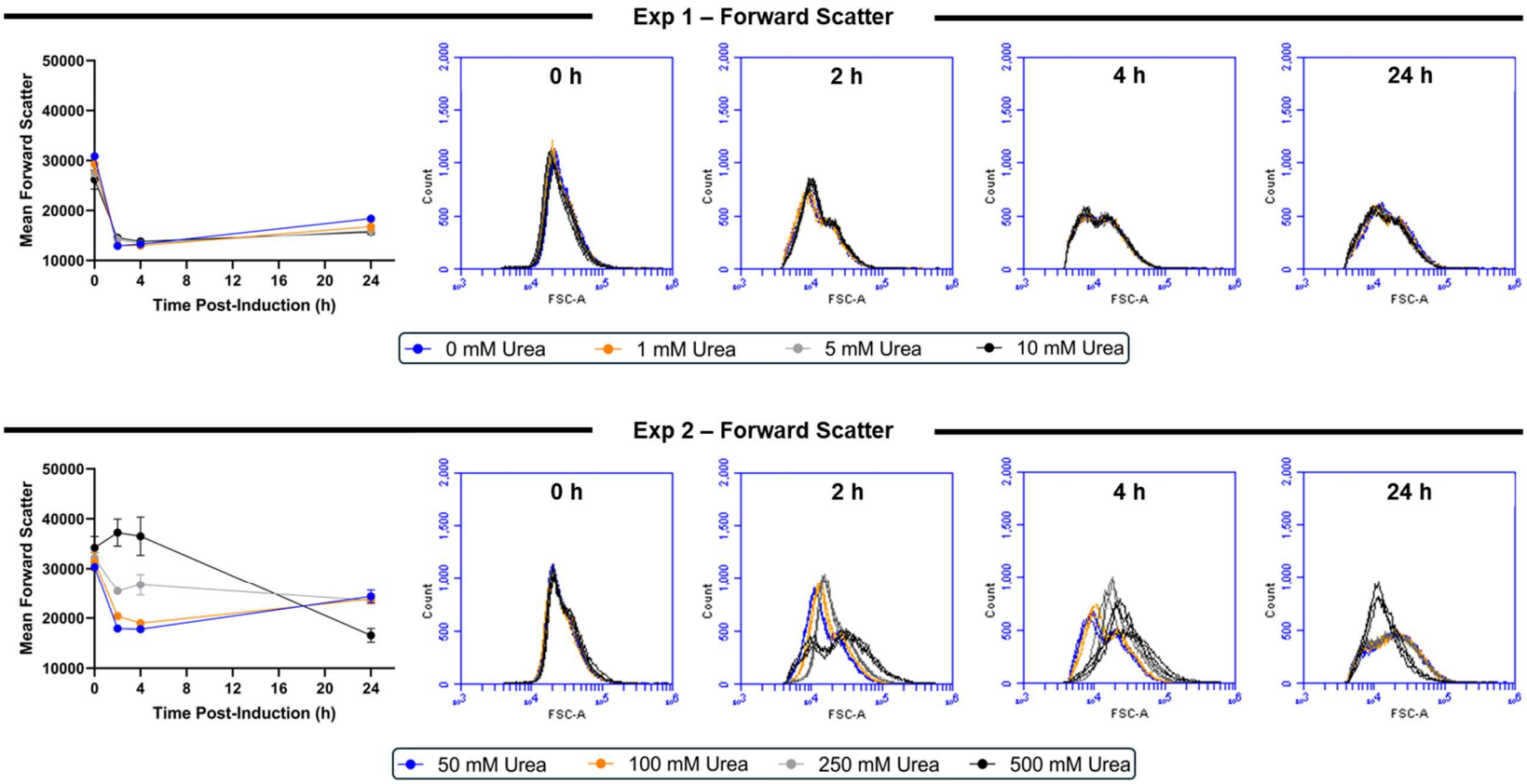


Figure 3.16: Forward scatter of JCB387 harbouring the pET15b-P*uti101*-*6xhis::gfp* construct and induced with varying concentrations of urea was measured using FCM. JCB387 was cultured in 50 mL LB + Amp and incubated at 37 °C, 200 rpm. At OD_{600} 0.4-0.6, urea was added to cultures in triplicate for each concentration. Data is shown for two separate experiments (Exp 1 and Exp 2). XY plots show mean forward scatter of whole cultures, error bars represent +/- SD from triplicate cultures. Histograms show forward scatter (FSC-A) at the single cell level, with each urea concentration shown for biological triplicates.

Top panel – Exp 1: There was little difference in mean forward scatter between cultures induced with 0 mM to 10 mM urea. At the single cell level there appeared to be some heterogeneity in all cultures from 2 – 24 h post-induction as indicated by two peaks on the histograms, although forward scatter in all conditions was like the 0 mM urea control.

Bottom panel – Exp 2: Mean forward scatter of cultures correlated with the concentration of urea used and increased between 0 h and 2 h post-induction in cultures induced with 500 mM urea. At the single cell level there appeared to be some heterogeneity in cultures induced with 500 mM urea at 2 h post-induction.

by two-way ANOVA (adjusted $p < 0.003$ for all comparisons). Notably, for cultures induced with 500 mM urea, FSC increased between 0 h and 2 h post-induction, reaching over 37000 at 2 h post-induction; a 2-fold difference compared with cultures induced with 50 mM which decreased to 18000 (Figure 3.16, bottom panel). Something similar was observed previously in JCB387 when inducing transformed cells with 500 mM urea (Figure 3.7B). At the single cell level, induction with higher concentrations of urea (50 mM – 500 mM) produced greater heterogeneity in FSC (raw data for histograms is provided in Chapter 8 – Appendix, Table 8.5). Cultures induced with 50 mM or 100 mM urea were similar, with those induced with 250 mM deviating slightly (Figure 3.16, bottom panel). Cultures induced with 500 mM urea were considerably different; populations were split based on FSC at 2 h post-induction (mean CV = 67.49 %) but had merged by 4 h post-induction (mean CV = 43.35 %) (Figure 3.16, bottom panel). It is possible this split population 2 h post-induction for cultures induced with 500 mM urea was due to shocking cells with a high solute concentration; by 4 hours post-induction, physiology had adjusted.

Once JCB387 physiology in response to induction with urea was established, we wanted to understand P_{uti101} characteristics and assess its performance for RPP. 6xHis::GFP expression was tracked via green fluorescence during growth, using FCM. In experiment 1, using low concentrations of urea (0 mM – 10 mM), uninduced cultures had low mean green fluorescence throughout growth (< 800 AU) (Figure 3.17, top panel), indicating basal expression from P_{uti101} was low. In induced cultures (1 mM – 10 mM) a similar pattern was evident; mean green fluorescence increased from induction, peaked at 4 h post-induction and decreased from this point by 24 h post-induction. Expression from P_{uti101} could be switched on with just 1 mM, although this was only a 4-fold increase in mean green fluorescence over uninduced cultures, reaching approximately 3000 AU at 4 h post-induction. Comparatively, inducing with 5 mM or 10 mM urea produced an approximately 40 to 50-fold increase in mean green fluorescence, reaching up to over 40000 AU at 4 h post-induction (Figure 3.17, top panel). No significant

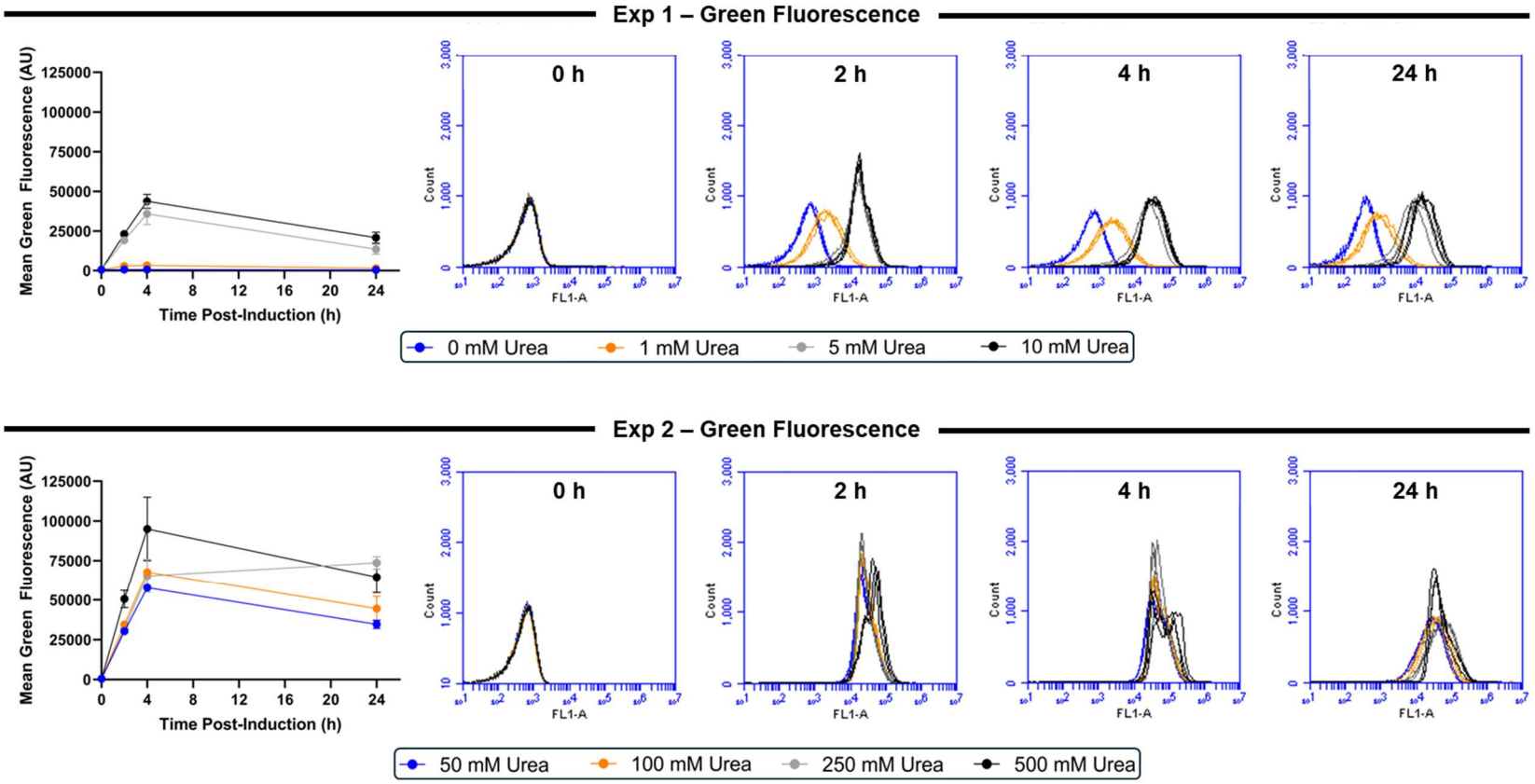


Figure 3.17: Green fluorescence of JCB387 harbouring the pET15b-P*uti101*-*6xhis::gfp* construct and induced with varying concentrations of urea was measured using FCM. JCB387 was cultured in 50 mL LB + Amp and incubated at 37 °C, 200 rpm. At OD_{600} 0.4-0.6, 6xHis::GFP expression was induced with urea, added to cultures in triplicate for each concentration. Data is shown for two replicate experiments (Exp 1 and Exp 2). XY plots show mean green fluorescence of whole cultures, error bars represent +/- SD from triplicate cultures. Histograms show green fluorescence (FL1-A) at the single cell level, with each urea concentration shown for biological triplicates.

Top panel – Exp 1: 6xHis::GFP expression from P*uti101* was switched on with just 1 mM urea, although there was little difference in mean green fluorescence between cultures induced with 5 mM and 10 mM urea. At the single cell level, regardless of the concentration of urea used for induction, populations were homogenous.

Bottom panel – Exp 2: 6xHis::GFP expression from P*uti101* did not appear particularly dose dependent, with mean green fluorescence similar after inducing with 50 – 250 mM urea. At the single cell level, induction with 500 mM urea caused heterogeneity in green fluorescence, particularly at 4 h post-induction.

difference in mean green fluorescence was found between cultures induced with 5 mM or 10 mM urea, even at 4 h post-induction when the difference appeared greatest (adjusted p = 0.18 for all comparisons using two-way ANOVA). At the single cell level, cultures induced with lower concentrations of urea (0 mM – 10 mM) in experiment 1 appeared as single populations with respect to green fluorescence (FL1-A) (Figure 3.17, top panel). Raw data for histograms is provided in Chapter 8 – Appendix, Table 8.6. In induced cultures (1 mM – 10 mM urea), CV% for green fluorescence (FL1-A) was lower for cultures induced with higher concentrations of urea. For example, at 4 h post-induction mean CV for cultures induced with 1 mM urea was 77.90 %; while for cultures induced with 10 mM urea, mean CV was 55.81 % (Table 8.6). It is likely when inducing with low concentrations of urea, any imbalances in uptake throughout the culture population are amplified, resulting in greater heterogeneity in 6xHis::GFP expression and thus green fluorescence.

In experiment 2, using high concentrations of urea (50 mM – 100 mM), mean green fluorescence was higher, reaching around 60000 AU (Figure 3.17, bottom panel). In experiment 2, a maximum mean green fluorescence was reached at 4 h post-induction, decreasing by 24 h post-induction for cultures induced with 50 mM, 100 mM or 500 mM urea. Interestingly, cultures induced with 250 mM urea diverged from this; mean green fluorescence increased between 4 h and 24 h post-induction. Inducing with 500 mM urea produced the highest mean green fluorescence reaching over 94000 AU at 4 h post-induction, although there was considerable variation between replicates; this was an approximately 1.6-fold increase over cultures induced with 50 mM urea at 57000 AU. Little difference in mean green fluorescence was observed between cultures induced with 50 mM, 100 mM or 250 mM urea and this was not significant (p = 0.2). At the single cell level, cultures induced with higher concentrations of urea (50 mM – 250 mM) in experiment 2 were mostly single populations and all with high green fluorescence (FL1-A) (Figure 3.17, bottom panel). In cultures induced with 500 mM urea, two populations of lower and higher green fluorescence were present, notably

at 4 h post-induction (Figure 3.17, bottom panel). Raw data for histograms is provided in Chapter 8 – Appendix, Table 8.7 and indicated greater heterogeneity in green fluorescence (FL1-A) for cultures induced with 500 mM urea at 4 h post-induction (mean CV = 65.93 %), compared with cultures induced with 50 mM – 250 mM urea (mean CV = 27.40 – 45.08 %). It was also noted that heterogeneity in green fluorescence appeared lower in cultures induced with 50 mM – 250 mM urea (Table 8.7), than for cultures induced with 1 – 10 mM urea (Table 8.6). Presumably when inducing with higher concentrations of urea, stochasticity in uptake has less of an effect as more urea is available.

As a final metric of P_{uti101} performance, rates of 6xHis::GFP expression were calculated through linear regression of mean green fluorescence values presented in Figure 3.17 for experiment 1 and 2, between 0 h and 4 h post-induction. For low urea concentrations in experiment 1, there was little difference in the rate of 6xHis::GFP expression between cultures induced with 5 mM and 10 mM urea (Figure 3.18A). At higher urea concentrations in experiment 2, the rate of 6xHis::GFP expression in cultures was also similar between 50 mM – 250 mM urea (Figure 3.18B). Rates of 6xHis::GFP expression appeared higher in cultures induced with 500 mM, although when analysed by one-way ANOVA, this was only significantly different from cultures induced with 50 mM urea (adjusted p = 0.0160). Overall, mean green fluorescence (Figure 3.17) and expression rate data (Figure 3.18) indicated that while there appeared to be some dose dependence, P_{uti101} did not appear highly tuneable in JCB387.

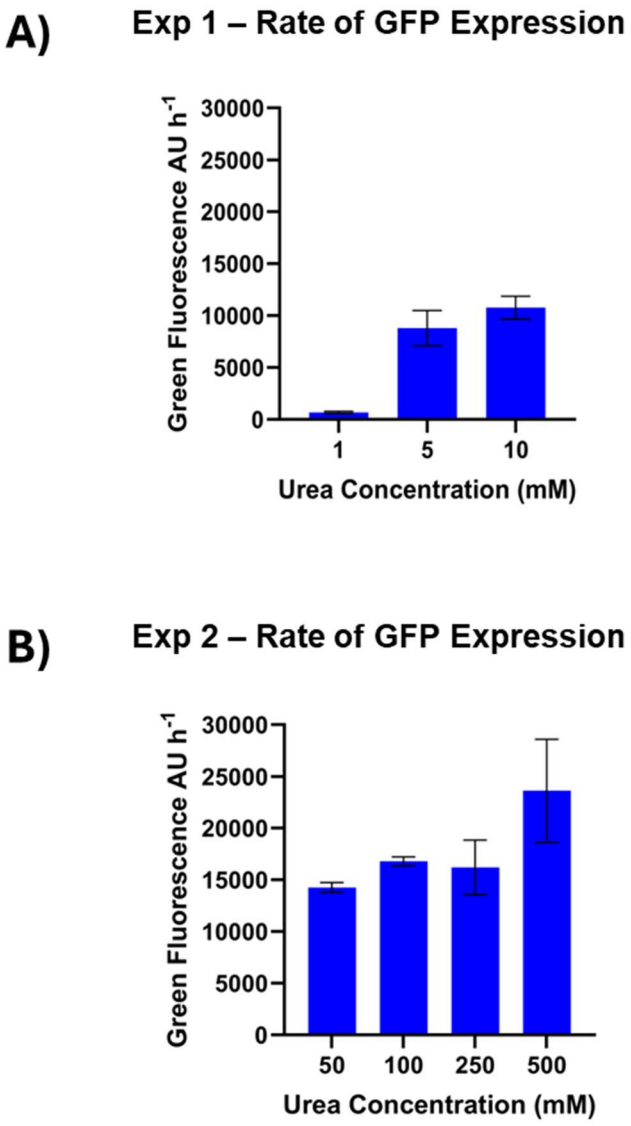


Figure 3.18: Rate of 6xHis::GFP expression from P_{uti101} in JCB387 induced with low (Experiment 1) and high (Experiment 2) concentrations of urea.

JCB387 was cultured in 50 mL LB + Amp and incubated at 37 °C, 200 rpm. At OD_{600} 0.4-0.6, urea was added to cultures in triplicate for each concentration. Data is shown for two separate experiments (Experiment 1 and Experiment 2). Rates of 6xHis::GFP expression (AU h^{-1}) were calculated by fitting a linear regression model to mean green fluorescence values (presented in Figure 3.17) between 0 h and 4 h post-induction. Error bars represent +/- SD from biological triplicates. R^2 following regression was > 0.95 for each replicate.

A) Expression rates for experiment 1 using low concentrations of urea to induce 6xHis::GFP indicated there was little difference between 5 mM and 10 mM urea.

B) Expression rates for experiment 2 using high concentrations of urea to induce 6xHis::GFP indicated there was little difference between 50 mM and 250 mM urea. Inducing cultures with 500 mM urea resulted in an increased rate of 6xHis::GFP expression, though this was only significantly different to 50 mM cultures when analysed by one-way ANOVA (adjusted p = 0.0160)

3.3.2 Expression in BL21

For consistency with the work of the Browning lab (Aston University), initial overexpression work using P_{uti101} was completed in *E. coli* JCB387, a K-12 derivative constructed for studying the regulation of nitrate reduction (Page et al., 1990). As BL21 is more relevant to RPP (Phue et al., 2005, Marisch et al., 2013, Jeong et al., 2015), we wanted to look further at P_{uti101} performance in this strain. Additionally, BL21 was observed to be less affected than JCB387 by higher concentrations of urea, based on growth characteristics (Figure 3.2) and FSC analysis (Figure 3.4). Thus, BL21 containing pET-15b-P_{uti101}-*6xhis*::*gfp* was aerated at 37 °C, 200 rpm in 50 mL LB (Lennox) + Amp in Erlenmeyer flasks. At OD_{600} 0.4-0.6, 6xHis::GFP expression from P_{uti101} was induced using 0 mM – 500 mM urea, in triplicate flasks for each concentration. Overexpression proceeded for a further 24 h.

Biomass accumulation of BL21 was monitored by OD_{600} (Figure 3.19A). OD_{600} correlated with the concentration of urea used for induction, up to a concentration of 100 mM urea; cultures induced with 500 mM urea increasing more steadily. Under all conditions, OD_{600} reached around 4.0 to 5.0 with uninduced cultures the lowest each time (Figure 3.19A); this was lower than in JCB387 which reached approximately OD_{600} 5.5 to over 6.0 for uninduced cultures (Figure 3.14). Specific growth rates for cultures were calculated using OD_{600} and were predictably similar across urea concentrations used for induction (Figure 3.19B). We would have expected induction with higher concentrations of urea to negatively affect biomass accumulation; its possible OD_{600} data did not accurately reflect cell growth in the cultures. BL21 cells were stained with PI and analysed using FCM to try and better quantify viability, but it was not possible to gate cells properly following urea addition (Figure 3.20). Dead cell controls were created at 24 h post-induction with 50 mM urea, via 15-minute treatment with 70 % (v/v) ethanol for 15 min. For dead cell controls, ideally over 99% of cells would reside within the PI+ gate. However, mixed populations of PI- and PI+ cells were observed in dead cell controls

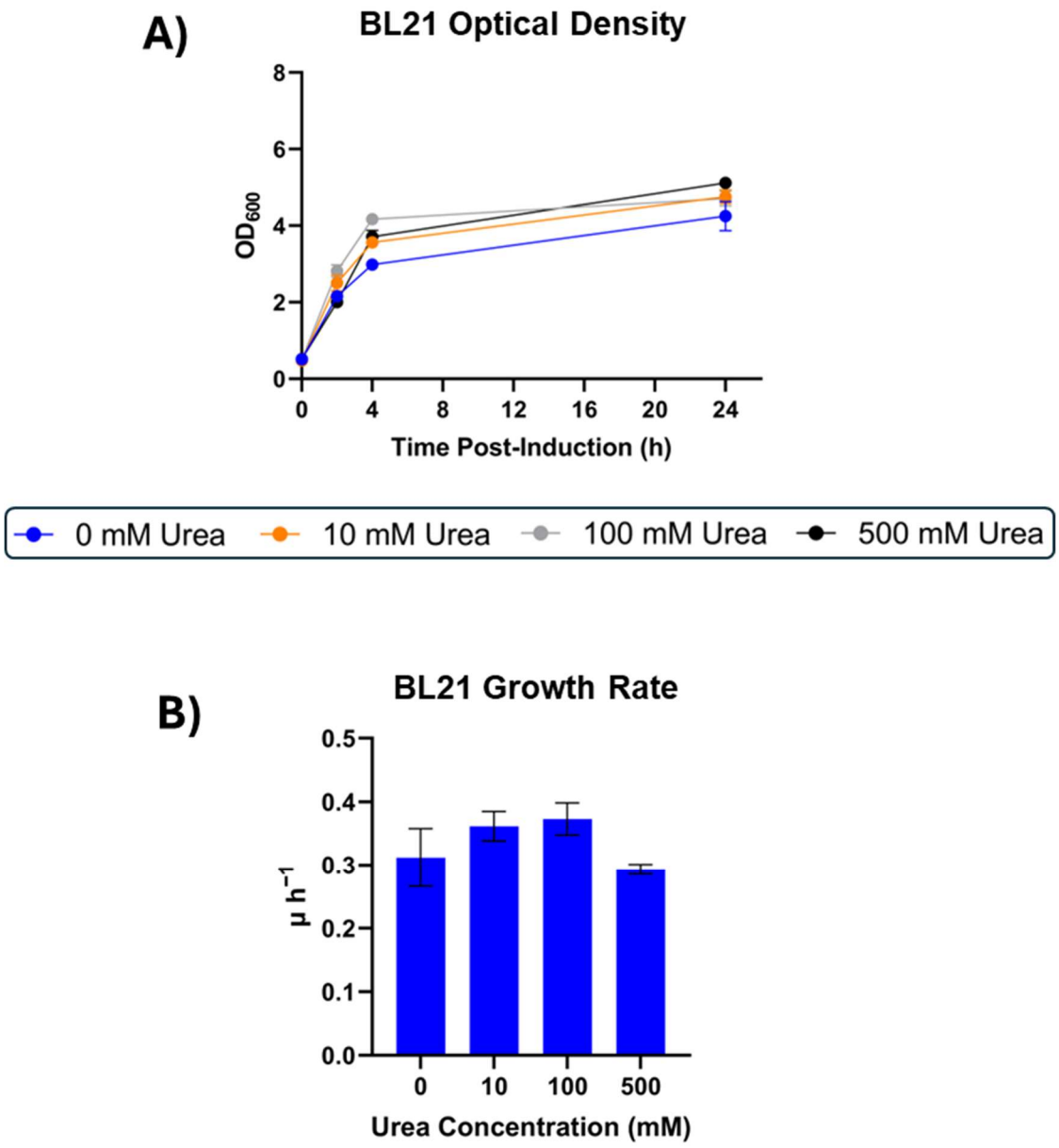


Figure 3.19: Growth data of BL21 harbouring the pET15b-P*uti101*-*6xhis::gfp* construct, with 6xHis::GFP expression from P*uti101* induced with varying concentrations of urea.

BL21 was cultured in 50 mL LB + Amp and incubated at 37 °C, 200 rpm. At OD_{600} 0.4-0.6, 6xHis::GFP expression was induced by adding urea to cultures in triplicate for each concentration. Error bars represent +/- SD from biological triplicates.

(A) OD_{600} was monitored to observe the effect of 6xHis::GFP expression and urea on biomass accumulation, which appeared similar for all conditions and lowest in the uninduced 0 mM control.

(B) Specific growth rate ($\mu\ h^{-1}$) was calculated from OD_{600} for both replicate experiments and was predictably similar for all conditions.

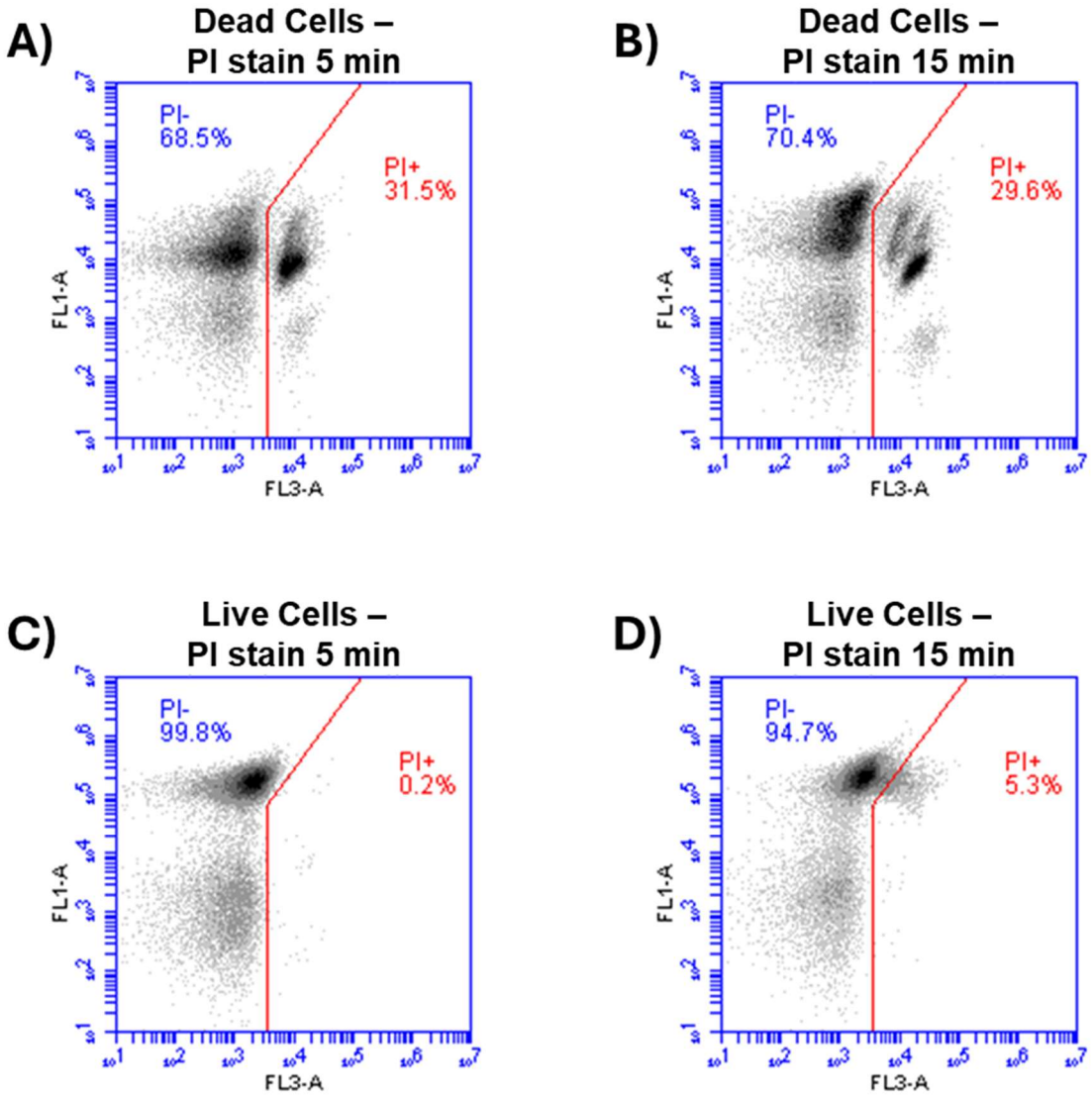


Figure 3.20: PI staining of cells as an indicator of cell viability was not possible in BL21 treated with urea.

BL21 harbouring the pET15b-P*uti101*-*6xhis::gfp* construct was cultured in 50 mL LB + Amp and incubated at 37 °C, 200 rpm. At OD_{600} 0.4-0.6 50 mM urea was added to cultures. At 24 h post-induction, live and dead cells were stained with 4 µg mL^{-1} PI. Live cells were diluted in PBS and stained with PI. Dead cells were resuspended in 70 % (v/v) ethanol for 15 min and then resuspended and diluted in PBS prior to staining with PI. Stained cells were analysed using FCM. Red fluorescence (FL3-A) increases when PI is bound to DNA. Green fluorescence was measured on the FL1-A channel (6xHis::GFP expression).

We attempted to create gates for PI- and PI+ cells but for dead cells, only 31.5 % of cells appeared within the PI+ gate after staining for 5 min **(A)** and increasing the length of staining to 15 min did not improve this **(B)**. For live cells, staining with PI for 5 min resulted in only 0.2 % of cells within the PI+ gate as expected **(C)**. Increasing the length of staining in live cells to 15 min resulted in 5.3 % of cells within the PI+ gate **(D)**. This meant that clear differentiation between PI- and PI+ cells was not possible.

stained with PI for 5 min (Figure 3.20A); increasing the length of staining to 15 min did not improve this (Figure 3.20B). Further, longer PI staining times meant it was not possible to gate live cells properly (Figure 3.20C - D).

In BL21, we had previously observed poor correlation between expression of 6xHis::GFP following induction with 500 mM urea and OD_{600} (Figure 3.6A). It was concluded in section 3.2.2 that this was because 6xHis::GFP overexpression increased cell size (assessed by FSC analysis) and in turn, scattering of light during optical density measurement (Figure 3.7). We wanted to see whether this applied at lower concentrations of urea too, so FSC was analysed using FCM. As observed in JCB387 (Figure 3.16), mean FSC of BL21 cultures correlated with the concentration of urea used (Figure 3.21A). At 4 h post-induction, where differences in mean FSC appeared greatest, the correlation between mean FSC and the concentration of urea used was significant when analysed by one-way ANOVA (adjusted $p < 0.02$ for all comparisons in both replicate experiments). Single-cell analysis of FSC indicated mostly single populations for BL21 induced with up to 100 mM urea (Figure 3.21B); at 24 h post-induction, cultures induced with 500 mM urea consisted of two FSC populations. Raw data for histograms is provided in Chapter 8 – Appendix, Table 8.8. It was noted that heterogeneity in FSC was higher in cultures induced with 50 mM – 100 mM between 2 h and 4 h post-induction (mean CV 42 – 48 %) compared with 500 mM cultures (mean CV 27 – 28%). Given urea concentration correlated with mean FSC (Figure 3.21A), higher concentrations of urea probably created a more consistent effect on cells within the cultures.

Once BL21 physiology in response to induction with urea was established, we wanted to understand P_{uti101} characteristics in this strain and assess its performance for RPP. Green fluorescence and thus 6xHis::GFP expression from P_{uti101} was monitored by FCM (Figure 3.22). Uninduced cultures maintained low mean green fluorescence throughout all 24 h (< 1000 AU) (Figure 3.22A), comparable with JCB387 (Figure 3.17, top panel). In induced

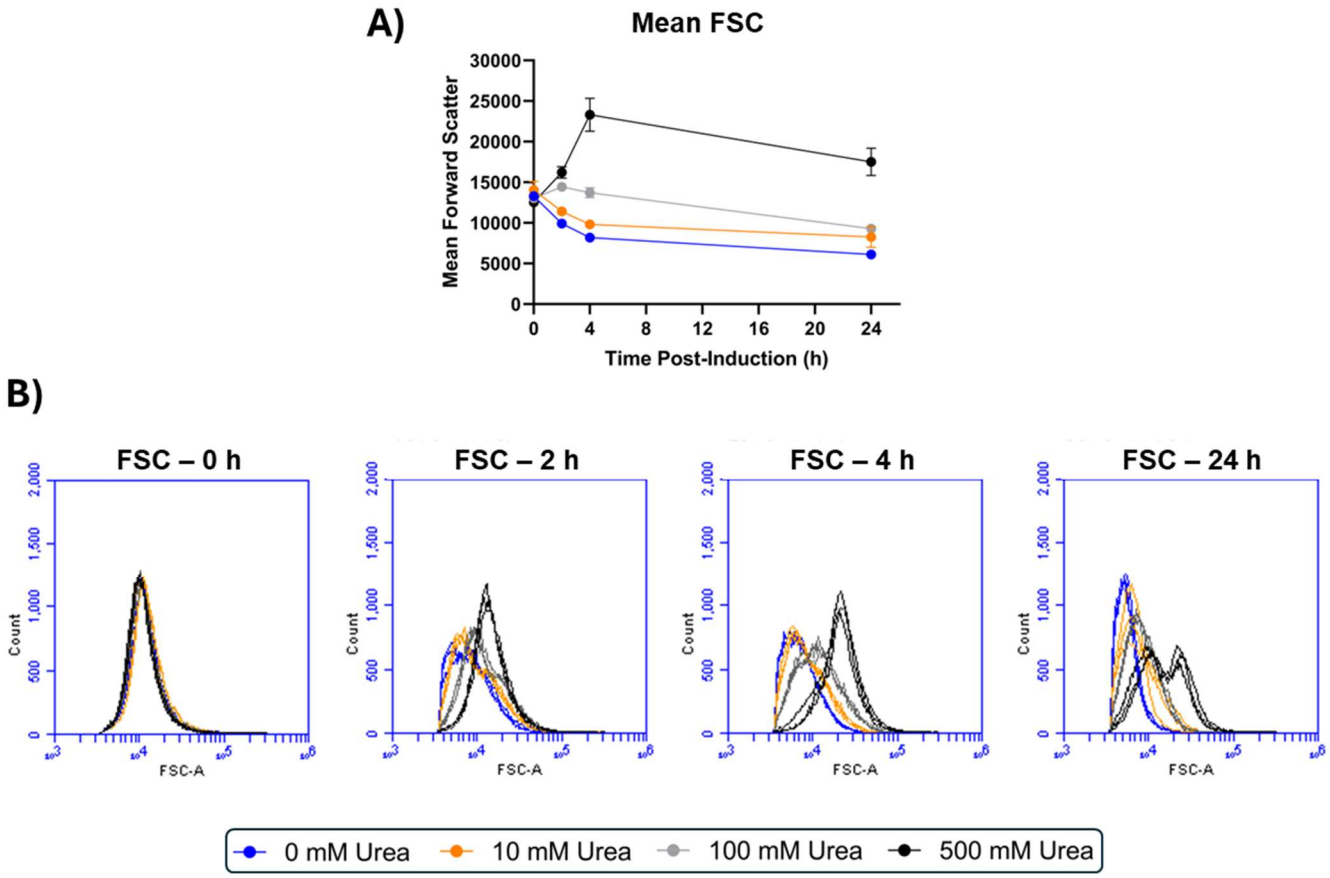


Figure 3.21: Forward scatter of BL21 harbouring the pET15b-P*uti101*-*6xhis::gfp* construct and induced with varying concentrations of urea was measured using FCM. BL21 was cultured in 50 mL LB + Amp and incubated at 37 °C, 200 rpm. At OD_{600} 0.4-0.6, urea was added to cultures in triplicate for each concentration. Plots for **(A)** and **(B)** use the same legend.

A) Mean forward scatter correlated with the concentration of urea used and increased between 0 h – 4 h post-induction in cultures induced with 500 mM urea. Error bars represent +/- SD from biological triplicates.

B) Forward scatter (FSC-A) analysis in single cells showed heterogeneity in all cultures, as indicated by the width of the peaks, although between 0 h and 4 h post-induction cultures were mostly one population. Data is shown for biological triplicates.

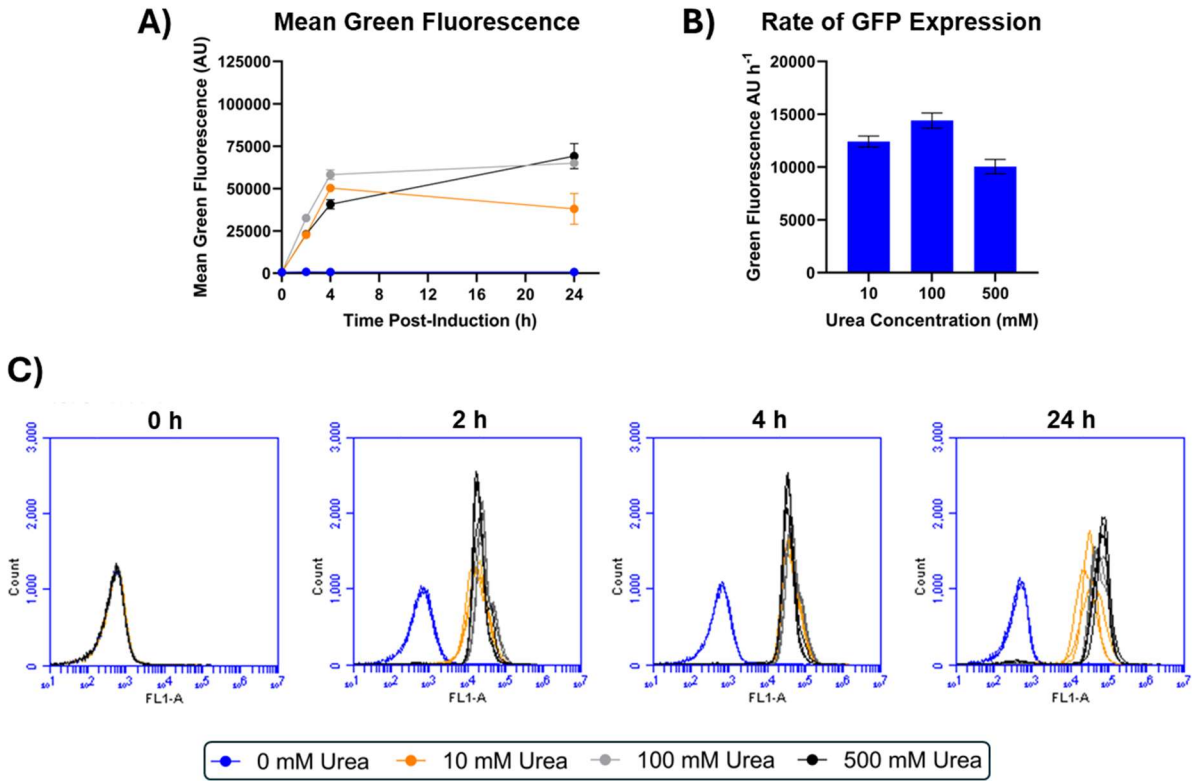


Figure 3.22: Green fluorescence of BL21 harbouring the pET15b-Puti101-6xhis::gfp construct and induced with varying concentrations of urea was measured using FCM. BL21 was cultured in 50 mL LB + Amp and incubated at 37 °C, 200 rpm. At OD_{600} 0.4-0.6, 6xHis::GFP expression was induced with urea, added to cultures in triplicate for each concentration. Plots for **(A)** and **(C)** use the same legend.

A) Mean green fluorescence and thus 6xHis::GFP expression appeared higher in cultures induced with 50 mM – 100 mM urea at 4 h post-induction although cultures induced with 500 mM urea were higher at 24 h post-induction. Error bars represent +/- SD from biological triplicates.

B) Rates of 6xHis::GFP expression (AU h^{-1}) were calculated by fitting a linear regression model to mean green fluorescence values (**A)** between 0 h and 4 h post-induction. Error bars represent +/- SD from triplicate cultures. R^2 following regression was > 0.95 for each replicate. Error bars represent +/- SD from biological triplicates.

C) At the single cell level one population was observed in all cultures and in those induced with urea, the population had high green fluorescence (FL1-A). Data is shown for biological triplicates.

cultures (10 mM – 500 mM urea) mean green fluorescence did not correlate with the concentration of urea added (Figure 3.22A). Instead mean green fluorescence in cultures induced with 500 mM urea increased steadily over time, comparable to cultures induced with 100 mM urea by 24 h post-induction. Little difference in mean green fluorescence was apparent between cultures induced with 10 mM or 100 mM urea, between induction and 4 h post-induction. Higher concentrations of urea did appear to prolong 6xHis::GFP expression; mean green fluorescence decreased more in cultures induced with 10 mM by 24 h post-induction. A maximum mean green fluorescence was observed in cultures induced with 100 mM urea, at around 58000 AU; this was slightly lower than that seen in JCB387 (Figure 3.17, bottom panel). Rates of 6xHis::GFP expression (Figure 3.22B) in BL21 were calculated through linear regression of mean green fluorescence values (Figure 3.22A) between 0 h and 4 h post-induction. Difference between the rates of GFP expression were significant when analysed by one-way ANOVA (adjusted $p < 0.03$ for all comparisons), with cultures induced with 100 mM urea the highest. This diverged from that observed in JCB387 (Figure 3.18), where cultures induced with 500 mM urea showed the highest rate of 6xHis::GFP expression. Given that JCB387 is a K12 strain and BL21 is a B strain, differences in in membrane structure could account for variations in urea uptake (Schneider et al., 2002).

At the single-cell level, cultures induced with urea (10 mM – 500 mM) consisted of one population with high green fluorescence (FL1-A) (Figure 3.22C). It was noted that there appeared to be lower heterogeneity in cultures induced with 500 mM urea. Raw data for histograms is provided in Chapter 8 – Appendix, Table 8.9 and supports this. At 4 h post-induction, mean CV in cultures induced with 10 mM – 100 mM urea was 42 – 46 %; in 500 mM cultures, mean CV was 27.47%. Overall, green fluorescence and expression rate data (Figure 3.22) indicated that while there appeared to be some dose dependence between 10 mM and 100 mM urea for P_{uti101}, the difference was small.

3.3.3 JCB387 and BL21 Seed cultures

In JCB387 and BL21, 6xHis::GFP expression from P_{uti101} in the absence of urea appeared low during growth, with little increase in mean green fluorescence over 24 h (Figure 3.17, top panel & Figure 3.22A). Such tight regulation is valuable in RPP, especially if the recombinant protein is toxic. To expand on this, green fluorescence was monitored using FCM for seed cultures of JCB387 and BL21 harbouring the pET-15b-P_{uti101}-*6xhis*::*gfp* construct, which were grown in 10 mL LB (Lennox) + Amp at 37 °C, 200 rpm for 16 – 18 h.

Using FCM, cells were gated as low (GFP-) or high (GFP+) green fluorescence using forward scatter (FSC-A) against green fluorescence (FL1-A) density plots. Background expression of 6xHis::GFP from P_{uti101} appeared low in JCB387 and BL21 seed cultures (Figure 3.23A). Of those seed cultures analysed, all had over 90 % of cells were within the GFP- gate, with the majority having over 96% of cells with low green fluorescence; in two instances for both strains, over 99% of cells were within the GFP- gate.

Due to the tight regulation of P_{uti101}, it was assumed harbouring the pET15b-P_{uti101}-*6xhis::gfp* construct would also have minimal impact on biomass accumulation in seed cultures. Transformed JCB387 and BL21 were compared with untransformed variants after overnight culture (Figure 3.23B). OD_{600} measurements indicated biomass accumulation was higher in seed cultures for JCB387, which were around 4.0 – 6.0; comparatively BL21 seed cultures reached 3.5 – 4.0. In both JCB387 and BL21, seed cultures for transformed strains were comparable with untransformed variants.

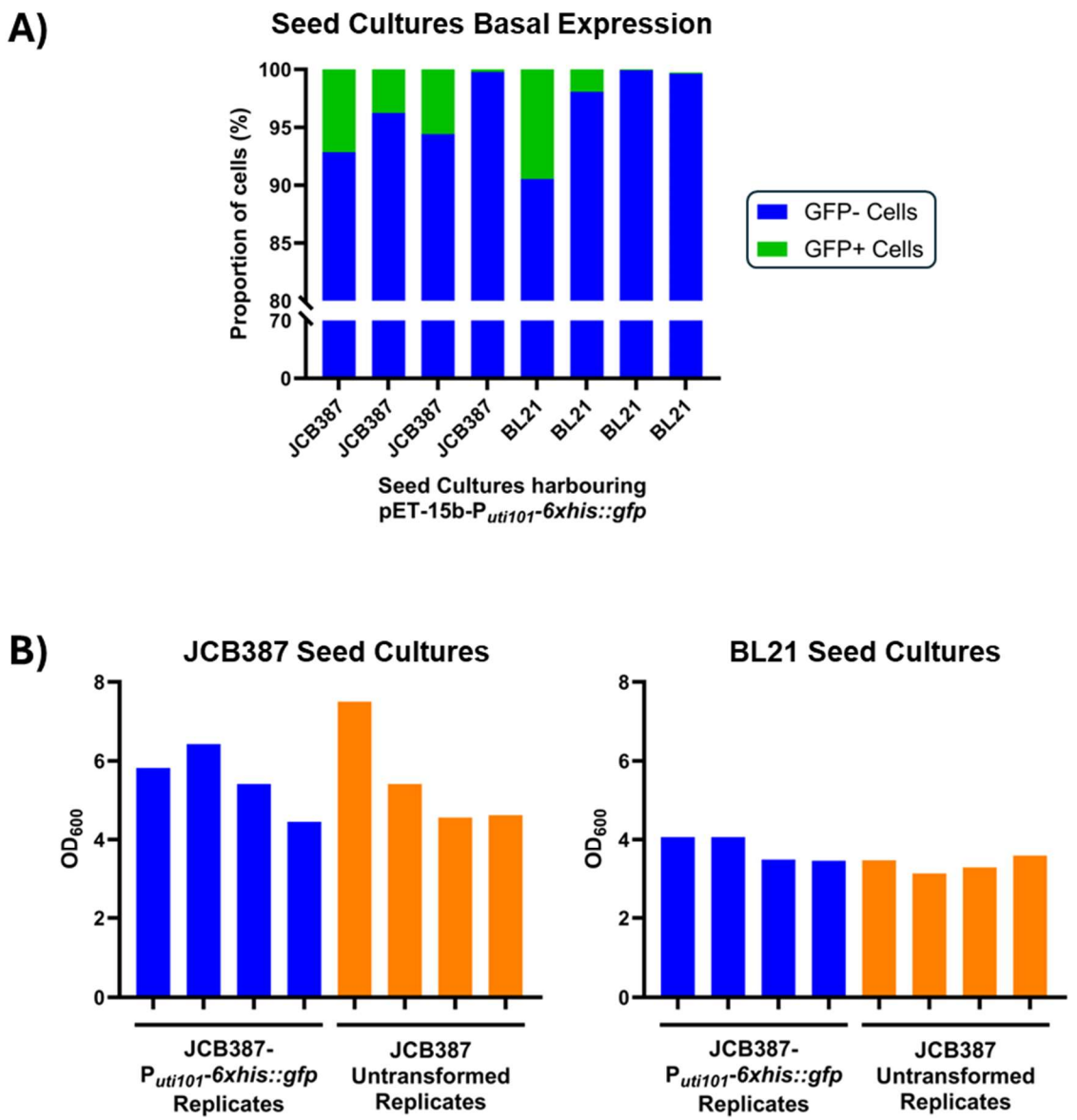


Figure 3.23: Analysis of JCB387 and BL21 seed cultures harbouring the pET15b-P*uti101*-*6xhis::gfp* construct.

Seed cultures of JCB387 and BL21 harbouring the pET15b-Puti101-6xhis::gfp construct were grown in 10 mL LB + Amp at 37 °C, 200 rpm for 16 – 18 h. Where provided for comparison with transformed strains, untransformed JCB387 and BL21 were grown in 10 mL LB at 37 °C, 200 rpm for 16 – 18 h.

(A) To monitor basal expression of 6xHis::GFP from P*uti101*, seed cultures were analysed using FCM and green fluorescence measured. Gates for low (GFP-) and high (GFP+) green fluorescence were created on forward scatter (FSC-A) vs. green fluorescence (FL1-A) plots using untransformed, uninduced and induced JCB387 and BL21 controls. Values for GFP- and GFP+ represent the proportion of cells (%) within each gate for replicate JCB387 and BL21 seed cultures. Each data point is for one biological replicate seed culture. Basal expression was tight during overnight growth with all seed cultures analysed having over 90% of cells within the GFP- gate; the majority being over 96%.

(B) Biomass accumulation measured via OD_{600} was monitored in seed cultures of JCB387 and BL21 harbouring the pET15b-P*uti101*-*6xhis::gfp* construct and compared with untransformed JCB387 and BL21. Each data point is for one biological replicate seed culture. In both JCB387 and BL21 seed cultures of cells containing the pET15b-P*uti101*-*6xhis::gfp* construct were comparable to untransformed variants.

3.3.4 Basal Expression

To understand regulation of P_{uti101}, untransformed and transformed JCB387 and BL21 cultures were compared in the absence of urea. JCB387 and BL21 harbouring the pET-15b-P_{uti101}-*6xhis*::*gfp* construct were aerated at 37 °C, 200 rpm in 50 mL LB (Lennox) + Amp in Erlenmeyer flasks. Untransformed JCB387 and BL21 were aerated at 37 °C, 200 rpm in 50 mL LB (Lennox) in Erlenmeyer flasks. Cultures were not induced with urea and growth proceeded for 24 h after reaching OD_{600} 0.4-0.6. For transformed JCB387 and BL21, data is from 6 replicate cultures each. For untransformed JCB387 and BL21, data is from 3 replicate cultures each.

Mean green fluorescence of cultures was monitored via FCM (Figure 3.24). In untransformed cells, mean green fluorescence was virtually unchanged over 24 h. In untransformed JCB387, mean green fluorescence remained around 300 AU; untransformed BL21 was slightly lower at approximately 200 AU. We had observed prior that at 0 h, untransformed JCB387 cells had higher FSC than BL21 (Figure 3.7B). Increased cell size could cause disparity in mean green fluorescence between strains; larger cells having more intracellular or surface components contributing to autofluorescence (Mihalcescu et al., 2015). In transformed JCB387 and BL21 harbouring the pET-15b-P_{uti101}-*6xhis*::*gfp* construct, mean green fluorescence of uninduced cultures was broadly similar between 500-800 AU; this was only 2 to 4-fold higher than untransformed variants. Transformed strains induced with 10 mM urea had reached 30000 – 50000 AU for JCB387 and BL21 respectively (Figure 3.17, top panel & Figure 3.22A). We concluded that with green fluorescence being only 2 to 4-fold higher than autofluorescence, basal expression from P_{uti101} was very low.

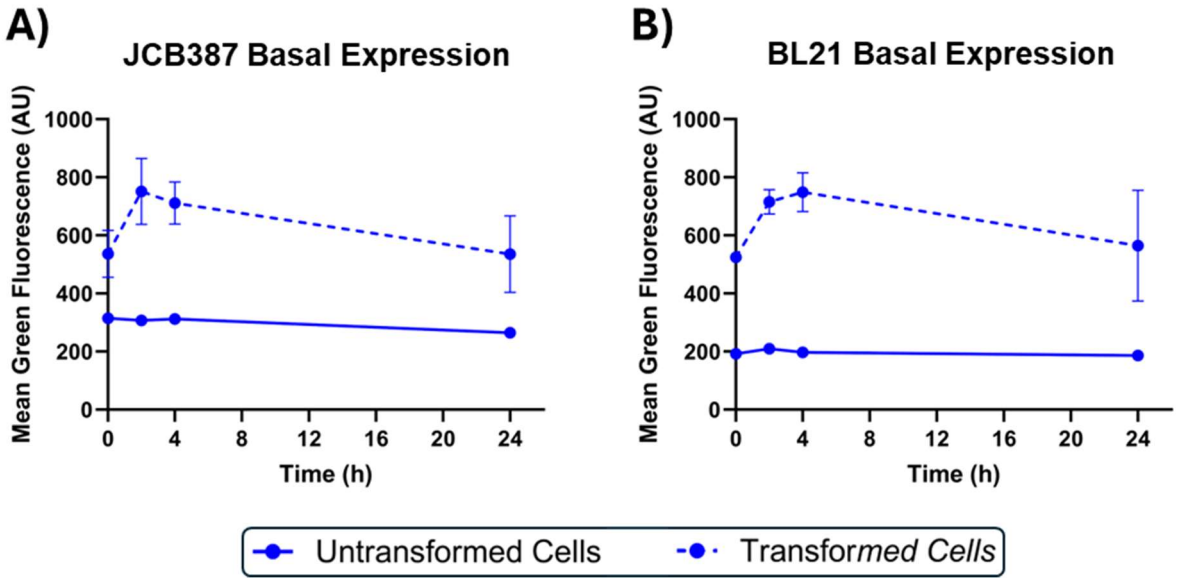


Figure 3.24: Analysis of basal expression of 6xHis::GFP from P_{uti101} in JCB387 and BL21 harbouring the pET15b-P_{uti101}-*6xhis::gfp* construct compared with autofluorescence of untransformed cells.

JCB387 and BL21 harbouring the pET15b-Puti101-6xhis::gfp construct were grown in 50 mL LB + Amp at 37 °C, 200 rpm. Untransformed JCB387 and BL21 were grown in 50 mL LB at 37 °C, 200 rpm. Urea was not added to cultures. Mean green fluorescence of cultures was monitored using FCM. Time (h) is from the point cultures reached OD_{600} 0.4-0.6. For untransformed cells, error bars represent +/- SD from biological triplicates cultures (not visible). For transformed cells, error bars represent +/- SD from six biological replicates.

In both JCB387 **(A)** and BL21 **(B)**, mean green fluorescence was only 2 to 3-fold higher in transformed cells than compared with untransformed variants. This indicated basal expression of 6xHis::GFP from P_{uti101} was low in the absence of urea.

3.4 Scale-up into baffled flasks

Initial work using the urea inducible system was done in 250 mL Erlenmeyer flasks using 50 mL LB (Lennox) media, but it was vital P_{uti101} was tested at increased scales and under more intensified growth to better understand the characteristics of the promoter. To improve aeration and thus growth rates and 6xHis::GFP expression, 500 mL baffled Erlenmeyer flasks were chosen. It was also decided to switch to richer TB medium, which is more amenable to high cell density growth than LB. TB uses glycerol as the carbon source which reduces overflow metabolism and acetate accumulation that would otherwise impair growth (Losen et al., 2004). At 50 mL scale, JCB387 and BL21 displayed similar expression of 6xHis::GFP up to 100 mM urea (Figure 3.17, bottom panel & Figure 3.22A). BL21 is widely used as a production host though and its physiology is better understood at scale, so it was decided to proceed with this strain for a better comparison to prior work (Selas Castiñeiras et al., 2018c).

3.4.1 Growth analysis in baffled flasks

Inducible systems and host behaviour may change in response to working at larger scales and use of different growth media. To provide a baseline for future analysis of the urea inducible system, uninduced BL21 harbouring the pET-15b-P_{uti101}-*6xhis::gfp* construct was grown in triplicate cultures, using baffled Erlenmeyer flasks and 100 mL TB + Amp at 37 °C, 150 rpm until 26 h post-inoculation. Shaking speed was reduced in 100 mL baffled flasks to 150 rpm (from 200 rpm in 50 mL flasks) due to foaming.

Biomass accumulation and cell density were monitored via OD_{600} and FCM respectively (Figure 3.25A and 3.25B). Both OD_{600} and cell density increased rapidly after 2 h post-inoculation as they reached log phase, slowing by about 5 h post-inoculation. A maximum OD_{600} of 19.6 and maximum cell density of 2.36×10^{10} cells mL^{-1} (as measured by FCM) were reached at 26 h post-inoculation; this was considerably higher than at 50 mL scale, where BL21 cultures

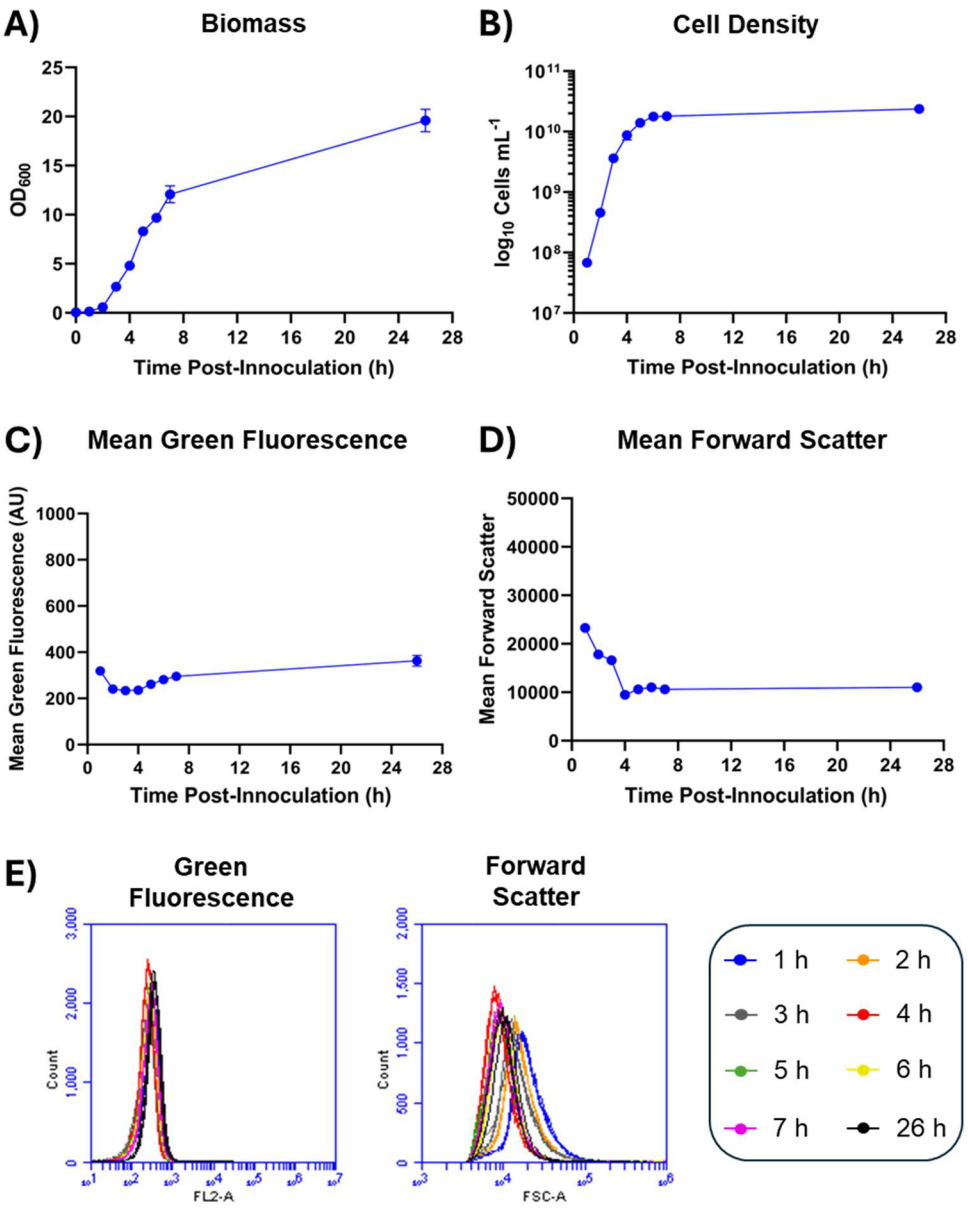


Figure 3.25: Analysis of uninduced BL21 carrying the pET-15b-P*uti101*-*6xhis::gfp* construct during scale-up.

During scale-up, uninduced BL21 carrying the pET-15b-P*uti101*-*6xhis::gfp* construct was aerated in 100 mL TB + Amp in baffled Erlenmeyer flasks at 37 °C, 150 rpm until 26 h post-inoculation.

Biomass accumulation measured via OD_{600} **(A)** was higher than observed at 50 mL scale using non-baffled flasks, reaching approximately 20. Cell density **(B)** was measured via FCM, with cultures saturating around 6 h post-inoculation and reaching a maximum of 2.38×10^{10} cells mL^{-1} at 24 h post-inoculation. Error bars represent +/- SD from biological triplicates.

Mean green fluorescence **(C)** measured via FCM was stable throughout growth, around just 300 AU. The lowest mean green fluorescence was at 3 h post-inoculation and highest at 24 h post-inoculation. Mean FSC **(D)** was also measured via FCM and decreased from 23000 AU at inoculation until 4 h post-induction where it remained more stable at around 9000 – 11000 AU until 24 h post-inoculation. When looking at single cells via FCM **(E)**, BL21 cultures appeared evenly distributed and as single populations with regards to green fluorescence (FL2-A) and FSC, throughout all 24 h of growth. Data is shown for biological triplicates

reached OD_{600} values around 4-6 (section 3.3.2). Specific growth rate was calculated from cell density; the mean for replicate cultures was 0.8615 $\mu\ h^{-1}$ (SD = 0.032). For reference with previous measurements of uninduced BL21, specific growth rate was calculated from OD_{600} too; the mean for replicate cultures was 0.6613 $\mu\ h^{-1}$ (SD = 0.005). This was also higher than observed for BL21 at 50 mL scale, where specific growth rate reached around 0.3 $\mu\ h^{-1}$ (section 3.3.2).

To evaluate whether richer TB medium, increased culture volume or improved growth characteristics affected basal expression from P_{uti101} in any way, mean green fluorescence of cultures was analysed by FCM (Figure 3.25C). Mean green fluorescence was low throughout growth at approximately 300 AU; it decreased following inoculation during lag-phase to 233 AU. From 4 h post-inoculation (during log-phase growth based on OD_{600} – Figure 3.25A) mean green fluorescence increased slightly, until 24 h post-inoculation where a maximum value of 363 AU was reached. This was comparable with basal expression observed in section 3.3.4 and so we concluded scale-up did not affect repression of the P_{uti101} promoter.

Mean FSC was monitored via FCM to confirm whether the change in culture scale or growth medium affected cell size (Figure 3.25D). Mean FSC decreased from 23000 following inoculation to around 9000 at 4 h post-inoculation. Mean FSC then increased slightly between 5 h and 7 h post-inoculation; this correlated with slightly elevated mean green fluorescence observed at these time-points (Figure 3.25C). Slight increases in FSC and thus cells size would have produced a higher green fluorescence signal and vice versa. Analysis of single cells using FCM indicated cultures were homogonous and composed of single populations with regards to green fluorescence (FL1-A) and forward scatter (FSC-A) (Figure 3.25E). Raw data for histograms is provided in Chapter 8 – Appendix (Table 8.10 & Table 8.11); distributions were quite tight for both green fluorescence and forward scatter (mean CV 29 – 31 % for FL1-A; mean CV 24 – 27 % for FSC-A).

3.4.2 Effect of urea on BL21 in TB medium

It was previously shown that even addition of 500 mM urea did not hugely affect BL21 growth in LB at 50 mL scale (Figure 3.2). To confirm scale-up did not affect this, BL21 physiology in response to urea was evaluated in TB at 100 mL scale. To uncouple any effects of urea from that of 6xHis::GFP expression, untransformed BL21 were aerated at 37 °C, 150 rpm in 100 mL TB in baffled Erlenmeyer flasks. At OD_{600} 0.4-0.6, 0 mM – 500 mM urea was added to flasks in duplicate, with growth proceeding for a further 24 h.

To monitor the effect of urea on growth at 100 mL scale, biomass accumulation was monitored via OD_{600} and cell density via FCM (Figure 3.26A and 3.26C). While cultures induced with 500 mM urea appeared to have slightly lower OD_{600}, particularly at 4 h and 24 h post-induction (Figure 3.26A), cell density measurements indicated there was a negligible difference; all cultures irrespective of the concentration of urea added reached over $1.00x10^{10}$ cells mL^{-1} (Figure 3.26C). Specific growth rates were calculated from OD_{600} (Figure 3.26B) and cell density (Figure 3.26D) and further highlight the little difference between concentrations of urea. Mean FSC of untransformed cultures was analysed by FCM (Figure 3.26E). Under all conditions, mean FSC decreased from induction at approximately 25000, to around 11000 by 2 h post-induction; mean FSC was stable from this point through until 24 h post-induction. Even addition of 500 mM urea had little effect on BL21 and was not significantly different from the untreated control; this was consistent with what was observed at 50 mL scale (Figure 3.4B). Thus in the absence of 6xHis::GFP expression, up to 500 mM urea had little effect on BL21 physiology under scaled-up conditions (Figure 3.26).

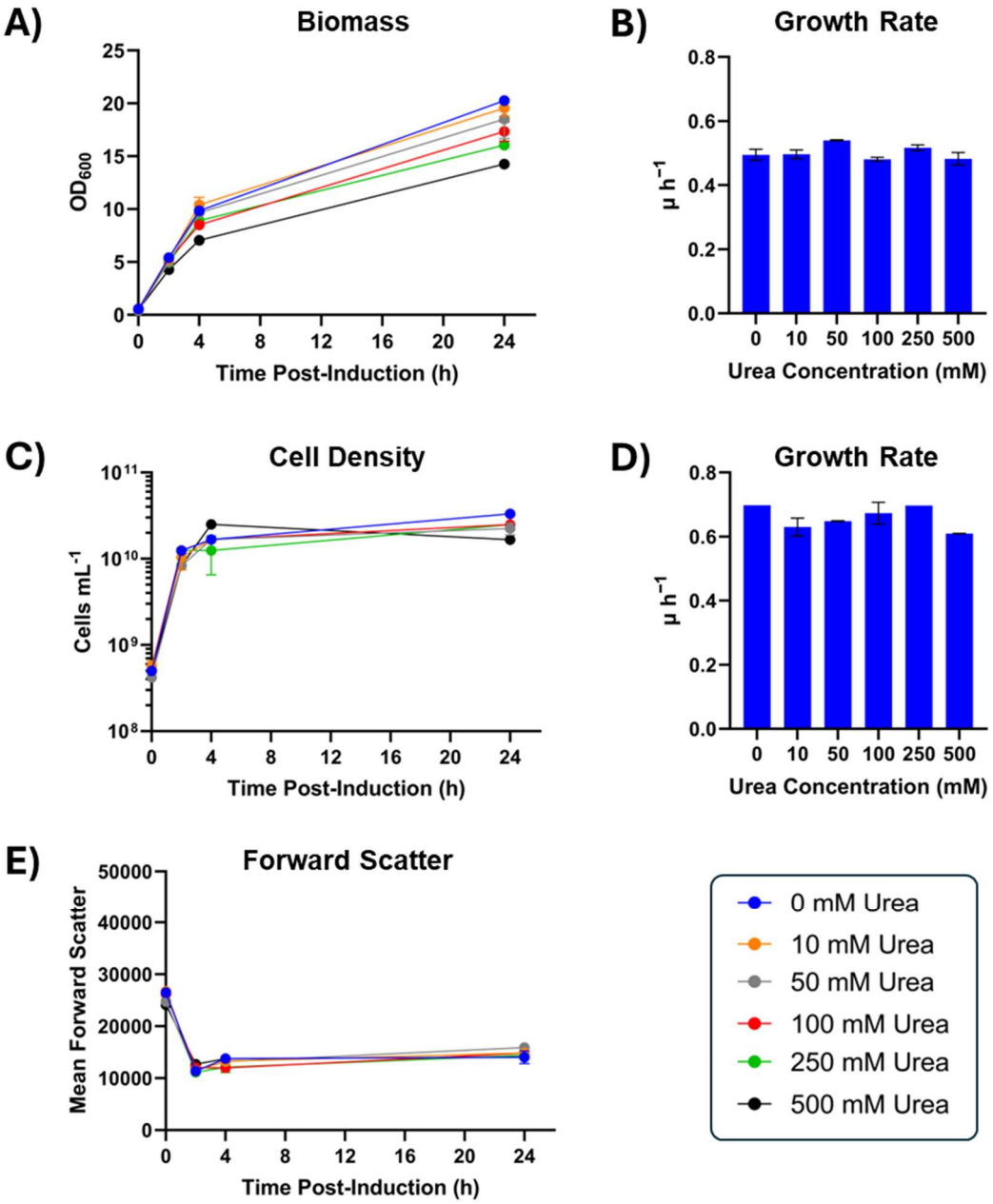


Figure 3.26: Analysis of the effect of urea on untransformed BL21 during scale-up.

To uncouple the effect of urea from 6xHis::GFP expression, untransformed BL21 was aerated in 100 mL TB in baffled Erlenmeyer flasks at 37 °C, 150 rpm. At OD_{600} 0.4-0.6, urea was added to cultures in duplicate for each concentration. Error bars represent +/- SD from biological duplicates. Plots **(A)**, **(C)** and **(E)** use the same legend (bottom right).

OD_{600} was monitored throughout **(A)**; some difference in biomass was observed, particularly in cultures treated with 500 mM urea. At 24 h post-induction, there was a clear correlation between OD_{600}, and the concentration of urea added. Specific growth rate ($\mu\ h^{-1}$) **(B)** was calculated from OD_{600} (0 – 2 h post-induction) and indicated little difference between conditions. Cell density was monitored via FCM **(C)**. While OD_{600} appeared to correlate with urea concentration, there was little difference in cells mL^{-1} between conditions; at 4 h post-induction cell density was highest in cultures treated with 500 mM urea. Specific growth rate ($\mu\ h^{-1}$) **(D)** was also calculated from cells mL^{-1} (0 – 2 h post-induction) and indicated little difference between conditions. Mean FSC was analysed using FCM **(E)**; little difference was apparent in untransformed BL21 treated with 0 mM – 500 mM urea.

3.4.3 P_{uti101} reproducibility in TB medium

BL21 biomass accumulation and growth rates appeared increased using baffled flasks and TB medium (section 3.4.1) and thus it was of interest to see whether improved physiology at scale led to increased 6xHis::GFP expression from P_{uti101}. BL21 containing pET-15b-P_{uti101}-*6xhis*::*gfp* was aerated at 37 °C, 150 rpm in 100 mL TB in baffled Erlenmeyer flasks. At OD_{600} 0.4-0.6, 6xHis::GFP production was induced in duplicate, using 0 mM – 500 mM urea; with overexpression continuing for a further 24 h. Two repeat experiments (Exp 1 and Exp 2) using the same conditions were performed.

Biomass accumulation and cell density of BL21 were monitored by OD_{600} and FCM respectively (Figure 3.27A and 3.27B). OD_{600} was far higher than at 50 mL scale (Figure 3.19A), reaching around 15-25 depending on the condition, although there was little discernible pattern (Figure 3.27A). In both experiments, cultures induced with 500 mM urea were lowest between induction and 4 h post-induction, but difference were negligible, and these cultures were higher than uninduced controls at 24 h post-induction. We had noted at 50 mL scale the poor concentration between $OD_{600,}$ and the concentration of urea used in BL21 (Figure 3.19); this was attributed to increases in cell size (predicted based on forward scatter) found at higher urea concentrations (see section 3.2.2).

Cell density measurements were more revealing (Figure 3.27B); cells mL^{-1} inversely correlated with the concentration of urea used; cultures induced with 500 mM displayed impaired growth for example. Cultures generally reached cell densities around

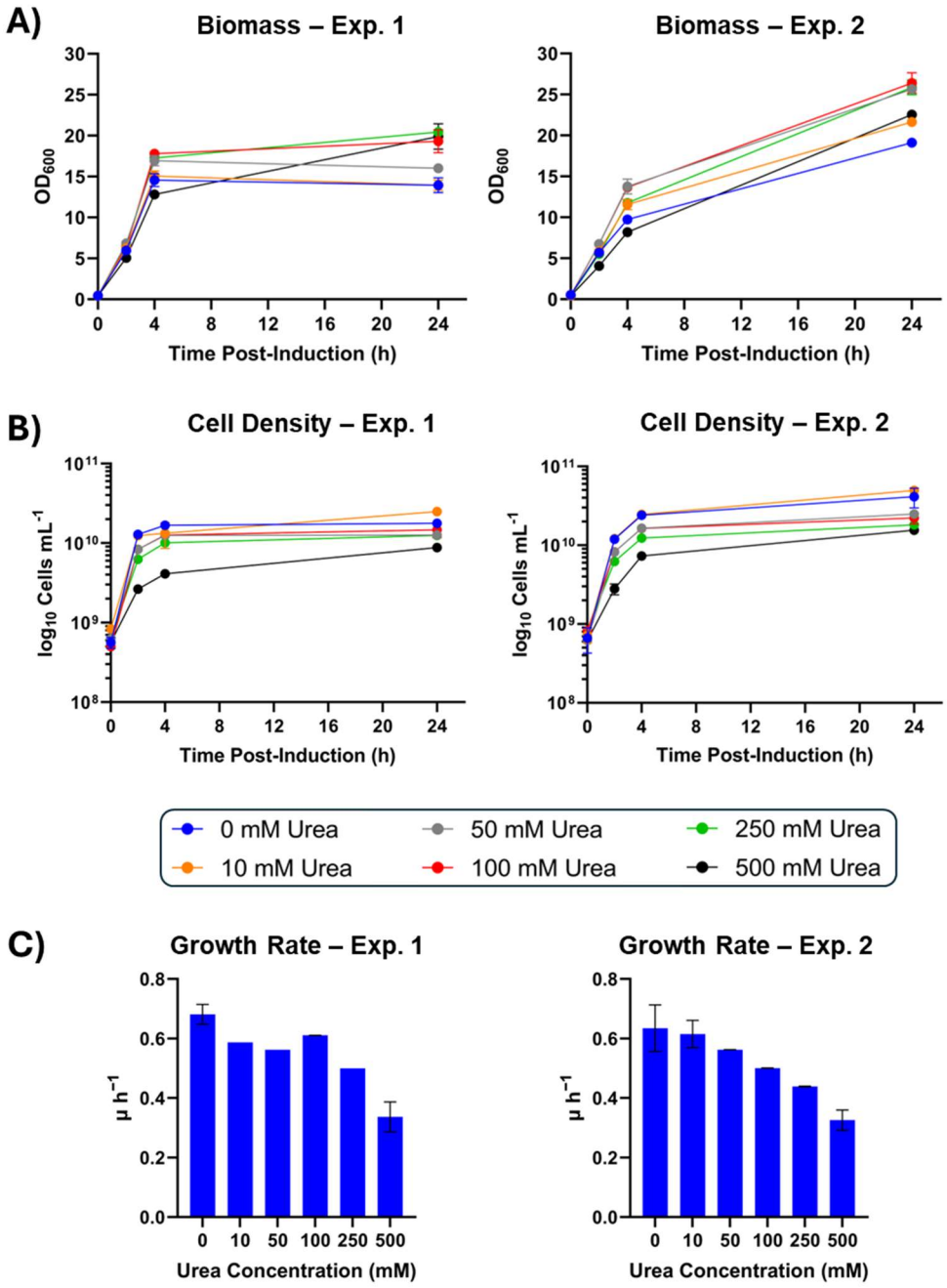


Figure 3.27: Growth data of induced BL21 carrying the pET-15b-P*uti101*-*6xhis::gfp* construct during scale-up.

BL21 carrying the pET-15b-P*uti101*-*6xhis::gfp* construct was aerated in 100 mL TB + Amp in baffled Erlenmeyer flasks at 37 °C, 150 rpm. At OD_{600} 0.4-0.6, 6xHis::GFP expression was induced with urea, added to cultures in duplicate for each concentration. Error bars represent +/- SD from biological duplicates. Data for two repeated experiments is shown, Exp 1 and Exp 2.

Biomass accumulation was monitored via OD_{600} **(A)** and no clear pattern was observed, with uninduced cultures having the lowest OD_{600} at 24 h post-induction. Cell density was monitored via FCM **(B)** and was broadly similar between cultures induced with 10 mM – 250 mM urea. Cultures induced with 500 mM urea appeared to have some growth arrest after induction, but cell density increased to a level comparable with other conditions by 24 h post-induction. Specific growth rates ($\mu\ h^{-1}$) **(C)** were calculated from cell density and were lowest in cultures induced with 500 mM urea. Interestingly, specific growth rate correlated with the concentration of urea used in Exp 2.

$2.00x10^{10}$ cells mL^{-1}. As OD_{600} did not appear to correlate well with the concentration of urea used (Figure 3.27A), cell density (Figure 3.27B) was used to calculated specific growth rate (Figure 3.27C). Specific growth rate appeared lowest in cultures induced with 500 mM urea. Interestingly, in experiment 2, specific growth rate inversely correlated with the concentration of urea used; this was not as clear in experiment 1. Overall, growth rates were improved in scale up for BL21 overexpressing 6xHis::GFP; for reference inducing with 500 mM urea at 50 mL scale, a specific growth rate of around 0.25 $\mu\ h^{-1}$ was observed (Figure 3.6C); at 100 mL scale this was around 0.35 $\mu\ h^{-1}$ (Figure 3.27C).

Mean forward scatter (FSC) was monitored via FCM following induction with urea (Figure 3.28A); a similar pattern was observed in both experiments. Mean FSC in uninduced cultures was comparable, at around 22000 AU. In cultures induced with 0 mM – 100 mM urea, mean FSC decreased between induction and 2 h post-induction to around 12000 AU. Mean FSC of cultures induced with 0 mM – 10 mM urea remained low at 4 h post-induction, while cultures induced with 50 mM – 100 mM urea increased to levels seen in 250 mM urea cultures, which had remained more stable or increased between induction and 2 h post-induction at around 25000 AU. Mean FSC of cultures induced with 500 mM urea increased massively to around 35000 – 40000 by 4 h post-induction (Figure 3.28A). Overall, at 100 mL scale, like at 50 mL scale (Figure 3.21), there was a clear correlation between the concentration of urea used and mean FSC of cultures. At 50 mL scale, we attributed this in section 3.2.2 and 3.3.2 to the observation that in BL21, cells overexpressing 6xHis::GFP had increased cell size; something similar involving multiple physiological effects presumably occurred at 100

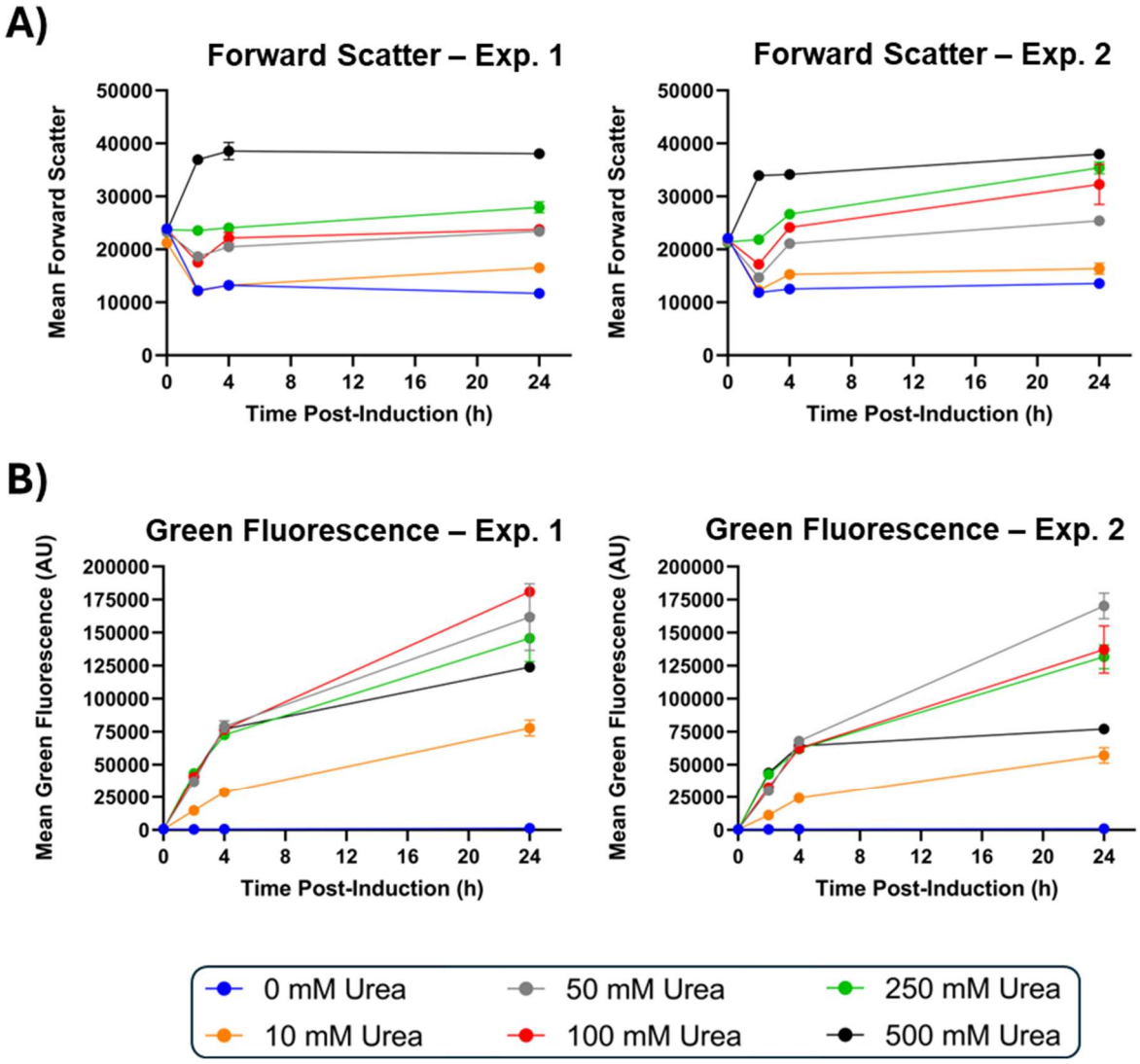


Figure 3.28: FCM data of induced BL21 carrying the pET-15b-P$_{uti101}$-*6xhis::gfp* construct during scale-up.

BL21 carrying the pET-15b-P$_{uti101}$-*6xhis::gfp* construct was aerated in 100 mL TB + Amp in baffled Erlenmeyer flasks at 37 °C, 150 rpm. At OD_{600} 0.4-0.6, 6xHis::GFP expression was induced with urea, added to cultures in duplicate for each concentration. Error bars represent +/- SD from biological duplicates. Data for two repeated experiments is shown, Exp 1 and Exp 2.

(A) Mean forward scatter of cultures was monitored via FCM and the concentration of urea used for induction correlated with higher FSC. Inducing with concentrations of urea over 250 mM prevented a drop in FSC between 0 h and 2 h post-induction seen at lower concentrations.

(B) Mean green fluorescence of cultures was monitored via FCM and based this, P$_{uti101}$ showed little dose dependence when inducing 6xHis::GFP expression with concentrations above 10 mM urea. At 24 h post-induction, cultures induced with 50 mM – 100 mM urea had higher mean green fluorescence.

mL scale too. For example, during RPP host cells are subjected to various stressors (section 1.4.2), in addition to effects high concentrations of solute like urea (500 mM) may cause (Record Jr et al., 1998, Jeong and Lee, 2003, Justice et al., 2008). Analysis of single cells via FCM indicated little heterogeneity in FSC when inducing with 0 mM – 100 mM urea (Figure 3.29). In cultures induced with 250 mM – 500 mM urea, multiple populations of lower and higher FSC were present at 4 h or 24 h post-induction. Raw FSC data for histograms is provided in Chapter 8 – Appendix for experiment 1 (Table 8.12) and experiment 2 (Table 8.13) further highlights the heterogeneity in FSC at 24 h post-induction in cultures induced with 250 mM – 500 mM urea (mean CV = 45 – 86%).

To see whether 6xHis::GFP expression from P_{uti101} increased through scale-up, mean green fluorescence was monitored by FCM (Figure 3.28B) and indicated similar patterns of 6xHis::GFP expression in both replicate experiments. Uninduced cultures had low mean green fluorescence throughout all 24 h. Between 0 h and 4 h post-induction, mean green fluorescence was similar in cultures induced with over 50 mM urea, reaching around 70000 – 75000 AU. In all conditions tested, mean green fluorescence was highest at 24 h post-induction; the highest observed was in cultures induced with 100 mM urea in experiment 1, reaching over 180000 AU. In experiment 2, cultures induced with 50 mM urea reached the highest mean green fluorescence, reaching 170000 AU at 24 h post-induction; this was much higher than at 50 mL scale (Figure 3.22A). Even at 24 h post-induction though, there was little difference in mean green fluorescence between cultures induced with 50 mM – 250 mM urea; thus, similarly to 50 mL scale (Figure 3.22A), P_{uti101} showed little dose dependence. It was

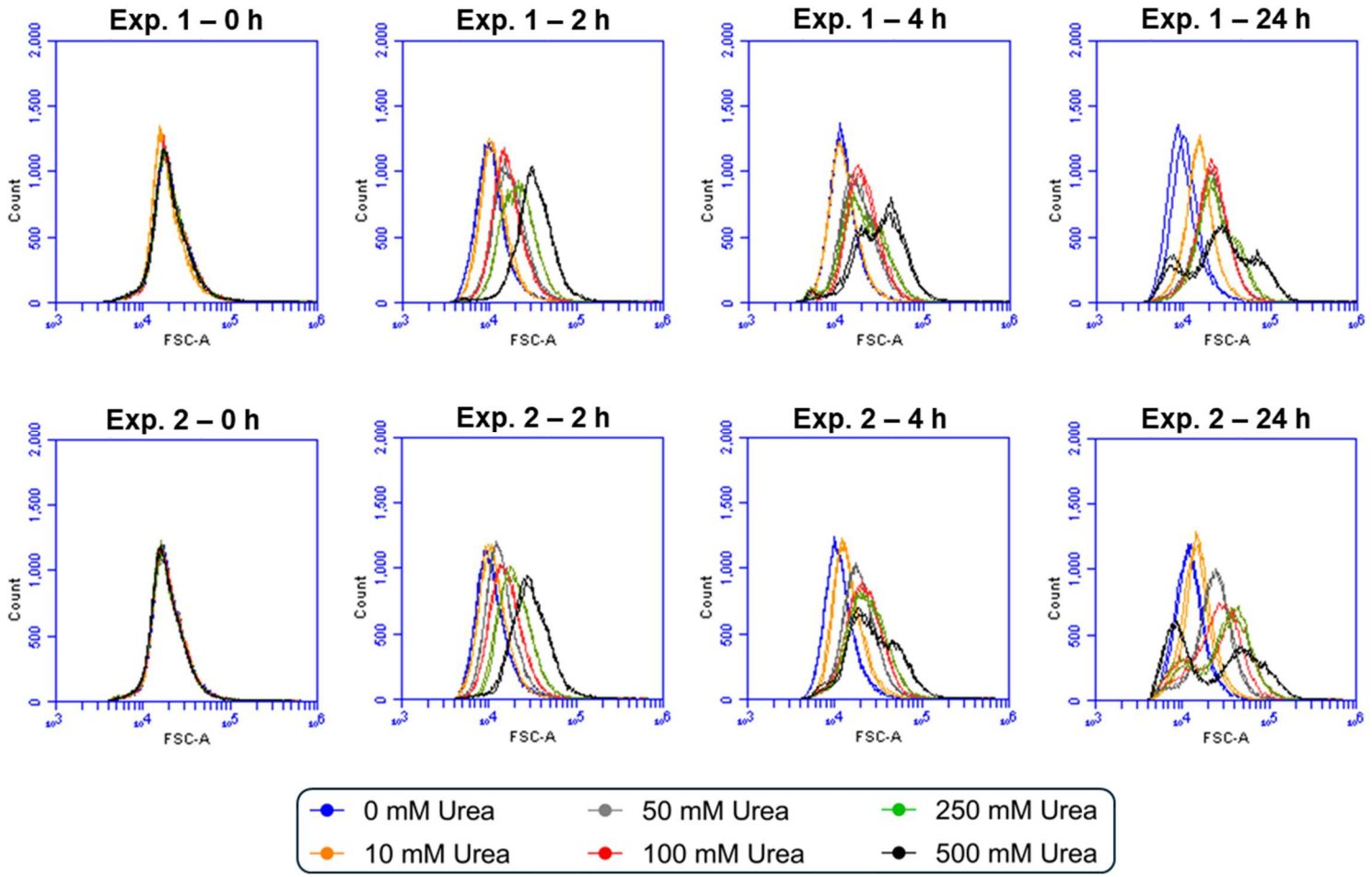


Figure 3.29: Forward scatter (FSC) data of induced BL21 carrying the pET-15b-P*uti101*-*6xhis::gfp* construct during scale-up.

BL21 carrying the pET-15b-P*uti101*-*6xhis::gfp* construct was aerated in 100 mL TB + Amp in baffled Erlenmeyer flasks at 37 °C, 150 rpm. At OD_{600} 0.4-0.6, 6xHis::GFP expression was induced with urea, added to cultures in duplicate for each concentration. Each concentration of urea is shown for biological duplicates. Data for two repeated experiments is shown, Exp 1 (top panel) and Exp 2 (bottom panel). Analysis of FSC in single cells via FCM indicated cultures induced with 0 mM – 250 mM urea were mostly single populations at 0 h to 4 h post-induction. Multiple populations were apparent in cultures induced with 500 mM urea at 4 h post-induction. At 24 h post-induction, cultures induced with over 250 mM urea had two populations of lower and higher FSC.

noted though that induction with 500 mM urea did appear to negatively affect mean green fluorescence; at 24 h post-induction, these cultures had lower mean green fluorescence than 50 – 250 mM urea cultures. Further, cultures induced with 10 mM urea had lower mean green fluorescence than all other conditions throughout. This diverged from that seen at 50 mL scale (Figure 3.22A), where cultures induced with 10 mM or 100 mM urea had similar mean green fluorescence. We attributed this to the improved growth conditions at scale (as seen for cell density in Figure 3.27B); at lower urea concentrations there is not sufficient urea available to compensate for increased biomass over time. Thus, it seemed apparent there was a tighter optimal range of urea concentrations required to maximise 6xHis::GFP expression (50 mM – 250 mM) at 100 mL than compared with 50 mL scale.

FCM analysis at the single-cell level indicated green fluorescence (FL1-A) of cell populations was homogenous in cultures induced with over 50 mM urea, between induction and 4 h post-induction (Figure 3.30). Cultures induced with 10 mM urea were more widely distributed but were still a single population of green fluorescent cells. At 24 h post-induction, there was more heterogeneity; populations of lower green fluorescence were apparent in all induced cultures and comparable to that of the uninduced controls. Interestingly, cultures induced with 500 mM urea not only had the largest low green fluorescence populations, but these populations were of lower than the uninduced controls. This is indicative of cells that had lost pET-15b-P_{uti101}-*6xhis*::*gfp* due to the burden associated with RPP and segregation instabilities (Sevastsyanovich et al., 2009); or mutations causing loss of GFP from the construct. However, this would need to be confirmed via replica plating to confirm plasmid loss

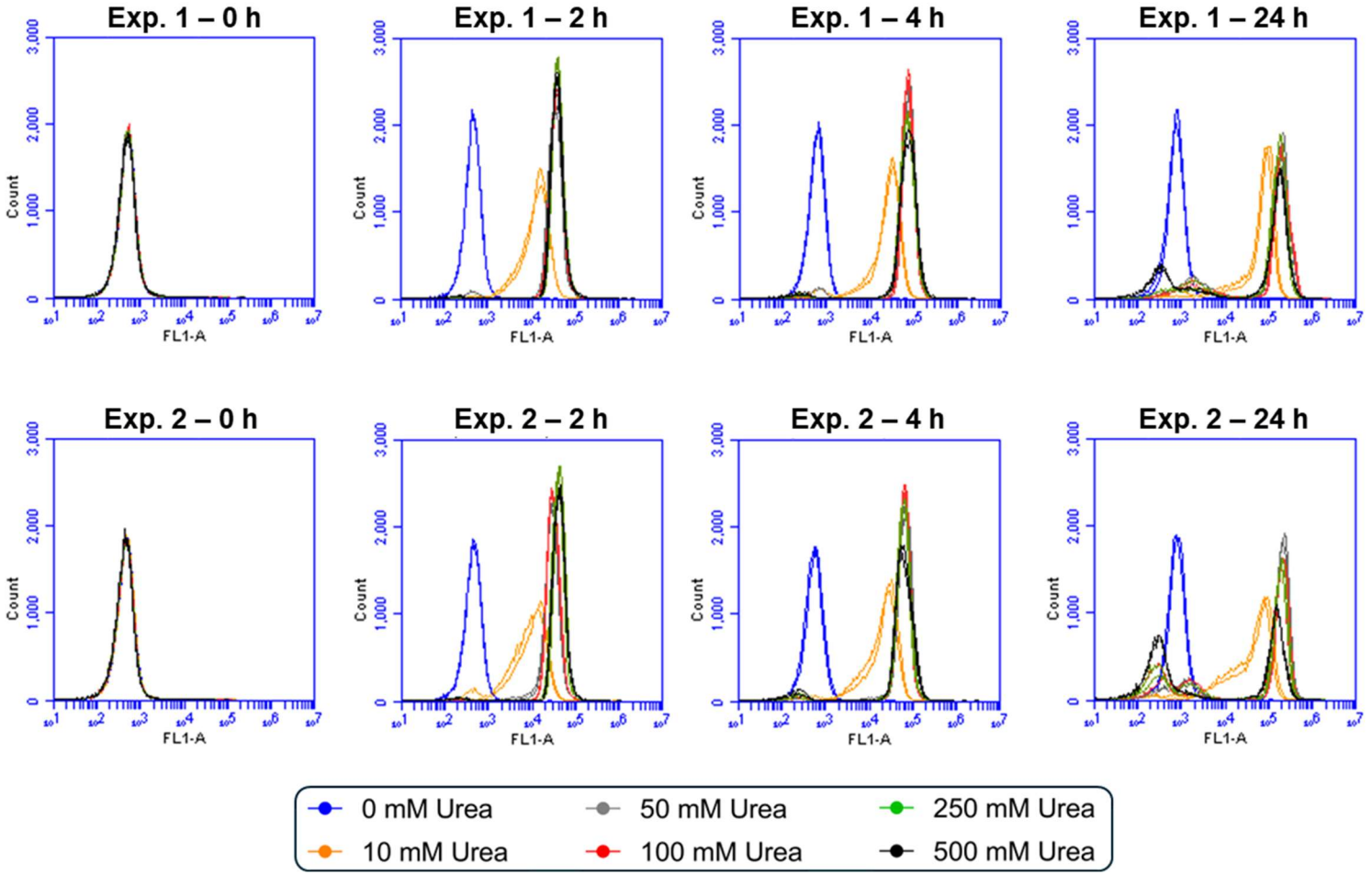


Figure 3.30: Green fluorescence (FL1-A) data of induced BL21 carrying the pET-15b-P*uti101*-*6xhis::gfp* construct during scale-up.

BL21 carrying the pET-15b-P*uti101*-*6xhis::gfp* construct was aerated in 100 mL TB + Amp in baffled Erlenmeyer flasks at 37 °C, 150 rpm. At OD_{600} 0.4-0.6, 6xHis::GFP expression was induced with urea, added to cultures in duplicate for each concentration. Each concentration of urea is shown for biological duplicates. Data for two repeated experiments is shown, Exp 1 (top panel) and Exp 2 (bottom panel). Analysis green fluorescence (FL1-A) in single cells via FCM indicated cultures induced with 50 mM – 500 mM were normally distributed and mostly single populations at 0 h to 4 h post-induction. By 24 h post-induction mixed populations of high and low green fluorescence were evident in all cultures induced with urea.

or sequencing purified constructs. Raw green fluorescence (FL1-A) data for histograms is provided in Chapter 8 – Appendix for experiment 1 (Table 8.14) and experiment 2 (Table 8.15) further highlights the heterogeneity (CV%) in green fluorescence at 24 h post-induction in cultures induced with 50 mM – 500 mM urea.

Given there was considerable heterogeneity in green fluorescence profiles at 24 h post-induction in cultures induced with 50 mM – 500 mM urea (Figure 3.30), we wanted to quantify the proportion of cells in cultures that were productive and overexpressing 6xHis::GFP. Density plots of FSC (FSC-A) against green fluorescence (FL1-A) were used to create low and high green fluorescence gates and quantify the proportion of cells within each. Data is shown for the proportion of cells (%) within each culture residing in the high green fluorescence gate (GFP+) (Figure 3.31). Predictably, the proportion of cells in uninduced cultures (0 mM urea) remained under 1 % throughout. Following induction, around 90 – 95% of cells were within the GFP+ gate between 2 h and 4 h post-inoculation for all conditions. By 24 h post-induction, proportion of cells within the GFP+ gate had dropped to around 80% for cultures induced with 50 mM – 250 mM urea; in cultures induced with 500 mM urea, this was around 50 – 60 %. Comparatively, in cultures induced with 10 mM urea, the proportion of cells within the GFP+ gate was around 95% at 24 h post-induction (Figure 3.31). This was attributed to improved growth (Figure 3.27) over that seen at 50 mL scale (Figure 3.19) and higher 6xHis::GFP expression when inducing at concentrations of urea over 10 mM (Figure 3.28B). Higher cell densities would have degraded the ampicillin (Amp) selectable marker more rapidly and coupled with increased stress from more intensified RPP and growth, would mean plasmid free cells were favoured.

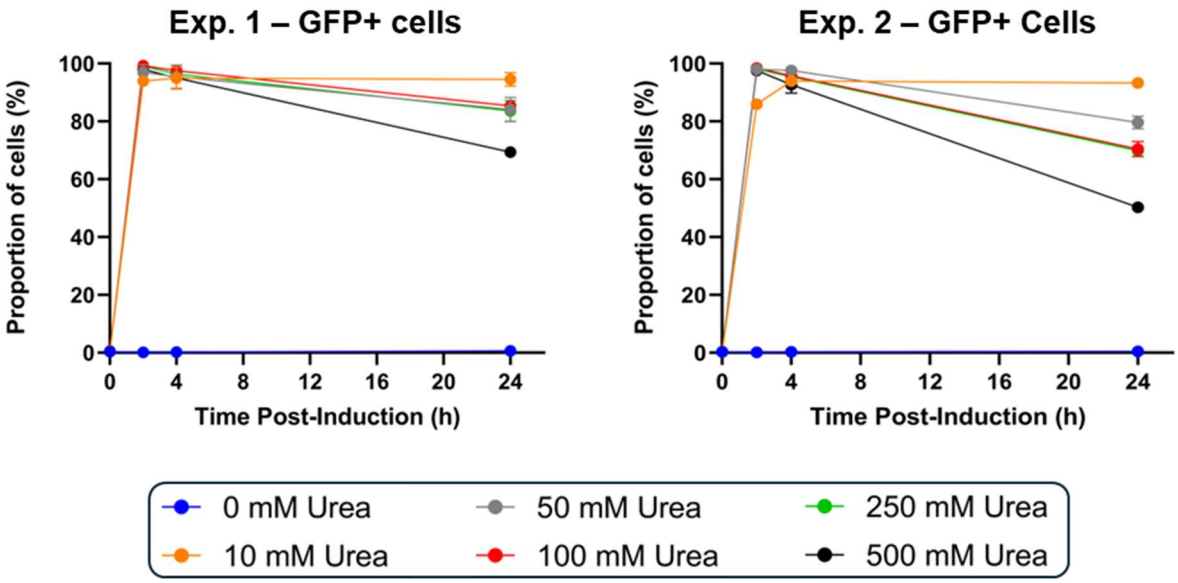


Figure 3.31: FCM gating of induced BL21 carrying the pET-15b-P$_{uti101}$-*6xhis::gfp* construct during scale-up.

BL21 carrying the pET-15b-P$_{uti101}$-*6xhis::gfp* construct was aerated in 100 mL TB + Amp in baffled Erlenmeyer flasks at 37 °C, 150 rpm. At OD_{600} 0.4-0.6, 6xHis::GFP expression was induced with urea, added to cultures in duplicate for each concentration. Error bars represent +/- SD from biological duplicates. Data for two repeated experiments is shown, Exp 1 and Exp 2.

Green fluorescence of cultures was monitored using FCM. Density plots of forward scatter (FSC-A) against green fluorescence (FL1-A) were used to create low and high green fluorescence gates and the proportion of cells within each gate calculated. Data is shown for the proportion of cells within each culture residing in the high green fluorescence gate (GFP+). In both experiments, around 90 % of BL21 cells induced with urea were within the GFP+ gate till 4 h post-induction. By 24 h post-induction, addition of higher concentrations of urea seemed to correlate with a lower percentage of cells within the GFP+ gate.

3.4.4 BL21 Seed Cultures in TB medium

In BL21, background expression from P_{uti101} in the absence of urea appeared low during growth in TB at 100 mL scale, with little increase in green fluorescence over 24 h (Figure 3.28B). Basal expression in seed cultures was found to be low at 50 mL scale using LB medium (Figure 3.23A), but we wanted to confirm this was also true when TB was used at the seed stage and check BL21 seed culture growth against untransformed cells. Seed cultures of BL21 harbouring the pET-15b-P_{uti101}-*6xhis*::*gfp* construct were grown in 10 mL TB + Amp at 37 °C, 200 rpm for 16 – 18 h. Seed cultures of untransformed BL21 were grown in 10 mL TB at 37 °C, 200 rpm for 16 – 18 h.

To check basal expression in TB medium, FCM was used to gate cells as low (GFP-) or high (GFP+) green fluorescence using forward scatter (FSC-A) against green fluorescence (FL1-A) density plots and the proportion of cells within each gate calculated (Figure 3.32A). Basal expression of 6xHis::GFP from P_{uti101} appeared low in BL21 seed cultures grown in TB. Of those analysed, all had over 97% of cells within the GFP- gate, with the majority being over 99%. Biomass accumulation (Figure 3.32B) and cell density (Figure 3.32C) were also monitored in seed cultures, measured by OD_{600} and FCM respectively. Both were consistent across all seed cultures monitored; OD_{600} generally reached around 4.0 and cell density saturated at approximately 4.00E+09 cells mL^{-1}. OD_{600} and cell density were lower in seed cultures than shake flasks (Figure 3.27A-B); this was expected though as baffled Erlenmeyer flasks provide a larger surface area for oxygen exchange into the culture. Crucially, there was little difference in OD_{600} or cell density between seed cultures of BL21 harbouring the pET-15b-P_{uti101}-*6xhis*::*gfp* construct and seed cultures of untransformed BL21 (3.32B-C).

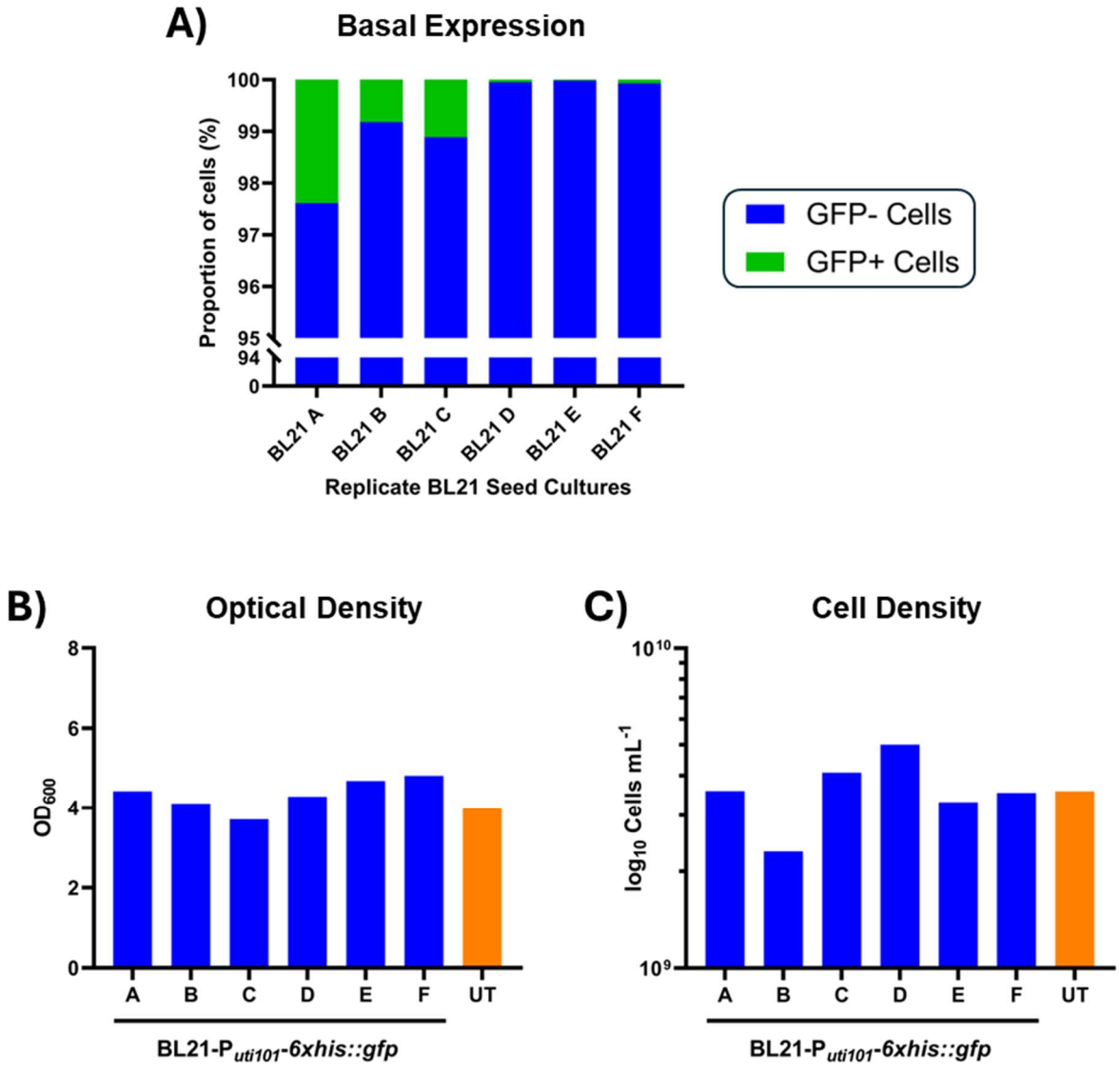


Figure 3.32: Analysis of BL21 seed cultures harbouring the pET15b-P*uti101*-*6xhis::gfp* construct in TB during scale-up.

Seed cultures of BL21 harbouring the pET15b-Puti101-6xhis::gfp construct were grown in 10 mL TB + Amp at 37 °C, 200 rpm for 16 – 18 h. Where provided for comparison with transformed strains, untransformed BL21 were grown in 10 mL TB at 37 °C, 200 rpm for 16 – 18 h.

(A) To monitor basal expression of 6xHis::GFP from P*uti101*, seed cultures were analysed using FCM and green fluorescence measured. Gates for low (GFP-) and high (GFP+) green fluorescence were created on forward scatter (FSC-A) vs. green fluorescence (FL1-A) plots using untransformed, uninduced and induced BL21 controls. Values for GFP- and GFP+ represent the proportion of cells (%) within each gate for six biological replicate BL21 seed cultures (A-F). Each data point is for one biological replicate seed culture. Basal expression was tight during overnight growth in TB, with all seed cultures analysed having over 97% of cells within the GFP- gate; half being over 99%.

(B-C) Growth of seed cultures of BL21 harbouring the pET15b-P*uti101*-*6xhis::gfp* construct (blue) was monitored and compared with untransformed BL21 (orange). Each data point is for one biological replicate seed culture. Biomass accumulation was measured via OD_{600} **(B)** and cell density via FCM **(C)**. For both, BL21 seed cultures of cells containing the pET15b-P*uti101*-*6xhis::gfp* construct were comparable to untransformed variants.

3.4.5 Basal expression from P_{uti101} in TB medium

During scale-up, low green fluorescence was observed in uninduced BL21 pET15b-P_{uti101}-*6xhis::gfp* cultures throughout growth (Figure 3.28B) and was comparable to that seen at 50 mL scale (Figure 3.22A). To fully understand how tight regulation of P_{uti101} was at 100 mL scale, BL21 pET15b-P_{uti101}-*6xhis::gfp* transformants were compared with untransformed BL21. Cultures of each were aerated in 100 mL TB (+ Amp for transformed cultures) using baffled flasks at 37 °C, 150 rpm. Cultures were not induced with urea, growth proceeded for 24 h after reaching OD_{600} 0.4-0.6. Data is shown for two replicate cultures of untransformed BL21 and four replicate cultures of transformed BL21.

Mean green fluorescence from duplicate cultures of untransformed BL21 was measured via FCM and compared to uninduced cultures of BL21 pET15b-P_{uti101}-*6xhis::gfp* (Figure 3.33A). In untransformed BL21, mean green fluorescence was stable over all 24 h, at around 200 AU; this was virtually the same as at 50 mL scale (Figure 3.24B). In transformed BL21, mean green fluorescence of uninduced cultures was similar at approximately 500-800 AU; this was only 3 to 4-fold higher than untransformed variants. Mean green fluorescence peaked at 24 h post-induction in transformed cultures.

To further quantify basal expression, FCM was used to gate cells as low or high green fluorescence using forward scatter (FSC-A) against green fluorescence (FL1-A) density plots. The proportion of cells (%) within the high green fluorescence gate (GFP+) are provided (Figure 3.33B). Untransformed BL21 had predictably 0% of cells

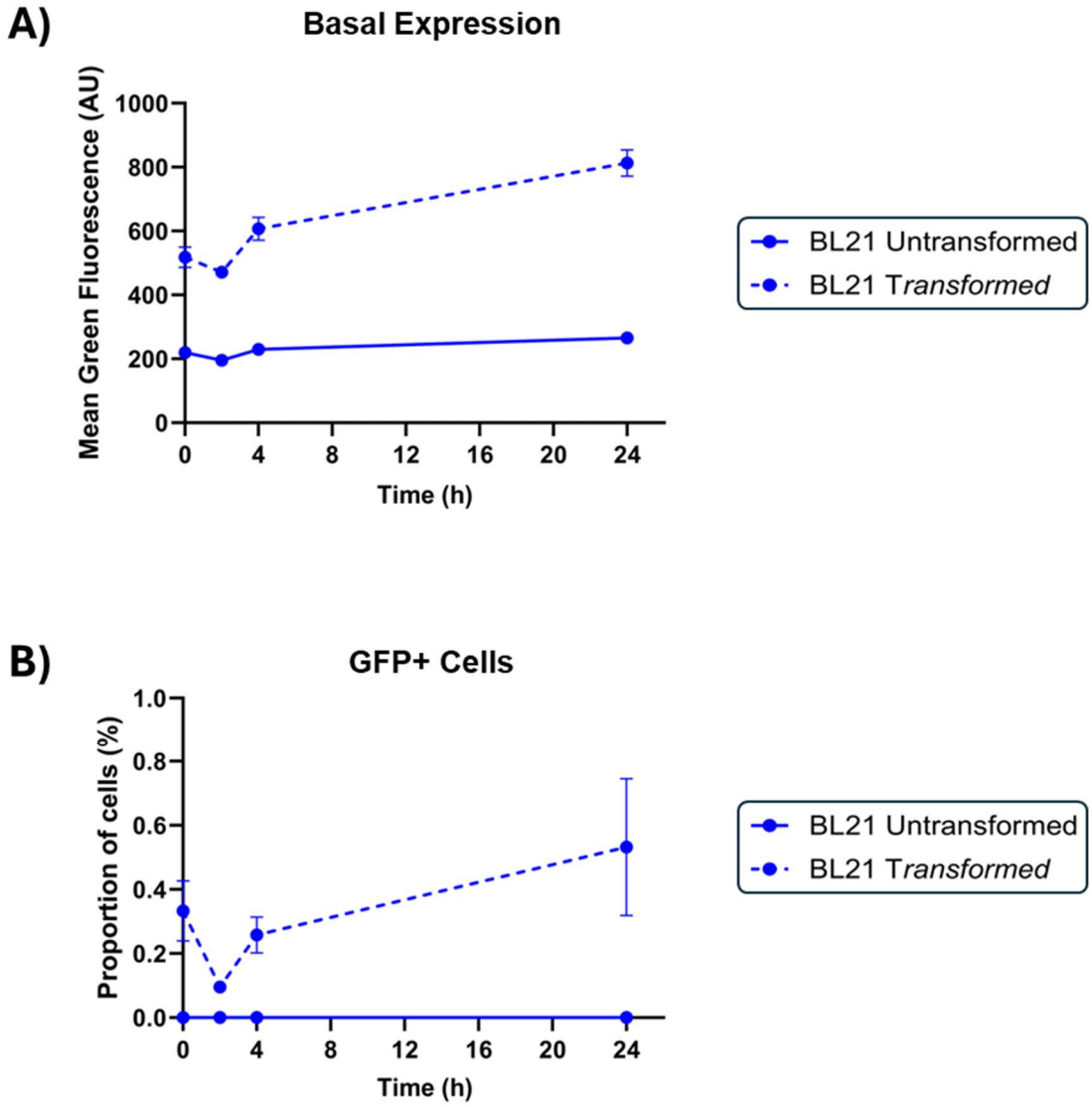


Figure 3.33: Basal expression of 6xHis::GFP from P_{uti101} in the absence of urea was monitored in BL21 during scale-up.

To monitor basal expression from P_{uti101} during scale-up using 100 mL TB and baffled flasks, transformed BL21 harbouring the pET15b-P_{uti101}-*6xhis::gfp* construct was compared with untransformed BL21. Transformed BL21 was grown in 100 mL TB + Amp in baffled Erlenmeyer flasks. Untransformed BL21 was grown in 100 mL TB in baffled Erlenmeyer flasks. Cultures were grown at 37 °C, 150 rpm.

(A) Mean green fluorescence was analysed using FCM. Basal expression from P_{uti101} in the absence of urea appeared very low; mean green fluorescence was only 2 to 3-fold higher in transformed cells. Error bars represent +/- SD from 4 biological replicates for transformed cells and 2 biological replicates for untransformed cells (too small to be visible in untransformed cultures).

(B) To further quantify basal expression, using FCM, density plots of forward scatter (FSC-A) against green fluorescence (FL1-A) were used to create low and high green fluorescence gates with the mean proportion of cells from replicates plotted over time. Regulation was tight throughout all 24 h, less than 1% of cells were in the high green fluorescence gate (GFP+). Error bars represent +/- SD from 4 biological replicates for transformed cells and 2 biological replicates for untransformed cells (too small to be visible in untransformed cultures).

within the GFP+ gate throughout all 24 h. Background expression of 6xHis::GFP from P_{uti101} was also very low in uninduced BL21 though; less than 1% of cells were within the GFP+ gate throughout all 24 h of growth. Proportions of transformed cells within the GFP+ gate was highest at 24 h and correlated with the higher mean green fluorescence observed at this time-point (Figure 3.33A).

3.4.6 Point of induction

Something not assayed at 50 mL scale was whether P_{uti101} could drive strong expression of 6xHis::GFP when induced during stationary phase growth of BL21. Uncoupling biomass accumulation from overexpression is often desirable if the protein of interest is toxic. Attempting to reach high cell densities while concurrently synthesising a protein inhibitory to the hosts growth is counterintuitive; the necessary concentrations of cells required will never be reached, limiting final yield. We knew basal expression from P_{uti101} was extremely low in the absence of urea, so if overexpression in stationary phase was comparable to log phase induction, the system could be an attractive option for synthesis of toxic proteins.

To test this, BL21 containing pET-15b-P_{uti101}-*6xhis*::*gfp* was aerated at 37 °C, 150 rpm in 100 mL TB + Amp using baffled Erlenmeyer flasks. Overexpression of 6xHis::GFP was induced with urea after growing cultures to approximately OD_{600} 0.5, 5 or 10; increasing concentrations of urea were used at higher OD_{600}, so that the strength of induction was relative to the concentration of cells at that point (Experiment 1). For cultures induced at OD_{600} = 0.5, 50 mM or 100 mM urea was added; for cultures induced at OD_{600} = 5, 250 mM or 500 mM urea was added; for cultures induced at

OD_{600} = 10, 500 mM or 1000 mM urea was added. Conditions were induced in duplicate, with overexpression continuing until 24 h post-induction. A control experiment was run in parallel to account for whether the higher concentrations of urea used to induce cultures at OD_{600} = 5 and 10 had a negative effect on 6xHis::GFP expression (Experiment 2). In this control experiment, cultures were induced at approximately OD_{600} 0.5, 5 or 10 using 50 mM or 100 mM urea, with all other parameters maintained.

Mean green fluorescence was monitored via FCM for experiment 1. Inducing P_{uti101} at OD_{600} = 5 and 10 was detrimental to 6xHis::GFP expression using higher concentrations of urea (Figure 3.34A). Cultures induced at OD_{600} 5 or 10 had significantly lower mean green fluorescence at all time-points following induction. Cultures induced at OD_{600} = 5 reached a maximum mean green fluorescence of around 20000 AU; for cultures induced at OD_{600} = 10, this was even lower at around 10000 AU (Figure 3.34A). Conversely, induction at OD_{600} = 0.5, mean green fluorescence was over 60000 AU, an up to 6-fold difference. The correlation between the density of cells at induction and the maximum mean green fluorescence at 24 h post-induction, favouring induction at OD_{600} = 0.5 (Figure 3.34A), was significant when analysed by one-way ANOVA (adjusted $p < 0.0001$ for all comparisons). Interestingly, for each induction condition (OD_{600} = 0.5, 5 or 10), mean green fluorescence for both concentrations of urea used was similar at 2 h and 4 h post-induction; however, the lower concentration was consistently higher at 24 h post-induction (Figure 3.34A).

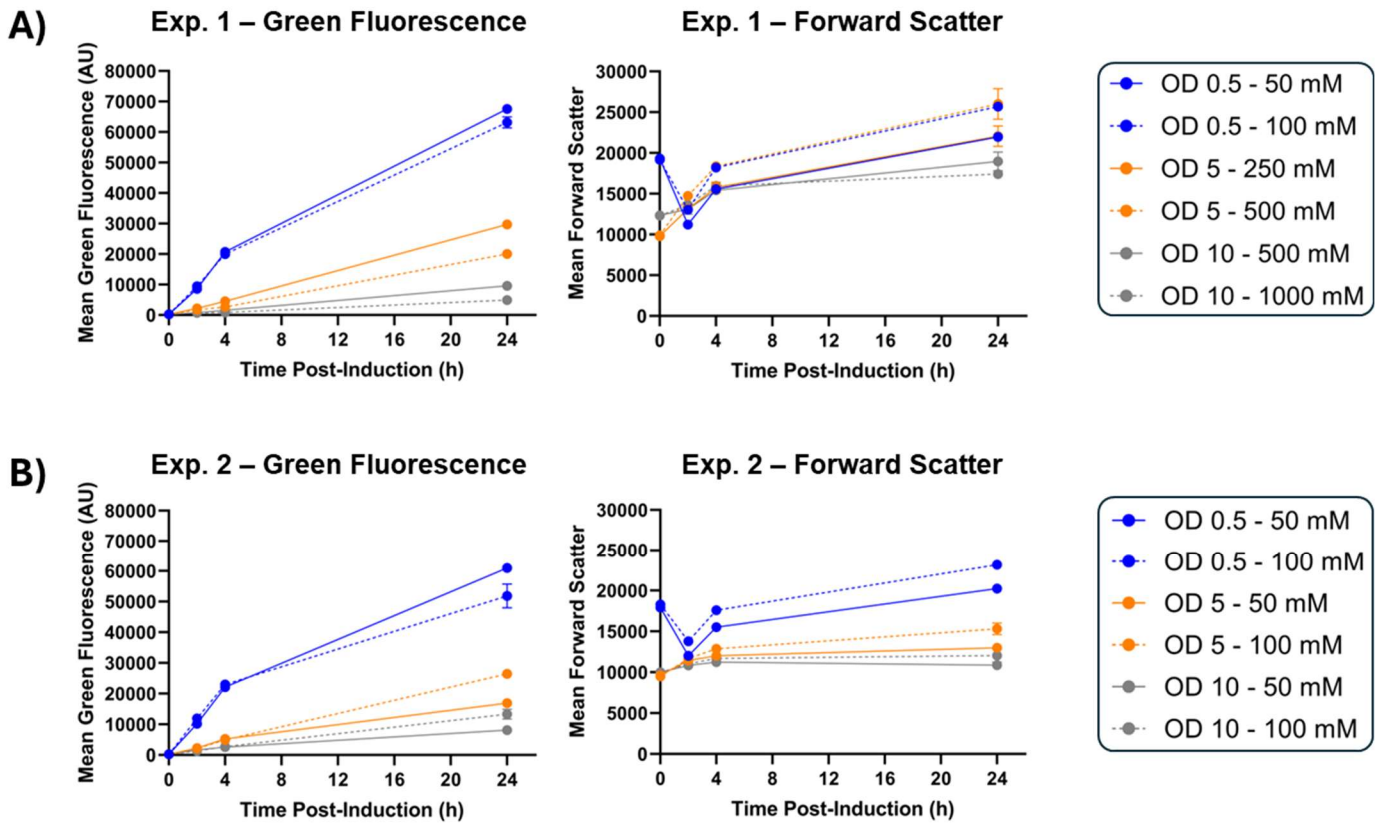


Figure 3.34: The effect of early and late induction on 6xHis::GFP expression was evaluated using FCM during scale-up.

BL21 carrying the pET-15b-P_{uti101}-*6xhis::gfp* construct was aerated in 100 mL TB + Amp in baffled Erlenmeyer flasks at 37 °C, 150 rpm. At OD_{600} = 0.5, 5 and 10, 6xHis::GFP expression was induced with urea in duplicate for each concentration. Data for two experiments is shown, Exp 1 **(A)** and Exp 2 **(B)**. Error bars represent +/- SD from 4 biological replicates.
(A) Exp 1 – BL21 was induced with the urea concentration scaled to the OD_{600} of the culture. Early induction at OD_{600} 0.5 produced much higher mean green fluorescence as measured via FCM. Mean forward scatter measured via FCM was similar between induction and 4 h post-induction in all cultures.

(B) Exp 2 – A control experiment for using high concentrations of urea in Exp 1, BL21 was induced with 50 mM or 100 mM urea. Mean green fluorescence measured via FCM indicated induction at OD_{600} 0.5 was better. Interestingly mean forward scatter also measured via FCM was also lower in cultures induced at a higher OD_{600}.

In experiment 2, reducing the urea concentration used for cultures induced at OD_{600} = 5 and 10 did little to improve 6xHis::GFP (Figure 3.34B). Mean green fluorescence of cultures measured using FCM was comparable to that seen when higher urea concentrations were used to induce cultures at OD_{600} = 5 and 10 (Figure 3.34A); thus, the high concentrations of urea used to induce cultures at OD_{600} = 5 and 10 in experiment 1 were presumably not responsible for poor expression of 6xHis::GFP. In experiment 2, mean green fluorescence was again over 3-fold lower in cultures induced at OD_{600} = 5 and 10 (Figure 3.34B); this was significant when analysed by one-way ANOVA at 24 h post-induction (adjusted $p < 0.0001$ for all comparisons). At all OD_{600} values used for induction, the two concentrations of urea used (50 mM and 100 mM) had little difference on mean green fluorescence at 2 h or 4 h post-induction.

Analysis of green fluorescence in single cells was checked in both experiment 1 and 2 using FCM, to confirm whether there was any heterogeneity in expression of 6xHis::GFP within the population. Regardless of the point of induction or concentration of urea used across both experiments, cultures were mostly homogenous with regards to green fluorescence (FL2-A) between induction and 4 h post induction (Figure 3.35). At 24 h post-induction, a second population of low green fluorescence was present in both experiments 1 and 2. Raw green fluorescence (FL1-A) data for histograms is provided in Chapter 8 – Appendix for experiment 1 (Table 8.16) and experiment 2 (Table 8.17) and further highlights the heterogeneity (CV%) in green fluorescence at 24 h post-induction in cultures.

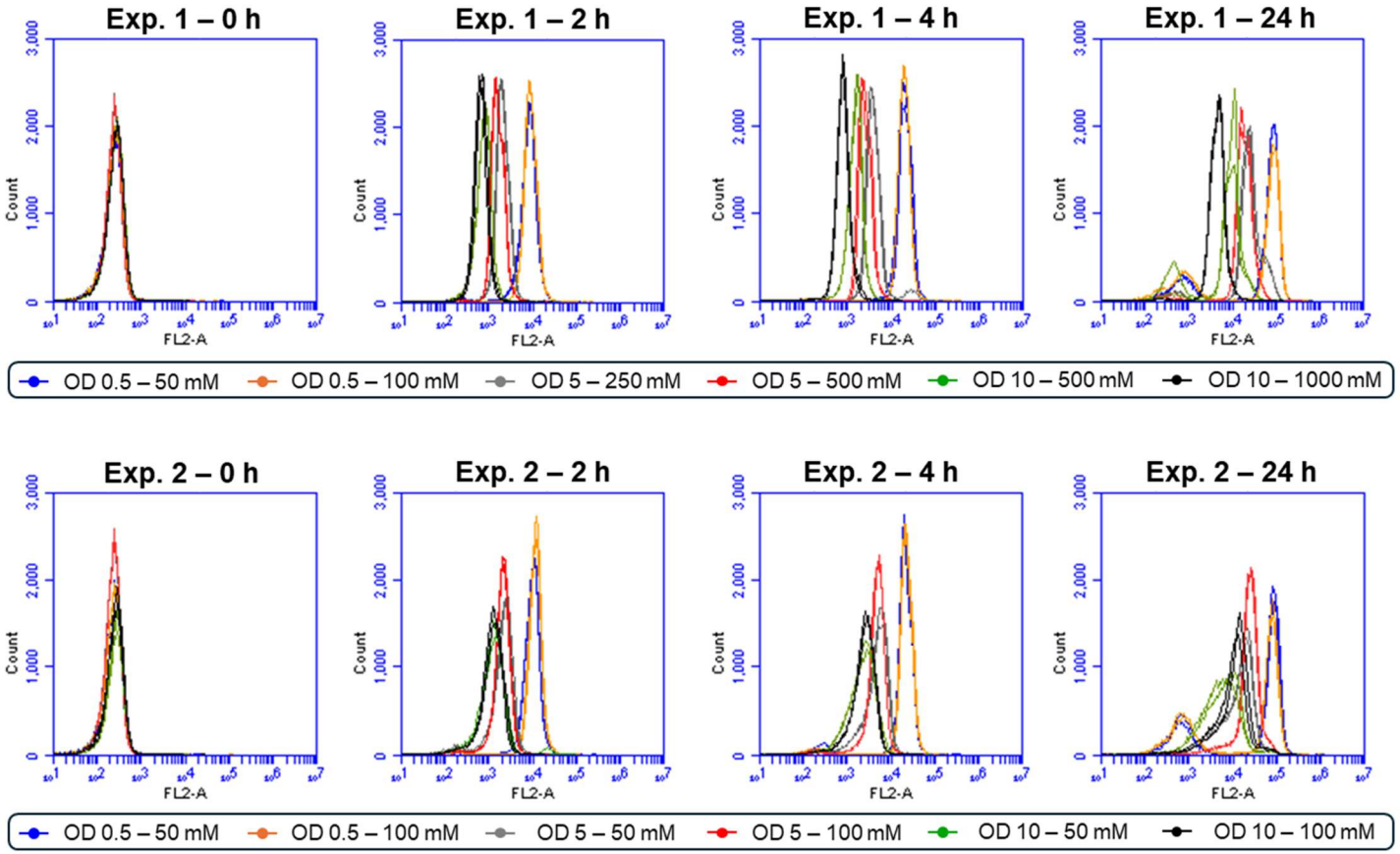


Figure 3.35: Histograms of green fluorescence (FL2-A) measured via FCM for Exp 1 and Exp 2 presented in Figure 3.34 A and Figure 3.34B.

BL21 carrying the pET-15b-P_{uti101}-*6xhis::gfp* construct was aerated in 100 mL TB + Amp in baffled Erlenmeyer flasks at 37 °C, 150 rpm. At OD_{600} = 0.5, 5 and 10, 6xHis::GFP expression was induced with urea. Data is shown for duplicate biological replicates. Data for two repeat experiments is shown, Exp 1 **(top panel)** and Exp 2 **(bottom panel)**.

Top panel Exp 1 – BL21 was induced with the urea concentration scaled to the OD_{600} of the culture. Cultures were mostly single populations until 24 h post-induction.

Bottom Panel Exp 2 – A control experiment for Exp 1, BL21 was induced with 50 mM or 100 mM urea. Cultures were mostly single populations until 24 h.

In both experiments 1 and 2, mean FSC was monitored by FCM to check physiology in response to induction of 6xHis::GFP at OD_{600} = 0.5, 5 or 10. In experiment 1, when inducing cultures at OD_{600} = 5 or 10 with higher urea concentrations mean FSC increased between induction and 2 h post-induction, unlike for cultures induced at OD_{600} = 0.5 (Figure 3.34A). However, this increase in FSC was not as big as that observed prior when adding 500 mM to cultures at OD_{600} = 0.4 – 0.6 (Figure 3.28A). It is possible cultures with higher biomass were more resistant to the effect of urea; alternatively, this was more likely due to lower 6xHis::GFP expression after inducing cells at higher OD_{600} (Figure 3.34) as this was previously shown to result in larger cells for BL21 (Figure 3.7B). To support this, at the single cell level, there was little heterogeneity in FSC when analysed by FCM, irrespective of the point of induction or concentration of urea used in either experiment 1 or 2 (Figure 3.36). Conversely for induction at OD_{600} = 0.4 – 0.6 in prior work, 500 mM urea was shown to produce multiple populations with different FSC (Figure 3.29). Raw forward scatter (FL1-A) data for histograms is provided in Chapter 8 – Appendix for experiment 1 (Table 8.18) and experiment 2 (Table 8.19) and further highlights the lower heterogeneity in FSC throughout (mean CV = 20-30%).

To monitor growth of cultures induced at OD_{600} = 0.5, 5 or 10, biomass accumulation and cell density were monitored by OD_{600} and FCM respectively (Figure 3.37). In experiment 1, inducing with urea at OD_{600} 0.5 or 5, biomass increased consistently between 0 h and 24 h post-induction (Figure 3.37A). For cultures induced at OD_{600} 10 in experiment 1, little increase in biomass was observed and it decreased between induction and 2 h post-induction (Figure 3.37A). Cell density increased in cultures

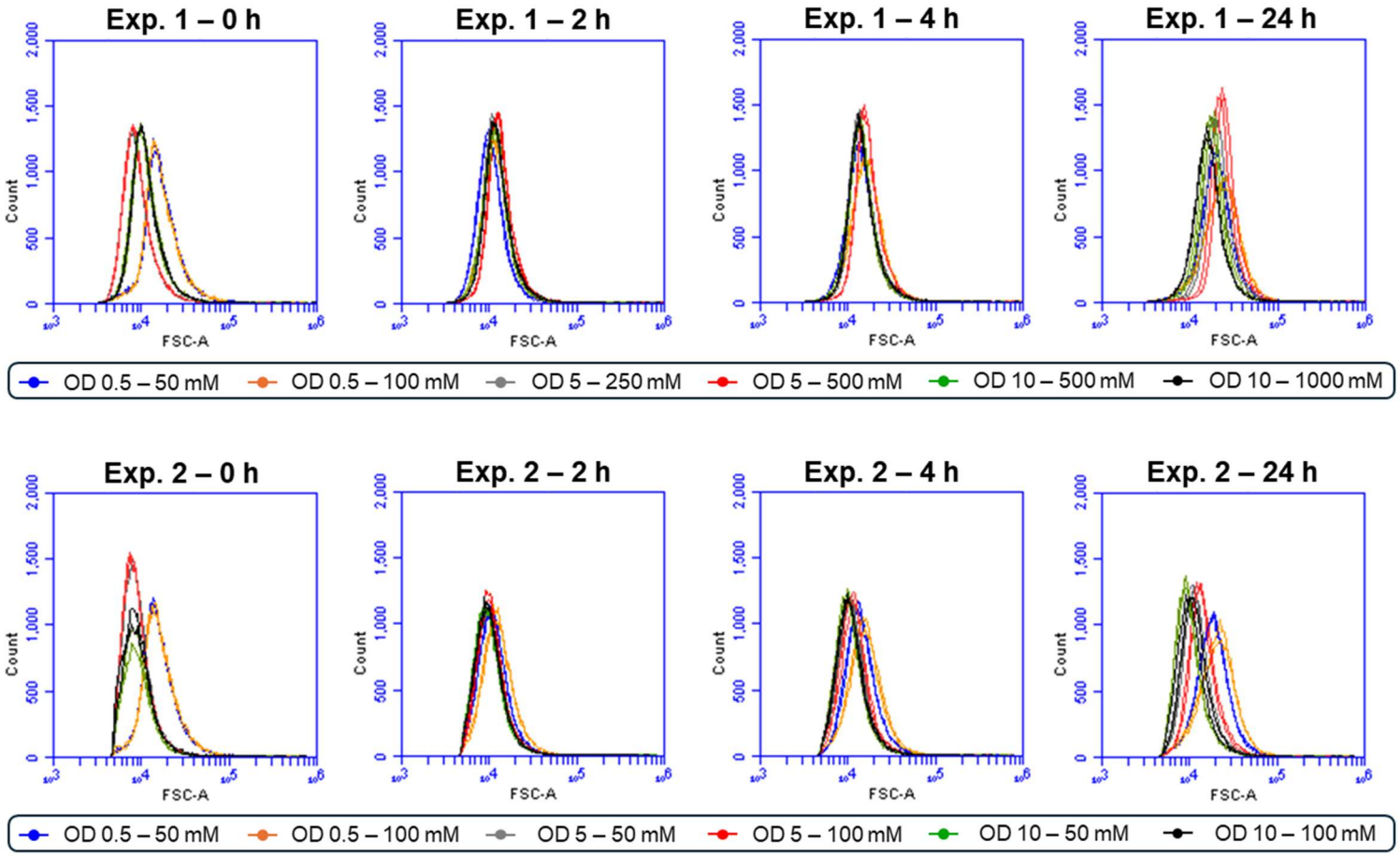


Figure 3.36: Histograms of forward scatter (FSC-A) measured via FCM for Exp 1 and Exp 2 presented in Figure 3.34 A and Figure 3.34B.

BL21 carrying the pET-15b-P*uti101*-*6xhis::gfp* construct was aerated in 100 mL TB + Amp in baffled Erlenmeyer flasks at 37 °C, 150 rpm. At OD_{600} = 0.5, 5 and 10, 6xHis::GFP expression was induced with urea. Data is shown for duplicate biological replicates. Data for two experiments is shown, Exp 1 **(top panel)** and Exp 2 **(bottom panel)**.
Top panel Exp 1 – BL21 was induced with the urea concentration scaled to the OD_{600} of the culture. Cultures were single populations across all time-points.

Bottom Panel Exp 2 – A control experiment for Exp 1, BL21 was induced with 50 mM or 100 mM urea. Cultures were single populations across all time-points.

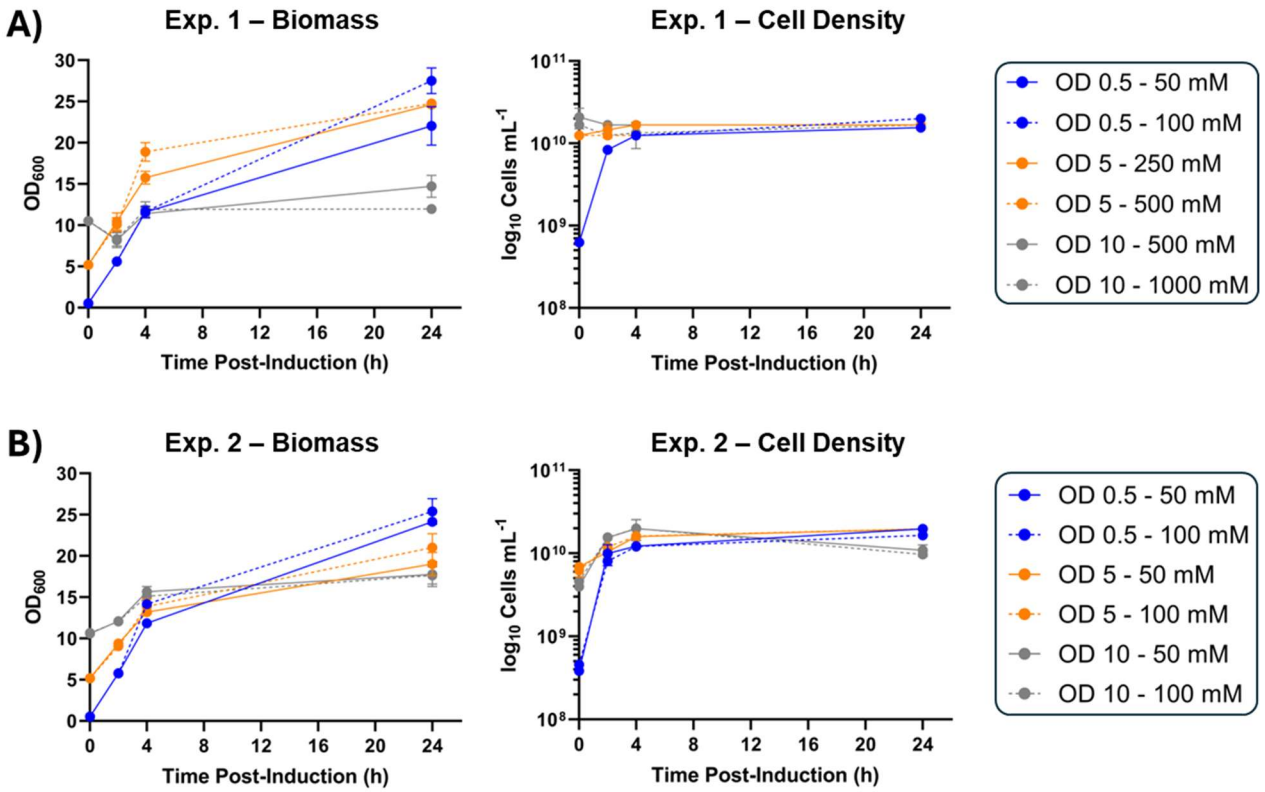


Figure 3.37: The effect of early and late induction of 6xHis::GFP on BL21 physiology was evaluated using FCM during scale-up.

BL21 carrying the pET-15b-P$_{uti101}$-*6xhis::gfp* construct was aerated in 100 mL TB + Amp in baffled Erlenmeyer flasks at 37 °C, 150 rpm. At OD_{600} = 0.5, 5 and 10, 6xHis::GFP expression was induced with urea in duplicate for each concentration. Data for two experiments is shown, Exp 1 **(A)** and Exp 2 **(B)**. Error bars represent +/- SD from duplicate biological replicates.

(A) Exp 1 – BL21 was induced with the urea concentration scaled to the OD_{600} of the culture. For cultures induced at OD_{600} 10 a drop occurred following induction. Cell density measured via FCM only increased in cultures induced at OD_{600} 0.5, with those induced at 5 or 10 remaining stable around 1.50×10^{10} cells mL^{-1}.

(B) Exp 2 – A control experiment for using high concentrations of urea in Exp 1, BL21 was induced with 50 mM or 100 mM urea. Inducing with lower concentrations of urea at higher OD_{600} had little effect on biomass. Cell density increased in all cultures following induction, although was slightly lower at 0 h than in cultures shown in (A).

induced at OD_{600} 0.5 and 5, with those induced at 10 remaining stable at around $1.50x10^{10}$ cells mL^{-1}, presumably having saturated (Figure 3.37A). In experiment 1, active growth of cultures thus seemed to correlate with 6xHis::GFP expression as cultures induced at OD_{600} = 0.5 had the highest mean green fluorescence (Figure 3.34A). Inducing with lower concentrations of urea (50 mM or 100 mM) at higher OD_{600} (5 or 10) did improve biomass accumulation in experiment 2 (Figure 3.37B). In experiment 2, cell density did increase in all cultures following induction (Figure 3.37B), although cell densities at 0 h post-induction were slightly lower than in cultures shown in Figure 3.37A for experiment 1.

3.4.7 Pulse-chase comparison of urea with IPTG

Thus far the dynamics of urea entry into cells were unclear. Being small and polar urea readily diffuses across the *E. coli* cytoplasmic membrane (Zeidel et al., 1992), but whether this occurred rapidly after addition or more stably during growth following addition was of interest. We tested this by inducing with urea, then removing the urea by centrifuging the cells, and resuspending in fresh medium. As a comparison for P_{uti101} and urea, the novel IPTG inducible P_{lac} derivative PAR4 was used (Hothersall et al., 2021). BL21 containing either pET-15b-P_{uti101}-*6xhis::gfp* or pET-22b-PAR4-*6xhis::gfp* was aerated in 50 mL TB, at 37 °C, 200 rpm until OD_{600} 0.4-0.6 and induced with 0 – 500 mM urea or 0 – 100 µM IPTG. Working volume for these experiments was decreased to facilitate easier processing. After 1 h, cells were centrifuged and resuspended in fresh TB medium to remove the inducer and growth resumed. This was compared with control cultures where either inducer was not removed.

To confirm resuspension in fresh medium did not majorly affect BL21 physiology and inhibit 6xHis::GFP expression from P_{uti101} or PAR4, cell density was monitored throughout growth via FCM (Figure 3.38). Cell density was slightly higher in BL21 cells where urea was not removed, reaching around $1x10^{10}$ cells mL^{-1}, although resuspended cultures still saturated at around $5x10^{9}$ cells mL^{-1} and were slightly lower at induction (Figure 3.38A). Similarly to BL21 induced with urea, cultures where IPTG was not removed after induction had slightly higher cell densities, reaching approximately $8.00x10^{9}$ cells mL^{-1}; resuspended cultures $6.00x10^{9}$ cells mL^{-1} (Figure 3.38B). Given this, we assumed removal of the inducer had minimal effect on BL21 physiology.

Mean green fluorescence was then monitored via FCM. In control cultures, where urea was not removed, mean green fluorescence was far higher, reaching around 150000 AU in cultures induced with 50 mM urea and 120000 AU in cultured induced with 500 mM urea (Figure 3.39A). When urea was removed at 1 h post-induction, mean green fluorescence dropped; cultures induced with 50 mM urea only reached around 5000 AU, a 30-fold drop in mean green fluorescence. When the inducer was removed, cultures induced with 500 mM urea had higher mean green fluorescence, at around 30000 AU (Figure 3.39A). IPTG entry into cells was comparable to urea and dose dependent (Figure 3.39B). Mean green fluorescence was far higher in cultures where IPTG was not removed. Interestingly, in cultures where IPTG was removed, basal expression from the P_{lac}-based PAR4 promoter meant the uninduced control had higher mean green fluorescence than cultures induced with 10 µm IPTG at 4 h post-induction (Figure 3.39B). However, complete removal of urea and IPTG was not

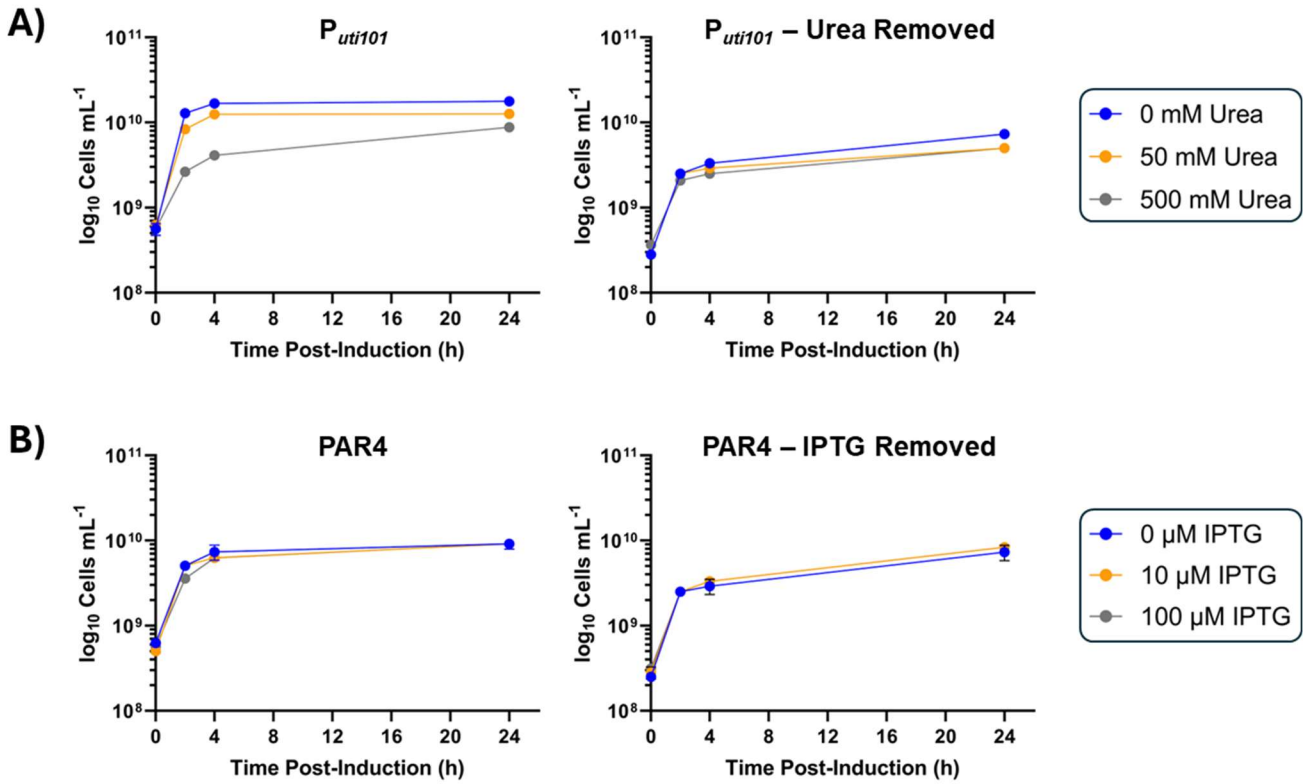


Figure 3.38: Cell density data for BL21 during analysis of urea entry into cells by comparison to IPTG.

P_{uti101} was compared with the IPTG inducible P_{lac} derivative PAR4 to assess urea entry into cells. BL21 containing constructs with either promoter driving expression of 6xHis::GFP was aerated in 50 mL TB + Amp, at 37 °C, 200 rpm until OD_{600} 0.4-0.6 and induced with urea or IPTG. After 1 h, cells were spun down and resuspended in fresh TB to remove the inducer and growth resumed. Cell density was monitored via FCM. Plots are from the point of induction, error bars represent +/- SD from duplicate biological replicates.

(A) Cell density was slightly higher in BL21 cells that were induced under normal conditions, reaching around $1.00x10^{10}$ cells mL^{-1}; although, resuspended cultures still saturated at around $5.00x10^{9}$ cells mL^{-1}.

(B) Similarly to BL21 induced with urea, cultures induced with IPTG under normal conditions had higher cell density reaching approximately $8.00x10^{9}$ cells mL^{-1}; resuspended cultures $6.00x10^{9}$ cells mL^{-1}.

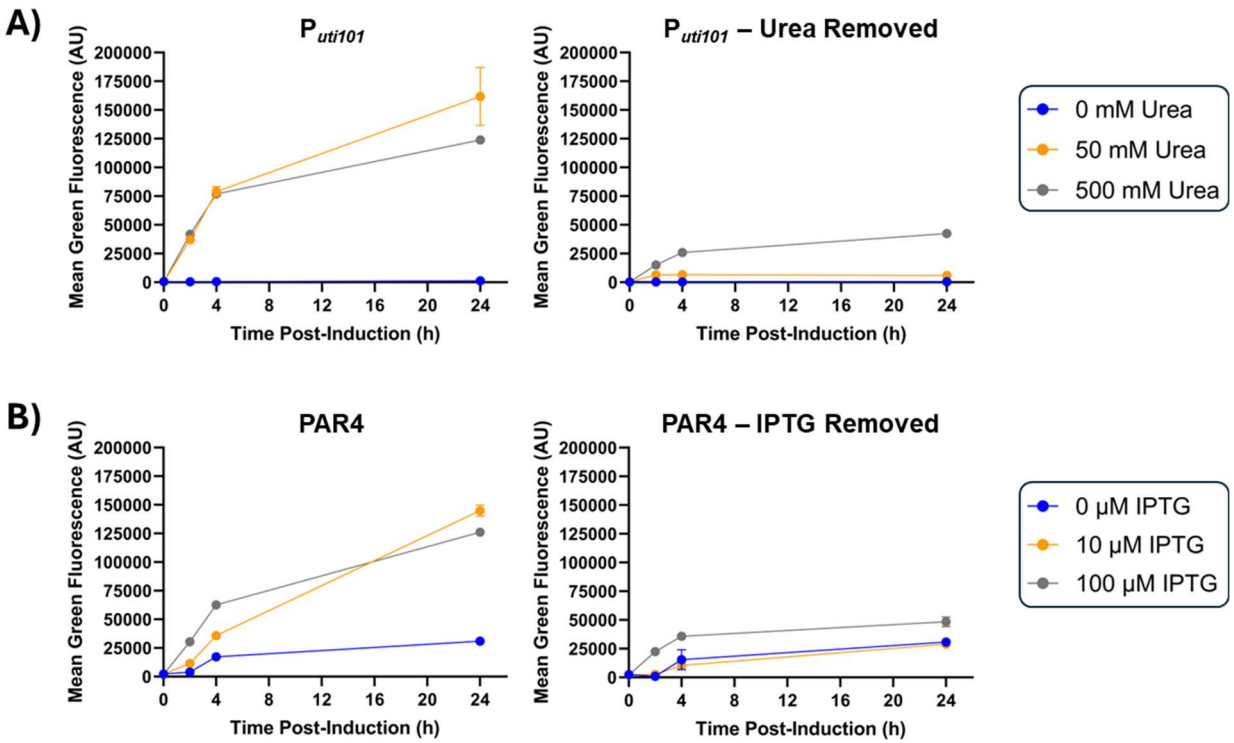


Figure 3.39: Urea entry into cells was compared with IPTG by resuspending cultures in fresh TB without inducers at 1 h post-induction.

P_{uti101} was compared with the IPTG inducible P_{lac} derivative PAR4 to assess urea entry into cells. BL21 containing constructs with either promoter driving expression of 6xHis::GFP was aerated in 50 mL TB + Amp, at 37 °C, 200 rpm until OD_{600} 0.4-0.6 and induced with urea or IPTG. After 1 h, cells were spun down and resuspended in fresh TB to remove the inducer and growth resumed. Mean green fluorescence was monitored via FCM. Plots are from the point of induction, error bars represent +/- SD from duplicate biological replicates.

(A) Urea entry into cells appeared to occur more steadily during growth and be somewhat dose dependent; mean green fluorescence was far higher in cultures induced under normal conditions. When removing urea at 1 h post-induction, mean green fluorescence dropped, particularly in cultures induced with 50 mM urea.

(B) IPTG entry into cells appeared like urea and also dose dependent; mean green fluorescence was far higher in cultures induced under normal conditions, dropping significantly if IPTG was removed at 1 h post-induction. Interestingly, in cultures where IPTG was removed, basal expression from P_{lac} meant the uninduced control had higher mean green fluorescence than cultures induced with 10 µm IPTG at 4 h post-induction.

confirmed by methods like HPLC, so its possible residual amount of either were still present.

As the inducers were present for only 1 h, we wondered whether the little that was taken up by cells was distributed evenly throughout the population or entered a subset of cells leading to heterogeneity. FCM analysis of green fluorescence (FL1-A) in single cells indicated that for both IPTG and urea, regardless of the concentrations added, only single populations of cells were present (Figure 3.40). Distributions were generally very tight and raw data for histograms is provided in Chapter 8 – Appendix for P_{uti101} (Table 8.20) and PAR4 (Table 8.21). Given the green fluorescence data (Figure 3.39 and Figure 3.40) urea did not seem to diffuse into cells quickly following induction; instead, it appeared like IPTG, urea moves into cells throughout the course of growth, and this is at least partly dependent on the concentration used.

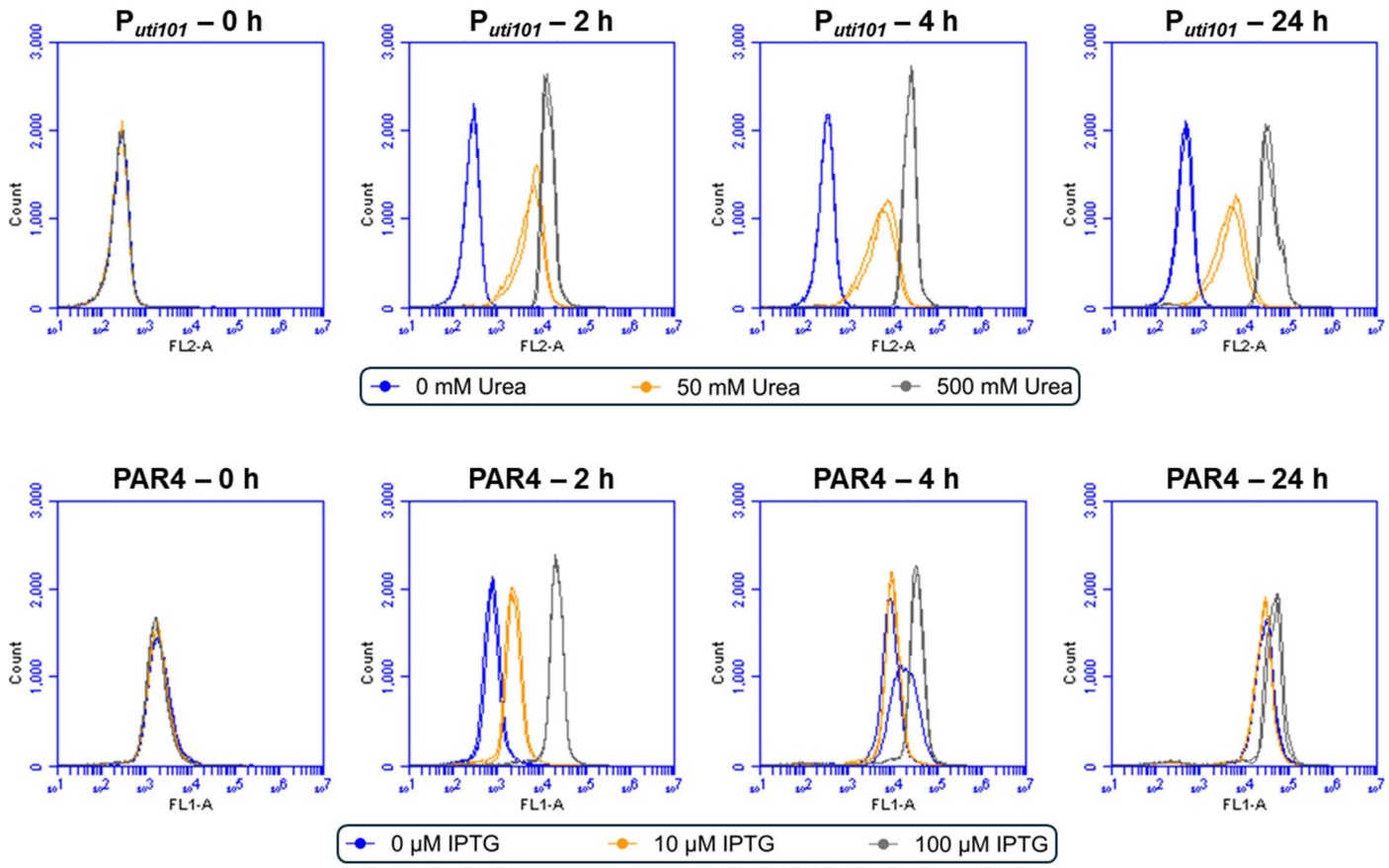


Figure 3.40: Histograms for green fluorescence data presented in Figure 3.39 (urea and IPTG removed).

P_{uti101} was compared with the IPTG inducible P_{lac} derivative PAR4 to assess urea entry into cells. BL21 containing constructs with either promoter driving expression of 6xHis::GFP was aerated in 50 mL TB + Amp, at 37 °C, 200 rpm until OD_{600} 0.4-0.6 and induced with urea or IPTG. After 1 h, cells were spun down and resuspended in fresh TB to remove the inducer and growth resumed. Green fluorescence was monitored via FCM. For each condition, data is shown for duplicate biological replicates.

Even when removing both urea and IPTG at 1 h post-induction, uptake of both inducers appeared to be evenly distributed amongst cells within each culture, irrespective of the concentration added. Under all conditions, a single population of cells was observed with regards to green fluorescence.

3.5 Scale-up into bioreactors

As a final test for the urea inducible system, cultures were scaled up into bioreactors to evaluate performance under conditions comparable to commercial RPP. A large increase in 6xHis::GFP expression was observed when scaling up from using 50 mL LB in 250 mL flasks (Figure 3.22A) to 100 mL TB in 500 mL baffled flasks (Figure 3.28B), richer medium and better growth rates due to aeration the likely cause. Thus, it was hoped that increased control over physical parameters during fed-batch fermentation would further improve expression from P_{uti101}.

3.5.1 Fed-batch fermentation trial

The urea inducible system was scaled up into bioreactors. BL21 harbouring the pET-15b-P_{uti101}-*6xhis::gfp* construct was grown in 1.5 L semi-defined medium + Amp, previously shown to be suitable for high cell density fermentation and high levels of protein production in *E. coli* (Wyre and Overton, 2014). Many fed-batch fermentation processes comprise an initial biomass-generation phase followed by induction of recombinant protein synthesis (Zulkifly et al., 2023). While it was previously shown that late induction with urea was detrimental to 6xHis::GFP expression (Figure 3.34), we speculated that feeding at high cell densities combined with better control over physical parameters may improve this. The vessel was inoculated to OD_{600} = 0.05 and cells aerated until OD_{600} ~ 50 (23 h post-inoculation). Prior work at flask scale had indicated 50 mM – 100 mM urea provided the best combination of high 6xHis::GFP expression without any significant negative impact on host physiology (Figure 3.27 & Figure 3.28). Thus, at OD_{600} ~ 50 (23 h post-inoculation), cells were induced with 100 mM urea and feeding with 714 g L^{-1} glycerol + 7.4 g L^{-1} $MgSO_4 \cdot 7H_2O$ started at 67.5 mL h^{-1}, the

composition and rate of which had previously been optimised (Wyre and Overton, 2014). Growth continued until 24 h post-induction (47 h post-inoculation) (Figure 3.41). In the bioreactor, pH was maintained at 6.3 +/- 0.1 using 10 % (w/v) NH4OH or 5 % (w/v) HCl. Air was sparged into the vessel from below at 3 L min-1 and DO was maintained at 30% by cascade to agitation at 200 – 800 rpm. Temperature was maintained at 37°C. Foaming was controlled by addition of PPG-2000.

Biomass accumulation and cell density were monitored throughout fermentation via OD_{600} and FCM respectively (Figure 3.41). OD_{600} continually increased throughout growth, reaching a maximum of 211 at 24 h post-induction (47 h post-inoculation). Similarly, cell density increased rapidly between inoculation and 6 h post-inoculation after which growth rates slowed but reached around $1x10^{11}$ cells mL^{-1} at 24 h post-induction (47 h post-inoculation). To check fermentation parameters were tolerated by BL21, cells were stained with PI. While previously shown to not fully stain BL21 exposed to urea (Figure 3.20), PI was used pre-induction in combination with FCM to gate cells into PI- GFP- (viable with low green fluorescence), PI- GFP+ (viable with high green fluorescence) and PI+ populations (non-viable) (Figure 3.42A). Pre-induction, low levels of PI+ cells (~ 2 %) were apparent, with over 90% of cells within the PI- GFP- gate.

After induction with urea, gating on only low green fluorescence (GFP-) and high green fluorescence (GFP+) populations were used; data is shown for cells residing within the GFP+ gate (Figure 3.42B). By approximately 3 h post-induction (26 h post-inoculation), over 95 % of cells were within the GFP+ gate and remained so until the process end.

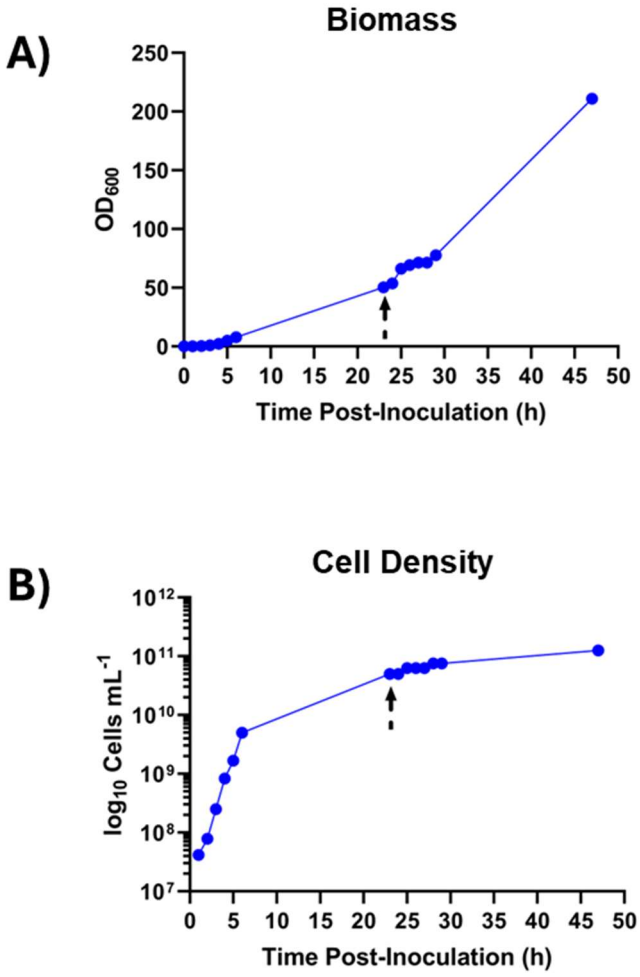


Figure 3.41: Growth data for bioreactor scale-up using late induction and late feeding.

BL21 harbouring the pET-15b-P_{uti101}-*6xhis::gfp* construct was grown in 1.5 L semi-defined medium + Amp. In the bioreactor, pH was maintained at 6.3 +/- 0.1 using 10 % (w/v) NH_4OH or 5 % (w/v) HCl. Air was sparged into the vessel from below at 3 L min^{-1} and DO was maintained at 30% by cascade to agitation at 200 – 800 rpm. Temperature was maintained at 37°C. Foaming was controlled by addition of PPG-2000. The bioreactor was inoculated to OD_{600} 0.05 and cells aerated until ~ OD_{600} 50 (23 h post-inoculation), induced with 100 mM urea **(black arrow)** and feeding (714 g L^{-1} glycerol + 7.4 g L^{-1} $MgSO_4 \cdot 7H_2O$) started at the same time at 67.5 mL h^{-1} **(black arrow)**. Aeration proceeded until 24 h post-induction (47 h post-inoculation). One repeat is shown.

(A) OD_{600} was used to monitor biomass accumulation which increased from the point of induction reaching a maximum of over 200.

(B) Cell density was monitored via FCM, increasing from inoculation and reaching approximately $1x10^{11}$ cells mL^{-1} at 47 h post-inoculation.

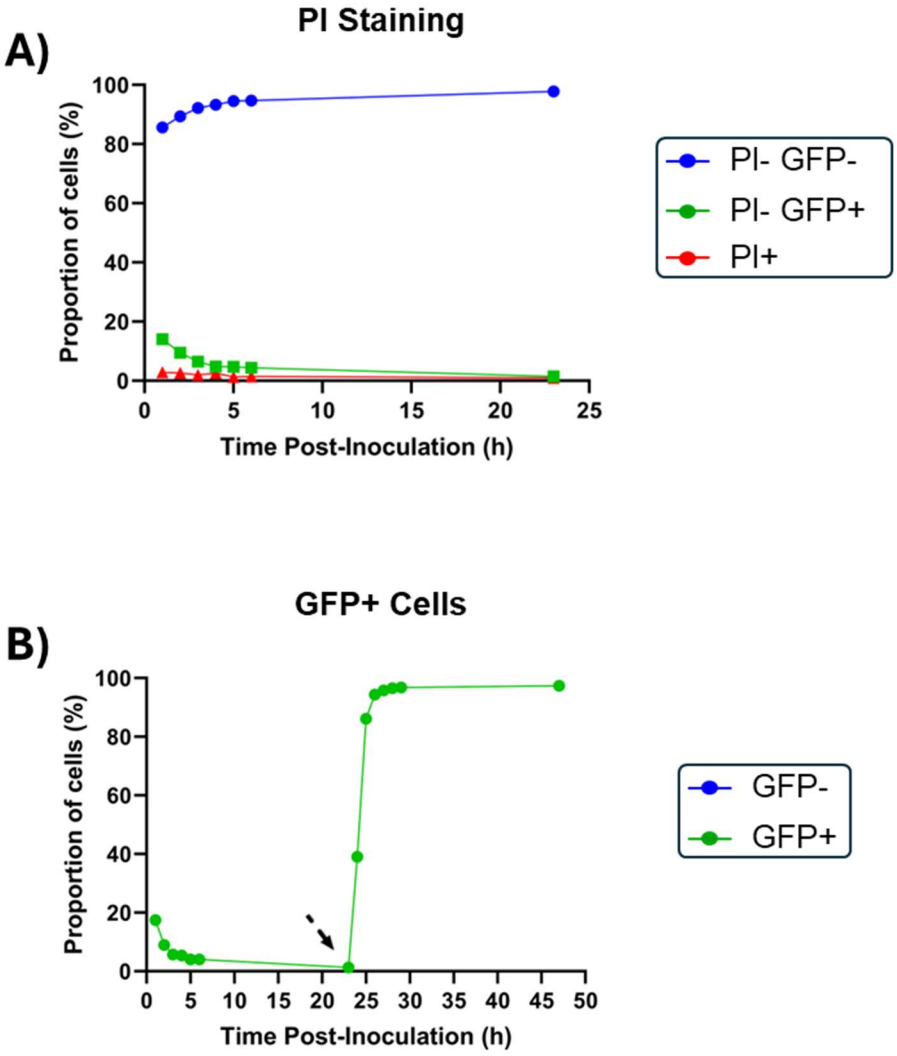


Figure 3.42: FCM data for bioreactor scale-up using late induction and late feeding.

BL21 harbouring the pET-15b-P*uti101*-*6xhis::gfp* construct was grown in 1.5 L semi-defined medium + Amp. In the bioreactor, pH was maintained at 6.3 +/- 0.1 using 10 % (w/v) NH_4OH or 5 % (w/v) HCl. Air was sparged into the vessel from below at 3 L min^{-1} and DO was maintained at 30% by cascade to agitation at 200 – 800 rpm. Temperature was maintained at 37°C. Foaming was controlled by addition of PPG-2000. The bioreactor was inoculated to OD_{600} 0.05 and cells aerated until ~ OD_{600} 50 (23 h post-inoculation), induced with 100 mM urea **(black arrow)** and feeding (714 g L^{-1} glycerol + 7.4 g L^{-1} $MgSO_4 \cdot 7H_2O$) started at the same time at 67.5 mL h^{-1} **(black arrow)**. Aeration proceeded until 24 h post-induction (47 h post-inoculation). One repeat is shown.

(A) Prior to induction with urea and addition of feed at 23 h post-inoculation, BL21 viability was assessed by staining cells with 4 µg mL^{-1} PI for 5 min and analysed via FCM. Cells were gated on red fluorescence (FL3-A) and green fluorescence (FL2-A) density plots. Gates were generated for cells which were PI- GFP- (viable and low green fluorescence), PI- GFP+ (viable and high green fluorescence) and PI+ (non-viable). Pre-induction, low levels of dead cells were apparent with over 90% of cells within the PI- GFP- gate.

(B) As PI staining was previously shown to be incompatible with BL21 treated with urea, FCM was also used to gate cells as low green fluorescence and high green fluorescence using forward scatter (FSC-A) and green fluorescence (FL2-A) density plots. Data is shown for cells residing in the high green fluorescence GFP+ gate. Pre-induction, few cells were within the GFP+ gate. By approximately 3 h post-induction (26 h post-inoculation), over 95 % of cells were within the GFP+ gate and remained so until the process end.

Given the proportion of cells with high green fluorescence (GFP+) was high (Figure 3.42B), we wanted to see what green fluorescence was reached. Hence, FCM was used to analyse mean green fluorescence (Figure 3.43A) which was low prior to induction. After addition of 100 mM urea, mean green fluorescence continually increased until fermentation was stopped at 24 h post-induction (47 h post-inoculation). Mean green fluorescence during fermentation was lower than that observed in baffled flasks (Figure 3.28B); only reaching around 35000 AU (Figure 3.43). We wondered whether cell size was affected during fermentation so mean FSC was analysed via FCM (Figure 3.43B). Mean FSC decreased from the point of inoculation, until 100 mM urea was added when it increased slightly; this increase was likely due overexpression of 6xHis::GFP. To check whether the low green fluorescence observed was due to partial induction or mixed populations, analysis of individual cells was checked via FCM (Figure 3.43C). At the single cell level, only single populations of cells were observed for green fluorescence (FL1-A) (Figure 3.43C). Similarly, for FSC, there was little heterogeneity apparent (Figure 3.43C).

Physical parameters were monitored during fermentation (Figure 3.44). Following inoculation, DO decreased rapidly until reaching setpoint (30 %), switching on the agitation cascade (200 – 800 rpm). DO was mostly maintained around 30% until approximately 8 h – 12 h post-inoculation where it dropped to around 1 % and then increased again. This coincided with large addition of base to maintain pH at 6.3 +/- 0.1, presumably due to overflow metabolism, which then stopped once DO increased back to 30%, presumably because cell growth slowed which is supported by Figure 3.41B. Between 15 h and 23 h post-inoculation DO increased to around 80 %, this

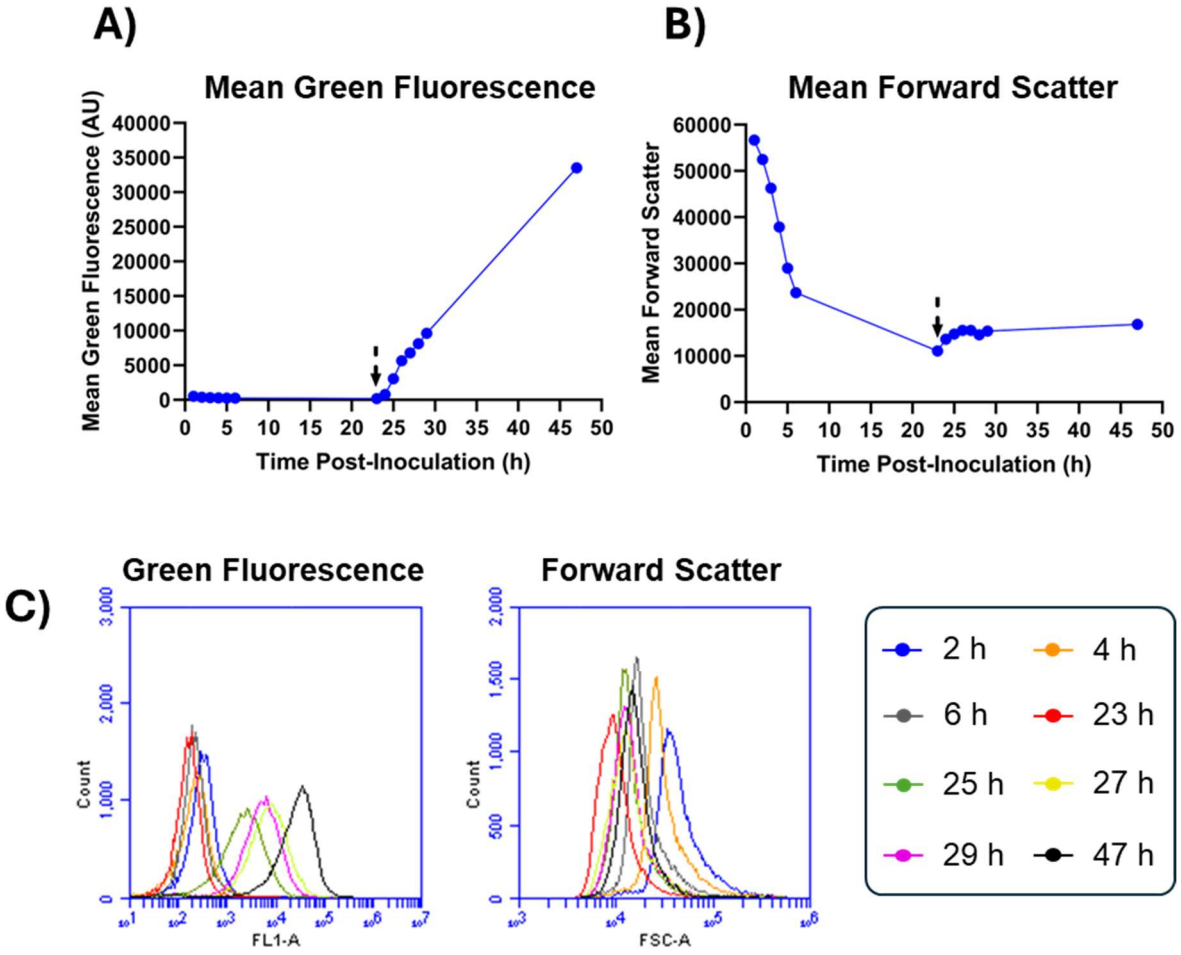


Figure 3.43: FCM data for bioreactor scale-up using late induction and late feeding.

BL21 harbouring the pET-15b-P_{uti101}-*6xhis::gfp* construct was grown in 1.5 L semi-defined medium + Amp. In the bioreactor, pH was maintained at 6.3 +/- 0.1 using 10 % (w/v) NH_4OH or 5 % (w/v) HCl. Air was sparged into the vessel from below at 3 L min^{-1} and DO was maintained at 30% by cascade to agitation at 200 – 800 rpm. Temperature was maintained at 37°C. Foaming was controlled by addition of PPG-2000. The bioreactor was inoculated to OD_{600} 0.05 and cells aerated until ~ OD_{600} 50 (23 h post-inoculation), induced with 100 mM urea **(black arrow)** and feeding (714 g L^{-1} glycerol + 7.4 g L^{-1} $MgSO_4 \cdot 7H_2O$) started at the same time at 67.5 mL h^{-1} **(black arrow)**. Aeration proceeded until 24 h post-induction (47 h post-inoculation). One repeat is shown.

(A) Mean green fluorescence was monitored using FCM and was low at all time-points between inoculation and addition of 100 mM urea **(black arrow)**; it steadily increased from induction reaching a maximum of around 35000 AU at 24 h post-induction (47 h post inoculation).

(B) Mean FSC, analysed by FCM, decreased from the point of inoculation until 100 mM urea was added **(black arrow)**, increasing slightly.

(C) At the single cell level FCM analysis indicated only single populations of cells were observed for green fluorescence (FL1-A) and forward scatter (FSC-A).

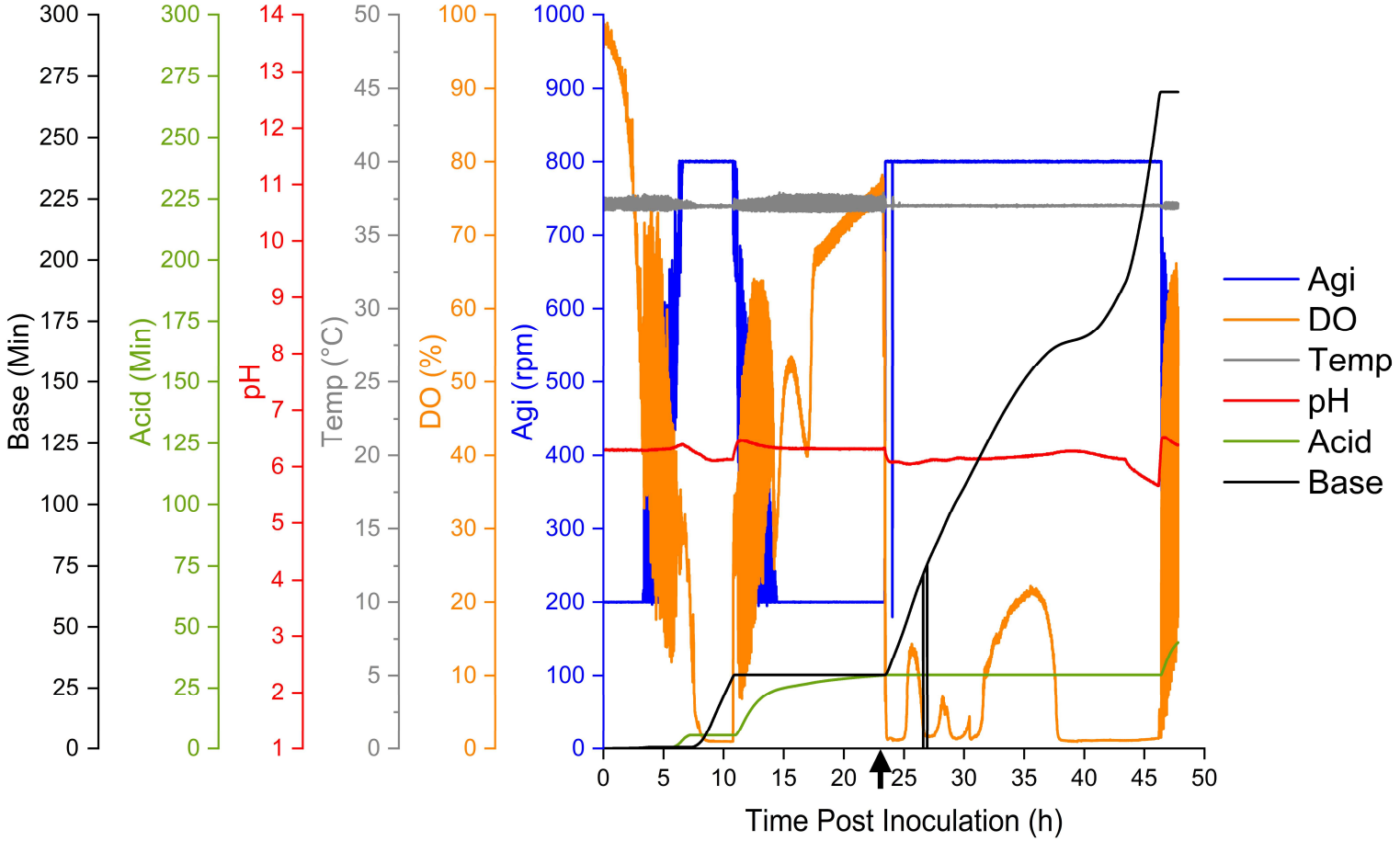


Figure 3.44: Bioreactor trace during scale-up using late induction and late feeding.

BL21 harbouring the pET-15b-P_{uti101}-*6xhis::gfp* construct was grown in 1.5 L semi-defined medium + Amp. In the bioreactor, pH was maintained at 6.3 +/- 0.1 using 10 % (w/v) NH_4OH or 5 % (w/v) HCl. Air was sparged into the vessel from below at 3 L min^{-1} and DO was maintained at 30% by cascade to agitation at 200 – 800 rpm. Temperature was maintained at 37°C. Foaming was controlled by addition of PPG-2000. The bioreactor was inoculated to OD_{600} 0.05 and cells aerated until ~ OD_{600} 50 (23 h post-inoculation), induced with 100 mM urea **(x-axis black arrow)** and feeding (714 g L^{-1} glycerol + 7.4 g L^{-1} $MgSO_4 \cdot 7H_2O$) started at the same time at 67.5 mL h^{-1} **(x-axis black arrow)**. Aeration proceeded until 24 h post-induction (47 h post-inoculation).

correlated with the point at which growth rates decreased (Figure 3.47A). Upon induction and initiation of feeding, DO almost immediately dropped from around 80 % to around 2 % and remained under set point until 46 h post-inoculation. Base addition again increased during this period, once again likely due to overflow metabolism triggering a drop in pH.

3.5.2 Adjusted fed-batch fermentation

From previous experiments it was shown that P_{uti101} induction and activity were restricted in stationary phase cells (Figure 3.34); similarly in section 3.5.1, it was observed that mean green fluorescence was lower in bioreactors (Figure 3.43) than in baffled flasks (Figure 3.28B). Hence, the point of induction was shifted to an earlier time-point (OD_{600} 0.4 – 0.6) to improve 6xHis::GFP expression in bioreactors. BL21 harbouring the pET-15b-P_{uti101}-*6xhis::gfp* construct was grown in 1.5 L semi-defined medium + Amp; cells were induced with 100 mM urea at OD_{600} ~ 0.4 – 0.6 (2 h post-inoculation). At OD_{600} 40 – 50 (23 h post-inoculation), feeding with 714 g L^{-1} glycerol + 7.4 g L^{-1} $MgSO_4 \cdot 7H_2O$ with 714 g L^{-1} glycerol + 7.4 g L^{-1} $MgSO_4 \cdot 7H_2O$ was initiated at a reduced rate of 18.5 mL h^{-1}, to try to decrease the overflow metabolism observed in the previous experiment (section 3.5.1). Growth continued until exhaustion of the feed (50 h post-inoculation) (Figure 3.45). In the bioreactor, pH was maintained at 6.3 +/- 0.1 using 10 % (w/v) NH4OH or 5 % (w/v) HCl. Air was sparged into the vessel from below at 3 L min-1 and DO was maintained at 30% by cascade to agitation at 200 – 800 rpm. Temperature was maintained at 37°C. Foaming was controlled by addition of PPG-2000. Two repeat fermentations using the above conditions were performed (Exp 1 and Exp 2).

Biomass accumulation and cell density were monitored throughout fermentation via OD_{600} and FCM respectively (Figure 3.45). OD_{600} continually increased throughout growth in both fermentations, reaching a maximum of 209 in the first fermentation and 184 in the second. Presumably lower biomass accumulation in the second fermentation was due to higher accumulation of 6xHis::GFP; the maximum cell density reached in both different to, at $6.25x10^{10}$ cells mL^{-1} and $5.03x10^{10}$ cells mL^{-1} respectively (Figure 3.45).

FCM was used to analyse mean green fluorescence during fermentation and was comparable in both experiments (Figure 3.46A). Mean green fluorescence was low prior to induction, between 1 h and 2 h post-inoculation. Upon addition of 100 mM urea (2 h post-inoculation), mean green fluorescence rapidly increased until 6 h post-inoculation, reaching around 50000 – 75000 AU in each fermentation; this was already higher than the maximum mean green fluorescence reached using late induction (Figure 3.43A). In both fed-batch fermentations (Exp 1 and Exp 2), increases mean green fluorescence slowed between 6 h and 23 h post-inoculation, having increased to around 60000 and 90000 AU respectively (Figure 3.46A). Feeding was initiated at 23 h post-inoculation and mean green fluorescence immediately increased, reflecting 6xHis::GFP accumulation. In the first fed-batch fermentation (Exp 1), mean green fluorescence plateaued around 26 h post-inoculation at approximately 150000 AU; in the second (Exp 2), at approximately 200000 AU around 28 h post-inoculation (Figure 3.46A). Maximum green fluorescence reached in each fed-batch fermentation was 163000 and 218000 for Exp 1 and Exp 2 respectively, at 50 h post-inoculation. Analysis of individual cells by FCM (Figure 3.47A) revealed multiple populations of cells with

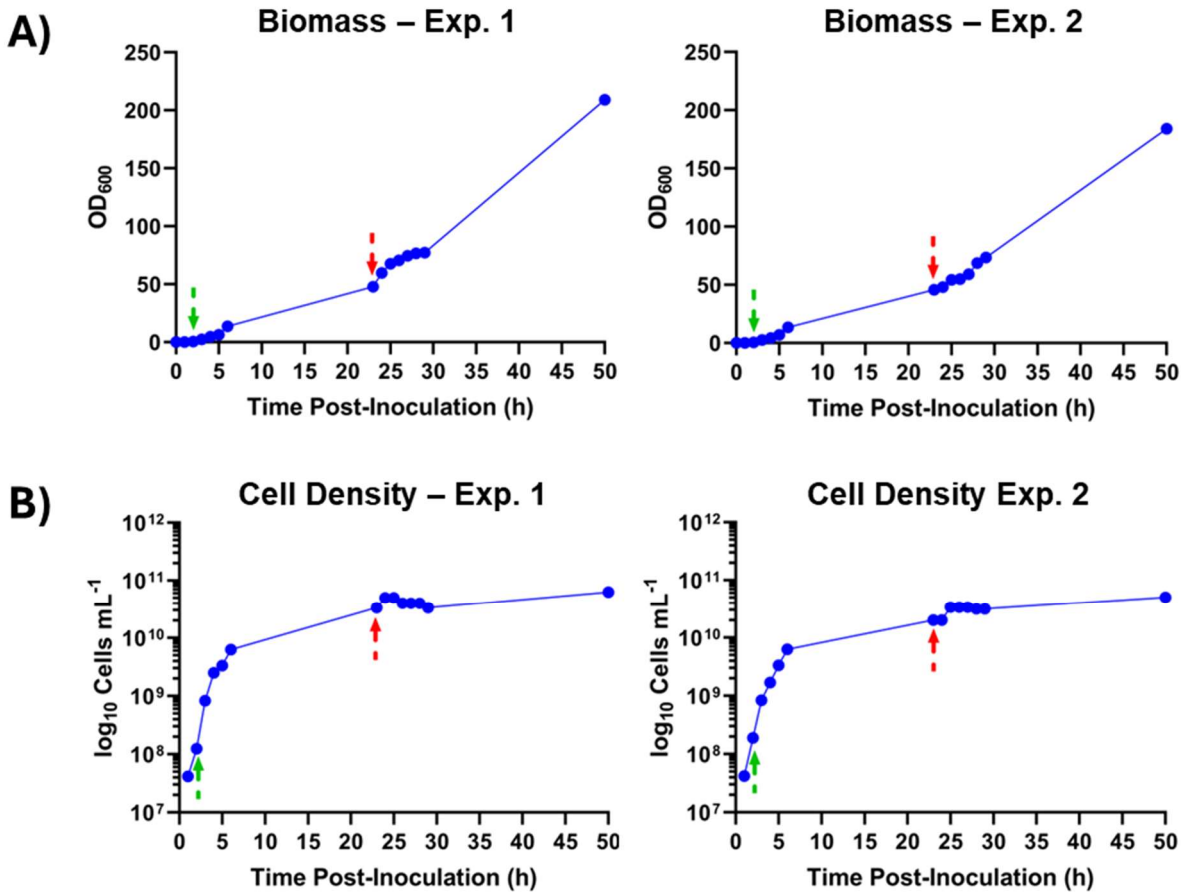


Figure 3.45: Growth data for bioreactor scale-up using early induction and late feeding.

BL21 harbouring the pET-15b-P*uti101*-*6xhis::gfp* construct was grown in 1.5 L semi-defined medium + Amp. In the bioreactor, pH was maintained at 6.3 +/- 0.1 using 10 % (w/v) NH_4OH or 5 % (w/v) HCl. Air was sparged into the vessel from below at 3 L min^{-1} and DO was maintained at 30% by cascade to agitation at 200 – 800 rpm. Temperature was maintained at 37°C. Foaming was controlled by addition of PPG-2000. The bioreactor was inoculated to OD_{600} 0.05 and cells aerated until ~ OD_{600} 0.4 – 0.6 (2 h post-inoculation), induced with 100 mM urea **(green arrow)**. At OD_{600} 40 – 50 feeding (714 g L^{-1} glycerol + 7.4 g L^{-1} $MgSO_4 \cdot 7H_2O$) was at 18.5 mL h^{-1} **(red arrow)**. Aeration proceeded until 24 h post-induction (47 h post-inoculation). Data is shown for two repeat fermentations (Exp 1 and Exp 2).

(A) OD_{600} was used to monitor biomass accumulation which increased from the point of induction reaching a maximum of around 200 in both experiments. No drop in OD_{600} was observed following induction and initiation of feeding did not lead to a large increase.

(B) Cell density was monitored via FCM, increasing from inoculation and reaching approximately $1x10^{11}$ cells mL^{-1} at 47 h post-inoculation.

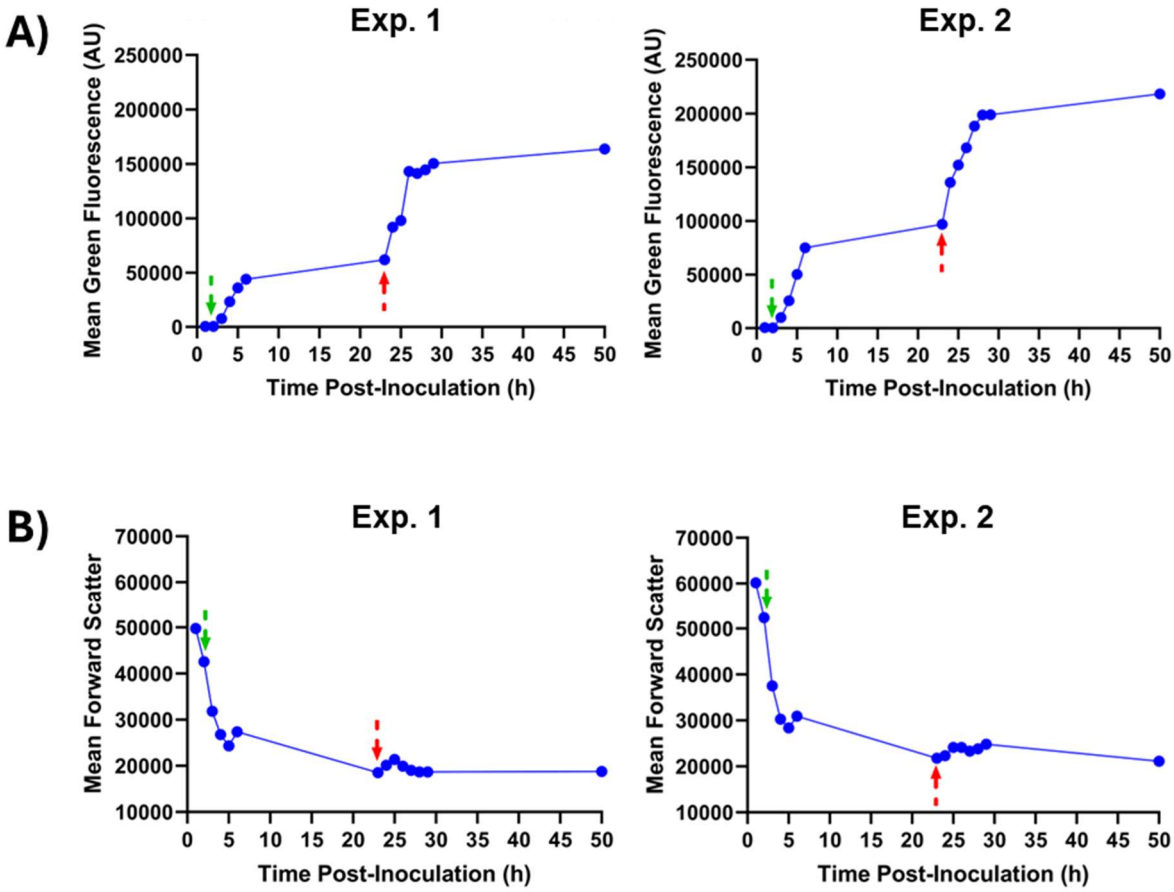


Figure 3.46: FCM data for bioreactor scale-up using early induction and late feeding.

BL21 harbouring the pET-15b-P_{uti101}-*6xhis::gfp* construct was grown in 1.5 L semi-defined medium + Amp. In the bioreactor, pH was maintained at 6.3 +/- 0.1 using 10 % (w/v) NH_4OH or 5 % (w/v) HCl. Air was sparged into the vessel from below at 3 L min^{-1} and DO was maintained at 30% by cascade to agitation at 200 – 800 rpm. Temperature was maintained at 37°C. Foaming was controlled by addition of PPG-2000. The bioreactor was inoculated to OD_{600} 0.05 and cells aerated until ~ OD_{600} 0.4 – 0.6 (2 h post-inoculation), induced with 100 mM urea **(green arrow)**. At OD_{600} 40 – 50 (23 h post-inoculation) feeding (714 g L^{-1} glycerol + 7.4 g L^{-1} $MgSO_4 \cdot 7H_2O$) was at 18.5 mL h^{-1} **(red arrow)**. Aeration proceeded until 24 h post-induction (50 h post-inoculation). Data is shown for two repeat fermentations (Exp 1 and Exp 2).

(A) Mean green fluorescence was measured using FCM and increased quickly between induction and 4 h post induction (6 h post-inoculation), slowing by 23 h post-inoculation. Initiation of feeding resulted in a massive increase in mean green fluorescence which continued until 26 h to 29 h post-inoculation in experiment 1 and 2 respectively.

(B) Mean FSC measured via FCM was similar in both experiments and dropped between inoculation and 5 h post-inoculation with a small increase at 6 h. After initiation of feeding a small increase in mean FSC was observed.

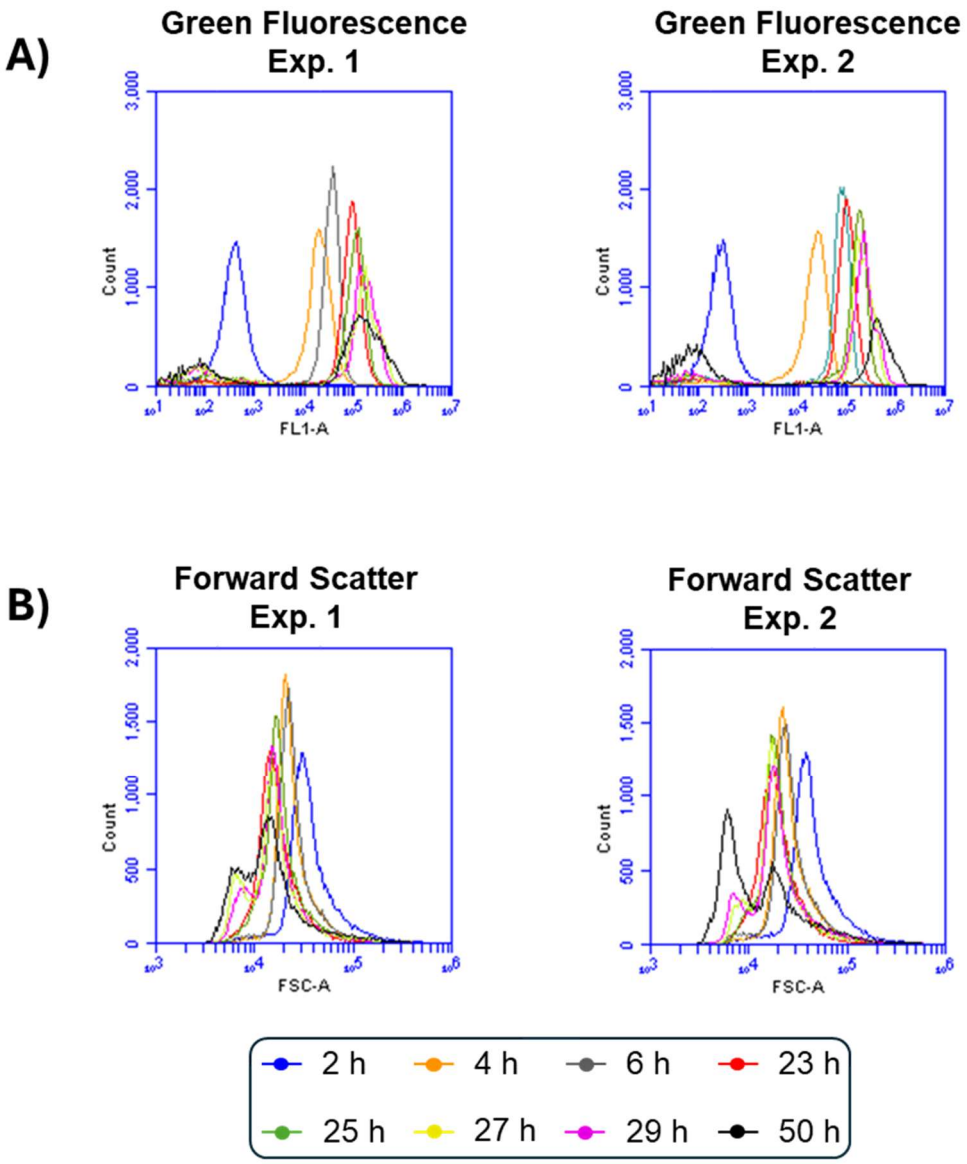


Figure 3.47: FCM data for bioreactor scale-up using early induction and late feeding.

BL21 harbouring the pET-15b-P_{uti101}-*6xhis::gfp* construct was grown in 1.5 L semi-defined medium + Amp. In the bioreactor, pH was maintained at 6.3 +/- 0.1 using 10 % (w/v) NH_4OH or 5 % (w/v) HCl. Air was sparged into the vessel from below at 3 L min^{-1} and DO was maintained at 30% by cascade to agitation at 200 – 800 rpm. Temperature was maintained at 37°C. Foaming was controlled by addition of PPG-2000. The bioreactor was inoculated to OD_{600} 0.05 and cells aerated until ~ OD_{600} 0.4 – 0.6 (2 h post-inoculation), induced with 100 mM urea **(green arrow)**. At OD_{600} 40 – 50 (23 h post-inoculation) feeding (714 g L^{-1} glycerol + 7.4 g L^{-1} $MgSO_4 \cdot 7H_2O$) was at 18.5 mL h^{-1} **(red arrow)**. Aeration proceeded until 24 h post-induction (50 h post-inoculation). Data is shown for two repeat fermentations (Exp 1 and Exp 2).

(A) Green fluorescence was measured at the single cell level using FCM; populations appeared to be predominantly highly green, fluorescent but with a second population of very low green fluorescence, particularly at 50 h post-inoculation in experiment 2.

(B) FSC was measured in single cells using FCM. Between 2 h and 25 h post-inoculation, there was mostly a single population with regards to FSC but notably two populations of lower and higher FSC at 27 h – 50 h post-inoculation.

respect to green fluorescence (FL1-A) at each time point after induction (2h post-inoculation). While the largest subpopulation was highly green fluorescent, a small subset with low green fluorescence was present, even at 4 h post-inoculation. In both fermentations (Exp 1 and Exp 2), this population appeared greatest at 50 h post-inoculation and was larger in the second experiment (Figure 3.47A). As 6xHis::GFP accumulation was higher in Exp 2, we assumed that greater numbers of low green fluorescence cells were due to increased burden.

Mean FSC was analysed by FCM, and a remarkably similar pattern was evident in both fed-batch fermentations (Figure 3.46B). Mean FSC decreased from the point of inoculation at around 50000 – 60000 to 25000 – 30000 by 5 h post-inoculation; induction with 100 mM urea at 2 h did not lead to any increase. Interestingly at 6 h post-inoculation, a slight increase in mean FSC occurred before decreasing to around 20000 AU by 23 h post-inoculation. At this point, feeding was initiated and mean FSC increased slightly until 25 h post-inoculation; this correlated with the point at which 6xHis::GFP increased massively (Figure 3.46A). Mean FSC was generally stable from this point with both fermentations finishing with cells at approximately 20000 AU. FCM analysis of single cells (Figure 3.47B) indicated that between 2 h and 25 h post-inoculation, there was mostly a single population with regards to FSC. At 27 h – 50 h post-inoculation, two populations of lower and higher FSC appeared to be present; the former group presumably not accumulating 6xHis::GFP as we know from prior work, high 6xHis::GFP expression correlated with higher FSC in BL21 (Figure 3.7B).

As an early induction protocol was used, staining cells with PI after 2 h post-inoculation was not possible due to the interaction of urea with BL21 (Figure 3.16A). So, as another measure of fermentation performance FCM was used to create FSC against green fluorescence (FL1-A) density plots and cells gated into low or high green fluorescence groups; the proportion within the high green fluorescence GFP+ gate was then plotted throughout all 50 h of growth (Figure 3.48). Both fed-batch fermentations were similar; between induction and 23 h post-induction, the proportion of cells within the GFP+ gate was around 90 – 95 %. Upon initiation of feeding however, the proportion of cells within the GFP+ gate began to drop, reaching around 75 - 80 % by 29 h post-induction (Figure 3.48). This was likely a combination of the feed permitting cells to increase 6xHis::GFP expression, increasing stress; and the presence of plasmid free cells, the antibiotic used for selection (100 μg mL^{-1} Amp during batch stage) presumably being exhausted by this point. Although plasmid loss is a well-known occurrence during RPP in *E. coli* (Sevastsyanovich et al., 2009), replica plating would be required to confirm this. One solution to this for further optimisation could have been use of carbenicillin over ampicillin (Wyre and Overton, 2014) as it is generally more resistant to degradation by β-lactamases (Overton, 2014). In the first fed-batch fermentation, proportions of cells within the GFP+ gate remained stable between 29 h and 50 h post-inoculation; in the second, only around 50% of cells were in the GFP+ gate (Figure 3.48). We assumed this was due to higher 6xHis::GFP expression in the second fed-batch fermentation (Exp 2).

Physical parameters were monitored during both fed batch fermentations and traces were very similar (Figure 3.49 and 3.50). Following inoculation, DO decreased rapidly,

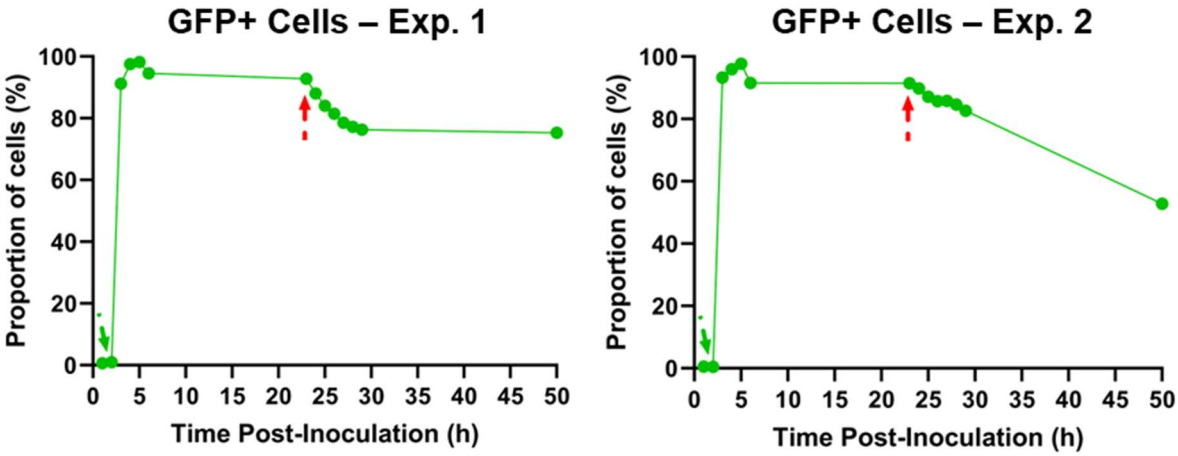


Figure 3.48: Gating cells based on fluorescence during bioreactor scale-up using early induction and late feeding.

BL21 harbouring the pET-15b-P_{uti101}-*6xhis::gfp* construct was grown in 1.5 L semi-defined medium + Amp. In the bioreactor, pH was maintained at 6.3 +/- 0.1 using 10 % (w/v) NH_4OH or 5 % (w/v) HCl. Air was sparged into the vessel from below at 3 L min^{-1} and DO was maintained at 30% by cascade to agitation at 200 – 800 rpm. Temperature was maintained at 37°C. Foaming was controlled by addition of PPG-2000. The bioreactor was inoculated to OD_{600} 0.05 and cells aerated until ~ OD_{600} 0.4 – 0.6 (2 h post-inoculation), induced with 100 mM urea **(green arrow)**. At OD_{600} 40 – 50 (23 h post-inoculation) feeding (714 g L^{-1} glycerol + 7.4 g L^{-1} $MgSO_4 \cdot 7H_2O$) was at 18.5 mL h^{-1} **(red arrow)**. Aeration proceeded until 24 h post-induction (50 h post-inoculation). Data is shown for two repeat fermentations (Exp 1 and Exp 2).

(A) As PI staining was previously shown to be incompatible with BL21 treated with urea, FCM was also used to gate cells as low green fluorescence and high green fluorescence using forward scatter (FSC-A) and green fluorescence (FL2-A) density plots. Data is shown for cells residing within the high green fluorescence (GFP+) gate. After induction with urea, around 90% of cells were within the GFP+ gate until 23 h post-inoculation, which corresponded with the initiation of feeding; the proportion of cells within the GFP- gate increased to around 20% in experiment 1 and 50% in experiment 2 by 50 h post-inoculation.

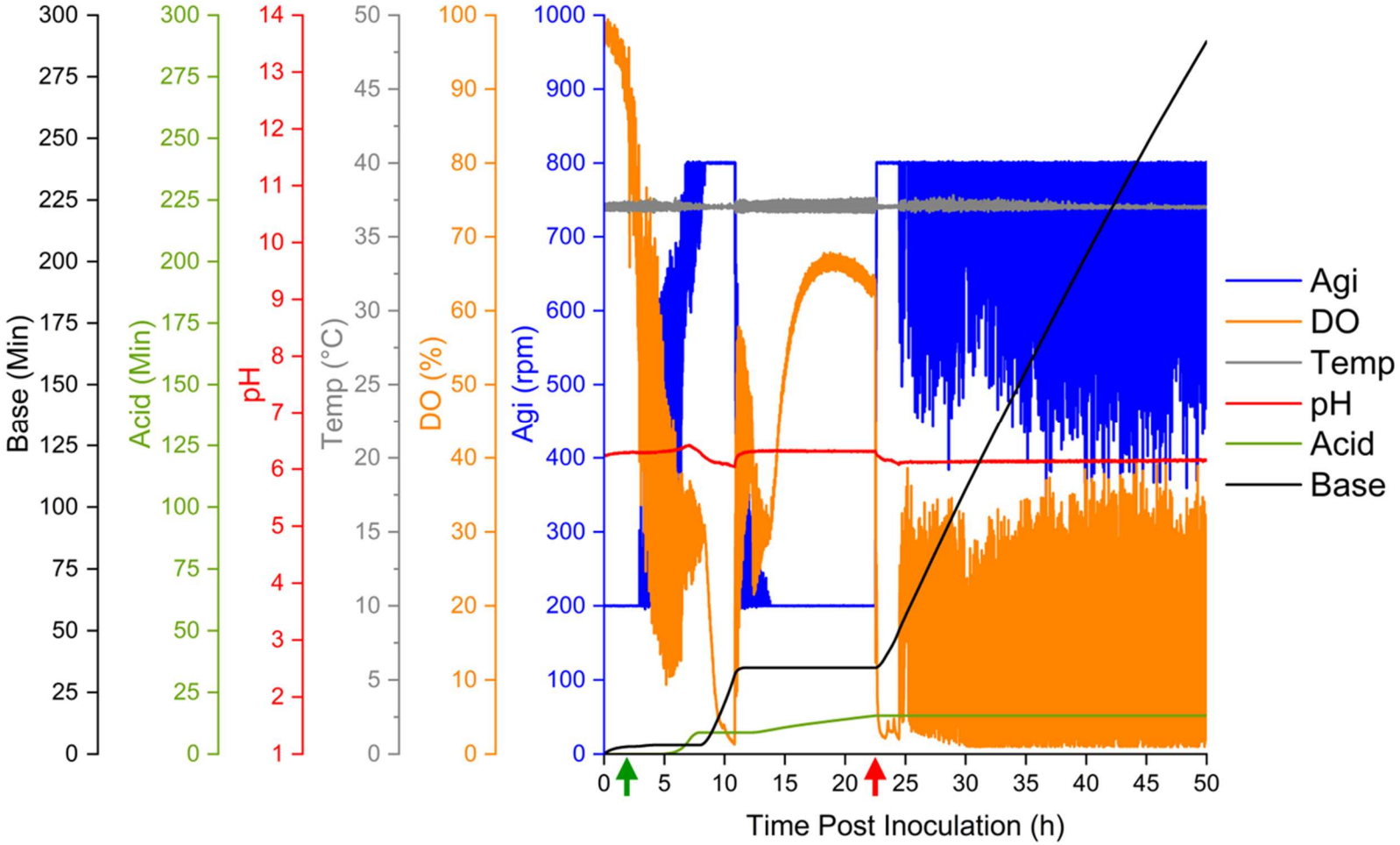


Figure 3.49: Bioreactor trace during scale-up using late induction and late feeding for Experiment 1.

BL21 harbouring the pET-15b-Puti101-6xhis::gfp construct was grown in 1.5 L semi-defined medium + Amp. In the bioreactor, pH was maintained at 6.3 +/- 0.1 using 10 % (w/v) NH4OH or 5 % (w/v) HCl. Air was sparged into the vessel from below at 3 L min^{-1} and DO was maintained at 30% by cascade to agitation at 200 – 800 rpm. Temperature was maintained at 37°C. Foaming was controlled by addition of PPG-2000. The bioreactor was inoculated to OD600 0.05 and cells aerated until ~ OD600 0.4 – 0.6 (2 h post-inoculation), induced with 100 mM urea (green arrow x-axis). At OD600 40 – 50 (23 h post-inoculation) feeding (714 g L−1 glycerol + 7.4 g L−1 MgSO4·7H2O) was at 18.5 mL h−1 (red arrow x-axis). Aeration proceeded until 24 h post-induction (50 h post-inoculation).

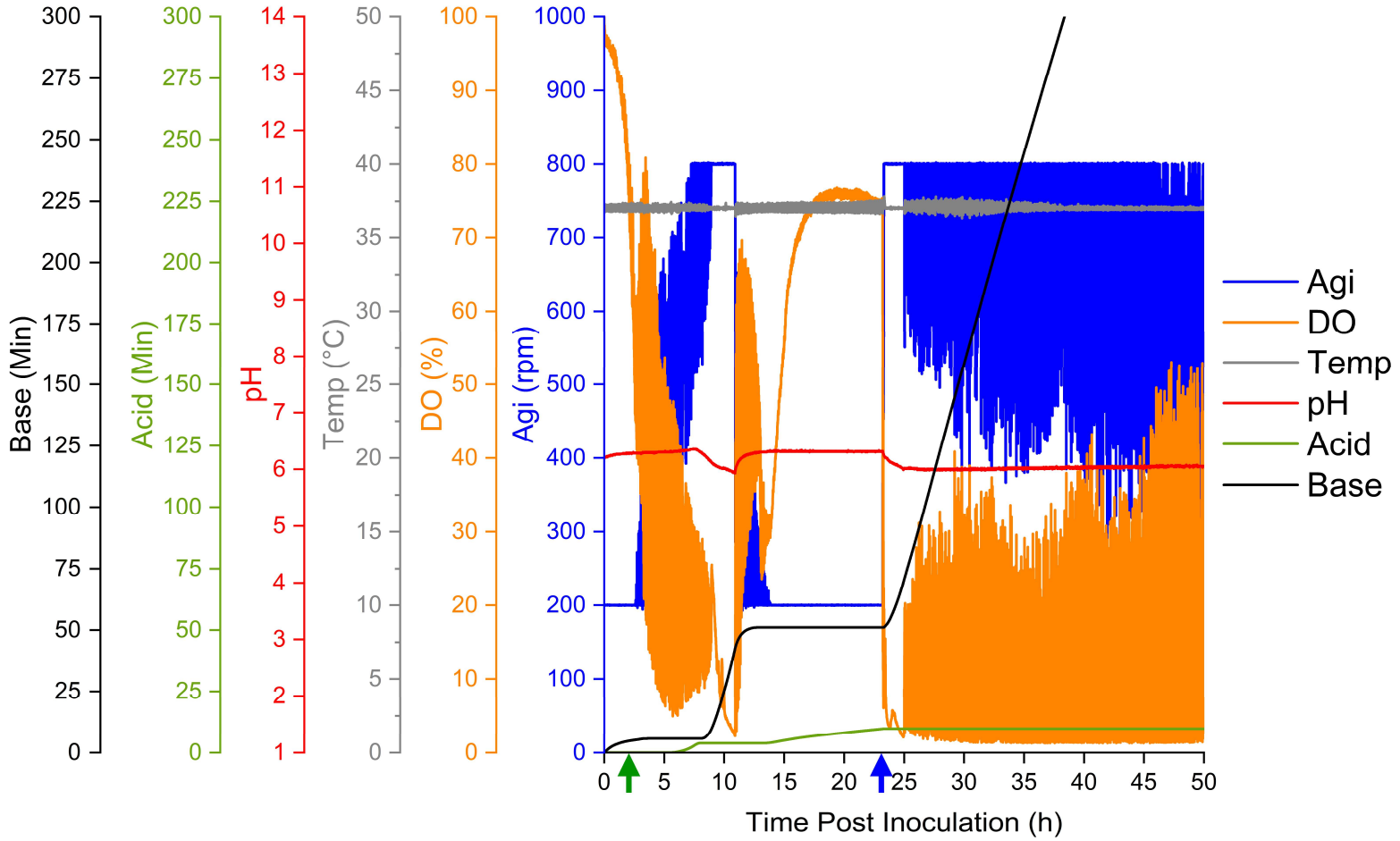


Figure 3.50: Bioreactor trace during scale-up using late induction and late feeding for Experiment 2.

BL21 harbouring the pET-15b-Puti101-6xhis::gfp construct was grown in 1.5 L semi-defined medium + Amp. In the bioreactor, pH was maintained at 6.3 +/- 0.1 using 10 % (w/v) NH4OH or 5 % (w/v) HCl. Air was sparged into the vessel from below at 3 L min^{-1} and DO was maintained at 30% by cascade to agitation at 200 – 800 rpm. Temperature was maintained at 37°C. Foaming was controlled by addition of PPG-2000. The bioreactor was inoculated to OD600 0.05 and cells aerated until ~ OD600 0.4 – 0.6 (2 h post-inoculation), induced with 100 mM urea (green arrow x-axis). At OD600 40 – 50 (23 h post-inoculation) feeding (714 g L−1 glycerol + 7.4 g L−1 MgSO4·7H2O) was at 18.5 mL h−1 (red arrow x-axis). Aeration proceeded until 24 h post-induction (50 h post-inoculation).

and continued to do so after induction (2 h post-inoculation), until reaching setpoint (30 %) and switching on the agitation cascade (200 – 800 rpm). DO was mostly maintained around 30% until approximately 8 h – 12 h post-inoculation where it dropped to around 2 % and then increased toward 30% again. This coincided with large addition of base, presumably due to overflow metabolism, which then stopped once DO increased back toward 30% as cell growth slowed (Figure 3.45B). Between 15 h and 23 h post-inoculation, DO increased to around 65 – 70 %, for fed-batch fermentation one and two respectively; this correlated with the point at which growth rates had decreased (Figure 3.54B) and during this point, base addition did not occur, although some acid was added. Upon initiation of feeding, DO almost immediately dropped from around 65 – 70 % to around 3 %; the agitation cascade switched on and DO increased, but it was not possible to maintain it at set point (30%), presumably due to density of cells growing. Base addition again increased during this period, once again likely due to overflow metabolism. DO remained fluctuating until the end of fermentation at 50 h post-inoculation.

3.5.3 Flow cytometer calibration

FCM analysis at 50 mL and 100 mL scales (section 3.2 – 3.4) were done using a BD Accuri C6 instrument; all fermentation work was completed using a BD Accuri C6 Plus. While the cytometer designs are near identical, to accurately compare fermentation work with that done previously a fed batch fermentation (Exp 1, discussed in section 3.5.2) was analysed using both the C6 and C6 Plus flow cytometers (C6 plus data was presented previously in section 3.5.2).

For reference, BL21 harbouring the pET-15b-P_{uti101}-*6xhis::gfp* construct was grown in 1.5 L semi-defined medium + Amp; cells were induced with 100 mM urea at OD_{600} ~ 0.4 – 0.6 (2 h post-inoculation). At OD_{600} 40 – 50 (23 h post-inoculation), feeding with 714 g L^{-1} glycerol + 7.4 g L^{-1} $MgSO_4 \cdot 7H_2O$ with 714 g L^{-1} glycerol + 7.4 g L^{-1} $MgSO_4 \cdot 7H_2O$ was initiated at 18.5 mL h^{-1}. Growth continued until exhaustion of the feed (50 h post-inoculation) (see section 3.5.2). In the bioreactor, pH was maintained at 6.3 +/- 0.1 using 10 % (w/v) NH4OH or 5 % (w/v) HCl. Air was sparged into the vessel from below at 3 L min-1 and DO was maintained at 30% by cascade to agitation at 200 – 800 rpm. Temperature was maintained at 37°C. Foaming was controlled by addition of PPG-2000. The fed batch fermentation was then analysed using BD Accuri C6 and BD Accuri C6 Plus flow cytometers.

Mean green fluorescence was comparable between cytometers until reaching approximately 60000 AU, where the C6 Plus appeared to have a greater range of detection at higher fluorescence values (Figure 3.51A). The C6 Plus showed a maximum mean green fluorescence value of around 160000 AU; on the C6 this value was around 1.6-fold lower at 100000 AU. Mean FSC was comparable in terms of pattern and comparable over the whole range of detection, R^2 being 0.96 (Figure 3.51B). The most notable difference was at 1 h post induction; FSC was 50000 AU on the C6 Plus but 30000 AU on the C6. Cell density was virtually the same across both cytometers, the C6 Plus detecting slightly lower cells mL^{-1} values at most time-points (Figure 3.51C).

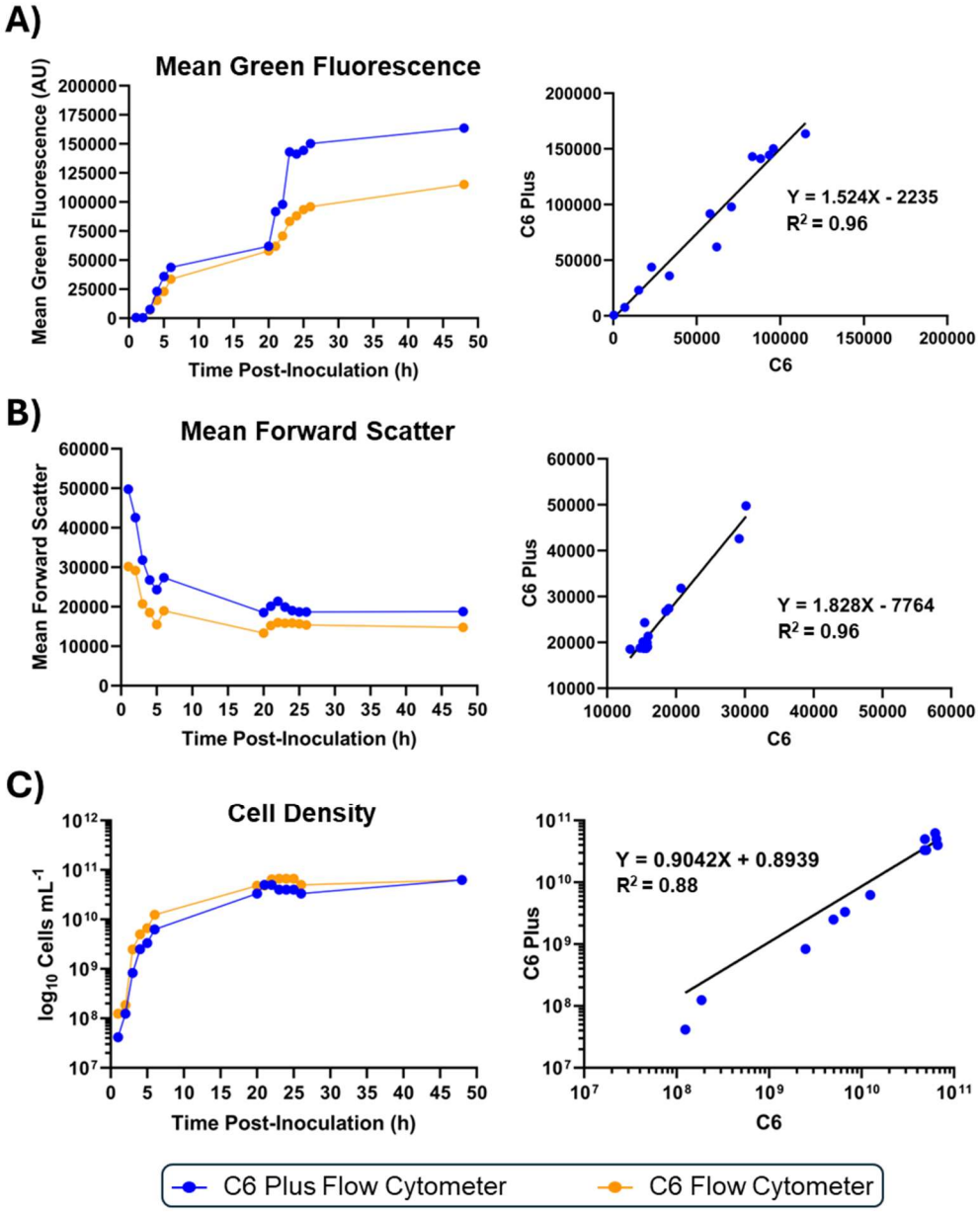


Figure 3.51: Comparison of C6 and C6 Plus flow cytometer performance during early induction late feeding fermentation (Exp 1).

BL21 harbouring the pET-15b-P*uti101*-*6xhis::gfp* construct was grown in 1.5 L semi-defined medium + Amp. In the bioreactor, pH was maintained at 6.3 +/- 0.1 using 10 % (w/v) NH_4OH or 5 % (w/v) HCl. Air was sparged into the vessel from below at 3 L min^{-1} and DO was maintained at 30% by cascade to agitation at 200 – 800 rpm. Temperature was maintained at 37°C. Foaming was controlled by addition of PPG-2000. The bioreactor was inoculated to OD_{600} 0.05 and cells aerated until ~ OD_{600} 0.4 – 0.6 (2 h post-inoculation), induced with 100 mM urea **(green arrow)**. At OD_{600} 40 – 50 (23 h post-inoculation) feeding (714 g L^{-1} glycerol + 7.4 g L^{-1} $MgSO_4 \cdot 7H_2O$) was at 18.5 mL h^{-1} **(red arrow)**. Aeration proceeded until 24 h post-induction (50 h post-inoculation). Data is shown for Exp 1 early induction late feeding fermentation (Exp 1). Calibration curves (right) are provided for each plot (left).

Mean green fluorescence measured via FCM **(A)** was similar between cytometers up till approximately 60000 AU, where the C6 plus appeared to have a greater range of detection at higher fluorescence values. Mean FSC measured via FCM **(B)** was broadly comparable and followed a similar pattern with the C6 plus showing a better range of detection at higher FSC values. Cell density measured via FCM **(C)** was virtually the same across both cytometers, the C6 plus detecting a slightly lower cells mL^{-1} value at 1 h post-inoculation.

3.5.4 Analysis of Recombinant proteins from Fermentation Analysis

For each fed-batch fermentation, samples were harvested and analysed by SDS PAGE to quantify 6xHis::GFP expression. Data is shown for fed-batch fermentations using early or late induction with urea; samples were resolved at 24 h post-induction (Ind) and the exhaustion of the feed (Feed). In all samples (Figure 3.52), bands were present above the 26 kDa marker, corresponding to the mass of 6xHis::GFP (~ 26.9 kDa). Late induction combined with feeding at a high cell density resulted in poor titre of 6xHis::GFP, this matched the mean green fluorescence data obtained during this fermentation (Figure 3.43A). Early induction with feeding at high cell densities (section 3.5.2) produced much denser bands and correlated with the far higher mean green fluorescence values seen during those fermentations (Figure 3.46A). Interestingly, in both repeat fed-batch fermentations (Exp 1 and Exp 2), bands were denser at 24 h post-induction (26 h post-inoculation) than after exhaustion of feed (48 h post-inoculation), possibly due to differences in 6xHis::GFP solubility at different time-points.

Intensity of bands resolved by SDS PAGE were analysed in ImageJ (Fiji) to quantify protein concentration. Titre of 6xHis::GFP (Figure 3.53A) using late induction with urea led to accumulation of approximately 0.03 g L^{-1} 6xHis::GFP at 24 h post induction (47 h post-inoculation). For early induction with urea, 0.12 g L^{-1} and 0.14 g L^{-1} 6xHis::GFP was accumulated in fed-batch fermentations at 24 h post-induction (26 h post-inoculation), a 4-fold increase over late induction. Upon exhaustion of feed (50 h post-inoculation), there was apparently lower 6xHis::GFP titre in fed-batch fermentations induced early, at 0.09 g L^{-1} and 0.13 g L^{-1} respectively. We assumed this was because

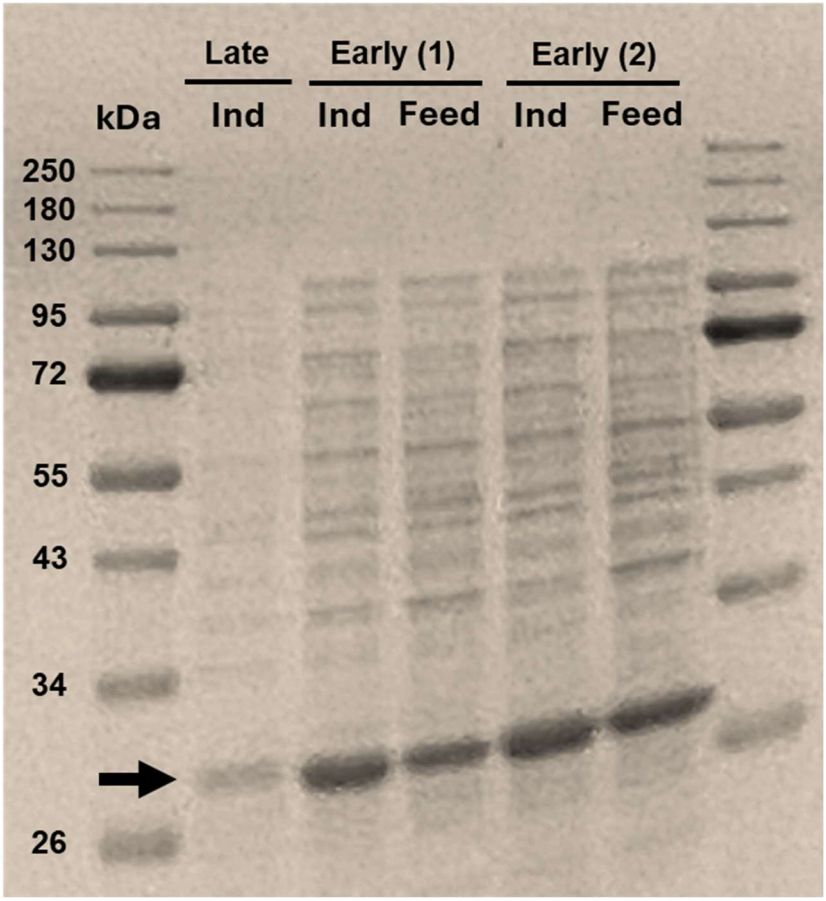


Figure 3.52: SDS PAGE analysis of 6xHis::GFP accumulation in fed-batch fermentations.

SDS PAGE was used to quantify 6xHis::GFP expression during fermentation. Whole cell lysates were normalised to OD_{600} 1.0 and 10 µL of a 1:1 mix with 2X SDS PAGE sample buffer was loaded into each well.

Data is shown for fed-batch fermentations using early or late induction with urea. Ladders are loaded in lanes 1 and 7. In lane 2, samples from fed batch fermentation using late induction (23 h post-inoculation) and late feeding (23 h post-inoculation). Lane 2 and 3, from fed batch fermentation using early induction (Exp 1); lane 2 represents (24 h post-induction/26 h post-inoculation); lane 3 represents exhaustion of feed (48 h post-induction/50 h post-inoculation). Lane 4 and 5, from fed batch fermentation using early induction (Exp 2); lane 4 represents (24 h post-induction/26 h post-inoculation); lane 5 represents exhaustion of feed (48 h post-induction/50 h post-inoculation).

In all samples resolved, bands were present above the 26 kDa marker, corresponding to the mass of 6xHis::GFP (~ 26.9 kDA). Late induction combined with feeding at a high cell density resulted in poor overexpression of 6xHis::GFP. Early induction with feeding at high cell densities produced much denser bands; in both repeats (1 and 2), bands were denser at 24 h post-induction/26 h post-inoculation than after exhaustion of feed.

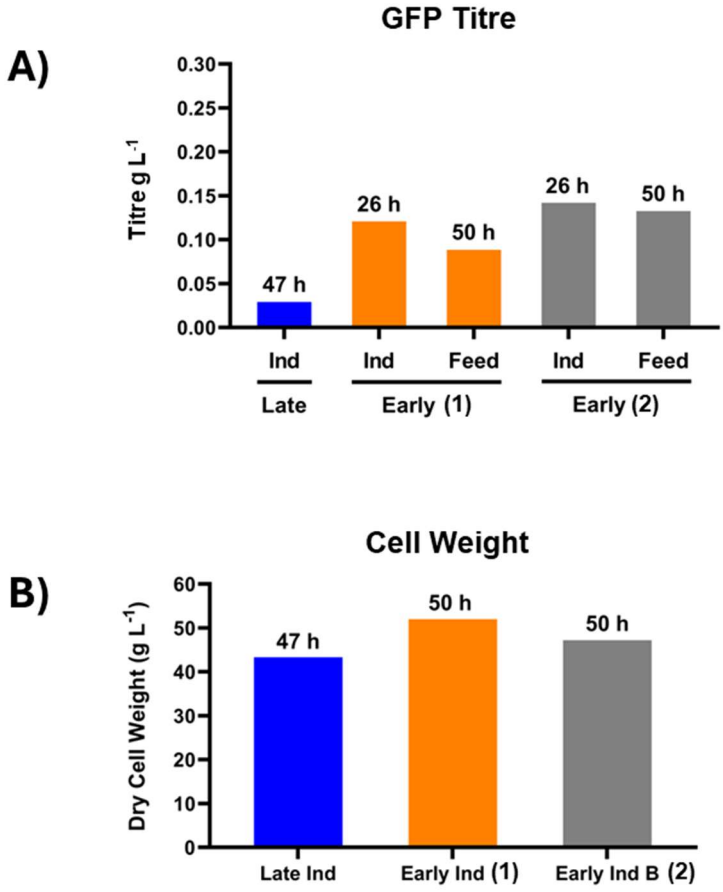


Figure 3.53: Fermentation performance based on GFP titre following SDS PAGE analysis and dry cell weight.

(A) SDS PAGE was used to quantify 6xHis::GFP expression during fermentation. Whole cell lysates were normalised to OD_{600} 1.0 and 10 µL of a 1:1 mix with 2X SDS PAGE sample buffer was loaded into each well. Band intensity for samples resolved via SDS PAGE was calculated in Fiji (ImageJ) and used to estimate protein concentration. Data is shown for fed-batch fermentations using early or late induction with urea. Two repeat fermentations are shown for early induction (1 and 2). Data shown is at 24 h post-induction/26 h post-inoculation (Ind) and exhaustion of feed at 48 h post-induction/50 h post-inoculation (Feed).

(B) Dry cell weight (DCW) was calculated at the end of each fermentation.

in these fermentations, higher percentages of low green fluorescence cells were present (Figure 3.48). Further, the discrepancy was attributed to differences in OD_{600} between fermentations (Figure 3.53A) affecting normalisation to 1.0 even though cell density was similar, or differences in 6xHis::GFP solubility and thus green fluorescence. Finally, DCW was calculated for each fed-batch fermentation, with each accumulating 40 – 50 g L^{-1} of cell biomass (Figure 3.58B); the two fed batch runs induced early being slightly higher.

3.6 Discussion

In this work, a novel urea inducible promoter from the urinary pathogen *P. mirablis* has been evaluated for use in RPP. Presently available inducible systems often have caveats with their use. Those incorporating *lac* promoters, including the popular T7 promoter, exhibit high basal expression (Spehr et al., 2000) and the available solutions are not always optimal (Studier, 1991a). Similarly, the P_{araBAD} promoter while tightly regulated is not tuneable at cellular level, due to all-or-nothing induction observed at sub-saturating inducer concentrations (Siegele and Hu, 1997, Carrier and Keasling, 1999). Further many inducers like IPTG, L-arabinose and L-rhamnose are expensive, some costing over £20000 kg^{-1} and thus induction can represent a sizeable cost at scale. Given inducible promoters are central to an expression system and major determinant of process efficiency (Giacalone et al., 2006, Wittmann et al., 2008, Zhao et al., 2021, García-Calvo et al., 2023), there was a desire to evaluate novel systems which may exhibit improved characteristics while utilising cheaper inducers. Using a GFP reporter and combined with FCM analysis, we optimised application of the

promoter from flask through to bioreactor scale. Various parameters which govern the properties of an inducible system were tested and will be discussed in turn.

Foremost is the strength of expression driven by the P_{uti101} promoter; the motive central to RPP being a desire to accumulate high concentrations of bioactive product. As transcription is the initial step of a process culminating in protein synthesis, maximising rates have often been desirable to improve final yield. Here, we found that P_{uti101} drove moderate overexpression of 6xHis::GFP, and was comparable to the novel lacUV5 promoter, PAR4 (Hothersall et al., 2021). In section 3.4.7, green fluorescence using the P_{uti101} promoter reached around 150000 AU while for PAR4, around 140000 AU was reached. Although in Chapter 3, we had seen PAR4 reach 150000 AU. PAR4 is weaker than WT lacUV5, but stronger than P_{lac}; the distal O3 axillary operator being replaced with the stronger O1 operator, although a p34G mutation in the -35 hexamer brings it closer to consensus (Browning et al., 2019). Comparison of P_{uti101} with other promoters analysed under similar conditions using the same BD Accuri flow cytometer in our lab further highlights that the urea inducible promoter was around PAR4 strength, driving stronger expression than promoters like PAR1 but weaker than T7 promoter systems (Table 3.1). However, a multitude of other factors such as the availability of chaperones (Mamipour et al., 2017) and host physiology (Rajacharya et al., 2024) during culture can affect expression levels, so the values are not a perfect comparison.

In isolation the lower strength of P_{uti101} seems suboptimal (see Table 3.1 for relative strength compared to other promoters tested under comparable conditions), but protein accumulation is complex and multifaceted – there is a point at which the rate

Table 3.1: Promoter characteristics from work completed in our lab. In each instance, GFP expression was measured via FCM on a BD Accuri flow cytometer. Strength is the maximum mean green fluorescence (AU) observed during culture. Tightness refers to whether high basal expression was observed. Tunability refers to whether the promoter displayed dose dependence.

Promoter	Max Green Fluorescence	Tightness	Tunable	Reference
Shake flask cultures				
P_{uti101}	150000 AU	Very tight	Limited	This work (Chapter 3)
PAR4	150000 AU	Leaky	Yes	This work (Chapter 3)
PAR1	50000 AU	Leaky	Yes	(Hothersall et al., 2021)
PAR4	175000 AU	Leaky	Yes	(Hothersall et al., 2021)
PAR7	225000 AU	Leaky	Yes	(Hothersall et al., 2021)
P_{araBAD}	65000 AU	Very tight	No	This work (Chapter 4)
T7 pET	180000 AU	Leaky	Yes	This work (Chapter 4)
T7 pBAD	400000 AU	Leaky	No	(Zulkifly et al., 2023)
Bioreactor cultures				
P_{uti101}	180000 AU	Very tight	Limited	This work
T7 pBAD	400000 AU	Leaky	No	(Zulkifly et al., 2023)

of transcription often becomes deleterious to yield. T7 systems drive extreme levels of transcription (Sastry and Ross, 1997); a high influx of mRNA for a heterologous protein quickly saturates translation machinery, preventing expression of native proteins. In addition, the protein folding machinery can become saturated, leading to accumulation of misfolded proteins, inclusion bodies, and prevention of successful folding of native host proteins (Hoffmann et al., 2004). Compounded by other metabolic stressors caused by overexpression, what follows is upregulation of multiple overlapping pathways; the general stress (RpoS), heat shock (RpoH) and stringent responses (ppGpp) instigating pleiotropic effects which shut down growth and limit protein expression (Hoffmann and Rinas, 2004, Singh et al., 2012, Carneiro et al., 2013). These issues plague stronger inducible systems and often stress minimisation protocols which limit the rate of transcription are required (Wyre and Overton, 2014, Selas Castiñeiras et al., 2018b, Kasli et al., 2019, Stargardt et al., 2021, Rajacharya et al., 2024).

Minimising stress often requires a titratable promoter system, where the relationship between inducer concentration and expression is more linear. Overall tunability of the urea inducible system was limited; dose dependence was only notable when comparing massively different concentrations (see section 3.3.1 and 3.4.3). There are not many truly titratable promoters; the *lac* and *araBAD* promoters exhibit all-or-nothing expression when induced at under sub-saturating conditions (Novick and Weiner, 1957, Siegele and Hu, 1997). In these instances, the cell population is split between those that are fully induced, and those which have up taken little to no inducer and remain inactive; globally this gives the appearance of tunability, until expression is

observed at the single cell level (Marschall et al., 2017). P_{rhaBAD} promoters have been shown to be capable of very precise and linear expression dependent on rhamnose concentration. L-rhamnose metabolism by *E. coli* can be problematic however and lead to lower expression (Boronat and Aguilar, 1979). Certainly, one advantage of the urea inducible system is that is orthologous; many *E. coli* strains like K-12 and B variants using for RPP not able to metabolise urea (Konieczna et al., 2012) To counteract this in P_{rhaBAD} switches to orthogonal inducers like L-mannose or promoter modification are required (Wagner et al., 2008, Kelly et al., 2016).

Mechanistically precise tunability can be affected by the influx of an inducer into the cell and heterogeneity in the availability of symporters at the point of addition – ITPG and L-arabinose may diffuse across the membrane but are also actively transported by LacY and AraE; at low inducer concentrations, this is weighted toward the latter (Marbach and Bettenbrock, 2012, Afroz et al., 2014, Fritz et al., 2014). Urea being small and polar enters *E. coli* by diffusion (Zeidel et al., 1992) although P_{uti101} did appear to conform to the all or nothing paradigm. At the lower range, expression was switched on with as little as 1 mM urea and while green fluorescence was considerably reduced, 6xHis::GFP expression appeared to be homogenous at the cellular level. Hence, we would describe expression from P_{uti101} as on-off; if there is any dose dependence, it is within a narrow range as a threshold seemed to be reached at around 50 – 100 mM urea.

Dose response is highlighted in Figure 3.54 providing the relative maximum green fluorescence (%) achieved after induction with various concentrations of urea. It is

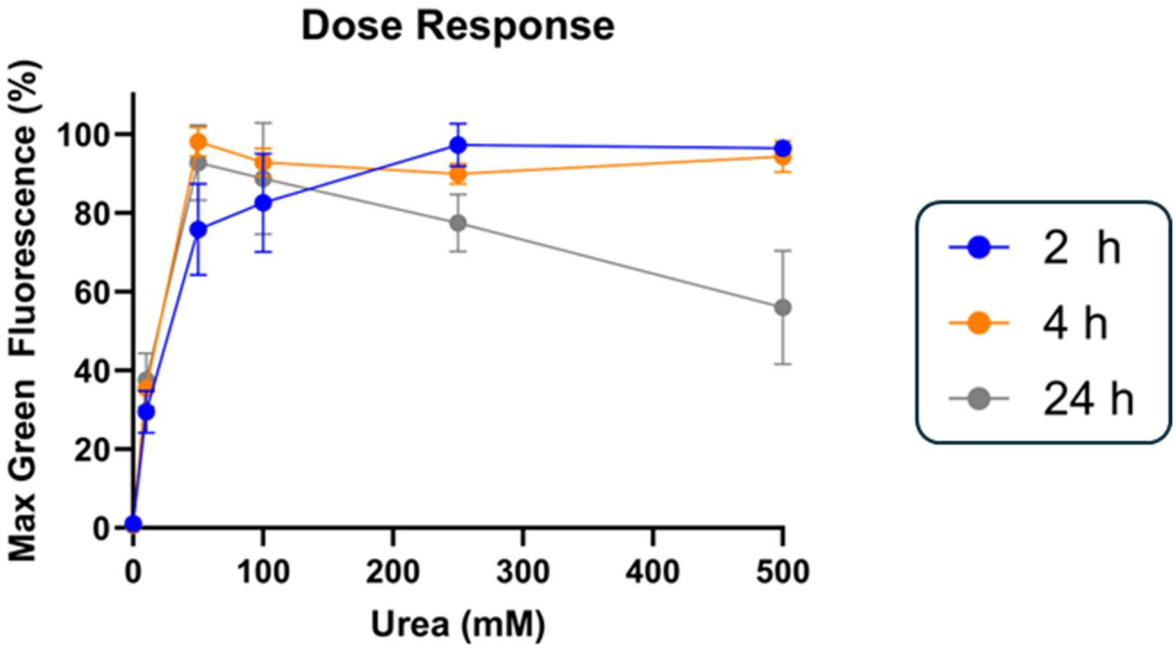


Figure 3.54: Dose response curves for urea (mM) concentrations used to induce 6xHis::GFP expression in BL21 harbouring the pET-15b-P$_{uti101}$-*6xhis::gfp* construct.

Data is shown for BL21 cultures in 100 mL TB + Amp using baffled Erlenmeyer flasks. This data was originally shown in Figure 3.28B for 2 repeat experiments. Maximum mean green fluorescence at each time-point (2 h, 4 h, 24 h) was identified and mean green fluorescence values converted to a percentage of this maximum. The mean percentage of the maximum green fluorescence is shown across both experiments for a total of 4 biological replicates with error bars representing +/- the SD. A threshold was reached at around 50 – 100 mM after which there was little benefit to 6xHis::GFP expression by increasing the concentration of urea and at 24 h, this was detrimental to the maximum green fluorescence achieved.

clear a threshold was reached at around 50 – 100 mM after which there was little benefit to 6xHis::GFP expression by increasing the concentration of urea and at 24 h, this was detrimental to the maximum green fluorescence achieved. We had initially wondered whether expression from P_{uti101} would increase at urea concentrations higher than 100 mM; the physiological concentration of urea reaches 500 mM in human urine (Fox-Moon and Shirtliff, 2015). However, as supported by Figure 3.54, at 50 – 100 mM urea, P_{uti101} appeared fully switched on without perturbation to the hosts physiology.

In section 3.4.6 we found P_{uti101} activity decreased significantly when inducing during stationary phase growth. For example, when inducing at OD_{600} 5 or 10, green fluorescence reached around 10000 – 30000 AU. When inducing earlier at OD_{600} 0.5, green fluorescence reached more than double at around 70000 AU. This partially limits the applicability of P_{uti101} to processes where it would advantageous to uncouple biomass accumulation from overexpression, such as when a protein is toxic (Ou et al., 2004). It is possible urea uptake was reduced in stationary phase; indeed permeability to various chemicals is known to change in the latter stages of growth (Whittle et al., 2021).

Alternatively, we considered the effects of the systems regulators. P_{uti101} is positively regulated by the AraC-like transcriptional activator UreR (D'Orazio and Collins, 1993, Nicholson et al., 1993) but negatively regulated by the nucleoid protein H-NS, the two competing for binding sites localised to the intergenic region between divergent promoters (Coker et al., 2000, Poore and Mobley, 2003). H-NS functions by structuring

the chromosome, condensing chromosomal DNA (Spurio et al., 1992) and thus in part, acting as a global transcriptional regulator. H-NS is autoregulated, but there are conflicting reports on whether its activity is lower (Falconi et al., 1993, Free and Dorman, 1995) or higher (Dersch et al., 1993, Ueguchi et al., 1993) in stationary phase cells. Certainly, if negative regulation of H-NS drops during stationary phase, this would account for lower expression from P_{uti101} when inducing at high cell densities. Further, HN-S activity is known to increase under cold shock however (La Teana et al., 1991, Brandi et al., 1994), and activity of P_{uti101} was shown to decrease when cells were grown at 25 °C (Hothersall et al., 2022b). Recent experiments in our laboratory have also demonstrated that RPP controlled from P_{uti101} is lower at 30 °C than 37 °C (Ashwathi Valiyaparambil, personal communication), presumably also due to H-NS. A final consideration for the poor expression during stationary phase is whether P_{uti101} is a σ^{70}-dependent (RpoD) promoter (Salgado et al., 2024). During stationary phase intracellular RpoD concentration is reduced and σ^{38} (RpoS) becomes the predominant sigma factor (Battesti et al., 2011, Schellhorn, 2020). It is possible lower RpoD concentration accounted for apparent lower activity of P_{uti101}.

A major advantage of P_{uti101} was shown to be its extremely tight regulation with only a low green fluorescence signal of around 700 AU observed prior to addition of urea. This was typically just 2 to 3-fold higher fluorescence than untransformed cells, which tended to have green fluorescence signals of around 200 – 300 AU. Importantly, basal expression remained low throughout growth till 24 h post-induction and was not affected by scale-up into baffled Erlenmeyer flasks (see sections 3.3.4 and 3.4.5). We found this was broadly comparable with the low background expression observed with

the P_{araBAD} promoter (Chapter 4), considered a very tightly regulated promoter (Guzman et al., 1995). Indeed the positive regulator for the system UreR is an AraC-like transcriptional activator (Poore et al., 2001). Presumably H-NS is also in part responsible for the extremely low background expression observed in seed cultures and uninduced cultures as it provides a second layer of regulation (Coker et al., 2000, Poore and Mobley, 2003). Regardless, in other expression systems, basal expression is considerably higher. When using PAR4, a P_{lac} derivative which is weaker and more tightly repressed than WT lacUV5 (Browning et al., 2019), we found basal fluorescence in the absence of IPTG reached around 25000 AU at 24 h post-induction (section 3.4.7), a 35-fold increase over P_{uti101}. Similarly, when using a T7*lac* system (chapter 4), basal green fluorescence, even pre-induction was at over 10000 AU.

It may be possible to improve promoter performance further. P_{uti101} is positively regulated by UreR when bound to urea (Thomas and Collins, 1999) and negatively by H-NS (Coker et al., 2000); both of which compete for binding of a curved A/T rich intergenic region between *ureR* and P_{uti101} promoters (Poore and Mobley, 2003). Modification of this intergenic region to reduce curvature by substituting A/T nucleotides would presumably reduce negative regulation and potentially increase expression. Without negative regulation, the system is then more dependent on the concentration of urea added which could improve tuneability. Knockout of the gene encoding H-NS is another option, although as a global negative transcriptional regulator its complete removal while not lethal, would have serious effects to physiology that could negatively affect RPP (Dorman, 2004). However, removal of H-

NS or reducing binding to intergenic regions would likely increase basal expression from P_{uti101} as only one level of regulation would be present.

Concentrations of urea 500 mM appeared to consistently increase FSC, and this correlated with increased cell length when analysed by fluorescence microscopy but was dependent on overexpression of 6xHis::GFP (section 3.2.2); the FSC of untransformed cells was far less affected by high urea concentrations. This was interesting; lower concentrations of urea (50 – 100 mM) appeared to induce similar or greater levels of 6xHis::GFP expression, yet FSC in these cultures was comparable to uninduced cells. High level overexpression of a recombinant protein is known to increase cell size (Jeong and Lee, 2003) and our lab has observed similar previously using a T7 system (Zulkifly et al., 2023), but here this was only in tandem with very high urea concentrations. During microscopy analysis, we observed significant filamentation in transformed cells induced with 500 mM urea, but not so much in untransformed variants.

Filamentation is a phenomenon resulting from inhibition to septation, the cause of which can be from a wide range of external stimuli, acting as a type of protective mechanism by inhibiting cell division (Justice et al., 2008). One pathway well associated with filamentation is the SOS response (Simmons et al., 2008), which is induced by DNA damage and division defects. For example, the protein SulA inhibits cell division via FtsZ and is upregulated during the SOS response (Trusca et al., 1998). Being chaotropic, urea will denature structure of nucleic acids in addition to proteins, so it is possible this had some effect. Regardless, we expected urea to have a greater

effect on host physiology, but only minimal growth arrest was observed at 500 mM, and in JCB387, very few dead cells were detected after viability staining. Further, we had looked at whether addition of 500 mM urea induced expression of the CpxAR periplasmic stress response utilising a P_{spy}-*gfp* reporter (see chapter 5) but did not observe any increase in green fluorescence (data not shown). Regardless, increased FSC and thus filamentation seemed restricted to 500 mM urea and thus a far higher concentration than would be needed for RPP; we found the optimal concentration for induction to be 50 – 100 mM. Besides doing little to improve expression from P_{uti101}, concentrations over 250 mM would prove unwieldly at scale – inducing a large vessel with 500 mM urea would require large volumes of concentrate and significantly dilute the culture.

Future work on the urea inducible P_{uti101} promoter must initially look at application of optimised conditions to a more industrially relevant recombinant protein. Optimising scale-up greatly improved green fluorescence and thus 6xHis::GFP expression (Table 3.2); it would be crucial to see how this applies to other recombinant proteins that are more difficult to express than GFP. Further, conditions normally considered difficult to express would be particularly relevant due to the tight regulation and not overly strong expression exhibited by P_{uti101}. It would also be useful to see how addition of urea affects various stress responses. Viability staining and growth rates indicated minimal impact on the host but filamentation in response to urea treatment and protein overexpression indicates some physiological change was occurring. We briefly looked at whether urea induced CpxAR and BaeSR utilising a P_{spy}::GFP sensor developed in Chapter 5 of this work, but did not observe a notable response (data not shown). Other

Table 3.2: A summary of the maximum green fluorescence, as measured via FCM analysis achieved for each strain used during scale-up.
It was clear that optimisation of growth through scaling from 50 mL to 100 mL and finally fed-batch fermentation, 6xHis::GFP expression could be increased.

50 mL LB			
Strain	**Urea Concentration (mM)**	**Mean Green Fluorescence (AU)**	**Section**
JCB387	500	94938	3.3.1
BL21	500	69907	3.3.2
100 mL TB			
BL21	100	180865	3.4.3
Fementation			
BL21	100	218249	3.5.2

stress pathways such as RpoS, RpoH and the SOS response all warrant investigation, and this could also be facilitated via GFP fusions to appropriately regulated promoters.

3.7 Conclusions

The aim of this project was to investigate the applicability of a novel promoter for RPP. To do so, we explored the use of a novel urea inducible promoter from *P. mirablis* and optimised expression of a model protein 6xHis::GFP from flask to bioreactor scale. Throughout the various stages of scale-up, we attempted to determine the strength and tuneability of expression, the levels of basal expression in the absence of urea, and the effect of the inducer urea on host cells.

When induced in early log phase cells, P_{uti101} drives expression of controlled genes comparable to medium strength *lac* promoters with little impact to growth characteristics. High cell density culture during fed-batch fermentation was able to improve this further, reaching over 20 g L^{-1} of recombinant 6xHis::GFP at a DCW of 45 g L^{-1}. To highlight this, a summary of expression of 6xHis::GFP based on the maximum mean green fluorescence observed at each stage of scale-up is provided in Table 3.2. However, we found that induction of P_{uti101} in the latter stages of growth was not possible. Given uncoupling proteins expression and biomass accumulation is an effective strategy, future work should look to probe the reasons for this, be it reduced influx of urea (Whittle et al., 2021) or the effects of increased negative regulation by H-NS (Free and Dorman, 1995, Dersch et al., 1993).

Unlike many inducible promoters, basal expression from P_{uti101} in the absence of urea was found to be extremely low and equivalent to the negative regulation seen with the frequently used P_{araBAD} promoter (Guzman et al., 1995). This was one of the greatest strengths of the urea inducible promoter. When looking at dose dependence and overall tunability of the system, it was observed that although an inducible range between 1 mM – 50 mM urea was evident, induction with higher concentrations resulted in diminishing returns for protein accumulation. P_{uti101} is regulated both positively via urea addition (Thomas and Collins, 1999) and negatively via HN-S (Coker et al., 2000, Poore and Mobley, 2003). Modification of the promoter to remove or reduce negative regulation so that expression is solely dependent on urea addition could possibly improve tunability, but at the expense of basal expression.

When combined with high level overexpression of 6xHis::GFP, we frequently observed filamentation at urea concentrations around 500 mM. This indicated possible stress and division defects like seen during SOS response (Simmons et al., 2008), although given it predominantly occurred in cells overexpressing 6xHis::GFP urea was clearly not the sole driver for this. In addition, urea concentrations required for this phenomenon were above the optimal found to achieve maximum expression, which was generally around 50 – 100 mM. Further, use of high concentrations of urea somewhat defeats one advantage of the urea inducible promoter, that it is a cheap inducer.

Future work should look to evaluate the promoter at fed-batch scale using an industrially relevant model protein and seek to improve promoter performance by

engineering of overall strength and tunability. Regardless, the work presented here shows the urea inducible system should be an asset in expanding the *E. coli* genetic toolbox. Its low basal expression which can be switched on by a cheap and readily available inducer provides a solid alternative to those currently available. Combining GFP with FCM provided great insight into promoter and inducer dynamics at the single cell level and further supports its use for optimisation of RPP in *E. coli*. Thus, in this work we have met the initial aims and objective set out initially and have thoroughly evaluated a new inducible platform with great applicability for future RPP work.

Chapter 4: Periplasmic GFP Reporters

4.1 Introduction

Much work on RPP in *E. coli* has focused on optimising overexpression of proteins within the cytoplasm, and owing to decades of research, localisation of recombinant proteins here is more of a known quantity (Sorensen and Mortensen, 2005, Overton, 2014, Rosano and Ceccarelli, 2014, Zhang et al., 2022). Several recombinant proteins are expressed in other cellular compartments like the periplasm (covered in section 1.5.5). Expression here is advantageous (section 1.5.3); offering a lower protein content with fewer proteases to aid product stability (Talmadge and Gilbert, 1982); simplifying downstream processing (Schimek et al., 2020) and crucially providing access to the Dsb system (Bardwell et al., 1991), disulphide bonding being essential for many recombinant proteins (Berkmen, 2012).

Screening is imperative to optimise a production system but has proven problematic in the periplasm. Traditionally this was done by liberating the periplasmic contents via chemical or physical means from spheroplasts and resolving the resulting fractions by SDS PAGE or immunoblotting (Lall et al., 1989, Davidson and Sun, 2002); this time-consuming and not conducive to a high throughput approach though. We have recently reviewed several methods for more rapid quantification of proteins localised to the periplasm (Osgerby and Overton, 2023) and this was covered in section 1.5.4. While methods such as halo (HT7) tags (Ke et al., 2016), tetracysteine (Tc) tags (Lee et al., 2016, Gao et al., 2018) and β-lactamase fusions (Heggeset et al., 2013, Selas Castiñeiras et al., 2018a, Mirzadeh et al., 2020) have proved useful in optimising periplasmic expression, they still require multiple processing steps after sampling to

detect recombinant proteins (Osgerby and Overton, 2023). GFP reporter fusions to a protein of interest combined with cytometric analysis would offer more real-time detection.

A huge assortment of GFP derivatives are currently available for use (Day and Davidson, 2009). Several mutations have improved usage in *E. coli*; F64L/S65T improve folding, fluorescence intensity and create a single excitation peak (Heim et al., 1995, Cormack et al., 1996); F99S, M153T, and V163A aid maturation at 37 °C (Crameri et al., 1996); A206K reduces propensity for GFP to dimerise (Zacharias et al., 2002). Unfortunately, most GFP derivatives are non-fluorescent in oxidising environments when delivered in an unfolded conformation (Figure 4.1); theorised due to two cysteine residues, C48 and C70, aberrant disulphide bonding resulting misfolding (Jain et al., 2001, Dammeyer and Tinnefeld, 2012). In support of this, other fluorescent proteins devoid of cysteine residues fluoresce in the periplasm, including the DsRed (Matz et al., 1999) derivatives mRFP1 (Chen et al., 2005) and mCherry (Dinh and Bernhardt, 2011); though red fluorescent proteins tend not to have optimal physical properties.

GFPmut3* was fluorescent when exported in a fully folded state via Tat (Thomas et al., 2001); C48 and C70 being internalised and protected from access by the Dsb system, though this not ideal as Sec is the primary export machinery in *E. coli* (Orfanoudaki and Economou, 2014). More recently, the derivative sfGFP was shown to be fluorescent when exported to the periplasm via Sec (Aronson et al., 2011, Dinh and Bernhardt, 2011). The superfolder mutations S30R, Y39N, N105T, Y145F, I171V

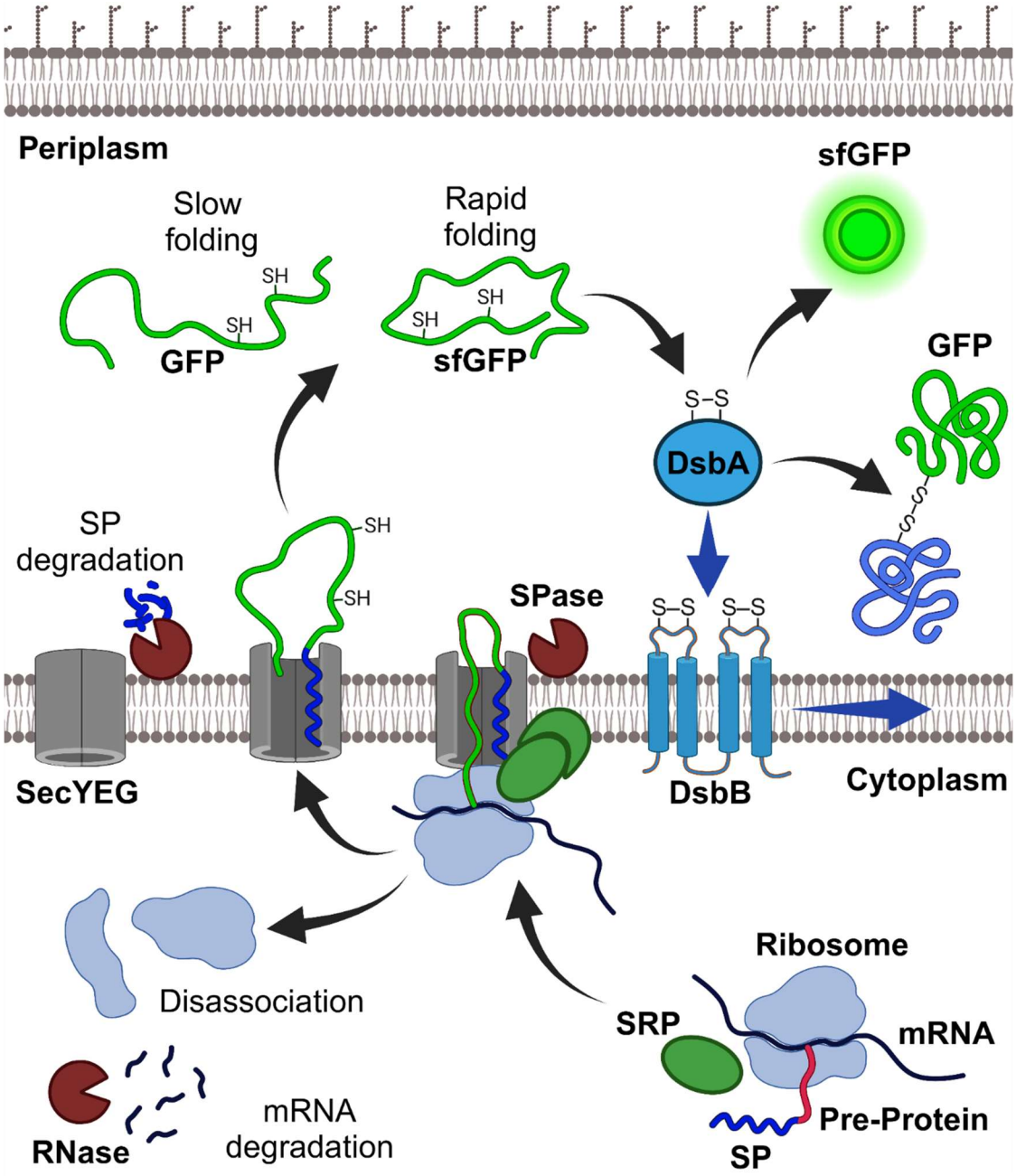


Figure 4.1: sfGFP supposedly fluoresces in the bacterial periplasm even when exported via Sec. Figure adapted from (Osgerby and Overton, 2023). Created with Biorender.com.

When exported via the post-translational of Sec, the RNC is coupled to SecYEG via SRP and its cognate receptor at the membrane FtsY. Translation occurs through the channel; upon termination the ribosome is recycled, and mRNA degraded.

On the periplasmic side, SPase degrades the signal peptide (SP) releasing nascent GFP into the periplasm. Rapid folding of sfGFP quickly buries cysteine residues with β-barrel while in other GFP derivatives, they remain exposed.

Cysteine residues are readily oxidised by the Dsb system; DsbA the donor which is recycled by the membrane bound DsbB. Activity of the Dsb system causes GFP to form mixed disulphides and misfold. Comparatively, folding kinetics of sfGFP prevent this allowing it to reach a fluorescent state.

which promote improved folding kinetics (Pédelacq et al., 2006), were proposed to allow nascent periplasmic sfGFP to reach a mature fluorescent state before disulphide bonding occurs (Figure 4.1). There were conflicting reports on periplasmic fluorescence however, prior work indicating sfGFP was non-fluorescent in the periplasm (Fisher and Delisa, 2008). This discrepancy was attributed to differences in expression, the former using a chromosomally encoded copy of *sfgfp* compared with expression from a plasmid (Dinh and Bernhardt, 2011).

We were very interested in utilising a GFP-based screening tool to aid in optimising expression of recombinant proteins in the periplasm. Little information on application of sfGFP for screening under conditions relevant to RPP was found and it could be combined with FCM to offer high throughput. Hence, we looked at exploiting the rapid folding kinetics of sfGFP for application in more easily quantifying recombinant proteins localised to the periplasm. In combination with FCM, we have evaluated the use of sfGFP using expression constructs with differing strengths to determine whether it could be utilised to screen for periplasmic expression of recombinant proteins.

4.2 Periplasmic msfGFP reporters using a T7*lac* system

Similar to prior work (Aronson et al., 2011, Dinh and Bernhardt, 2011), we utilised a sfGFP derivative msfGFP, containing the super folder mutations S30R, Y39N, N105T, Y145F, I171V and a monomerising A206K mutation (Zacharias et al., 2002, Pédelacq et al., 2006).

To direct msfGFP for translocation, two signal peptides were selected. PelB^{SP} from the *Erwinia carotovora* pectate lyase B protein directs post-translational export (Lei et al., 1987) and chosen as a model for this pathway due to prior use (Selas Castiñeiras et al., 2018a). The second signal peptide DsbA^{SP}, has been consistently described as directing co-translational export of cargo proteins, although even in the original publication, this was not clear (Schierle et al., 2003). It has since been shown DsbA^{SP} is in fact unlikely to be an SRP substrate (Schibich et al., 2016). Regardless, DsbA^{SP} is presumably exported differently to PelB^{SP} and has been shown to direct more efficient export than other signal peptides (Selas Castiñeiras et al., 2018a). Further, DsbA^{SP} was shown necessary for export of msfGFP that reached a fluorescent conformation in the periplasm (Dinh and Bernhardt, 2011).

A T7*lac* system was selected to drive expression of msfGFP under the notion it would direct high level expression. A suite of constructs were generated directing msfGFP for export to the periplasm using pET-26b(+)-*pelB^{SP}*::*msfgfp* and pET-26b(+)Δ-*dsbA^{SP}*::*msfgfp*. A further construct pET-26b(+)-*msfgfp* expressing cytoplasmic msfGFP was generated as a control.

4.2.1 Expressing exported msfGFP via T7*lac*

To test the suite of T7*lac* driven msfGFP constructs, pET-26b(+)-*pelB^{SP}*::*msfgfp* and pET-26b(+)Δ-*dsbA^{SP}*::*msfgfp* and pET-26b(+)-*msfgfp* were transformed into BL21(DE3). Cultures were aerated at 30 °C, 200 rpm in 50 mL TB + Kan and induced with 50 µM IPTG at OD_{600} 0.4-0.6 with expression continuing until 24 h post-induction.

Untransformed BL21(DE3) was used as a further control; each strain was performed in duplicate.

Overexpression of msfGFP was tracked by measuring mean green fluorescence via FCM (Figure 4.2A). Mean green fluorescence in cultures expressing cytoplasmic msfGFP or PelB^{SP}::msfGFP were similar, reaching 112000 and 180000 AU at 4 h post-induction respectively; we were surprised this was higher in the latter. This was not verified by SDS PAGE or Western blotting, however. Comparatively mean green fluorescence for cultures expressing DsbA^{SP}::msfGFP was over 10-fold lower than cultures expressing cytoplasmic msfGFP or PelB^{SP}::msfGFP, reaching 10000 AU at 4 h post-induction, though this was still 50-fold higher than the untransformed control (Figure 4.2A). It was noted that background expression of msfGFP from T7*lac* appeared to be high; pre-induction, mean green fluorescence in all cultures was approximately 50-fold higher than the untransformed control. Expression of msfGFP in single cells was additionally monitored via FCM (Figure 4.3). Between induction and 4 h post-induction, cultures expressing cytoplasmic msfGFP or PelB^{SP}::msfGFP were mostly homogenous. DsbA^{SP}::msfGFP cultures were apparently split between low and high fluorescent populations, the former comparable with the untransformed control suggesting some type of mutation occurred to inactivate msfGFP expression or plasmid loss. Ideally we would have used replica plating to confirm whether cells retained the plasmid, although we thought it was more unlikely at 2 h and 4 h post-induction due to selection with kanamycin. At 24 h post-induction, all cultures bar the untransformed control had mixed populations of low and high green fluorescence, though more apparent in cultures expressing PelB^{SP}::msfGFP or DsbA^{SP}::msfGFP.

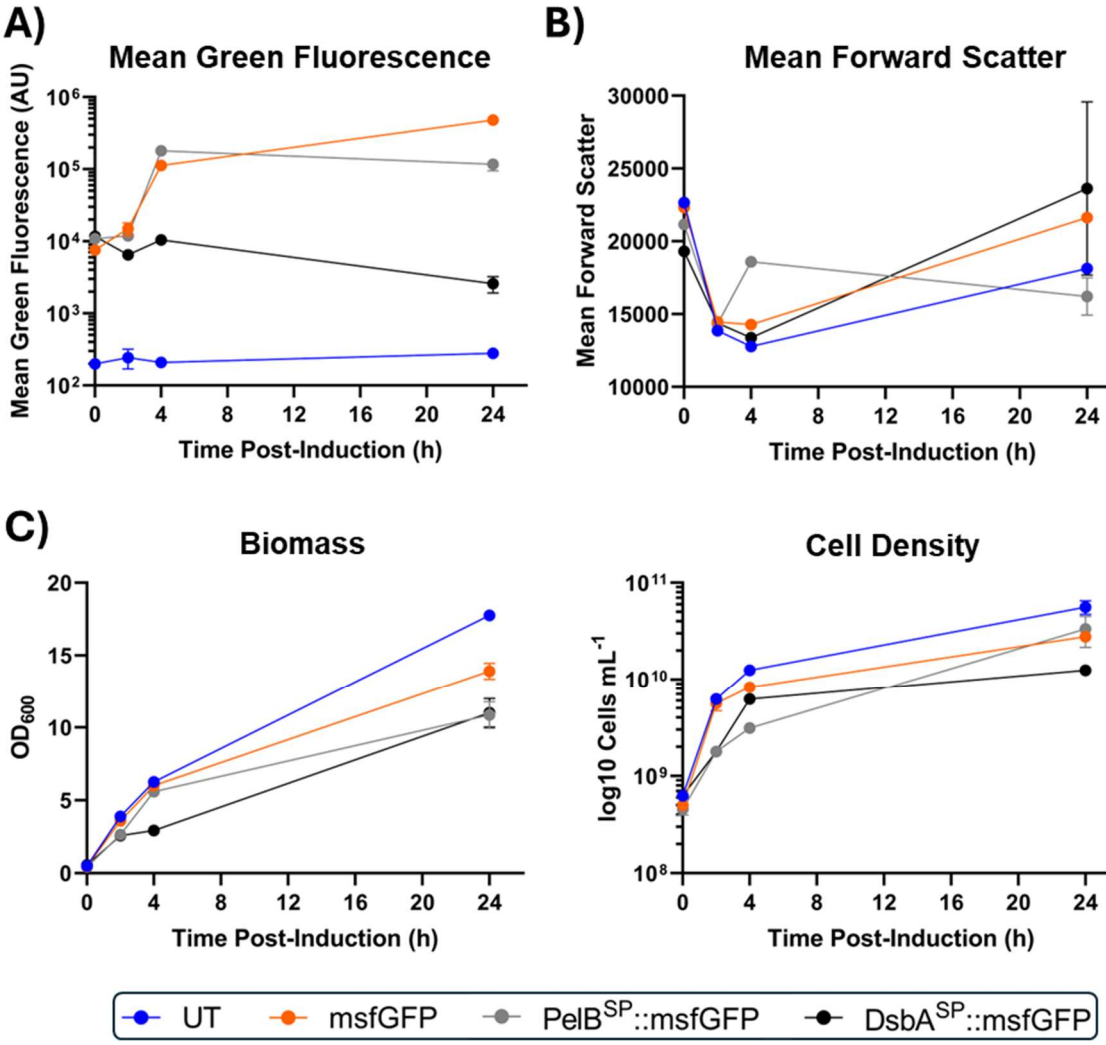


Figure 4.2: Effect of msfGFP expression on BL21(DE3) from T7*lac* constructs.

msfGFP expressed from T7*lac* was exported to the periplasm via fusion to PelB^{SP} or DsbA^{SP}; cytoplasmic and untransformed (UT) variants were used as controls. Cultures were aerated at 30 °C, 200 rpm in 50 mL TB + kan and induced with 50 µM IPTG at OD_{600} 0.4-0.6. Expression continued for a further 24 h. Error bars represent +/- SD from biological duplicates.

(A) Mean green fluorescence was monitored via FCM. Expression of PelB^{SP}::msfGFP was similar to the cytoplasmic control, albeit lower at 24 h post-induction. Mean green fluorescence in DsbA^{SP}::msfGFP cultures was about 10-fold lower than the cytoplasmic control.

(B) Mean FSC was monitored via FCM and was elevated in PelB^{SP}::msfGFP cultures at 4 h post-induction, most likely due to high expression, although this wasn't observed in the cytoplasmic control.

(C) Biomass accumulation and cell density were monitored via OD_{600} and FCM. PelB^{SP}::msfGFP and DsbA^{SP}::msfGFP cultures had some growth arrest following induction; the latter recovered somewhat but it appeared to be expressing little msfGFP.

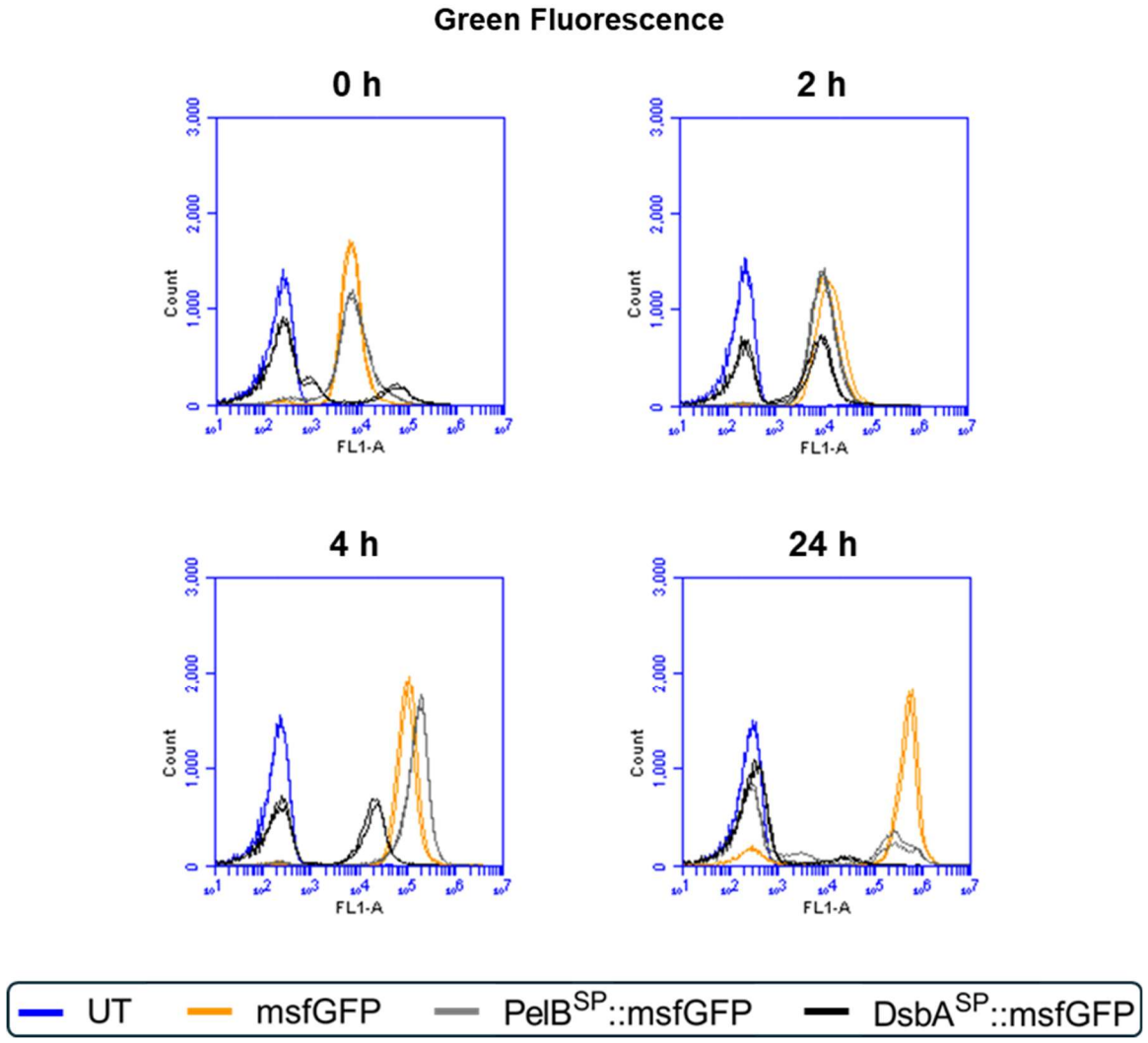


Figure 4.3: FCM analysis of green fluorescence from msfGFP expression in BL21(DE3) using T7*lac* constructs.

msfGFP expressed from T7*lac* was exported to the periplasm via fusion to $PelB^{SP}$ or $DsbA^{SP}$; cytoplasmic and untransformed (UT) variants were used as controls. Cultures were aerated at 30 °C, 200 rpm in 50 mL TB + kan and induced with 50 µM IPTG at OD_{600} 0.4-0.6. Expression continued for a further 24 h. Each condition is shown for biological duplicates.

Green fluorescence (FL1-A) was monitored in single cells using FCM. Populations were mostly homogenous until 24 h post-induction; $PelB^{SP}$::msfGFP and $DsbA^{SP}$::msfGFP cultures had large populations of cells with low green fluorescence at levels comparable with the UT control.

Based on green fluorescence analysis in single cells (Figure 4.3), it was clear expression of PelB^{SP}::msfGFP or DsbA^{SP}::msfGFP was not as well tolerated as expression of cytoplasmic msfGFP due to the heterogeneity observed in the former. To check for effects to physiology, mean FSC was monitored via FCM (Figure 4.2B). At 4 h post-induction, mean FSC in cultures expressing PelB^{SP}::msfGFP was elevated although it was not clear whether this was due to higher level expression of msfGFP or export as both the cytoplasmic control and DsbA^{SP}::msfGFP were similar. Biomass accumulation and cell density were also monitored via FCM (Figure 4.2C). At different time-points, cultures expressing PelB^{SP}::msfGFP or DsbA^{SP}::msfGFP appeared to have some growth arrest compared to the cytoplasmic control, dependent on whether obseerving OD_{600} or cell density.

To further quantify viability, cells were stained with PI and gated via FCM using red fluorescence (FL3-A) and green fluorescence (FL1-A) density plots. Cells were gated as viable with low green fluorescence (PI- GFP-), viable with high green fluorescence (PI- GFP+) or non-viable (PI+) populations (Figure 4.4). The cytoplasmic control appeared to have most cells within the PI- GFP+ gate indicating expression affected physiology less. In PelB^{SP}::msfGFP cultures, 20 % of cells were within the PI+ gate by 4 h post-induction, suggesting poor tolerance to export of msfGFP. Similarly, in DsbA^{SP}::msfGFP cultures, 10 % of cells were within the PI+ gate by 4 h post-induction. Even at induction, there were considerable numbers of cells within the PI+ gate for cultures expressing PelB^{SP}::msfGFP or DsbA^{SP}::msfGFP; presumably this was due to extremely poor growth between inoculation and induction for these strains. To even get cultures expressing PelB^{SP}::msfGFP or DsbA^{SP}::msfGFP to OD_{600} 0.4-0.6 for

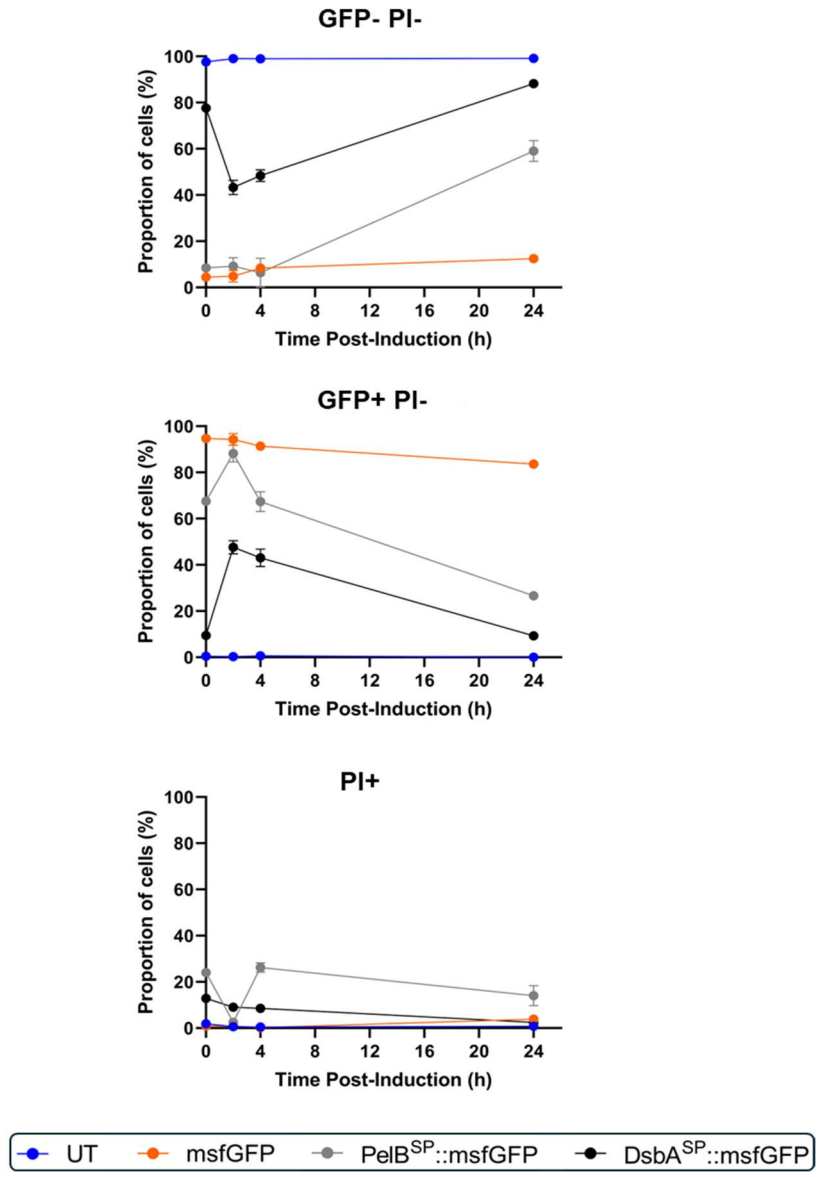


Figure 4.4: PI staining was used to assess viability of BL21(DE3) expressing msfGFP from T7*lac* constructs.

msfGFP expressed from T7*lac* was exported to the periplasm via fusion to PelB^{SP} or DsbA^{SP}; cytoplasmic and untransformed (UT) variants were used as controls. Cultures were aerated at 30 °C, 200 rpm in 50 mL TB + Kan and induced with 50 µM IPTG at OD_{600} 0.4-0.6. Expression continued for a further 24 h. Error bars represent +/- SD for biological duplicates.

To assess viability 4 µg mL^{-1} PI was used to stain cells. Cultures were gated as viable with low green fluorescence (GFP- PI-), viable with high green fluorescence (GFP+ PI-), or non-viable (PI+) using FCM and red fluorescence (FL3-A) and green fluorescence (FL1-A) density plots. In PelB^{SP}::msfGFP cultures, 20 % of cells were within the PI+ gate at 4 h post-induction suggesting poor tolerance to export of msfGFP. Similarly, in DsbA^{SP}::msfGFP cultures, 10 % of cells were in the PI+ gate at 4 h post-induction. Cells for the cytoplasmic control cultures were mostly within the PI- GFP+ gate throughout.

induction in a useful time-frame, the concentration of inoculum had to be increased from 0.05 to 0.1 and 0.15 respectively likely transferring over many plasmid free cells from the seed cultures although this was not assessed through replica plating as those strains were difficult to cultivate on solid medium. While PI technically measures membrane integrity, it is an indicator that cells are non-viable; taken together with growth data (Figure 4.2C), we concluded that expressing PelB^{SP}::msfGFP or DsbA^{SP}::msfGFP was likely detrimental to BL21(DE3).

To check if any msfGFP accumulated in the periplasm, cultures were fractioned into cytoplasmic (CF) and periplasmic (PF) fractions and resolved via SDS PAGE (Figure 4.5). In PelB^{SP}::msfGFP cultures, there were dense bands in PF fractions consistent with msfGFP (26.9 kDa) from 4 h post-induction. In cultures expressing DsbA^{SP}::msfGFP only faint bands consistent with msfGFP were present but partly expected due to the low levels of green fluorescence observed (Figure 4.2). Densitometry of SDS PAGE gels at 4 h post-induction using ImageJ (Fiji) indicated that for PelB^{SP}::msfGFP cultures, 22.27% of the msfGFP was in the periplasmic fraction. Interestingly for DsbA^{SP}::msfGFP cultures, densitometry analysis indicated 34.66% of msfGFP was in the periplasmic fraction; bands on the gel were faint though so this should be interpreted with caution. However, it has been suggested before though that DsbA^{SP} is an efficient exporter compared with other signal peptides (Horga et al., 2018, Selas Castiñeiras et al., 2018a). As periplasmic expression can place considerable stress on the host (Schlegel et al., 2013, Karyolaimos et al., 2019a), if DsbA^{SP} was more efficiently exporting msfGFP, this could be a reason for the poor viability observed in growth analysis (Figure 4.2C) and during PI staining (Figure 4.4).

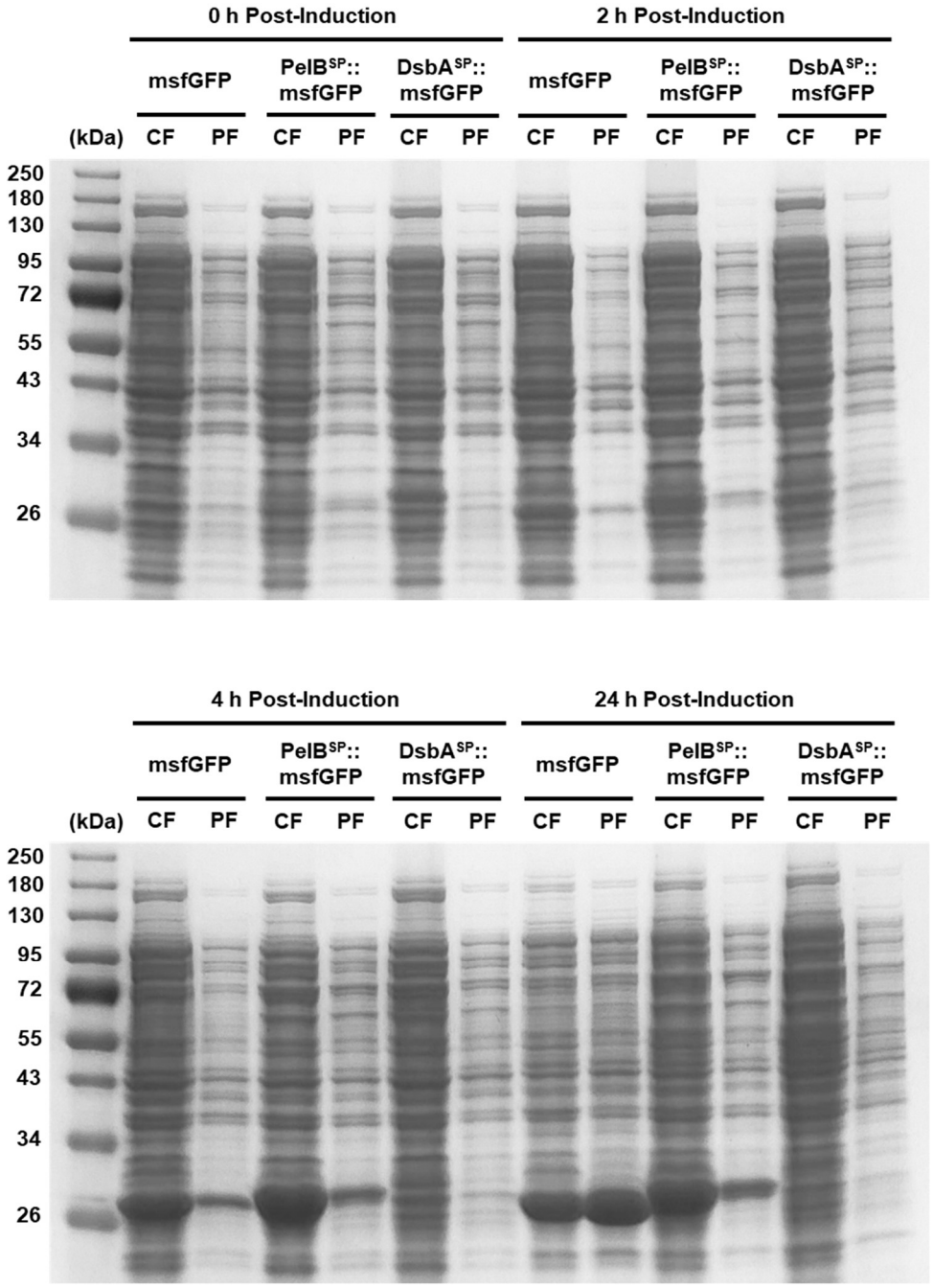


Figure 4.5: SDS PAGE analysis of BL21(DE3) expressing msfGFP from T7*lac* constructs.

msfGFP expressed from T7*lac* was exported to the periplasm via fusion to PelB^{SP} or DsbA^{SP}; cytoplasmic and untransformed (UT) variants were used as controls. Cultures were aerated at 30 °C, 200 rpm in 50 mL TB + Kan and induced with 50 µM IPTG at OD_{600} 0.4-0.6. Expression continued for a further 24 h.

Cultures were fractioned into cytoplasmic (CF) and periplasmic (PF) fractions and resolved via SDS PAGE. In PelB^{SP}::msfGFP cultures, there were dense bands in PF fractions consistent with msfGFP (26.9 kDa) from 4 h post-induction; however, there appeared to be considerable leakage between CF and PF fractions, as evidenced by the cytoplasmic control. Densitometry analysis of gels indicated 23.49% of msfGFP was periplasmic for PelB^{SP}::msfGFP cultures and 34.66% for DsbA^{SP}::msfGFP cultures, although in DsbA cultures expression was very low.

There appeared to be considerable leakage between CF and PF fractions though, as evidenced by the cytoplasmic control (Figure 4.5). It is possible the high expression from T7*lac* made cells particularly fragile and prone to damage during spheroplasting. However, it has been shown that during overexpression of recombinant proteins, excretion of cytoplasmic proteins across the IM and into the periplasm can occur in a mechanosensitive channel (MscL)-dependent manner (Morra et al., 2018). This would account for the observed presence of cytoplasmic msfGFP in periplasmic fractions (Figure 4.5). This does raise the question of whether periplasmic msfGFP seen in PelB^{SP}::msfGFP and DsbA^{SP}::msfGFP cultures was due to export or leakage. It is also possible that msfGFP leaked from the periplasm into extracellular medium (Kastenhofer et al., 2021). Additional SDS PAGE analysis of growth medium or western blotting for more accurate identification of msfGFP could have been performed but given the low percentages of msfGFP calculated in periplasmic fractions, there were clearly issues with the system.

4.2.2 Background expression from T7*lac*

As expression of PelB^{SP}::msfGFP or DsbA^{SP}::msfGFP from T7*lac* proved poorly tolerated by the BL21(DE3) host during growth in flasks. Part of the issue appeared to be high background expression pre-induction (Figure 4.2A) necessitating higher concentrations of inoculum be used to get cultures to an appropriate OD_{600} for induction.

Seed cultures for each strain were monitored; grown at 30 °C, 200 rpm for 16 – 18 h in 10 mL TB + Kan + 0.4 % (w/v) D-glucose for additional repression of T7*lac*. OD_{600}

of PelB^{SP}::msfGFP and DsbA^{SP}::msfGFP seed cultures were comparable with the cytoplasmic control (Figure 4.6A), reaching between 4.0 – 5.0 after overnight growth. As an indication of viability, seed cultures were stained using PI and gated via FCM using red fluorescence (FL3-A) and green fluorescence (FL1-A) density plots. Cells were gated as viable with low green fluorescence (GFP- PI-), viable with high green fluorescence (GFP+ PI-) or non-viable populations (PI+) (Figure 4.6B). Only around 1 – 2 % of cells were within the PI+ gate for PelB^{SP}::msfGFP and DsbA^{SP}::msfGFP seed cultures; over 95 % of cells were within the GFP+ gate, however highlighting the high basal expression from T7*lac*.

There was clearly some disconnect between what was observed after inoculation and at the seed stage. Cells in PelB^{SP}::msfGFP and DsbA^{SP}::msfGFP seed cultures were still expressing msfGFP and so likely not to be plasmid free, although replica plating would need to be used to confirm this. It is entirely possible some form of inactivating mutation to prevent export msfGFP had occurred, but constructs would need to be purified and sequenced to confirm this. However, if an inactivating mutation to export had occurred, large inoculums (0.1-0.15 instead of 0.05), would not have been required to get PelB^{SP}::msfGFP and DsbA^{SP}::msfGFP cultures to OD_{600} 0.4 – 0.6 in a meaningful timeframe during shake flask work (section 4.2.1). Further, growth after inoculation would presumably have been better during shake flask analysis as evidenced by cell density measurements (Figure 4.2C). Regardless, high background expression at the seed stage was clearly an issue which would limit the effectiveness of T7*lac*-msfGFP construct being utilised for a periplasmic screening system.

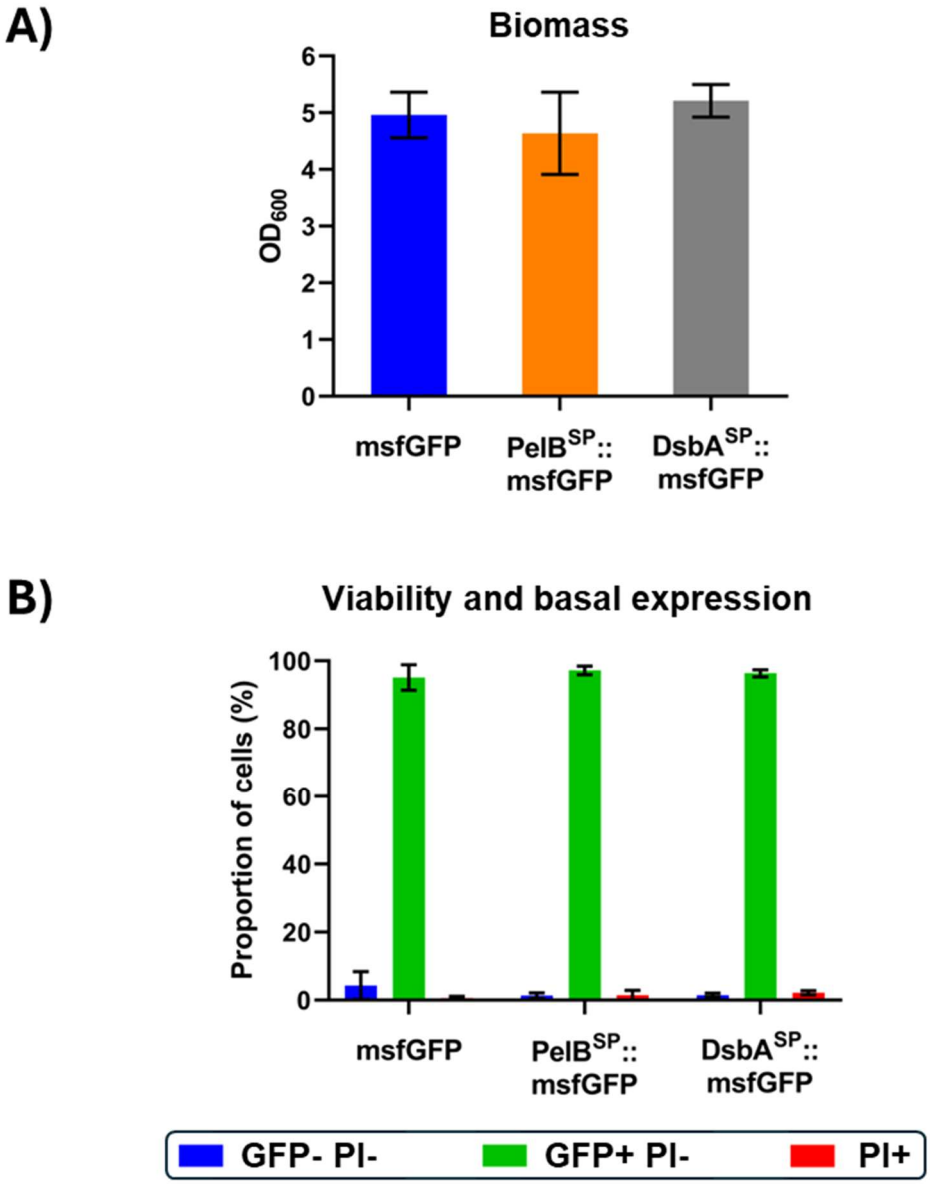


Figure 4.6: Analysis of basal expression and viability in seed cultures for BL21(DE3) expressing msfGFP from T7*lac* constructs.

msfGFP expressed from T7*lac* was exported to the periplasm via fusion to PelB^{SP} or DsbA^{SP}; cytoplasmic variants were used as controls. Seed cultures were aerated at 30 °C, 200 rpm in 50 mL TB + Kan + 0.4 % (w/v) D-glucose. Error bars represent +/- SD from for biological triplicate seed cultures.

(A) Regardless of whether cells expressed cytoplasmic or periplasmic msfGFP, biomass accumulation in seed cultures was similar.

(B) To assess viability 4 µg mL^{-1} PI was used to stain cells. Cultures were gated as viable with low green fluorescence (GFP- PI-), viable with high green fluorescence (GFP+ PI-), or non-viable (PI+) using FCM and red fluorescence (FL3-A) and green fluorescence (FL1-A) density plots. High basal msfGFP expression from T7*lac* was evident in all cultures, over 90 % of cells being within the GFP+ PI- gate. This presumably compounded the poor tolerance seen when expressing PelB^{SP}::msfGFP or DsbA^{SP}::msfGFP.

4.3 Periplasmic msfGFP reporters using a P_{araBAD} system

Expression of PelB^{SP}::msfGFP or DsbA^{SP}::msfGFP proved poorly tolerated by the BL21(DE3) host compounded by high basal expression of msfGFP from T7*lac* (section 4.2.1). This was not workable as a screening system, which would ideally have had minimal impact on the hosts physiology. We reasoned a tighter system was required which directed lower levels of expression. Tuning T7*lac* using T7 lysozyme to inhibit T7 RNA polymerase was considered (Studier, 1991b), but we decided a two plasmid system would be non-optimal. Instead, it was decided to switch promoters. P_{araBAD} is known to have low basal expression in the absence of its inducer L-arabinose (Guzman et al., 1995), so was used to generate a series of constructs driving expression of exported or cytoplasmic msfGFP; pBAD30-*kanR-pelB^{SP}::msfgfp*, pBAD30-*kanR-dsbA^{SP}::msfgfp* and pBAD30-*kanR-msfgfp*. The pBAD30 backbone was further chosen to reduce the gene dosage as it had a lower copy p15A origin rather than the high copy pBR322 variant found in pET vectors. Additionally, *ampR* in pBAD30 was replaced with *kanR* in an opposing direction to provide tighter selection and prevent readthrough from P_{araBAD}.

4.3.1 Background expression from P_{araBAD}

To ensure the suite of P_{araBAD} constructs were tightly regulated, seed cultures for each were monitored. BL21 seed cultures harbouring pBAD30-*kanR-pelB^{SP}::msfgfp*, pBAD30-*kanR-dsbA^{SP}::msfgfp* or pBAD30-*kanR-msfgfp* were grown at 30 °C, 200 rpm for 16 – 18 h in 10 mL TB + Kan + 0.4 % (w/v) D-glucose for additional repression of P_{araBAD}.

OD_{600} of $PelB^{SP}$::msfGFP and $DsbA^{SP}$::msfGFP seed cultures were comparable with the cytoplasmic control (Figure 4.7A), reaching over 4.0 after overnight growth; this was comparable with seed cultures for the T7*lac* system (Figure 4.6A). Viability of seed cultures was further quantified using PI and cells gated via FCM using red fluorescence (FL3-A) and green fluorescence (FL1-A) density plots. Cells were gated as viable with low green fluorescence (GFP- PI-), viable with high green fluorescence (GFP+ PI-) or non-viable populations (PI+) (Figure 4.7B). Few cells were within PI+ gates in any seed culture, at around just 0.5 % of the population. Further, over 99 % of cells were within the GFP- PI- gate indicating regulation of P_{araBAD} was indeed tight and prevented any basal msfGFP expression.

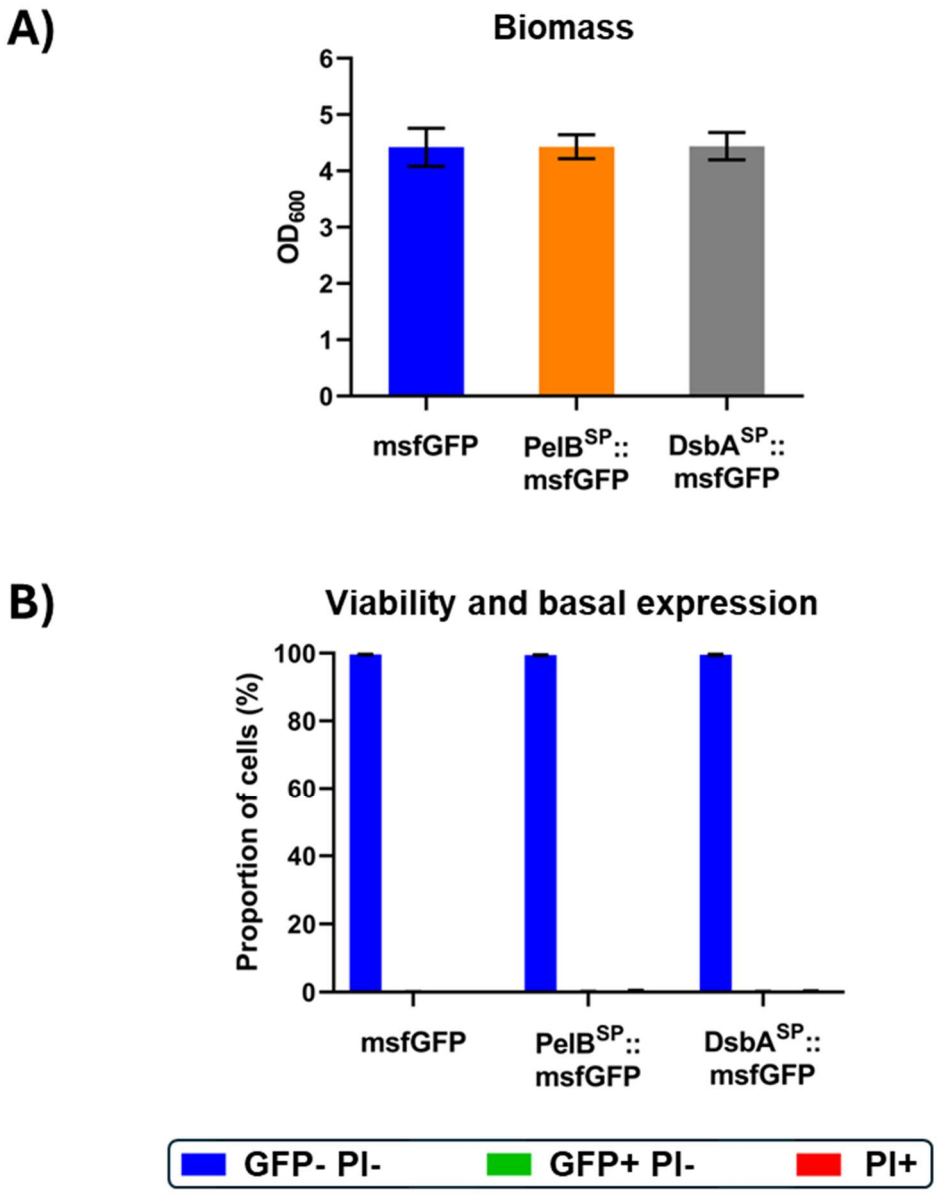


Figure 4.7: Analysis of basal expression and viability in seed cultures for BL21 expressing msfGFP from P_{araBAD} constructs.

Due to basal expression from T7*lac*, the system was swapped to one with tighter regulation. msfGFP expressed from P_{araBAD} was exported to the periplasm via fusion to $PelB^{SP}$ or $DsbA^{SP}$; cytoplasmic variants were used as controls. Seed cultures were aerated at 30 °C, 200 rpm in 10 mL TB + Kan + 0.4 % (w/v) D-glucose. Error bars represent +/- SD from for biological triplicate seed cultures.

(A) Regardless of whether cells expressed cytoplasmic or periplasmic msfGFP, biomass accumulation in seed cultures was similar.

(B) To assess viability 4 µg mL^{-1} PI was used to stain cells. Cultures were gated as viable with low green fluorescence (GFP- PI-), viable with high green fluorescence (GFP+ PI-), or non-viable (PI+) using FCM and red fluorescence (FL3-A) and green fluorescence (FL1-A) density plots. Basal msfGFP expression from P_{araBAD} was almost non-existent in all seed cultures with nearly 100 % of cells within the GFP- PI- gate.

4.3.2 Expressing exported msfGFP via P_{araBAD}

Tight regulation from P_{araBAD} and hence low basal expression of msfGFP (Figure 4.7B) meant cultures expressing PelB^{SP}::msfGFP and DsbA^{SP}::msfGFP should have been more viable between inoculation and induction. It was hoped this would permit better expression of exported msfGFP following initiation. To test the suite of P_{araBAD} driven msfGFP constructs, pBAD30-*kanR-pelB^{SP}*::*msfgfp*, pBAD30-*kanR-dsbA^{SP}*::*msfgfp* and pBAD30-*kanR-msfgfp* were transformed into BL21. Cultures were aerated at 30 °C, 200 rpm in 50 mL TB + kan and induced with 0.2 % (w/v) L-arabinose at OD_{600} 0.4-0.6, with expression continuing until 24 h post-induction. Untransformed BL21 was run as an additional control, with each strain repeated in duplicate cultures.

Overexpression of msfGFP was tracked by measuring mean green fluorescence via FCM (Figure 4.8A). Predictably, compared with T7*lac* (Figure 4.2A), mean green fluorescence was lower in general when driving expression from P_{araBAD}. Cultures expressing cytoplasmic msfGFP reached the highest mean green fluorescence observed, at around 60000 AU at 4 h post-induction. Comparatively, mean green fluorescence for cultures expressing PelB^{SP}::msfGFP or DsbA^{SP}::msfGFP was lower, reaching around 50000 AU and 30000 AU respectively at 4 h post-induction. For DsbA^{SP}::msfGFP cultures though this marked a large improvement in expression over that observed when using T7*lac* (Figure 4.2A). By 24 h, green fluorescence had decreased considerably in all cultures; for PelB^{SP}::msfGFP and DsbA^{SP}::msfGFP cultures, this was approximately 3000 AU and 1500 AU respectively. We wondered whether lower green fluorescence at 24 h was because BL21 had metabolised L-arabinose during the latter stages of growth (Stargardt et al., 2021), meaning less

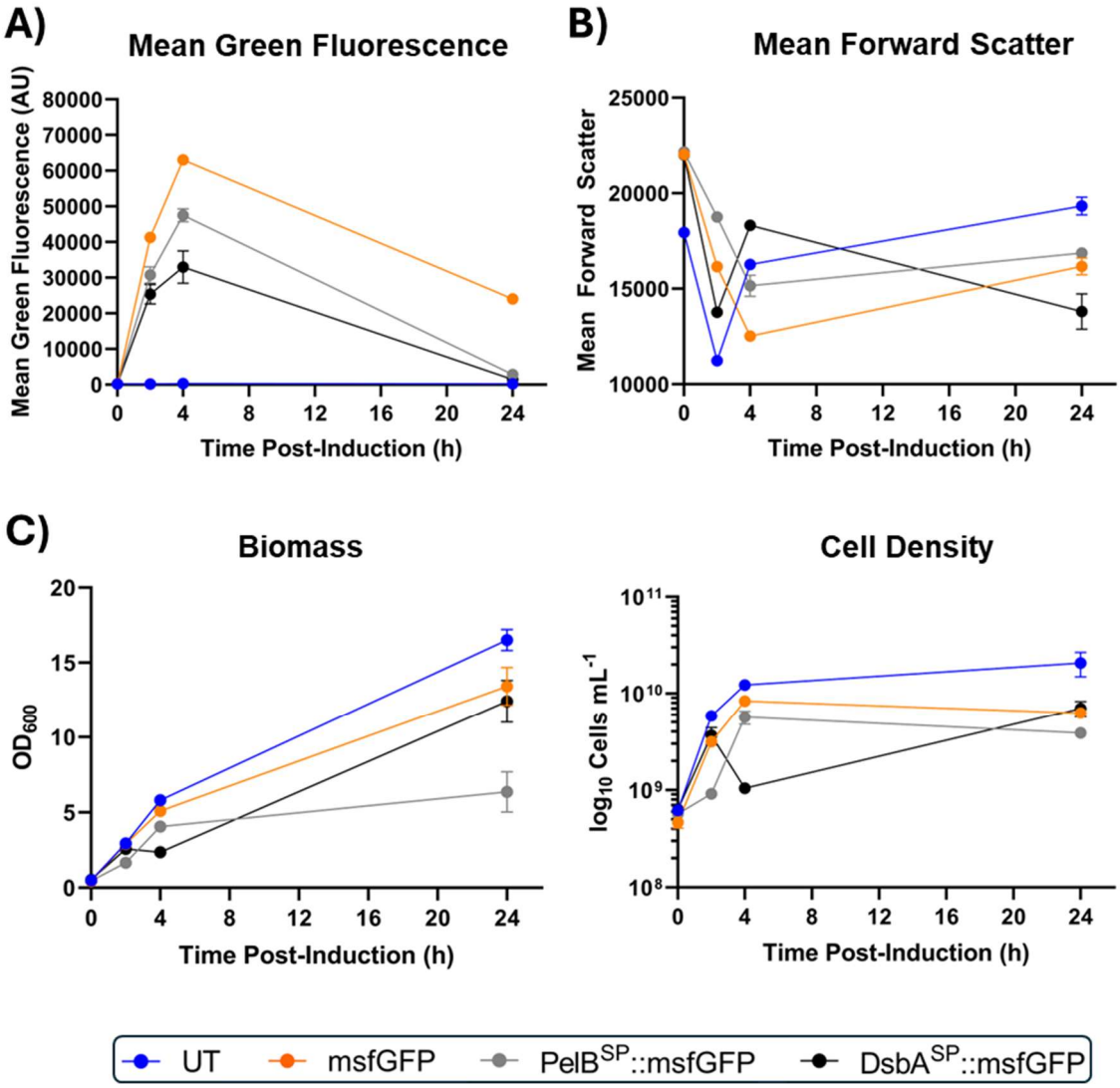


Figure 4.8: Effect of msfGFP expression from P_{araBAD} constructs on BL21.

msfGFP expressed from P_{araBAD} was exported to the periplasm via fusion to $PelB^{SP}$ or $DsbA^{SP}$; a cytoplasmic variant and untransformed strain (UT) used as controls. Cultures were aerated at 30 °C, 200 rpm in 50 mL TB + Kan and induced with 0.2 % (w/v) L-arabinose at OD_{600} 0.4-0.6. Expression continued for a further 24 h. Error bars represent +/- SD for biological duplicates.

(A) Mean green fluorescence was monitored via FCM. Expression of $PelB^{SP}$::msfGFP $DsbA^{SP}$::msfGFP appeared lower than for the cytoplasmic control. In all cultures, a considerable drop in mean green fluorescence was observed between 4 h and 24 h post-induction.

(B) Mean FSC was monitored via FCM and was elevated in $PelB^{SP}$::msfGFP and $DsbA^{SP}$::msfGFP cultures at 4 h post-induction indicating cells were larger.

(C) Biomass accumulation and cell density were monitored via OD_{600} and FCM. $PelB^{SP}$::msfGFP cultures had some growth arrest following induction, although recovered to levels similar to the cytoplasmic control. $DsbA^{SP}$::msfGFP cultures had a drop in cell density at 4 h post-induction.

inducer was available to activate expression. Although mean green fluorescence from cultures expressing cytoplasmic msfGFP was still higher at 24 h than those expressing PelB^{SP}::msfGFP or DsbA^{SP}::msfGFP. Green fluorescence in single cells was also monitored via FCM (Figure 4.9) and cultures were found to be homogenous throughout growth. Most cells within DsbA^{SP}::msfGFP cultures had low green fluorescence comparable with the untransformed control suggesting the expression plasmid had been lost or inactivated in some way, but this would have to be confirmed via replica plating.

To confirm whether expression of exported msfGFP from P_{araBAD} affected host physiology, mean FSC was monitored via FCM (Figure 4.8B). At 4 h post-induction, corresponding with the point of maximum green fluorescence for each culture, mean FSC was higher in cultures expressing PelB^{SP}::msfGFP or DsbA^{SP}::msfGFP compared with the cytoplasmic control; this was significant when analysed by one-way ANOVA ($p < 0.05$ for all comparisons). Something similar was observed when using T7*lac* to drive expression of msfGFP (Figure 4.2B); DsbA^{SP}::msfGFP cultures likely being lower in that instance due to lower expression. Biomass accumulation and cell density were also monitored via OD_{600} and FCM respectively. Even with lower expression from P_{araBAD}, there were still instances where some growth arrest was apparent in PelB^{SP}::msfGFP and DsbA^{SP}::msfGFP cultures compared with controls; this looked to occur earlier in PelB^{SP}::msfGFP cultures.

As an indication of viability, cells were stained using PI and gated via FCM using red fluorescence (FL3-A) and green fluorescence (FL1-A) density plots. Cells were gated

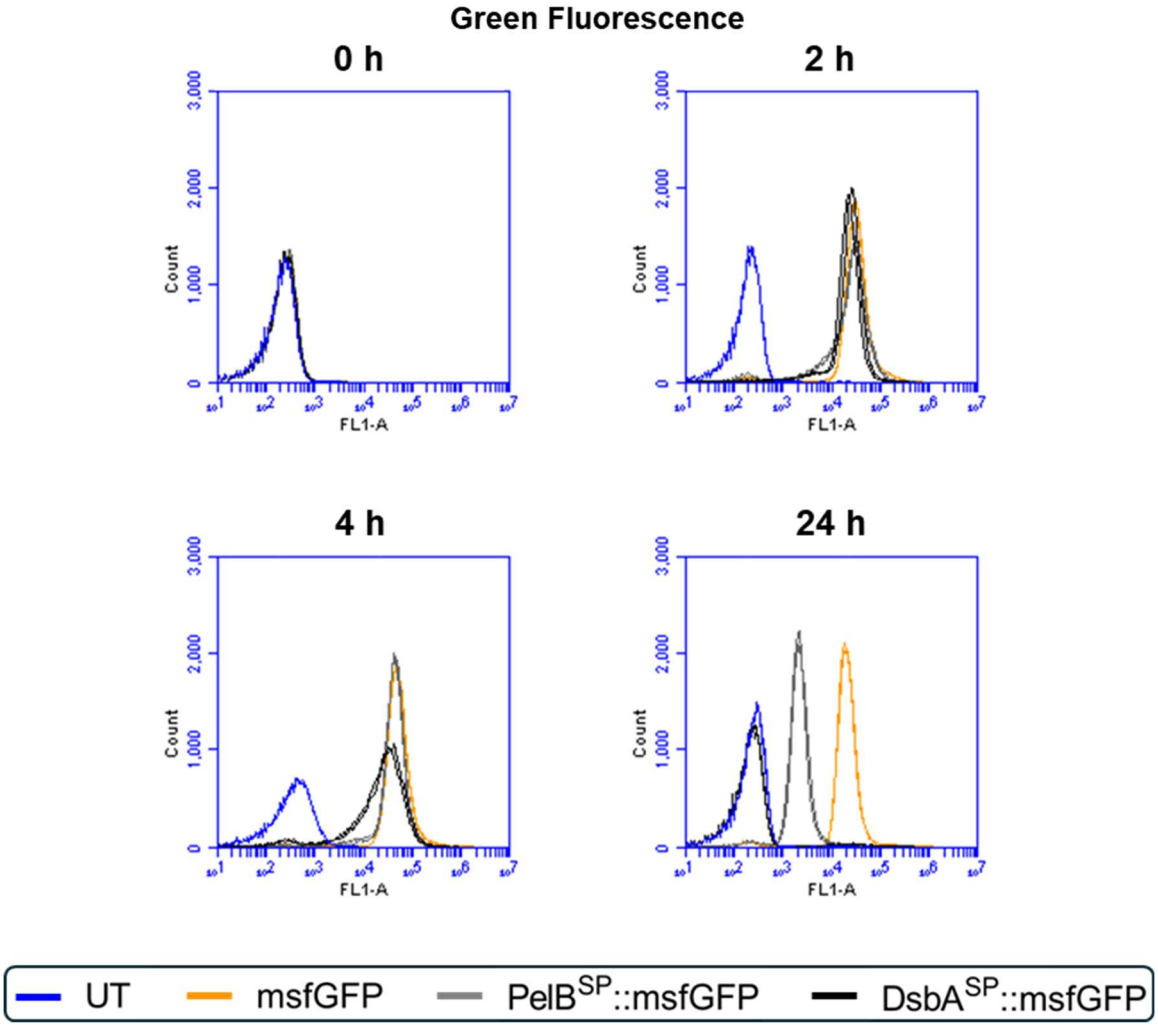


Figure 4.9: FCM analysis of green fluorescence from msfGFP expression in BL21 using P_{araBAD} constructs.

msfGFP expressed from P_{araBAD} was exported to the periplasm via fusion to $PelB^{SP}$ or $DsbA^{SP}$; a cytoplasmic variant and untransformed strain (UT) used as controls. Cultures were aerated at 30 °C, 200 rpm in 50 mL TB + Kan and induced with 0.2 % (w/v) L-arabinose at OD_{600} 0.4-0.6. Expression continued for a further 24 h. Each condition is shown for biological duplicates.

Green fluorescence (FL1-A) was monitored in single cells using FCM. Populations were mostly homogenous in all cultures throughout growth, showing one population.

as viable with low green fluorescence (GFP- PI-), viable with high green fluorescence (GFP+ PI-) or non-viable populations (PI+) (Figure 4.10). Untransformed and cytoplasmic controls had almost no cells within the PI+ gate throughout growth, the latter having over 95 % of cells within the GFP+ PI- gate following induction. Due to tighter regulation from P_{araBAD} only around 1 – 2 % of cells were within the PI+ gate in PelB^{SP}::msfGFP and DsbA^{SP}::msfGFP cultures pre-induction. However, after addition of 0.2% (w/v) L-arabinose, 20 % of cells within PelB^{SP}::msfGFP cultures were within the PI+ gate by 4 h post-induction. Worse still, in DsbA^{SP}::msfGFP cultures, over 35 % of cells were within the PI+ gate by 4 h post-induction.

Care must be taken when assessing data for PI staining as it is strictly a measure of membrane integrity and permeability, which is used to infer on the viability of a cell. While done in yeast, it was shown that some sub populations of *S. cerevisiae* which are stained as PI+ can subsequently repair damage to the membrane such that viability is restored and cells stain as PI- (Davey and Hexley, 2011). In the bacteria *Shewanella decolorationis*, shifts in metabolism were shown to produce a comparable effect with PI+ cells seemingly repairing their membranes and were subsequently stained as PI- (Yang et al., 2015). However, there are caveats in all methods for measuring viability, plating on to solid media frequently results in the viable but not culturable (VBNC) paradigm, especially if cells are stressed (Boaretti et al., 2003). However, taking the results from PI staining (Figure 4.10) together with biomass and cell density analysis (Figure 4.8C), it was likely that expression of PelB^{SP}::msfGFP and DsbA^{SP}::msfGFP was not well tolerated using P_{araBAD} constructs either.

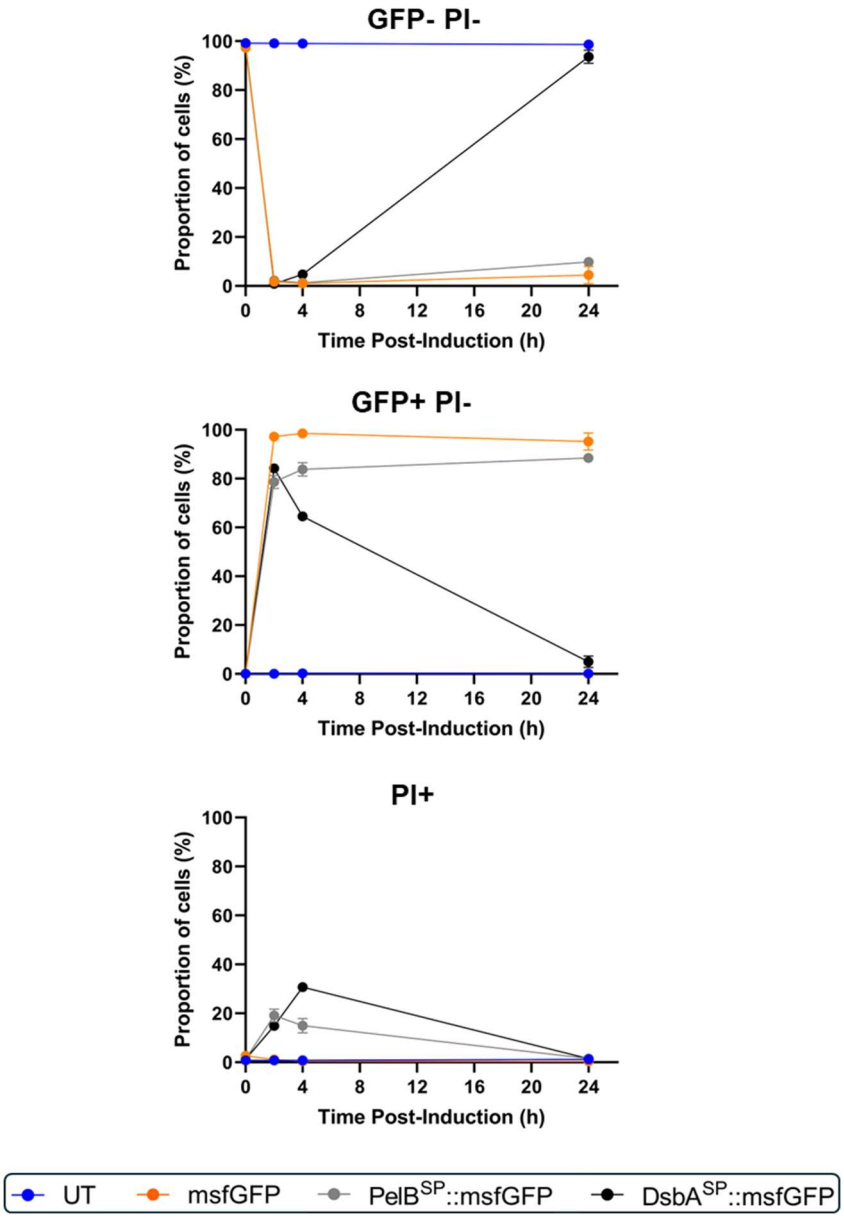


Figure 4.10: PI staining was used to assess viability of BL21 expressing msfGFP from P_{araBAD} constructs.

msfGFP expressed from P_{araBAD} was exported to the periplasm via fusion to $PelB^{SP}$ or $DsbA^{SP}$; a cytoplasmic variant and untransformed strain (UT) used as controls. Cultures were aerated at 30 °C, 200 rpm in 50 mL TB + Kan and induced with 0.2 % (w/v) L-arabinose at OD_{600} 0.4-0.6. Expression continued for a further 24 h. Error bars represent +/- SD for biological duplicates.

To assess viability 4 μg mL^{-1} PI was used to stain cells. Cultures were gated as viable with low green fluorescence (GFP- PI-), viable with high green fluorescence (GFP+ PI-), or non-viable (PI+) using FCM and red fluorescence (FL3-A) and green fluorescence (FL1-A) density plots. Low background fluorescence pre-induction was observed in all cultures (GFP- PI-). In $PelB^{SP}$::msfGFP cultures, 20 % of cells were within the PI+ gate by 2 h post-induction; similarly, in $DsbA^{SP}$::msfGFP cultures, over 30 % of cells within the PI+ gate by 4 h post-induction. The cytoplasmic control appeared to be well tolerated with over 95% of cells within the GFP+ PI- gate following induction.

4.3.3 Tuning expression of exported msfGFP from P_{araBAD}

Even with lower expression from P_{araBAD}, expression of PelB^{SP}::msfGFP and DsbA^{SP}::msfGFP still appeared to be poorly tolerated based on analysis of biomass, cell density and PI staining (Figures 4.8C and 4.10). Induction with 0.2 % (w/v) L-arabinose is considered enough to fully switch on transcription from P_{araBAD} (Guzman et al., 1995), hence we wondered whether tuning expression would permit better tolerance to export of msfGFP. The msfGFP constructs pBAD30-*kanR-pelB^{SP}::msfgfp*, pBAD30-*kanR-dsbA^{SP}::msfgfp* and pBAD30-*kanR-msfgfp* were transformed into BL21. Cultures were aerated at 30 °C, 200 rpm in 50 mL TB + Kan and induced with 0.02 % or 0.2 % (w/v) L-arabinose at OD_{600} 0.4-0.6, with expression continuing until 24 h post-induction. Each strain and condition were repeated in duplicate cultures.

Overexpression of msfGFP was tracked by measuring mean green fluorescence via FCM (Figure 4.11A). Predictably, mean green fluorescence was higher in cultures induced with 0.2 % L-arabinose. At 0.2 % L-arabinose, msfGFP expression from each strain was comparable with that observed prior (Figure 4.8A); cultures expressing cytoplasmic msfGFP or PelB^{SP}::msfGFP having higher mean green fluorescence than those expressing DsbA^{SP}::msfGFP. When inducing cultures with 0.02 % L-arabinose, expression was approximately 3-fold lower than at 0.2 %. However, tuning of P_{araBAD} was on a global rather than per cell basis and expression was mixed when inducing sub-saturating concentrations of L-arabinose. Analysis of green fluorescence in single cells using FCM indicated two populations of higher and lower green fluorescence were present when using 0.02 % L-arabinose (Figure 4.12). This was consistent with

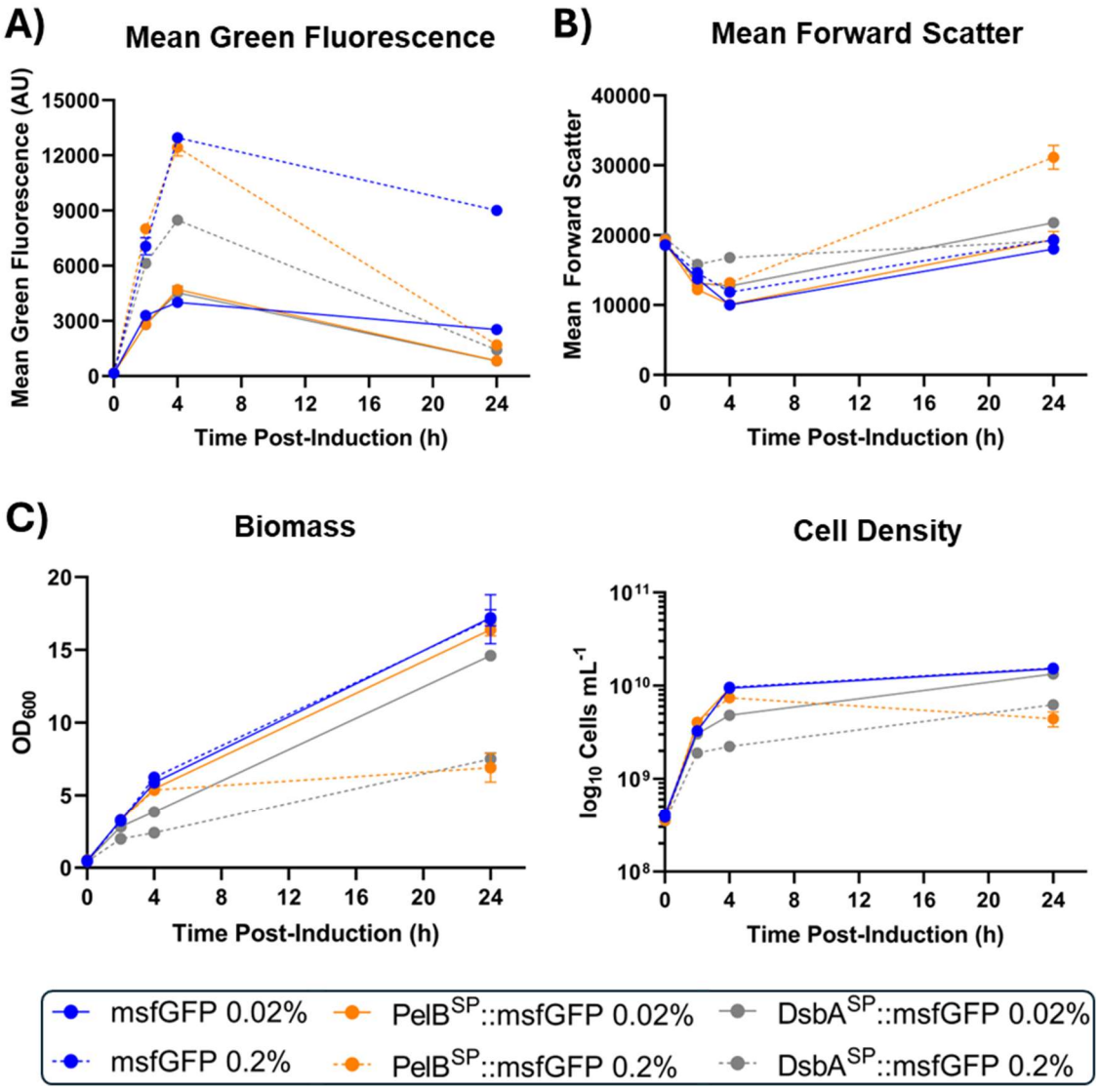


Figure 4.11: Effect of tuning msfGFP expression from P_{araBAD} constructs on BL21.

msfGFP expressed from P_{araBAD} was exported to the periplasm via fusion to PelB^{SP} or DsbA^{SP}; a cytoplasmic variant used as a control. Cultures were aerated at 30 °C, 200 rpm in 50 mL TB + Kan and induced with 0.02 % or 0.2 % L-arabinose at OD_{600} 0.4-0.6. Expression continued for a further 24 h. Error bars represent +/- SD for biological duplicates.

(A) Mean green fluorescence was monitored via FCM. Predictably, msfGFP expression was lower in cultures indued with 0.02 % L-arabinose. In cultures induced with 0.2 % L-arabinose, mean green fluorescence for PelB^{SP}::msfGFP cultures were like the cytoplasmic control; DsbA^{SP}::msfGFP cultures were lower.

(B) Mean FSC was monitored via FCM and was elevated in DsbA^{SP}::msfGFP cultures induced with 0.2 % L-arabinose at 4 h post-induction indicating cells were larger.

(C) Biomass accumulation and cell density were monitored via OD_{600} and FCM. DsbA^{SP}::msfGFP cultures had some growth arrest following induction. Cell density in PelB^{SP}::msfGFP cultures had notably dropped at 24 h post-induction.

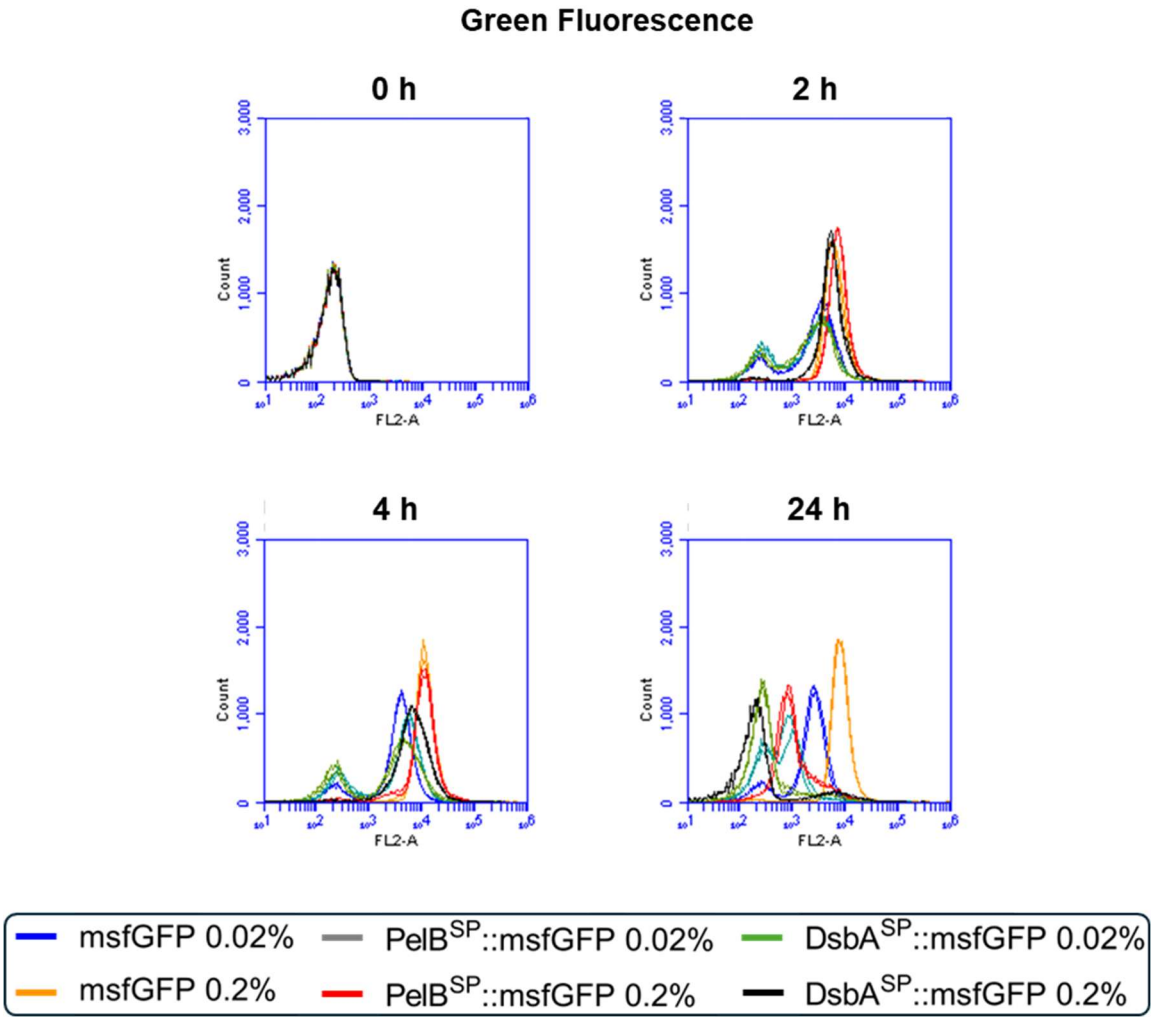


Figure 4.12: FCM analysis of green fluorescence during attempts to tune msfGFP expression in BL21 using P_{araBAD} constructs.

msfGFP expressed from P_{araBAD} was exported to the periplasm via fusion to $PelB^{SP}$ or $DsbA^{SP}$; a cytoplasmic variant used as a control. Cultures were aerated at 30 °C, 200 rpm in 50 mL TB + Kan and induced with 0.02 % or 0.2 % (w/v) L-arabinose at OD_{600} 0.4-0.6. Expression continued for a further 24 h. Each condition is shown for biological duplicates.

Green fluorescence (FL2-A) was monitored in single cells using FCM. In cultures induced with 0.2 % L-arabinose, populations were mostly homogenous throughout growth; although, $DsbA^{SP}$::msfGFP were mixed at 24 h post-induction. In cultures induced with 0.02 % L-arabinose, populations of low and high green fluorescence were observed even at 2 h post-induction, suggesting tunability of P_{araBAD} was on a per culture basis.

all-or-nothing induction and was partially expected being a known issue with P_{araBAD} at sub-saturating L-arabinose concentrations (see section 1.4.3) (Siegele and Hu, 1997).

Mean FSC was monitored via FCM and was quite like that seen previously (Figure 4.8B) when inducing cytoplasmic and PelB^{SP}::msfGFP cultures with 0.2 % L-arabinose; mean FSC decreasing between induction and 4 h post-induction, then increasing by 24 h post-induction (Figure 4.11). In DsbA^{SP}::msfGFP cultures induced with 0.2 % L-arabinose we observed the same (Figure 4.11), but this was a departure from that seen previously where mean FSC had increased between 2 h and 4 h post-induction (Figure 4.8B). However, in this experiment, there was little difference in mean FSC between cultures regardless of the condition (Figure 4.11B). To check further differences in physiology between cultures induced with different concentrations of L-arabinose, biomass accumulation and cell density were monitored via OD_{600} and FCM respectively (Figure 4.11C). Growth arrest in DsbA^{SP}::msfGFP cultures was apparent, even when inducing with 0.02 % L-arabinose, although for PelB^{SP}::msfGFP cultures, this only appeared to occur at 24 h post-induction.

As an indication of viability, cells were stained using PI and gated via FCM using red fluorescence (FL3-A) and green fluorescence (FL1-A) density plots. Cells were gated as viable (PI-) or non-viable populations (PI+) (Figure 4.13). It was not possible to gate cells into low (GFP-) or high (GFP+) green fluorescence groups due to populations of cells induced with 0.02 % L-arabinose bisecting the gate; due to the heterogeneity in induction observed (Figure 4.12). After 4 h post-induction, approximately 20 % of cells in cultures expressing PelB^{SP}::msfGFP or DsbA^{SP}::msfGFP induced with 0.2 % L-

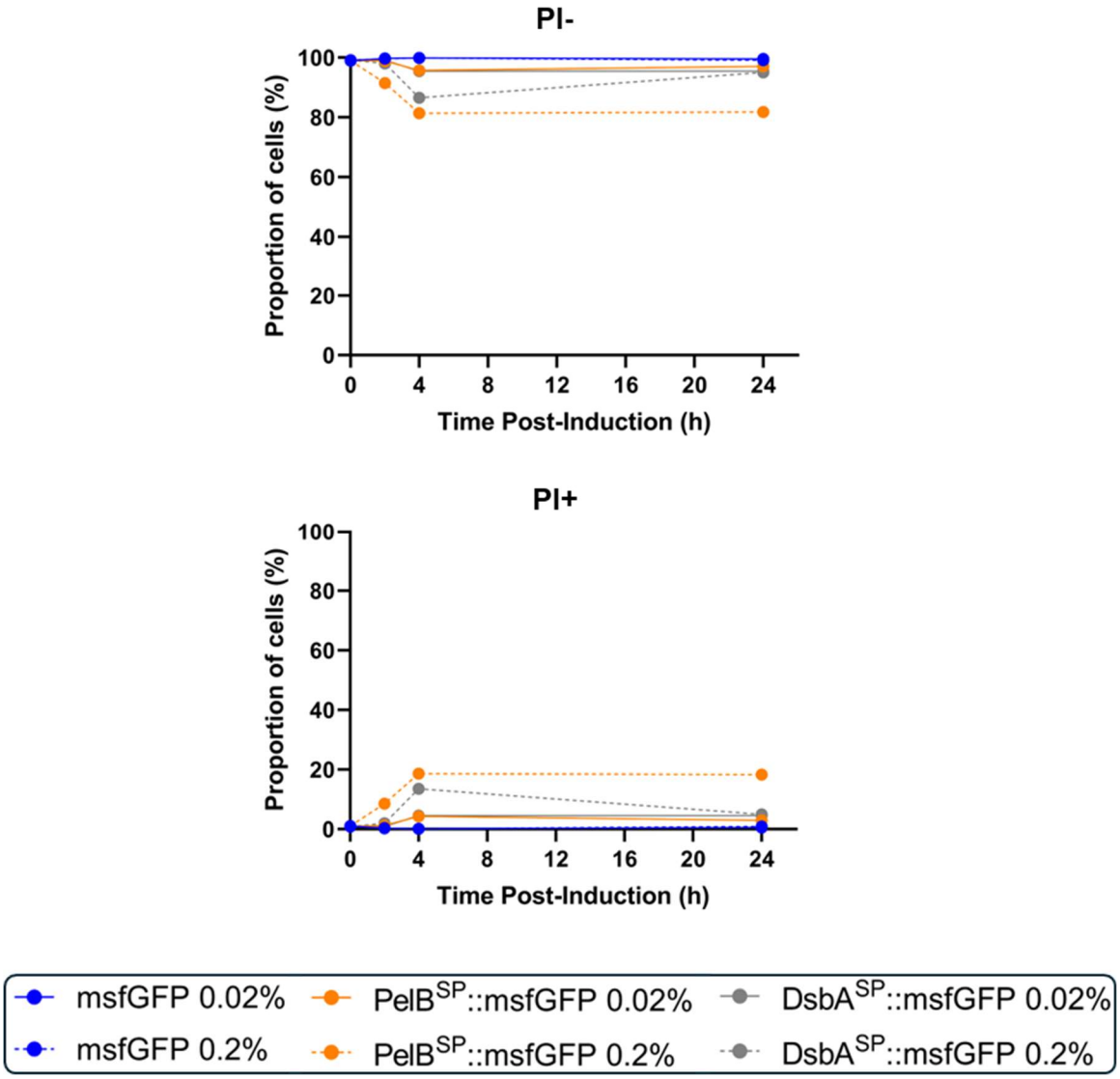


Figure 4.13: PI staining was used to assess viability of BL21 after attempting to tune expression of msfGFP from P_{araBAD} constructs.

msfGFP expressed from P_{araBAD} was exported to the periplasm via fusion to $PelB^{SP}$ or $DsbA^{SP}$; a cytoplasmic variant used as a control. Cultures were aerated at 30 °C, 200 rpm in 50 mL TB + Kan and induced with 0.02 % or 0.2 % (w/v) L-arabinose at OD_{600} 0.4-0.6. Expression continued for a further 24 h. Error bars represent +/- SD for biological duplicates.

To assess viability 4 µg mL^{-1} PI was used to stain cells. Cultures were gated as viable (PI-), viable or non-viable (PI+) using FCM and red fluorescence (FL3-A) and green fluorescence (FL1-A) density plots. In $PelB^{SP}$::msfGFP and $DsbA^{SP}$::msfGFP cultures induced with 0.2 % L-arabinose, around 20 % of cells were within the PI+ gate by 4 h post-induction. Predictably, due to lower expression, $PelB^{SP}$::msfGFP and $DsbA^{SP}$::msfGFP cultures induced with 0.02 % L-arabinose, far fewer PI+ cells were observed. Cytoplasmic controls had over 95% cells within the PI- gate throughout culture.

arabinose were within the PI+ gate (Figure 4.13), consistent with that observed prior (Figure 4.10).

At 4 h post-induction, where the proportion of cells within the PI+ gate seemed to peak in cultures induced with 0.2% L-arabinose, there were significantly less in PelB^{SP}::msfGFP or DsbA^{SP}::msfGFP cultures induced with 0.02 % L-arabinose (Figure 4.13). This was significant when t-tests were used to compare cultures at 0.02 % and 0.2 % L-arabinose ($p < 0.0019$ for PelB^{SP}::msfGFP; $p < 0.0039$ for DsbA^{SP}::msfGFP). As mentioned previously, care must still be taken in analysing PI data as it is not a complete measure of viability (Davey and Hexley, 2011, Yang et al., 2015). However, taking the results from PI staining (Figure 4.13) together with biomass and cell density analysis (Figure 4.11C), it was probable that tuning expression from P_{araBAD} using 0.02% L-arabinose improved physiology, but at the expense of msfGFP expression (Figure 4.11A and Figure 4.12).

To check if any msfGFP accumulated in the periplasm, cultures were fractioned into cytoplasmic (CF) and periplasmic (PF) fractions and resolved via SDS PAGE (Figure 4.14 – 4.15). At induction, there were bands in all lanes consistent with msfGFP (26.9 kDa) although it was difficult to determine whether these were from a native protein. At 2 h and 4 h post-induction, bands around the 26 kDA marker were denser in cytoplasmic fractions. For PelB^{SP}::msfGFP cultures, there were bands just above the 26 kDa marker in periplasmic fractions. By 24 h post-induction, bands consistent with msfGFP were far fainter; GFP is well known to be relatively stable and resistant to

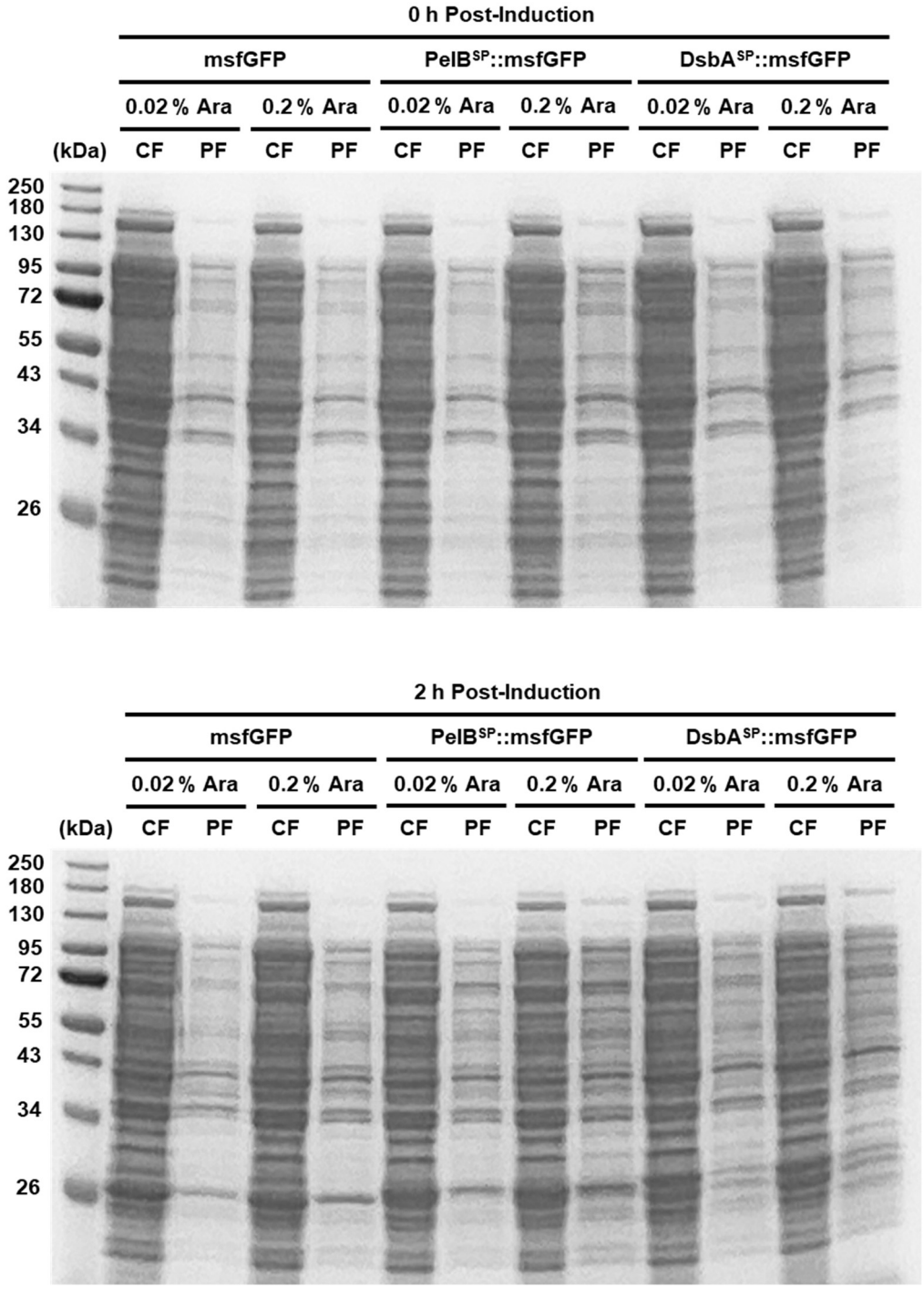


Figure 4.14: SDS PAGE analysis of BL21 expressing msfGFP from P_{araBAD} constructs.

msfGFP expressed from P_{araBAD} was exported to the periplasm via fusion to PelB^{SP} or DsbA^{SP}; a cytoplasmic variant used as a control. Cultures were aerated at 30 °C, 200 rpm in TB and induced with 0.02 % or 0.2 % L-arabinose at OD_{600} 0.4-0.6. Expression continued for a further 24 h.

Cultures were fractioned into cytoplasmic (CF) and periplasmic (PF) fractions and resolved via SDS PAGE. In PelB^{SP}::msfGFP cultures, there were bands in PF fractions consistent with msfGFP (26.8 kDa) from 4 h post-induction; though, there appeared to be some leakage between CF and PF fractions, as evidenced by the cytoplasmic control.

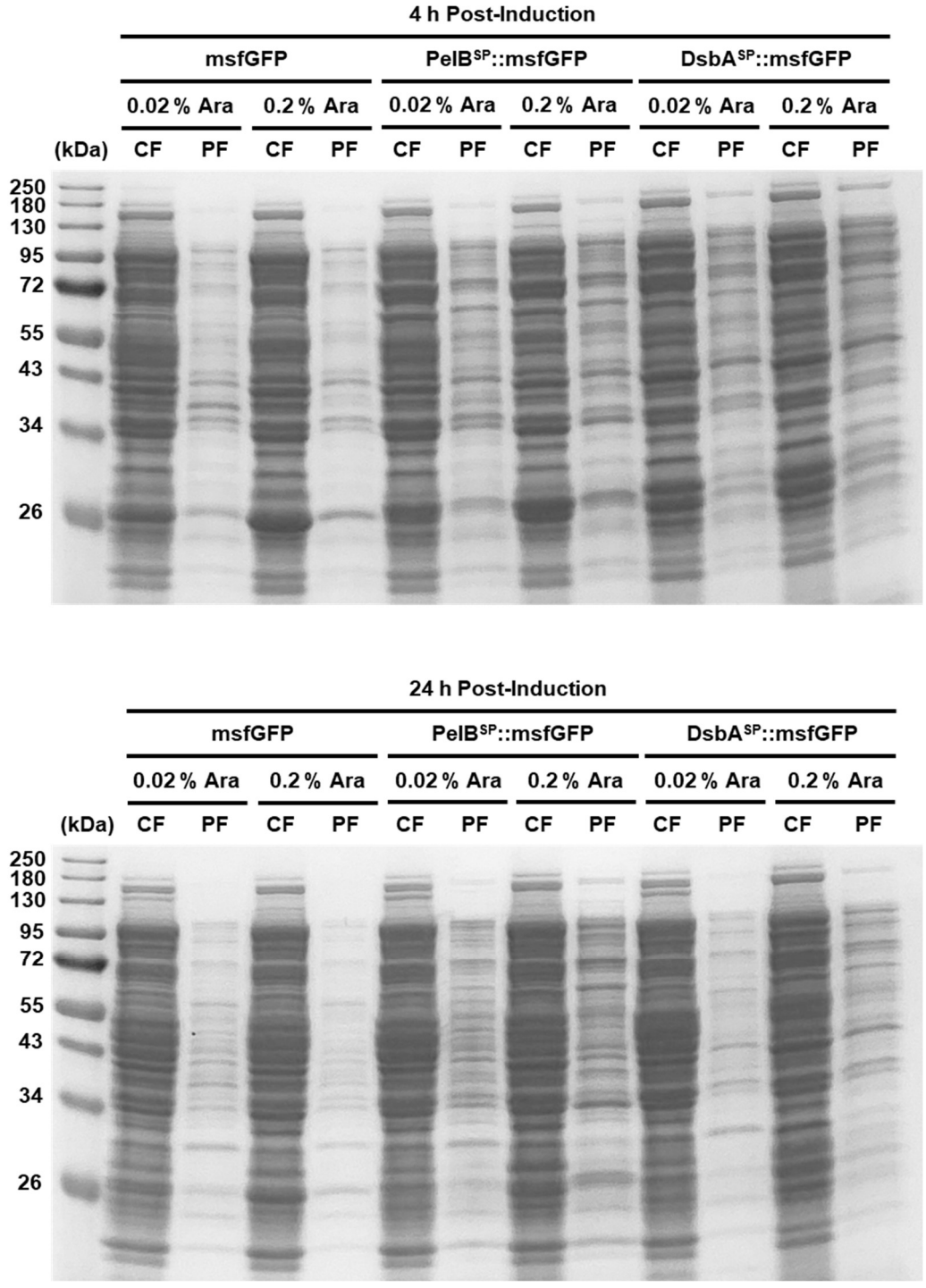


Figure 4.15: SDS PAGE analysis of BL21 expressing msfGFP from P_{araBAD} constructs.

msfGFP expressed from P_{araBAD} was exported to the periplasm via fusion to PelB^{SP} or DsbA^{SP}; a cytoplasmic variant used as a control. Cultures were aerated at 30 °C, 200 rpm in TB and induced with 0.02 % or 0.2 % L-arabinose at OD_{600} 0.4-0.6. Expression continued for a further 24 h.

Cultures were fractioned into cytoplasmic (CF) and periplasmic (PF) fractions and resolved via SDS PAGE. In PelB^{SP}::msfGFP cultures, there were bands in PF fractions consistent with msfGFP (26.8 kDa) from 4 h post-induction; though, there appeared to be some leakage between CF and PF fractions, as evidenced by the cytoplasmic control.

proteolytic degradation (Khmelinskii et al., 2016), so it is possible leakage into the extracellular medium had occurred, but this would need to be confirmed.

At 2 h post-induction, densitometry of SDS PAGE gels using ImageJ (Fiji) indicated that for PelB^{SP}::msfGFP cultures the percentage of periplasmic msfGFP was 15.64% for those induced with 0.02% L-arabinose and 26.09% for those induced with 0.2% L-arabinose. For DsbA^{SP}::msfGFP cultures, the percentage of periplasmic msfGFP at 2 h post-induction was calculated as 19.81% for those induced with 0.02% L-arabinose and 23.72% for those induced with 0.2% L-arabinose. At 4 h post-induction for PelB^{SP}::msfGFP cultures the percentage of periplasmic msfGFP was calculated as 15.72% for those induced with 27.72% and 25.79% for those induced with 0.2% L-arabinose. For DsbA^{SP}::msfGFP cultures, the percentage of periplasmic msfGFP at 4 h post-induction was calculated as 14.32% for those induced with 0.02% L-arabinose and 23.82% for those induced with 0.2% L-arabinose.

As with T7*lac* constructs (Figure 4.5), there appeared to be leakage of cytoplasmic msfGFP into periplasmic fractions (Figure 4.14 – 4.15), which as referenced in section 4.2.1, can occur during overexpression of recombinant proteins (Morra et al., 2018). Although the method has been used previously (Selas Castiñeiras et al., 2018a), we wondered whether the fractionation assay itself was a problem, while some bands were consistent across fractions, not all proteins visualised in the cytoplasmic fraction were visible in the periplasmic fraction. As an example, at 2 h post-induction in the cytoplasmic fraction for PelB^{SP}::msfGFP induced with 0.02% L-arainose (Figure 4.14), there is a band between 43 and 55 kDa markers which is not found in the periplasmic

fraction. Regardless, given the generally poor growth and physiological characteristics of cultures expressing PelB^{SP}::msfGFP or DsbA^{SP}::msfGFP (Figures 4.11C and 4.13), the system was still not workable.

4.4 Periplasmic cfSGFP2 reporters using a P$_{araBAD}$ system

Lower concentrations of L-arabinose were able to improve viability in response to exported msfGFP (Figure 4.11C and Figure 4.13), but expression was negatively affected (Figure 4.11A and Figure 4.12). Hence, msfGFP would not be useful as a screening tool in to optimise periplasmic RPP. The primary reason given for msfGFP resistance to oxidative environments was rapid folding protecting cysteine residues from forming disulphide bridges; however rapid folding may also lead to blockages of Sec when exporting via the post-translational branch (Aronson et al., 2011, Dinh and Bernhardt, 2011). In general, we wondered whether a GFP derivative without superfolder mutations, but devoid of cysteine residues would be better tolerated by the host. Hence cystine-free SGFP2 (cfSGFP2) was chosen which has the mutations C48S and C70M and had previously been used in mammalian oxidising environments (Suzuki et al., 2012). Constructs driving expression of exported or cytoplasmic cfSGFP2 were generated using the P$_{araBAD}$ system; pBAD30-*kanR-dsbA*^{SP}::*cfsgfp2* and pBAD30-*kanR-cfsgfp2*.

4.4.1 Expressing exported cfSGFP2 via P$_{araBAD}$

To test cfSGFP2, constructs pBAD30-*kanR-dsbA*^{SP}::*cfsgfp2* and pBAD30-*kanR-cfsgfp2* were transformed into BL21. Cultures were aerated at 30 °C, 200 rpm in 50 mL TB + Kan and induced with 0.02 % (w/v) or 0.2 % (w/v) L-arabinose at OD_{600} 0.4-0.6, with expression continuing until 24 h post-induction. Each strain was repeated in duplicate cultures.

Overexpression of cfSGFP2 was tracked by measuring mean green fluorescence via FCM (Figure 4.16A). Mean green fluorescence was far higher in cultures expressing cytoplasmic cfSGFP2 compared with DsbA^{SP}::cfSGFP2; in cultures induced with 0.2 % L-arabinose, this difference was over 20-fold at 2 h post-induction (Figure 4.16A). In all cultures, mean green fluorescence peaked at 2 h post-induction and decreased over time. At the single cell level (Figure 4.17), even cultures induced with 0.02 % L-arabinose appeared as a single population. We wondered whether this was due to the apparent overall low expression of cfSGFP2; as while P_{araBAD} is known to suffer from all-or-nothing induction (Siegele and Hu, 1997), if expression is already very low, separate peaks may not be distinguishable on histograms. What is more revealing is that the peak widths, indicating heterogeneity, for cultures induced with 0.02% L-arabinose were wider (CV ~ 36%) than for cultures induced with 0.2% L-arabinose (CV ~ 22%) (Figure 4.17).

Mean FSC was monitored using FCM to check for any effects to host physiology (Figure 4.16B). It was difficult to determine a clear pattern; however, mean FSC was higher in DsbA^{SP}::cfSGFP2 cultures at 2 h and 4 h post-induction, but lower at 6 h and 24 h post-induction. Monitoring biomass accumulation and cell density via OD_{600} and FCM was more revealing (Figure 4.16C). From 2 h post-induction, DsbA^{SP}::cfSGFP2 cultures underwent notable growth arrest, an over half a log difference in cells mL^{-1} apparent at 6 h post-induction. By 24 h post-induction, cell density of DsbA^{SP}::cfSGFP2 cultures had increased somewhat to levels comparable with the cytoplasmic control.

Membrane integrity, as a measure of cell viability, was further checked by staining cells with PI and gating via FCM using red fluorescence (FL3-A) and green fluorescence (FL1-A) density plots. Cells were gated as viable (PI-) or non-viable populations (PI+) (Figure 4.18). It was not possible to gate cells into low (GFP-) or high (GFP+) green fluorescence groups due to populations of cells induced with 0.02 % L-arabinose bisecting the gates. While expression

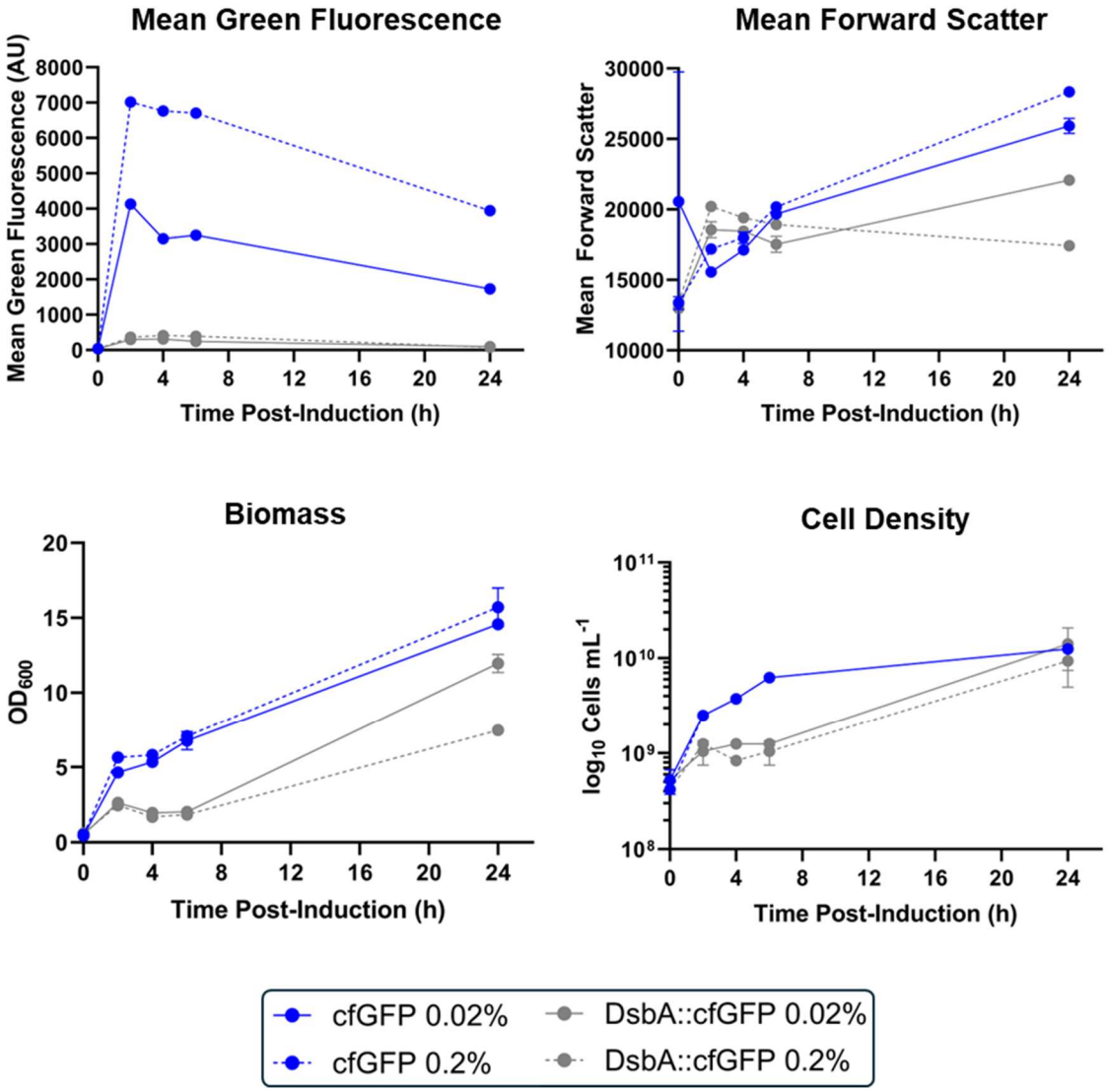


Figure 4.16: Effect of cfSGFP2 expression from P_{araBAD} constructs on BL21.

cfSGFP2 expressed from P_{araBAD} was exported to the periplasm via fusion to $DsbA^{SP}$; a cytoplasmic variant used as a control. Cultures were aerated at 30 °C, 200 rpm in 50 mL TB + Kan and induced with 0.02 % or 0.2 % (w/v) L-arabinose at OD_{600} 0.4-0.6. Expression continued for a further 24 h. Error bars represent +/- SD for biological duplicates.

(A) Mean green fluorescence was monitored via FCM. cfSGFP2 expression was far lower when fused to $DsbA^{SP}$ compared with cytoplasmic controls.

(B) Mean FSC was monitored via FCM. $DsbA^{SP}$::msfGFP cultures had higher mean FSC than cytoplasmic controls at 2 h and 4 h post-induction, but lower at 6 h and 24 h post-induction.

(C) Biomass accumulation and cell density were monitored via OD_{600} and FCM. $DsbA^{SP}$::msfGFP cultures had some growth arrest following induction indicating exported cfSGFP2 was not well tolerated.

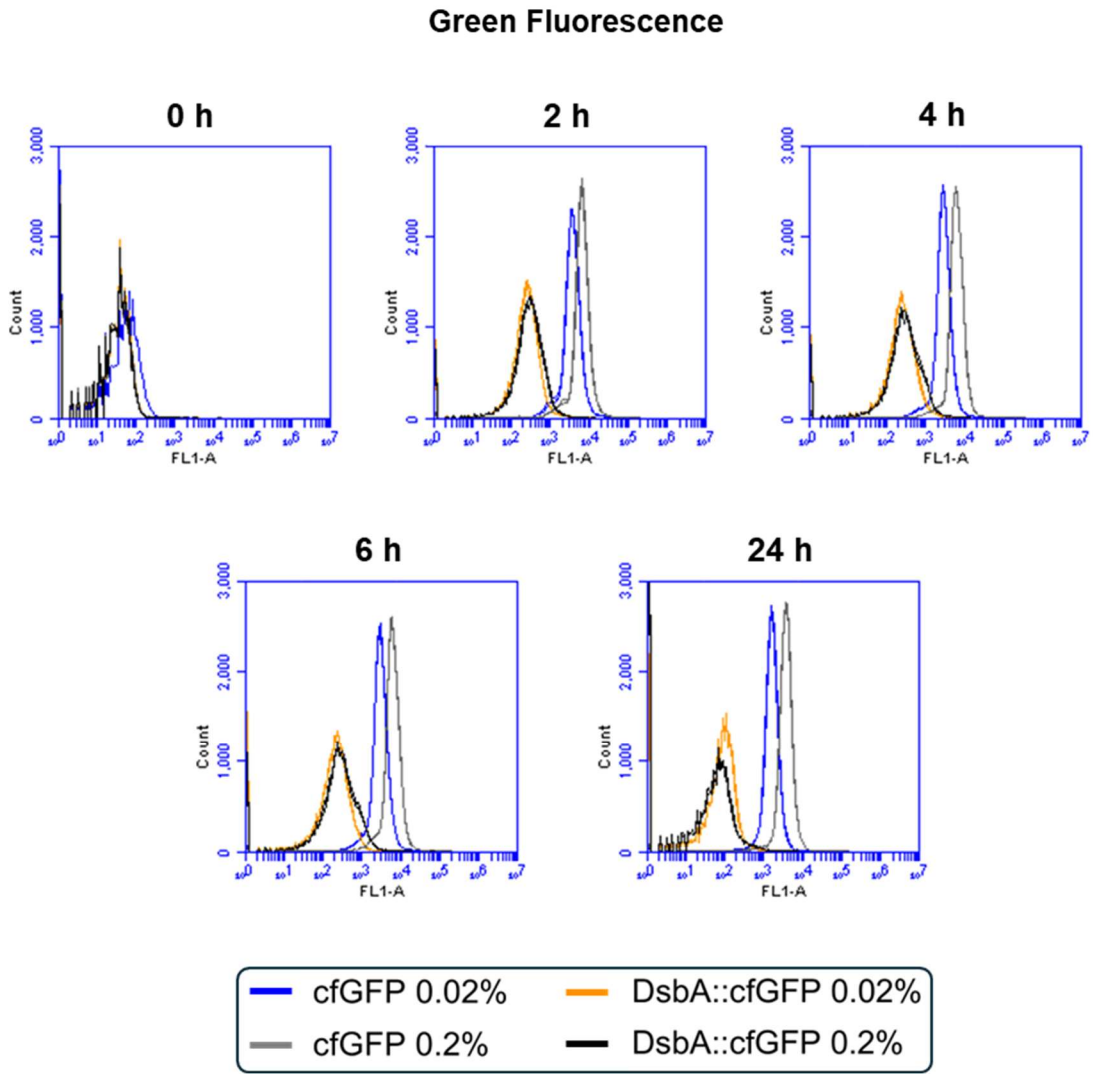


Figure 4.17: FCM analysis of green fluorescence during cfSGFP2 expression in BL21 using P_{araBAD} constructs.

cfSGFP2 expressed from P_{araBAD} was exported to the periplasm via fusion to $DsbA^{SP}$; a cytoplasmic variant used as a control. Cultures were aerated at 30 °C, 200 rpm in 50 mL TB + Kan and induced with 0.02 % (w/v) or 0.2 % (w/v) L-arabinose at OD_{600} 0.4-0.6. Expression continued for a further 24 h. Error bars represent +/- SD for biological duplicates.

Green fluorescence (FL1-A) was monitored in single cells using FCM; at all time-points following induction, cultures presented as a single population.

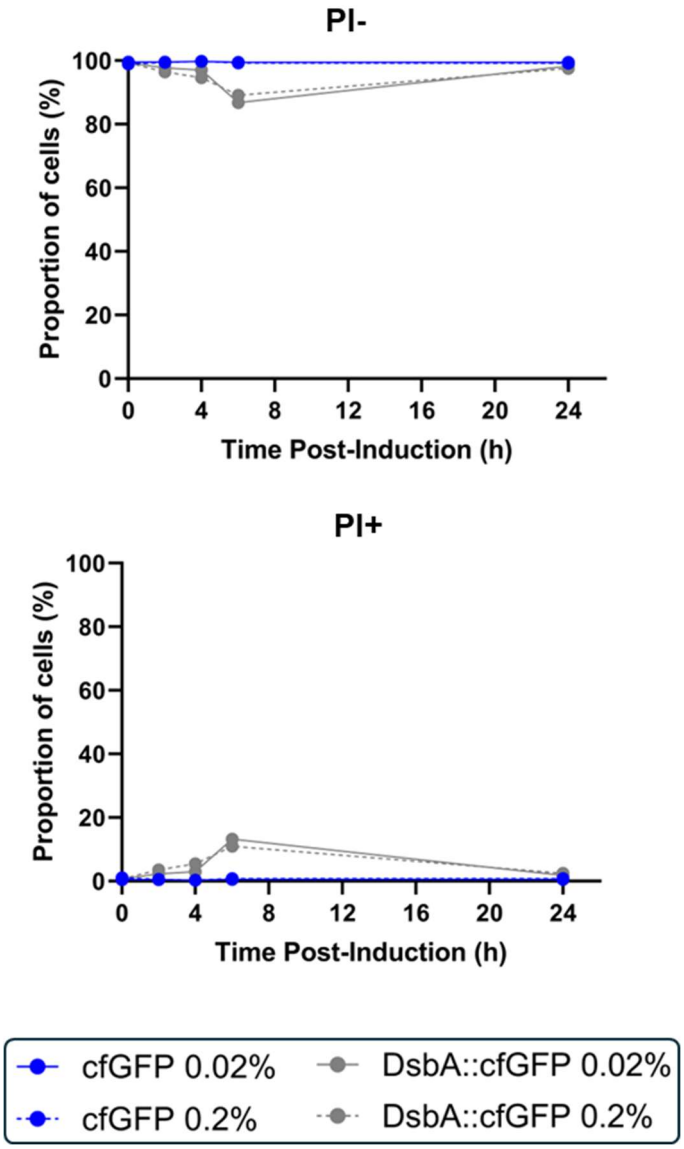


Figure 4.18: PI staining was used to assess viability of BL21 during expression of cfSGFP2 from P_{araBAD} constructs.

cfSGFP2 expressed from P_{araBAD} was exported to the periplasm via fusion to $DsbA^{SP}$; a cytoplasmic variant was used as a control. Cultures were aerated at 30 °C, 200 rpm in 50 mL TB + Kan and induced with 0.02 % (w/v) or 0.2 % (w/v) L-arabinose at OD_{600} 0.4-0.6. Expression continued for a further 24 h. Error bars represent +/- SD for biological duplicates.

To assess viability 4 µg mL^{-1} PI was used to stain cells. Cultures were gated as viable (PI-), viable or non-viable (PI+) using FCM and red fluorescence (FL3-A) and green fluorescence (FL1-A) density plots. In $DsbA^{SP}$::msfGFP cultures, regardless of the concentration of L-arabinose used for induction, around 15 % of cells were within the PI+ gate at 6 h post-induction. Cytoplasmic controls appeared to be well tolerated with over 95% of cells within the PI- gate.

was low (Figure 4.16A), cytoplasmic cfSGFP2 seemed to be well tolerated with near 100 % of cells within the PI- gate throughout growth (Figure 4.18). Comparatively, even with extremely low green fluorescence and thus likely cfSGFP2 expression, over 10 % of cells in $DsbA^{SP}$::cfSGFP2 cultures were dead at 6 h post-induction.

Overall, this seemed to imply cfSGFP2 does not express well in *E. coli* and is detrimental to growth when fused to $DsbA^{SP}$. The alternative was cfSGFP2 had lower brightness, so to check accumulation, cultures were fractioned into cytoplasmic (CF) and periplasmic (PF) fractions and resolved via SDS PAGE (Figure 4.19). We were unable to identify any bands consistent with the size of cfSGFP2 (26.9 kDa) present after induction with L-arabinose which were not visible at 0 h. This was consistent with cfSGFP2 being poorly expressed, presumably due to optimisation for mammalian hosts (Suzuki et al., 2012).

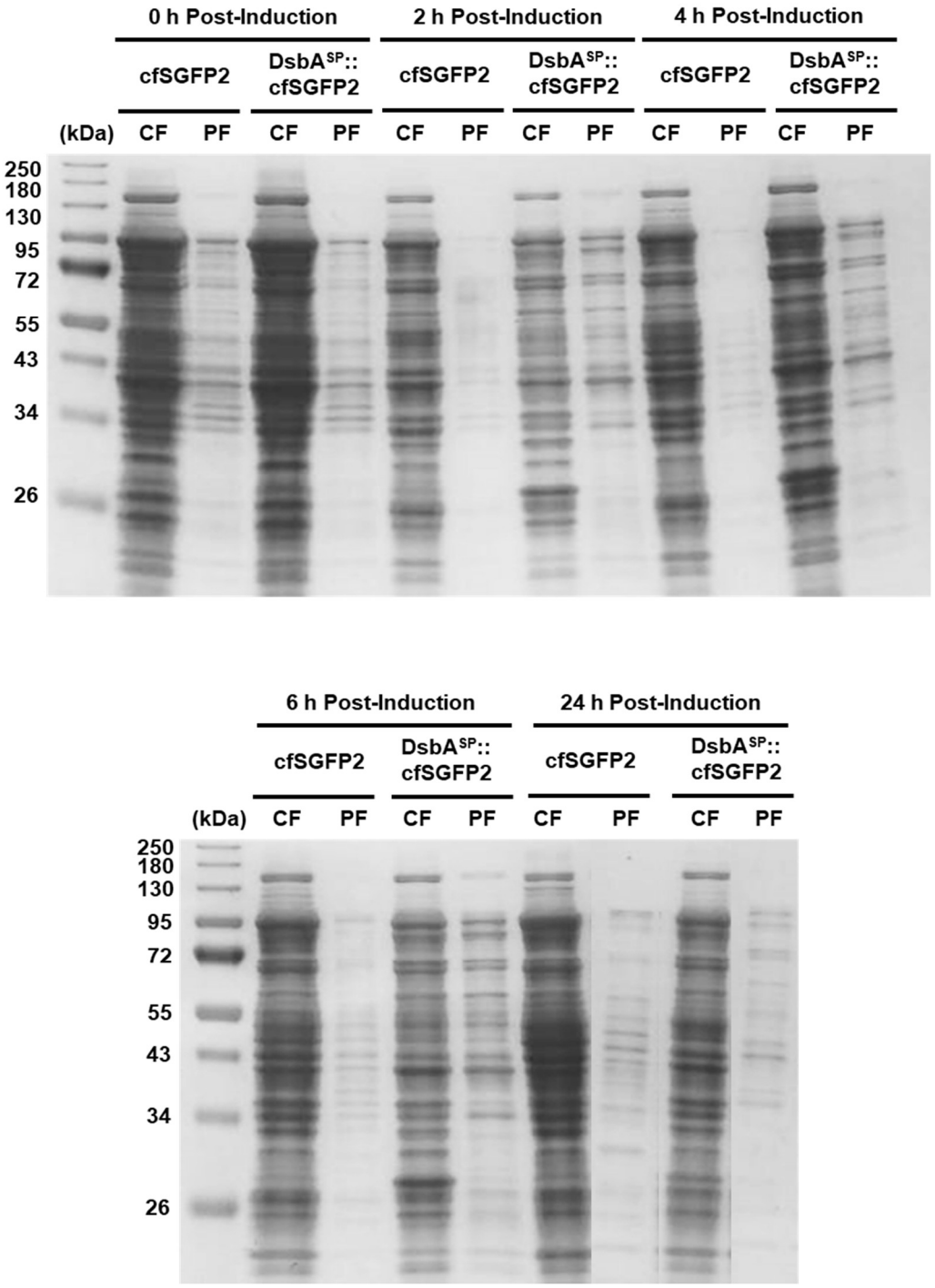


Figure 4.19: SDS PAGE analysis of BL21 expressing cfSGFP2 from P_{araBAD} constructs.

cfSGFP2 expressed from P_{araBAD} was exported to the periplasm via fusion to $DsbA^{SP}$; a cytoplasmic variant was used as a control. Cultures were aerated at 30 °C, 200 rpm in 50 mL TB + Kan and induced with 0.02 % (w/v) or 0.2 % (w/v) L-arabinose at OD_{600} 0.4-0.6. Expression continued for a further 24 h. Error bars represent +/- SD from duplicate flasks.

Cultures were fractioned into cytoplasmic (CF) and periplasmic (PF) fractions and resolved via SDS PAGE. We did not observe any notably dense bands consistent with cfSGFP2 (26.9 kDa), likely due to the overall poor expression.

4.5 Microscopy Analysis

4.5.1 Fluorescence microscopy for T7*lac* and P_{araBAD} constructs

It was clear msfGFP was not useful as a periplasmic screening tool for RPP, but we still wondered whether it was fluorescent if exported to the periplasm. Thus, msfGFP expressed from T7*lac* was exported to the periplasm via fusion to $PelB^{SP}$ or $DsbA^{SP}$. Cultures were aerated at 30 °C, 200 rpm in TB and induced with 50 µM IPTG at OD_{600} 0.4-0.6. At 4 h post-induction cells were visualised using fluorescence microscopy and a 100X oil immersion objective. In both cultures expressing $PelB^{SP}$::msfGFP and $DsbA^{SP}$::msfGFP, accumulation of msfGFP at specific foci was apparent, with cells appearing punctate (Figure 4.20). It was clear when expressed via T7*lac* msfGFP fused to $PelB^{SP}$ or $DsbA^{SP}$ accumulated at the boundaries of the cell, but we did not observe any fluorescent halos that would suggest msfGFP was localised to the periplasm. Similarly, msfGFP expressed from P_{araBAD} was exported to the periplasm via fusion to $PelB^{SP}$ or $DsbA^{SP}$. Cultures were aerated at 30 °C, 200 rpm in TB and induced with 50 µM IPTG at OD_{600} 0.4-0.6. At 4 h post-induction cells were visualised using fluorescence microscopy and a 100X oil immersion objective. Predictably cells expressing cytoplasmic msfGFP were uniformly fluorescent (Figure 4.21). Green fluorescence in cells expressing $PelB^{SP}$::msfGFP for P_{araBAD} constructs also appeared homogenous, somewhat different from that observed with the T7*lac* version (Figure 4.20). In cells expressing $DsbA^{SP}$::msfGFP however, accumulation of msfGFP again appeared to cluster at discrete regions, though cells with uniform fluorescence were also present. As with T7*lac* constructs, we did not observe any fluorescent halos for P_{araBAD} constructs which may be indicative that msfGFP was localised to the periplasm.

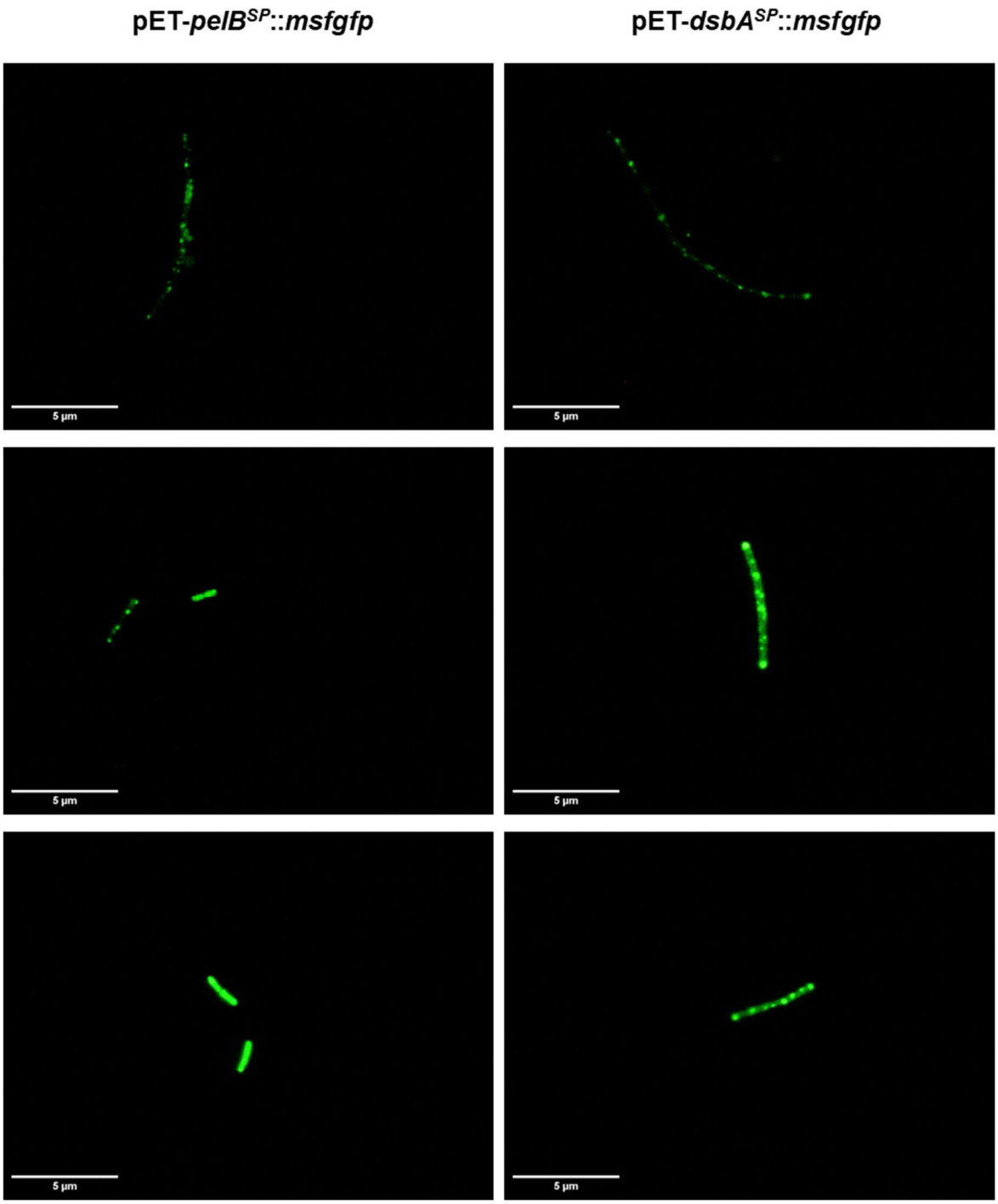


Figure 4.20: Fluorescence microscopy of BL21(DE3) expressing msfGFP from T7*lac*.

msfGFP expressed from T7*lac* was exported to the periplasm via fusion to PelB^{SP} or DsbA^{SP}. Cultures were aerated at 30 °C, 200 rpm in 50 mL TB + Kan and induced with 50 µM IPTG at OD_{600} 0.4-0.6. At 4 h post-induction cells were visualised using fluorescence microscopy and a 100X oil immersion objective. Data for each condition is shown from one culture.

In both cultures expressing PelB^{SP}::msfGFP and DsbA^{SP}::msfGFP, accumulation of msfGFP at specific foci was apparent, with cells appearing punctate. We did not observe any fluorescent halos that would suggest msfGFP was localised to the periplasm.

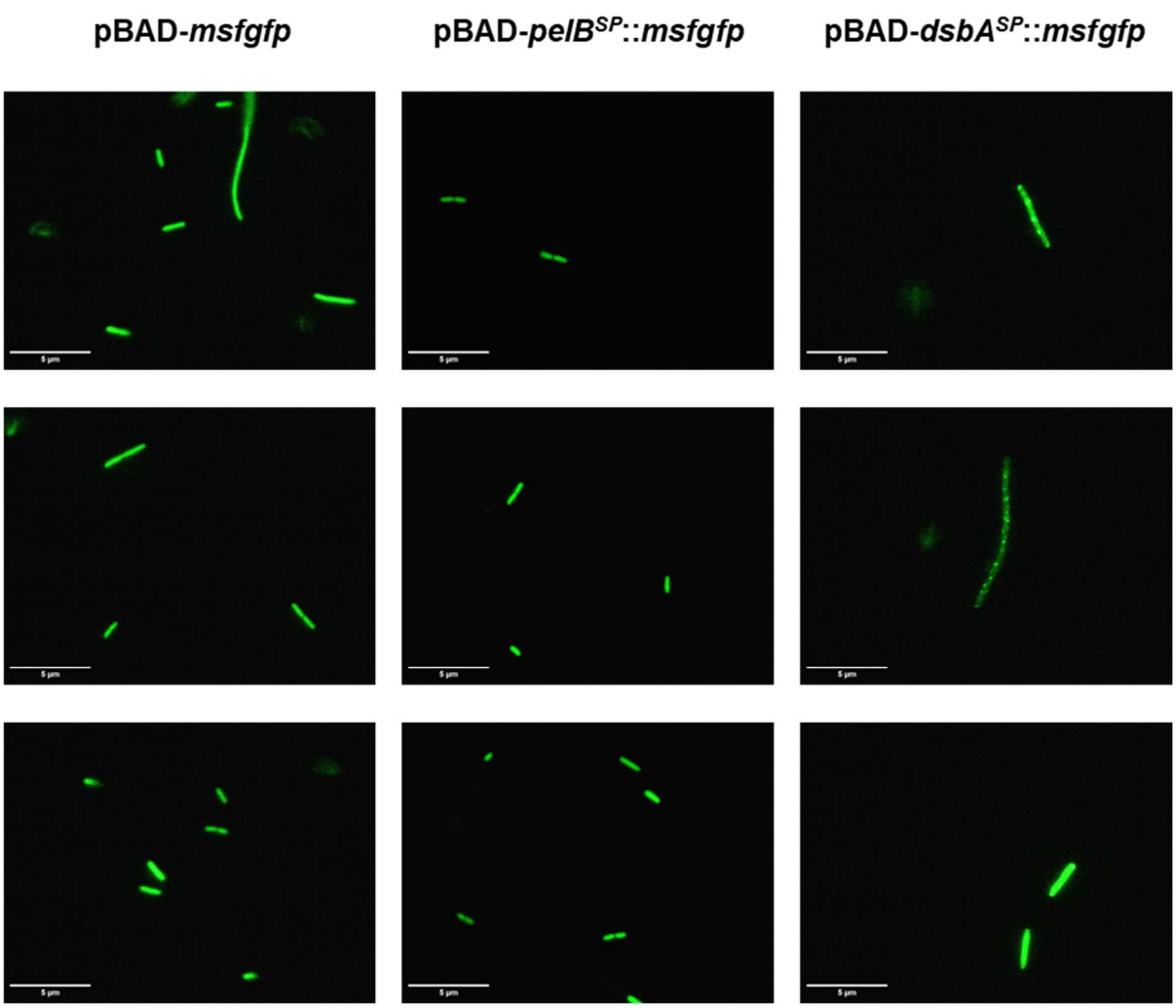


Figure 4.21: Fluorescence microscopy of BL21 expressing msfGFP from P_{araBAD}.

msfGFP expressed from P_{araBAD} was exported to the periplasm via fusion to PelB^{SP} or DsbA^{SP}, a cytoplasmic variant was used a control. Cultures were aerated at 30 °C, 200 rpm in 50 mL TB + Kan and induced with 0.2 % L-arabinose at OD_{600} 0.4-0.6. At 4 h post-induction cells were visualised using fluorescence microscopy and a 100X oil immersion objective. Data for each condition is shown from one culture.

In cultures expressing cytoplasmic msfGFP and PelB^{SP}::msfGFP, green fluorescence appeared homogenous throughout the cells. In DsbA^{SP}::msfGFP, accumulation of msfGFP at specific foci was apparent, with cells appearing punctate. We did not observe any fluorescent halos that would suggest msfGFP was localised to the periplasm.

4.5.2 Structured illumination microscopy

Fluorescence microscopy has limited resolution to visualise small regions like the periplasm, we wondered whether structured illumination microscopy (SIM) would provide more detail. To check this, msfGFP expressed from P_{araBAD} was exported to the periplasm via fusion to $PelB^{SP}$ and $DsbA^{SP}$::msfGFP. Cultures were aerated at 30 °C, 200 rpm in TB and induced with 0.2 % L-arabinose at OD_{600} 0.4-0.6. To define either the inner or outer membrane, at 4 h post-induction cells were stained with Nile red and then visualised via SIM using green and red fluorescence channels.

Cells expressing cytoplasmic msfGFP from P_{araBAD} were very small although uniformly fluorescent (Figure 4.22). Those expressing $PelB^{SP}$::msfGFP were larger but also had consistent green fluorescence throughout the cell (Figure 4.23). When staining cells expressing either cytoplasmic msfGFP or $PelB^{SP}$::msfGFP with Nile red and merging green and red fluorescence channels during analysis, it was difficult to determine cell boundaries. Comparatively, cells expressing $DsbA^{SP}$::msfGFP again had accumulation of msfGFP at specific foci localised toward the exterior. Interestingly one cell appeared to exhibit a green fluorescent halo (Figure 4.24, bottom left). When merging red and green channels (Figure 4.25), red fluorescence appeared in the same position as green fluorescence. It was not clear which membrane Nile red was staining though there is evidence that it stains the inner membrane (Ilangumaran Ponmalar et al., 2022). If this was the outer membrane, this combined with the visualisation of a fluorescent halo supported the notion msfGFP was fluorescent in the periplasm when exported using $DsbA^{SP}$.

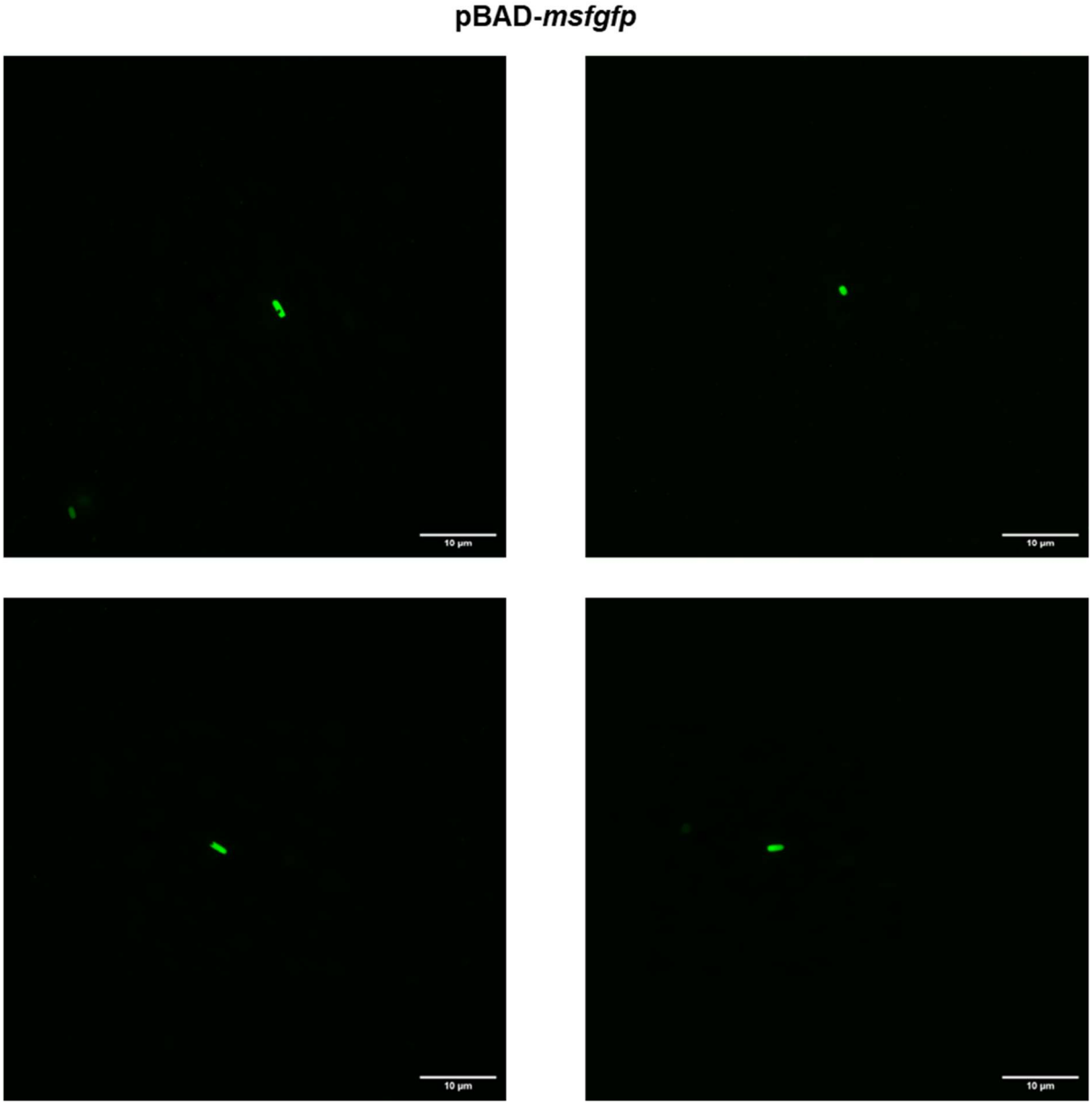


Figure 4.22: SIM analysis of BL21 expressing msfGFP from P_{araBAD}.

Cytoplasmic msfGFP expressed from P_{araBAD} was aerated at 30 °C, 200 rpm in 50 mL TB + Kan and induced with 0.2 % L-arabinose at OD_{600} 0.4-0.6. To define either the inner or outer membrane, at 4 h post-induction cells were stained with Nile red and then visualised via SIM using green and red fluorescence channels. Data for each condition is shown from one culture.

Shown are images from the green fluorescence channel. In cells expressing cytoplasmic msfGFP, green fluorescence appeared homogenous throughout. Staining cells with Nile red was inefficient and we were unable to merge channels.

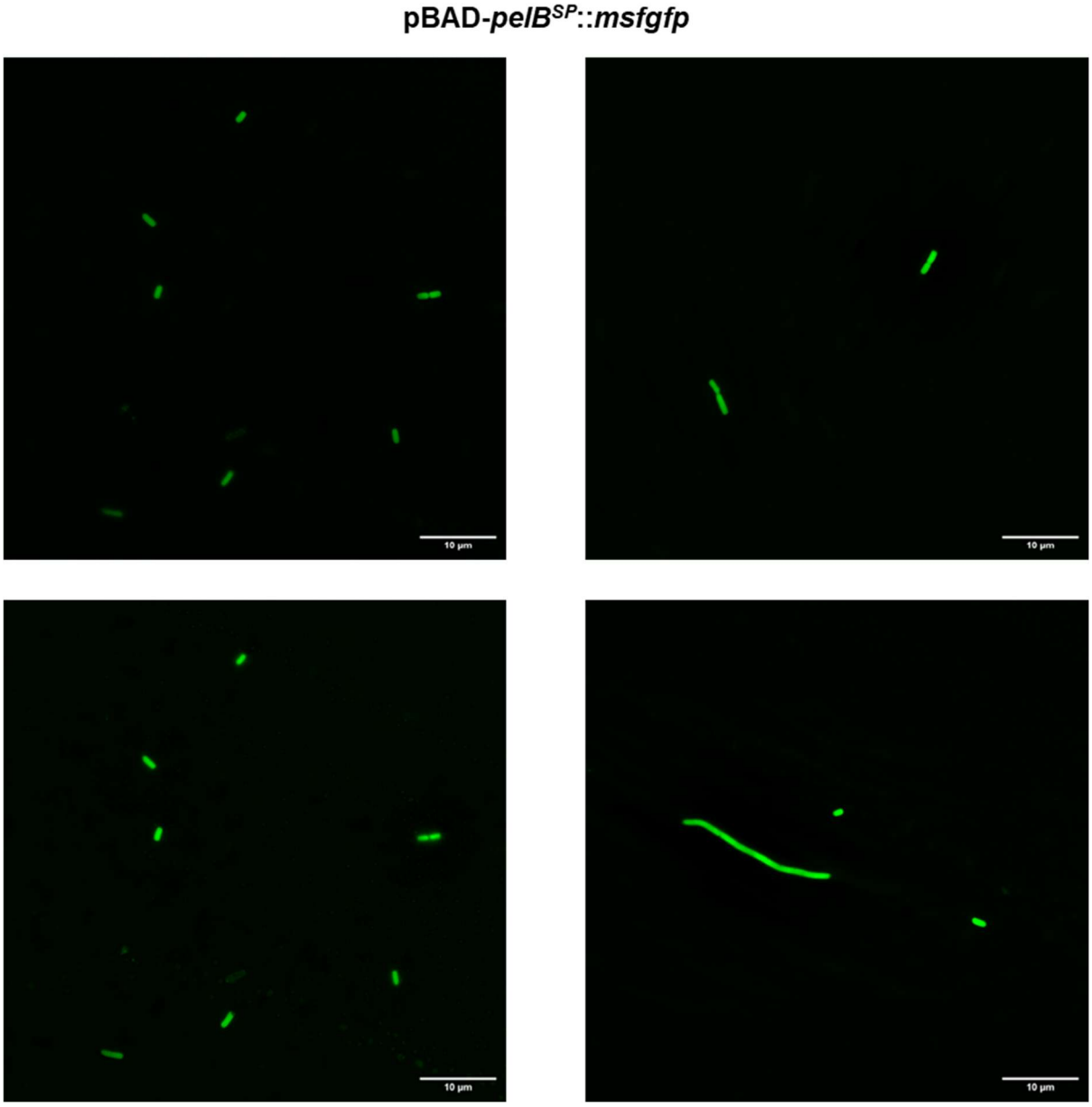


Figure 4.23: SIM analysis of BL21 expressing PelB^{SP}::msfGFP from P_{araBAD}.

msfGFP expressed from P_{araBAD} was exported to the periplasm via fusion to PelB^{SP}. Cultures were aerated at 30 °C, 200 rpm in 50 mL TB + Kan and induced with 0.2 % L-arabinose at OD_{600} 0.4-0.6. To define either the inner or outer membrane, at 4 h post-induction cells were stained with Nile red and then visualised via SIM using green and red fluorescence channels. Data for each condition is shown from one culture.

Shown are images from the green fluorescence channel. In cells expressing PelB^{SP}::msfGFP, green fluorescence appeared homogenous throughout. Staining cells expressing PelB^{SP}::msfGFP with Nile red was inefficient and we were unable to merge channels.

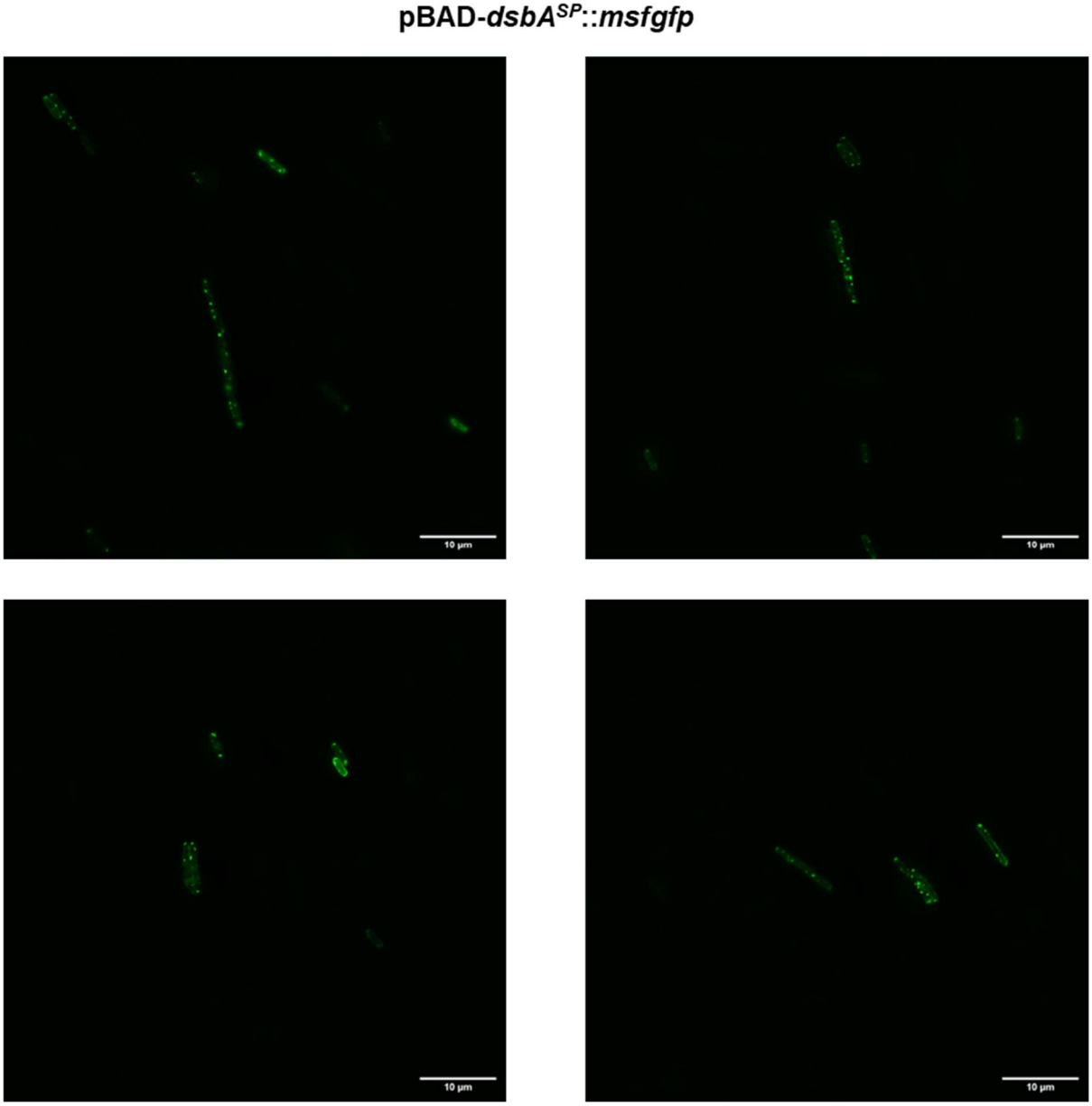


Figure 4.24: SIM analysis of BL21 expressing DsbA^{SP}::msfGFP from P_{araBAD}.

msfGFP expressed from P_{araBAD} was exported to the periplasm via fusion to DsbA^{SP}. Cultures were aerated at 30 °C, 200 rpm in 50 mL TB + Kan and induced with 0.2 % L-arabinose at OD_{600} 0.4-0.6. To define either the inner or outer membrane, at 4 h post-induction cells were stained with Nile red and then visualised via SIM using green and red fluorescence channels. Data for each condition is shown from one culture.

Shown are images from the green fluorescence channel. In cells expressing DsbA^{SP}::msfGFP, accumulation of msfGFP at specific foci was apparent, with cells appearing punctate. In a single cell (bottom left image), there was what appeared to be a green, fluorescent halo.

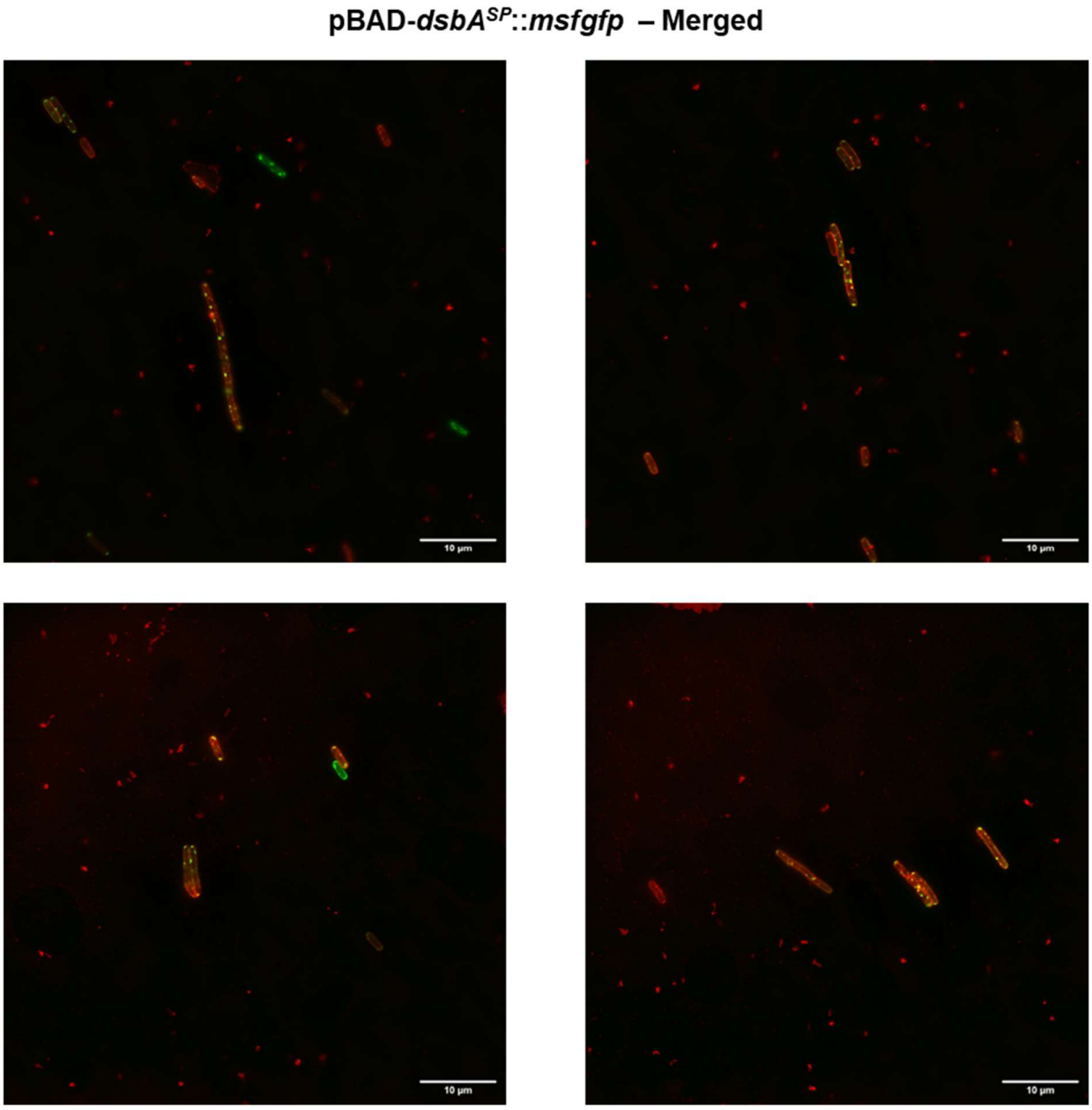


Figure 4.25: SIM analysis of BL21 expressing DsbA^{SP}::msfGFP from P_{araBAD} – merged channels.

msfGFP expressed from P_{araBAD} was exported to the periplasm via fusion to DsbA^{SP}. Cultures were aerated at 30 °C, 200 rpm in 50 mL TB + Kan and induced with 0.2 % L-arabinose at OD_{600} 0.4-0.6. To define either the inner or outer membrane, at 4 h post-induction cells were stained with Nile red and then visualised via SIM using green and red fluorescence channels. Data for each condition is shown from one culture.

Shown are images after merging red and green fluorescence channels. In a single cell (bottom left image), there was what appeared to be a green, fluorescent halo; red fluorescence was not noticeable around this region.

4.6 Discussion

Expression of recombinant proteins in the periplasm is a hugely attractive option, particularly for the many biotherapeutics which require disulphide bonding for activity (Walsh and Walsh, 2022). Quantifying recombinant proteins localised to the periplasm is often time-intensive due to typically requiring fractionation SDS PAGE analysis. As optimisation is so crucial RPP, higher throughputs are desirable (Sun et al., 2023). While some more rapid methods for protein quantification in the periplasm have been evaluated (Osgerby and Overton, 2023); we attempted to create a screening tool utilising GFP. Unlike nearly all other GFP derivatives, msfGFP has been proposed to fluoresce when exported to oxidising environments like the bacterial periplasm (Aronson et al., 2011, Dinh and Bernhardt, 2011). Hence, in this work, we evaluated the use of msfGFP for detecting overexpression of recombinant proteins localised to the periplasm via fusion to $PelB^{SP}$ or $DsbA^{SP}$; use of FCM and viability staining allowed impact of expression the host to be observed at the single cell level.

Interestingly, fusion of msfGFP to $PelB^{SP}$ was consistently shown to have better expression compared with $DsbA^{SP}$; we also found that cells expressing $DsbA^{SP}$::msfGFP grew poorly in general. Work in our lab and others previously during signal peptide screening seemed to suggest $DsbA^{SP}$ was a more efficient ‘exporter’ than $PelB^{SP}$, which was found to be a better ‘expresser’ (Selas Castiñeiras et al., 2018a, Horga et al., 2018). It was also suggested fusions to $PelB^{SP}$ may become trapped in the cytoplasm; such fusions are exported post-translationally and due to the fast folding kinetics of msfGFP means it may reach an active state before export (Aronson et al., 2011, Dinh and Bernhardt, 2011).

This is somewhat consistent with what we observed during fluorescence microscopy analysis (section 4.5). Expression of PelB^{SP}::GFP more frequently gave rise to cells with homogenous fluorescence comparable to cytoplasmic controls. Conversely, expression DsbA^{SP}::msfGFP frequently resulted in concentrated green, fluorescent foci near the boundary of the cell. In support of prior work, we did observe some cells potentially consistent with msfGFP fluorescence in the periplasm when expressing DsbA^{SP}::msfGFP and visualisation using SIM, although in the majority exhibited punctate expression. Further, high level expression of msfGFP was previously suggested as preventing fluorescence of msfGFP in the periplasm (Fisher and Delisa, 2008, Dinh and Bernhardt, 2011).

Two expression systems were tested, a T7*lac* based system and a P$_{araBAD}$ version. In both instances overexpression of msfGFP directed for export via fusion to PelB^{SP} or DsbA^{SP} resulted in considerable proportions of PI+ cells shortly after induction (10-30%). It is likely this was not specifically an issue with msfGFP; indeed, these findings are consistent with what we have observed during production of other periplasmic proteins. Export of a PelB^{SP}::scFv fusion via expression from a strong P$_{lac}$ derivative PAR7 (Hothersall et al., 2021) also resulted in a high number of PI+ cells, upwards of 30%, very quickly after induction (see chapter 5). It is likely the high proportions of PI+ cells observed was due to poor compatibility between overexpression and export. We selected the Sec pathway as it is the predominant export machinery (Orfanoudaki and Economou, 2014); while export of folded proteins via Tat has been looked at previously (Browning et al., 2017), export via this route would prevent access to a primary reason

for localising proteins to the periplasm, the Dsb system (Matos et al., 2014); disulphide bonds being essential for many recombinant proteins (Rathore and Batra, 2016).

Besides the typical stressors placed on cells during RPP (Hoffmann and Rinas, 2004), periplasmic expression adds additional stress to translocation systems. Capacity of Sec is presumably limited; *E. coli* is not known to be a prolific exporter in general (Francetic, 2000). High level expression of recombinant proteins through Sec must quickly lead to saturation and an export deficient state (Mergulhão et al., 2004, Schlegel et al., 2013, Baumgarten et al., 2018). This is obviously problematic for the host, sec being essential. Around 25 % of the proteome is localised to the envelope, and of those exported proteins, approximately 98 % are Sec dependent (Beckwith, 2013, Orfanoudaki and Economou, 2014). With this in mind, it is clear why high level expression directed through Sec could quickly result in cell death, export of native proteins required for survival is prevented; indeed, overexpression of periplasmic recombinant proteins was shown to upregulated Sec components like the ATPase SecA and insertase YidC (Karyolaimos et al., 2020). When we reduced expression levels using a P_{araBAD} promoter induced with 0.02 % L-arabinose, the proportion of PI+ cells noticeably dropped to under 5% (section 4.3.4). However, P_{araBAD} is poorly titratable with sub-saturating L-arabinose concentrations resulting in all-or-nothing induction (Siegele and Hu, 1997) and we observed significant heterogeneity when inducing at 0.02 %. Co-expression of an inducible variant of L-arabinose transporter AraE improves homogeneity at lower inducer concentrations but adds additional complexity to the system (Khlebnikov et al., 2000). Further, being restricted to such low expression is not at all ideal for an optimisation and screening system.

Precise tuning of expression is obviously a requirement for better tolerance of the host to export of recombinant proteins (Simmons and Yansura, 1996), and mimics what has been observed during cytoplasmic expression; minimising stress through slower growth and production synthesis improves yield (Sevastsyanovich et al., 2009, Wyre and Overton, 2014, Selas Castiñeiras et al., 2018b, Chen et al., 2021, Zulkifly et al., 2023). Indeed, much research into periplasmic expression has focused on the use of more highly regulated systems (Karyolaimos and de Gier, 2021). P_{rhaBAD} promoters are capable of very precise and linear expression dependent on rhamnose concentration; though L-rhamnose is metabolised by *E. coli* (Boronat and Aguilar, 1979). Shifting P_{rhaBAD} to orthogonal inducers like L-mannose is possible however by removing the requirement to activate two regulators (Kelly et al., 2016). A system, Lemo21(DE3), utilising a rhamnose inducible promoter to control expression of the T7 RNA RNA polymerase inhibitor T7 lysozyme was developed (Wagner et al., 2008), allowing more precise control of expression levels. This was applied to periplasmic expression of recombinant proteins and found to be necessary to not overload the cell (Schlegel et al., 2013).

Further work indicated tunability of P_{rhaBAD} was dependent on L-rhamnose metabolism by the host (Hjelm et al., 2017). Mutagenising *rhaB* which encodes the catabolic protein RhaB rendered it inactive; deletion of transporter RhaT meant L-rhamnose entry into cells was via diffusion and the concentration remained stable allowing even more precise tuning exported protein expression. This P_{rhaBAD} system was once again used in a screen to optimise signal peptides (Karyolaimos et al., 2019a). Continuing in this

vein, a system utilising an orthogonal pyrimido[4,5-d]pyrimidine-2,4-diamin (PPDA) riboswitch was developed to regulate translation in T7 based systems (Morra et al., 2016). This was subsequently applied to optimise production of proteins exported to the periplasm (Horga et al., 2018). Thus, if msfGFP is to be used as a screening tool, it must be allied to systems with additional layers of control.

Besides the detriment to host physiology and perhaps the most important point is that throughout this work, we typically saw around 10 – 30% of expressed GFP translocated to the periplasm, based on SDS PAGE analysis. This is perhaps the biggest issue with application of the GFP derivatives tested toward screening of periplasmic proteins. If export efficiency is so low, there is little point in screening. Prior work also using $DsbA^{SP}$, achieved over 60% of the expressed recombinant protein as periplasmic (Horga et al., 2018). Although this was through the application of a novel system allowing tuning of transcription and translation rates to better harmonise with translocation, and during fed-batch fermentation where host physiology can be maximised. Some studies have utilised plasmids harbouring various chaperones such as GroELS, DnaKJE or FkpA to assist folding or prevent aggregation of Fab fragments during expression (Farajnia et al., 2020, Levy et al., 2013).

Besides msfGFP, we also looked at a cysteine free derivative cfSGFP2 (section 4.4) (Suzuki et al., 2012); cysteine residues purportedly responsible for misfolding GFP in oxidising environments (Jain et al., 2001, Dammeyer and Tinnefeld, 2012). We found that even cytoplasmic cfSGFP2 appeared to be expressed poorly in *E. coli*, with low green fluorescence observed even during full induction of P_{araBAD} with 0.2 % L-

arabinose. cfSGFP2 is less bright than msfGFP, having an extinction coefficient of 45000 M^{-1} cm^{-1} and quantum yield of 0.75; comparatively msfGFP has a quantum yield of 0.65 but extinction coefficient of 83300 M^{-1} cm^{-1} (Pédelacq et al., 2006, Suzuki et al., 2012). When analysing cfSGFP2 content in cells by SDS PAGE however, we could not identify notable bands consistent with high level cfSGFP2 accumulation (26.9 kDa) that were not visible pre-induction.

Though cfSGFP2 was originally developed for use in mammalian systems, it does contain some mutations that improve expression in bacteria, namely F64L, S65T, M153T, and V163A (Heim et al., 1995, Cormack et al., 1996, Crameri et al., 1996); though, A206K/A206V are replaced with an alternate monomerising mutation A206L (Nakagawa et al., 2012). We had initially considered codon optimising the sequence prior to cloning. But, using various tools, we found the CAI for cfSGFP2 in *E. coli* K-12 MG1655 to be around 0.69; this is less than ideal but we also found msfGFP had a CAI even lower at around 0.59. It is worth noting though that such tools are only predictive and do not necessarily reflect how a protein will express *in vivo*; indeed, we observed high green fluorescence when expressing cytoplasmic msfGFP but not cfSGFP2. A further point is that even with extremely low green fluorescence, expression of $DsbA^{SP}$::cfSGFP2 still resulted in high levels of dead cells after just a few hours. cfSGFP2 was clearly not applicable for use in *E. coli* but other cysteine free derivatives have been developed. moxGFP is monomeric msfGFP derivative with the C48S/C70S mutations found in cfSGFP2 but retaining the S30R, Y39N, N105T, Y145F, I171V mutations for more robust folding (Costantini et al., 2015). While not yet

demonstrated as fluorescent in the *E. coli* periplasm, moxGFP presents an opportunity for future work.

It is also of worth noting some of the caveats of this work, namely the utility of the fluorescent dye PI, which intercalates between bases of nucleic acids such as DNA. Upon binding, PI emission maximum is shifted to 617 nm and fluorescence is greatly increased. The application of PI is frequently as a measure of cell viability and indeed, it has been used regularly to quantify this using FCM (Steinkamp et al., 1999, Crowley et al., 2016). However, as we have discussed throughout this chapter, it is more strictly a measure of permeability and the integrity of the membrane. PI is non-permeable to intact membranes, being a cationic and a relatively large molecule it will not readily diffuse across lipid bilayers. If integrity of the membrane is lost and becomes permeable, it can enter cells. This is used as a barometer for cell viability as fundamentally, the membrane is essential for life.

However, several reports have indicated that PI sometimes incorrectly stains cells, be this because the loss of membrane integrity was reversed (Davey and Hexley, 2011, Yang et al., 2015); or extracellular DNA was stained, as was the case during analysis of biofilms (Rosenberg et al., 2019). Given this, it was important to utilise PI analysis with other standard methods for measuring cell physiology including optical and cell density analysis using FCM. We could have plated cells onto solid growth medium as an alternative to the latter, but as we frequently observed during periplasmic expression, cells are often stressed during RPP (Hoffmann and Rinas, 2004, Mergulhão et al., 2004, Schlegel et al., 2013, Baumgarten et al., 2018) and this can

often result in a VBNC phenotype which can also misrepresent culture viability (Boaretti et al., 2003).

Other observations which should be addressed in any continuation of this work include replica plating experiments to quantify plasmid loss (Sevastsyanovich et al., 2009) and further probe potential reasons for the often-low green fluorescence seen in cultures expressing exported msfGFP. Further, given issues with leakage of cells during fractionation and SDS PAGE analysis (Morra et al., 2018), analysis of growth medium fractions would be productive to further clarify this. However, overall, the systems tested were clearly not workable for use as screening tools.

4.7 Conclusions

The aim of this project was to investigate whether GFP derivatives resistant to oxidising environments could be utilised as a periplasmic screening system. We evaluated the use of the robust folding GFP derivative msfGFP for detecting overexpression of recombinant proteins localised to the periplasm.

To do so, we initially utilised a T7*lac* system to drive expression of msfGFP fused to either $PelB^{SP}$ or $DsbA^{SP}$. However, we found that upon induction of either $PelB^{SP}$::msfGFP or $DsbA^{SP}$::msfGFP, considerable drops in cell density, biomass accumulation and large proportions of PI+ cells were observed and taken as indications of generally poor tolerance or loss to viability. Further, the efficiency of export of $PelB^{SP}$::msfGFP or $DsbA^{SP}$::msfGFP, based on the proportion of msfGFP estimated to be periplasmic, was frequently low.

Given the high levels of expression from T7*lac* promoters, attempts were made to tune expression to levels which would be more tolerable and less detrimental to host physiology. However, when using a weaker P_{araBAD} system a similar drop in cell density, biomass accumulation and large proportions of PI+ cells were observed. Improved host physiology was seen at very low L-arabinose concentrations, indicating more tuneable systems are required for delivery of msfGFP to the periplasm. A second derivative cfSGFP2 was found to express poorly in *E. coli* and thus has limited scope for future use without modification. However, in support of prior work, using SIM, we did observe some cells, which had exported msfGFP via $DsbA^{SP}$, that would be considered consistent with msfGFP fluorescence in the periplasm.

While we had set out to develop a screening system, overall, we found that applicability of msfGFP, when expressed from T7*lac* or P_{araBAD} systems was not suitable for use as such a tool to quantify periplasmic recombinant proteins. Regardless we hope that this work will further cement the notion that localisation of recombinant proteins to the periplasm requires significant control over expression using highly regulated systems. It also further highlights the benefits of FCM analysis to observe expression at the single cell level, and combined with viability staining, can be used to further identify problems with host physiology during RPP optimisation.

Chapter 5: Biosensors and Feedback Loops

5.1 Introduction

In Chapter 4 we tried utilising novel GFP derivatives such as sfGFP, resistant to folding in oxidative environments (Aronson et al., 2011, Dinh and Bernhardt, 2011, Suzuki et al., 2012), to quickly screen for localisation of recombinant proteins to the *E.* coli periplasmic space. This proved difficult, and while other methods exist for screening (Osgerby and Overton, 2023), all come with caveats. Like previously suggested (Schlegel et al., 2013, Baumgarten et al., 2018), we suspected high level expression of a recombinant protein directed to the periplasm quickly saturates translocation machinery, preventing export of native proteins and leading to cell death. Our attention thus changed from screening to ways in which we could detect stress arising from export of a recombinant protein and then use this to modulate expression accordingly.

In section 1.5.2, we described several of the stress response networks found within the *E. coli* cell envelope (Mitchell and Silhavy, 2019), such as σ^E (Mecsas et al., 1993), CpxAR (Raivio, 2014), BaeSR (Raffa and Raivio, 2002), Psp (Flores-Kim and Darwin, 2016) and Rcs (Meng et al., 2021). Stress response pathways in general provide a form of feedback control, sensing signals arising from perturbations within the cell and responding to contain the originating problem. We began to think more about applicability of such feedback to RPP; in theory, following initial induction, this sort of control offers a novel way to regulate recombinant protein production without user input. Such self-regulating systems would be required to detect specific stressors, triggering a cascade of events culminating in the cessation of expression. Ideally upon a reduction in stress, expression resumes creating a cyclical expression system which

is directly coupled to host physiology. This seemed particularly attractive for expression of periplasmic proteins, where the stress placed upon the cell is presumably great. Indeed, reports on successful periplasmic expression seem to utilise highly regulated systems with precise tunability such as with the rhamnose inducible promoter (Schlegel et al., 2013, Hjelm et al., 2017, Karyolaimos et al., 2019a, Karyolaimos et al., 2020). Taking this further, riboswitches have been incorporated to provide additional tuneable control over translation and align transcription and translation rates with translocation (Horga et al., 2018).

Feedback systems have been developed for use in *E. coli*. One has looked at regulating expression in response to stress associated with production of integral membrane proteins (IMPs) (Guidi et al., 2022). The system utilised part of the CpxAR stress response pathway, specifically an untranslated region of *cpxP* mRNA which is cleaved by RNase E, forming *cpxQ*. An sRNA (Urban and Vogel, 2007), *cpxQ* purportedly regulates translation of proteins involved in IMP synthesis via interaction with target mRNA (Chao and Vogel, 2016). The CpxP promoter and region encoding the sRNA were co-expressed on a plasmid alongside an expression construct containing an IMP. The cyclical nature of the system proceeded as overexpression of the IMP increasing stress levels which induced *cpxQ*; downregulation of the IMP then occurred, which in turn reduced upregulation of *cpxQ*.

Another self-regulating circuit for recombinant protein production was designed previously (Dragosits et al., 2012), which exploited the *ibpAB* promoter to control expression of cytoplasmic GFP. P_{ibpAB} is a σ^{32} dependent promoter, encoded by *rpoH*

(Narberhaus and Balsiger, 2003). σ^{32} is the regulator for the cytoplasmic heat shock response; predictably this is induced by elevated temperatures, although the resulting effect on misfolding and aggregation of cytoplasmic proteins seems to be the main driver (Miwa et al., 2021). For the feedback loop, Dragosits et al. (2012) utilised the TetR repressor and inserted a *tet* operator downstream of a T7 promoter. A degradation tag was fused to *tetR* to allow for cycling of the system.

A generalised example of such a system is provided using BL21(DE3) and a T7 expression system as an example (Figure 5.1A). In BL21(DE3), the IPTG inducible promoter lacUV5 controls expression of a chromosomal copy of T7 RNA polymerase necessary for transcription from the T7 promoter, which drives expression of a gene of interest on a plasmid (Studier and Moffatt, 1986). During overexpression of the recombinant protein increased stress levels which are detrimental to growth or lower yields would trigger expression from a feedback construct (Figure 5.1B). The trigger is key to the systems function and define under what conditions feedback is initiated. Regardless, the result would be expression of a repressor which targets operator sequences inserted downstream of the T7 promoter, sterically blocking T7 RNA polymerase and shutting off expression. For reference, operator sequences could in theory be additionally inserted downstream of lacUV5 on the chromosome preventing expression of T7 RNA polymerase entirely. For cycling of the system, the repressor must be continually degraded, lest it remain bound to the operator. Reduced expression would translate to lower stress, improving expression.

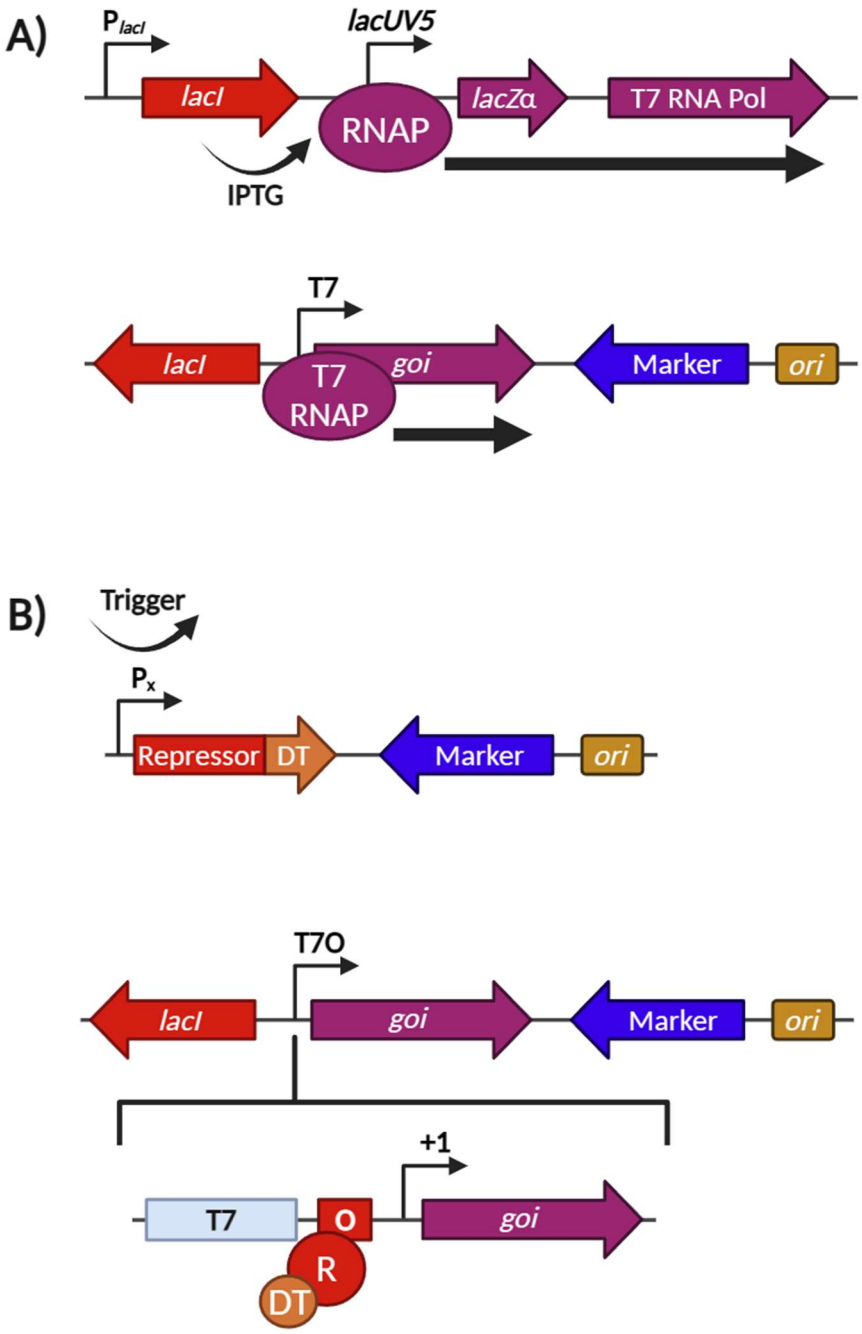


Figure 5.1: Feedback loops are an interesting proposition for recombinant protein production in *E. coli*; adjustment of expression levels without any additional input is possible. A generalised overview of how such a system may be implemented is provided.

(A) T7 systems are widely used for RPP in *E. coli*. In the strain BL21(DE3), the IPTG inducible promoter *lacUV5* controls expression of a chromosomal copy of T7 RNA polymerase which is required to transcribe from the T7 promoter driving expression of a gene of interest on an exogenous plasmid.

(B) Central to the system is a trigger which senses when expression levels reach a point where the host is placed under stress detrimental to efficient protein production. Such a trigger would be used to activate expression of a repressor fused to a degradation tag. Insertion of a compatible operator site downstream of the T7 promoter would sterically block T7 RNA polymerase from binding. Degradation tags fused to the repressor would facilitate cycling of the system.

We were interested to see whether a comparable system could be developed for expression of periplasmic proteins. By utilising FCM and GFP expression combined with overexpression of periplasmic recombinant proteins, we attempted to identify triggers which could be utilised in generation of such a feedback circuit. This was followed by evaluating novel application of mutagenised repressors to regulate expression and combination with triggers to regulate expression in a stress-dependent manner.

5.2 SecM as a Periplasmic Biosensor

Being the primary export system (Orfanoudaki and Economou, 2014), we decided to focus ways to detect stress resulting from high level translocation via Sec. Further, a primary reason for export of recombinant proteins to the periplasm is access to the Dsb system (Bardwell et al., 1991, Berkmen, 2012), allowing synthesis of biotherapeutics like antibodies which required disulphide bonding for activity (Rathore and Batra, 2016). Without an oxidising cytoplasm, such proteins cannot fold correctly prior to export, which does not appear compatible with Tat mediated translocation (Delisa et al., 2003, Matos et al., 2014). Thus, our aim was to directly detect export stress and more specifically, when the translocon had become saturated.

5.2.1 Design of a SecM Periplasmic Biosensor

In *E. coli*, the Sec machinery has a native detection system for translocon saturation. Central to the post-translational branch of Sec is the ATPase SecA, which drives export (Ambroziak et al., 2021). SecA expression is tightly controlled by the secretion monitor protein SecM. Both SecM and SecA are transcribed together as an operon (Figure

5.2A); it is the resulting bicistronic mRNA which regulates SecA at the translational level (Oliver et al., 1998). SecM is a small 19 kDa protein and translated first and exported co-translationally via SRP to the periplasm (Rajapandi et al., 1991, Sarker et al., 2000); here it is swiftly degraded by tail specific protease (Nakatogawa and Ito, 2001) and appears to have no function besides regulating SecA. There are two parts key to translational regulation; first is a 17 amino acid arrest sequence at the C-terminus of SecM; the key residues being FXXXXWIXXXXGIRAGP (Nakatogawa and Ito, 2002). Upon loading the terminal Proline-166 to the ribosomal A-site during elongation, the ribosome stalls (Nakatogawa and Ito, 2002). Exact mechanics behind the stalling are apparently complex and potentially involve multiple contacts of SecM outside of the arrest sequence with ribosomal proteins, particularly around the exit site (Gumbart et al., 2012, Zhang et al., 2015, Bracken and Woolhead, 2019, Muta et al., 2020).

The second part of regulation is the localisation of the *secA* Shine-Dalgarno sequence within a region prone to hairpin formation (McNicholas et al., 1997). During synthesis and translocation of SecM through SecYEG, stalling occurs causing the ribosome to disrupt the mRNA secondary structure enclosing the *secA* Shine-Dalgarno sequence. Under conditions amenable to translocation, the pause in translation is transient due to the pulling action of Sec (Butkus et al., 2003, Yap and Bernstein, 2011). Under translocation deficient conditions, where transfer of nascent SecM through SecYEG is impaired, the length of the translational stall increases revealing the *secA* RBS, due to the ribosome disrupting the hairpin in this part of the mRNA (Butkus et al., 2003, Yap and Bernstein, 2011); hence, increased SecA translation occurs.

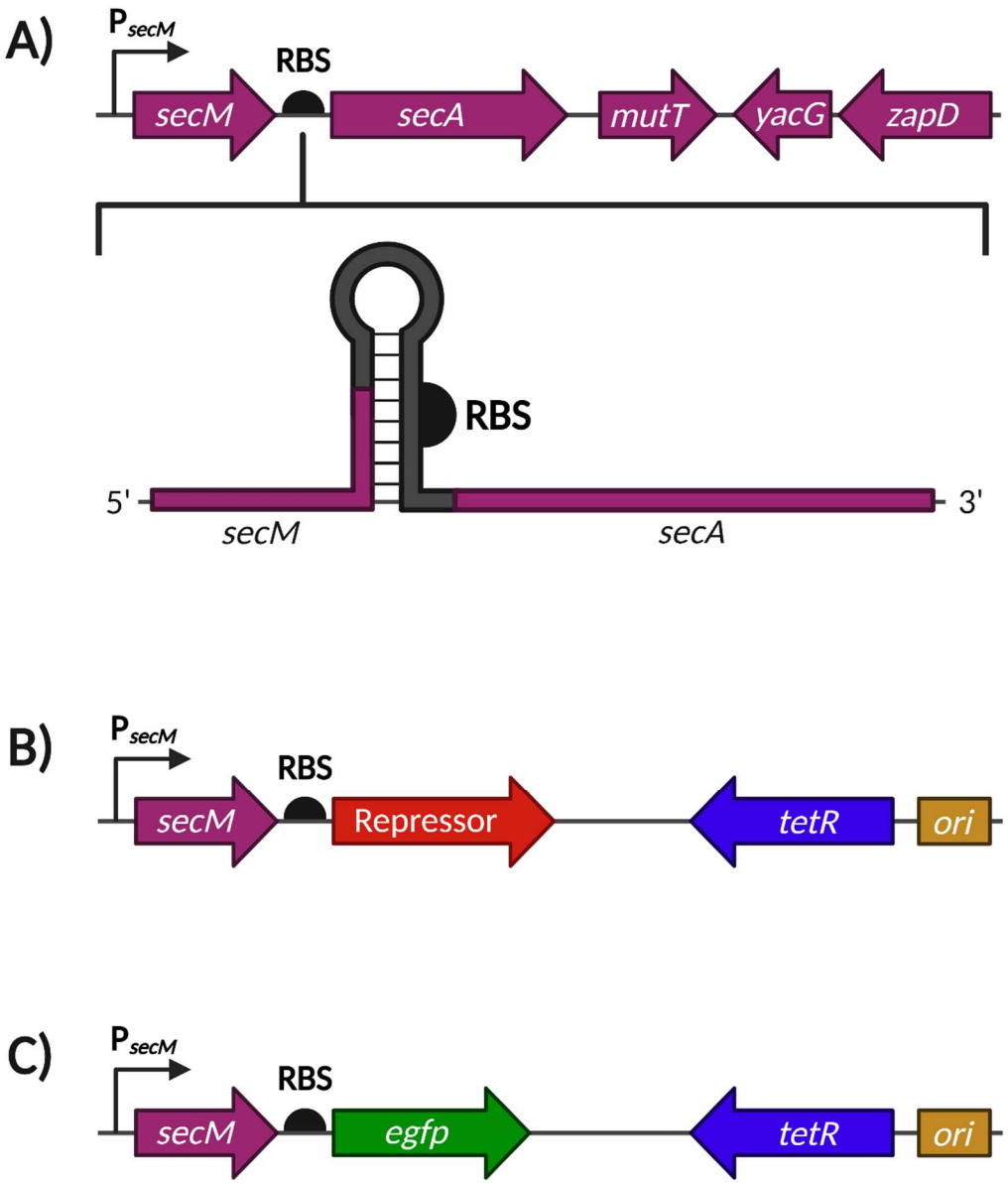


Figure 5.2: Central to a functional feedback loop is a trigger which can sense a desired intercellular condition such as saturation of translocation machinery.

(A) In *E. coli* the ATPase SecA is the driving force behind post-translational export via Sec and thus its expression is tightly regulated translationally by a co-expressed protein, SecM. Bi-cistronic *secM*::*secA* mRNA forms a tight hairpin shielding the SecA RBS from access by the ribosome. As SecM is co-translationally exported via Sec, a pause is induced once P166 reaches the ribosome A site. This conformation of the complex flattens the hairpin allowing another ribosome to assemble around the SecA RBS. The length of the pause directly correlates with the secretion status of the cell; if SecM is not translocated due to saturation of Sec, the pause is longer, and more SecA is translated.

(B) We theorised SecM could be used as a trigger to sense whether Sec was saturated due to overexpression of exported recombinant proteins. Shown is a region on a low copy pRW50 plasmid which uses Tet for selection. We theorised that if we cloned a region up to the *secA* start codon and replaced *secA* with a repressor, co-expression of this construct could allow negative feed back into an expression vector, shutting off protein production if saturation of Sec occurred.

(C) To first evaluate the efficacy of SecM as a sensor for recombinant protein-mediated export stress, a SecM expression cassette including the SecA RBS was cloned into a plasmid backbone, upstream of *egfp*.

We theorised that SecM could be exploited as a trigger for regulating expression of a recombinant protein, in response to export mediated stress (Figure 5.2B). The *secA* gene would be replaced with that encoding a repressor. Under translocation deficient conditions, SecM stalling of the ribosome would provide access to the intergenic Shine-Dalgarno sequence upregulating translation of the repressor. This repressor would downregulate expression of the recombinant protein. To test this theory, the *secM-secA* operon was cloned and *msfgfp* inserted in place of *secA* (Figure 5.2C); a low copy pRW50 backbone was selected, the pSC101 origin would prevent too much SecM being exported which might have stressed translocation even further. By exposing the cell to conditions which saturate Sec, it was hoped green fluorescence would increase.

5.2.2 Analysis of a SecM Periplasmic Biosensor

Analysis of SecM as a sensor for periplasmic stress required growth of cells under conditions which overloaded translocation machinery. Thus, the sensor construct pRW50Δ-*secM*::*msfgfp* was co-transformed with expression plasmids pET-26b(+)-PAR1-*pelB*^{SP}::anti-*il-1β* scFv, pET-26b(+)-PAR4-*pelB*^{SP}::anti-*il-1β* scFv or pET-26b(+)-PAR7-*pelB*^{SP}::anti-*il-1β* scFv. Each PAR promoter drives expression of an anti-IL-1β scFv used as a model recombinant protein; the PelB^{SP} directs its export to the periplasm via the post-translational branch of Sec (Steiner et al., 2006). Promoters are P_{lac} derivatives and were designed to increase in strength in the order PAR1<PAR4<PAR7 (Browning et al., 2019, Hothersall et al., 2021).

PAR1 was P_{lac} O1O1, having the upstream O3 auxiliary operator replaced with O1 and is much weaker than WT P_{lac}. PAR4 was P_{lacUV5} O1O1 p34G, the upstream O3 auxiliary operator replaced with O1 and a mutation in the -35 hexamer to match consensus; its strength was between P_{lac} and P_{lacUV5}. PAR7 was P_{tac} O1O1, an additional O1 operator added at -82 of the WT P_{tac} and was thus slightly weaker. The SecM sensor construct, and PAR promoter constructs were co-expressed in BL21 and aerated in 50 mL LB (Miller) in Erlenmeyer flasks at 37 °C, 200 rpm. At OD_{600} 0.4-0.6, overexpression of $PelB^{SP}$::anti-IL-1β scFv was induced in duplicate using 100 μM IPTG. Uninduced cultures for each strain were ran in parallel as a control. Expression was allowed to proceed for a further 24 h.

Accumulation of msfGFP due to stress from overexpression of exported $PelB^{SP}$::anti-IL-1β scFv was monitored by measuring mean green fluorescence using FCM (Figure 5.3A). Between 2 h and 6 h post-inoculation, mean green fluorescence was elevated in induced cultures containing PAR4 or PAR7. This increase in mean green fluorescence was only small; at 6 h post-induction it was around 1.1-fold for PAR4 and 1.4-fold for PAR7. Fluorescence of uninduced controls and induced PAR1 remained low. Although small, increased mean green fluorescence could have been due to increased expression of msfGFP but also due to changes in physiology from high level overexpression of $PelB^{SP}$::anti-IL-1β scFv (as described in chapter 4).

To confirm this, mean FSC was also monitored using FCM (Figure 5.3B); larger cells could have accounted for higher fluorescence. Mean FSC correlated with mean green fluorescence; at 6 h post-induction, PAR7+ cultures had around 6-fold higher FSC than

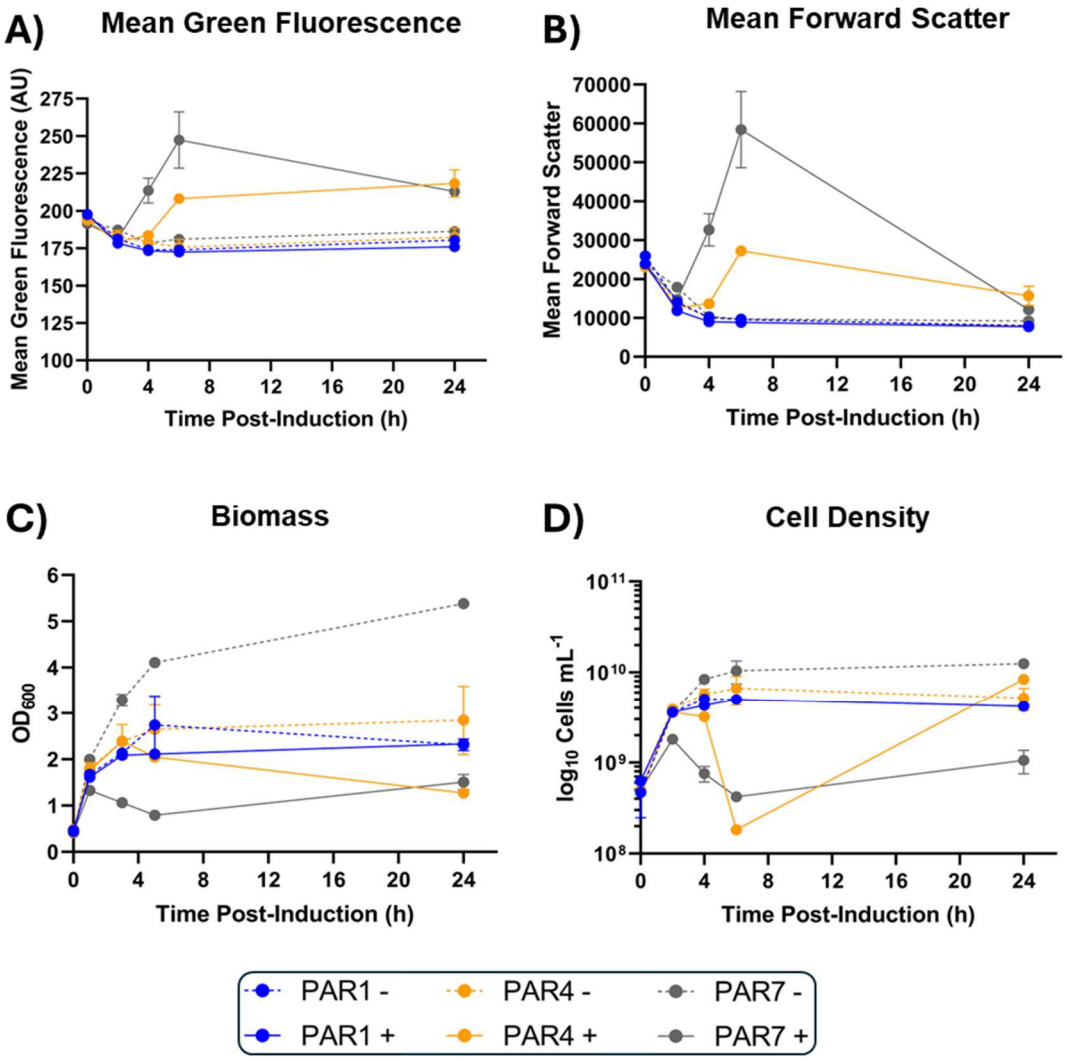


Figure 5.3: Analysis of SecM as a sensor for export stress.

Overexpression of periplasmic recombinant proteins should saturate translocation machinery and stall SecM export, upregulating GFP translation. In BL21 pRW50Δ-*secM::gfp* construct was co-expressed alongside PAR promoter plasmids driving expression of an exported scFv; pET-26b(+)-PAR1-*pelB*^{SP}::anti *il-1β* scFv, pET-26b(+)-PAR4-*pelB*^{SP}::anti *il-1β* scFv, pET-26b(+)-PAR7-*pelB*^{SP}::anti *il-1β* scFv. PAR promoters are derivatives of P_{lac} with increasing strengths. Cultures were grown at 37 °C, 200 rpm in 50 mL LB + Kan + Tet. At OD_{600} 0.4-0.6, cultures were induced with 100 µM IPTG (+) and were compared with uninduced ones (-). Error bars represent +/- SD from biological duplicates.

(A) Mean green fluorescence was measured via FCM and changed little after induction. PAR7+ cultures had the highest mean green fluorescence at 6 h post-induction but only reached 250 AU, only a small increase over uninduced controls.

(B) Mean FSC was measured via FCM and correlated with mean green fluorescence suggesting an increase in FSC was responsible for the small increase observed in (A) for cultures overexpressing high levels of the exported scFv. At 6 h post-induction, PAR7+ cultures were 6-fold larger than the uninduced controls.

(C) OD_{600} indicated biomass accumulation was impacted by induction of scFv expression from PAR promoters, in particular PAR7 which drives the strongest expression.

(D) Cell density measurement was tracked via FCM. PAR4+ or PAR7+ experienced significant growth arrest; at 6 h post-induction there was an almost 2-log difference in cells mL^{-1}.

uninduced controls. At the single cell level, increases in FSC were due to a subset of cells (Figure 5.4); at 6 h post-induction, both induced PAR4 and PAR7 cultures had left skewed distributions with smaller populations exhibiting extremely high FSC. This all suggested increased cell size was at least partially responsible for the small increase observed in mean green fluorescence for cultures overexpressing exported PelB^{SP}::anti-IL-1β scFv.

To check the BL21 host was under stress from overexpression of PelB^{SP}::anti-IL-1β scFv, biomass accumulation and cell density were monitored via OD_{600} and FCM respectively (Figure 5.3C – D). Between induction and 6 h post-induction OD_{600} for induced PAR4 cultures was not too different from uninduced controls. Comparatively, induced PAR7 cultures experienced notable growth arrest beginning at 1 h post-induction; although both induced PAR4 and PAR7 cultures were under OD_{600} 2.0 at 24 h post-induction, indicating severe growth restriction. Cell density measurement was more revealing; at 6 h post-induction, both induced PAR4 and PAR7 cultures had an over 1-log drop in cells mL^{-1} compared with uninduced controls.

It was assumed that induced cells expressing PelB^{SP}::anti-IL-1β scFv from PAR4 or PAR7 were under considerable stress. PI staining was used as a measure of cell viability via membrane integrity; after staining cells, FCM was used to gate cells on red fluorescence (FL3-A) and green fluorescence (FL1-A) density plots. Gates were created for cells not stained by PI, indicating viability, and cells stained by PI, indicating non-viability. Data is shown for cells stained by PI (PI+) (Figure 5.5). In PAR4 and PAR7 cultures, there were considerable numbers of cells within the PI+ gate following

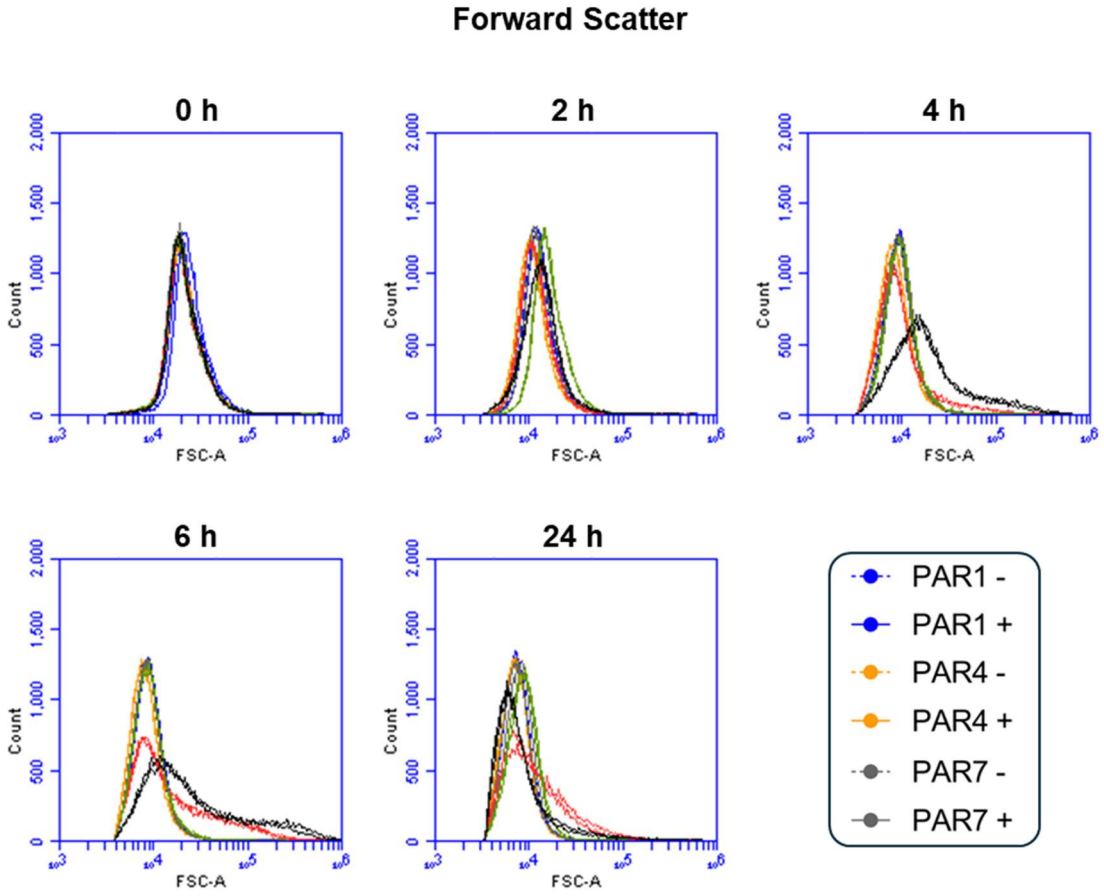


Figure 5.4: FSC analysis of BL21 expressing the SecM sensor construct using FCM.

Overexpression of periplasmic recombinant proteins should saturate translocation machinery and stall SecM export, upregulating GFP translation. In BL21 pRW50Δ-*secM::gfp* construct was co-expressed alongside PAR promoter plasmids driving expression of an exported scFv; pET-26b(+)-PAR1-*pelB*^{SP}::anti *il-1β* scFv, pET-26b(+)-PAR4-*pelB*^{SP}::anti *il-1β* scFv, pET-26b(+)-PAR7-*pelB*^{SP}::anti *il-1β* scFv. PAR promoters are derivatives of P_{lac} with increasing strengths. Cultures were grown at 37 °C, 200 rpm in 50 mL LB + Kan + Tet. At OD_{600} 0.4-0.6, cultures were induced with 100 µM IPTG (+) and were compared with uninduced ones (-). Data for each condition is shown for biological duplicates.

FSC was analysed using FCM and was elevated in conditions where high level expression of the exported scFv. In PAR4+ and PAR7+ cultures; at 4 h and 6 h post-induction, the distribution of cells was left skewed indicating a mixed population of larger and smaller cells.

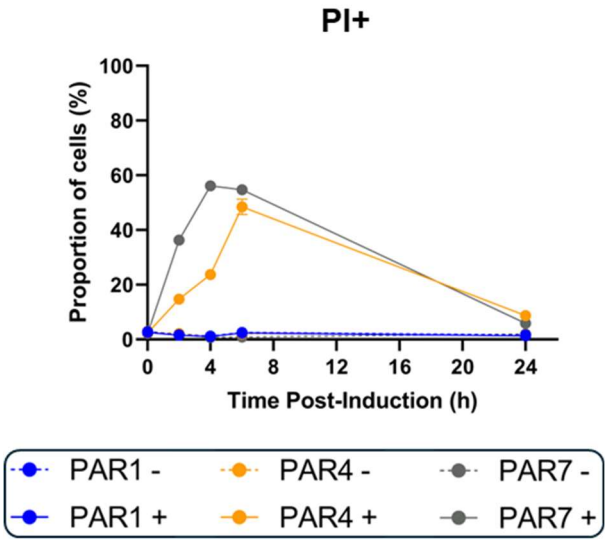


Figure 5.5: Viability of BL21 co-expressing SecM sensor and PAR scFv construct was assessed using PI.

Overexpression of periplasmic recombinant proteins should saturate translocation machinery and stall SecM export, upregulating GFP translation. In BL21 pRW50Δ-*secM::gfp* construct was co-expressed alongside PAR promoter plasmids driving expression of an exported scFv; pET-26b(+)-PAR1-*pelB*^{SP}::anti *il-1β* scFv, pET-26b(+)-PAR4-*pelB*^{SP}::anti *il-1β* scFv, pET-26b(+)-PAR7-*pelB*^{SP}::anti *il-1β* scFv. PAR promoters are derivatives of P_{lac} with increasing strengths. Cultures were grown at 37 °C, 200 rpm in 50 mL LB + Kan + Tet. At OD_{600} 0.4-0.6, cultures were induced with 100 µM IPTG (+) and were compared with uninduced ones (-). Error bars represent +/- SD from biological duplicates.

To assess viability, 4 µg mL^{-1} PI was used to stain cells. Using FCM, cells were gated using red fluorescence (FL3-A) and green fluorescence (FL1-A) density plots. Gates were created for viable and non-viable cells based on staning as PI- (viable) or PI+ (non-viable). Data is shown for cells residing within the PI+ gate.

In PAR4+ and PAR7+ cultures expressing the anti-IL-1β scFv, considerable numbers of cells, around 50 %, were within the PI+ gate by 6 h post-induction indicating they were non-viable. Conversely, in PAR1+ cultures expressing the anti-IL-1β scFv, few cells were within the PI+ gate.

induction with IPTG; at 6 h post-induction this was around 50 % of cells. This was indicative that these cells were not viable, presumably due to overexpression of PelB^{SP}::anti-IL-1β scFv.

Several reports have indicated PI can incorrectly stain cells, due to reversal of lost membrane integrity (Davey and Hexley, 2011, Yang et al., 2015); or staining extracellular DNA in biofilm analysis (Rosenberg et al., 2019). However, given data for biomass accumulation (Figure 5.3C) and cell density (Figure 5.3D) also indicated poor growth in induced PAR4+ and PAR7+ cultures compared with uninduced controls, we thought it was likely the former was causing considerable physiological issues to BL21 cells. Other considerations were that we would ideally check either plasmid free or empty vector controls for the SecM construct to observe the effect on growth and further determine if there is any interference with native SecM function. However, as induced PAR1+ and all uninduced control cultures saturated around $1x10^{10}$ cells mL^{-1} (Figure 5.3D), we assumed if there was perturbation to native SecM, it was not hugely detrimental to growth. A final consideration is that ultimately, we did not observe any notable response from the system; mean green fluorescence only increasing by around 75 AU at 6 h post-induction (Figure 5.3A). Hence we decided instead to proceed with developing a new system utilising a different sensor.

5.3 P_{spy} as a Periplasmic Biosensor

It was clear the SecM biosensor did not function as intended; even if the small increase in mean green fluorescence was in part caused by increased periplasmic stress from overexpression of PelB^{SP}::anti-IL-1β scFv, the low levels of msfGFP expression driven

by SecM would presumably not be enough for a repressor in a feedback system. This inability to respond appropriately to stress mediated by export of recombinant proteins meant a new biosensor was required. A primary advantage of the SecM system was it was directly coupled to the export status of the cell. However, it was decided to try a simpler approach and utilise a promoter activated under specific conditions which had a large fold-change in expression when switched on.

5.3.1 Design of a Periplasmic Stress Biosensor

Spheroplast Protein Y (Spy) is a periplasmic chaperone with holdase and foldase functionality, preventing aggregation or assisting folding while bound to substrates (Koldewey et al., 2016, Kwon et al., 2010, Mitra et al., 2021). Spy has also been used as a fusion tag to improve recombinant protein solubility (Ruan et al., 2020). The promoter P_{spy} is regulated by two stress response systems, BaeSR and CpxAR (Raivio et al., 2000, Raffa and Raivio, 2002, Nishino et al., 2005, Yamamoto and Ishihama, 2005); it has two BaeR sites and a single CpxR site (Yamamoto and Ishihama, 2006, Yamamoto et al., 2008, Srivastava et al., 2014). Under periplasmic stress conditions (for example ethanol, tannins, indole, Zn^{2+}, Cu^{2+}), expression of Spy is massively upregulated (Nishino et al., 2005, Bury-Moné et al., 2009, Quan et al., 2011).

We predicted that P_{spy} would respond strongly to stress induced by overexpression of periplasmic recombinant proteins and could be used as a biosensor. P_{spy} was cloned into a low copy pBAD30Δ backbone with *ara* genes deleted; the p15A origin limiting additional stress on the host from high gene dosage. To monitor activity in response

to various conditions, *6xhis::gfp* was inserted downstream, creating the sensor construct pBAD30Δ-P_{spy}-*6xhis::gfp*.

5.3.2 Validation of a P_{spy} biosensor

Using truncations of P_{spy} it was previously shown that responses to various stressors are mediated by either BaeSR or CpxAR (Srivastava et al., 2014); it also highlighted the use of fusing GFP downstream of P_{spy} to monitor activity. Ethanol was chosen as a general stressor to evaluate activity of the P_{spy} biosensor and confirm it was working as intended. BL21 harbouring the sensor construct pBAD30Δ-P_{spy}-*6xhis::gfp* was aerated in 50 mL LB (Miller) + Amp in Erlenmeyer flasks at 37 °C, 200 rpm. At OD_{600} 0.4-0.6, the P_{spy} promoter was induced using 4 % (v/v) ethanol, a sub-lethal concentration that should stress cells. Growth continued till 24 h post-induction. Untreated controls were run in parallel; each condition was repeated in triplicate.

Accumulation of 6xHis::GFP due to stress from treatment with 4 % (v/v) ethanol was monitored by measuring mean green fluorescence using FCM (Figure 5.6A). After addition of ethanol, 6xHis::GFP expression massively increased. At 4 h post-induction, ethanol treated cultures reached a mean green fluorescence of 40000 AU; by 24 h post-induction this was around 100000 AU. Comparatively, uninduced cultures were mostly stable at around 1000 AU between 0 h and 4 h; at 24 h, mean green fluorescence increased slightly to ~4000 AU. This was still quite low; previously we have seen untransformed BL21 had a mean green fluorescence ~200 AU; uninduced BL21 transformed with a construct containing GFP regulated by a very tight urea promoter was ~800 AU (Chapter 3). Nevertheless, activity of P_{spy} increased over

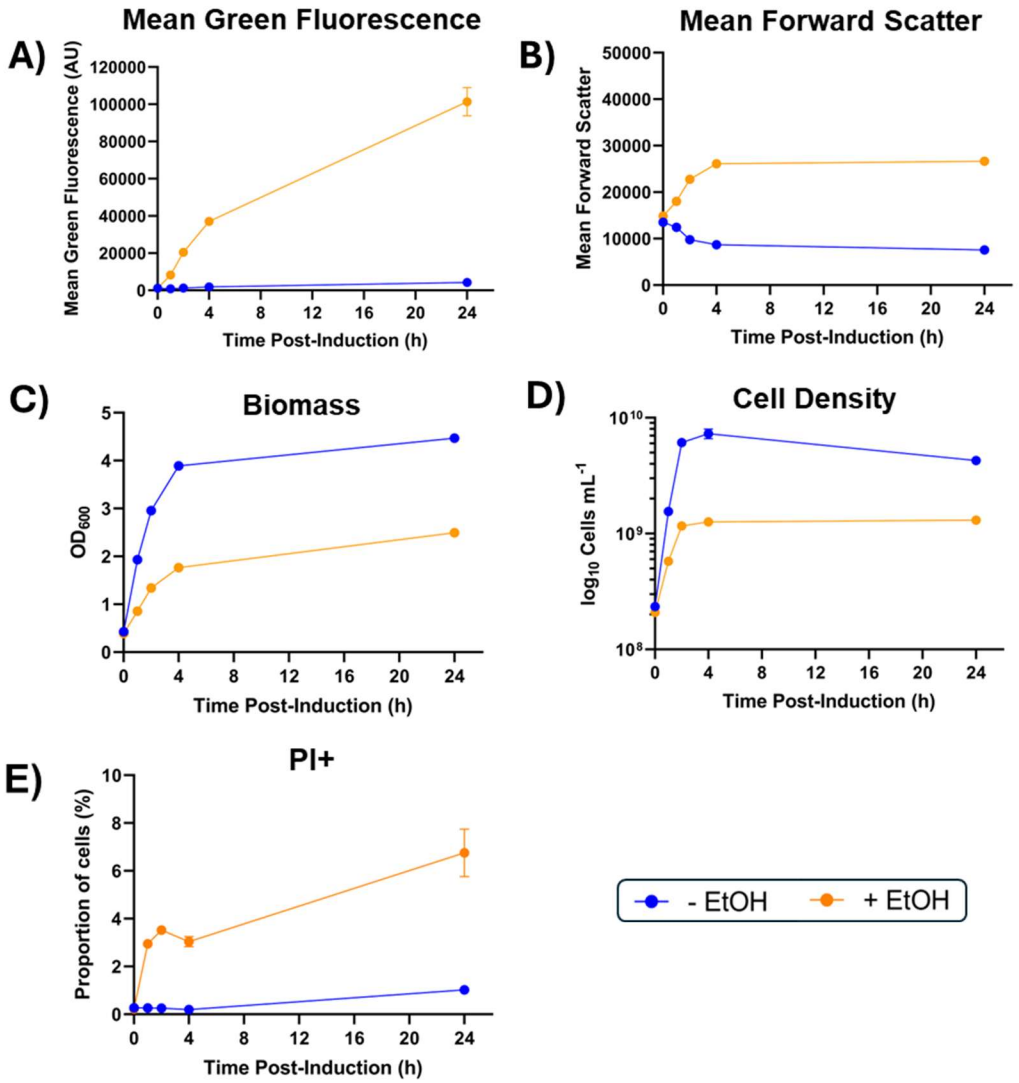


Figure 5.6: Analysis of the response of the P_{spy} sensor to ethanol treatment.

A P_{spy}-*gfp* sensor was constructed to report on periplasmic stress. BL21 harbouring the pBAD30Δ-P_{spy}-*gfp* construct were cultured at 37 °C, 200 rpm in 50 mL LB + Amp. At OD_{600} 0.4-0.6, cultures were treated (induced) with 4 (v/v) % ethanol (+ EtOH); untreated controls (- EtOH) were ran in parallel. Error bars represent +/- SD from biological duplicates.

(A) Mean green fluorescence was measured via FCM. After addition of ethanol mean green fluorescence increased massively reaching around 100000 AU at 24 h, a 25-fold increase over the untreated control indicating the sensor was switched on under envelope stress.

(B) Mean FSC was measured via FCM and increased massively in cultures treated with EtOH indicating cell size increased due to stress from envelope damage.

(C) OD_{600} and **(D)** cell density measured via FCM indicated biomass accumulation was impacted by addition of ethanol; there was a near 1 $\log_{10}$ difference in cells mL^{-1} observed between treated and untreated cultures.

(E) To assess viability, 4 μg mL^{-1} PI was used to stain cells. Using FCM, cells were gated using red fluorescence (FL3-A) and green fluorescence (FL2-A) density plots. Gates were created for viable and non-viable cells based on staining. Data is shown for stained cells residing within the PI+ gate. While biomass accumulation dropped in treated cultures, only 6 % of the culture were stained as non-viable (PI+).

time and this was expected as presumably BL21 was under more envelope stress during latter stages of growth, irrespective of ethanol treatment. However, overall, we observed a near 25-fold increase in expression of 6xHis::GFP in cultures treated with ethanol. The P_{spy} biosensor clearly functioned as intended in response to ethanol treatment; this increase in green fluorescence was significant when analysed by multiple t-tests at 1 – 24 h post-induction (adjusted p <0.000001 for all comparisons, values were log transformed to better meet assumption of normality). To check whether expression of 6xHis::GFP from P_{spy} was consistent throughout the culture, green fluorescence (FL2-A) of single cells was monitored using FCM (Figure 5.7A). Between induction and 4 h post-induction, cultures consisted of mostly a single population with regards to green fluorescence. In ethanol treated cultures, there were very small low green fluorescence populations present at 2 h, 4 h, with a larger one at 24 h post-induction. Particularly at 24 h, as is commonly encountered (Sevastsyanovich et al., 2009), these were assumed to be plasmid-free cells although this would need to be confirmed by replica plating. However, given cultures at 2 h and 4 h post-induction were mostly homogenous this was not done. Alternatively, it was possible that 6xHis::GFP expression was inactivated in some way due to additional stress imposed by ethanol treatment, though this would require confirmation by sequencing purified P_{spy} constructs.

Increased FSC and thus cell size would be indicative of stress so was monitored via FCM (Figure 5.6B). Predictably, mean FSC increased in ethanol treated cultures peaking just under 30000 AU at 4 h post-induction, remaining stable until 24 h. This was a near 3-fold increase in mean FSC over the untreated controls, which decreased

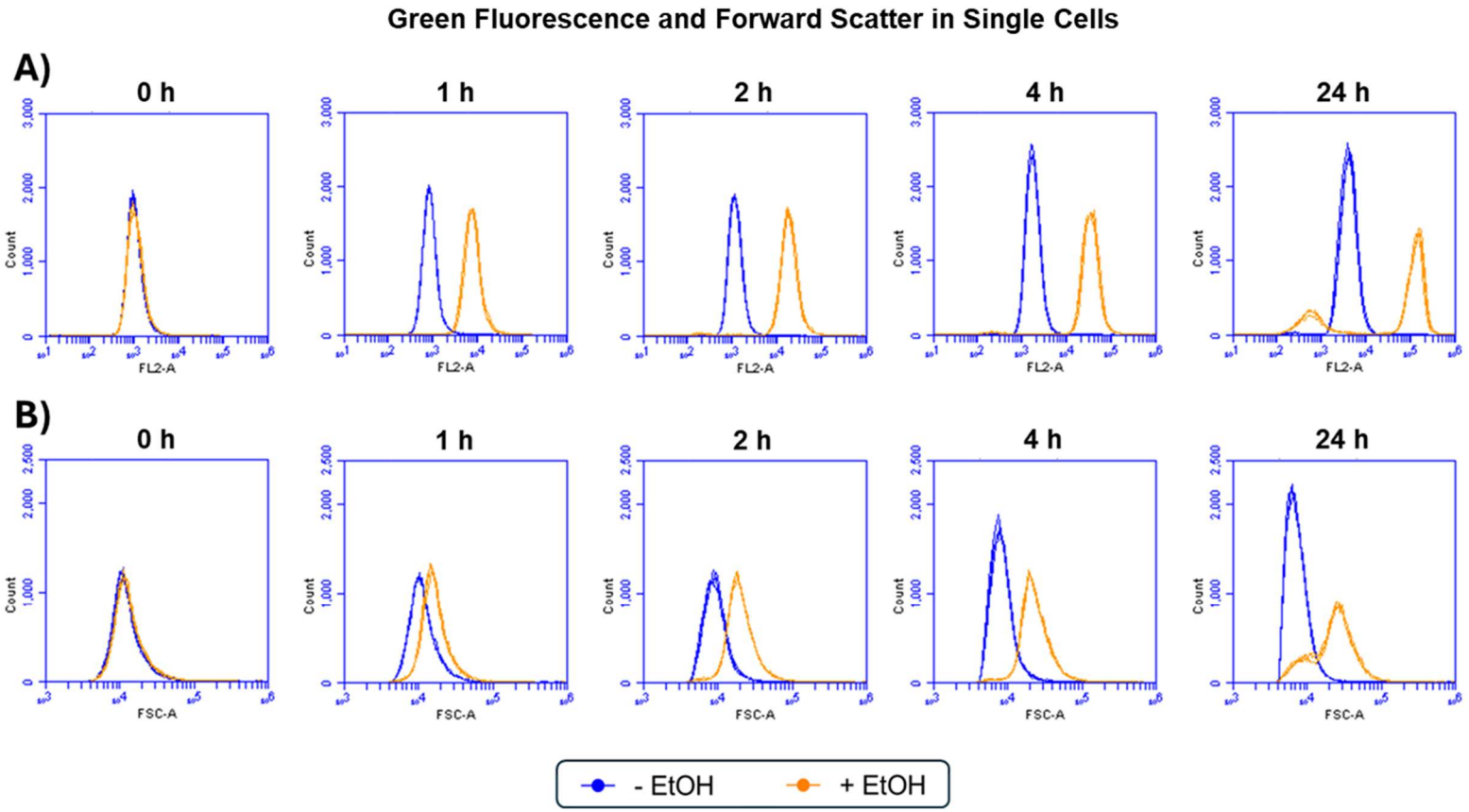


Figure 5.7: Single cell analysis of green fluorescence and forward scatter analysis in BL21 expressing the P_{spy} construct.

A P_{spy}-*gfp* sensor was constructed to report on periplasmic stress. BL21 harbouring the pBAD30Δ-P_{spy}-*gfp* construct were cultured at 37 °C, 200 rpm in 50 mL LB + Amp. At OD_{600} 0.4-0.6, cultures were treated (induced) with 4 (v/v) % ethanol (+ EtOH); untreated controls (- EtOH) were ran in parallel. Data shown for each condition is from biological triplicates.

Green fluorescence (FL2-A) **(A)** and forward scatter (FSC-A) **(B)** were used to monitor single cells via FCM; in all cultures a single populations were present between 0 h and 4 h, indicating any GFP expression from P_{spy} and the ethanol treatment were homogenous. At 24 h, a secondary population of cells with lower green fluorescence and FSC was present in ethanol treated cultures.

from 0 h to under 10000 AU until 24 h. Increased mean FSC for ethanol treated cultures was significant at 1 h – 24 h post-induction when analysed by multiple t-tests (adjusted $p < 0.0002$ for all comparisons). FSC was checked in single cells using FCM to confirm whether a subset, or the entire population of ethanol treated cells were larger (Figure 5.7). Between 1 h and 4 h, populations of both treated and untreated cultures were homogenous and normally distributed; thus, the ethanol treatment affected all cells in the culture and is presumably why green fluorescence at these time points was consistent. At 24 h post-induction, two populations of smaller and larger FSC were present in ethanol treated cultures; gating using FCM indicated the smaller-FSC population had lower green fluorescence (data not shown). Treated and untreated cultures were analysed using fluorescence and brightfield microscopy at 2 h and 4 h post-induction (Figures 5.8 – 5.9). Mean FSC was higher in ethanol treated cultures and indeed, cells in these generally appeared larger. Cells in untreated cultures were broadly around 1 – 3 µm in length; in treated cultures, some were larger at 4 – 5 µm with some as big as 16 µm.

Biomass accumulation (Figure 5.6C) and cell density (Figure 5.6D) were monitored via OD_{600} and FCM respectively. Predictably, in ethanol treated cultures, growth was inhibited; a near 1-$\log_{10}$ reduction in cell density was observed at 4 h post-induction. In untreated controls without ethanol treatment, cultures reached an OD_{600} of over 4.0 and the final cell density was just under $1x10^{10}$ cells mL^{-1}. PI staining was used as a measure of cell viability via membrane integrity; after staining cells, FCM was used to gate cells on red fluorescence (FL3-A) and green fluorescence (FL1-A) density plots. Gates were created for cells not stained by PI, indicating viability, and cells stained by

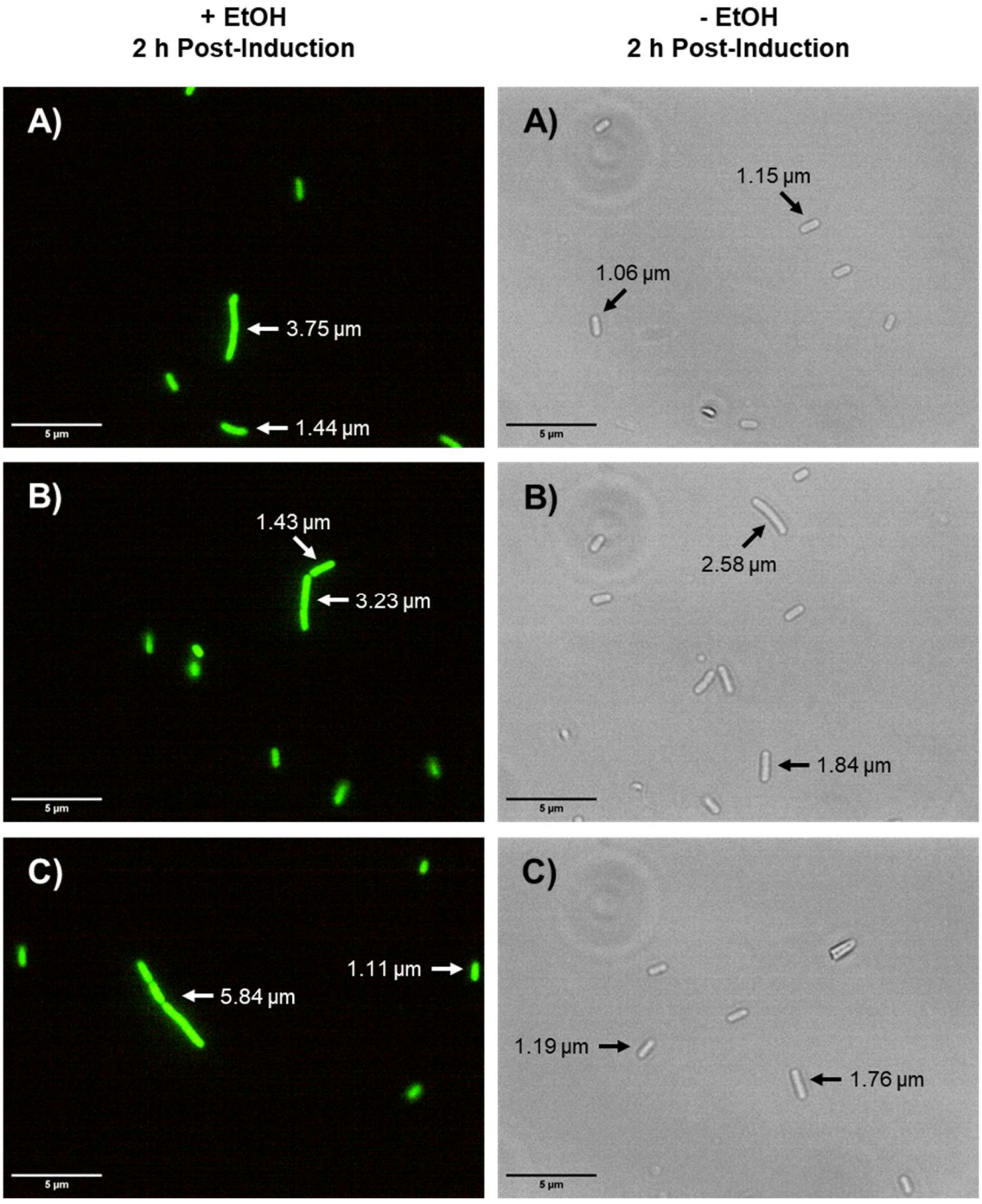


Figure 5.8: Microscopy analysis of BL21 expressing the P_{spy} construct at 2 h following ethanol treatment.

A P_{spy}-*gfp* sensor was constructed to report on periplasmic stress. BL21 harbouring the pBAD30Δ-P_{spy}-*gfp* construct were cultured at 37 °C, 200 rpm in 50 mL LB + Amp. At OD_{600} 0.4-0.6, cultures were treated (induced) with 4 (v/v) % ethanol (+ EtOH); untreated controls (- EtOH) were ran in parallel. Each image is from one biological replicate **(A, B, C)**.

To confirm ethanol treated cells had filamented, cells were imaged using fluorescence microscopy for + EtOH cultures and brightfield microscopy for - EtOH cultures. At 2 h post-induction, larger filamented cells were observed in + EtOH cultures compared with the untreated control. This was not homogenous throughout the culture though, with some cells being considerably larger than others.

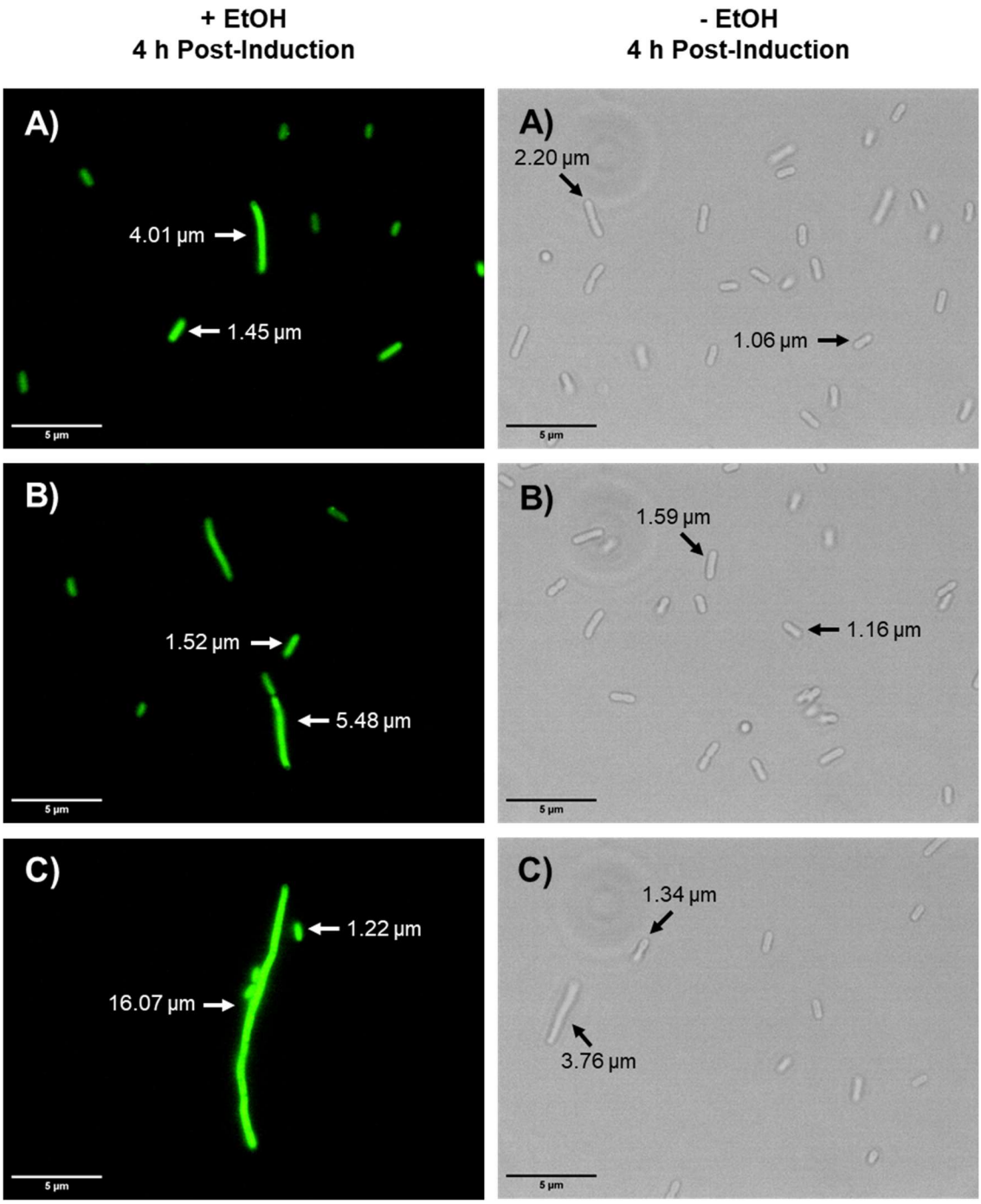


Figure 5.9: Microscopy analysis of BL21 expressing the P_{spy} construct at 4 h following ethanol treatment.

A P_{spy}-*gfp* sensor was constructed to report on periplasmic stress. BL21 harbouring the pBAD30Δ-P_{spy}-*gfp* construct were cultured at 37 °C, 200 rpm in 50 mL LB + Amp. At OD_{600} 0.4-0.6, cultures were treated (induced) with 4 (v/v) % ethanol (+ EtOH); untreated controls (- EtOH) were ran in parallel. Each image is from one biological replicate **(A, B, C)**.

To confirm ethanol treated cells had filamented, cells were imaged using fluorescence microscopy for + EtOH cultures and brightfield microscopy for - EtOH cultures. At 4 h post-induction, larger filamented cells were observed in + EtOH cultures compared with the untreated control. This was not homogenous throughout the culture though, with some cells being considerably larger than others.

PI, indicating non-viability. Data is shown for cells stained by PI (PI+) (Figure 5.6E). Even in ethanol treated cultures, the proportion of cells within the PI+ gate never increased above 8 %. In untreated cultures, the proportion of cells within the PI+ gate was only around 1 % throughout all 24 h of growth.

It is worth noting that plasmid free or empty vector controls would have been useful to further probe the effect of the P_{spy} sensor on BL21 physiology, and in any future analysis of P_{spy} response to chemical treatment, this would be a necessary step. However, given the biomass (Figure 5.6C) and cell density (Figure 5.6D) data aligned with what we have observed consistently for BL21 (see chapter 3 and 4) and supported by data from PI staining (Figure 5.6E) we assumed the presence of the P_{spy} sensor was not hugely detrimental to physiology.

5.3.3 Other stressors of a P_{spy} biosensor

The P_{spy} biosensor responded as expected to treatment of cells with sub-lethal concentrations of ethanol and the promoter has been proposed to respond to several envelope stressors via both stress response pathways regulating it (Hagenmaier et al., 1997, Garbe et al., 2000, Bury-Moné et al., 2009, Quan et al., 2011, He et al., 2021). We were curious whether the P_{spy} biosensor would respond to other stressors. Undergraduate project students in our lab demonstrated that P_{spy} was activated by growth at higher temperatures and EDTA although not urea (data not shown). We also measured P_{spy} activity in efflux pump mutants. Efflux pumps are ubiquitous in all cells, responsible for exporting noxious substances. The major efflux pump of *E. coli* is AcrAB-TolC, a member of the RND family of efflux pumps, with a broad substrate range

of endogenous and exogenous compounds including many antibiotics (Alav et al., 2021). Indeed, inactivation of AcrAB-TolC results in increased susceptibility to many antibiotics (Nikaido and Zgurskaya, 2001). Given that AcrAB-TolC pumps compounds from the periplasm to outside the cell, we predicted that efflux pump mutants would have increased periplasmic stress.

To test this, *E. coli* MG1655 and strains with deletions in *acrA* (encoding the periplasmic component of the AcrAB-TolC pump), *acrB* (the inner membrane component), and *tolC* (outer membrane component) were transformed with pBAD30Δ-P_{spy}-*6xhis::gfp*. A mutant *acrB*, D408A, in which the efflux pump can assemble but is nonfunctional (Wang-Kan et al., 2021) was also tested. Cultures were aerated in 50 mL LB (Miller) + Amp in Erlenmeyer flasks at 37 °C, 200 rpm. At OD_{600} 0.4-0.6, 200 µL of cultures were transferred to 96-well microtiter plates and treated with 0, 1 or 4 % (v/v) ethanol. The 96-well plate was incubated at 37 °C with orbital shaking in a plate reader for a further 24 h with OD_{600} and green fluorescence monitored at 15-minute intervals. Each strain and condition were repeated in quadruplet wells taken from the same culture.

None of the mutants had significant growth defects compared with WT MG1655 (Figure 5.10A); monitoring OD_{600} indicated all untreated cultures were comparable and in fact, Δ*acrA* and *acrB*^{D408A} strains grew slightly faster than WT. In treated cultures, Δ*tolC* and *acrB*^{D408A} strains exposed to 4 % (v/v) ethanol appeared to exhibit greatest growth arrest. During green fluorescence measurement (Figure 5.10B), the dynamic range of the plate reader meant that adjusting fluorescence gain to encompass all

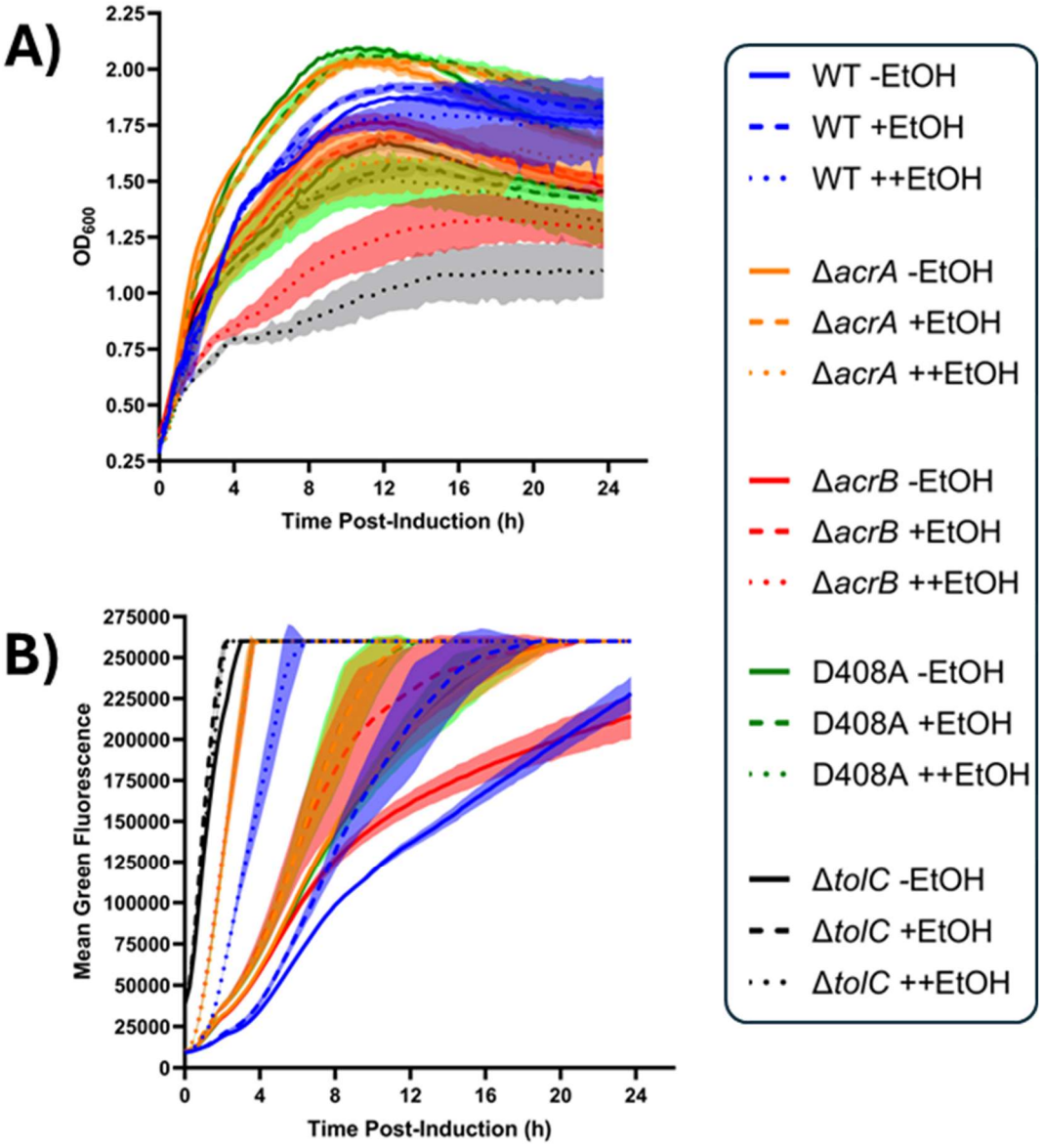


Figure 5.10: Analysis of the P_{spy} construct in MG1655 efflux mutants.

To see if other stressors induced P_{spy}, MG1655 derivatives were used with knockouts in components of AcrAB-TolC and an *acrB*^{D408A} strain which had a non-functional pump. MG1655 strains (1 culture each) were grown at 37 °C, 200 rpm in 50 mL LB + Amp. At OD_{600} 0.4-0.6, 200 µL of cultures were transferred to 96-well plates and treated with 0 % (- EtOH), 1 % (+ EtOH) or 4 % (++ EtOH) (v/v) ethanol. In the plate reader, cells were cultured at 37°C, with orbital shaking for a further 24 h. Each condition was repeated in quadruplet wells. Error envelopes represent +/- the SD from 4 technical repeats.

(A) OD_{600} was monitored throughout growth, the mean from quadruplet wells is provided. None of the untreated mutants had growth defects compared with the WT, although *ΔtolC* and D408A cultures exposed to 4 % EtOH experienced considerable growth arrest compared to others.

(B) Green fluorescence was monitored throughout growth, the mean from quadruplet wells is provided. The dynamic range of the plate reader meant that adjusting fluorescence gain to encompass all conditions with useful separation was difficult. While green fluorescence data must be interpreted with caution, we can infer that Δ*tolC* cultures regardless of EtOH treatment maxed green fluorescence much quicker than other efflux mutants assayed, indicating P_{spy} responds more strongly to stress associated with knockout of this gene. In untreated cultures, Δ*acrA* and D408A had a higher mean green fluorescence than Δ*acrB* or WT cultures.

conditions with useful separation was difficult. For example, adjustment of the gain to accurately measure green fluorescence of Δ*tolC* strains resulted in poor resolution for remaining strains. If a similar more focused experiment were to be done, application of FCM would be useful; due to smaller volumes and analysis at the single cell level, it has orders of magnitude greater range for fluorescence measurement. However, given this was just an exploratory experiment and the large number of conditions we wanted to analyse, it was determined use of a plate reader would be more appropriate initially.

Thus, while green fluorescence data from the plate reader must be interpreted with caution, we can draw some conclusions from the speed at which green fluorescence was maxed out (Figure 5.10B). In Δ*tolC* strains, even without ethanol treatment, GFP expression from P_{spy} rapidly increased and after 3 h, green fluorescence had reached the maximum the plate reader could detect based on gain settings. Ethanol further accelerated the increase in green fluorescence in Δ*tolC.* In untreated cultures, Δ*acrA* and *acrB*^{D408A} strains had a more rapid increase in mean green fluorescence than Δ*acrB* or WT variants; ethanol appeared to further increase green fluorescence in a dose-dependent manner.

Based on time taken to max green fluorescence (Figure 5.10B), Δ*tolC* seemed to switch on P_{spy} more so than other mutants and we wondered why this might be. In addition to its role in the AcrAB-TolC RND efflux pump (Alav et al., 2021), TolC is an OM component in efflux pumps (Zgurskaya et al., 2011) so presumably its loss has a greater effect on physiology than deletion of AcrA or AcrB for example. Further a Δ*tolC* mutant has been shown previously to switch on expression of P_{spy} (Rosner and Martin,

2013); this was suggested as being CpxA-dependent and due to the iron chelating compound enterobactin (Guest et al., 2019). As P_{spy} is regulated by CpxAR (in addition to BaeSR), this further supports what we observed (Figure 5.10) (Yamamoto and Ishihama, 2006, Yamamoto et al., 2008, Srivastava et al., 2014).

5.4 P_{spy} response to recombinant proteins and export stressors

Validation of the P_{spy} biosensor using sub-lethal concentrations of ethanol confirmed the construct was working as intended and responded to known periplasmic stressors. Our overall desire however was to utilise the sensor for detecting stress arising from overexpressing recombinant proteins in the periplasm and more specifically when export machinery was overloaded or impaired.

5.4.1 P_{spy} response to recombinant protein stressors

To test P_{spy} sensor response to recombinant proteins, pBAD30Δ-P_{spy}-*6xhis::gfp* was co-transformed in BL21, alongside PAR promoter plasmids pET-26b(+)-PAR1-*pelB*^{SP}::anti-*il-1β* scFv, pET-26b(+)-PAR4-*pelB*^{SP}::anti-*il-1β* scFv or pET-26b(+)-PAR7-*pelB*^{SP}::anti-*il-1β* scFv. When co-expressed with the SecM biosensor, overexpression of exported PelB^{SP}::anti-IL-1β scFv from PAR4 and PAR7 was shown to be extremely deleterious to growth (section 5.2.2). While some effect from the SecM biosensor could not be discounted, based on physiological analysis (Figure 5.3C-D and Figure 5.5), we attributed this more to the effect of overexpressing PelB^{SP}::anti-IL-1β scFv. Thus, we wanted to use these constructs to test the sensing capabilities of P_{spy} in response to overexpression of exported recombinant proteins. In two repeated experiments using the same conditions, BL21 was aerated in 50 mL TB + Amp + Kan in Erlenmeyer flasks

at 30 °C, 200 rpm. At OD_{600} 0.4-0.6, overexpression of $PelB^{SP}$::anti-IL-1β scFv was induced in duplicate cultures for each strain using 100 µM IPTG. Uninduced duplicate cultures for each strain were run in parallel as controls. Expression was allowed to proceed for a further 24 h.

Mean green fluorescence was monitored throughout growth using FCM and both replicate experiments were very similar (Figure 5.11A). In uninduced controls, mean green fluorescence was low throughout growth; between induction and 3 h post-induction it was under 1000 AU. At 24 h post-induction, mean green fluorescence had increased in uninduced cultures to around 1000 – 2000 AU, like observed during P_{spy} biosensor validation experiments (Figure 5.6A), presumably cells in stationary phase being under increased periplasmic stress. Crucially, when inducing cultures containing PAR4 or PAR7 constructs with IPTG, mean green fluorescence increased. At 3 h post-induction induced PAR4 and PAR7 cultures had a mean green fluorescence around 2000 – 3000 AU. Interestingly, mean green fluorescence continued to increase in induced PAR4 cultures to 5 h post-induction, reaching 6000 – 7000 AU; induced PAR7 cultures decreased slightly though, possibly being too stressed to even synthesise 6xHis::GFP. PAR1 cultures changed little irrespective of induction with IPTG; RP expression presumably not being high enough. Another consideration was green fluorescence at 24 h post-induction; we expected this to be lower due to plasmid loss, but in all cultures there was a level of green fluorescence comparable to induction. This suggested that the pBAD30Δ-P_{spy}-*6xhis::gfp* construct was still present and stable. Regardless, differences in mean green fluorescence between induced and uninduced cultures containing PAR4 or PAR7 were significant at 3 h and 5 h post-induction, when

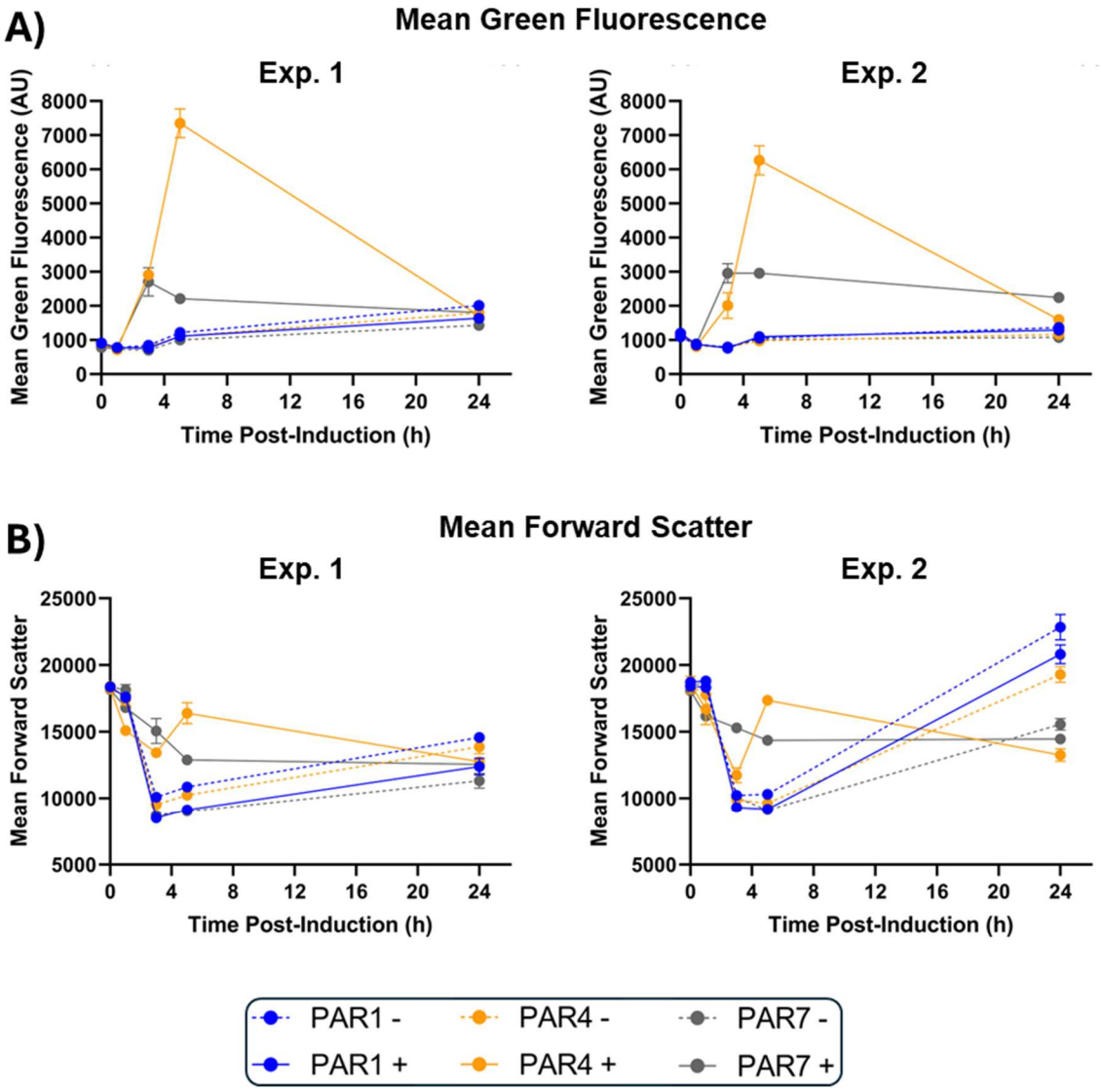


Figure 5.11: FCM analysis of the P_{spy} sensor response to expression of PelB^{SP}::anti-IL-1β scFv.

Response of the P_{spy}-*gfp* sensor to ethanol indicated general envelope stress switched it on. For use in feedback control during RPP, it should be activated by stressors associated with overexpression of exported proteins. To test this, BL21 harbouring the pBAD30Δ-P_{spy}-*gfp* construct and co-expressing PAR promoter plasmids driving expression of an exported scFv; pET-26b(+)-PAR1-*pelB*^{SP}::anti-*il-1β* scFv, pET-26b(+)-PAR4-*pelB*^{SP}::anti *il-1β* scFv, pET-26b(+)-PAR7-*pelB*^{SP}::anti *il-1β* scFv. PAR promoters are derivatives of P_{lac} with increasing strengths. Cultures were grown at 37 °C, 200 rpm in 50 mL TB + Amp + Kan. At OD_{600} 0.4-0.6, cultures were induced with 100 µM IPTG (+) and were compared with uninduced ones (-). For each condition, duplicate cultures were used. Data is provided for two repeat experiments (Exp.1 and Exp. 2). Error bars represent +/- SD from biological duplicates.

(A) Mean green fluorescence was monitored throughout growth using FCM. At 3 h post-induction, mean green fluorescence was elevated in PAR4+ and PAR7+ cultures; a 3-fold increase compared with PAR1+ or uninduced controls. At 5 h post-induction, mean green fluorescence in PAR4 cultures continued to increase, now approximately 7-fold higher than uninduced controls. This indicated high level overexpression of exported recombinant proteins switches on P_{spy}.

(B) Mean FSC was monitored using FCM and was elevated in PAR4+ and PAR7+ cultures at 3 h and 5 h post-induction. Based on green fluorescence measurements, this was largely consistent with the estimated time at which overexpression of the PelB^{SP}::anti-IL-1β scFv would've been highest.

analysed by two sample t-tests (adjusted $p < 0.03$ for all comparisons) indicating the sensor responded to periplasmic recombinant protein stressors.

While mean green fluorescence increased in response to induction of PelB^{SP}::anti-IL-1β scFv from PAR4 and PAR7 promoters, it was not clear whether upregulated expression of 6xHis::GFP from P_{spy} was consistent throughout the culture. Thus, in both replicate experiments, green fluorescence (FL2-A) was monitored in single cells using FCM (Figure 5.12). In PAR1 and uninduced PAR4 and PAR7 cultures, cells remained a single population of low green fluorescence. Induction of PAR4 and PAR7 cultures led to considerable heterogeneity at 3 h and 5 h post-induction; this correlated with the point at which mean green fluorescence was highest. Cells in induced PAR4 and PAR7 cultures had varying levels of 6xHis::GFP expression, at 3 h – 5 h post-induction (Figure 5.12); particularly for PAR7, 3 subpopulations with green fluorescence lower than, comparable to and higher than uninduced cultures. Thus, induction of PAR4 and PAR7 promoters did not switch on expression from P_{spy} homogenously. There were several potential reasons for this; firstly, we assumed this was, at least in part, due to the deleterious nature of overexpressing PelB^{SP}::anti-IL-1β scFv, in addition to trying to synthesise 6xHis::GFP from the P_{spy} construct.

While not an exact comparison, we know from other work with BL21 using comparable growth conditions (Chapter 3 and Chapter 4), green autofluorescence values for untransformed cells observed using the same BD Accuri C6 flow cytometer were around 10^2 on the FL2-A channel. As an example, for induced PAR7 cultures at 3 h post-induction (Figure 5.12), the mean fluorescence of the lowest green fluorescence

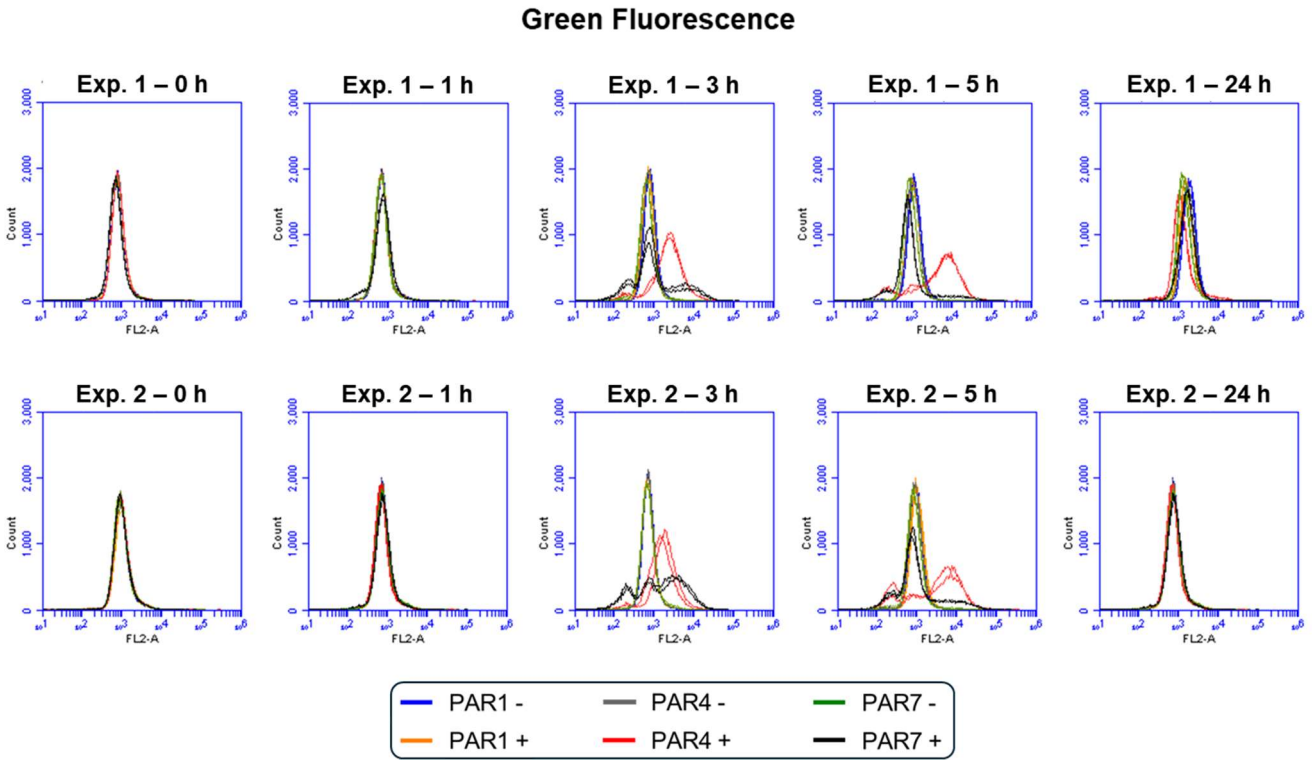


Figure 5.12: Green fluorescence analysis in single cells of the P_{spy} sensor response to expression of PelB^{SP}::anti-IL-1β scFv using FCM.

Response of the P_{spy}-*gfp* sensor to ethanol indicated general envelope stress switched it on. For use in feedback control during RPP, it should be activated by stressors associated with overexpression of exported proteins. To test this, BL21 harbouring the pBAD30Δ-P_{spy}-*gfp* construct and co-expressing PAR promoter plasmids driving expression of an exported scFv; pET-26b(+)-PAR1-*pelB*^{SP}::anti-*il-1β* scFv, pET-26b(+)-PAR4-*pelB*^{SP}::anti *il-1β* scFv, pET-26b(+)-PAR7-*pelB*^{SP}::anti *il-1β* scFv. PAR promoters are derivatives of P_{lac} with increasing strengths. Cultures were grown at 37 °C, 200 rpm in 50 mL TB + Amp + Kan. At OD_{600} 0.4-0.6, cultures were induced with 100 µM IPTG (+) and were compared with uninduced ones (-). Data is provided for two repeat experiments (Exp.1 and Exp. 2). Data for each condition is shown for biological duplicates.

To check homogenous expression of GFP from P_{spy} activated by overexpression of PelB^{SP}::anti-IL-1β, green fluorescence (FL2-A) was monitored at the single cell level using FCM. At 3 h and 5 h post-induction, multiple populations of cells were present in PAR4+ and PAR7+ cultures; a subset of cells experiencing enough stress from overexpression to activate P_{spy}. Interestingly, in PAR7+ cultures at 3 h and 5 h post-induction, populations with green fluorescence lower than in uninduced controls were apparent. Generally, this would've been indicative of untransformed cells, but this population was not apparent at 24 h post-induction.

peak was measured at 2.4×10^2. This would suggest that populations with green fluorescence around this level had either lost the P_{spy} sensor construct or 6xHis::GFP from it. We had assumed cultures would still be under selection with ampicillin (Amp) at 3 h post-induction, although β-lactamase leakage across the OM and into extracellular medium where it degrades ampicillin is known (Domingues et al., 2017). What is interesting is that at 24 h post-induction and across both repeat experiments, all cultures were single populations with green fluorescence (FL2-A) values at or over 10^3 (Figure 5.12); a level that is more consistent with the presence of 6xHis::GFP. Again, we assumed if plasmid free-cells were present, they would have a physiological advantage over transformed cells, and so at 24 h, more of the population would have green fluorescence (FL2-A) values around 10^2. It is possible that remaining transformed cells conferred protection through β-lactamase leakage (Domingues et al., 2017) whilst ampicillin was still present in the culture and any plasmid free cells were eventually lost from the culture during further growth between 3 h and 24 h post-induction. Replica plating would ideally have been used to probe this further, but as we had seen the P_{spy} sensor responded to induced PAR4 and PAR7 cultures (Figure 5.11A) we did not consider this critical to development of the system at this stage.

Mean FSC was also monitored via FCM throughout growth for both repeat experiments (Figure 5.11B), increased FSC and thus larger cells being known to occur under stress and high-level protein expression (see chapter 3) (Jeong and Lee, 2003). Compared with uninduced cultures, mean FSC was elevated in induced PAR4 and PAR7 cultures between 1 h and 5 h post-induction, when analysed by two sample t-tests this was significant (adjusted $p < 0.04$ for all comparisons). Timing of elevated FSC was

consistent with the observed point of maximum 6xHis::GFP expression, and therefore stress from overexpression of PelB^{SP}::anti-IL-1β scFv. In both experiments, induced PAR4 and PAR7 cultures had approximately 1.5 – 2-fold greater mean FSC at around 15000. At 24 h post-induction, uninduced and PAR1 cultures increased in mean FSC, whereas induced PAR1 and PAR4 cultures remained stable or decreased. To further monitor stress, biomass accumulation and cell density were monitored via OD_{600} and FCM respectively (Figure 5.13A-B). Growth arrest was apparent in induced PAR4 and PAR7 cultures; being a stronger promoter, this predictably occurred earlier for PAR7 at 3 h post-induction. Regardless, at 5 h post-induction, both induced PAR4 and PAR7 cultures had just under a 1-log drop in cells mL^{-1}; this correlated with the point at which maximum 6xHis::GFP expression was observed from P_{spy}. By 24 h post-induction all cultures reached close to $1x10^{10}$ cells mL^{-1}, again matching the point at which 6xHis::GFP expression appeared to decrease.

PI staining was used as a measure of cell viability via membrane integrity; after staining cells, FCM was used to gate cells on red fluorescence (FL3-A) and green fluorescence (FL1-A) density plots. Gates were created for cells not stained by PI, indicating viability, and cells stained by PI, indicating non-viability. Data is shown for cells stained by PI (PI+) (Figure 5.14) and cultures of PAR4 and PAR7 induced with IPTG had considerable levels of cells within the PI+ gate. Supporting OD_{600} and cell density data (Figure 5.13), this occurred earlier for PAR7 cultures in which over 20 % of cells were within the PI+ gate after just 1 h. By 3 h post-induction, over 40 % of cells in induced PAR7 cultures were within the PI+ gate, although this decreased back to around 20 % by 5 h post-induction. For induced PAR4 cultures over 40 % of cells were within the

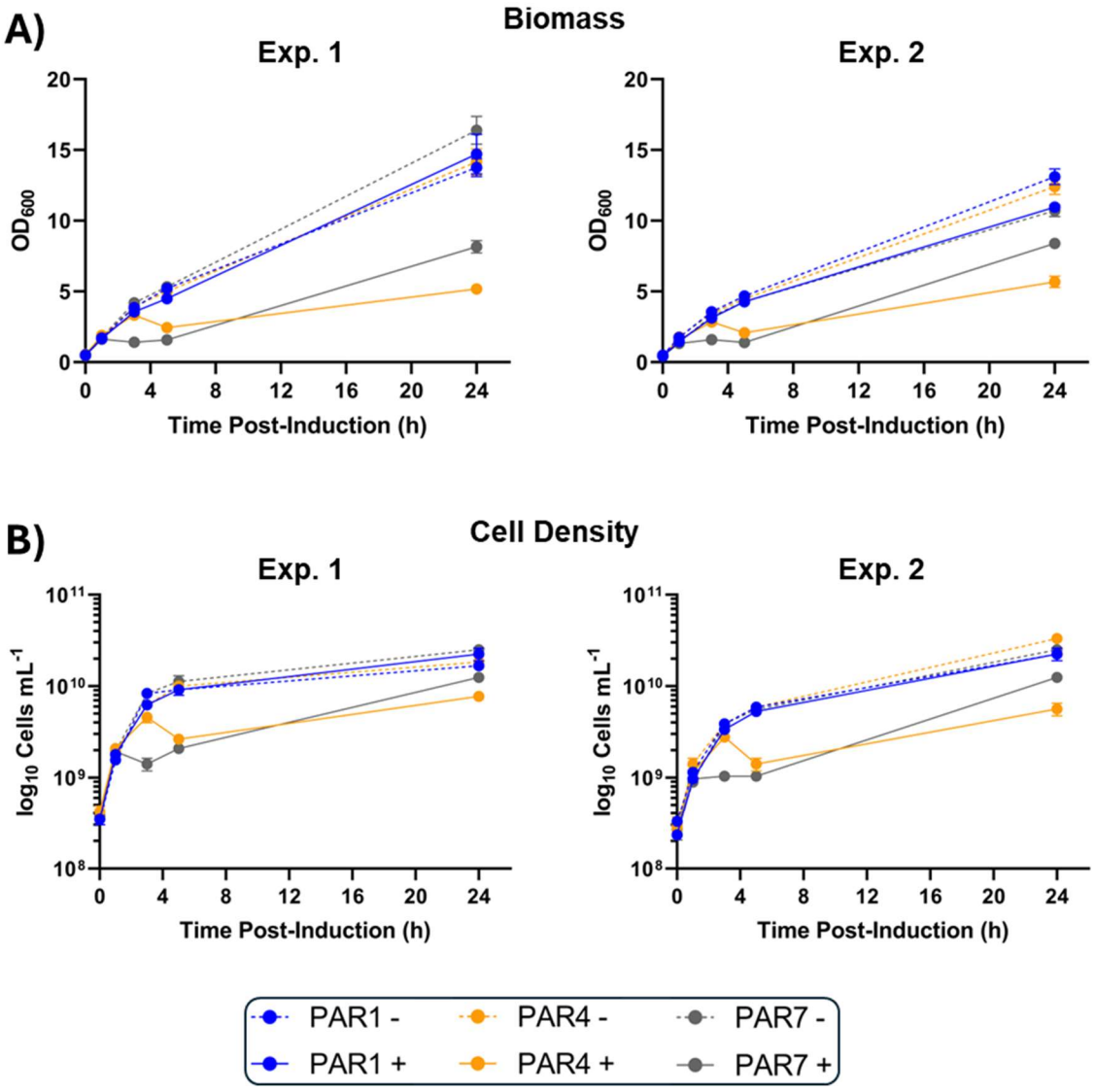


Figure 5.13: Growth data for BL21 harbouring the P_{spy} sensor and expressing PelB^{SP}::anti-IL-1β scFv.

Response of the P_{spy}-*gfp* sensor to ethanol indicated general envelope stress switched it on. For use in feedback control during RPP, it should be activated by stressors associated with overexpression of exported proteins. To test this, BL21 harbouring the pBAD30Δ-P_{spy}-*gfp* construct and co-expressing PAR promoter plasmids driving expression of an exported scFv; pET-26b(+)-PAR1-*pelB^{SP}*::anti-*il-1β* scFv, pET-26b(+)-PAR4-*pelB^{SP}*::anti *il-1β* scFv, pET-26b(+)-PAR7-*pelB^{SP}*::anti *il-1β* scFv. PAR promoters are derivatives of P_{lac} with increasing strengths. Cultures were grown at 37 °C, 200 rpm in 50 mL TB + Amp + Kan. At OD_{600} 0.4-0.6, cultures were induced with 100 µM IPTG (+) and were compared with uninduced ones (-). For each condition, duplicate cultures were used. Data is provided for two repeat experiments (Exp.1 and Exp. 2). Error bars represent +/- SD from biological duplicates.

(A) Biomass accumulation was monitored throughout growth via OD_{600}. PAR4+ and PAR7+ cultures experienced growth arrest at 5 h and 3 h post-induction respectively. We assumed this arrest was delayed in PAR4+ cultures due to the weaker promoter driving lower expression of the PelB^{SP}::anti-IL-1β scFv.

(B) Cell density was monitored throughout via FCM. Analysis supported OD_{600} data; PAR4+ and PAR7+ cultures experienced growth arrest at 5 h and 3 h post-induction respectively. Although by 24 h post-induction these cultures somewhat recovered and saturated at just under $1x10^{10}$ cells mL^{-1}.

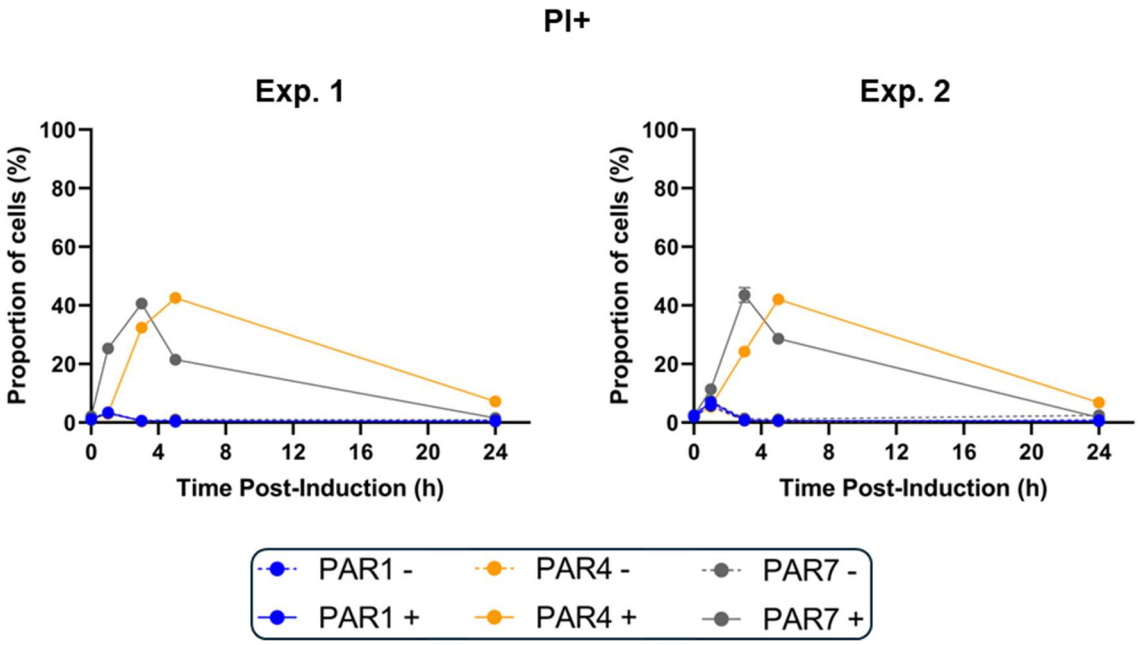


Figure 5.14: PI staining data for BL21 harbouring the P_{spy} sensor and expressing PelB^{SP}::anti-IL-1β scFv.

Response of the P_{spy}-*gfp* sensor to ethanol indicated general envelope stress switched it on. For use in feedback control during RPP, it should be activated by stressors associated with overexpression of exported proteins. To test this, BL21 harbouring the pBAD30Δ-P_{spy}-*gfp* construct and co-expressing PAR promoter plasmids driving expression of an exported scFv; pET-26b(+)-PAR1-*pelB^{SP}*::anti-*il-1β* scFv, pET-26b(+)-PAR4-*pelB^{SP}*::anti *il-1β* scFv, pET-26b(+)-PAR7-*pelB^{SP}*::anti *il-1β* scFv. PAR promoters are derivatives of P_{lac} with increasing strengths. Cultures were grown at 37 °C, 200 rpm in 50 mL TB + Amp + Kan. At OD_{600} 0.4-0.6, cultures were induced with 100 µM IPTG (+) and were compared with uninduced ones (-). For each condition, duplicate cultures were used. Data is provided for two repeat experiments (Exp.1 and Exp. 2). Error bars represent +/- SD from biological duplicates.

To assess viability, 4 µg mL^{-1} PI was used to stain cells. Using FCM, cells were gated using red fluorescence (FL3-A) and green fluorescence (FL2-A) density plots. Gates were created for viable and non-viable cells based on staining. Data is shown for stained cells residing within the PI+ gate. In PAR4+ and PAR7+ cultures, considerable around 40 % of cells were within the PI+ gate by 5 h and 3 h post-induction respectively. This could have been delayed in PAR4+ cultures due to the weaker promoter driving lower expression of the PelB^{SP}::anti-IL-1β scFv.

PI+ gate by 5 h post-induction. Taken together with OD_{600} and cell density data (Figure 5.14), this highlights the fact that even PAR4 was strong enough to put the BL21 host under considerable physiological burden when expressing $PelB^{SP}$::anti-IL-1β scFv. Predictably, PAR1 and uninduced PAR4 and PAR7 cultures had almost no cells within the PI+ gate throughout growth.

5.4.2 P_{spy} response to export stressors

Several SecA inhibitors exist, sodium azide perhaps being the best-known (Oliver et al., 1990); although, it is also a potent inhibitor of other ATPases including mammalian variants so we were reticent to use it (Noumi et al., 1987, Bowler et al., 2006). Rose Bengal (RB) is a xanthene dye which has been shown to inhibit SecA at sub-micromolar concentrations (Hsieh et al., 2014), although being non-permeant required permeabilization of the OM using polymyxin B nonapeptide (PMBN) (Jin et al., 2016). We hypothesised that sub-MIC concentrations of RB could be used alongside PMBN to inhibit SecA without cell death, mimicking saturation of translocation machinery and observing the response of the P_{spy} sensor. To test this, BL21 harbouring pBAD30Δ-P_{spy}-*6xhis::gfp* was aerated in 50 mL LB + Amp in Erlenmeyer flasks at 37 °C, 200 rpm. At OD_{600} 0.4-0.6, RB and PMBN were added. RB was used at concentrations of 1.59 and 7.95 μg mL^{-1}, equivalent to 1/10 and 1/2 MIC, supplemented with 25 μg mL^{-1} PMBN (Jin et al., 2016). Controls of 7.95 μg mL^{-1} RB and 25 μg mL^{-1} PMBN were used. Untreated cultures were run as additional controls. Growth was allowed to proceed for until 24 h post-induction. Each condition was repeated in duplicate cultures.

Mean green fluorescence was monitored throughout growth using FCM (Figure 5.15A) and increased rapidly in cultures treated with ½ MIC RB + PMBN, reaching around 12000 AU at 1 h post-induction, a greater than 10-fold change over the untreated control. Even treatment with just 1/10 MIC RB + PMBN appeared to upregulate P_{spy}, mean green fluorescence increasing to around 2500 AU, approximately 2.5-fold greater than the untreated control. Speed of the response was notable; production of recombinant anti-IL-1β scFv had taken around 3 – 5 h to induce P_{spy} to similar levels (Figure 5.11A). We assumed RB + PMBN was more fast-acting as there was no requirement by the cell to overexpress a recombinant protein. Crucially, RB and PMBN in isolation had little effect on green fluorescence (Figure 5.15A). Expression of 6xHis::GFP was further checked in single cells using FCM (Figure 5.15C). In all cultures, green fluorescence (FL2-A) appeared to be mostly homogenous between induction and 5 h post-induction. At 24 h post-induction, there was a small population of low green fluorescence present in all cultures, but we attributed this to loss of the P_{spy} sensor construct.

Previously mean FSC monitored via FCM was shown to be elevated in response to high level expression of recombinant proteins (Figure 5.11B) but treatment with RB + PMBN had little effect (Figure 5.15B). There was a slight elevation in mean FSC for cultures treated with 1/2 MIC RB + PMBN although overlap between error bars (+/- SD) was present. Further, biomass accumulation (Figure 5.16A) and cell density (Figure 5.16B) were also monitored via OD_{600} and FCM respectively. Similarly to FSC, growth of cultures treated with 1/2 MIC RB + PMBN appeared lower but not hugely different from the untreated control.

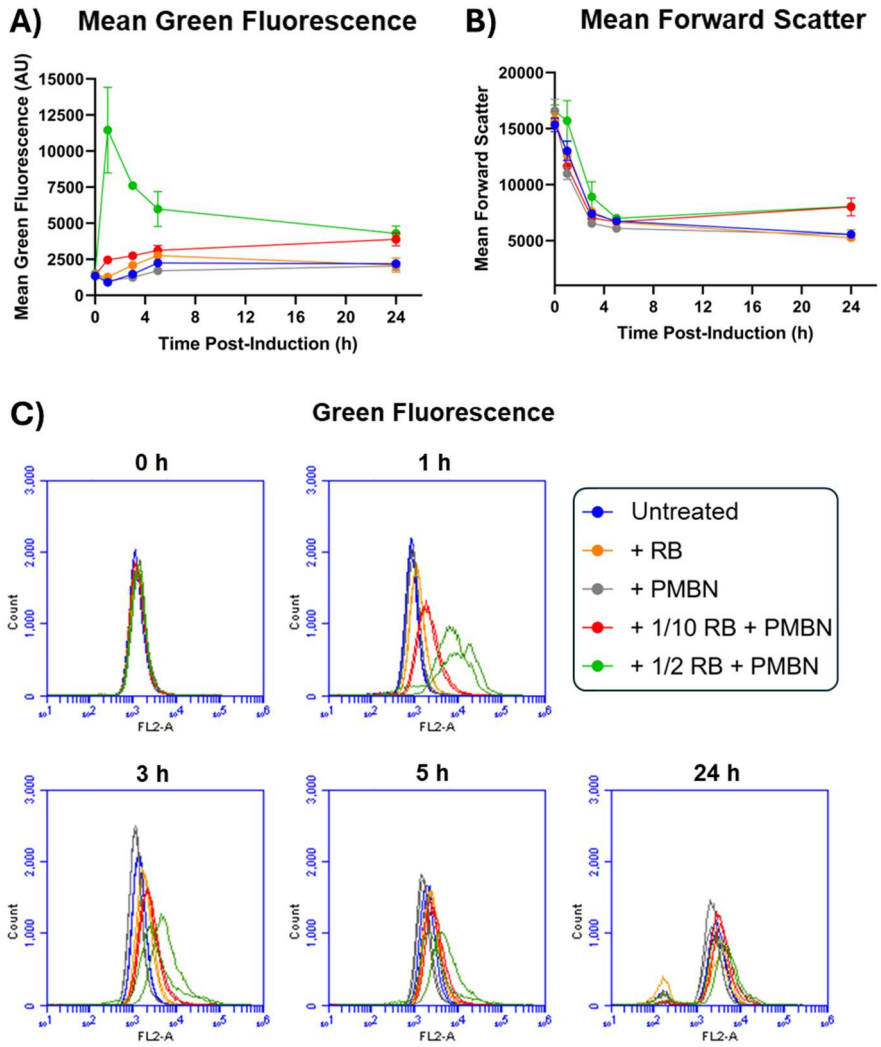


Figure 5.15: FCM analysis of the P_{spy} sensors response to treatment of BL21 with Rose Bengal.

The response of P_{spy} to Rose Bengal (RB), a potent SecA inhibitor was investigated. RB requires permeabilization with polymyxin B nonapeptide (PMBN) to enter cells. BL21 harbouring the pBAD30Δ-P_{spy}-*gfp* construct were grown at 37 °C, 200 rpm in 50 mL LB + Amp. At OD_{600} 0.4-0.6, cultures were treated with combinations of RB and PMBN. RB was used at 1/10 (1.59 µg mL^{-1}) and 1/2 (7.95 µg mL^{-1}) MIC concentrations, the RB only control was used at 1/2 MIC concentration (7.95 µg mL^{-1}), PMBN concentration was kept constant (25 µg mL^{-1}). An untreated control was used in parallel. Following addition, cultures were grown for a further 24 h. For each condition, duplicate cultures were used.

(A) Mean green fluorescence was monitored using FCM. Treatment of BL21 with 1/2 MIC RB + PMBN resulted in an increase in mean green fluorescence. Even treatment with 1/10 MIC RB produced a slight increase in mean green fluorescence at 1 h post-induction. Mean green fluorescence was low in RB and PMBN control cultures indicating the P_{spy}-*gfp* sensor responds specifically to inhibition of the Sec export machinery. Error bars represent +/- SD from biological duplicates.

(B) Mean FSC was monitored throughout using FCM, but little difference was observed between conditions. Error bars represent +/- SD from biological duplicates.

(C) To check the response to RB was consistent throughout the population, green fluorescence (FL2-A) was monitored in single cells using FCM. Between induction and 5 h post-induction, cultures appeared to be a single population for all conditions. At 24 h post-induction, secondary low green fluorescence populations were observed in all cultures indicating plasmid loss. Data for each condition is shown for duplicate cultures.

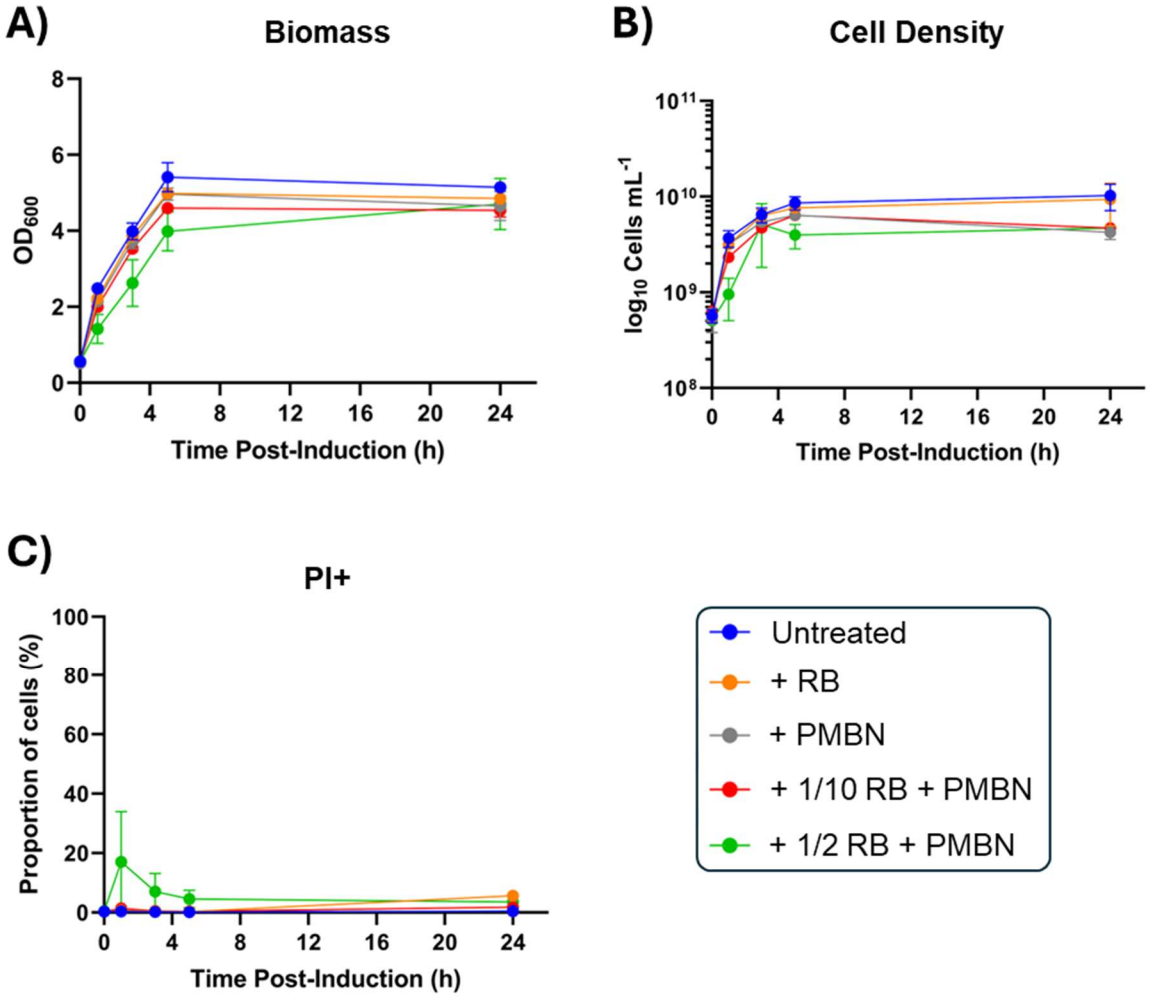


Figure 5.16: Analysis of BL21 physiology in response to treatment with Rose Bengal.

The response of P_{spy} to Rose Bengal (RB), a potent SecA inhibitor was investigated. RB requires permeabilization with polymyxin B nonapeptide (PMBN) to enter cells. BL21 harbouring the pBAD30Δ-P_{spy}-*gfp* construct were grown at 37 °C, 200 rpm in 50 mL LB + Amp. At OD_{600} 0.4-0.6, cultures were treated with combinations of RB and PMBN. RB was used at 1/10 (1.59 µg mL^{-1}) and 1/2 (7.95 µg mL^{-1}) MIC concentrations, the RB only control was used at 1/2 MIC concentration (7.95 µg mL^{-1}), PMBN concentration was kept constant (25 µg mL^{-1}). An untreated control was used in parallel. Following addition, cultures were grown for a further 24 h. For each condition, duplicate cultures were used. Error bars represent +/- SD from biological duplicates.

(A) Biomass accumulation and **(B)** cell density were monitored throughout via OD_{600} and FCM respectively. Biomass accumulation and cell density were minimally impacted at 1/2 MIC RB + PMBN.

(C) To assess viability, 4 µg mL^{-1} PI was used to stain cells. Using FCM, cells were gated using red fluorescence (FL3-A) and green fluorescence (FL2-A) density plots. Gates were created for viable and non-viable cells based on staining. Data is shown for stained cells residing within the PI+ gate. Cultures treated with 1/2 MIC RB + PMBN had around 20 % of cells within the PI+ gate by 1 h post-induction.

PI staining was used as a measure of cell viability via membrane integrity; after staining cells, FCM was used to gate cells on red fluorescence (FL3-A) and green fluorescence (FL1-A) density plots. Gates were created for cells not stained by PI, indicating viability, and cells stained by PI, indicating non-viability. Data is shown for cells stained by PI (PI+) (Figure 5.16C). Cultures treated with 1/2 MIC RB + PMBN had around 17 % of cells within the PI+ gate at 1 h, although this decreased to under 5 % by 5 h post-induction, mirroring the data observed for green fluorescence (Figure 5.15A). Overall, this indicated treatment of BL21 with 1/2 MIC RB + PMBN induced 6xHis::GFP expression from P_{spy} suggesting it responded to inhibition of Sec-dependent export. Based on OD_{600}, cell density and PI staining data (Figure 5.16), it appeared treatment of BL21 with 1/2 MIC RB + PMBN affected host physiology less than when P_{spy} was assayed using recombinant protein stressors (Figure 5.13 and 5.14). It is possible this was because treatment with 1/2 MIC RB + PMBN was more targeted (SecA inhibition) and was used at sub inhibitory concentrations by design. Conversely, overexpression of recombinant proteins can produce a multitude of negative effects to host physiology (Hoffmann and Rinas, 2004, Schlegel et al., 2013, Baumgarten et al., 2018, Guleria et al., 2020).

5.5 Designing a negative feedback system

Response of the P_{spy} sensor construct to stress induced by overexpression of exported $PelB^{SP}$::anti-IL-1β scFv and more targeted inhibition of translocation using RB + PMBN was evidence that it could be exploited as part of a feedback system to regulate expression during periplasmic RPP. A feedback construct containing P_{spy} driving expression of a repressor would be used to regulate an expression plasmid (Figure

5.17A). Prevalence of *lac* regulated T7 systems meant the *lac* repressor would be a simple option, although a ligand unresponsive (LU) variant would be required to prevent immediate de-repression due to the presence of IPTG. To prevent permanent repression, and to allow cycling of expression levels, LacI LU would need a degradation tag (DT) attached to reduce its half-life.

Using BL21(DE3) and T7*lac* driving expression of an exported recombinant protein as an example, the following was envisioned. During high level synthesis of an exported recombinant protein, saturation of the Sec translocation machinery would occur triggering P_{spy} expression of LacI LU-DT. Effects of this would be pleiotropic; feedback to the chromosomal lacUV5 promoter would prevent expression of T7 RNA polymerase, limiting expression from T7*lac* (Figure 5.17B); the expression plasmid would also be targeted, shutting down transcription of the gene encoding the recombinant protein (Figure 5.17C). Reduced expression strength should reduce RP synthesis and thus reduce Sec saturation, which in turn would reduce expression of LacI LU-DT from P_{spy}. Reduced stress would mean expression could be ramped up again, facilitated by continual degradation of LacI LU-DT.

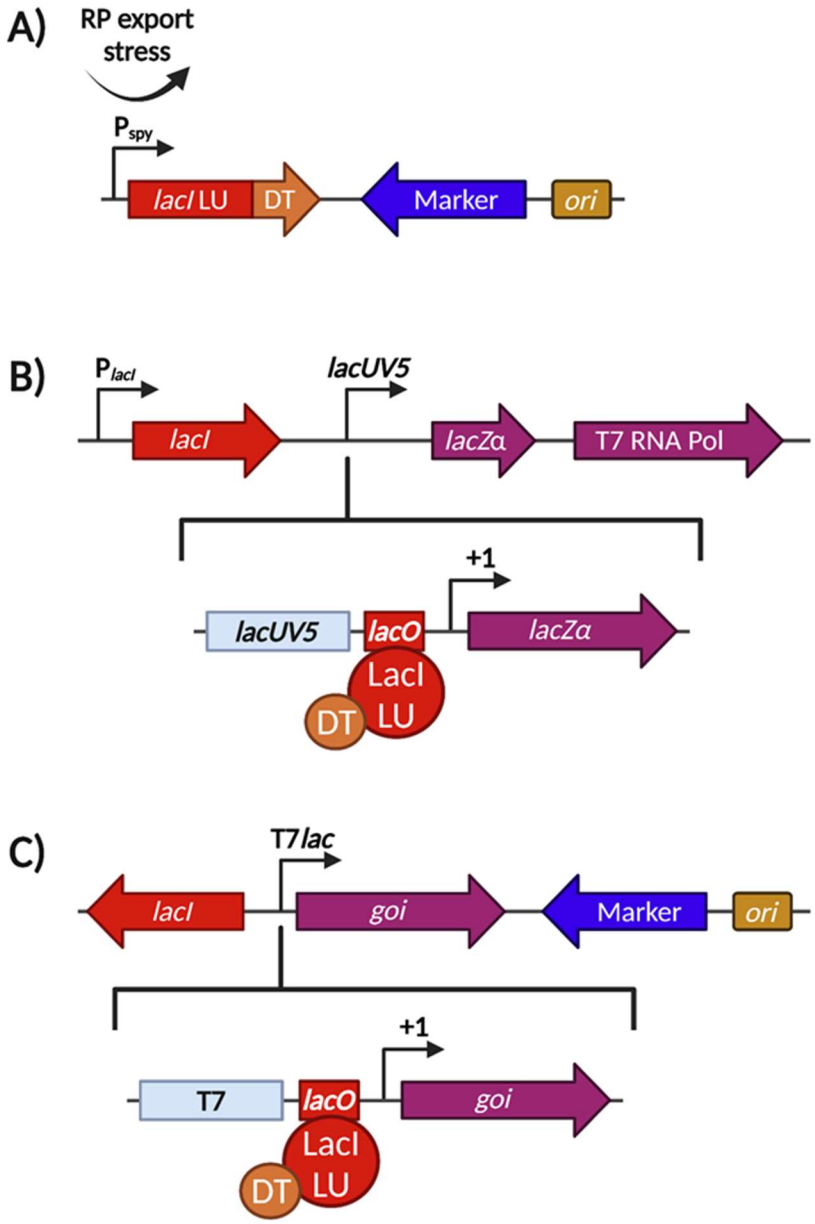


Figure 5.17: Application of the P_{spy} sensor for construction of a feedback loop.

It was decided the P_{spy} sensor could be used as a trigger for a novel feedback system to regulate expression of a periplasmic recombinant protein. An overview of how we theorised implementing such a system is provided.

(A) The feedback construct would have P_{spy} driving expression of a ligand unresponsive (LU) derivative of LacI which remains bound to *lac* operator sequences even in the presence of IPTG. A degradation tag (DT) would facilitate cycling of the feedback system between off and on states, preventing LacI LU from remaining permanently bound once stress had reduced.

(B) LacI was selected as the repressor for the system as *lac* regulated T7 promoters are widely used for RPP in *E. coli*. In the strain BL21(DE3), the IPTG inducible promoter *lacUV5* controls expression of a chromosomal copy of T7 RNA polymerase required to transcribe from the T7 promoter. Stress from periplasmic RPP would trigger expression of LacI LU-DT from P_{spy} and it would bind the operator preventing synthesis of T7 RNA polymerase.

(C) In systems using a T7*lac* promoter, LacI LU-DT would additionally bind *lac* operator sequences on the expression construct, directly preventing expression of the gene of interest (*goi*).

5.6 Ligand Unresponsive LacI

The feedback system required a ligand unresponsive (LU) variant of LacI to regulate expression of a recombinant protein in response to stress. Several mutations in LacI prevent interaction with inducing sugars without disrupting operator binding. Two mutants were chosen, $LacI^{R197G}$ (Spotts et al., 1991) and $LacI^{T276F}$ (Suckow et al., 1996) and the genes encoding them inserted downstream of P_{araBAD} on a pBAD30 backbone. L-arabinose inducible control of LacI LU would permit repression control over an IPTG inducible GFP driven by T7*lac*, and expression monitored using FCM. WT LacI would provide a suitable control.

5.6.1 Evaluating $LacI^{R197G}$ and $LacI^{T276F}$

To test LacI LU, BL21(DE3) harbouring pBAD30-*lacI*^{R197G}, pBAD30-*lacI*^{T276F} or pBAD30-*lacI* and co-transformed with pET-26b(+)Δ-ATG-*msfgfp* (expresses cytoplasmic msfGFP from T7*lac*) was grown in 50 mL LB + Amp + Kan in Erlenmeyer flasks at 37 °C, 200 rpm. At OD_{600} 0.4-0.6, expression of LacI variants and msfGFP were induced with combinations of 0.2 % (w/v) L-arabinose and 100 µM IPTG with expression proceeding until 24 h post-induction. Variants of ligand unresponsive LacI were assayed in separate experiments with their own controls. Conditions were repeated in duplicate cultures.

Mean green fluorescence was monitored throughout growth using FCM (Figure 5.18A). Predictably in cultures induced with only IPTG, mean green fluorescence increased rapidly, reaching nearly 100000 AU by 5 h post-induction. Likewise, in cultures only induced with L-arabinose, mean green fluorescence was low throughout growth,

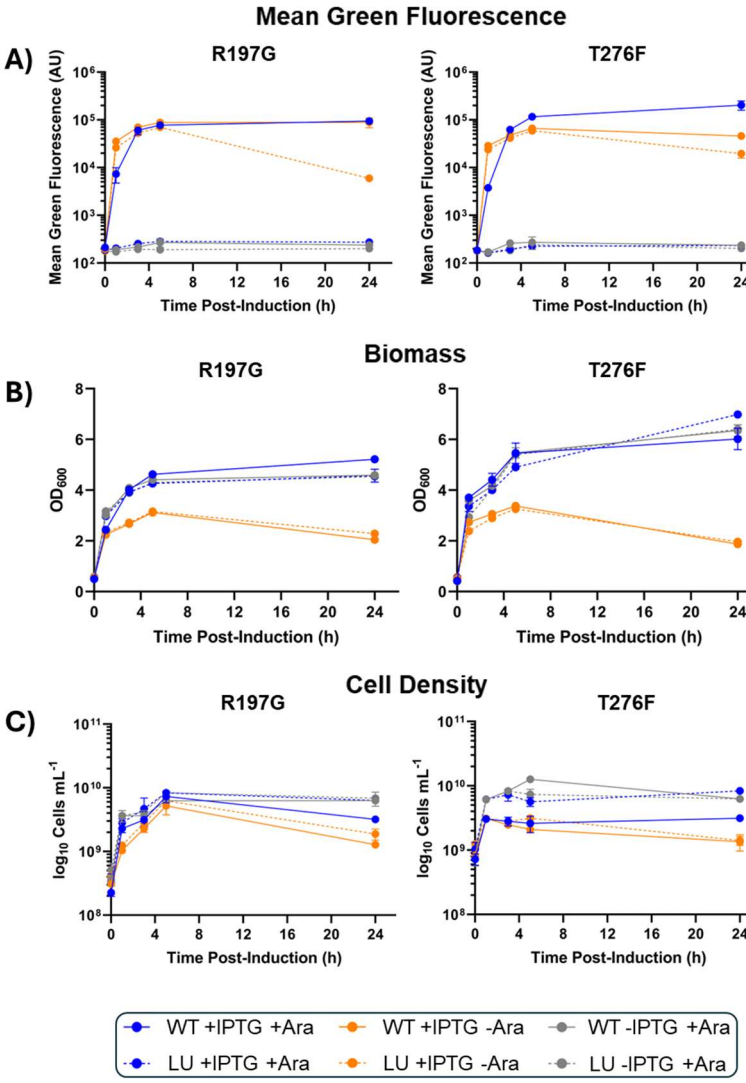


Figure 5.18: Analysis of ligand unresponsive LacI expression.

The feedback system required a ligand unresponsive (LU) variant of LacI to regulate expression of a recombinant protein in response to stress. Mutants LacI^{R197G} and LacI^{T276F} were chosen with WT LacI used as a control. In BL21(DE3) pBAD30-lacI^{R197G}, pBAD30-lacI^{T276F} or pBAD30-lacI were co-expressed alongside a T7*lac*-msfGFP construct. BL21(DE3) was cultured at 37°C, 200 rpm in LB + Amp + Kan. At OD_{600} 0.4-0.6, LacI or Lac LU variants were induced using 0.2 % (w/v) L-arabinose and msfGFP expression induced with 100 µM IPTG. Combinations (+/-) of 0.2 % (w/v) L-arabinose and 100 µM IPTG were used as controls. Each condition was repeated in duplicate cultures. Error bars represent +/- SD from biological duplicates.

(A) Mean green fluorescence was monitored throughout using FCM. Both LacI^{R197G} and LacI^{T276F}, were able to shut off expression of msfGFP in the presence of IPTG, and mean green fluorescence was comparable to controls without IPTG added. In cultures using WT LacI and inducing with IPTG and L-arabinose, mean green fluorescence and thus msfGFP expression was comparable with conditions where L-arabinose was not added. Data is shown as $\log_{10}$ mean green fluorescence.

(B) Biomass accumulation was monitored via OD_{600} throughout and both WT and LU cultures induced with IPTG but not L-arabinose appeared to some growth arrest beginning at 3 h post-induction.

(C) Cell density was monitored via FCM throughout. Based on OD_{600}, it was expected that WT and LU cultures induced with IPTG but not L-arabinose would have lower cell density, but this was not too dissimilar from other cultures.

remaining stable at around 200 AU. When inducing with IPTG and L-arabinose, mean green fluorescence also increased in cultures co-expressing WT LacI, reaching around 100000 AU by 5 h post-induction. However, in cultures co-expressing $LacI^{R197G}$ or $LacI^{T276F}$, mean green fluorescence remained extremely low at around 200 AU, comparable to cultures without IPTG. When analysed by two-sample t-tests, the difference in mean green fluorescence between WT LacI and $LacI^{R197G}$ or $LacI^{T276F}$ cultures induced with IPTG and L-arabinose was significant (adjusted $p < 0.05$ for all comparisons). At the single cell level, mean green fluorescence (FL2-A) measured via FCM was mostly homogenous (Figure 5.19). In cultures induced with only IPTG, or in cultures containing WT LacI induced with IPTG and L-arabinose, there were small populations with low green fluorescence. These populations were largest at 24 h post-induction and more notable in cultures only induced with IPTG, suggesting co-expression of WT LacI tuned expression from T7*lac* to be more amenable to the host.

Biomass accumulation was monitored via OD_{600} (Figure 5.18B). High level expression of msfGFP from T7*lac* meant cultures induced with only IPTG had impaired growth rates; in both experiments OD_{600} reached a maximum point of around 3.0 at 5 h post-induction. Importantly, induction of cultures expressing $LacI^{R197G}$ or $LacI^{T276F}$ with IPTG and L-arabinose had little negative effect on OD_{600} compared with other controls. Cell density was also monitored via FCM (Figure 5.18C); cultures only induced with IPTG were lower but still reached above $1x10^9$ cells mL^{-1} after 24h. Importantly, for cultures expressing $LacI^{R197G}$ or $LacI^{T276F}$ induced with IPTG and L-arabinose, cell density approached $1x10^{10}$ cells mL^{-1} at 5 h post-induction, suggesting mutant LacI had no aberrant effects on the host. PI staining was used as a measure of cell viability via

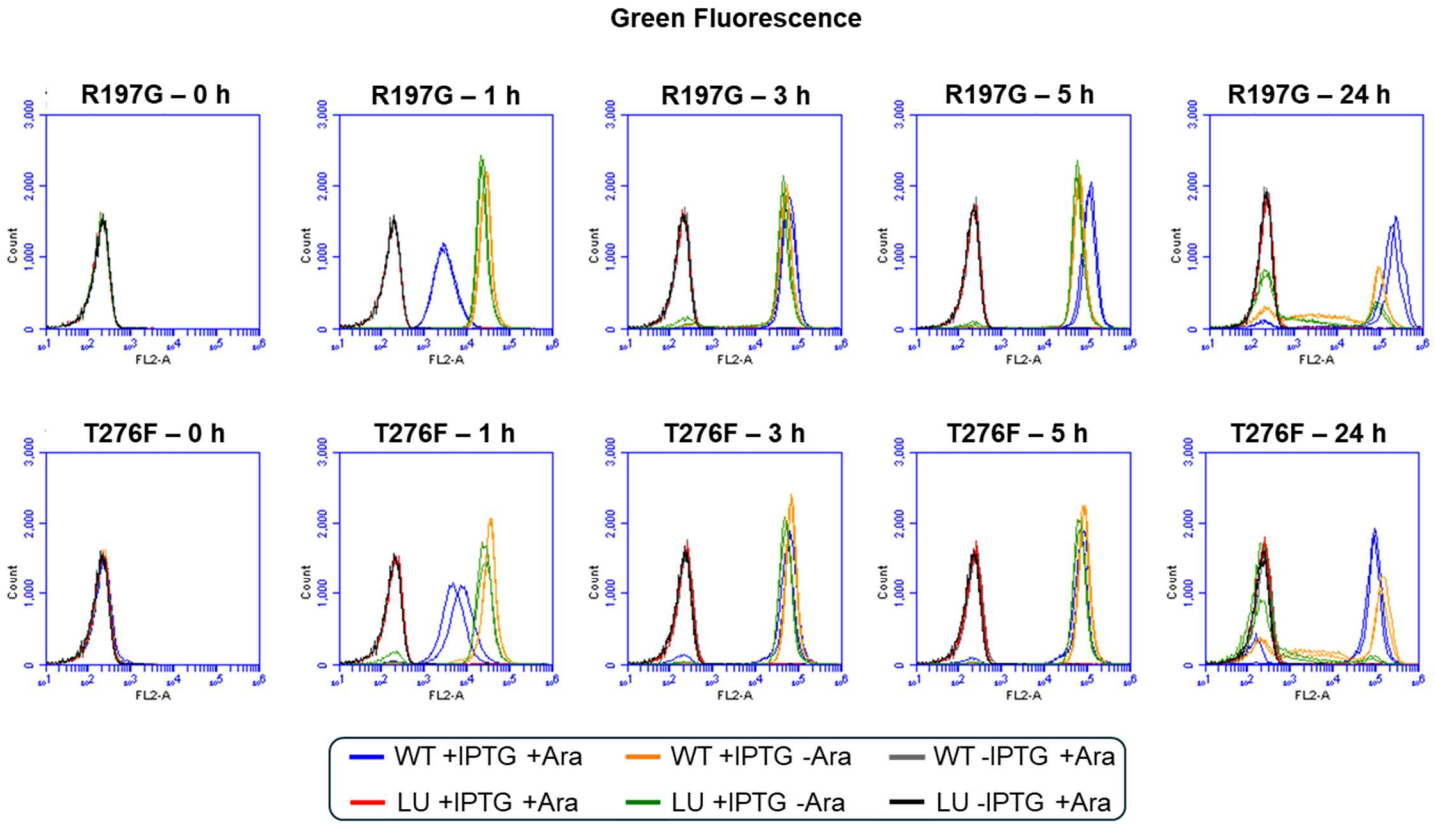


Figure 5.19: FCM analysis of green fluorescence in single cells during expression of ligand unresponsive LacI.

The feedback system required a ligand unresponsive (LU) variant of LacI to regulate expression of a recombinant protein in response to stress. Mutants LacI^{R197G} and LacI^{T276F} were chosen with WT LacI used as a control. In BL21(DE3) pBAD30-lacI^{R197G}, pBAD30-lacI^{T276F} or pBAD30-lacI were co-expressed alongside a T7*lac*-msfGFP construct. BL21(DE3) was cultured at 37°C, 200 rpm in LB + Amp + Kan. At OD_{600} 0.4-0.6, LacI or Lac LU variants were induced using 0.2 % (w/v) L-arabinose and msfGFP expression induced with 100 µM IPTG. Combinations (+/-) of 0.2 % (w/v) L-arabinose and 100 µM IPTG were used as controls. Each condition was repeated in duplicate cultures. Data for each condition is shown for biological duplicates.

Green fluorescence (FL2-A) of single cells was monitored using FCM. Between induction and 5 h post-induction regardless of condition, cultures were mostly homogenous. Some small populations of low green fluorescence were present for WT cultures induced with IPTG but at 24 h post-induction, these were much greater.

membrane integrity; after staining cells, FCM was used to gate cells on red fluorescence (FL3-A) and green fluorescence (FL1-A) density plots. Gates were created for cells not stained by PI, indicating viability, and cells stained by PI, indicating non-viability. Data is shown for cells stained by PI (PI+) (Figure 5.20). Predictably, due to higher levels of expression from T7*lac*, PI+ cells were predominantly seen within cultures only induced with IPTG and this was generally at 24 h post-induction.

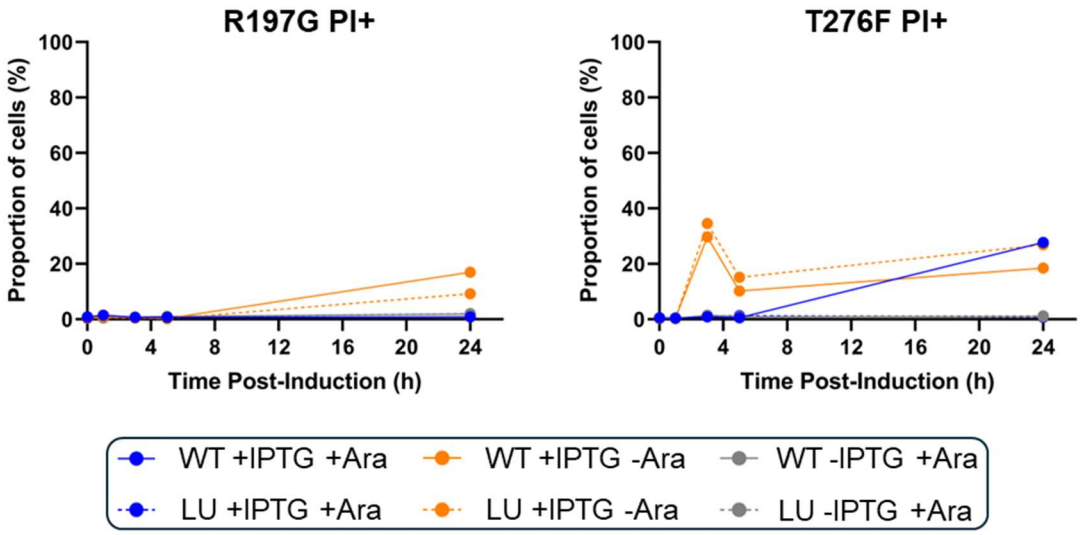


Figure 5.20: PI staining of BL21(DE3) during expression of ligand unresponsive LacI

The feedback system required a ligand unresponsive (LU) variant of LacI to regulate expression of a recombinant protein in response to stress. Mutants LacI^{R197G} and LacI^{T276F} were chosen with WT LacI used as a control. In BL21(DE3) pBAD30-lacI^{R197G}, pBAD30-lacI^{T276F} or pBAD30-lacI were co-expressed alongside a T7*lac*-msfGFP construct. BL21(DE3) was cultured at 37°C, 200 rpm in LB + Amp + Kan. At OD_{600} 0.4-0.6, LacI or Lac LU variants were induced using 0.2 % (w/v) L-arabinose and msfGFP expression induced with 100 µM IPTG. Combinations (+/-) of 0.2 % (w/v) L-arabinose and 100 µM IPTG were used as controls. Each condition was repeated in duplicate cultures. Error bars represent +/- SD from biological duplicates.

To assess viability, 4 µg mL^{-1} PI was used to stain cells. Using FCM, cells were gated using red fluorescence (FL3-A) and green fluorescence (FL2-A) density plots. Gates were created for cells based on staining as viable or non-viable (PI+). Data is shown for stained cells residing within the PI+ gate.

Between induction and 5 h post-induction, low percentages of cells were within the PI+ gate, although this increased at 24 h post-induction to up to 20% of cells. It was noted that the percentage of PI+ cells for WT lacI and LacI^{T276F} cultures treated with +IPTG -Ara increased and decreased between 1 h and 5 h post-induction.

5.6.2 SsrA tagged LacI^{R197G}

There were not major differences between LacI^{R197G} and LacI^{T276F} and both were effective in shutting down expression of msfGFP from T7*lac* (section 5.6.1) but we selected LacI^{R197G} to move forward with. For effective regulation during negative feedback, the repressor would have to be degraded, or expression would be repressed over very long timescales. *E. coli* natively possess a quality control system to tag proteins for degradation via SsrA (Karzai et al., 2000), a 363 bp RNA with functionality as tRNA and mRNA (Komine et al., 1994, Keiler et al., 1996); its purpose being to rescue stalled ribosomes from defective mRNA. During rescue, a short tag is attached to substrate mRNA with the sequence AANDENYALAA (Tu et al., 1995) and translation terminated. SsrA tagged polypeptides are degraded by AAA+ proteases (Lies and Maurizi, 2008), primarily ClpXP (Gottesman et al., 1998), assisted by the enhancing protein SspB (Levchenko et al., 2000). Degradation rates are influenced by three C-terminal residues of the tag and mutagenesis can be exploited for tuning (Keiler and Sauer, 1996, Andersen et al., 1998, Flynn et al., 2001). A modified variant of the SsrA tag with the sequence AANDENYADAS was selected; shown to have medium rates of degradation and far lower than the WT (Klimecka et al., 2021). Hence, LacI^{R197G} was tagged at its C-terminus with the AANDENYADAS SsrA tag, in the construct pBAD30-*lacI*^{R197G}-M.

To test LacI^{R197G}-M, it was assayed against untagged LacI^{R197G} in regulating expression of T7*lac* driven msfGFP. Expression of msfGFP was extremely low when using LacI^{R197G} but very high when using WT lacI (Figure 5.18), so it was hoped the tagged variant would provide a middle ground in terms of repression. BL21(DE3)

harbouring pBAD30-*lacI*^{R197G} or pBAD30-*lacI*^{R197G}-M and co-expressing pET-26b(+)Δ-ATG-*msfgfp* (T7*lac*) was grown in 50 mL LB + Amp + Kan in Erlenmeyer flasks at 37 °C, 200 rpm. At OD_{600} 0.4-0.6, expression of LacI^{R197G} or LacI^{R197G}-M and msfGFP were induced with 0.2 % (w/v) L-arabinose and 100 µM IPTG. Conditions were repeated in duplicate cultures with expression proceeding until 24 h post-induction.

Mean green fluorescence was monitored via FCM (Figure 5.21A). Predictably, induction of either LacI^{R197G} or LacI^{R197G}-M cultures with only IPTG resulted in high mean green fluorescence, reaching over 160000 AU by 5 h post-induction. Further, as observed prior (Figure 5.18A), even when inducing with IPTG and L-arabinose, mean green fluorescence and thus msfGFP expression was low in LacI^{R197G} cultures, at around 200 AU (Figure 5.21A). When inducing with IPTG and L-arabinose, mean green fluorescence in LacI^{R197G}-M cultures was higher than LacI^{R197G}, and steadily increased over time, suggesting degradation reduced repression. At 5 h post-induction, LacI^{R197G}-M cultures induced with IPTG and L-arabinose reached a mean green fluorescence of approximately 40000 AU; this was a 4-fold reduction in mean green fluorescence against cultures induced with only IPTG, and a 10-fold increase over cultures induced with only L-arabinose (Figure 5.21A) (adjusted $p < 0.004$ for all comparisons when analysed by one-way ANOVA). LacI^{R197G}-M cultures only induced with L-arabinose had higher green fluorescence than LacI^{R197G} cultures, confirming reduced repression (Figure 5.21A). There was little heterogeneity in green fluorescence (FL1-A) between induction and 5 h post-induction when measured via FCM (Figure 5.21B); though, LacI^{R197G}-M cultures induced with IPTG and L-arabinose had a widely distributed population at 1 h post-induction. By 24 h post-induction,

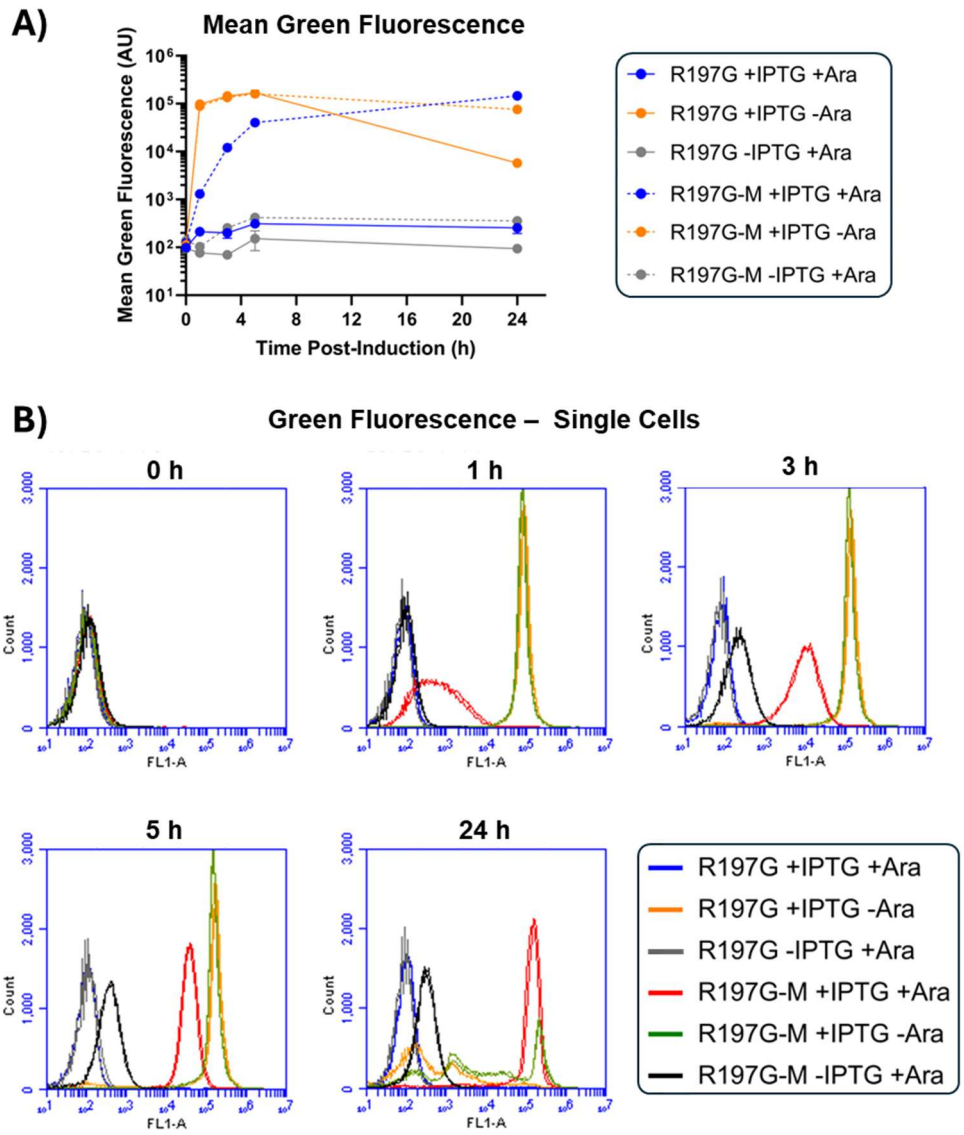


Figure 5.21: FCM green fluorescence analysis of degradation tagged LacI^{R197G}-M.

LacI^{R197G} was shown to be effective in shutting down expression from a T7*lac* promoter, but a feedback loop necessitated a degradation tag be attached for system turnover. A modified SsrA tag was fused to the LacI^{R197G} C-terminus. Constructs containing P_{araBAD} driving expression of LacI^{R197G} or the tagged derivative LacI^{R197G}-M were co-expressed alongside a T7*lac*-msfGFP construct. Cultures of BL21(DE3) were grown at 37°C, 200 rpm in 50 mL LB + Amp + Kan. At OD_{600} 0.4-0.6 LacI^{R197G} was induced using 0.2 % (w/v) L-arabinose and msfGFP expression induced with 100 µM IPTG. Combinations (+/-) of 0.2 % (w/v) L-arabinose and 100 µM IPTG were used as controls. Each condition was repeated in duplicate cultures.

(A) Mean green fluorescence was monitored via FCM and as previously seen, was very low for R197G cultures when inducing with IPTG and L-arabinose. Comparatively, for R197G-M cultures, when inducing with IPTG and L-arabinose, mean green fluorescence steadily increased over time and was higher than in cultures not induced with L-arabinose by 24 h post-induction. Error bars represent +/- SD from biological duplicates.

(B) Green fluorescence (FL1-A) of single cells was monitored using FCM. Between induction and 5 h post-induction regardless of condition, cultures were mostly homogenous although R197G-M cultures induced with IPTG and L-arabinose were widely distributed at 1 h post-induction. At 24 h post-induction, there was considerable heterogeneity in cultures only in induced with IPTG; comparatively R197G-M cultures had a tight population of high green fluorescence. Data for each condition is shown for biological duplicates.

multiple green fluorescent populations were observed for LacI^{R197G} cultures induced with only IPTG; this was expected due to strong expression from T7*lac*. Interestingly, at 24 h post-induction, LacI^{R197G}-M cultures were a single population; presumably the lower expression facilitated improved host physiology allowing homogenous expression of msfGFP to proceed for longer.

There was concern that high expression of SsrA tagged LacI would titrate away proteases required for normal cellular function and have a negative impact on physiology. Biomass accumulation (Figure 5.22A) and cell density (Figure 5.22B) were monitored via OD_{600} and FCM respectively. Cultures containing LacI^{R197G}-M induced with L-arabinose reached slightly lower OD_{600} and cell density than untagged LacI^{R197G}, although both reached over $1x10^9$ cells mL^{-1}. Comparatively, cultures only induced with IPTG exhibited growth arrested after induction, presumably due to unrestricted expression of msfGFP from T7*lac*. PI staining was used as a measure of cell viability via membrane integrity; after staining cells, FCM was used to gate cells on red fluorescence (FL3-A) and green fluorescence (FL1-A) density plots. Gates were created for cells not stained by PI, indicating viability, and cells stained by PI, indicating non-viability. Data is shown for cells stained by PI (PI+) (Figure 5.22C). Proportions of cells within the PI+ gate were generally below 5 % between induction and 5 h post-induction for all cultures. At 24 h post-induction, the proportion of cells within the PI+ gate in cultures only induced with IPTG was approximately 10 – 15 %. However, LacI^{R197G}-M cultures induced with IPTG and L-arabinose had the highest levels of cells within the PI+ gate at 24 h post-induction, reaching around 35 %. We assumed this

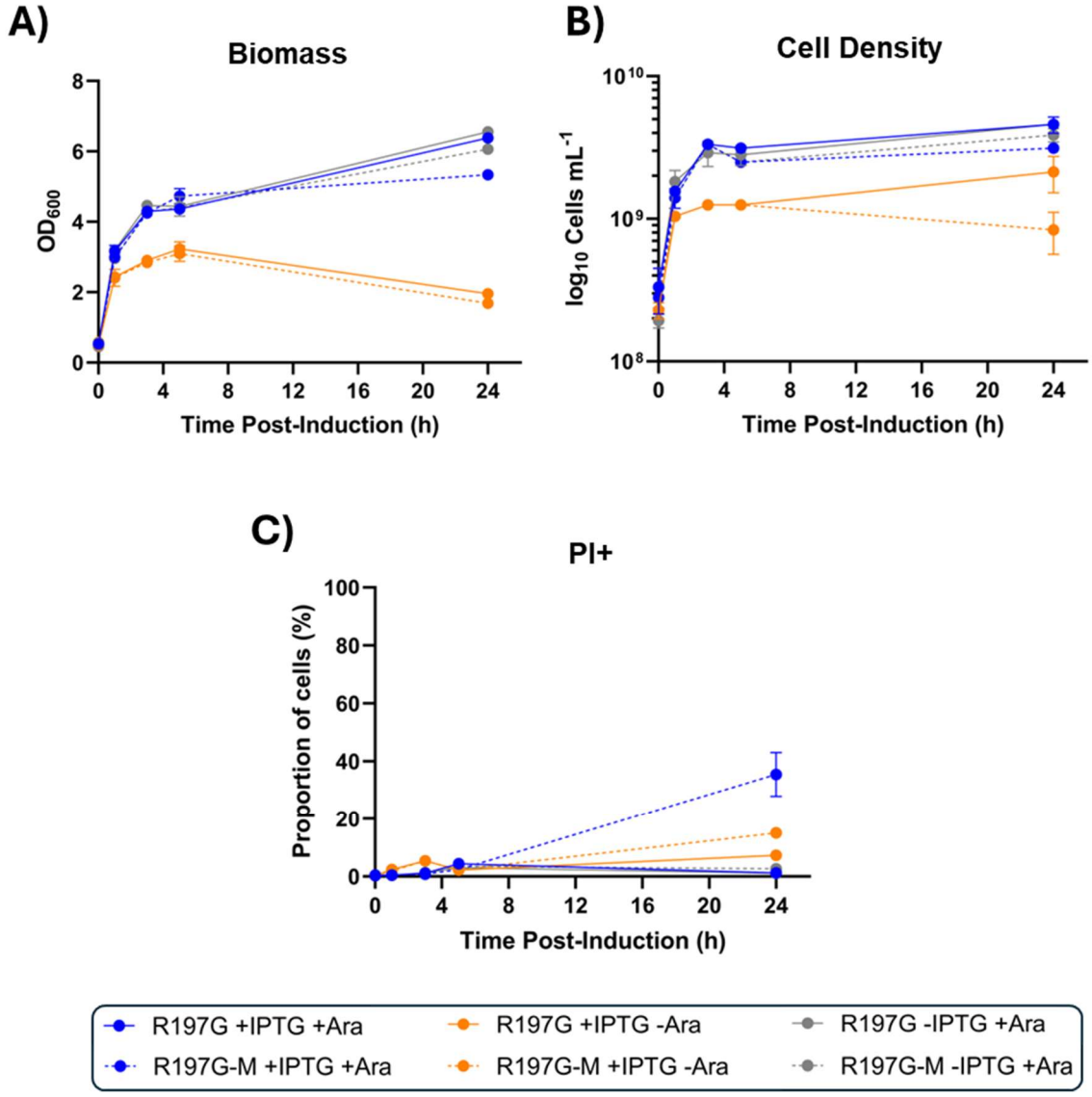


Figure 5.22: Growth data for BL21(DE3) expressing degradation tagged LacI^{R197G}-M.

LacI^{R197G} was shown to be effective in shutting down expression from a T7*lac* promoter, but a feedback loop necessitated a degradation tag be attached for system turnover. A modified SsrA tag was fused to the LacI^{R197G} C-terminus. Constructs containing P_{araBAD} driving expression of LacI^{R197G} or the tagged derivative LacI^{R197G}-M were co-expressed alongside a T7*lac*-msfGFP construct. Cultures of BL21(DE3) were grown at 37°C, 200 rpm in 50 mL LB + Amp + Kan. At OD_{600} 0.4-0.6 LacI^{R197G} was induced using 0.2 % (w/v) L-arabinose and msfGFP expression induced with 100 µM IPTG. Combinations (+/-) of 0.2 % (w/v) L-arabinose and 100 µM IPTG were used as controls. Each condition was repeated in duplicate cultures. Error bars represent +/- SD from biological duplicates.

(A) Biomass accumulation and **(B)** cell density was monitored via OD_{600} and FCM respectively. As expected, cultures only induced with IPTG had some growth arrest presumably due to higher level expression of msfGFP. Interestingly, induction of R197G-M cultures with IPTG and L-arabinose did not significantly impact growth until it dropped slightly at 24 h post-induction.

(C) To assess viability, 4 µg mL^{-1} PI was used to stain cells. Using FCM, cells were gated using red fluorescence (FL3-A) and green fluorescence (FL2-A) density plots. Gates were created for cells based on staining as viable or non-viable (PI+). Data is shown for stained cells residing within the PI+ gate. Highest levels of PI+ cells were in R197G-M cultures induced with IPTG and L-arabinose at 24 h post-induction, reaching around 35%. We assumed this was due to high level expression of msfGFP and LacI^{R197G}-M.

was in part due to the combined effect of high level msfGFP and LacI^{R197G}-M expression.

Overall, we found that in cultures induced with IPTG and L-arabinose, expression of msfGFP appeared to increase over time when repressed by LacI^{R197G}-M, suggesting a decrease in repression (Figure 5.21A). Conversely, in cultures induced with IPTG and L-arabinose expression of msfGFP repressed by LacI^{R197G} appeared extremely low (Figure 5.21A) and was consistent with that observed previously for this variant of ligand unresponsive LacI (Figure 5.18A). We theorised two potential explanations for what was observed in fully induced LacI^{R197G}-M cultures: increased degradation of LacI^{R197G}-M by proteases like ClpXP over time; and / or decreased expression of LacI^{R197G}-M over time. For the former, there are reports that degradation of SsrA tags increases (Farrell et al., 2005) and decreases (Lies and Maurizi, 2008) during stationary. The latter could be due to decreasing L-arabinose concentrations as BL21 can metabolise this (Stargardt et al., 2021). We did observe that green fluorescence of fully induced cultures repressed by LacI^{R197G} also increased slightly between 1 h and 5 h post-induction but then remained stable through till 24 h post-induction.

5.6.3 Supplementation with additional arabinose

As green fluorescence of fully induced msfGFP cultures repressed by LacI^{R197G}-M increased over time (Figure 5.21A), we wanted to assess whether this was caused by L-arabinose metabolism resulting in lower availability of inducer. To do so, we decided check whether additional supplementation with L-arabinose during growth could offset decreasing repression. BL21(DE3) harbouring pBAD30-*lacI*^{R197G} or pBAD30-*lacI*^{R197G}-M and pET-26b(+)Δ-ATG-*msfgfp* was grown in 50 mL LB (Miller) + Amp + Kan in Erlenmeyer flasks at 37 °C, 200 rpm. At OD_{600} 0.4-0.6, expression of LacI^{R197G} or LacI^{R197G}-M and msfGFP were induced with combinations of 0.2 % (w/v) L-arabinose and 100 µM IPTG; some cultures were supplemented with additional 0.2 % (w/v) L-arabinose at 3 h post-induction. Conditions were repeated in duplicate cultures.

Mean green fluorescence was monitored via FCM (Figure 5.23A). Supplementation with additional L-arabinose at 3 h post-induction did not decrease msfGFP expression in any strain; in fact, it slightly increased green fluorescence in many conditions. Further, single cell analysis via FCM indicated cultures under all conditions were homogenous throughout growth (Figure 5.24). OD_{600} was similar in all cultures (Figure 5.23B), although cell density measured via FCM indicated there was some effect to supplementing with L-arabinose at 3 h post-induction (Figure 5.23C). Cell density of all supplemented cultures dropped between 3 h and 7 h post-induction, suggesting more LacI^{R197G} and LacI^{R197G}-M were being synthesised.

PI staining was used as a measure of cell viability via membrane integrity; after staining cells, FCM was used to gate cells on red fluorescence (FL3-A) and green fluorescence

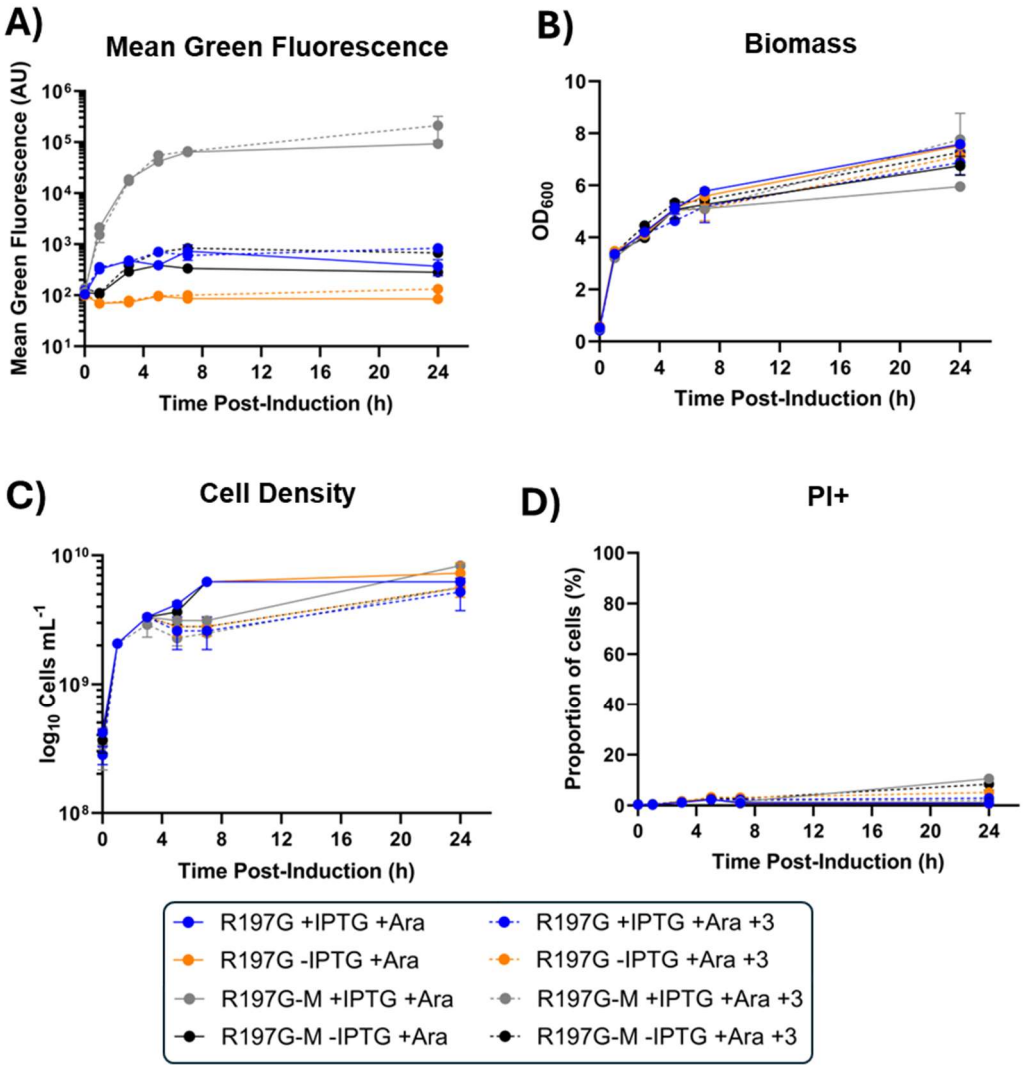


Figure 5.23: Analysis of BL21(DE3) expressing degradation tagged LacI^{R197G}-M.

The degradation rate of LacI^{R197G}-M previously appeared to increase during growth resulting in green fluorescence increasing over time. We wondered whether supplementing with additional arabinose after induction would decrease the rate of LacI^{R197G}-M degradation. Constructs containing P_{araBAD} driving expression of LacI^{R197G} or the tagged derivative LacI^{R197G}-M were co-expressed alongside a T7*lac*-msfGFP construct. Cultures of BL21(DE3) were grown at 37°C, 200 rpm in 50 mL LB + Amp + Kan. At OD_{600} 0.4-0.6 LacI^{R197G} was induced using 0.2 % (w/v) L-arabinose and msfGFP expression induced with 100 µM IPTG. At 3 h post-induction, some cultures were induced again with 0.2% L-arabinose (+3). Combinations (+/-) of 0.2 % (w/v) L-arabinose and 100 µM IPTG were used as controls. Each condition was repeated in duplicate cultures. Error bars represent +/- SD from biological duplicates.

(A) Mean green fluorescence was monitored via FCM and steadily increased over time for R197G-M cultures. Supplementing with additional L-arabinose at 3 h post-induction appeared to have the reverse effect, mean green fluorescence being higher than the non-supplemented culture at 5 h and 24 h post-induction.

(B) Biomass measured via OD_{600} and **(C)** cell density measured via FCM were used check whether supplementing with L-arabinose affected growth; there was a slight drop in cell density but OD_{600} was similar.

(D) To assess viability, 4 µg mL^{-1} PI was used to stain cells. Using FCM, cells were gated using red fluorescence (FL3-A) and green fluorescence (FL2-A) density plots. Gates were created for cells based on staining as viable or non-viable (PI+). Data is shown for stained cells residing within the PI+ gate. Proportion of PI+ cells was low throughout, the highest being R197G-M cultures where 10 % of cells were within the PI+ gate at 24 h post-induction.

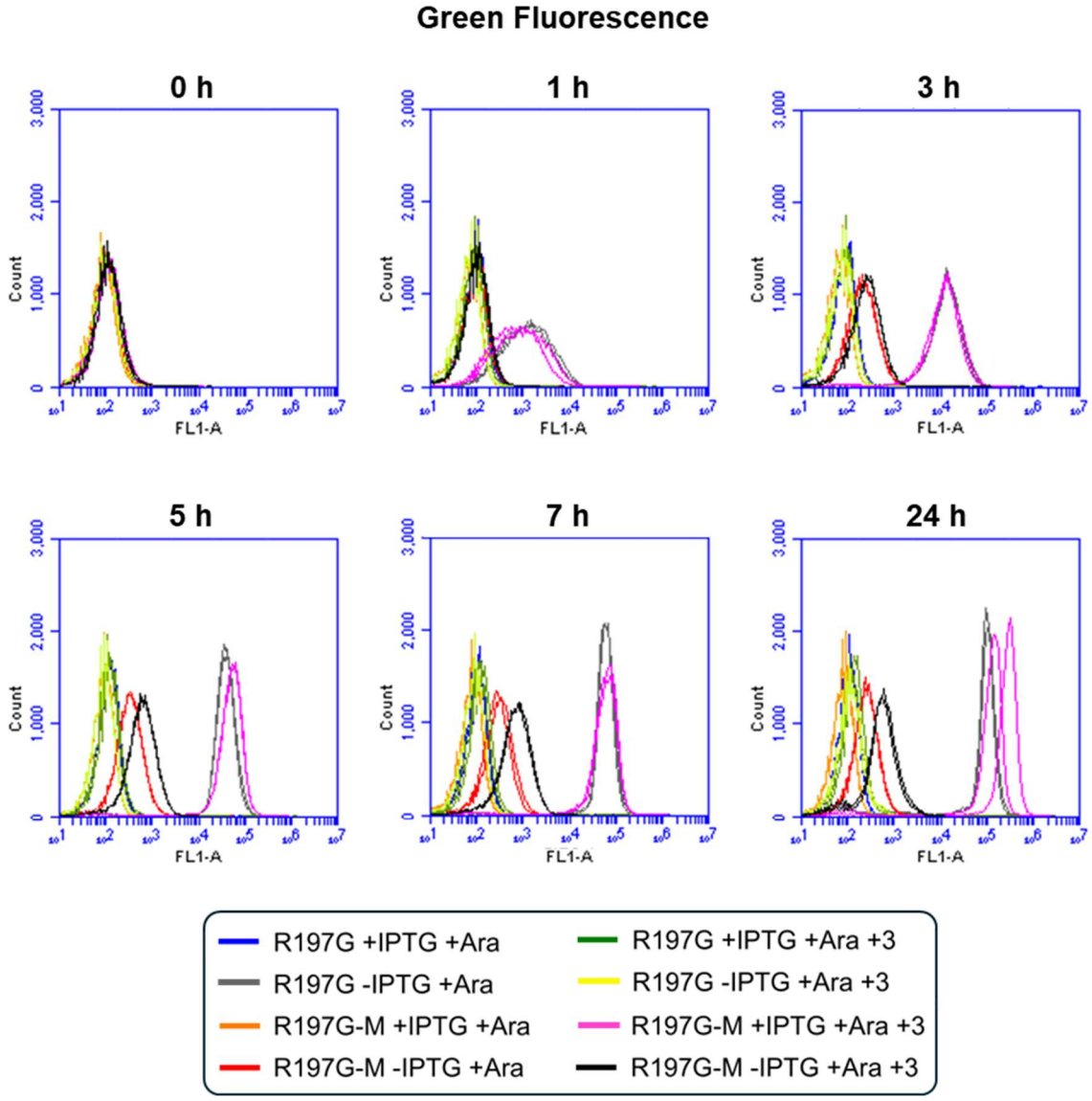


Figure 5.24: FCM green fluorescence analysis during expression of degradation tagged LacI^{R197G}-M.

The degradation rate of LacI^{R197G}-M previously appeared to increase during growth resulting in green fluorescence increasing over time. We wondered whether supplementing with additional arabinose after induction would decrease the rate of LacI^{R197G}-M degradation. Constructs containing P_{araBAD} driving expression of LacI^{R197G} or the tagged derivative LacI^{R197G}-M were co-expressed alongside a T7*lac*-msfGFP construct. Cultures of BL21(DE3) were grown at 37°C, 200 rpm in 50 mL LB + Amp + Kan. At OD_{600} 0.4-0.6 LacI^{R197G} was induced using 0.2 % (w/v) L-arabinose and msfGFP expression induced with 100 µM IPTG. At 3 h post-induction, some cultures were induced again with 0.2% L-arabinose (+3). Combinations (+/-) of 0.2 % (w/v) L-arabinose and 100 µM IPTG were used as controls. Each condition was repeated in duplicate cultures. Data is shown for biological duplicates.

Green fluorescence (FL1-A) of single cells was monitored using FCM to see if there was any heterogeneity resulting from supplementing with additional L-arabinose at 3 h post-induction. Across all time point, cultures were mostly homogenous although R197G-M cultures induced with IPTG, and L-arabinose were widely distributed at 1 h post-induction.

(FL1-A) density plots. Gates were created for cells not stained by PI, indicating viability, and cells stained by PI, indicating non-viability. Data is shown for cells stained by PI (PI+) (Figure 5.23D). Proportions of PI+ cells were generally below 3 % between induction and 7 h post-induction for all cultures. At 24 h post-induction the proportion of PI+ cells in all cultures increased slightly, with $LacI^{R197G}$-M cultures induced with ITPG and L-arabinose the highest at 10 %, also observed previously (Figure 5.22C).

It was clear then that supplementation with additional L-arabinose was not able to prevent an increase in fluorescence, and thus msfGFP expression when using the SsrA tagged variant $LacI^{R197G}$-M (Figure 5.23A). Further, in untagged $LacI^{R197G}$, we also noticed a slight drop in green fluorescence in cultures not treated with L-arabinose (Figure 5.23A). Hence, it seemed the L-arabinose concentration was not the cause of increased fluorescence when using the SsrA tagged variant $LacI^{R197G}$-M. As degradation tags on any repressor will eventually be critical to system turnover in a feedback loop (Figure 5.17A) (Dragosits et al., 2012), future work could look at variants of a pulse chase experiment; we utilised something similar during Chapter 3. Expression of $LacI^{R197G}$ variants would be induced with L-arabinose, along with msfGFP expression using IPTG. Shortly after induction, cells would be spun down and only IPTG added back into fresh medium. This would allow determination of the permanency of repression from $LacI^{R197G}$ with and without the SsrA tags.

5.8 Negative Feedback system

Response of the P_{spy} sensor construct to stress induced by overexpression of exported $PelB^{SP}$::anti-IL-1β scFv and targeted inhibition of SecA using RB + PMBN was evidence it could be exploited as a trigger for feedback control of expression during

RPP (section 5.4). Further, LacI^{R197G} effectively shut off expression of msfGFP from T7*lac* and would be an effective repressor for the system (section 5.6.1). The SsrA tagged variant LacI^{R197G}-M appeared to provide lower repression of T7*lac* than the untagged LacI^{R197G}, but repression was not stable and increased considerably over time (section 5.6.2). There was concern whether P_{spy} could drive high enough expression of LacI^{R197G} to counteract the notoriously strong T7*lac* promoter; coupled with high degradation rates observed with the SsrA tag, control over expression could potentially be limited. Instead, we decided to test the system without the SsrA tag; LacI^{R197G} was inserted downstream of P_{spy}, on the sensor construct pBAD30Δ-P_{spy}-LacI^{R197G}.

To assay the system, constructs expressing periplasmic msfGFP via fusion to PelB^{SP} and DsbA^{SP}, or cytoplasmic msfGFP, all driven by T7*lac* were used. These constructs were those generated in Chapter 3 of this work. While the PelB^{SP}::msfGFP and DsbA^{SP}::msfGFP constructs were shown to function poorly during that work, typically exporting around 20% of msfGFP to the periplasm, they were found to be deleterious to cell growth, presumably due to conflicts between overexpression and attempting to export the recombinant protein to the periplasm (Schlegel et al., 2013, Baumgarten et al., 2018). Hence we thought they would be useful as a first test of the feedback construct; if host physiology was improved in strains co-expressing both, this would be a good indication that the system could work. Hence, BL21(DE3) co-transformed with pBAD30Δ-P_{spy}-LacI^{R197G} and pET-26b(+)-*pelB^{SP}*::*msfgfp*, pET-26b(+)Δ-*dsbA^{SP}*::*msfgfp* or pET-26b(+)Δ-*msfgfp* were grown in 50 mL TB + Amp + Kan in Erlenmeyer flasks at 30 °C, 200 rpm. At OD_{600} 0.4-0.6, expression of msfGFP was

induced with 100 μM IPTG. Expression was allowed to proceed for a further 24 h. Controls not containing the pBAD30Δ-P_{spy}-LacI^{R197G} construct were run in parallel. Each condition was repeated in duplicate cultures.

Expression of msfGFP was monitored by mean green fluorescence measurement using FCM (Figure 5.25A). In strains not harbouring the P_{spy} feedback construct, mean green fluorescence was high at induction, highlighting background expression from T7*lac*; for cultures expressing PelB^{SP}::msfGFP, this was over 45000 AU. In strains harbouring the P_{spy} feedback construct, mean green fluorescence was far lower, ranging from 200 – 1000 AU; presumably this was due to basal expression of LacI^{R197G} from P_{spy}. In cultures not containing the P_{spy} feedback construct, IPTG induction caused an increase in mean green fluorescence for cytoplasmic msfGFP; PelB^{SP}::msfGFP initially decreased then increased, whereas DsbA^{SP}::msfGFP decreased (Figure 5.25A). In all strains harbouring the P_{spy} feedback construct, mean green fluorescence decreased after induction with IPTG, suggesting that P_{spy} detected periplasmic stress and repressed msfGFP expression (Figure 5.25A). Between 1 h post-induction and 24 h post-induction, mean green fluorescence in all cultures harbouring the P_{spy} feedback construct increased. This could be due to P_{spy} activity decreasing during stationary phase (as observed during expression of periplasmic anti-*il-1β* scFv in Figure 5.11), and / or decreased periplasmic stress causing declining activation of P_{spy}, resulting in lower expression of LacI^{R197G}.

It was interesting that the P_{spy} feedback construct appeared to respond to induction of cytoplasmic msfGFP; this suggests effects of cytoplasmic expression have effects on

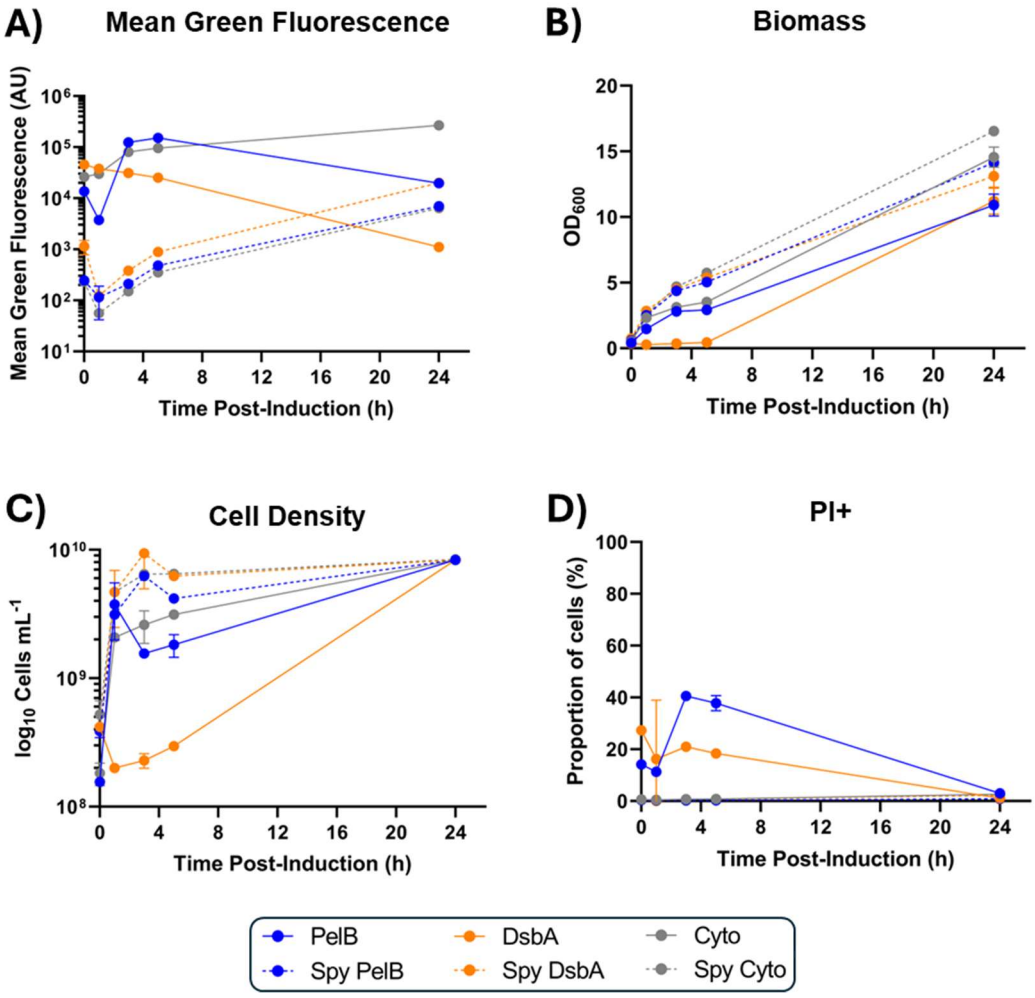


Figure 5.25: Analysis of a P_{spy} negative feedback construct.

Due to the fast and unstable degradation rate observed for $LacI^{R197G}$-M, it was decided to test a P_{spy} feedback construct using untagged $LacI^{R197G}$, which was expressed from P_{spy}. Constructs containing T7*lac* driving expression of $PelB^{SP}$::msfGFP, $DsbA^{SP}$::msfGFP and msfGFP were co-expressed. Strains harbouring only the msfGFP expression constructs were used as controls. BL21(DE3) was cultured in 50 mL TB + Amp + Kan at 30 °C, 200 rpm. At OD_{600} 0.4-0.6 msfGFP expression was induced with 100 µM IPTG. Each condition was repeated in duplicate cultures. Error bars represent +/- SD from biological duplicates.

(A) Mean green fluorescence was monitored via FCM. Background expression of msfGFP was high in cultures not co-expressing the P_{spy} feedback construct, but considerably lower in those that were. Induction with IPTG caused mean green fluorescence to decrease in cultures expressing $PelB^{SP}$::msfGFP and $DsbA^{SP}$::msfGFP. In cultures harbouring the P_{spy} feedback construct, mean green fluorescence decreased following induction but began to increase over time. Interestingly, overexpression of cytoplasmic msfGFP also appeared to further switch on P_{spy}.

(B) Biomass was monitored via OD_{600} and **(C)** cell density via FCM. Overexpression of exported msfGFP severely affected growth, cultures expressing $DsbA^{SP}$::msfGFP had a near 1 log drop in cell density following induction. In cultures co-expressing the P_{spy} feedback construct, growth was much improved.

(D) To assess viability, 4 µg mL^{-1} PI was used to stain cells. Using FCM, cells were gated using red fluorescence (FL3-A) and green fluorescence (FL2-A) density plots. Gates were created for cells based on staining as viable or non-viable (PI+). Data is shown for stained cells residing within the PI+ gate. Proportions of cells within the PI+ gate for cultures expressing $PelB^{SP}$::msfGFP or $DsbA^{SP}$::msfGFP were high at between 20 – 40 %; comparatively in those cultures co-expressing the P_{spy} feedback construct, PI+ cells remained extremely low throughout growth.

the envelope. It must also be noted however, that this could be due to actual leakage of cytoplasmic proteins into the periplasm; this has been shown to occur in cells undergoing high level expression due to translational stress (Morra et al., 2018). Such a process could also activate envelope stress responses like CpxAR and BaeSR which regulate the P_{spy} promoter (Yamamoto and Ishihama, 2006, Yamamoto et al., 2008, Srivastava et al., 2014).

Analysis of green fluorescence in single cells using FCM indicated cultures harbouring the P_{spy} feedback construct were composed of a single population throughout growth (Figure 5.26). Comparatively, there was considerable heterogeneity in cultures only expressing PelB^{SP}::msfGFP and DsbA^{SP}::msfGFP, indicating expression was poorly tolerated (as seen in chapter 4). However, cultures only expressing cytoplasmic msfGFP were more homogenous. To further observe tolerance, OD_{600} (Figure 5.25B) and cell density (Figure 5.25C) were monitored via FCM; predictably growth arrest in cultures only expressing PelB^{SP}::msfGFP and DsbA^{SP}::msfGFP was observed, both decreasing not long after induction (Figure 5.25B and 5.25C). Comparatively cell density for cultures only expressing cytoplasmic msfGFP continued to increase after induction (Figure 5.25C). Cultures harbouring the P_{spy} feedback construct had far better growth; as an example, at 5 h post-induction there was a near 2-log difference in cell density between cultures expressing DsbA^{SP}::msfGFP (Figure 5.25C).

PI staining was used as a measure of cell viability via membrane integrity; after staining cells, FCM was used to gate cells on red fluorescence (FL3-A) and green fluorescence (FL1-A) density plots. Gates were created for cells not stained by PI, indicating viability,

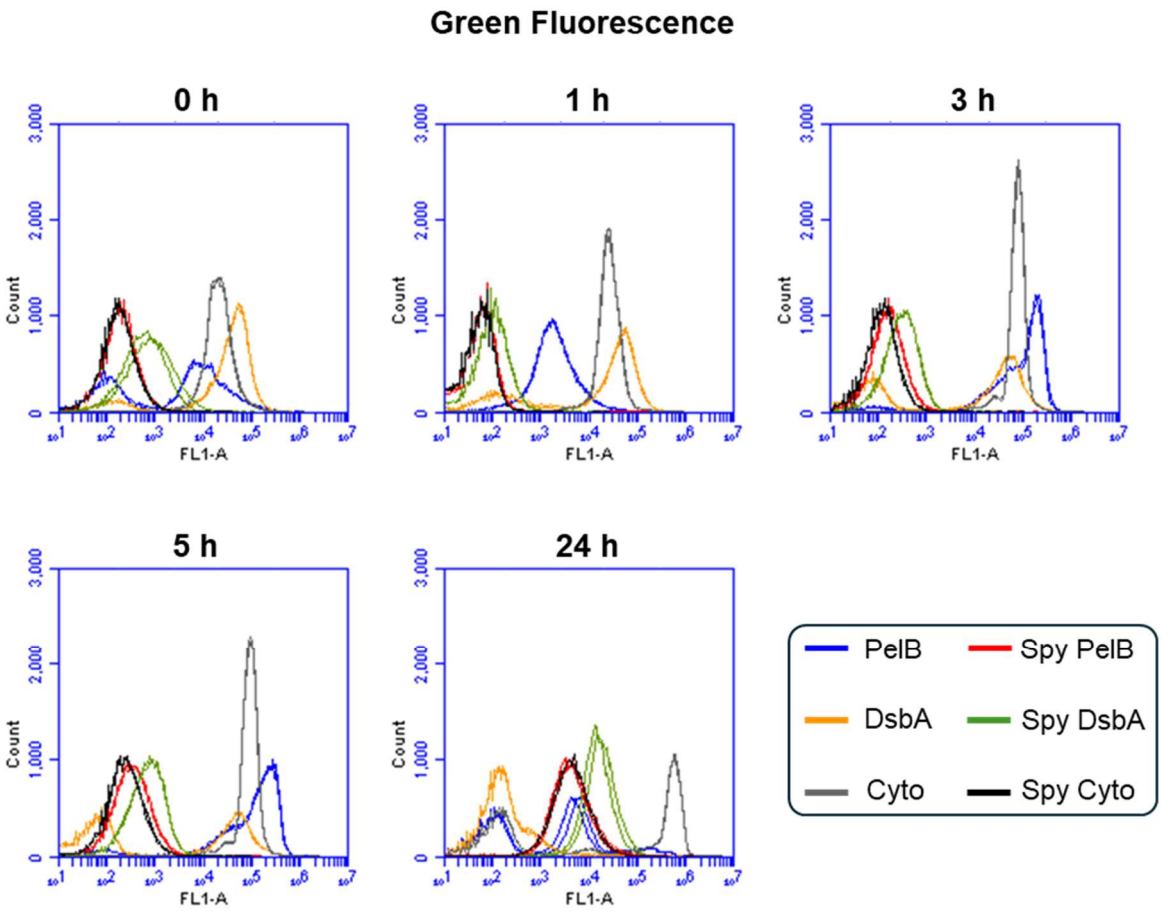


Figure 5.26: Analysis of a P_{spy} negative feedback construct.

Due to the fast and unstable degradation rate observed for $LacI^{R197G}$-M, it was decided to test a P_{spy} feedback construct using untagged $LacI^{R197G}$, which was expressed from P_{spy}. Constructs containing T7*lac* driving expression of $PelB^{SP}$::msfGFP, $DsbA^{SP}$::msfGFP and msfGFP were co-expressed. Strains harbouring only the msfGFP expression constructs were used as controls. BL21(DE3) was cultured in 50 mL TB + Amp + Kan at 30 °C, 200 rpm. At OD_{600} 0.4-0.6 msfGFP expression was induced with 100 µM IPTG. Each condition was repeated in duplicate cultures. Data for each condition is shown for biological duplicates.

Green fluorescence (FL1-A) of single cells was monitored using FCM to see if there was any heterogeneity resulting from co-expression of the P_{spy} feedback construct; at all time points, these cultures were a single population. Comparatively, for $PelB^{SP}$::msfGFP and $DsbA^{SP}$::msfGFP cultures not co-expressing the feedback construct, there was considerable heterogeneity throughout growth; control cultures expressing cytoplasmic msfGFP were a single population until 24 h post-induction.

and cells stained by PI, indicating non-viability. Data is shown for cells stained by PI (PI+) (Figure 5.25D). Proportions of within the PI+ gate were high in cultures only expressing PelB^{SP}::msfGFP and DsbA^{SP}::msfGFP, ranging from 20 – 40 %; this is consistent with what we observed when using these constructs previously (see chapter 4). When co-expressing the P_{spy} feedback construct, the proportion of live cells was near 100 % throughout growth (Figure 5.25D).

Overall, it was clear that the P_{spy} feedback construct was able to shut off expression of msfGFP from T7*lac* (Figure 5.25A) and the fact that host physiology was seemingly improved (Figure 5.25B-D) was reassuring. However, a main concern was that green fluorescence increased continually between 1 h post-induction and 24 h post-induction (Figure 5.25A). This suggested expression from P_{spy} is not consistent throughout all stages of growth and possibly decreases during stationary phase. We had in fact seen something similar before, when P_{spy} was used to express 6xHis::GFP in response to overexpression of PelB^{SP}::anti-IL-1β scFv but had attributed this to possible plasmid loss during the latter stages of growth (Figure 5.11). P_{spy} is bound by RNA polymerase with the σ^{70} subunit (Salgado et al., 2024); in stationary phase the alternative σ^{S} is predominant (Schellhorn, 2020); this could be one possibility for reduced activity. P_{spy} activity not being consistent is problematic for its use in a feedback loop as this would result in poor control of the target recombinant protein.

5.9 Discussion

We have attempted to identify novel ways to detect stress during export of recombinant proteins to the bacterial periplasm and then utilise this to tune overexpression. Many

recombinant proteins require disulphide bonding for activity, including many biotherapeutics (Walsh and Walsh, 2022). Hence, periplasmic expression is often desirable in *E. coli* to permit access the Dsb system (Bardwell et al., 1991); but it is often more difficult to overexpress recombinant proteins here than in the cytoplasm, due to limitations with the capacity of the *E. coli* translocation machinery (Schlegel et al., 2013, Baumgarten et al., 2018). A system utilising the BaeSR/CpxAR regulated P_{spy} promoter from the periplasmic chaperone Spy (Koldewey et al., 2016, Kwon et al., 2010, Mitra et al., 2021) was found to respond to recombinant protein stressors and an additional assay utilising Rose Bengal to specifically target the ATPase SecA, responsible for driving post-translational export (Oswald et al., 2021). To create a feedback system, the P_{spy} biosensor was combined with a ligand unresponsive mutant of LacI (R197G) (Spotts et al., 1991), and subsequently shown to switch on in response to overexpression of exported recombinant proteins.

Prior to developing the P_{spy} negative feedback system, in our initial work we tried to exploit the translational regulation of SecA by SecM for use as a biosensor. Poor expression of proteins in the periplasm is considered a result of saturating export machinery (Mergulhão et al., 2004, Schlegel et al., 2013, Baumgarten et al., 2018). We reasoned that as SecA translation is directly coupled to the export status of the cell by SecM (Nakatogawa et al., 2005), it could be exploited to report on stress arising during RPP. The gene encoding sfGFP was inserted downstream of the *secA* SD sequence but stressing the cells via overexpression of a $PelB^{SP}$::anti-IL-1β scFv did not produce a notable signal. We observed a slight increase in green fluorescence signal following induction but FSC and thus cell size had also increased; larger cells are known to

exhibit an increased fluorescent signal. Our first thought as to why the system did not respond as intended was use of the low copy plasmid pRW50 (Lodge, 1992) to express SecM::GFP, the pSC101 origin maintains about 4 copies per cell (Shao et al., 2021), so the gene dosage for the system could have simply been too low.

Alternatively, perhaps SecA is not highly abundant. There are conflicting reports on the concentration of SecA present within the cell; some place the number as high as 13000 copies (Or, 2002, Kusters and Driessen, 2011), others were more conservative at 518 (Ishihama et al., 2008) and 750 copies per cell (Oliver et al., 1998). Higher values seem extreme given the number of Sec translocons in the cell at a given time was estimated at around 500 copies (Matsuyama et al., 1992), although the number of copies of SecB, a chaperone which works in tandem with SecA during export, were predicted at over 6000 (Findik and Randall, 2017). Most recently fusion of SecA to the yellow fluorescent protein YpeT was used to more accurately determine SecA concentration at between 86 – 154 copies per cell (Seinen et al., 2021).

A further consideration is the effect of translation initiation on protein expression (Vimberg et al., 2007). During cloning, we took a region incorporating up to the SecA start codon. The translation initiation region (TIR) comprises the Shine-Dalgarno (SD) sequence (Chen et al., 1994), start codon (Gren, 1984), and upstream (Hook-Barnard et al., 2007) and downstream (Stenström and Isaksson, 2002) flanking regions commonly termed enhancers. Thus fusion of msfGFP to SecM in place of SecA will alter the TIR and may be less efficient; this is crucial as initiation is a rate-limiting step during translation (Reeve et al., 2014) and optimisation of this region has been used

to improve expression of recombinant proteins (Mirzadeh et al., 2015). As a solution to this, it would be interesting to clone 5' regions of *secA* upstream of *msfgfp* in the SecM construct to see whether this improves expression.

Failure of the SecM::GFP biosensor led us to evaluate one utilising the promoter from the periplasmic chaperone Spy (Hagenmaier et al., 1997, Garbe et al., 2000, Bury-Moné et al., 2009, Quan et al., 2011, He et al., 2021). P_{spy}::*gfp* was shown to respond to overexpression of a $PelB^{SP}$::anti-IL-1β scFv and the SecA inhibitor RB when delivered in combination with PMBN (Hsieh et al., 2014, Jin et al., 2016). While both switched on expression from P_{spy}, GFP expression profiles, based on green fluorescence measurement, appeared quite different between $PelB^{SP}$::anti-IL-1β scFv and the SecA inhibitor RB. For the former, green fluorescence increased over time reaching a maximum fluorescence of around 7000 AU at 5 h post-induction. At 1/2 MIC in combination with PMBN, RB increased green fluorescence rapidly, reaching around 11000 AU after just 1 h. Without PMBN, RB had less effect on green fluorescence reaching around 2500 AU at 5 h post-induction; given its poor permeability into cells though, this was expected (Jin et al., 2016). We assumed RB acted more immediately than $PelB^{SP}$::anti-IL-1β scFv as there was no requirement by the cell to ramp up expression of a recombinant protein.

The latter screen was insightful as it showed P_{spy}::*gfp* responded specifically to stress arising from impairment of translocation. Further, assaying cells with RB + PMBN could potentially be utilised to screen for novel mutations which promote more efficient export under stress when combined with methods for detection of periplasmic localisation

(Osgerby and Overton, 2023). We also found the P_{spy}::*gfp* sensor was switched on in a Δ*tolC* strain and considerably more so than in Δ*acrA* and Δ*acrB* strains. Besides complex in the AcrAB-TolC RND efflux pump (Alav et al., 2021), TolC forms the OM part of other efflux pumps (Zgurskaya et al., 2011) so presumably its loss is more problematic. Previously a Δ*tolC* strain was shown to switch on expression of P_{spy} (Rosner and Martin, 2013); this was suggested as being CpxA-dependent and due to the iron chelating compound enterobactin (Guest et al., 2019).

P_{spy}::*gfp* responded well to the target stress but could potentially be optimised further; mean green fluorescence being elevated in the absence target stressors. P_{spy} is regulated by two systems, BaeSR and CpxAR, with the former apparently not activated by recombinant protein stress (Leblanc et al., 2011). Truncations to P_{spy} and removal of BaeR or CpxA binding sites were shown to alter induction of the promoter to stressors the WT responded to (Srivastava et al., 2014). This could potentially reduce off target induction of the system. Other stress response promoters could presumably provide comparable utility for detection of periplasmic stress, particularly those regulated by σ^E and CpxAR pathways (Mutalik et al., 2009, Raivio, 2014). Besides promoters encoding sRNAs like MicA and RybB (Thompson et al., 2007, Udekwu and Wagner, 2007) σ^E target promoters that are strongly upregulated include those for: the protease DegP (Huber and Bukau, 2008); a phospholipid biogenesis protein, PlsB (Noga et al., 2020); MdoG, involved in periplasmic glucan synthesis (Hanoulle et al., 2004) and RpoE itself (Mutalik et al., 2009), although the latter is activated by several regulators (Gopalkrishnan et al., 2014). Highly upregulated (Price and Raivio, 2009) CpxAR target promoters potentially of interest include those for: LdtC, required for cell

wall biosynthesis (Sanders and Pavelka, 2013); the PPIase PpiA (Justice et al., 2005); and YccA, a regulator of the protease FtsH (Kihara et al., 1995).

Nevertheless, P_{spy} appeared to be triggered as intended and was combined with the ligand unresponsive derivative $LacI^{R197G}$ to create a feedback system for regulating export of RPP. $LacI^{R197G}$ and $LacI^{T276F}$ were extremely effective in shutting off expression from T7 promoters and we demonstrated their own application in tuning protein expression. Many ligand insensitive variants of LacI have been reported (Markiewicz et al., 1994); in general mutagenesis of residues within the inducer binding pocket that interact with IPTG are capable of abolishing inducibility (Daber et al., 2009). Indeed R197 can also be mutagenised to leucine or lysine with similar effect (Spotts et al., 1991). Further the C43(DE3) strain (Miroux and Walker, 1996), well known for tolerance to expression of otherwise recalcitrant membrane protein contains the ligand unresponsive V192F mutation in the chromosomal copy of *lacI* (Kwon et al., 2015). Due to the tight regulation of $LacI^{R197G}$ to operator sequences, we tried attaching an SsrA tag to the C-terminus to eventually facilitate system turnover of our feedback loop, as had been done prior (Dragosits et al., 2012).

When assaying SsrA degradation tags, we found that expression of msfGFP, repressed by L-arabinose induced $LacI^{R197G}$-M increased over time, suggesting a drop in repression (section 5.6). We expected msfGFP expression to be more stable over time and considered whether metabolism of L-arabinose by the host may have occurred; supplementation with additional arabinose at 3 h post-induction had little effect on msfGFP expression though. It is possible entry of L-arabinose into cells

changes over time, AraE and AraF promoters have been shown to reach peak activity during exponential growth and decrease in stationary phase (Madar et al., 2013); although, induction of P_{araBAD} is possible during stationary phase (Kasli et al., 2019). As we discussed in section 5.6.3, it would be prudent to probe the permanency of repression from $LacI^{R197G}$, with and without the SsrA tags, using a pulse chase experiment to remove L-arabinose after induction.

The alternative is increased degradation of the SsrA tag during stationary phase and this has been suggested before (Farrell et al., 2005), although there are conflicting reports on this (Lies and Maurizi, 2008). SsrA tags are primarily degraded by the ClpXP complex (Lies and Maurizi, 2008), but other AAA+ proteases are purported to degrade SsrA tagged polypeptides including ClpAP (Farrell et al., 2005) and Lon (Choy et al., 2007). Specifically ClpAP degradation was shown to increase during stationary phase (Farrell et al., 2005). An alternative degradation system could employ something similar to (Cronan and Kuzminov, 2024). SspB enhances delivery of SsrA tagged substrates to ClpXP (Levchenko et al., 2000). SsrA tags dependent on SsrB were devloped (McGinness et al., 2006); by using tight inducible promoter to control SsrB expression, degradation rates of SsrA tags could be controlled (Cronan and Kuzminov, 2024).

The final part of this work encompassed feedback control using P_{spy}::*lacI*^{R197G} to regulate T7*lac* driven expression of $PelB^{SP}$::msfGFP and $DsbA^{SP}$::msfGFP. A summary table is provided (Table 5.1), highlighting the performance of the P_{spy} negative feedback construct when used to regulate expression of model recombinant

Table 5.1: Performance of the P_{spy} negative feedback construct.

In section 5.8, a P_{spy} negative feedback construct was used to regulate expression of msfGFP, PelB^{SP}::msfGFP and DsbA^{SP}::msfGFP from T7*lac* constructs. As a measure of performance, data is provided for various assays used during analysis at 5 h post-induction and compared with data from strains not harbouring the feedback construct. Green fluorescence is provided to assess whether feedback improved expression of target proteins, OD_{600} and cell density provide a measure of whether growth characteristics improved, and PI staining used to infer any loss of membrane integrity which may be indicative of non-viable cells.

Performance	msfGFP	P_{spy} Sensor Construct + msfGFP	PelBSP::msfGFP	P_{spy} Sensor Construct + PelB^{SP}::msfGFP	DsbASP::msfGFP	P_{spy} Sensor Construct + DsbA^{SP}::msfGFP
Mean Green Fluorescence (AU)	95347.50	353.50	151978.00	479.00	25230.50	889.00
OD_{600}	3.52	5.74	2.93	5.04	0.45	5.37
Cell Density (cells mL^{-1})	6.49E+09	4.17E+09	1.82E+09	3.13E+09	2.96E+08	6.25E+09
Cells stained PI+ (%)	0.80	0.33	37.77	0.25	18.36	0.68

proteins msfGFP, PelBSP::msfGFP and DsbASP::msfGFP from T7lac constructs in section 5.8. As a measure of performance, data is provided for various assays used during analysis at 5 h post-induction and compared with data from strains not harbouring the feedback construct. We found that co-expression of the P_{spy} negative feedback construct greatly improved host physiology, based on OD_{600}, cell density and membrane integrity assayed via PI staining. This appeared to be predominantly due to hugely reduced msfGFP expression, based on green fluorescence analysis, in strains co-expressing the P_{spy} negative feedback construct. However, as evidenced in Table 5.1, green fluorescence and thus msfGFP expression was reduced to levels too low for RPP by the P_{spy} negative feedback construct. This was because while we had a strong system off switch in $LacI^{R197G}$, there was little ability for turnover without the presence of an SsrA degradation tag.

In addition, it was found that from 1 h post-induction green fluorescence in cultures co-expressing the P_{spy} negative feedback construct increased, reaching around 10000 AU by 24 h post-induction; this was comparable with non-repressed $PelB^{SP}$ and $DsbA^{SP}$ controls. This indicated a loss of control. This also occurred during initial experiments using $PelB^{SP}$::anti-IL-1β scFv to induce P_{spy}::*gfp*, suggesting P_{spy} activity changed once cells had entered stationary phase. In addition to being regulated by BaeSR and CpxAR, P_{spy} is a σ^{70}-dependent (RpoD) promoter (Srivastava et al., 2014, Salgado et al., 2024). During stationary phase intracellular RpoD concentration is reduced and σ^{38} (RpoS) becomes the predominant sigma factor (Battesti et al., 2011, Schellhorn, 2020). It is possible lower RpoD concentration accounted for apparent lower activity of P_{spy}; however, when treating cells expressing P_{spy}::*gfp* with 4 % (v/v) ethanol, green

fluorescence remained high at 24 h. Its possible addition of ethanol had some effect on induction of RpoS, preventing its expression from being fully switched on as was shown previously (Cao et al., 2017).

We also found that P_{spy}::*lacI*^{R197G} was active in cultures expressing cytoplasmic msfGFP. While it is possible leakage occurred from the cytoplasm and activated P_{spy} (Morra et al., 2018), an important control for future development of the system will be to use the P_{spy}::*gfp* biosensor to monitor expression of cytoplasmic proteins. In addition, to better understand the nature of WT P_{spy} activity during various growth phases, with and without external stressors, RT-qPCR could be used to quantify mRNA transcripts (Nagao et al., 2023). A final consideration is engineering the dynamics of the system, first at the transcriptional level via promoter modification to alter P_{spy} performance. Promoters can be tuned in different ways such as modification of the -35 and -10 hexamers to change closeness to the consensus, improving or reducing recruitment of RNA polymerase (Li and Zhang, 2014, Einav and Phillips, 2019). Spacing between -35 and -10 hexamers also affects performance, 17 bp +/- 1 bp generally considered optimal (Klein et al., 2021, Forquet et al., 2022). In P_{spy}, addition and removal of CpxAR and BaeSR sites was shown to alter response to different stressors (Srivastava et al., 2014). Finally, modification of the TIR to tune translation of the downstream repressor would affect system dynamics (Vimberg et al., 2007), and this was used during optimisation of a cytoplasmic negative feedback loop (Dragosits et al., 2012). Such tuning should encompass the Shine-Dalgarno (SD) sequence (Chen et al., 1994), start codon (Gren, 1984), and any upstream (Hook-Barnard et al., 2007) or downstream (Stenström and Isaksson, 2002) enhancers.

5.10 Conclusion

The aim of this project was to develop a system able to detect stress arising during periplasmic overexpression of a recombinant protein, then exploiting this sensing capability as a trigger to tune expression to a physiologically tolerable level via negative feedback. As such, we have evaluated the use of different biosensors for detection of stress arising from export of recombinant proteins to the bacterial periplasm. In addition, we have attempted to optimise various that would be required for construction of a feedback loop.

We found that application of SecM-GFP as a monitor for saturation of Sec did not result in high enough levels of GFP expression to be exploited as a trigger. Further optimisation of the system to improve response may be possible through engineering the translation initiation region. As an alternative system, a P_{spy}::*gfp* biosensor was found to respond to the intended periplasmic recombinant protein signal and supports the identification and exploitation of other stress response promoters that could be used to detect and report on various perturbations to host physiology during RPP. Further, a novel assay using RB to measure P_{spy} performance could potentially be exploited in other ways to screen for mutations which promote more efficient export under stress.

To create a feedback system utilising P_{spy} as a trigger, ligand unresponsive variants of LacI were analysed to control expression of T7*lac* and were shown to be an extremely effective off switch. For system turnover, we were unable to engineer effective turnover due to increasing degradation rates from SsrA tags over time. Further work will be

required to assess the dynamics of repression when using ligand unresponsive LacI. Firstly, probing inducible expression $LacI^{R197G}$ with and without SsrA tags using a pulse chase experiment, to observe the dynamics of repression over time. Tuneable degradation must also be explored; if the rate at which de-repression of the system occurs can be modulated, this would offer far more control over system turnover during optimisation of different recombinant proteins.

To create a negative feedback loop, P_{spy} was utilised alongside untagged ligand unresponsive LacI as a system proof of concept. Here we found feedback control was switched on in response to overexpression of periplasmic recombinant proteins. Given the lack of system turnover due to an absence of any degradation tag, expression of the target recombinant protein GFP was reduced to levels not suitable for RPP. However, host physiology was greatly improved during feedback control and certainly cements the potential for the use of such systems during RPP, particularly when expression is otherwise detrimental to the host. It was also found that expression from the trigger used for feedback, the P_{spy} promoter, appeared to decrease over time resulting in a loss of repression. Hence, further engineering will be required to alter the dynamics of the system.

A final point is that the P_{spy} trigger was also switched-on during overexpression of cytoplasmic recombinant proteins. Certainly, future work must analyse the response of the P_{spy}::GFP sensor to cytoplasmic overexpression. Meanwhile, construction of a cytoplasmic sensor and analysing its response to periplasmic overexpression would be illuminating. Though, given the considerable overlap between stressors imposed

upon cells by recombinant proteins regardless of the compartment they are directed to, it may be difficult to develop a system which only responds to one stressor. However, given the intended periplasmic recombinant protein stress was detected and showed that utilising this to tune expression resulted in improved host physiology, we believe this work met many of our initial aims and objectives and provides a solid platform for future work.

Chapter 6: General conclusions and future work

E. coli has a long history of use as a host for RPP and was used to synthesise the first recombinant protein somatostatin (Itakura et al., 1977). More recently, due to their ability to synthesise many post-translational modifications (Jenkins et al., 2008), mammalian hosts have become preferred for biotherapeutic production, used for the synthesis of over 40% of approved biotherapeutics (Walsh and Walsh, 2022). However, *E. coli* is still hugely relevant due to its amenable processing characteristics (Overton, 2014, Rosano and Ceccarelli, 2014). Further, access to the Dsb system (Bardwell et al., 1993) via export to the periplasm allows *E. coli* to synthesise disulphide bonds required for many complex recombinant proteins (Berkmen, 2012, Rathore and Batra, 2016).

During the aims and objectives section of this work (section 1.7), we identified several areas of research that would be useful to further improve and optimise RPP in *E. coli*. Within this thesis we have presented the results from three areas of research including optimising the use of a novel urea inducible promoter (Hothersall et al., 2022b), evaluating the applicability of oxidation resistant GFP derivatives for use as a periplasmic screening tool (Osgerby and Overton, 2023), and development of biosensors able to detect stress arising from periplasmic expression and attempting to exploit this as a negative feedback loop. This chapter will be used to summarise the findings and conclusions of the three areas of research and discuss future work applicable to each.

6.1 Urea inducible promoter

Many available inducible systems for RPP often have caveats with their use. The most common include *lac* promoters along T7 expression systems, both of which suffer from high basal expression (Spehr et al., 2000). Others like P_{araBAD} promoter tuned on a per cell basis due to all-or-nothing induction (Siegele and Hu, 1997, Carrier and Keasling, 1999). Meanwhile many inducers have considerable costs associate with their use, IPTG being over £20000 kg^{-1} and requires an appropriate cold chain for stability.

Hence, in chapter 3 of this work, we evaluated and optimised a novel urea inducible promoter P_{uti101}, originally from *P. mirabilis* (Hothersall et al., 2022b). Being central to any expression system (Giacalone et al., 2006, Wittmann et al., 2008, Zhao et al., 2021, García-Calvo et al., 2023), there was an obvious desire to evaluate a new inducible promoter and determine its functionality in RPP. Further, the orthologous nature of the system was attractive given many *E. coli* strains used in RPP are unable to metabolise urea (Konieczna et al., 2012). To explore the use of P_{uti101}, GFP was used as a reporter and combined with FCM analysis to observe expression at the single cell level and detect any heterogeneity arising from the inducer urea, or characteristics of P_{uti101}. Using these methods, sue of P_{uti101} for RPP was optimised from flask through to bioreactor scale. Various parameters which govern the properties of an inducible system were tested and will be discussed in turn.

Our first finding from this work was on the strength of expression from the urea inducible system (sections 3.3.1, 3.3.2, 3.4.3). P_{uti101} appeared to drive expression comparable with the novel lacUV5 derivative PAR4 (Browning et al., 2019), which while

weaker than the WT, is still stronger than the *lac* promoter. However, based on work in chapter 4, P_{uti101} was weaker than a T7*lac* promoter. This is not necessarily bad, the extreme levels of transcription generated by T7 systems quickly saturates translation machinery preventing expression of native proteins (Sastry and Ross, 1997). In such cases, this often to the determent of the host and final titre of recombinant protein. This is due to upregulation of multiple stress responses (Hoffmann et al., 2004), including the general stress response (Battesti et al., 2011), the heat shock response is mediated (Arsène et al., 2000) and the stringent response (Haseltine and Block, 1973).

Another consideration was tunability and whether the dose of urea used had a linear relationship with expression. This is important because it allows more precise control over the level of expression depending on the recombinant protein being used (Marschall et al., 2017). We found that P_{uti101} was not particularly dose-dependent and differences in expression were only notable between much lower and higher concentrations (section 3.3.1, 3.4.3). While it appeared expression could be switched on with as little as 1 mM urea, in general, we found that at around 50 mM – 100 mM urea, a threshold was reached. Increasing the concentration to 250 mM – 500 mM urea resulted in either diminishing increases in expression or negatively affected it (Figure 3.54). However, this was when expressing GFP and may be different when a more difficult to express protein is used. Future work should certainly prioritise evaluating expression of a more industrially relevant recombinant protein and the optimisation done in this work will help to facilitate that. In addition, engineering of P_{uti101} to possibly improve tunability should be considered. P_{uti101} regulated at two separate points, positively by UreR when bound to urea (Thomas and Collins, 1999) and negatively by

the global regulator H-NS (Coker et al., 2000). UreR and H-NS appear to compete for binding of an intergenic region between *ureR* and P_{uti101} promoters (Poore and Mobley, 2003). Modification of this region to make HN-S binding less favourable increases the systems dependence on urea potentially altering tunability, but at the expense of overall regulation.

Tight regulation was in fact found to be a major advantage of the urea inducible promoter (sections 3.3.4 and 3.4.5). Here we observed that in the absence of urea, basal expression of GFP from P_{uti101} resulted in only 2 to 3-fold higher fluorescence than the autofluorescence untransformed cells. Further, basal expression remained constantly low throughout culture and was not impacted by scaling the system. Overall basal expression was comparable with the tightly regulated P_{araBAD} promoter (chapter 4). Compared with something like a T7*lac* promoter (chapter 4), basal expression from P_{uti101} was around 35-fold lower. Given this, care must be taken when attempting to tune the promoter so as not to dramatically increase basal expression.

With how tightly regulated P_{uti101} appeared, it would have been ideal in some instances to uncouple protein expression from biomass accumulation. This is useful when a recombinant protein is toxic, allowing cultures to reach a high biomass before inducing expression can greatly improve titres (Ou et al., 2004). However, we observed that P_{uti101} activity decreased considerably when inducing at OD_{600} 5 or 10, compared with inducing at OD_{600} 0.5. During flask work (section 3.4.6), early induction typically resulted in over double the green fluorescence compared with late induction. Similarly,

during bioreactor scale-up, late induction (section 3.5.1) resulted in around a 6-fold lower maximum green fluorescence compared with early induction (section 3.5.2).

It is possible urea uptake was reduced at OD_{600} 5 or 10 as cells were in stationary phase. It has been shown before the permeability to various chemicals is changes in the latter stages of growth (Whittle et al., 2021). Alternatively the systems negative regulator H-NS may be more active in stationary phase although there are reports lower (Falconi et al., 1993, Free and Dorman, 1995) and higher (Dersch et al., 1993, Ueguchi et al., 1993) in stationary phase cells. In future work it would be interesting to see how induction changes in a HN-S knockout although given the global activity of H-NS, such a strain would likely not be useful for RPP (Dorman, 2004).

During this work we tested concentrations of urea up to 500 mM using untransformed cells to ascertain its effect. Urea is chaotropic and is commonly used to denature proteins, albeit at high concentrations. We found that even at 500 mM, there appeared to be little effect of urea on the growth of cells that would indicate poor tolerance to the inducer (section 3.2.1 and 3.4.1). One interesting observation was that in both JCB387 and BL21 cells overexpressing GFP and induced with 500 mM urea, higher forward scatter was found during FCM analysis (section 3.2.2). During microscopy analysis, cells were highly filamented, but these effects were not particularly noticeable in untransformed cells. Similarly, at concentrations of 50 – 100 mM and high level GFP expression, we did not observe higher forward scatter values. There seemed to be some combined effect between 500 mM urea and overexpression of GFP which contributed to the increased cell size. Perhaps at such high urea concentrations,

osmolarity was more problematic to cells undergoing expression. However, induction with 500 mM urea was found to offer little benefit over lower concentrations so is not particularly relevant to RPP.

6.2 Periplasmic screening tools

In *E. coli* optimising of the overexpression of proteins within the cytoplasm is well studied (Sorensen and Mortensen, 2005, Overton, 2014, Rosano and Ceccarelli, 2014, Zhang et al., 2022). However, expression of recombinant proteins within the periplasm offers several advantages, primarily access to the Dsb system (Bardwell et al., 1991), but also lower concentrations of proteases (Talmadge and Gilbert, 1982) and simpler purification (Schimek et al., 2020). Due to this, periplasmic expression is attractive for biotherapeutic production in *E. coli*, with disulphide bonding being essential for many (Berkmen, 2012). One issue with expressing recombinant proteins in the periplasm is how to easily quantify the levels that have accumulated. Traditionally, fractionation and SDS PAGE have been used but such methods are time consuming and prevent high throughput approaches.

Hence, in chapter 4 of this work, we attempted to develop a screening tool utilising GFP derivatives resistant to oxidising environments. Most GFP derivatives exported in an unfolded state are non-fluorescent in the periplasm, due misfolding via activity of the Dsb system on cysteine residues (Jain et al., 2001, Dammeyer and Tinnefeld, 2012). The derivative msfGFP had been shown previously to fluoresce in the periplasm, due to improved folding kinetics, so we were interested in whether it could be used for screening (Aronson et al., 2011, Dinh and Bernhardt, 2011). To do so, we

constructed a suite of msfGFP expression vectors directing it for export to the periplasm via PelB or DsbA signal peptides.

We found that overexpression of PelB^{SP}::msfGFP or DsbA^{SP}::msfGFP using a T7*lac* promoter was deleterious to growth (section 4.2.1). During FCM analysis, we stained cells using PI to monitor viability and found that anywhere from 10 – 30 % of cells stained as PI+ shortly after induction. This indicated cells expressing PelB^{SP}::msfGFP or DsbA^{SP}::msfGFP had possibly lost membrane integrity and were non-viable. However, it is worth noting some of the limitations of PI. It is frequently used to measure cell viability, it has been used regularly to quantify this using FCM (Steinkamp et al., 1999, Crowley et al., 2016) and is available as commercial kits to do so. PI is a DNA intercalating agent which is not permeable to cells with intact membranes. Upon binding DNA fluorescence is greatly increased, hence PI is a measure of cell permeability. The assumption is that cells which have lost membrane integrity are not viable although it has been shown previously that reversal of this is possible (Davey and Hexley, 2011, Yang et al., 2015). Thus, while PI data must be interpreted with caution, combined with growth analysis, it became clear that neither PelB^{SP}::msfGFP or DsbA^{SP}::msfGFP were well tolerated.

Given the high basal expression observed using T7*lac* (section 4.2.2) and poor tolerance to overexpression of PelB^{SP}::msfGFP or DsbA^{SP}::msfGFP, we tried using the more tightly regulated P_{araBAD} promoter (Guzman et al., 1995) to drive expression (section 4.3). Predictably, basal expression in uninduced cells was low, but upon induction of PelB^{SP}::msfGFP or DsbA^{SP}::msfGFP, we still found BL21 cells exhibited

extremely poor growth with high levels of cells stained as PI+. However, utilising the P_{araBAD} expression systems combined with SIM analysis of cells stained with Nile red, we were able to potentially support prior work (Aronson et al., 2011, Dinh and Bernhardt, 2011) that msfGFP is fluorescent in the periplasm (section 4.5.2).

Attempts to tune expression of P_{araBAD} further using lower concentrations of L-arabinose were not successful, as while growth improved considerably, populations of higher and lower expression were evident at the single cell level. Such heterogeneity in expression is well known with P_{araBAD} though (Siegele and Hu, 1997). Further, having to restrict expression to such low levels is not viable for a screening tool. Using the P_{araBAD} system we tried using a different GFP derivative which was resistant to oxidising environments via a different mechanism to msfGFP. The cfSGFP2 derivative is devoid of cysteine residues and was shown to fluoresce in mammalian oxidising environments comparable to the periplasm (Suzuki et al., 2012). However, expression was extremely poor and even given this, we still found cell growth to be affected (section 4.4).

Using both T7*lac* and P_{araBAD} expression systems (section 4.2 and 4.3), we attempted to determine the level of msfGFP that was exported via fusion to PelB or DsbA signal peptides using fractionation and SDS PAGE. While there were bands observed consistent with msfGFP in periplasmic fractions, we consistently saw that in samples taken from cytoplasmic msfGFP control cultures, there was leakage into the periplasmic fraction. It is possible the fractionation method was not effective for cells highly stressed during RPP although this has been used previously (Selas Castiñeiras

et al., 2018a). An alternative is that is was shown that during overexpression, due to translational stress, cytoplasmic proteins can be excreted across the IM and OM without interaction with export machinery (Morra et al., 2018).

Another issue in both T7*lac* and P_{araBAD} systems is that consistently during fractionation and SDS PAGE analysis, the proportion of msfGFP found within the periplasm was typically around 20%. If efficiency for export using these systems is so low, they are not suited for screening. Prior work also using $DsbA^{SP}$, achieved over 60% of the expressed recombinant protein as periplasmic (Horga et al., 2018). Although this work utilised a novel system to harmonise transcription, translation and export along with fed-batch fermentation. It is clear from our work that any future attempts to develop a screening tool must at the least utilise highly tuneable systems, one example being the rhamnose inducible promoter which is extremely dose dependent and tightly regulated (Hjelm et al., 2017, Karyolaimos et al., 2019a). However, given the observed poor tolerance to msfGFP export, even systems like this may not be useful. Instead, there are other periplasmic screening tools which we reviewed as part of this work which have been shown to be more effective (Osgerby and Overton, 2023).

6.1 Biosensors and negative feedback loops

In Chapter 4 we attempted to use novel GFP derivatives such as msfGFP, resistant to folding in oxidative environments (Aronson et al., 2011, Dinh and Bernhardt, 2011, Suzuki et al., 2012), to screen for localisation of recombinant proteins to the *E.* coli periplasmic space. This proved difficult due to poor growth of cells following expression of exported msfGFP. As has been previously suggested (Schlegel et al., 2013,

Baumgarten et al., 2018), high level expression of a recombinant protein directed to the periplasm quickly saturates translocation machinery, preventing export of native proteins and leading to cell death. Thus, we wondered whether we could detect stress arising from export of recombinant proteins and use this to modulate expression accordingly.

Hence in chapter 5 of this work, our aim was to determine whether we could create a sensor which would firstly report on stress associated with periplasmic expression. This sensor would then be used as a trigger to initiate a feedback response to shut off expression until stress levels dropped. Feedback loops for RPP had been generated previously in *E. coli* for cytoplasmic (Dragosits et al., 2012) and membrane proteins (Guidi et al., 2022), but not for periplasmic proteins. We determined that for the feedback loop we would need a sensing component acting as the trigger, a repressor to serve as an off switch, and a degradation tag to allow system turnover.

We initially looked at SecM for use as sensing component of our system. Natively SecM fulfils a similar role, it is responsible for detecting saturation of SecYEG (Nakatogawa and Ito, 2002) and responding by translationally upregulating the driving force behind export, SecA (Ambroziak et al., 2021). SecM and SecA are transcribed together (Oliver et al., 1998), and the presence of an mRNA hairpin conceals the SecA RBS (McNicholas et al., 1997). During export of SecM, if translocation is prevented due to saturation, an arrest sequence on the SecM mRNA causes the ribosome to stall, disrupting the hairpin and allowing access to the SecA RBS (Nakatogawa and Ito, 2002). We cloned *secM* up to the *secA* start codon and inserted GFP in its place.

However, when we probed its response using an exported PelB^{SP}::anti-IL-1β scFv, we did not see any meaningful response in green fluorescence (section 5.2.2). We had cloned the SecM-GFP sensor onto a low copy pRW50 plasmid (Lodge, 1992) and considered whether the gene dose was high enough. Alternatively, given recent reports have indicated the number of copies of SecA within the cell are around 86 – 154 copies (Seinen et al., 2021), it could be that SecM does not need to direct strong translation. However, future work on this system should evaluate the effect of the TIR (Vimberg et al., 2007). As we replaced SecA with GFP, this will have altered the TIR and given this is a rate limiting step in translation (Reeve et al., 2014), could have affected expression.

We shifted our attention to the P$_{spy}$ promoter from the periplasmic chaperone Spy which is massively upregulated during envelope stress (Hagenmaier et al., 1997, Garbe et al., 2000, Bury-Moné et al., 2009, Quan et al., 2011, He et al., 2021). P$_{spy}$ is regulated by both CpxAR and BaeSR stress responses (Koldewey et al., 2016, Kwon et al., 2010, Mitra et al., 2021). We found that P$_{spy}$::*gfp* was shown to respond to overexpression of a PelB^{SP}::anti-IL-1β scFv (section 5.4.1) and the SecA inhibitor RB when delivered in combination with PMBN (Hsieh et al., 2014, Jin et al., 2016) (Section 5.4.2). We also found that P$_{spy}$ responded to deletion of TolC (section 5.4.2); given this we feel future work should look at other stressors the P$_{spy}$::*gfp* sensor responds to.

With a potential trigger identified, we began to look at potential repressors for use as an off switch. We chose ligand unresponsive derivatives of LacI, LacI^{R197G} (Spotts et al., 1991) and LacI^{T276F} (Suckow et al., 1996). Through inducible expression from

P_{araBAD} both variants of LacI ligand unresponsive were shown to be extremely effective in shutting off expression of msfGFP from a T7*lac* promoter (section 5.6.1) and there was little difference between the two. We selected the $LacI^{R197G}$ variant to take forward and attached an SsrA tag to the C-terminus so any eventual feedback loop would have sufficient turnover. This degradation tag was a modified variant of the SsrA tag with the sequence AANDENYADAS was selected; shown to have medium rates of degradation and far lower than the WT (Klimecka et al., 2021). Upon testing this, based on increases in green fluorescence, we observed that the degradation rate of the tagged variant $LacI^{R197G}$-M appeared to increase over time (section 5.6.2). L-arabinose metabolism by the BL21 host was thought of as a potential cause (Stargardt et al., 2021), lower inducer availability meaning less $LacI^{R197G}$-M was expressed over time. However, supplementing cultures with additional L-arabinose did little to change the increasing degradation rate (section 5.6.3).

It is possible entry of L-arabinose into cells changes over time, AraE and AraF promoters have been shown to reach peak activity during exponential growth and decrease in stationary phase (Madar et al., 2013). Similarly, increased degradation of the SsrA tag by ClpXP could have occurred (Farrell et al., 2005), although there are conflicting reports on whether this is true (Lies and Maurizi, 2008). An essential experiment for future work would be to utilise a pulse chase experiment to remove L-arabinose shortly after induction and observe permanency of $LacI^{R197G}$ repression with and without the degradation tag.

As we were not confident in the degradation tags performance, we decided to test the proof of concept of the feedback system without them attached to $LacI^{R197G}$. Thus, $LacI^{R197G}$ was inserted downstream of P_{spy} to create a feedback construct and assayed against $PelB^{SP}$::msfGFP and $DsbA^{SP}$::msfGFP constructs generated during chapter 4 of this work. We found that the P_{spy} feedback construct responded to induction by shutting off expression of $PelB^{SP}$::msfGFP or $DsbA^{SP}$::msfGFP based on a drop in green fluorescence (section 5.8). Further, based on analysis of growth and PI staining, physiology of cells co-expressing the P_{spy} feedback construct was greatly improved. However, this was presumably because expression was mostly shut off due to the lack of any degradation tag for system turnover. Still this clearly provided a good proof of concept that feedback control could be utilised to improve host physiology in response to overexpression of periplasmic recombinant proteins.

One point of concern and something that will need to be addressed in future work was that repression of $PelB^{SP}$::msfGFP and $DsbA^{SP}$::msfGFP by the P_{spy} feedback construct appeared to decrease over time. In addition to being regulated by BaeSR and CpxAR, P_{spy} is a σ^{70}-dependent (RpoD) promoter (Srivastava et al., 2014, Salgado et al., 2024). During stationary phase σ^{38} (RpoS) predominates (Battesti et al., 2011, Schellhorn, 2020) which could have accounted for lower P_{spy} activity over time. It would be prudent to assay WT P_{spy} activity during various growth phases, with and without external stressors using RT-qPCR to quantify mRNA transcripts (Nagao et al., 2023).

Finally future work to the system, preferably once suitable turnover of the system has been developed must look to engineer the overall dynamics. Firstly, via promoter

modification to alter P_{spy} performance such as altering the -35 and -10 hexamers to change closeness to the consensus, improving or reducing recruitment of RNA polymerase (Li and Zhang, 2014, Einav and Phillips, 2019). Finally, modification of the TIR to tune translation of the downstream repressor would affect system dynamics (Vimberg et al., 2007), and this was used during optimisation of a cytoplasmic negative feedback loop (Dragosits et al., 2012).

Chapter 7: References

ABABI, M., TRIDGETT, M., OSGERBY, A. & JARAMILLO, A. 2022. Scarless Recombineering of Phage in Lysogenic State.

ABRAMSON, J., SMIRNOVA, I., KASHO, V., VERNER, G., IWATA, S. & KABACK, H. R. 2003. The lactose permease of Escherichia coli: overall structure, the sugar-binding site and the alternating access model for transport. *FEBS Letters,* 555**,** 96-101.

ADAMS, S. R., CAMPBELL, R. E., GROSS, L. A., MARTIN, B. R., WALKUP, G. K., YAO, Y., LLOPIS, J. & TSIEN, R. Y. 2002. New Biarsenical Ligands and Tetracysteine Motifs for Protein Labeling in Vitro and in Vivo: Synthesis and Biological Applications. *Journal of the American Chemical Society,* 124**,** 6063-6076.

ADES, S. E., CONNOLLY, L. E., ALBA, B. M. & GROSS, C. A. 1999. The Escherichia coli sigma E-dependent extracytoplasmic stress response is controlled by the regulated proteolysis of an anti-sigma factor. *Genes & Development,* 13**,** 2449-2461.

AFROZ, T., BILIOURIS, K., KAZNESSIS, Y. & BEISEL, C. L. 2014. Bacterial sugar utilization gives rise to distinct single-cell behaviours. *Molecular Microbiology,* 93**,** 1093-1103.

AKOPIAN, D., SHEN, K., ZHANG, X. & SHAN, S.-O. 2013. Signal Recognition Particle: An Essential Protein-Targeting Machine. *Annual Review of Biochemistry,* 82**,** 693-721.

AKSNES, H., REE, R. & ARNESEN, T. 2019. Co-translational, Post-translational, and Non-catalytic Roles of N-Terminal Acetyltransferases. *Molecular Cell,* 73**,** 1097-1114.

ALAV, I., KOBYLKA, J., KUTH, M. S., POS, K. M., PICARD, M., BLAIR, J. M. A. & BAVRO, V. N. 2021. Structure, Assembly, and Function of Tripartite Efflux and Type 1 Secretion Systems in Gram-Negative Bacteria. *Chem Rev,* 121**,** 5479-5596.

ALBA, B. M., LEEDS, J. A., ONUFRYK, C., LU, C. Z. & GROSS, C. A. 2002. DegS and YaeL participate sequentially in the cleavage of RseA to activate the sigma(E)-dependent extracytoplasmic stress response. *Genes & Development,* 16**,** 2156-2168.

AMBROZIAK, P., RZEPKA, I. & SKORKO-GLONEK, J. 2021. SecA – a multidomain and multitask bacterial export protein. *Acta Biochimica Polonica,* 68.

ANDERSEN, J. B., STERNBERG, C., POULSEN, L. K., BJØRN, S. P., GIVSKOV, M. & MOLIN, S. 1998. New Unstable Variants of Green Fluorescent Protein for Studies of Transient Gene Expression in Bacteria. *Applied and Environmental Microbiology,* 64**,** 2240-2246.

ANTON, B. P. & RALEIGH, E. A. 2016. Complete Genome Sequence of NEB 5-alpha, a Derivative of Escherichia coli K-12 DH5α. *Genome Announc,* 4.

ARDITO, F., GIULIANI, M., PERRONE, D., TROIANO, G. & LO MUZIO, L. 2017. The crucial role of protein phosphorylation in cell signaling and its use as targeted therapy (Review). *Int J Mol Med,* 40**,** 271-280.

ARDITTI, R. R., SCAIFE, J. G. & BECKWITH, J. R. 1968. The nature of mutants in the lac promoter region. *Journal of Molecular Biology,* 38**,** 421-426.

ARNESEN, T. 2011. Towards a Functional Understanding of Protein N-Terminal Acetylation. *PLoS Biology,* 9**,** e1001074.

ARONSON, D. E., COSTANTINI, L. M. & SNAPP, E. L. 2011. Superfolder GFP Is Fluorescent in Oxidizing Environments When Targeted via the Sec Translocon. *Traffic,* 12**,** 543-548.

ARSÈNE, F., TOMOYASU, T. & BUKAU, B. 2000. The heat shock response of Escherichia coli. *International Journal of Food Microbiology,* 55**,** 3-9.

ASSENBERG, R., WAN, P. T., GEISSE, S. & MAYR, L. M. 2013. Advances in recombinant protein expression for use in pharmaceutical research. *Current Opinion in Structural Biology,* 23**,** 393-402.

AUCLAIR, S. M., BHANU, M. K. & KENDALL, D. A. 2012. Signal peptidase I: Cleaving the way to mature proteins. *Protein Science,* 21**,** 13-25.

BAESHEN, M. N., AL-HEJIN, A. M., BORA, R. S., AHMED, M. M., RAMADAN, H. A., SAINI, K. S., BAESHEN, N. A. & REDWAN, E. M. 2015. Production of Biopharmaceuticals in E. coli: Current Scenario and Future Perspectives. *J Microbiol Biotechnol,* 25**,** 953-62.

BALZER, S., KUCHAROVA, V., MEGERLE, J., LALE, R., BRAUTASET, T. & VALLA, S. 2013. A comparative analysis of the properties of regulated promoter systems commonly used for recombinant gene expression in Escherichia coli. *Microbial Cell Factories,* 12**,** 26.

BARDWELL, J. C., LEE, J. O., JANDER, G., MARTIN, N., BELIN, D. & BECKWITH, J. 1993. A pathway for disulfide bond formation in vivo. *Proceedings of the National Academy of Sciences,* 90**,** 1038-1042.

BARDWELL, J. C. A., MCGOVERN, K. & BECKWITH, J. 1991. Identification of a Protein Required for Disulfide Bond Formation In Vivo. *Cell,* 67**,** 581-589.

BARONE, P. W., WIEBE, M. E., LEUNG, J. C., HUSSEIN, I. T. M., KEUMURIAN, F. J., BOURESSA, J., BRUSSEL, A., CHEN, D., CHONG, M., DEHGHANI, H., GERENTES, L., GILBERT, J., GOLD, D., KISS, R., KREIL, T. R., LABATUT, R., LI, Y., MÜLLBERG, J., MALLET, L., MENZEL, C., MOODY, M., MONPOEHO, S., MURPHY, M., PLAVSIC, M., ROTH, N. J., ROUSH, D., RUFFING, M., SCHICHO, R., SNYDER, R., STARK, D., ZHANG, C., WOLFRUM, J., SINSKEY, A. J. & SPRINGS, S. L. 2020. Viral contamination in biologic manufacture and implications for emerging therapies. *Nature Biotechnology,* 38**,** 563-572.

BATES, A. & POWER, C. A. 2019. David vs. Goliath: The Structure, Function, and Clinical Prospects of Antibody Fragments. *Antibodies,* 8**,** 28.

BATTESTI, A., MAJDALANI, N. & GOTTESMAN, S. 2011. The RpoS-mediated general stress response in Escherichia coli. *Annual Review of Microbiology,* 65**,** 189-213.

BAUMGARTEN, T., YTTERBERG, A. J., ZUBAREV, R. A. & DE GIER, J.-W. 2018. Optimizing Recombinant Protein Production in the Escherichia coli Periplasm Alleviates Stress. *Applied and Environmental Microbiology,* 84**,** e00270-18.

BECKWITH, J. 2013. The Sec-dependent pathway. *Research in Microbiology,* 164**,** 497-504.

BENNION, B. J. & DAGGETT, V. 2003. The molecular basis for the chemical denaturation of proteins by urea. *Proceedings of the National Academy of Sciences,* 100**,** 5142-5147.

BERG, P. & MERTZ, J. 2010. Personal Reflections on the Origins and Emergence of Recombinant DNA Technology. *Genetics,* 184**,** 9-17.

BERINI, F., MARINELLI, F. & BINDA, E. 2020. Streptomycetes: Attractive Hosts for Recombinant Protein Production. *Frontiers in Microbiology,* 11.

BERKMEN, M. 2012. Production of disulfide-bonded proteins in Escherichia coli. *Protein Expr Purif,* 82**,** 240-51.

BERNSTEIN, H. D., PORITZ, M. A., STRUB, K., HOBEN, P. J., BRENNER, S. & WALTER, P. 1989. Model for signal sequence recognition from amino-acid sequence of 54K subunit of signal recognition particle. 340**,** 482-486.

BISSWANGER, H. 2014. Enzyme assays. *Perspectives in Science,* 1**,** 41-55.

BLATTNER, F. R., PLUNKETT, G., 3RD, BLOCH, C. A., PERNA, N. T., BURLAND, V., RILEY, M., COLLADO-VIDES, J., GLASNER, J. D., RODE, C. K., MAYHEW, G. F., GREGOR, J., DAVIS, N. W., KIRKPATRICK, H. A., GOEDEN, M. A., ROSE, D. J., MAU, B. & SHAO, Y. 1997. The complete genome sequence of Escherichia coli K-12. *Science,* 277**,** 1453-62.

BOARETTI, M., LLEÒ, M. M., BONATO, B., SIGNORETTO, C. & CANEPARI, P. 2003. Involvement of rpoS in the survival of Escherichia coli in the viable but non-culturable state. *Environ Microbiol,* 5**,** 986-96.

BOLHUIS, A. 2004. The archaeal Sec–dependent protein translocation pathway. *Philosophical Transactions of the Royal Society of London. Series B: Biological Sciences,* 359**,** 919-927.

BOOS, W. & SHUMAN, H. 1998. Maltose/maltodextrin system of Escherichia coli: transport, metabolism, and regulation. *Microbiology and Molecular Biology Reviews,* 62**,** 204-229.

BORONAT, A. & AGUILAR, J. 1979. Rhamnose-induced propanediol oxidoreductase in Escherichia coli: purification, properties, and comparison with the fucose-induced enzyme. *Journal of Bacteriology,* 140**,** 320-326.

BOWLER, M. W., MONTGOMERY, M. G., LESLIE, A. G. W. & WALKER, J. E. 2006. How azide inhibits ATP hydrolysis by the F-ATPases. *Proceedings of the National Academy of Sciences,* 103**,** 8646-8649.

BRACKEN, H. A. & WOOLHEAD, C. A. 2019. Increased freedom of movement in the nascent chain results in dynamic changes in the structure of the SecM arrest motif. *Biosci Rep,* 39.

BRANDI, A., PON, C. L. & GUALERZI, C. O. 1994. Interaction of the main cold shock protein CS7.4 (CspA) of Escherichia coli with the promoter region of hns. *Biochimie,* 76**,** 1090-1098.

BRAUN, V. 1975. Covalent lipoprotein from the outer membrane of escherichia coli. *Biochimica et Biophysica Acta (BBA) - Reviews on Biomembranes,* 415**,** 335-377.

BRENNAN, R. G. & MATTHEWS, B. W. 1989. The helix-turn-helix DNA binding motif. *J Biol Chem,* 264**,** 1903-6.

BROOKS, S. A. 2004. Appropriate Glycosylation of Recombinant Proteins for Human Use: Implications of Choice of Expression System. *Molecular Biotechnology,* 28**,** 241-256.

BROSIUS, J., ERFLE, M. & STORELLA, J. 1985. Spacing of the -10 and -35 Regions in the Tac Promoter. Effect on Its in Vivo Activity. *Journal of Biological Chemistry,* 260**,** 3539-3541.

BROWN, C. E. & HOGG, R. W. 1972. A Second Transport System for L-Arabinose in Escherichia coli B Controlled by the araC Gene. *Journal of Bacteriology,* 111**,** 606-613.

BROWNING, D. F., GODFREY, R. E., RICHARDS, K. L., ROBINSON, C. & BUSBY, S. J. W. 2019. Exploitation of the Escherichia coli lac operon promoter for controlled recombinant protein production. *Biochemical Society Transactions,* 47**,** 755-763.

BROWNING, D. F., RICHARDS, K. L., PESWANI, A. R., ROOBOL, J., BUSBY, S. J. W. & ROBINSON, C. 2017. Escherichia coli "TatExpress" strains super-secrete human growth hormone into the bacterial periplasm by the Tat pathway. *Biotechnology and Bioengineering,* 114**,** 2828-2836.

BURY-MONÉ, S., NOMANE, Y., REYMOND, N., BARBET, R., JACQUET, E., IMBEAUD, S., JACQ, A. & BOULOC, P. 2009. Global Analysis of Extracytoplasmic Stress Signaling in Escherichia coli. *PLoS Genetics,* 5**,** e1000651.

BUTKUS, M. E., PRUNDEANU, L. B. & OLIVER, D. B. 2003. Translocon "Pulling" of Nascent SecM Controls the Duration of Its Translational Pause and Secretion-Responsive secA Regulation. 185**,** 6719-6722.

BUTLER, M. & SPEARMAN, M. 2014. The choice of mammalian cell host and possibilities for glycosylation engineering. *Current Opinion in Biotechnology,* 30**,** 107-112.

CALLEWAERT, L., VANOIRBEEK, K. G. A., LURQUIN, I., MICHIELS, C. W. & AERTSEN, A. 2009. The Rcs Two-Component System Regulates Expression of Lysozyme Inhibitors and Is Induced by Exposure to Lysozyme. *Journal of Bacteriology,* 191**,** 1979-1981.

CALOS, M. P. 1978. DNA sequence for a low-level promoter of the lac repressor gene and an 'up' promoter mutation. *Nature,* 274**,** 762-765.

CAO, H., WEI, D., YANG, Y., SHANG, Y., LI, G., ZHOU, Y., MA, Q. & XU, Y. 2017. Systems-level understanding of ethanol-induced stresses and adaptation in E. coli. *Scientific Reports,* 7**,** 44150.

CARNEIRO, S., FERREIRA, E. C. & ROCHA, I. 2013. Metabolic responses to recombinant bioprocesses in Escherichia coli. *Journal of Biotechnology,* 164**,** 396-408.

CARRIER, T. A. & KEASLING, J. D. 1999. Investigating Autocatalytic Gene Expression Systems through Mechanistic Modeling. *Journal of Theoretical Biology,* 201**,** 25-36.

CASTIÑEIRAS, T., WILLIAMS, S., HITCHCOCK, A., COLE, J., SMITH, D. & OVERTON, T. 2018. Optimizing host cell physiology and stress avoidance for the production of recombinant human tumour necrosis factor α in Escherichia coli. *Microbiology,* 164.

CATIPOVIC, M. A., BAUER, B. W., LOPARO, J. J. & RAPOPORT, T. A. 2019. Protein translocation by the SecA ATPase occurs by a power-stroke mechanism. *The EMBO Journal,* 38**,** e101140.

ÇELIK, E. & ÇALıK, P. 2012. Production of recombinant proteins by yeast cells. *Biotechnology Advances,* 30**,** 1108-1118.

CHABA, R., ALBA, B. M., GUO, M. S., SOHN, J., AHUJA, N., SAUER, R. T. & GROSS, C. A. 2011. Signal integration by DegS and RseB governs the σE-mediated envelope stress response in Escherichia coli. *Proc Natl Acad Sci U S A,* 108**,** 2106-11.

CHAMBERLIN, M., MCGRATH, J. & WASKELL, L. 1970. New RNA Polymerase from Escherichia coli infected with Bacteriophage T7. *Nature,* 228**,** 227-231.

CHAMBERLIN, M. & RING, J. 1973. Characterization of T7-specific ribonucleic acid polymerase. 1. General properties of the enzymatic reaction and the template specificity of the enzyme. *J Biol Chem,* 248**,** 2235-44.

CHAO, Y. & VOGEL, J. 2016. A 3' UTR-Derived Small RNA Provides the Regulatory Noncoding Arm of the Inner Membrane Stress Response. *Molecular Cell,* 61**,** 352-363.

CHEN, B., LIU, W., LI, Y., MA, B., SHANG, S. & TAN, Z. 2022. Impact of N-Linked Glycosylation on Therapeutic Proteins. *Molecules,* 27**,** 8859.

CHEN, H., BJERKNES, M., KUMAR, R. & JAY, E. 1994. Determination of the optimal aligned spacing between the Shine – Dalgarno sequence and the translation initiation codon of Escherichia coli m RNAs. *Nucleic Acids Research,* 22**,** 4953-4957.

CHEN, J. C., VIOLLIER, P. H. & SHAPIRO, L. 2005. A membrane metalloprotease participates in the sequential degradation of a Caulobacter polarity determinant. *Molecular Microbiology,* 55**,** 1085-1103.

CHEN, R. 2012. Bacterial expression systems for recombinant protein production: E. coli and beyond. *Biotechnology Advances,* 30**,** 1102-1107.

CHEN, X., LI, C. & LIU, H. 2021. Enhanced Recombinant Protein Production Under Special Environmental Stress. *Frontiers in Microbiology,* 12.

CHOU, C. H., ARISTIDOU, A. A., MENG, S. Y., BENNETT, G. N. & SAN, K. Y. 1995. Characterization of a pH-inducible promoter system for high-level expression of recombinant proteins in Escherichia coli. *Biotechnol Bioeng,* 47**,** 186-92.

CHOU, M. M. & KENDALL, D. A. 1990. Polymeric sequences reveal a functional interrelationship between hydrophobicity and length of signal peptides. *Journal of Biological Chemistry,* 265**,** 2873-2880.

CHOY, J. S., AUNG, L. L. & KARZAI, A. W. 2007. Lon Protease Degrades Transfer-Messenger RNA-Tagged Proteins. *Journal of Bacteriology,* 189**,** 6564-6571.

CHU, B. C. H., DEWOLF, T. & VOGEL, H. J. 2013. Role of the Two Structural Domains from the Periplasmic Escherichia coli Histidine-binding Protein HisJ *. *Journal of Biological Chemistry,* 288**,** 31409-31422.

CIUSA, M. L., MARSHALL, R. L., RICCI, V., STONE, J. W. & PIDDOCK, L. J. V. 2022. Absence, loss-of-function, or inhibition of Escherichia coli AcrB does not increase expression of other efflux pump genes supporting the discovery of AcrB inhibitors as antibiotic adjuvants. *J Antimicrob Chemother,* 77**,** 633-640.

COHEN, S. N., CHANG, A. C. Y., BOYER, H. W. & HELLING, R. B. 1973. Construction of Biologically Functional Bacterial Plasmids In Vitro. *Proceedings of the National Academy of Sciences,* 70**,** 3240-3244.

COHEN, S. N., CHANG, A. C. Y. & HSU, L. 1972. Nonchromosomal Antibiotic Resistance in Bacteria: Genetic Transformation of Escherichia coli by R-Factor DNA. *Proceedings of the National Academy of Sciences,* 69**,** 2110-2114.

COKER, C., BAKARE, O. O. & MOBLEY, H. L. T. 2000. H-NS Is a Repressor of the Proteus mirabilis Urease Transcriptional Activator Gene ureR. *Journal of Bacteriology,* 182**,** 2649-2653.

COLEMAN, J. E. 1992. Structure and mechanism of alkaline phosphatase. *Annu Rev Biophys Biomol Struct,* 21**,** 441-83.

CORMACK, B. P., VALDIVIA, R. H. & FALKOW, S. 1996. FACS-optimized mutants of the green fluorescent protein (GFP). *Gene,* 173**,** 33-38.

CORTÉS-AVALOS, D., MARTÍNEZ-PÉREZ, N., ORTIZ-MONCADA, M. A., JUÁREZ-GONZÁLEZ, A., BAÑOS-VARGAS, A. A., PAULINA, PÉREZ-RUEDA, E. & IBARRA, J. A. 2021. An update of the unceasingly growing and diverse AraC/XylS family of transcriptional activators. *FEMS Microbiology Reviews,* 45.

COSTANTINI, L. M., BALOBAN, M., MARKWARDT, M. L., RIZZO, M. A., GUO, F., VERKHUSHA, V. V. & SNAPP, E. L. 2015. A palette of fluorescent proteins optimized for diverse cellular environments. *Nature Communications,* 6**,** 7670.

CRAMERI, A., WHITEHORN, E. A., TATE, E. & STEMMER, W. P. C. 1996. Improved Green Fluorescent Protein by Molecular Evolution Using DNA Shuffling. *Nature Biotechnology,* 14**,** 315-319.

CRANE, J. M. & RANDALL, L. L. 2017. The Sec System: Protein Export in Escherichia coli. *EcoSal Plus,* 7.

CRANFORD-SMITH, T. & HUBER, D. 2018. The way is the goal: how SecA transports proteins across the cytoplasmic membrane in bacteria. *FEMS Microbiology Letters,* 365.

CRONAN, G. E. & KUZMINOV, A. 2024. Degron-Controlled Protein Degradation in Escherichia coli: New Approaches and Parameters. *ACS Synthetic Biology,* 13**,** 669-682.

CROSET, A., DELAFOSSE, L., GAUDRY, J.-P., AROD, C., GLEZ, L., LOSBERGER, C., BEGUE, D., KRSTANOVIC, A., ROBERT, F., VILBOIS, F., CHEVALET, L. & ANTONSSON, B. 2012. Differences in the glycosylation of recombinant proteins expressed in HEK and CHO cells. *Journal of Biotechnology,* 161**,** 336-348.

CROWLEY, L. C., SCOTT, A. P., MARFELL, B. J., BOUGHABA, J. A., CHOJNOWSKI, G. & WATERHOUSE, N. J. 2016. Measuring Cell Death by Propidium Iodide Uptake and Flow Cytometry. *Cold Spring Harb Protoc,* 2016.

D'ORAZIO, S. E. & COLLINS, C. M. 1993. The plasmid-encoded urease gene cluster of the family Enterobacteriaceae is positively regulated by UreR, a member of the AraC family of transcriptional activators. *Journal of Bacteriology,* 175**,** 3459-3467.

D'ORAZIO, S. E. F., THOMAS, V. & COLLINS, C. M. 1996. Activation of transcription at divergent urea-dependent promoters by the urease gene regulator UreR. *Molecular Microbiology,* 21**,** 643-655.

DABER, R., SHARP, K. & LEWIS, M. 2009. One Is Not Enough. *Journal of Molecular Biology,* 392**,** 1133-1144.

DAMMEYER, T. & TINNEFELD, P. 2012. ENGINEERED FLUORESCENT PROTEINS ILLUMINATE THE BACTERIAL PERIPLASM. *Computational and Structural Biotechnology Journal,* 3**,** e201210013.

DARTIGALONGUE, C. & RAINA, S. 1998. A new heat shock gene, ppiD, encodes a peptidyl prolyl isomerase required for folding of outer membrane proteins in Escherichia coli. *The EMBO Journal,* 17**,** 3968-3980-3980.

DATTELBAUM, J. D., LOCKATELL, C. V., JOHNSON, D. E. & MOBLEY, H. L. T. 2003. UreR, the Transcriptional Activator of the Proteus mirabilis Urease Gene Cluster, Is Required for Urease Activity and Virulence in Experimental Urinary Tract Infections. *Infection and Immunity,* 71**,** 1026-1030.

DAVEY, H. M. & HEXLEY, P. 2011. Red but not dead? Membranes of stressed Saccharomyces cerevisiae are permeable to propidium iodide. *Environ Microbiol,* 13**,** 163-171.

DAVIDSON, V. L. & SUN, D. 2002. [12] - Lysozyme-Osmotic Shock Methods for Localization of Periplasmic Redox Proteins in Bacteria. *In:* SEN, C. K. & PACKER, L. (eds.) *Methods in Enzymology.* Academic Press.

DAY, R. N. & DAVIDSON, M. W. 2009. The fluorescent protein palette: tools for cellular imaging. *Chemical Society Reviews,* 38**,** 2887.

DE BOER, H. A., COMSTOCK, L. J. & VASSER, M. 1983. The tac promoter: a functional hybrid derived from the trp and lac promoters. *Proceedings of the National Academy of Sciences,* 80**,** 21-25.

DE LAS PEÑAS, A., CONNOLLY, L. & GROSS, C. A. 1997. The σE-mediated response to extracytoplasmic stress in Escherichia coli is transduced by RseA and RseB, two negative regulators of σE. *Molecular Microbiology,* 24**,** 373-385.

DEEKS, E. D. 2016. Certolizumab Pegol: A Review in Inflammatory Autoimmune Diseases. *BioDrugs,* 30**,** 607-617.

DEKKER, C., KRUIJFF, B. D. & GROS, P. 2003. Crystal structure of SecB from Escherichia coli. *Journal of Structural Biology,* 144**,** 313-319.

DELISA, M. P., LI, J., RAO, G., WEIGAND, W. A. & BENTLEY, W. E. 2000. Monitoring GFP-operon fusion protein expression during high cell density cultivation of Escherichia coli using an on-line optical sensor. *Biotechnology and Bioengineering,* 65**,** 54-64.

DELISA, M. P., TULLMAN, D. & GEORGIOU, G. 2003. Folding quality control in the export of proteins by the bacterial twin-arginine translocation pathway. *Proceedings of the National Academy of Sciences,* 100**,** 6115-6120.

DEMAIN, A. L. & VAISHNAV, P. 2009. Production of recombinant proteins by microbes and higher organisms. *Biotechnology Advances,* 27**,** 297-306.

DEMIRHAN, D., KUMAR, A., ZHU, J., POULSEN, P. C., MAJEWSKA, N. I., SEBASTIAN, Y., CHAERKADY, R., YU, W., ZHU, W., ZHUANG, L., SHAH, P., LEKSTROM, K., COLE, R. N., ZHANG, H., BETENBAUGH, M. J. & BOWEN, M. A. 2022. Comparative systeomics to elucidate physiological differences between CHO and SP2/0 cell lines. *Scientific Reports,* 12.

DENKS, K., VOGT, A., SACHELARU, I., PETRIMAN, N.-A., KUDVA, R. & KOCH, H.-G. 2014. The Sec translocon mediated protein transport in prokaryotes and eukaryotes. *Molecular Membrane Biology,* 31**,** 58-84.

DERSCH, P., SCHMIDT, K. & BREMER, E. 1993. Synthesis of the Escherichia coli K-12 nucleoid-associated DNA-binding protein H-NS is subjected to growth-phase control and autoregulation. *Mol Microbiol,* 8**,** 875-89.

DHARA, V. G., NAIK, H. M., MAJEWSKA, N. I. & BETENBAUGH, M. J. 2018. Recombinant Antibody Production in CHO and NS0 Cells: Differences and Similarities. *BioDrugs,* 32**,** 571-584.

DIGIUSEPPE, P. A. & SILHAVY, T. J. 2003. Signal Detection and Target Gene Induction by the CpxRA Two-Component System. *Journal of Bacteriology,* 185**,** 2432-2440.

DINH, T. & BERNHARDT, T. G. 2011. Using Superfolder Green Fluorescent Protein for Periplasmic Protein Localization Studies. *Journal of Bacteriology,* 193**,** 4984-4987.

DIXON, N. E., GAZZOLA, C., BLAKELEY, R. L. & ZERNER, B. 1975. Jack bean urease (EC 3.5.1.5). Metalloenzyme. Simple biological role for nickel. *Journal of the American Chemical Society,* 97**,** 4131-4133.

DOMINGUES, I. L., GAMA, J. A., CARVALHO, L. M. & DIONISIO, F. 2017. Social behaviour involving drug resistance: the role of initial density, initial frequency and population structure in shaping the effect of antibiotic resistance as a public good. *Heredity,* 119**,** 295-301.

DORMAN, C. J. 2004. H-NS: a universal regulator for a dynamic genome. *Nature Reviews Microbiology,* 2**,** 391-400.

DRAGOSITS, M., NICKLAS, D. & TAGKOPOULOS, I. 2012. A synthetic biology approach to self-regulatory recombinant protein production in Escherichia coli. *Journal of Biological Engineering,* 6**,** 2.

DRAZIC, A., MYKLEBUST, L. M., REE, R. & ARNESEN, T. 2016. The world of protein acetylation. *Biochim Biophys Acta,* 1864**,** 1372-401.

DU PLESSIS, D. J. F., BERRELKAMP, G., NOUWEN, N. & DRIESSEN, A. J. M. 2009. The Lateral Gate of SecYEG Opens during Protein Translocation. *Journal of Biological Chemistry,* 284**,** 15805-15814.

EINAV, T. & PHILLIPS, R. 2019. How the avidity of polymerase binding to the –35/–10 promoter sites affects gene expression. *Proceedings of the National Academy of Sciences,* 116**,** 13340-13345.

EJAZ, U., SOHAIL, M. & GHANEMI, A. 2021. Cellulases: From Bioactivity to a Variety of Industrial Applications. *Biomimetics (Basel),* 6.

ENGLESBERG, E. 1961. Enzymatic characterization of 17 L-arabinose negative mutants of Escherichia coli. *Journal of Bacteriology,* 81**,** 996-1006.

ERICKSON, J. W. & GROSS, C. A. 1989. Identification of the sigma E subunit of Escherichia coli RNA polymerase: a second alternate sigma factor involved in high-temperature gene expression. *Genes & Development,* 3**,** 1462-1471.

FABIA, B.-U., BINGWA, J., PARK, J., HIEU, N.-M. & AHN, J.-H. 2021. Utilizing the ABC Transporter for Growth Factor Production by fleQ Deletion Mutant of Pseudomonas fluorescens. *Biomedicines,* 9**,** 679.

FALCH, E. A. 1991. Industrial enzymes — Developments in production and application. *Biotechnology Advances,* 9**,** 643-658.

FALCONI, M., HIGGINS, N. P., SPURIO, R., PON, C. L. & GUALERZI, C. O. 1993. Expression of the gene encoding the major bacterial nucleoid protein H-NS is subject to transcriptional auto-repression. *Molecular Microbiology,* 10**,** 273-282.

FANG, J. & WEI, Y. 2011. Expression, purification and characterization of the Escherichia coli integral membrane protein YajC. *Protein Pept Lett,* 18**,** 601-8.

FARAJNIA, S., GHORBANZADEH, V. & DARIUSHNEJAD, H. 2020. Effect of Molecular Chaperone on the Soluble Expression of Recombinant Fab Fragment in E. coli. *International Journal of Peptide Research and Therapeutics,* 26**,** 251-258.

FARRELL, C. M., GROSSMAN, A. D. & SAUER, R. T. 2005. Cytoplasmic degradation of ssrA-tagged proteins. *Molecular Microbiology,* 57**,** 1750-1761.

FINDIK, B. T. & RANDALL, L. L. 2017. Determination of the intracellular concentration of the export chaperone SecB in Escherichia coli. *PLOS ONE,* 12**,** e0183231.

FISHER, A. C. & DELISA, M. P. 2008. Laboratory Evolution of Fast-Folding Green Fluorescent Protein Using Secretory Pathway Quality Control. *PLoS ONE,* 3**,** e2351.

FLIER, J. S. & KAHN, C. R. 2021. Insulin: A pacesetter for the shape of modern biomedical science and the Nobel Prize. *Mol Metab,* 52**,** 101194.

FLORES-KIM, J. & DARWIN, A. J. 2016. The Phage Shock Protein Response. *Annual Review of Microbiology,* 70**,** 83-101.

FLORES-MIRELES, A. L., WALKER, J. N., CAPARON, M. & HULTGREN, S. J. 2015. Urinary tract infections: epidemiology, mechanisms of infection and treatment options. *Nature Reviews Microbiology,* 13**,** 269-284.

FLYNN, J. M., LEVCHENKO, I., SAUER, R. T. & BAKER, T. A. 2004. Modulating substrate choice: the SspB adaptor delivers a regulator of the extracytoplasmic-stress response to the AAA+ protease ClpXP for degradation. *Genes & Development,* 18**,** 2292-2301.

FLYNN, J. M., LEVCHENKO, I., SEIDEL, M., WICKNER, S. H., SAUER, R. T. & BAKER, T. A. 2001. Overlapping recognition determinants within the ssrA degradation tag allow modulation of proteolysis. *Proceedings of the National Academy of Sciences,* 98**,** 10584-10589.

FORQUET, R., NASSER, W., REVERCHON, S. & MEYER, S. 2022. Quantitative contribution of the spacer length in the supercoiling-sensitivity of bacterial promoters. *Nucleic Acids Research,* 50**,** 7287-7297.

FOX-MOON, S. M. & SHIRTLIFF, M. E. 2015. Chapter 77 - Urinary Tract Infections Caused by Proteus mirabilis. *In:* TANG, Y.-W., SUSSMAN, M., LIU, D., POXTON, I. & SCHWARTZMAN, J. (eds.) *Molecular Medical Microbiology (Second Edition).* Boston: Academic Press.

FRAIN, K. M., ROBINSON, C. & VAN DIJL, J. M. 2019. Transport of Folded Proteins by the Tat System. *The Protein Journal,* 38**,** 377-388.

FRANCETIC, O. 2000. Expression of the endogenous type II secretion pathway in Escherichia coli leads to chitinase secretion. *The EMBO Journal,* 19**,** 6697-6703.

FRANCIS, D. M. & PAGE, R. 2010. Strategies to Optimize Protein Expression in E. coli. *Current Protocols in Protein Science,* 61**,** 5.24.1-5.24.29.

FREE, A. & DORMAN, C. J. 1995. Coupling of Escherichia coli hns mRNA levels to DNA synthesis by autoregulation: implications for growth phase control. *Mol Microbiol,* 18**,** 101-13.

FREUDL, R. 2018. Signal peptides for recombinant protein secretion in bacterial expression systems. *Microbial Cell Factories,* 17.

FRITZ, G., MEGERLE, J. A., WESTERMAYER, S. A., BRICK, D., HEERMANN, R., JUNG, K., RÄDLER, J. O. & GERLAND, U. 2014. Single Cell Kinetics of Phenotypic Switching in the Arabinose Utilization System of E. coli. *PLoS ONE,* 9**,** e89532.

GAO, W., YIN, J., BAO, L., WANG, Q., HOU, S., YUE, Y., YAO, W. & GAO, X. 2018. Engineering Extracellular Expression Systems in Escherichia coli Based on Transcriptome Analysis and Cell Growth State. *ACS Synthetic Biology,* 7**,** 1291-1302.

GARBE, T. R., KOBAYASHI, M. & YUKAWA, H. 2000. Indole-inducible proteins in bacteria suggest membrane and oxidant toxicity. *Archives of Microbiology,* 173**,** 78-82.

GARCÍA-CALVO, L., RANE, D. V., EVERSON, N., HUMLEBREKK, S. T., MATHIASSEN, L. F., MÆHLUM, A. H. M., MALMO, J. & BRUHEIM, P. 2023. Central carbon metabolite profiling reveals vector-associated differences in the recombinant protein production host Escherichia coli BL21. *Frontiers in Chemical Engineering,* 5.

GENDLINA, I., GUTMAN, D. M., THOMAS, V. & COLLINS, C. M. 2002. Urea-dependent Signal Transduction by the Virulence Regulator UreR *. *Journal of Biological Chemistry,* 277**,** 37349-37358.

GHASEMIAN, A. & MORADPOUR, Z. 2019. Chapter 8 - Production of Recombinant Microbial Thermostable Lipases. *In:* SINGH, H. B., GUPTA, V. K. & JOGAIAH, S. (eds.) *New and Future Developments in Microbial Biotechnology and Bioengineering.* Amsterdam: Elsevier.

GIACALONE, M. J., GENTILE, A. M., LOVITT, B. T., BERKLEY, N. L., GUNDERSON, C. W. & SURBER, M. W. 2006. Toxic protein expression in Escherichia coli using a rhamnose-based tightly regulated and tunable promoter system. *BioTechniques,* 40**,** 355-364.

GILBERT, W., MAJORS, J. & MAXAM, A. 1976. In Dahlem Workshop on Chromosomes. 1976. Berlin: Abakon Verlagsgesellschaft, 167-178.

GIOVANNONI, M., GRAMEGNA, G., BENEDETTI, M. & MATTEI, B. 2020. Industrial Use of Cell Wall Degrading Enzymes: The Fine Line Between Production Strategy and Economic Feasibility. *Frontiers in Bioengineering and Biotechnology,* 8.

GOPALKRISHNAN, S., NICOLOFF, H. & ADES, S. E. 2014. Co-ordinated regulation of the extracytoplasmic stress factor, sigmaE, with other Escherichia coli sigma factors by (p)ppGpp and DksA may be achieved by specific regulation of individual holoenzymes. *Molecular Microbiology,* 93**,** 479-493.

GOTTESMAN, S., ROCHE, E., ZHOU, Y. & SAUER, R. T. 1998. The ClpXP and ClpAP proteases degrade proteins with carboxy-terminal peptide tails added by the SsrA-tagging system. *Genes Dev,* 12**,** 1338-47.

GREENFIELD, N. J. 2006. Using circular dichroism spectra to estimate protein secondary structure. *Nature Protocols,* 1**,** 2876-2890.

GREN, E. J. 1984. Recognition of messenger RNA during translational initiation in Escherichia coli. *Biochimie,* 66**,** 1-29.

GUBELLINI, F., VERDON, G., KARPOWICH, N. K., LUFF, J. D., BOËL, G., GAUTHIER, N., HANDELMAN, S. K., ADES, S. E. & HUNT, J. F. 2011. Physiological response to membrane protein overexpression in E. coli. *Mol Cell Proteomics,* 10**,** M111.007930.

GUEST, R. L., COURT, E. A., WALDON, J. L., SCHOCK, K. A. & RAIVIO, T. L. 2019. Impaired Efflux of the Siderophore Enterobactin Induces Envelope Stress in Escherichia coli. *Frontiers in Microbiology,* 10.

GUIDI, C., DE WANNEMAEKER, L., DE BAETS, J., DEMEESTER, W., MAERTENS, J., DE PAEPE, B. & DE MEY, M. 2022. Dynamic feedback regulation for efficient membrane protein production using a small RNA-based genetic circuit in Escherichia coli. *Microbial Cell Factories,* 21.

GULERIA, R., JAIN, P., VERMA, M. & MUKHERJEE, K. J. 2020. Designing next generation recombinant protein expression platforms by modulating the cellular stress response in Escherichia coli. *Microbial Cell Factories,* 19.

GUMBART, J., SCHREINER, E., DANIEL, BECKMANN, R. & SCHULTEN, K. 2012. Mechanisms of SecM-Mediated Stalling in the Ribosome. *Biophysical Journal,* 103**,** 331-341.

GUO, H., SUN, J., LI, X., XIONG, Y., WANG, H., SHU, H., ZHU, R., LIU, Q., HUANG, Y., MADLEY, R., WANG, Y., CUI, J., ARVAN, P. & LIU, M. 2018. Positive charge in the n-region of the signal peptide contributes

to efficient post-translational translocation of small secretory preproteins. *Journal of Biological Chemistry,* 293**,** 1899-1907.

GUPTA, S. K. & SHUKLA, P. 2018. Glycosylation control technologies for recombinant therapeutic proteins. *Applied Microbiology and Biotechnology,* 102**,** 10457-10468.

GUZMAN, L. M., BELIN, D., CARSON, M. J. & BECKWITH, J. 1995. Tight regulation, modulation, and high-level expression by vectors containing the arabinose PBAD promoter. *J Bacteriol,* 177**,** 4121-30.

HACKER, D. L. & BALASUBRAMANIAN, S. 2016. Recombinant protein production from stable mammalian cell lines and pools. *Current Opinion in Structural Biology,* 38**,** 129-136.

HAGENMAIER, S., STIERHOF, Y. D. & HENNING, U. 1997. A new periplasmic protein of Escherichia coli which is synthesized in spheroplasts but not in intact cells. *Journal of Bacteriology,* 179**,** 2073-2076.

HAHN, S., DUNN, T. & SCHLEIF, R. 1984. Upstream repression and CRP stimulation of the Escherichia coli L-arabinose operon. *J Mol Biol,* 180**,** 61-72.

HANOULLE, X., ROLLET, E., CLANTIN, B., LANDRIEU, I., ÖDBERG-FERRAGUT, C., LIPPENS, G., BOHIN, J.-P. & VILLERET, V. 2004. Structural Analysis of Escherichia coli OpgG, a Protein Required for the Biosynthesis of Osmoregulated Periplasmic Glucans. *Journal of Molecular Biology,* 342**,** 195-205.

HANTKE, K. & BRAUN, V. 1973. Covalent Binding of Lipid to Protein: Diglyceride and Amide-Linked Fatty Acid at the N-Terminal End of the Murein-Lipoprotein of the Escherichia coli Outer Membrane. *European Journal of Biochemistry,* 34**,** 284-296.

HASELTINE, W. A. & BLOCK, R. 1973. Synthesis of Guanosine Tetra- and Pentaphosphate Requires the Presence of a Codon-Specific, Uncharged Transfer Ribonucleic Acid in the Acceptor Site of Ribosomes. *Proceedings of the National Academy of Sciences,* 70**,** 1564-1568.

HE, W., YU, G., LI, T., BAI, L., YANG, Y., XUE, Z., PANG, Y., REICHMANN, D., HILLER, S., HE, L., LIU, M. & QUAN, S. 2021. Chaperone Spy Protects Outer Membrane Proteins from Folding Stress via Dynamic Complex Formation. *mBio,* 12.

HEGGESET, T. M. B., KUCHAROVA, V., NÆRDAL, I., VALLA, S., SLETTA, H., ELLINGSEN, T. E. & BRAUTASET, T. 2013. Combinatorial Mutagenesis and Selection of Improved Signal Sequences and Their Application for High-Level Production of Translocated Heterologous Proteins in Escherichia coli. *Applied and Environmental Microbiology,* 79**,** 559-568.

HEIM, R., CUBITT, A. B. & TSIEN, R. Y. 1995. Improved green fluorescence. *Nature,* 373**,** 663-664.

HJELM, A., KARYOLAIMOS, A., ZHANG, Z., RUJAS, E., VIKSTRÖM, D., SLOTBOOM, D. J. & DE GIER, J.-W. 2017. Tailoring Escherichia coli for the l-Rhamnose PBAD Promoter-Based Production of Membrane and Secretory Proteins. *ACS Synthetic Biology,* 6**,** 985-994.

HOFFMAN, C. S. & WRIGHT, A. 1985. Fusions of secreted proteins to alkaline phosphatase: an approach for studying protein secretion. *Proceedings of the National Academy of Sciences,* 82**,** 5107-5111.

HOFFMANN, F., HEUVEL, J., ZIDEK, N. & RINAS, U. 2004. Minimizing inclusion body formation during recombinant protein production in Escherichia coli at bench and pilot plant scale. *Enzyme and Microbial Technology,* 34**,** 235-241.

HOFFMANN, F. & RINAS, U. 2004. Stress Induced by Recombinant Protein Production in Escherichia col. *Advances in Biochemical Engineering/Biotechnology,* 89**,** 73-92.

HOGG, R. W. & ENGLESBERG, E. 1969. L-Arabinose Binding Protein from Escherichia coli B. *Journal of Bacteriology,* 100**,** 423-432.

HOMMA, T., YOSHIHISA, T. & ITO, K. 1997. Subunit interactions in the Escherichia coli protein translocase: SecE and SecG associate independently with SecY. *FEBS Letters,* 408**,** 11-15.

HOOK-BARNARD, I. G., BRICKMAN, T. J. & MCINTOSH, M. A. 2007. Identification of an AU-rich Translational Enhancer within the Escherichia coli fepB Leader RNA. *Journal of Bacteriology,* 189**,** 4028-4037.

HORGA, L. G., HALLIWELL, S., CASTIÑEIRAS, T. S., WYRE, C., MATOS, C. F. R. O., YOVCHEVA, D. S., KENT, R., MORRA, R., WILLIAMS, S. G., SMITH, D. C. & DIXON, N. 2018. Tuning recombinant protein expression to match secretion capacity. *Microbial Cell Factories,* 17.

HOTHERSALL, J., GODFREY, R. E., FANITSIOS, C., OVERTON, T. W., BUSBY, S. J. W. & BROWNING, D. F. 2021. The PAR promoter expression system: Modified lac promoters for controlled recombinant protein production in Escherichia coli. *New Biotechnology,* 64**,** 1-8.

HOTHERSALL, J., LAI, S., ZHANG, N., GODFREY, R. E., RUANTO, P., BISCHOFF, S., ROBINSON, C., OVERTON, T. W., BUSBY, S. J. W. & BROWNING, D. F. 2022a. Inexpensive protein overexpression driven by the NarL transcription activator protein. *Biotechnol Bioeng,* 119**,** 1614-1623.

HOTHERSALL, J., OSGERBY, A., GODFREY, R. E., OVERTON, T. W., BUSBY, S. J. W. & BROWNING, D. F. 2022b. New vectors for urea-inducible recombinant protein production. *New Biotechnology,* 72**,** 89-96.

HSIEH, Y.-H., HUANG, Y.-J., JIN, J.-S., YU, L., YANG, H., JIANG, C., WANG, B. & TAI, P. C. 2014. Mechanisms of Rose Bengal inhibition on SecA ATPase and ion channel activities. *Biochemical and Biophysical Research Communications,* 454**,** 308-312.

HU, Y., CHENG, K., HE, L., ZHANG, X., JIANG, B., JIANG, L., LI, C., WANG, G., YANG, Y. & LIU, M. 2021. NMR-Based Methods for Protein Analysis. *Analytical Chemistry,* 93**,** 1866-1879.

HUANG, M., BAO, J. & NIELSEN, J. 2014. Biopharmaceutical protein production bySaccharomyces cerevisiae: current state and future prospects. *Pharmaceutical Bioprocessing,* 2**,** 167-182.

HUBER, D. & BUKAU, B. 2008. DegP: a Protein "Death Star". *Structure,* 16**,** 989-990.

HUBER, D., JAMSHAD, M., HANMER, R., SCHIBICH, D., DÖRING, K., MARCOMINI, I., KRAMER, G. & BUKAU, B. 2017. SecA Cotranslationally Interacts with Nascent Substrate Proteins In Vivo. *Journal of Bacteriology,* 199**,** JB.00622-16.

HUBER, D., RAJAGOPALAN, N., PREISSLER, S., ROCCO, M. A., MERZ, F., KRAMER, G. & BUKAU, B. 2011. SecA Interacts with Ribosomes in Order to Facilitate Posttranslational Translocation in Bacteria. *Molecular Cell,* 41**,** 343-353.

HUGHES, J., REES, S., KALINDJIAN, S. & PHILPOTT, K. 2011. Principles of early drug discovery. *British Journal of Pharmacology,* 162**,** 1239-1249.

ILANGUMARAN PONMALAR, I., SWAIN, J. & BASU, J. K. 2022. Escherichia coli response to subinhibitory concentrations of colistin: insights from a study of membrane dynamics and morphology. *Biomaterials Science,* 10**,** 2609-2617.

IRVING, S. E., CHOUDHURY, N. R. & CORRIGAN, R. M. 2021. The stringent response and physiological roles of (pp)pGpp in bacteria. *Nature Reviews Microbiology,* 19**,** 256-271.

ISHIHAMA, Y., SCHMIDT, T., RAPPSILBER, J., MANN, M., HARTL, F. U., KERNER, M. J. & FRISHMAN, D. 2008. Protein abundance profiling of the Escherichia coli cytosol. *BMC Genomics,* 9**,** 102.

ISLAND, M. D. & MOBLEY, H. L. 1995. Proteus mirabilis urease: operon fusion and linker insertion analysis of ure gene organization, regulation, and function. *Journal of Bacteriology,* 177**,** 5653-5660.

ITAKURA, K., HIROSE, T., CREA, R., RIGGS, A. D., HEYNEKER, H. L., BOLIVAR, F. & BOYER, H. W. 1977. Expression in Escherichia coli of a Chemically Synthesized Gene for the Hormone Somatostatin. *Science,* 198**,** 1056-1063.

ITO, K., WITTEKIND, M., NOMURA, M., SHIBA, K., YURA, T., MIURA, A. & NASHIMOTO, H. 1983. A Temperature-Sensitive Mutant of E. Coli Exhibiting Slow Processing of Exported Proteins. *Cell,* 32**,** 789-797.

JACKSON, D. A., SYMONS, R. H. & BERG, P. 1972. Biochemical Method for Inserting New Genetic Information into DNA of Simian Virus 40: Circular SV40 DNA Molecules Containing Lambda Phage Genes and the Galactose Operon of Escherichia coli. *Proceedings of the National Academy of Sciences,* 69**,** 2904-2909.

JACOB, F. & MONOD, J. 1961. Genetic regulatory mechanisms in the synthesis of proteins. *Journal of Molecular Biology,* 3**,** 318-356.

JAIN, R. K., JOYCE, P. B. M., MOLINETE, M., HALBAN, P. A. & GORR, S.-U. 2001. Oligomerization of green fluorescent protein in the secretory pathway of endocrine cells. *Biochemical Journal,* 360**,** 645.

JENKINS, N., MURPHY, L. & TYTHER, R. 2008. Post-translational Modifications of Recombinant Proteins: Significance for Biopharmaceuticals. *Molecular Biotechnology,* 39**,** 113-118.

JEONG, H., KIM, H. J. & LEE, S. J. 2015. Complete Genome Sequence of Escherichia coli Strain BL21. *Genome Announc,* 3.

JEONG, K. J. & LEE, S. Y. 2003. Enhanced Production of Recombinant Proteins in Escherichia coli by Filamentation Suppression. *Applied and Environmental Microbiology,* 69**,** 1295-1298.

JIN, B.-K., ODONGO, S., RADWANSKA, M. & MAGEZ, S. 2023. NANOBODIES®: A Review of Diagnostic and Therapeutic Applications. *International Journal of Molecular Sciences,* 24**,** 5994.

JIN, J., HSIEH, Y. H., CUI, J., DAMERA, K., DAI, C., CHAUDHARY, A. S., ZHANG, H., YANG, H., CAO, N., JIANG, C., VAARA, M., WANG, B. & TAI, P. C. 2016. Using Chemical Probes to Assess the Feasibility of Targeting SecA for Developing Antimicrobial Agents against Gram-Negative Bacteria. *ChemMedChem,* 11**,** 2511-2521.

JOHNSON, K. C., YONGKY, A., VISHWANATHAN, N., JACOB, N. M., JAYAPAL, K. P., GOUDAR, C. T., KARYPIS, G. & HU, W.-S. 2014. Exploring the transcriptome space of a recombinant BHK cell line through next generation sequencing. *Biotechnology and Bioengineering,* 111**,** 770-781.

JOHNSON, LOUISE N. 2009. The regulation of protein phosphorylation. *Biochemical Society Transactions,* 37**,** 627-641.

JOLY, N., ENGL, C., JOVANOVIC, G., HUVET, M., TONI, T., SHENG, X., STUMPF, M. P. H. & BUCK, M. 2010. Managing membrane stress: the phage shock protein (Psp) response, from molecular mechanisms to physiology. *FEMS Microbiology Reviews,* 34**,** 797-827.

JONES, B. D. & MOBLEY, H. L. 1989. Proteus mirabilis urease: nucleotide sequence determination and comparison with jack bean urease. *Journal of Bacteriology,* 171**,** 6414-6422.

JUSTICE, S. S., HUNSTAD, D. A., CEGELSKI, L. & HULTGREN, S. J. 2008. Morphological plasticity as a bacterial survival strategy. *Nature Reviews Microbiology,* 6**,** 162-168.

JUSTICE, S. S., HUNSTAD, D. A., HARPER, J. R., DUGUAY, A. R., PINKNER, J. S., BANN, J., FRIEDEN, C., SILHAVY, T. J. & HULTGREN, S. J. 2005. Periplasmic Peptidyl Prolyl cis-trans Isomerases Are Not Essential for Viability, but SurA Is Required for Pilus Biogenesis in Escherichia coli. *Journal of Bacteriology,* 187**,** 7680-7686.

KAPPAUN, K., PIOVESAN, A. R., CARLINI, C. R. & LIGABUE-BRAUN, R. 2018. Ureases: Historical aspects, catalytic, and non-catalytic properties – A review. *Journal of Advanced Research,* 13**,** 3-17.

KARASZ, D. C., WEAVER, A. I., BUCKLEY, D. H. & WILHELM, R. C. 2022. Conditional filamentation as an adaptive trait of bacteria and its ecological significance in soils. *Environmental Microbiology,* 24**,** 1-17.

KARBALAEI, M., REZAEE, S. A. & FARSIANI, H. 2020. Pichia pastoris: A highly successful expression system for optimal synthesis of heterologous proteins. *Journal of Cellular Physiology,* 235**,** 5867-5881.

KARYOLAIMOS, A., AMPAH-KORSAH, H., HILLENAAR, T., MESTRE BORRAS, A., DOLATA, K. M., SIEVERS, S., RIEDEL, K., DANIELS, R. & DE GIER, J.-W. 2019a. Enhancing Recombinant Protein Yields in the E. coli Periplasm by Combining Signal Peptide and Production Rate Screening. *Frontiers in Microbiology,* 10.

KARYOLAIMOS, A., AMPAH-KORSAH, H., HILLENAAR, T., MESTRE BORRAS, A., DOLATA, K. M., SIEVERS, S., RIEDEL, K., DANIELS, R. & DE GIER, J. W. 2019b. Enhancing Recombinant Protein Yields in the E. coli Periplasm by Combining Signal Peptide and Production Rate Screening. *Front Microbiol,* 10**,** 1511.

KARYOLAIMOS, A. & DE GIER, J. W. 2021. Strategies to Enhance Periplasmic Recombinant Protein Production Yields in Escherichia coli. *Front Bioeng Biotechnol,* 9**,** 797334.

KARYOLAIMOS, A., DOLATA, K. M., ANTELO-VARELA, M., MESTRE BORRAS, A., ELFAGEIH, R., SIEVERS, S., BECHER, D., RIEDEL, K. & DE GIER, J.-W. 2020. Escherichia coli Can Adapt Its Protein Translocation Machinery for Enhanced Periplasmic Recombinant Protein Production. *Frontiers in Bioengineering and Biotechnology,* 7.

KARZAI, A. W., ROCHE, E. D. & SAUER, R. T. 2000. The SsrA–SmpB system for protein tagging, directed degradation and ribosome rescue. *Nature Structural Biology,* 7**,** 449-455.

KASLI, I. M., THOMAS, O. R. T. & OVERTON, T. W. 2019. Use of a design of experiments approach to optimise production of a recombinant antibody fragment in the periplasm of Escherichia coli: selection of signal peptide and optimal growth conditions. *AMB Express,* 9.

KASTENHOFER, J., RAJAMANICKAM, V., LIBISELLER-EGGER, J. & SPADIUT, O. 2021. Monitoring and control of E. coli cell integrity. *J Biotechnol,* 329**,** 1-12.

KE, N., LANDGRAF, D., PAULSSON, J. & BERKMEN, M. 2016. Visualization of Periplasmic and Cytoplasmic Proteins with a Self-Labeling Protein Tag. *Journal of Bacteriology,* 198**,** 1035-1043.

KEILER, K. C. & SAUER, R. T. 1996. Sequence Determinants of C-terminal Substrate Recognition by the Tsp Protease. *Journal of Biological Chemistry,* 271**,** 2589-2593.

KEILER, K. C., WALLER, P. R. H. & SAUER, R. T. 1996. Role of a Peptide Tagging System in Degradation of Proteins Synthesized from Damaged Messenger RNA. *Science,* 271**,** 990-993.

KELLY, C. L., LIU, Z., YOSHIHARA, A., JENKINSON, S. F., WORMALD, M. R., OTERO, J., ESTÉVEZ, A., KATO, A., MARQVORSEN, M. H., FLEET, G. W., ESTÉVEZ, R. J., IZUMORI, K. & HEAP, J. T. 2016. Synthetic Chemical Inducers and Genetic Decoupling Enable Orthogonal Control of the rhaBAD Promoter. *ACS Synth Biol,* 5**,** 1136-1145.

KHLEBNIKOV, A., DATSENKO, K. A., SKAUG, T., WANNER, B. L. & KEASLING, J. D. 2001. Homogeneous expression of the P(BAD) promoter in Escherichia coli by constitutive expression of the low-affinity high-capacity AraE transporter. *Microbiology (Reading),* 147**,** 3241-7.

KHLEBNIKOV, A. & KEASLING, J. D. 2002. Effect of lacY expression on homogeneity of induction from the P(tac) and P(trc) promoters by natural and synthetic inducers. *Biotechnol Prog,* 18**,** 672-4.

KHLEBNIKOV, A., RISA, Ø., SKAUG, T., CARRIER, T. A. & KEASLING, J. D. 2000. Regulatable Arabinose-Inducible Gene Expression System with Consistent Control in All Cells of a Culture. *Journal of Bacteriology,* 182**,** 7029-7034.

KHMELINSKII, A., MEURER, M., HO, C.-T., BESENBECK, B., FÜLLER, J., LEMBERG, M. K., BUKAU, B., MOGK, A. & KNOP, M. 2016. Incomplete proteasomal degradation of green fluorescent proteins in the context of tandem fluorescent protein timers. *Molecular Biology of the Cell,* 27**,** 360-370.

KIHARA, A., AKIYAMA, Y. & ITO, K. 1995. FtsH is required for proteolytic elimination of uncomplexed forms of SecY, an essential protein translocase subunit. *Proceedings of the National Academy of Sciences,* 92**,** 4532-4536.

KIM, J. Y., KIM, Y.-G. & LEE, G. M. 2012. CHO cells in biotechnology for production of recombinant proteins: current state and further potential. *Applied Microbiology and Biotechnology,* 93**,** 917-930.

KLEIN, C. A., TEUFEL, M., WEILE, C. J. & SOBETZKO, P. 2021. The bacterial promoter spacer modulates promoter strength and timing by length, TG-motifs and DNA supercoiling sensitivity. *Scientific Reports,* 11**,** 24399.

KLIMECKA, M. M., ANTOSIEWICZ, A., IZERT, M. A., SZYBOWSKA, P. E., TWARDOWSKI, P. K., DELAUNAY, C. & GÓRNA, M. W. 2021. A Uniform Benchmark for Testing SsrA-Derived Degrons in the Escherichia coli ClpXP Degradation Pathway. *Molecules,* 26**,** 5936.

KOBAYASHI, T. 1999. Respiratory chain strongly oxidizes the CXXC motif of DsbB in the Escherichia coli disulfide bond formation pathway. *The EMBO Journal,* 18**,** 1192-1198.

KOLDEWEY, P., STULL, F., HOROWITZ, S., MARTIN, R. & BARDWELL, J. C. A. 2016. Forces Driving Chaperone Action. *Cell,* 166**,** 369-379.

KOLODRUBETZ, D. & SCHLEIF, R. 1981a. L-arabinose transport systems in Escherichia coli K-12. *Journal of Bacteriology,* 148**,** 472-479.

KOLODRUBETZ, D. & SCHLEIF, R. 1981b. Regulation of the l-arabinose transport operons in Escherichia coli. *Journal of Molecular Biology,* 151**,** 215-227.

KOMINE, Y., KITABATAKE, M., YOKOGAWA, T., NISHIKAWA, K. & INOKUCHI, H. 1994. A tRNA-like structure is present in 10Sa RNA, a small stable RNA from Escherichia coli. *Proceedings of the National Academy of Sciences,* 91**,** 9223-9227.

KONIECZNA, I., ZARNOWIEC, P., KWINKOWSKI, M., KOLESINSKA, B., FRACZYK, J., KAMINSKI, Z. & KACA, W. 2012. Bacterial Urease and its Role in Long-Lasting Human Diseases. *Current Protein and Peptide Science,* 13**,** 789-806.

KONOVALOVA, A., MITCHELL, A. M. & SILHAVY, T. J. 2016. A lipoprotein/β-barrel complex monitors lipopolysaccharide integrity transducing information across the outer membrane. *eLife,* 5**,** e15276.

KRÄMER, H., NIEMÖLLER, M., AMOUYAL, M., REVET, B., VON WILCKEN-BERGMANN, B. & MÜLLER-HILL, B. 1987. lac repressor forms loops with linear DNA carrying two suitably spaced lac operators. *The EMBO Journal,* 6**,** 1481-1491.

KREWULAK, K. D., PEACOCK, R. S. & VOGEL, H. J. 2004. Periplasmic Binding Proteins Involved in Bacterial Iron Uptake. *Iron Transport in Bacteria.*

KUMAR, A., GROVER, S., SHARMA, J. & BATISH, V. K. 2010. Chymosin and other milk coagulants: sources and biotechnological interventions. *Critical Reviews in Biotechnology,* 30**,** 243-258.

KUMAZAKI, K., CHIBA, S., TAKEMOTO, M., FURUKAWA, A., NISHIYAMA, K.-I., SUGANO, Y., MORI, T., DOHMAE, N., HIRATA, K., NAKADA-NAKURA, Y., MATURANA, A. D., TANAKA, Y., MORI, H., SUGITA, Y., ARISAKA, F., ITO, K., ISHITANI, R., TSUKAZAKI, T. & NUREKI, O. 2014. Structural basis of Sec-independent membrane protein insertion by YidC. *Nature,* 509**,** 516-520.

KURIAKOSE, A., CHIRMULE, N. & NAIR, P. 2016. Immunogenicity of Biotherapeutics: Causes and Association with Posttranslational Modifications. *Journal of Immunology Research,* 2016**,** 1-18.

KUSTERS, I. & DRIESSEN, A. J. M. 2011. SecA, a remarkable nanomachine. *Cellular and Molecular Life Sciences,* 68**,** 2053-2066.

KWON, E., KIM, D. Y., GROSS, C. A., GROSS, J. D. & KIM, K. K. 2010. The crystal structure Escherichia coli Spy. *Protein Science,* 19**,** 2252-2259.

KWON, S.-K., KIM, S. K., LEE, D.-H. & KIM, J. F. 2015. Comparative genomics and experimental evolution of Escherichia coli BL21(DE3) strains reveal the landscape of toxicity escape from membrane protein overproduction. *Scientific Reports,* 5**,** 16076.

LA TEANA, A., BRANDI, A., FALCONI, M., SPURIO, R., PON, C. L. & GUALERZI, C. O. 1991. Identification of a cold shock transcriptional enhancer of the Escherichia coli gene encoding nucleoid protein H-NS. *Proceedings of the National Academy of Sciences,* 88**,** 10907-10911.

LALL, S. D., ERIHO, B. E. & JAY, J. M. 1989. Comparison for four methods for extracting periplasmic proteins. *Journal of Microbiological Methods,* 9**,** 195-199.

LAMBERT, D. & DRAPER, D. E. 2012. Denaturation of RNA Secondary and Tertiary Structure by Urea: Simple Unfolded State Models and Free Energy Parameters Account for Measured m-Values. *Biochemistry,* 51**,** 9014-9026.

LANG, B., BLOT, N., BOUFFARTIGUES, E., BUCKLE, M., GEERTZ, M., GUALERZI, C. O., MAVATHUR, R., MUSKHELISHVILI, G., PON, C. L., RIMSKY, S., STELLA, S., BABU, M. M. & TRAVERS, A. 2007. High-affinity DNA binding sites for H-NS provide a molecular basis for selective silencing within proteobacterial genomes. *Nucleic Acids Res,* 35**,** 6330-7.

LEBLANC, S. K. D., OATES, C. W. & RAIVIO, T. L. 2011. Characterization of the Induction and Cellular Role of the BaeSR Two-Component Envelope Stress Response of Escherichia coli. *Journal of Bacteriology,* 193**,** 3367-3375.

LEE, H. C. & BERNSTEIN, H. D. 2001. The targeting pathway of Escherichia coli presecretory and integral membrane proteins is specified by the hydrophobicity of the targeting signal. *Proceedings of the National Academy of Sciences,* 98**,** 3471-3476.

LEE, J. M., HAMMARÉN, H. M., SAVITSKI, M. M. & BAEK, S. H. 2023. Control of protein stability by post-translational modifications. *Nature Communications,* 14**,** 201.

LEE, S. K. & KEASLING, J. D. 2005. A Propionate-Inducible Expression System for Enteric Bacteria. *Applied and Environmental Microbiology,* 71**,** 6856-6862.

LEE, Y. J., LEE, R., LEE, S. H., YIM, S. S. & JEONG, K. J. 2016. Enhanced secretion of recombinant proteins via signal recognition particle (SRP)-dependent secretion pathway by deletion of rrsE in Escherichia coli. *Biotechnology and Bioengineering,* 113**,** 2453-2461.

LEI, S. P., LIN, H. C., WANG, S. S., CALLAWAY, J. & WILCOX, G. 1987. Characterization of the Erwinia carotovora pelB gene and its product pectate lyase. *Journal of Bacteriology,* 169**,** 4379-4383.

LEVCHENKO, I., SEIDEL, M., SAUER, R. T. & BAKER, T. A. 2000. A Specificity-Enhancing Factor for the ClpXP Degradation Machine. *Science,* 289**,** 2354-2356.

LEVY, R., AHLUWALIA, K., BOHMANN, D. J., GIANG, H. M., SCHWIMMER, L. J., ISSAFRAS, H., REDDY, N. B., CHAN, C., HORWITZ, A. H. & TAKEUCHI, T. 2013. Enhancement of antibody fragment secretion into the Escherichia coli periplasm by co-expression with the peptidyl prolyl isomerase, FkpA, in the cytoplasm. *Journal of Immunological Methods,* 394**,** 10-21.

LI, J. & ZHANG, Y. 2014. Relationship between promoter sequence and its strength in gene expression. *Eur Phys J E Soft Matter,* 37**,** 44.

LI, L., PARK, E., LING, J., INGRAM, J., PLOEGH, H. & RAPOPORT, T. A. 2016. Crystal structure of a substrate-engaged SecY protein-translocation channel. *Nature,* 531**,** 395-399.

LI, X., SHEN, J., CHEN, X., CHEN, L., WAN, S., QIU, X., CHEN, K., CHEN, C. & TAN, H. 2022. Humanization of Yeasts for Glycan-Type End-Products. *Frontiers in Microbiology,* 13.

LIES, M. & MAURIZI, M. R. 2008. Turnover of Endogenous SsrA-tagged Proteins Mediated by ATP-dependent Proteases in Escherichia coli. *Journal of Biological Chemistry,* 283**,** 22918-22929.

LINTON, D., ALLAN, E., KARLYSHEV, A. V., CRONSHAW, A. D. & WREN, B. W. 2002. Identification of N-acetylgalactosamine-containing glycoproteins PEB3 and CgpA in Campylobacter jejuni. *Molecular Microbiology,* 43**,** 497-508.

LISSEMORE, J. L., JANKOWSKI, J. T., THOMAS, C. B., MASCOTTI, D. P. & DEHASETH, P. L. 2000. Green fluorescent protein as a quantitative reporter of relative promoter activity in E. coli. *Biotechniques,* 28**,** 82-84.

LODGE, J. 1992. Broad host range plasmids carrying the Escherichia coli lactose and galactose operons. 95**,** 271-276.

LODGE, J., FEAR, J., BUSBY, S., GUNASEKARAN, P. & KAMINI, N. R. 1992. Broad host range plasmids carrying the Escherichia coli lactose and galactose operons. *FEMS Microbiol Lett,* 74**,** 271-6.

LOSEN, M., FRÖLICH, B., POHL, M. & BÜCHS, J. 2004. Effect of Oxygen Limitation and Medium Composition on Escherichia coli Fermentation in Shake-Flask Cultures. *Biotechnology Progress,* 20**,** 1062-1068.

LOW, K. O., MUHAMMAD MAHADI, N. & MD. ILLIAS, R. 2013. Optimisation of signal peptide for recombinant protein secretion in bacterial hosts. *Applied Microbiology and Biotechnology,* 97**,** 3811-3826.

MADAR, D., DEKEL, E., BREN, A., ZIMMER, A., PORAT, Z. & ALON, U. 2013. Promoter activity dynamics in the lag phase of Escherichia coli. *BMC Systems Biology,* 7**,** 136.

MAMIPOUR, M., YOUSEFI, M. & HASANZADEH, M. 2017. An overview on molecular chaperones enhancing solubility of expressed recombinant proteins with correct folding. *International Journal of Biological Macromolecules,* 102**,** 367-375.

MANSELL, T. J., LINDERMAN, S. W., FISHER, A. C. & DELISA, M. P. 2010. A rapid protein folding assay for the bacterial periplasm. *Protein Science,* 19**,** 1079-1090.

MANTA, B., BOYD, D. & BERKMEN, M. 2019. Disulfide Bond Formation in the Periplasm of Escherichia coli. *EcoSal Plus,* 8**,** 10.1128/ecosalplus.ESP-0012-2018.

MAO, C., CHEADLE, C. E., HARDY, S. J. S., LILLY, A. A., SUO, Y., SANGANNA GARI, R. R., KING, G. M. & RANDALL, L. L. 2013. Stoichiometry of SecYEG in the active translocase of Escherichia coli varies with precursor species. *Proceedings of the National Academy of Sciences,* 110**,** 11815-11820.

MAO, L., SCHNEIDER, J. W. & ROBINSON, A. S. 2022. Progress toward rapid, at-line N-glycosylation detection and control for recombinant protein expression. *Current Opinion in Biotechnology,* 78**,** 102788.

MARBACH, A. & BETTENBROCK, K. 2012. lac operon induction in Escherichia coli: Systematic comparison of IPTG and TMG induction and influence of the transacetylase LacA. *Journal of Biotechnology,* 157**,** 82-88.

MARISCH, K., BAYER, K., SCHARL, T., MAIRHOFER, J., KREMPL, P. M., HUMMEL, K., RAZZAZI-FAZELI, E. & STRIEDNER, G. 2013. A Comparative Analysis of Industrial Escherichia coli K–12 and B Strains in High-Glucose Batch Cultivations on Process-, Transcriptome- and Proteome Level. *PLoS ONE,* 8**,** e70516.

MARKIEWICZ, P., KLEINA, L. G., CRUZ, C., EHRET, S. & MILLER, J. H. 1994. Genetic Studies of the lac Repressor. XIV. Analysis of 4000 Altered Escherichia coli lac Repressors Reveals Essential and Non-essential Residues, as well as "Spacers" which do not Require a Specific Sequence. *Journal of Molecular Biology,* 240**,** 421-433.

MARSCHALL, L., SAGMEISTER, P. & HERWIG, C. 2017. Tunable recombinant protein expression in E. coli: promoter systems and genetic constraints. *Applied Microbiology and Biotechnology,* 101**,** 501-512.

MARTIN, R. G. & ROSNER, J. L. 2001. The AraC transcriptional activators. *Current Opinion in Microbiology,* 4**,** 132-137.

MATIAS, V. R. F. & BEVERIDGE, T. J. 2005. Cryo-electron microscopy reveals native polymeric cell wall structure in Bacillus subtilis 168 and the existence of a periplasmic space. *Molecular Microbiology,* 56**,** 240-251.

MATIAS, V. R. R. F. & BEVERIDGE, T. J. 2006. Native Cell Wall Organization Shown by Cryo-Electron Microscopy Confirms the Existence of a Periplasmic Space in Staphylococcus aureus. *Journal of Bacteriology,* 188**,** 1011-1021.

MATOS, C. F., ROBINSON, C., ALANEN, H. I., PRUS, P., UCHIDA, Y., RUDDOCK, L. W., FREEDMAN, R. B. & KESHAVARZ-MOORE, E. 2014. Efficient export of prefolded, disulfide-bonded recombinant proteins to the periplasm by the Tat pathway in Escherichia coli CyDisCo strains. *Biotechnol Prog,* 30**,** 281-90.

MATSUYAMA, S.-I., FUJITA, Y., SAGARA, K. & MIZUSHIMA, S. 1992. Overproduction, purification and characterization of SecD and SecF, integral membrane components of the protein translocation machinery of Escherichia coli. *Biochimica et Biophysica Acta (BBA) - Protein Structure and Molecular Enzymology,* 1122**,** 77-84.

MATZ, M. V., FRADKOV, A. F., LABAS, Y. A., SAVITSKY, A. P., ZARAISKY, A. G., MARKELOV, M. L. & LUKYANOV, S. A. 1999. Fluorescent proteins from nonbioluminescent Anthozoa species. *Nature Biotechnology,* 17**,** 969-973.

MAVEYRAUD, L. & MOUREY, L. 2020. Protein X-ray Crystallography and Drug Discovery. *Molecules,* 25**,** 1030.

MCGINNESS, K. E., BAKER, T. A. & SAUER, R. T. 2006. Engineering Controllable Protein Degradation. *Molecular Cell,* 22**,** 701-707.

MCNICHOLAS, P., SALAVATI, R. & OLIVER, D. 1997. Dual regulation of Escherichia coli secA translation by distinct upstream elements. *Journal of Molecular Biology,* 265**,** 128-141.

MECSAS, J., ROUVIERE, P. E., ERICKSON, J. W., DONOHUE, T. J. & GROSS, C. A. 1993. The activity of sigma E, an Escherichia coli heat-inducible sigma-factor, is modulated by expression of outer membrane proteins. *Genes & Development,* 7**,** 2618-2628.

MENG, J., YOUNG, G. & CHEN, J. 2021. The Rcs System in Enterobacteriaceae: Envelope Stress Responses and Virulence Regulation. *Frontiers in Microbiology,* 12.

MERCIER, E., HOLTKAMP, W., RODNINA, M. V. & WINTERMEYER, W. 2017. Signal recognition particle binds to translating ribosomes before emergence of a signal anchor sequence. *Nucleic Acids Research,* 45**,** 11858-11866.

MERCIER, E., WANG, X., MAITI, M., WINTERMEYER, W. & RODNINA, M. V. 2021. Lateral gate dynamics of the bacterial translocon during cotranslational membrane protein insertion. *Proceedings of the National Academy of Sciences,* 118**,** e2100474118.

MERGULHÃO, F. J. M., TAIPA, M. A., CABRAL, J. M. S. & MONTEIRO, G. A. 2004. Evaluation of bottlenecks in proinsulin secretion by Escherichia coli. *Journal of Biotechnology,* 109**,** 31-43.

MERTZ, J. E. & DAVIS, R. W. 1972. Cleavage of DNA by R1 Restriction Endonuclease Generates Cohesive Ends. *Proceedings of the National Academy of Sciences,* 69**,** 3370-3374.

MIHALCESCU, I., VAN-MELLE GATEAU, M., CHELLI, B., PINEL, C. & RAVANAT, J.-L. 2015. Green autofluorescence, a double edged monitoring tool for bacterial growth and activity in micro-plates. *Physical Biology,* 12**,** 066016.

MIROUX, B. & WALKER, J. E. 1996. Over-production of Proteins inEscherichia coli: Mutant Hosts that Allow Synthesis of some Membrane Proteins and Globular Proteins at High Levels. *Journal of Molecular Biology,* 260**,** 289-298.

MIRZADEH, K., MARTÍNEZ, V., TODDO, S., GUNTUR, S., HERRGÅRD, M. J., ELOFSSON, A., NØRHOLM, M. H. H. & DALEY, D. O. 2015. Enhanced Protein Production inEscherichia coliby Optimization of Cloning Scars at the Vector–Coding Sequence Junction. *ACS Synthetic Biology,* 4**,** 959-965.

MIRZADEH, K., SHILLING, P. J., ELFAGEIH, R., CUMMING, A. J., CUI, H. L., RENNIG, M., NØRHOLM, M. H. H. & DALEY, D. O. 2020. Increased production of periplasmic proteins in Escherichia coli by directed evolution of the translation initiation region. *Microbial Cell Factories,* 19.

MITCHELL, A. M. & SILHAVY, T. J. 2019. Envelope stress responses: balancing damage repair and toxicity. *Nature Reviews Microbiology,* 17**,** 417-428.

MITRA, R., GADKARI, V. V., MEINEN, B. A., VAN MIERLO, C. P. M., RUOTOLO, B. T. & BARDWELL, J. C. A. 2021. Mechanism of the small ATP-independent chaperone Spy is substrate specific. *Nature Communications,* 12**,** 851.

MIWA, T., CHADANI, Y. & TAGUCHI, H. 2021. Escherichia coli small heat shock protein IbpA is an aggregation-sensor that self-regulates its own expression at posttranscriptional levels. *Molecular Microbiology,* 115**,** 142-156.

MIYADA, C. G., STOLTZFUS, L. & WILCOX, G. 1984. Regulation of the araC gene of Escherichia coli: catabolite repression, autoregulation, and effect on araBAD expression. *Proceedings of the National Academy of Sciences,* 81**,** 4120-4124.

MOBLEY, H. L. & HAUSINGER, R. P. 1989. Microbial ureases: significance, regulation, and molecular characterization. *Microbiological Reviews,* 53**,** 85-108.

MOBLEY, H. L., ISLAND, M. D. & MASSAD, G. 1994. Virulence determinants of uropathogenic Escherichia coli and Proteus mirabilis. *Kidney Int Suppl,* 47**,** S129-36.

MORRA, R., DEL CARRATORE, F., MUHAMADALI, H., HORGA, L. G., HALLIWELL, S., GOODACRE, R., BREITLING, R. & DIXON, N. 2018. Translation Stress Positively Regulates MscL-Dependent Excretion of Cytoplasmic Proteins. *mBio,* 9.

MORRA, R., SHANKAR, J., ROBINSON, C. J., HALLIWELL, S., BUTLER, L., UPTON, M., HAY, S., MICKLEFIELD, J. & DIXON, N. 2016. Dual transcriptional-translational cascade permits cellular level tuneable expression control. *Nucleic Acids Research,* 44**,** e21-e21.

MUTA, M., IIZUKA, R., NIWA, T., GUO, Y., TAGUCHI, H. & FUNATSU, T. 2020. Nascent SecM chain interacts with outer ribosomal surface to stabilize translation arrest. *Biochemical Journal,* 477**,** 557-566.

MUTALIK, V. K., NONAKA, G., ADES, S. E., RHODIUS, V. A. & GROSS, C. A. 2009. Promoter Strength Properties of the Complete Sigma E Regulon of Escherichia coli and Salmonella enterica. *Journal of Bacteriology,* 191**,** 7279-7287.

NAGAI, H., YUZAWA, H. & YURA, T. 1991. Regulation of the heat shock response in E coli: involvement of positive and negative cis-acting elements in translation control of sigma 32 synthesis. *Biochimie,* 73**,** 1473-9.

NAGAMORI, S., NISHIYAMA, K.-I. & TOKUDA, H. 2002. Membrane Topology Inversion of SecG Detected by Labeling with a Membrane-Impermeable Sulfhydryl Reagent that Causes a Close Association of SecG with SecA. *The Journal of Biochemistry,* 132**,** 629-634.

NAGAO, Y., KOH, S., TAGUCHI, S. & SHIMADA, T. 2023. Cell-growth phase-dependent promoter replacement approach for improved poly(lactate-co-3-hydroxybutyrate) production in Escherichia coli. *Microbial Cell Factories,* 22.

NAGASAWA, S., ISHIGE, K. & MIZUNO, T. 1993. Novel Members of the Two-Component Signal Transduction Genes in Escherichia coli1. *The Journal of Biochemistry,* 114**,** 350-357.

NAKAGAWA, C., NISHIMURA, S., SENDA-MURATA, K. & SUGIMOTO, K. 2012. A Rapid and Simple Method of Evaluating the Dimeric Tendency of Fluorescent Proteins in Living Cells Using a Truncated Protein of Importin α as Fusion Tag. *Bioscience, Biotechnology, and Biochemistry,* 76**,** 388-390.

NAKATOGAWA, H. & ITO, K. 2001. Secretion Monitor, SecM, Undergoes Self-Translation Arrest in the Cytosol. *Molecular Cell,* 7**,** 185-192.

NAKATOGAWA, H. & ITO, K. 2002. The Ribosomal Exit Tunnel Functions as a Discriminating Gate. *Cell,* 108**,** 629-636.

NAKATOGAWA, H., MURAKAMI, A., MORI, H. & ITO, K. 2005. SecM facilitates translocase function of SecA by localizing its biosynthesis. *Genes & Development,* 19**,** 436-444.

NARBERHAUS, F. & BALSIGER, S. 2003. Structure-Function Studies of Escherichia coli RpoH (σ 32) by In Vitro Linker Insertion Mutagenesis. *Journal of Bacteriology,* 185**,** 2731-2738.

NARITA, T., WEINERT, B. T. & CHOUDHARY, C. 2019. Functions and mechanisms of non-histone protein acetylation. *Nature Reviews Molecular Cell Biology,* 20**,** 156-174.

NGUYEN, H., PARK, J., KANG, S. & KIM, M. 2015. Surface Plasmon Resonance: A Versatile Technique for Biosensor Applications. *Sensors,* 15**,** 10481-10510.

NICHOLSON, E. B., CONCAUGH, E. A., FOXALL, P. A., ISLAND, M. D. & MOBLEY, H. L. 1993. Proteus mirabilis urease: transcriptional regulation by UreR. *Journal of Bacteriology,* 175**,** 465-473.

NIEHAUS, F., GABOR, E., WIELAND, S., SIEGERT, P., MAURER, K. H. & ECK, J. 2011. Enzymes for the laundry industries: tapping the vast metagenomic pool of alkaline proteases. *Microbial Biotechnology,* 4**,** 767-776.

NIKAIDO, H. & ZGURSKAYA, H. I. 2001. AcrAB and related multidrug efflux pumps of Escherichia coli. *J Mol Microbiol Biotechnol,* 3**,** 215-8.

NISHI, H., HASHIMOTO, K. & ANNA 2011. Phosphorylation in Protein-Protein Binding: Effect on Stability and Function. *Structure,* 19**,** 1807-1815.

NISHINO, K., HONDA, T. & YAMAGUCHI, A. 2005. Genome-Wide Analyses of Escherichia coli Gene Expression Responsive to the BaeSR Two-Component Regulatory System. *Journal of Bacteriology,* 187**,** 1763-1772.

NISHIYAMA, K., HANADA, M. & TOKUDA, H. 1994. Disruption of the gene encoding p12 (SecG) reveals the direct involvement and important function of SecG in the protein translocation of Escherichia coli at low temperature. *The EMBO Journal,* 13**,** 3272–3277.

NOGA, M. J., BÜKE, F., BROEK, N. J. F. V. D., IMHOLZ, N. C. E., SCHERER, N., YANG, F. & BOKINSKY, G. 2020. Posttranslational Control of PlsB Is Sufficient To Coordinate Membrane Synthesis with Growth in Escherichia coli. *mBio,* 11**,** 10.1128/mbio.02703-19.

NORRANDER, J., KEMPE, T. & MESSING, J. 1983. Construction of improved M13 vectors using oligodeoxynucleotide-directed mutagenesis. *Gene,* 26**,** 101-106.

NOUMI, T., MAEDA, M. & FUTAI, M. 1987. Mode of inhibition of sodium azide on H+-ATPase of Escherichia coli. *FEBS Letters,* 213**,** 381-384.

NOVICK, A. & WEINER, M. 1957. ENZYME INDUCTION AS AN ALL-OR-NONE PHENOMENON. *Proceedings of the National Academy of Sciences,* 43**,** 553-566.

NOVOTNY, C. P. & ENGLESBERG, E. 1966. The L-arabinose permease system in Escherichia coli B/r. *Biochim Biophys Acta,* 117**,** 217-30.

OEHLER, S., AMOUYAL, M., KOLKHOF, P., VON WILCKEN-BERGMANN, B. & MÜLLER-HILL, B. 1994. Quality and position of the three lac operators of E. coli define efficiency of repression. *The EMBO Journal,* 13**,** 3348-3355.

OEHLER, S., EISMANN, E. R., KRÄMER, H. & MÜLLER-HILL, B. 1990. The three operators of the lac operon cooperate in repression. *Embo j,* 9**,** 973-9.

OGDEN, S., HAGGERTY, D., STONER, C. M., KOLODRUBETZ, D. & SCHLEIF, R. 1980. The Escherichia coli L-arabinose operon: binding sites of the regulatory proteins and a mechanism of positive and negative regulation. *Proc Natl Acad Sci U S A,* 77**,** 3346-50.

OKUDA, S., FREINKMAN, E. & KAHNE, D. 2012. Cytoplasmic ATP Hydrolysis Powers Transport of Lipopolysaccharide Across the Periplasm in E. coli. *Science,* 338**,** 1214-1217.

OLIVER, D., NORMAN, J. & SARKER, S. 1998. Regulation of Escherichia coli secA by Cellular Protein Secretion Proficiency Requires an Intact Gene X Signal Sequence and an Active Translocon. *Journal of Bacteriology,* 180**,** 5240-5242.

OLIVER, D. B., CABELLI, R. J., DOLAN, K. M. & JAROSIK, G. P. 1990. Azide-resistant mutants of Escherichia coli alter the SecA protein, an azide-sensitive component of the protein export machinery. *Proceedings of the National Academy of Sciences,* 87**,** 8227-8231.

OLSEN, J. V., BLAGOEV, B., GNAD, F., MACEK, B., KUMAR, C., MORTENSEN, P. & MANN, M. 2006. Global, In Vivo, and Site-Specific Phosphorylation Dynamics in Signaling Networks. *Cell,* 127**,** 635-648.

OMOYA, K., KATO, Z., MATSUKUMA, E., LI, A., HASHIMOTO, K., YAMAMOTO, Y., OHNISHI, H. & KONDO, N. 2004. Systematic optimization of active protein expression using GFP as a folding reporter. *Protein Expression and Purification,* 36**,** 327-332.

OR, E. 2002. Dissociation of the dimeric SecA ATPase during protein translocation across the bacterial membrane. *The EMBO Journal,* 21**,** 4470-4479.

ORFANOUDAKI, G. & ECONOMOU, A. 2014. Proteome-wide Subcellular Topologies ofE. coliPolypeptides Database (STEPdb). *Molecular & Cellular Proteomics,* 13**,** 3674-3687.

OSGERBY, A. & OVERTON, T. 2023. Approaches for High-throughput Quantification of Periplasmic Recombinant Proteins. *New Biotechnology,* 77.

OSWALD, J., NJENGA, R., NATRIASHVILI, A., SARMAH, P. & KOCH, H.-G. 2021. The Dynamic SecYEG Translocon. *Frontiers in Molecular Biosciences,* 8.

OTTONE, S., NGUYEN, X., BAZIN, J., BÉRARD, C., JIMENEZ, S. & LETOURNEUR, O. 2007. Expression of hepatitis B surface antigen major subtypes in Pichia pastoris and purification for in vitro diagnosis. *Protein Expression and Purification,* 56**,** 177-188.

OU, J., WANG, L., DING, X., DU, J., ZHANG, Y., CHEN, H. & XU, A. 2004. Stationary phase protein overproduction is a fundamental capability of Escherichia coli. *Biochemical and biophysical research communications,* 314**,** 174-80.

OVERTON, T. W. 2014. Recombinant protein production in bacterial hosts. *Drug Discovery Today,* 19**,** 590-601.

PAGE, L., GRIFFITHS, L. & COLE, J. A. 1990. Different physiological roles of two independent pathways for nitrite reduction to ammonia by enteric bacteria. *Arch Microbiol,* 154**,** 349-54.

PANYACHARIWAT, N. & STECKEL, H. 2014. Stability of urea in solution and pharmaceutical preparations. *J Cosmet Sci,* 65**,** 187-95.

PARAPOULI, M., VASILEIADIS, A., AFENDRA, A. S. & HATZILOUKAS, E. 2020. Saccharomyces cerevisiae and its industrial applications. *AIMS Microbiol,* 6**,** 1-31.

PATIL, R. S., ANUPA, A., GUPTA, J. A. & RATHORE, A. S. 2022. Challenges in Expression and Purification of Functional Fab Fragments in E. coli: Current Strategies and Perspectives. *Fermentation,* 8**,** 175.

PÉDELACQ, J.-D., CABANTOUS, S., TRAN, T., TERWILLIGER, T. C. & WALDO, G. S. 2006. Engineering and characterization of a superfolder green fluorescent protein. *Nature Biotechnology,* 24**,** 79-88.

PERLMAN, D. & HALVORSON, H. O. 1983. A putative signal peptidase recognition site and sequence in eukaryotic and prokaryotic signal peptides. *Journal of Molecular Biology,* 167**,** 391-409.

PETERSON, R. T. & SCHREIBER, S. L. 1999. Kinase phosphorylation: Keeping it all in the family. *Current Biology,* 9**,** R521-R524.

PHUE, J. N., NORONHA, S. B., HATTACHARYYA, R., WOLFE, A. J. & SHILOACH, J. 2005. Glucose metabolism at high density growth of E. coli B and E. coli K: Differences in metabolic pathways are responsible for efficient glucose utilization in E. coli B as determined by microarrays and Northern blot analyses. *Biotechnology and Bioengineering,* 90**,** 805-820.

POGLIANO, J., LYNCH, A. S., BELIN, D., LIN, E. C. & BECKWITH, J. 1997. Regulation of Escherichia coli cell envelope proteins involved in protein folding and degradation by the Cpx two-component system. *Genes & Development,* 11**,** 1169-1182.

POLLARD, T. D. 2010. A Guide to Simple and Informative Binding Assays. *Molecular Biology of the Cell,* 21**,** 4061-4067.

POORE, C. A., COKER, C., DATTELBAUM, J. D. & MOBLEY, H. L. T. 2001. Identification of the Domains of UreR, an AraC-Like Transcriptional Regulator of the Urease Gene Cluster in Proteus mirabilis. *Journal of Bacteriology,* 183**,** 4526-4535.

POORE, C. A. & MOBLEY, H. L. T. 2003. Differential regulation of the Proteus mirabilis urease gene cluster by UreR and H-NS. *Microbiology,* 149**,** 3383-3394.

POTEL, C. M., LIN, M.-H., HECK, A. J. R. & LEMEER, S. 2018. Widespread bacterial protein histidine phosphorylation revealed by mass spectrometry-based proteomics. *Nature Methods,* 15**,** 187-190.

PRICE, N. L. & RAIVIO, T. L. 2009. Characterization of the Cpx Regulon in Escherichia coli Strain MC4100. *Journal of Bacteriology,* 191**,** 1798-1815.

PRINZ, W. A., ÅSLUND, F., HOLMGREN, A. & BECKWITH, J. 1997. The Role of the Thioredoxin and Glutaredoxin Pathways in Reducing Protein Disulfide Bonds in the Escherichia coliCytoplasm*. *Journal of Biological Chemistry,* 272**,** 15661-15667.

QUAN, S., KOLDEWEY, P., TAPLEY, T., KIRSCH, N., RUANE, K. M., PFIZENMAIER, J., SHI, R., HOFMANN, S., FOIT, L., REN, G., JAKOB, U., XU, Z., CYGLER, M. & BARDWELL, J. C. A. 2011. Genetic selection designed to stabilize proteins uncovers a chaperone called Spy. *Nature Structural & Molecular Biology,* 18**,** 262-269.

QUIANZON, C. C. & CHEIKH, I. 2012. History of insulin. *Journal of Community Hospital Internal Medicine Perspectives,* 2**,** 18701.

RAFFA, R. G. & RAIVIO, T. L. 2002. A third envelope stress signal transduction pathway in Escherichia coli. *Molecular Microbiology,* 45**,** 1599-1611.

RAIVIO, T. L. 2014. Everything old is new again: An update on current research on the Cpx envelope stress response. *Biochimica et Biophysica Acta (BBA) - Molecular Cell Research,* 1843**,** 1529-1541.

RAIVIO, T. L., LAIRD, M. W., JOLY, J. C. & SILHAVY, T. J. 2000. Tethering of CpxP to the inner membrane prevents spheroplast induction of the Cpx envelope stress response. *Molecular Microbiology,* 37**,** 1186-1197.

RAIVIO, T. L., LEBLANC, S. K. D. & PRICE, N. L. 2013. The Escherichia coli Cpx Envelope Stress Response Regulates Genes of Diverse Function That Impact Antibiotic Resistance and Membrane Integrity. *Journal of Bacteriology,* 195**,** 2755-2767.

RAIVIO, T. L., POPKIN, D. L. & SILHAVY, T. J. 1999. The Cpx Envelope Stress Response Is Controlled by Amplification and Feedback Inhibition. *Journal of Bacteriology,* 181**,** 5263-5272.

RAIVIO, T. L. & SILHAVY, T. J. 2001. Periplasmic Stress and ECF Sigma Factors. *Annual Review of Microbiology,* 55**,** 591-624.

RAJACHARYA, G. H., SHARMA, A. & YAZDANI, S. S. 2024. Proteomics and metabolic burden analysis to understand the impact of recombinant protein production in E. coli. *Scientific Reports,* 14.

RAJAPANDI, T., DOLAN, K. M. & OLIVER, D. B. 1991. The first gene in the Escherichia coli secA operon, gene X, encodes a nonessential secretory protein. *Journal of Bacteriology,* 173**,** 7092-7097.

RAMAZI, S. & ZAHIRI, J. 2021. Posttranslational modifications in proteins: resources, tools and prediction methods. *Database (Oxford),* 2021.

RANDALL, L. L., CRANE, J. M., LIU, G. & HARDY, S. J. S. 2004. Sites of interaction between SecA and the chaperone SecB, two proteins involved in export. *Protein Science,* 13**,** 1124-1133.

RASHID, M. H. 2022. Full-length recombinant antibodies from Escherichia coli: production, characterization, effector function (Fc) engineering, and clinical evaluation. *mAbs,* 14.

RATHORE, A. & BATRA, J. 2016. Antibody production in microbial hosts. *Biopharm International,* 28**,** 18-23.

RECORD JR, M. T., COURTENAY, E. S., CAYLEY, D. S. & GUTTMAN, H. J. 1998. Responses of E. coli to osmotic stress: large changes in amounts of cytoplasmic solutes and water. *Trends in Biochemical Sciences,* 23**,** 143-148.

REEVE, B., HARGEST, T., GILBERT, C. & ELLIS, T. 2014. Predicting Translation Initiation Rates for Designing Synthetic Biology. *Frontiers in Bioengineering and Biotechnology,* 2.

REZNIKOFF, W. S., WINTER, R. B. & HURLEY, C. K. 1974. The Location of the Repressor Binding Sites in the lac Operon. *Proceedings of the National Academy of Sciences,* 71**,** 2314-2318.

RICKSEN, YAN, J. & LINDA 2015. H-NS Regulates Gene Expression and Compacts the Nucleoid: Insights from Single-Molecule Experiments. *Biophysical Journal,* 109**,** 1321-1329.

RIETSCH, A., BESSETTE, P., GEORGIOU, G. & BECKWITH, J. 1997. Reduction of the periplasmic disulfide bond isomerase, DsbC, occurs by passage of electrons from cytoplasmic thioredoxin. *Journal of Bacteriology,* 179**,** 6602–6608.

RIGGS, P. D., DERMAN, A. I. & BECKWITH, J. 1988. A Mutation Affecting the Regulation of a secA-lac2 Fusion Defines a New sec Gene. *Genetics,* 118**,** 571-579.

ROBINSON, P. J. & BULLEID, N. J. 2020. Mechanisms of Disulfide Bond Formation in Nascent Polypeptides Entering the Secretory Pathway. *Cells,* 9**,** 1994.

ROSANO, G. L. & CECCARELLI, E. A. 2014. Recombinant protein expression in Escherichia coli: advances and challenges. *Frontiers in Microbiology,* 5.

ROSANO, G. L., MORALES, E. S. & CECCARELLI, E. A. 2019. New tools for recombinant protein production in Escherichia coli: A 5-year update. *Protein Science,* 28**,** 1412-1422.

ROSENBERG, A. H., LADE, B. N., DAO-SHAN, C., LIN, S.-W., DUNN, J. J. & STUDIER, F. W. 1987. Vectors for selective expression of cloned DNAs by T7 RNA polymerase. *Gene,* 56**,** 125-135.

ROSENBERG, M., AZEVEDO, N. F. & IVASK, A. 2019. Propidium iodide staining underestimates viability of adherent bacterial cells. *Scientific Reports,* 9.

ROSNER, J. L. & MARTIN, R. G. 2013. Reduction of Cellular Stress by TolC-Dependent Efflux Pumps in Escherichia coli Indicated by BaeSR and CpxARP Activation of spy in Efflux Mutants. *Journal of Bacteriology,* 195**,** 1042-1050.

ROWE, L. W. & CIULLA, T. A. 2024. Long-acting delivery and therapies for neovascular age-related macular degeneration. *Expert Opinion on Biological Therapy,* 24**,** 799-814.

RUAN, A., REN, C. & QUAN, S. 2020. Conversion of the molecular chaperone Spy into a novel fusion tag to enhance recombinant protein expression. *Journal of Biotechnology,* 307**,** 131-138.

SALGADO, H., GAMA-CASTRO, S., LARA, P., MEJIA-ALMONTE, C., ALARCÓN-CARRANZA, G., LÓPEZ-ALMAZO, A. G., BETANCOURT-FIGUEROA, F., PEÑA-LOREDO, P., ALQUICIRA-HERNÁNDEZ, S., LEDEZMA-TEJEIDA, D., ARIZMENDI-ZAGAL, L., MENDEZ-HERNANDEZ, F., DIAZ-GOMEZ, A. K., OCHOA-PRAXEDIS, E., MUÑIZ-RASCADO, L. J., GARCÍA-SOTELO, J. S., FLORES-GALLEGOS, F. A., GÓMEZ, L., BONAVIDES-

MARTÍNEZ, C., VÍCTOR, M., HERNÁNDEZ-ALVAREZ, A. J., SANTOS-ZAVALETA, A., CAPELLA-GUTIERREZ, S., GELPI, J. L. & COLLADO-VIDES, J. 2024. RegulonDB v12.0: a comprehensive resource of transcriptional regulation in E. coli K-12. *Nucleic Acids Research,* 52**,** D255-D264.

SANDERS, A. N. & PAVELKA, M. S. 2013. Phenotypic analysis of Eschericia coli mutants lacking l,d-transpeptidases. *Microbiology,* 159**,** 1842-1852.

SARKER, S., RUDD, K. E. & OLIVER, D. 2000. Revised translation start site for secM defines an atypical signal peptide that regulates Escherichia coli secA expression. *J Bacteriol,* 182**,** 5592-5.

SASTRY, S. S. & ROSS, B. M. 1997. Nuclease Activity of T7 RNA Polymerase and the Heterogeneity of Transcription Elongation Complexes. *Journal of Biological Chemistry,* 272**,** 8644-8652.

SCHAFFER, J. N. & PEARSON, M. M. 2017. Proteus mirabilis and Urinary Tract Infections. *Urinary Tract Infections.*

SCHAFFITZEL, C., OSWALD, M., BERGER, I., ISHIKAWA, T., ABRAHAMS, J. P., KOERTEN, H. K., KONING, R. I. & BAN, N. 2006. Structure of the E. coli signal recognition particle bound to a translating ribosome. *Nature,* 444**,** 503-506.

SCHELLHORN, H. E. 2020. Function, Evolution, and Composition of the RpoS Regulon in Escherichia coli. *Frontiers in Microbiology,* 11.

SCHIBICH, D., GLOGE, F., PÖHNER, I., BJÖRKHOLM, P., WADE, R. C., VON HEIJNE, G., BUKAU, B. & KRAMER, G. 2016. Global profiling of SRP interaction with nascent polypeptides. *Nature,* 536**,** 219-223.

SCHIERLE, C. F., BERKMEN, M., HUBER, D., KUMAMOTO, C., BOYD, D. & BECKWITH, J. 2003. The DsbA Signal Sequence Directs Efficient, Cotranslational Export of Passenger Proteins to the Escherichia coli Periplasm via the Signal Recognition Particle Pathway. *Journal of Bacteriology,* 185**,** 5706-5713.

SCHIMEK, C., EGGER, E., TAUER, C., STRIEDNER, G., BROCARD, C., CSERJAN-PUSCHMANN, M. & HAHN, R. 2020. Extraction of recombinant periplasmic proteins under industrially relevant process conditions: Selectivity and yield strongly depend on protein titer and methodology. *Biotechnology Progress,* 36**,** e2999.

SCHLEGEL, S., RUJAS, E., YTTERBERG, A. J., ZUBAREV, R. A., LUIRINK, J. & DE GIER, J.-W. 2013. Optimizing heterologous protein production in the periplasm of E. coli by regulating gene expression levels. *Microbial Cell Factories,* 12**,** 24.

SCHLEIF, R. 1969. An l-arabinose binding protein and arabinose permeation in Escherichia coli. *Journal of Molecular Biology,* 46**,** 185-196.

SCHLEIF, R. 2000. Regulation of the l-arabinose operon of Escherichia coli. *Trends in Genetics,* 16**,** 559-565.

SCHLEIF, R. 2010. AraC protein, regulation of the l-arabinose operon in Escherichia coli, and the light switch mechanism of AraC action. *FEMS Microbiology Reviews,* 34**,** 779-796.

SCHLEIF, R. 2021. A Career's Work, the l-Arabinose Operon: How It Functions and How We Learned It. *EcoSal Plus,* 10**,** eESP-0012-2021.

SCHNEIDER, D., DUPERCHY, E., DEPEYROT, J., COURSANGE, E., LENSKI, R. E. & BLOT, M. 2002. Genomic comparisons among Escherichia coli strains B, K-12, and O157:H7 using IS elements as molecular markers. *BMC Microbiology,* 2**,** 18.

SCHULZE, R. J., KOMAR, J., BOTTE, M., ALLEN, W. J., WHITEHOUSE, S., GOLD, V. A. M., LYCKLAMA A NIJEHOLT, J. A., HUARD, K., BERGER, I., SCHAFFITZEL, C. & COLLINSON, I. 2014. Membrane protein insertion and proton-motive-force-dependent secretion through the bacterial holo-translocon SecYEG–SecDF–YajC–YidC. *Proceedings of the National Academy of Sciences, USA,* 111**,** 4844-4849.

SCHÜTZ, A., BERNHARD, F., BERROW, N., BUYEL, J. F., FERREIRA-DA-SILVA, F., HAUSTRAETE, J., VAN DEN HEUVEL, J., HOFFMANN, J. E., DE MARCO, A., PELEG, Y., SUPPMANN, S., UNGER, T., VANHOUCKE, M., WITT, S. & REMANS, K. 2023. A concise guide to choosing suitable gene expression systems for recombinant protein production. *STAR Protoc,* 4**,** 102572.

SCRIPTURE, J. B., VOELKER, C., MILLER, S., O'DONNELL, R. T., POLGAR, L., RADE, J., HORAZDOVSKY, B. F. & HOGG, R. W. 1987. High-affinity l-arabinose transport operon: Nucleotide sequence and analysis of gene products. *Journal of Molecular Biology,* 197**,** 37-46.

SCULLY, M., CATALAND, S. R., PEYVANDI, F., COPPO, P., KNÖBL, P., KREMER HOVINGA, J. A., METJIAN, A., DE LA RUBIA, J., PAVENSKI, K., CALLEWAERT, F., BISWAS, D., DE WINTER, H. & ZELDIN, R. K. 2019. Caplacizumab Treatment for Acquired Thrombotic Thrombocytopenic Purpura. *New England Journal of Medicine,* 380**,** 335-346.

SEINEN, A.-B., SPAKMAN, D., VAN OIJEN, A. M. & DRIESSEN, A. J. M. 2021. Cellular dynamics of the SecA ATPase at the single molecule level. *Scientific Reports,* 11.

SELAS CASTIÑEIRAS, T., WILLIAMS, S. G., HITCHCOCK, A., COLE, J. A., SMITH, D. C. & OVERTON, T. W. 2018a. Development of a generic β-lactamase screening system for improved signal peptides for periplasmic targeting of recombinant proteins in Escherichia coli. *Scientific Reports,* 8.

SELAS CASTIÑEIRAS, T., WILLIAMS, S. G., HITCHCOCK, A., COLE, J. A., SMITH, D. C. & OVERTON, T. W. 2018b. Optimizing host cell physiology and stress avoidance for the production of recombinant human tumour necrosis factor α in Escherichia coli. *Microbiology,* 164**,** 440-452.

SELAS CASTIÑEIRAS, T., WILLIAMS, S. G., HITCHCOCK, A. G. & SMITH, D. C. 2018c. E. coli strain engineering for the production of advanced biopharmaceutical products. *FEMS Microbiology Letters,* 365.

SEVASTSYANOVICH, Y., ALFASI, S., OVERTON, T., HALL, R., JONES, J., HEWITT, C. & COLE, J. 2009. Exploitation of GFP fusion proteins and stress avoidance as a generic strategy for the production of high-quality recombinant proteins. *FEMS Microbiology Letters,* 299**,** 86-94.

SHAO, B., RAMMOHAN, J., ANDERSON, D. A., ALPEROVICH, N., ROSS, D. & VOIGT, C. A. 2021. Single-cell measurement of plasmid copy number and promoter activity. *Nature Communications,* 12.

SHARMA, A. K., SHUKLA, E., JANOTI, D. S., MUKHERJEE, K. J. & SHILOACH, J. 2020. A novel knock out strategy to enhance recombinant protein expression in Escherichia coli. *Microbial Cell Factories,* 19.

SHEVCHIK, V. E., CONDEMINE, G. & ROBERT-BAUDOUY, J. 1994. Characterization of DsbC, a periplasmic protein of Erwinia chrysanthemi and Escherichia coli with disulfide isomerase activity. *The EMBO Journal,* 13**,** 2007-2012-2012.

SHIMOMURA, O., JOHNSON, F. H. & SAIGA, Y. 1962. Extraction, purification and properties of aequorin, a bioluminescent protein from the luminous hydromedusan, Aequorea. *J Cell Comp Physiol,* 59**,** 223-39.

SHRIMAL, S., CHEREPANOVA, N. A. & GILMORE, R. 2015. Cotranslational and posttranslocational N-glycosylation of proteins in the endoplasmic reticulum. *Semin Cell Dev Biol,* 41**,** 71-8.

SIEGELE, D. A. & HU, J. C. 1997. Gene expression from plasmids containing the araBAD promoter at subsaturating inducer concentrations represents mixed populations. *Proceedings of the National Academy of Sciences,* 94**,** 8168-8172.

SILHAVY, T. J., KAHNE, D. & WALKER, S. 2010. The Bacterial Cell Envelope. *Cold Spring Harbor Perspectives in Biology,* 2**,** a000414-a000414.

SIMMONS, L. A., FOTI, J. J., COHEN, S. E. & WALKER, G. C. 2008. The SOS Regulatory Network. *EcoSal Plus,* 3**,** 10.1128/ecosalplus.5.4.3.

SIMMONS, L. C. & YANSURA, D. G. 1996. Translational level is a critical factor for the secretion of heterologous proteins in Escherichia coli. *Nat Biotechnol,* 14**,** 629-34.

SINGH, A. B., SHARMA, A. K. & MUKHERJEE, K. J. 2012. Analyzing the metabolic stress response of recombinant Escherichia coli cultures expressing human interferon-beta in high cell density fed batch cultures using time course transcriptomic data. *Mol. BioSyst.,* 8**,** 615-628.

SKERRA, A. 1994. Use of the tetracycline promoter for the tightly regulated production of a murine antibody fragment in Escherichia coli. *Gene,* 151**,** 131-5.

SKINNER, S. O., SEPÚLVEDA, L. A., XU, H. & GOLDING, I. 2013. Measuring mRNA copy number in individual Escherichia coli cells using single-molecule fluorescent in situ hybridization. *Nature Protocols,* 8**,** 1100-1113.

SOCHACKI, K. A., SHKEL, I. A., RECORD, M. T. & WEISSHAAR, J. C. 2011. Protein Diffusion in the Periplasm of E. coli under Osmotic Stress. *Biophysical Journal,* 100**,** 22-31.

SOHN, J. & SAUER, R. T. 2009. OMP Peptides Modulate the Activity of DegS Protease by Differential Binding to Active and Inactive Conformations. *Molecular Cell,* 33**,** 64-74.

SORENSEN, H. P. & MORTENSEN, K. K. 2005. Soluble expression of recombinant proteins in the cytoplasm of Escherichia coli. *Microb Cell Fact,* 4**,** 1.

SPEHR, V., FRAHM, D. & MEYER, T. F. 2000. Improvement of the T7 expression system by the use of T7 lysozyme. *Gene,* 257**,** 259-267.

SPOHNER, S. C., MÜLLER, H., QUITMANN, H. & CZERMAK, P. 2015. Expression of enzymes for the usage in food and feed industry with Pichia pastoris. *Journal of Biotechnology,* 202**,** 118-134.

SPOTTS, R. O., CHAKERIAN, A. E. & MATTHEWS, K. S. 1991. Arginine 197 of lac repressor contributes significant energy to inducer binding. Confirmation of homology to periplasmic sugar binding proteins. *J Biol Chem,* 266**,** 22998-3002.

SPURIO, R., DÜRRENBERGER, M., FALCONI, M., LA TEANA, A., PON, C. L. & GUALERZI, C. O. 1992. Lethal overproduction of the Escherichia coli nucleoid protein H-NS: ultramicroscopic and molecular autopsy. *Molecular and General Genetics MGG,* 231**,** 201-211.

SRIVASTAVA, S. K., LAMBADI, P. R., GHOSH, T., PATHANIA, R. & NAVANI, N. K. 2014. Genetic regulation of spy gene expression in Escherichia coli in the presence of protein unfolding agent ethanol. *Gene,* 548**,** 142-8.

STARGARDT, P., STRIEDNER, G. & MAIRHOFER, J. 2021. Tunable expression rate control of a growth-decoupled T7 expression system by l-arabinose only. *Microbial Cell Factories,* 20.

STEINBERG, R., KNÜPFFER, L., ORIGI, A., ASTI, R. & KOCH, H.-G. 2018. Co-translational protein targeting in bacteria. *FEMS Microbiology Letters,* 365.

STEINER, D., FORRER, P., STUMPP, M. T. & PLÜCKTHUN, A. 2006. Signal sequences directing cotranslational translocation expand the range of proteins amenable to phage display. *Nature Biotechnology,* 24**,** 823-831.

STEINKAMP, J. A., LEHNERT, B. E. & LEHNERT, N. M. 1999. Discrimination of damaged/dead cells by propidium iodide uptake in immunofluorescently labeled populations analyzed by phase-sensitive flow cytometry. *Journal of Immunological Methods,* 226**,** 59-70.

STENSTRÖM, C. M. & ISAKSSON, L. A. 2002. Influences on translation initiation and early elongation by the messenger RNA region flanking the initiation codon at the 3' side. *Gene,* 288**,** 1-8.

STIEFEL, P., SCHMIDT-EMRICH, S., MANIURA-WEBER, K. & REN, Q. 2015. Critical aspects of using bacterial cell viability assays with the fluorophores SYTO9 and propidium iodide. *BMC Microbiology,* 15**,** 36.

STOCK, J. B., RAUCH, B. & ROSEMAN, S. 1977. Periplasmic space in Salmonella typhimurium and Escherichia coli. *J Biol Chem,* 252**,** 7850-61.

STOEBEL, D. M., FREE, A. & DORMAN, C. J. 2008. Anti-silencing: overcoming H-NS-mediated repression of transcription in Gram-negative enteric bacteria. *Microbiology,* 154**,** 2533-2545.

STRIEDNER, G., CSERJAN-PUSCHMANN, M., PÖTSCHACHER, F. & BAYER, K. 2003. Tuning the transcription rate of recombinant protein in strong Escherichia coli expression systems through repressor titration. *Biotechnol Prog,* 19**,** 1427-32.

STUDIER, F. W. 1991a. Use of bacteriophage T7 lysozyme to improve an inducible T7 expression system. *J Mol Biol,* 219**,** 37-44.

STUDIER, F. W. 1991b. Use of Bacteriophage T7 Lysozyme to Improve an Inducible T7 Expression System. *Journal of Molecular Biology,* 219**,** 37-44.

STUDIER, F. W. 2005. Protein production by auto-induction in high density shaking cultures. *Protein Expr Purif,* 41**,** 207-34.

STUDIER, F. W. & MOFFATT, B. A. 1986. Use of bacteriophage T7 RNA polymerase to direct selective high-level expression of cloned genes. *Journal of Molecular Biology,* 189**,** 113-130.

STÜLKE, J. & HILLEN, W. 1999. Carbon catabolite repression in bacteria. *Current Opinion in Microbiology,* 2**,** 195-201.

SU, W. W. 2005. Fluorescent proteins as tools to aid protein production. *Microb Cell Fact,* 4**,** 12.

SUCKOW, J., MARKIEWICZ, P., KLEINA, L. G., MILLER, J., KISTERS-WOIKE, B. & MÜLLER-HILL, B. 1996. Genetic Studies of the Lac Repressor XV: 4000 Single Amino Acid Substitutions and Analysis of the Resulting Phenotypes on the Basis of the Protein Structure. *Journal of Molecular Biology,* 261**,** 509-523.

SUN, M., GAO, A. X., LIU, X., YANG, Y., LEDESMA-AMARO, R. & BAI, Z. 2023. High-throughput process development from gene cloning to protein production. *Microbial Cell Factories,* 22.

SUZUKI, T., ARAI, S., TAKEUCHI, M., SAKURAI, C., EBANA, H., HIGASHI, T., HASHIMOTO, H., HATSUZAWA, K. & WADA, I. 2012. Development of Cysteine-Free Fluorescent Proteins for the Oxidative Environment. *PLoS ONE,* 7**,** e37551.

TABOR, S. & RICHARDSON, C. C. 1985. A bacteriophage T7 RNA polymerase/promoter system for controlled exclusive expression of specific genes. *Proc Natl Acad Sci U S A,* 82**,** 1074-8.

TAGOMORI, B. Y., DOS SANTOS, F. C. & BARBOSA-TESSMANN, I. P. 2021. Recombinant expression, purification, and characterization of an alpha-amylase from Massilia timonae. *3 Biotech,* 11**,** 13.

TAKAHASHI, Y.-H., INABA, K. & ITO, K. 2004. Characterization of the Menaquinone-dependent Disulfide Bond Formation Pathway of Escherichia coli. *Journal of Biological Chemistry,* 279**,** 47057-47065.

TALMADGE, K. & GILBERT, W. 1982. Cellular location affects protein stability in Escherichia coli. *Proceedings of the National Academy of Sciences,* 79**,** 1830-1833.

TAMARA, S., DEN BOER, M. A. & HECK, A. J. R. 2022. High-Resolution Native Mass Spectrometry. *Chemical Reviews,* 122**,** 7269-7326.

TAN, E., CHIN, C. S. H., LIM, Z. F. S. & NG, S. K. 2021. HEK293 Cell Line as a Platform to Produce Recombinant Proteins and Viral Vectors. *Front Bioeng Biotechnol,* 9**,** 796991.

TAW, M. N., BOOCK, J. T., KIM, D., ROCCO, M. A., WARAHO-ZHMAYEV, D. & DELISA, M. P. 2020. Twin-arginine translocase component TatB performs folding quality control via a general chaperone activity. Cold Spring Harbor Laboratory.

THOMAS, J. D., DANIEL, R. A., ERRINGTON, J. & ROBINSON, C. 2001. Export of active green fluorescent protein to the periplasm by the twin-arginine translocase (Tat) pathway in Escherichia coli. *Molecular Microbiology,* 39**,** 47-53.

THOMAS, V. J. & COLLINS, C. M. 1999. Identification of UreR binding sites in the Enterobacteriaceae plasmid-encoded and Proteus mirabilis urease gene operons. *Molecular Microbiology,* 31**,** 1417-1428.

THOMPSON, K. M., RHODIUS, V. A. & GOTTESMAN, S. 2007. σE Regulates and Is Regulated by a Small RNA in Escherichia coli. *Journal of Bacteriology,* 189**,** 4243-4256.

THOMPSON, N. & WAKARCHUK, W. 2022. O-glycosylation and its role in therapeutic proteins. *Biosci Rep,* 42.

TIDBLAD, A. 2022. The history, physiology and treatment safety of growth hormone. *Acta Paediatrica,* 111**,** 215-224.

TOOKE, C. L., HINCHLIFFE, P., BRAGGINTON, E. C., COLENSO, C. K., HIRVONEN, V. H. A., TAKEBAYASHI, Y. & SPENCER, J. 2019. β-Lactamases and β-Lactamase Inhibitors in the 21st Century. *J Mol Biol,* 431**,** 3472-3500.

TRIDGETT, M., ABABI, M., OSGERBY, A., RAMIREZ GARCIA, R. & JARAMILLO, A. 2021. Engineering Bacteria to Produce Pure Phage-like Particles for Gene Delivery. *ACS Synthetic Biology,* 10**,** 107-114.

TRUSCA, D., SCOTT, S., THOMPSON, C. & BRAMHILL, D. 1998. Bacterial SOS Checkpoint Protein SulA Inhibits Polymerization of Purified FtsZ Cell Division Protein. *Journal of Bacteriology,* 180**,** 3946-3953.

TSIRIGOTAKI, A., DE GEYTER, J., ŠOŠTARIC´, N., ECONOMOU, A. & KARAMANOU, S. 2017. Protein export through the bacterial Sec pathway. *Nature Reviews Microbiology,* 15**,** 21-36.

TSUKAZAKI, T. 2018. Structure-based working model of SecDF, a proton-driven bacterial protein translocation factor. *FEMS Microbiology Letters,* 365.

TU, G.-F., REID, G. E., ZHANG, J.-G., MORITZ, R. L. & SIMPSON, R. J. 1995. C-terminal Extension of Truncated Recombinant Proteins in Escherichia coli with a 10Sa RNA Decapeptide. *Journal of Biological Chemistry,* 270**,** 9322-9326.

TU, Q., YIN, J., FU, J., HERRMANN, J., LI, Y., YIN, Y., STEWART, A. F., MÜLLER, R. & ZHANG, Y. 2016. Room temperature electrocompetent bacterial cells improve DNA transformation and recombineering efficiency. *Scientific Reports,* 6**,** 24648.

TUNGEKAR, A. A., FULEWAR, P., KUMTHEKAR, R. & BHAMBURE, R. 2024. Understanding in-vivo refolding of antibody fragments (Fab): Biosimilar Ranibizumab a case study. *Process Biochemistry,* 146**,** 484-497.

TÜRKANOĞLU ÖZÇELIK, A., YILMAZ, S. & INAN, M. 2019. Pichia pastoris Promoters. Springer New York.

UDEKWU, K. I. & WAGNER, E. G. H. 2007. Sigma E controls biogenesis of the antisense RNA MicA. *Nucleic Acids Research,* 35**,** 1279-1288.

UEGUCHI, C., KAKEDA, M. & MIZUNO, T. 1993. Autoregulatory expression of the Escherichia coli hns gene encoding a nucleoid protein: H-NS functions as a repressor of its own transcription. *Molecular and General Genetics MGG,* 236-236**,** 171-178.

ULLERS, R. S., LUIRINK, J., HARMS, N., SCHWAGER, F., GEORGOPOULOS, C. & GENEVAUX, P. 2004. SecB is a bona fide generalized chaperone in Escherichia coli. *Proc Natl Acad Sci U S A,* 101**,** 7583-8.

URBAN, J. H. & VOGEL, J. 2007. Translational control and target recognition by Escherichia coli small RNAs in vivo. *Nucleic Acids Research,* 35**,** 1018-1037.

VALDEZ-CRUZ, N. A., CASPETA, L., PÉREZ, N. O., RAMÍREZ, O. T. & TRUJILLO-ROLDÁN, M. A. 2010. Production of recombinant proteins in E. coli by the heat inducible expression system based on the phage lambda pL and/or pR promoters. *Microbial Cell Factories,* 9**,** 18.

VAN HEIJENOORT, J. 2011. Peptidoglycan Hydrolases of Escherichia coli. *Microbiology and Molecular Biology Reviews,* 75**,** 636-663.

VANDRISSE, C. M. & ESCALANTE-SEMERENA, J. C. 2019. Protein Acetylation in Bacteria. *Annual Review of Microbiology,* 73**,** 111-132.

VARY, P. S., BIEDENDIECK, R., FUERCH, T., MEINHARDT, F., ROHDE, M., DECKWER, W.-D. & JAHN, D. 2007. Bacillus megaterium—from simple soil bacterium to industrial protein production host. *Applied Microbiology and Biotechnology,* 76**,** 957-967.

VEENENDAAL, A. K. J., VAN DER DOES, C. & DRIESSEN, A. J. M. 2001. Mapping the Sites of Interaction between SecY and SecE by Cysteine Scanning Mutagenesis. *Journal of Biological Chemistry,* 276**,** 32559-32566.

VIEIRA GOMES, A., SOUZA CARMO, T., SILVA CARVALHO, L., MENDONÇA BAHIA, F. & PARACHIN, N. 2018. Comparison of Yeasts as Hosts for Recombinant Protein Production. *Microorganisms,* 6**,** 38.

VIMBERG, V., TATS, A., REMM, M. & TENSON, T. 2007. Translation initiation region sequence preferences in Escherichia coli. *BMC Molecular Biology,* 8**,** 100.

VOLLMER, W. & BERTSCHE, U. 2008. Murein (peptidoglycan) structure, architecture and biosynthesis in Escherichia coli. *Biochimica et Biophysica Acta (BBA) - Biomembranes,* 1778**,** 1714-1734.

WAGNER, S., KLEPSCH, M. M., SCHLEGEL, S., APPEL, A., DRAHEIM, R., TARRY, M., HOGBOM, M., VAN WIJK, K. J., SLOTBOOM, D. J., PERSSON, J. O. & DE GIER, J. W. 2008. Tuning Escherichia coli for membrane protein overexpression. *Proceedings of the National Academy of Sciences, USA,* 105**,** 14371-14376.

WALSH, G. 2010. Post-translational modifications of protein biopharmaceuticals. *Drug Discovery Today,* 15**,** 773-780.

WALSH, G. & WALSH, E. 2022. Biopharmaceutical benchmarks 2022. *Nature Biotechnology,* 40**,** 1722-1760.

WANG-KAN, X., RODRÍGUEZ-BLANCO, G., SOUTHAM, A. D., WINDER, C. L., DUNN, W. B., IVENS, A. & PIDDOCK, L. J. V. 2021. Metabolomics Reveal Potential Natural Substrates of AcrB in Escherichia coli and Salmonella enterica Serovar Typhimurium. *mBio,* 12.

WANG, H., ZHANG, X., QIU, J., WANG, K., MENG, K., LUO, H., SU, X., MA, R., HUANG, H. & YAO, B. 2019. Development of Bacillus amyloliquefaciens as a high-level recombinant protein expression system. *Journal of Industrial Microbiology and Biotechnology,* 46**,** 113-123.

WEINER, L., BRISSETTE, J. L. & MODEL, P. 1991. Stress-induced expression of the Escherichia coli phage shock protein operon is dependent on sigma 54 and modulated by positive and negative feedback mechanisms. *Genes & Development,* 5**,** 1912-1923.

WELLES, H. L., GIAQUINTO, A. R. & LINDSTROM, R. E. 1971. Degradation of Urea in Concentrated Aqueous Solution. *Journal of Pharmaceutical Sciences,* 60**,** 1212-1216.

WHITTLE, E. E., MCNEIL, H. E., TRAMPARI, E., WEBBER, M., OVERTON, T. W. & BLAIR, J. M. A. 2021. Efflux Impacts Intracellular Accumulation Only in Actively Growing Bacterial Cells. *mBio,* 12.

WHITTLE, E. E., ORABABA, O., OSGERBY, A., SIASAT, P., ELEMENT, S. J., BLAIR, J. M. A. & OVERTON, T. W. 2024. Efflux pumps mediate changes to fundamental bacterial physiology via membrane potential. *mBio,* 15**,** e02370-24.

WIEDEMANN, C., KUMAR, A., LANG, A. & OHLENSCHLÄGER, O. 2020. Cysteines and Disulfide Bonds as Structure-Forming Units: Insights From Different Domains of Life and the Potential for Characterization by NMR. *Frontiers in Chemistry,* 8.

WINTER, R. B., BERG, O. G. & VON HIPPEL, P. H. 1981. Diffusion-driven mechanisms of protein translocation on nucleic acids. 3. The Escherichia coli lac repressor-operator interaction: kinetic measurements and conclusions. *Biochemistry,* 20**,** 6961-6977.

WITTMANN, C., WEBER, J., BETIKU, E., KRÖMER, J., BOEHM, D. & RINAS, U. 2008. Response of fluxome and metabolome to temperature-induced recombinant protein synthesis in Escherichia coli. *Journal of biotechnology,* 132**,** 375-84.

WYRE, C. & OVERTON, T. W. 2014. Use of a stress-minimisation paradigm in high cell density fed-batch Escherichia coli fermentations to optimise recombinant protein production. *Journal of Industrial Microbiology and Biotechnology,* 41**,** 1391-1404.

XI, X., SUN, W., LI, H., FAN, Q., ZHANG, X. & SUN, F. 2021. A comparative study and evaluation of anti-EGFR nanobodies expressed in Pichia pastoris and Escherichia coli as antitumor moieties. *Protein Expression and Purification,* 184**,** 105888.

YAMADA, H., MURAMATSU, S. & MIZUNO, T. 1990. An Escherichia coli Protein That Preferentially Binds to Sharply Curved DNA1. *The Journal of Biochemistry,* 108**,** 420-425.

YAMAMOTO, K. & ISHIHAMA, A. 2005. Transcriptional response of Escherichia coli to external copper. *Molecular Microbiology,* 56**,** 215-227.

YAMAMOTO, K. & ISHIHAMA, A. 2006. Characterization of Copper-Inducible Promoters Regulated by CpxA/CpxR in Escherichia coli. *Bioscience, Biotechnology, and Biochemistry,* 70**,** 1688-1695.

YAMAMOTO, K., OGASAWARA, H. & ISHIHAMA, A. 2008. Involvement of multiple transcription factors for metal-induced spy gene expression in Escherichia coli. *Journal of Biotechnology,* 133**,** 196-200.

YANG, H., QU, J., ZOU, W., SHEN, W. & CHEN, X. 2021. An overview and future prospects of recombinant protein production in Bacillus subtilis. *Applied Microbiology and Biotechnology,* 105**,** 6607-6626.

YANG, X.-J. & SETO, E. 2008. Lysine Acetylation: Codified Crosstalk with Other Posttranslational Modifications. *Molecular Cell,* 31**,** 449-461.

YANG, Y., XIANG, Y. & XU, M. 2015. From red to green: the propidium iodide-permeable membrane of Shewanella decolorationis S12 is repairable. *Scientific Reports,* 5**,** 18583.

YAP, M. N. & BERNSTEIN, H. D. 2011. The translational regulatory function of SecM requires the precise timing of membrane targeting. *Molecular Microbiology,* 81**,** 540-553.

YIN, J., LI, G., REN, X. & HERRLER, G. 2007. Select what you need: A comparative evaluation of the advantages and limitations of frequently used expression systems for foreign genes. *Journal of Biotechnology,* 127**,** 335-347.

YIP, K. M., FISCHER, N., PAKNIA, E., CHARI, A. & STARK, H. 2020. Atomic-resolution protein structure determination by cryo-EM. *Nature,* 587**,** 157-161.

ZACHARIAS, D. A., VIOLIN, J. D., NEWTON, A. C. & TSIEN, R. Y. 2002. Partitioning of lipid-modified monomeric GFPs into membrane microdomains of live cells. *Science,* 296**,** 913-6.

ZEIDEL, M. L., AMBUDKAR, S. V., SMITH, B. L. & AGRE, P. 1992. Reconstitution of functional water channels in liposomes containing purified red cell CHIP28 protein. *Biochemistry,* 31**,** 7436-40.

ZGURSKAYA, H. I., KRISHNAMOORTHY, G., NTREH, A. & LU, S. 2011. Mechanism and Function of the Outer Membrane Channel TolC in Multidrug Resistance and Physiology of Enterobacteria. *Frontiers in Microbiology,* 2.

ZHANG, J., PAN, X., YAN, K., SUN, S., GAO, N. & SUI, S. F. 2015. Mechanisms of ribosome stalling by SecM at multiple elongation steps. *Elife,* 4.

ZHANG, P., GAO, Q., WANG, T., KE, Y., MO, F., JIA, R., LIU, W., LIU, L., ZHENG, S., LIU, Y., LI, L., WANG, Y., XU, L., HAO, K., MIN, W., LIU, X., YANG, R., LI, S., LIN, C. & ZHAO, Y. 2021. Development and evaluation of a serological test for diagnosis of COVID-19 with selected recombinant spike proteins. *European Journal of Clinical Microbiology & Infectious Diseases,* 40**,** 921-928.

ZHANG, X., SCHAFFITZEL, C., BAN, N. & SHAN, S.-O. 2009. Multiple conformational switches in a GTPase complex control co-translational protein targeting. *Proceedings of the National Academy of Sciences,* 106**,** 1754-1759.

ZHANG, Z.-X., NONG, F.-T., WANG, Y.-Z., YAN, C.-X., GU, Y., SONG, P. & SUN, X.-M. 2022. Strategies for efficient production of recombinant proteins in Escherichia coli: alleviating the host burden and enhancing protein activity. *Microbial Cell Factories,* 21.

ZHAO, C., WANG, L., LI, D., LI, J., GE, Y., LIANG, T., ZHU, Y. & YU, R. 2021. High-cell-density fermentation of Escherichia coli for expression of a recombinant phenylalanine dehydrogenase mutant and its purification. *Journal of Chemical Technology & Biotechnology,* 96**,** 199-206.

ZHENG, Z., BLUM, A., BANERJEE, T., WANG, Q., DANTIS, V. & OLIVER, D. 2016. Determination of the Oligomeric State of SecYEG Protein Secretion Channel Complex Using in Vivo Photo- and Disulfide Cross-linking. *Journal of Biological Chemistry,* 291**,** 5997-6010.

ZHONG, Q., XIAO, X., QIU, Y., XU, Z., CHEN, C., CHONG, B., ZHAO, X., HAI, S., LI, S., AN, Z. & DAI, L. 2023. Protein posttranslational modifications in health and diseases: Functions, regulatory mechanisms, and therapeutic implications. *MedComm,* 4**,** e261.

ZLATINA, K. & GALUSKA, S. P. 2021. Immunoglobulin Glycosylation - An Unexploited Potential for Immunomodulatory Strategies in Farm Animals. *Front Immunol,* 12**,** 753294.

ZOPF, D., BERNSTEIN, H. D., JOHNSON, A. E. & WALTER, P. 1990. The methionine-rich domain of the 54 kd protein subunit of the signal recognition particle contains an RNA binding site and can be crosslinked to a signal sequence. *The EMBO Journal,* 9**,** 4511-4517.

ZULKIFLY, N. A. H., SELAS CASTIÑEIRAS, T. & OVERTON, T. W. 2023. Optimisation of recombinant TNFα production in Escherichia coli using GFP fusions and flow cytometry. *Frontiers in Bioengineering and Biotechnology,* 11.

Chapter 8: Appendix

Table 8.1: Untransformed JCB387 FCM raw forward scatter (mean FSC-A) and CV (% at peak mid-height) data for Chapter 3, Figure 3.5A, histograms. Mean CV% and SD are provided.

Untransformed JCB387 was cultured in 50 mL LB and incubated at 37 °C, 200 rpm. At OD_{600} 0.4-0.6 urea was added to cultures in triplicate for each concentration (0 mM, 10 mM, 100 mM and 500 mM urea). Samples were analysed by FCM at 0 h, 2 h, 4 h and 24 h post-induction.

Time Post Induction (h)	Urea Concentration (mM)	Replicate	FSC-A	CV	Mean CV	SD
0	0	A	28730.66	23.74%	23.85%	1.41%
		B	30827.74	22.50%		
		C	26141.34	25.32%		
	10	A	25143.88	25.93%	26.08%	0.26%
		B	25974.04	25.93%		
		C	24924.30	26.38%		
	100	A	25117.16	26.33%	26.49%	0.52%
		B	23121.62	27.08%		
		C	25928.82	26.07%		
	500	A	25396.46	25.47%	25.06%	0.51%
		B	26779.17	25.21%		
		C	26871.48	24.49%		
2	0	A	14941.75	44.73%	45.20%	0.41%
		B	14919.73	45.38%		
		C	14837.70	45.50%		
	10	A	15188.16	44.65%	43.68%	2.56%
		B	16941.33	40.78%		
		C	15325.00	45.61%		
	100	A	17180.53	41.40%	43.22%	1.99%
		B	16090.34	42.91%		
		C	15343.07	45.34%		
	500	A	28651.90	44.61%	45.01%	0.46%
		B	28530.23	45.51%		
		C	28692.83	44.90%		
4	0	A	17048.79	54.53%	54.47%	0.06%
		B	17356.12	54.41%		
		C	17221.63	54.46%		
	10	A	17035.60	54.65%	54.37%	0.27%
		B	18396.31	54.12%		
		C	17878.95	54.34%		
	100	A	18074.89	53.49%	54.25%	0.89%
		B	18156.59	54.03%		
		C	17122.93	55.22%		
	500	A	19706.73	26.44%	25.88%	0.56%
		B	21840.64	25.86%		
		C	22959.01	25.33%		
24	0	A	26973.99	71.86%	70.55%	1.34%
		B	31804.54	69.18%		
		C	28534.41	70.62%		
	10	A	26989.01	71.34%	69.23%	2.83%
		B	36231.41	66.02%		
		C	28697.37	70.34%		
	100	A	35851.24	65.92%	67.60%	2.71%
		B	35128.80	66.16%		
		C	27616.07	70.73%		
	500	A	30156.43	49.21%	35.56%	11.83%
		B	39802.63	29.16%		
		C	39945.59	28.32%		

Table 8.2: Untransformed BL21 FCM raw forward scatter (mean FSC-A) and CV (% at peak mid-height) data for Chapter 3, Figure 3.5B, histograms. Mean CV% and SD are provided.

Untransformed BL21 was cultured in 50 mL LB and incubated at 37 °C, 200 rpm. At OD_{600} 0.4-0.6 urea was added to cultures in triplicate for each concentration (0 mM, 10 mM, 100 mM and 500 mM urea). Samples were analysed by FCM at 0 h, 2 h, 4 h and 24 h post-induction.

Time Post Induction (h)	Urea Concentration (mM)	Replicate	FSC-A	CV	Mean CV	SD
0	0	A	16410.98	23.15%	23.01%	0.27%
		B	17274.97	22.70%		
		C	16834.65	23.17%		
	10	A	16743.62	23.69%	24.12%	0.40%
		B	14971.78	24.47%		
		C	14560.79	24.20%		
	100	A	16501.40	23.06%	22.85%	0.19%
		B	17558.85	22.78%		
		C	17395.92	22.70%		
	500	A	17286.87	23.17%	23.32%	0.30%
		B	16663.96	23.13%		
		C	15867.08	23.67%		
2	0	A	8775.36	23.20%	23.37%	0.16%
		B	8478.78	23.50%		
		C	8694.34	23.42%		
	10	A	8902.01	23.46%	23.22%	0.22%
		B	9202.54	23.17%		
		C	9139.20	23.02%		
	100	A	8698.57	23.42%	23.47%	0.06%
		B	8668.97	23.54%		
		C	8565.61	23.46%		
	500	A	11827.43	24.91%	24.90%	0.24%
		B	11195.09	25.14%		
		C	11753.20	24.66%		
4	0	A	7287.18	23.67%	23.59%	0.17%
		B	7339.11	23.70%		
		C	7571.27	23.39%		
	10	A	7106.31	23.51%	23.53%	0.13%
		B	7156.49	23.41%		
		C	7382.23	23.66%		
	100	A	7975.46	23.28%	23.21%	0.07%
		B	7848.69	23.20%		
		C	8029.15	23.15%		
	500	A	9041.43	24.03%	23.76%	0.29%
		B	9433.52	23.79%		
		C	9903.58	23.45%		
24	0	A	6016.02	24.09%	24.04%	0.10%
		B	6072.97	24.10%		
		C	6008.27	23.92%		
	10	A	5916.38	23.78%	23.65%	0.15%
		B	5962.51	23.48%		
		C	5976.22	23.69%		
	100	A	6024.86	23.29%	23.14%	0.19%
		B	6130.20	22.92%		
		C	6018.89	23.20%		
	500	A	6507.08	24.33%	24.09%	0.21%
		B	6465.40	23.98%		
		C	6709.61	23.96%		

Table 8.3: JCB387 and BL21 FCM raw forward scatter (mean FSC-A) and CV (% at peak mid-height) data for Chapter 3, Figure 3.7C, histograms. Mean CV% and SD are provided.

Untransformed JCB387 and BL21 (UT) were compared with transformed JCB387 and BL21 (GFP) harbouring the urea inducible promoter construct pET15b-P_{uti101}-*6xhis::gfp*. Untransformed strains were grown in LB, transformed strains were grown in 50 mL LB + Amp. Cultures were incubated at 37 °C, 200 rpm. At OD_{600} 0.4-0.5, 500 mM urea was added to cultures in duplicate for each strain (JCB387-UT, JCB387-GFP, BL21-UT, BL21-GFP). Samples were analysed by FCM at 0 h, 2 h, 4 h and 24 h post-induction.

Time Post Induction (h)	Strain	Replicate	FSC-A	CV	Mean CV	SD
0	JCB387-UT	A	26253.06	27.67%	27.71%	0.06%
		B	25177.32	27.75%		
	JCB387-GFP	A	24564.31	27.63%	27.93%	0.42%
		B	23649.71	28.22%		
	BL21-UT	A	17676.09	23.36%	23.38%	0.03%
		B	16435.33	23.40%		
	BL21-GFP	A	16269.31	23.77%	23.80%	0.04%
		B	15852.00	23.82%		
2	JCB387-UT	A	20854.61	29.23%	29.09%	0.20%
		B	22695.31	28.95%		
	JCB387-GFP	A	28852.06	32.97%	32.80%	0.24%
		B	29234.27	32.63%		
	BL21-UT	A	12380.78	22.53%	22.29%	0.35%
		B	12794.72	22.04%		
	BL21-GFP	A	25737.53	26.15%	26.16%	0.01%
		B	25683.47	26.16%		
4	JCB387-UT	A	16568.04	22.93%	22.48%	0.64%
		B	18481.82	22.02%		
	JCB387-GFP	A	33163.51	39.46%	39.29%	0.25%
		B	32557.17	39.11%		
	BL21-UT	A	10583.97	20.69%	20.77%	0.11%
		B	10399.55	20.84%		
	BL21-GFP	A	30955.03	23.74%	23.92%	0.25%
		B	31100.72	24.10%		
24	JCB387-UT	A	18525.04	25.38%	24.83%	0.78%
		B	20702.82	24.28%		
	JCB387-GFP	A	31537.50	39.19%	39.24%	0.06%
		B	29765.44	39.28%		
	BL21-UT	A	8773.74	19.65%	19.61%	0.06%
		B	8754.21	19.57%		
	BL21-GFP	A	28879.65	39.04%	38.75%	0.41%
		B	29240.40	38.46%		

Table 8.4: JCB387 FCM raw forward scatter (mean FSC-A) and CV (% at peak mid-height) data for Chapter 3, Figure 3.16, Top Panel, Exp 1 histograms. Mean CV% and SD are provided.

JCB387 harbouring the pET15b-P_{uti101}-*6xhis::gfp* construct was cultured in 50 mL LB + Amp and incubated at 37 °C, 200 rpm. At OD_{600} 0.4-0.6, 6xHis::GFP expression was induced by adding urea to cultures in triplicate for each concentration (0 mM, 1 mM, 5 mM and 10 mM urea). Samples were analysed by FCM at 0 h, 2 h, 4 h and 24 h post-induction.

Time Post Induction (h)	Urea Concentration (mM)	Replicate	FSC-A	CV	Mean CV	SD
0	0	A	31301.88	29.31%	29.73%	0.43%
		B	31140.21	29.73%		
		C	30088.81	30.16%		
	1	A	29191.02	30.47%	30.97%	0.57%
		B	31006.46	30.84%		
		C	27701.36	31.59%		
	5	A	27021.14	32.33%	31.48%	0.83%
		B	28259.23	30.67%		
		C	26991.39	31.43%		
	10	A	26058.99	31.18%	31.35%	1.05%
		B	24332.99	32.48%		
		C	28129.10	30.40%		
2	0	A	13278.80	42.66%	43.54%	0.76%
		B	12719.51	43.89%		
		C	12797.29	44.06%		
	1	A	12827.81	43.48%	43.90%	0.46%
		B	12882.22	43.83%		
		C	13318.09	44.40%		
	5	A	14258.92	41.95%	41.99%	0.49%
		B	13834.59	42.49%		
		C	14520.56	41.52%		
	10	A	14300.25	41.80%	41.86%	0.45%
		B	14707.30	42.34%		
		C	14623.22	41.45%		
4	0	A	13392.96	56.73%	56.61%	0.11%
		B	13161.76	56.51%		
		C	13334.69	56.58%		
	1	A	12682.71	57.33%	56.75%	0.51%
		B	13192.43	56.36%		
		C	13094.07	56.55%		
	5	A	13092.40	56.70%	57.11%	0.36%
		B	13351.45	57.26%		
		C	13751.43	57.36%		
	10	A	13766.30	56.64%	56.57%	0.26%
		B	13409.99	56.79%		
		C	14236.83	56.28%		
24	0	A	17891.97	54.84%	54.52%	0.61%
		B	18381.27	54.91%		
		C	18836.31	53.82%		
	1	A	17988.22	54.79%	56.15%	1.19%
		B	16183.71	57.03%		
		C	16133.02	56.63%		
	5	A	14956.98	57.48%	56.51%	0.88%
		B	16151.45	56.27%		
		C	16711.54	55.78%		
	10	A	15789.36	57.30%	57.27%	0.45%
		B	15216.14	57.70%		
		C	16046.12	56.80%		

Table 8.5: JCB387 FCM raw forward scatter (mean FSC-A) and CV (% at peak mid-height) data for Chapter 3, Figure 3.16, Bottom Panel, Exp 2 histograms. Mean CV% and SD are provided.

JCB387 harbouring the pET15b-P_{uti101}-*6xhis::gfp* construct was cultured in 50 mL LB + Amp and incubated at 37 °C, 200 rpm. At OD_{600} 0.4-0.6, 6xHis::GFP expression was induced by adding urea to cultures in triplicate for each concentration (50 mM, 100 mM, 250 mM and 500 mM urea). Samples were analysed by FCM at 0 h, 2 h, 4 h and 24 h post-induction.

Time Post Induction (h)	Urea Concentration (mM)	Replicate	FSC-A	CV	Mean CV	SD
0	50	A	30756.51	24.28%	24.53%	0.23%
		B	30628.38	24.71%		
		C	29624.84	24.61%		
	100	A	31747.03	24.53%	24.48%	0.36%
		B	32994.30	24.10%		
		C	29456.26	24.81%		
	250	A	31520.05	28.26%	28.23%	0.33%
		B	33555.89	27.89%		
		C	31499.22	28.54%		
	500	A	36596.37	27.59%	27.95%	0.47%
		B	32042.13	28.49%		
		C	34020.33	27.78%		
2	50	A	17861.11	35.46%	35.26%	0.20%
		B	17881.86	35.26%		
		C	18049.69	35.06%		
	100	A	20682.78	35.69%	36.02%	0.68%
		B	20484.30	35.57%		
		C	19961.67	36.81%		
	250	A	24823.14	34.10%	33.28%	0.77%
		B	25196.46	32.57%		
		C	26228.34	33.16%		
	500	A	37186.06	67.22%	67.49%	2.93%
		B	39970.39	64.70%		
		C	34580.14	70.55%		
4	50	A	17201.32	51.96%	51.34%	0.70%
		B	18382.99	50.58%		
		C	17760.17	51.48%		
	100	A	19342.56	48.47%	49.03%	0.80%
		B	19082.73	48.67%		
		C	18558.79	49.94%		
	250	A	24425.93	38.02%	35.08%	2.58%
		B	28645.68	33.18%		
		C	27028.87	34.03%		
	500	A	32859.41	43.44%	43.35%	1.88%
		B	36166.44	41.43%		
		C	40550.06	45.19%		
24	50	A	24059.74	59.16%	59.05%	0.80%
		B	25753.73	58.21%		
		C	23175.51	59.79%		
	100	A	24492.02	60.53%	60.38%	0.47%
		B	24211.35	60.75%		
		C	22730.32	59.85%		
	250	A	23122.60	60.02%	59.55%	0.41%
		B	23518.76	59.36%		
		C	23939.87	59.27%		
	500	A	15115.26	28.71%	28.85%	0.41%
		B	17860.86	28.52%		
		C	16678.02	29.31%		

Table 8.6: JCB387 FCM raw green fluorescence (mean FL1-A) and CV (% at peak mid-height) data for Chapter 3, Figure 3.17, Top Panel, Exp 1 histograms. Mean CV% and SD are provided.

JCB387 harbouring the pET15b-P_{uti101}-*6xhis::gfp* construct was cultured in 50 mL LB + Amp and incubated at 37 °C, 200 rpm. At OD_{600} 0.4-0.6, 6xHis::GFP expression was induced by adding urea to cultures in triplicate for each concentration (0 mM, 1 mM, 5 mM and 10 mM urea). Samples were analysed by FCM at 0 h, 2 h, 4 h and 24 h post-induction.

Time Post Induction (h)	Urea Concentration (mM)	Replicate	FL1-A	CV	Mean CV	SD
0	0	A	628.34	39.42%	39.43%	0.05%
		B	602.75	39.48%		
		C	597.62	39.38%		
	1	A	592.91	39.55%	39.59%	0.04%
		B	609.45	39.58%		
		C	583.37	39.63%		
	5	A	586.20	39.57%	39.63%	0.21%
		B	611.89	39.86%		
		C	594.04	39.46%		
	10	A	604.37	39.61%	39.66%	0.07%
		B	578.54	39.74%		
		C	602.14	39.64%		
2	0	A	727.89	50.23%	50.78%	0.47%
		B	608.67	51.03%		
		C	643.15	51.07%		
	1	A	2675.90	72.26%	71.59%	1.36%
		B	2575.78	72.49%		
		C	3374.77	70.03%		
	5	A	19456.62	45.73%	45.67%	0.12%
		B	17913.34	45.75%		
		C	19906.80	45.53%		
	10	A	21631.09	44.82%	44.56%	0.28%
		B	23524.76	44.60%		
		C	24328.82	44.26%		
4	0	A	696.40	51.69%	52.07%	0.44%
		B	615.16	52.55%		
		C	634.23	51.98%		
	1	A	2876.19	79.93%	77.90%	2.03%
		B	3156.70	77.89%		
		C	3643.29	75.88%		
	5	A	38198.38	60.00%	60.95%	1.35%
		B	27726.64	62.50%		
		C	38639.40	60.36%		
	10	A	40248.89	55.82%	55.81%	0.20%
		B	43906.37	56.00%		
		C	47315.15	55.61%		
24	0	A	393.81	48.56%	48.55%	0.24%
		B	426.01	48.31%		
		C	441.10	48.78%		
	1	A	1814.69	74.48%	77.38%	2.58%
		B	1282.23	79.42%		
		C	1345.44	78.23%		
	5	A	15254.91	60.57%	61.94%	2.83%
		B	9845.81	65.20%		
		C	15291.84	60.06%		
	10	A	21280.18	61.09%	62.25%	3.66%
		B	23860.17	59.32%		
		C	17028.22	66.35%		

Table 8.7: JCB387 FCM raw green fluorescence (mean FL1-A) and CV (% at peak mid-height) data for Chapter 3, Figure 3.17, Bottom Panel, Exp 2 histograms. Mean CV% and SD are provided.

JCB387 harbouring the pET15b-P_{uti101}-*6xhis::gfp* construct was cultured in 50 mL LB + Amp and incubated at 37 °C, 200 rpm. At OD_{600} 0.4-0.6, 6xHis::GFP expression was induced by adding urea to cultures in triplicate for each concentration (50 mM, 100 mM, 250 mM and 500 mM urea). Samples were analysed by FCM at 0 h, 2 h, 4 h and 24 h post-induction.

Time Post Induction (h)	Urea Concentration (mM)	Replicate	FL1-A	CV	Mean CV	SD
0	50	A	511.85	36.15%	36.11%	0.05%
		B	500.77	36.06%		
		C	508.92	36.11%		
	100	A	485.40	36.05%	36.13%	0.09%
		B	497.03	36.22%		
		C	488.11	36.12%		
	250	A	491.41	35.91%	36.15%	0.21%
		B	513.51	36.26%		
		C	491.49	36.28%		
	500	A	514.79	35.99%	35.97%	0.09%
		B	515.41	35.88%		
		C	506.76	36.05%		
2	50	A	29768.27	34.25%	33.98%	0.33%
		B	30262.82	34.08%		
		C	30690.09	33.61%		
	100	A	33377.74	31.29%	30.61%	0.64%
		B	35412.48	30.03%		
		C	34610.76	30.50%		
	250	A	31302.74	31.07%	31.36%	0.88%
		B	32593.21	30.66%		
		C	30806.82	32.35%		
	500	A	51087.41	42.77%	42.79%	0.91%
		B	44703.13	41.90%		
		C	55469.71	43.71%		
4	50	A	58162.78	44.60%	44.56%	0.79%
		B	59004.63	43.75%		
		C	55445.25	45.32%		
	100	A	65890.64	45.26%	45.08%	0.66%
		B	69318.97	44.34%		
		C	67752.74	45.63%		
	250	A	60575.33	27.13%	27.40%	0.98%
		B	77393.92	26.59%		
		C	57892.40	28.49%		
	500	A	85914.09	68.74%	65.93%	2.97%
		B	81080.89	66.22%		
		C	117821.15	62.82%		
24	50	A	32919.50	55.84%	55.56%	0.76%
		B	37500.41	54.70%		
		C	33060.14	56.13%		
	100	A	45169.35	64.48%	63.60%	0.97%
		B	51728.64	62.56%		
		C	36414.55	63.77%		
	250	A	75532.82	61.41%	61.37%	0.38%
		B	76250.64	60.97%		
		C	69134.99	61.72%		
	500	A	53057.81	47.62%	45.78%	1.62%
		B	71360.96	44.56%		
		C	69191.03	45.15%		

Table 8.8: BL21 FCM raw forward scatter (mean FSC-A) and CV (% at peak mid-height) data for Chapter 3, Figure 3.21B histograms. Mean CV% and SD are provided.

BL21 harbouring the pET15b-P*uti101*-*6xhis::gfp* construct was cultured in 50 mL LB + Amp and incubated at 37 °C, 200 rpm. At OD_{600} 0.4-0.6, 6xHis::GFP expression was induced by adding urea to cultures in triplicate for each concentration (0 mM, 10 mM, 100 mM and 500 mM urea). Samples were analysed by FCM at 0 h, 2 h, 4 h and 24 h post-induction.

Time Post Induction (h)	Urea Concentration (mM)	Replicate	FSC-A	CV	Mean CV	SD
0	0	A	13823.56	22.93%	23.29%	0.34%
		B	12756.82	23.61%		
		C	13283.83	23.34%		
	10	A	14515.52	22.42%	22.80%	0.90%
		B	14807.59	22.16%		
		C	12809.70	23.83%		
	100	A	13370.47	23.30%	23.47%	0.17%
		B	12377.88	23.64%		
		C	13381.14	23.48%		
	500	A	12687.28	23.56%	23.69%	0.23%
		B	12087.97	23.95%		
		C	12804.75	23.55%		
2	0	A	9445.90	41.73%	41.18%	0.65%
		B	9720.01	41.35%		
		C	10553.69	40.46%		
	10	A	11092.34	48.61%	48.11%	0.53%
		B	11393.12	47.55%		
		C	11737.48	48.17%		
	100	A	14008.97	47.08%	46.66%	1.18%
		B	14370.34	47.58%		
		C	14935.87	45.33%		
	500	A	15819.81	28.01%	27.80%	0.22%
		B	15776.86	27.81%		
		C	17009.98	27.57%		
4	0	A	8190.82	36.51%	36.21%	0.29%
		B	8177.51	36.19%		
		C	8199.11	35.93%		
	10	A	9363.41	43.02%	42.53%	0.44%
		B	9987.63	42.38%		
		C	10103.67	42.18%		
	100	A	13177.46	48.35%	48.11%	0.21%
		B	13579.89	48.02%		
		C	14368.06	47.97%		
	500	A	21156.70	27.99%	27.51%	0.43%
		B	23599.87	27.18%		
		C	25202.62	27.36%		
24	0	A	6144.82	19.08%	18.99%	0.21%
		B	6045.30	19.15%		
		C	6165.08	18.75%		
	10	A	6906.57	31.56%	35.71%	3.65%
		B	8381.78	37.16%		
		C	9480.28	38.41%		
	100	A	9132.75	35.78%	35.84%	0.05%
		B	9213.37	35.86%		
		C	9507.01	35.88%		
	500	A	15774.99	55.90%	53.65%	2.02%
		B	17649.17	51.99%		
		C	19141.96	53.05%		

Table 8.9: BL21 FCM raw green fluorescence (mean FL1-A) and CV (% at peak mid-height) data for Chapter 3, Figure 3.21C histograms. Mean CV% and SD are provided.

BL21 harbouring the pET15b-P*uti101*-*6xhis::gfp* construct was cultured in 50 mL LB + Amp and incubated at 37 °C, 200 rpm. At OD_{600} 0.4-0.6, 6xHis::GFP expression was induced by adding urea to cultures in triplicate for each concentration (0 mM, 10 mM, 50 mM and 500 mM urea). Samples were analysed by FCM at 0 h, 2 h, 4 h and 24 h post-induction.

Time Post Induction (h)	Urea Concentration (mM)	Replicate	FL1-A	CV	Mean CV	SD
0	0	A	526.21	38.00%	38.27%	0.24%
		B	518.64	38.38%		
		C	527.98	38.43%		
	10	A	557.32	37.95%	37.95%	0.03%
		B	557.94	37.92%		
		C	514.02	37.98%		
	100	A	520.43	38.09%	38.21%	0.13%
		B	515.23	38.20%		
		C	534.45	38.34%		
	500	A	515.04	38.60%	38.37%	0.23%
		B	502.68	38.37%		
		C	505.51	38.15%		
2	0	A	703.42	46.68%	46.30%	0.33%
		B	721.28	46.06%		
		C	794.21	46.16%		
	10	A	22975.97	47.38%	47.70%	1.60%
		B	23851.73	46.29%		
		C	21026.88	49.44%		
	100	A	33429.71	40.08%	40.95%	2.53%
		B	30210.53	43.80%		
		C	33892.82	38.98%		
	500	A	21815.60	29.85%	30.46%	1.28%
		B	21355.28	29.60%		
		C	25624.49	31.94%		
4	0	A	674.92	41.84%	42.01%	0.18%
		B	685.12	42.19%		
		C	710.62	41.99%		
	10	A	49703.36	45.70%	46.04%	0.60%
		B	52522.04	45.69%		
		C	48403.32	46.74%		
	100	A	59896.88	41.39%	42.27%	1.52%
		B	54802.46	44.02%		
		C	59719.22	41.39%		
	500	A	39792.63	26.92%	27.47%	1.09%
		B	38527.53	26.76%		
		C	43682.90	28.72%		
24	0	A	948.49	37.48%	37.35%	0.12%
		B	525.94	37.24%		
		C	457.51	37.32%		
	10	A	35160.47	40.80%	47.37%	5.98%
		B	30690.83	52.51%		
		C	48123.50	48.79%		
	100	A	66215.55	41.36%	41.39%	2.33%
		B	65421.66	39.07%		
		C	63119.02	43.73%		
	500	A	64812.31	36.63%	34.63%	2.25%
		B	64788.44	35.07%		
		C	77690.16	32.19%		

Table 8.10: BL21 FCM raw green fluorescence (mean FL1-A) and CV (% at peak mid-height) data for Chapter 3, Figure 3.25E, histograms. Mean CV% and SD are provided.

BL21 harbouring the pET15b-P_{uti101}-*6xhis::gfp* construct was cultured in 100 mL TB + Amp and incubated at 37 °C, 150 rpm in triplicate. Samples were analysed by FCM at 1 h, 2 h, 3h, 4 h, 5 h, 6 h, 7 h and 26 h post-inoculation.

Time Post Inoculation (h)	Replicate	FL1-A	CV	Mean CV	SD
1	A	328.99	31.00%	31.41%	0.39%
	B	312.60	31.78%		
	C	314.41	31.46%		
2	A	237.06	30.20%	30.37%	0.15%
	B	239.63	30.42%		
	C	245.53	30.48%		
3	A	226.91	30.97%	30.95%	0.04%
	B	236.97	30.98%		
	C	237.03	30.90%		
4	A	234.91	28.81%	29.05%	0.21%
	B	236.43	29.16%		
	C	235.80	29.19%		
5	A	259.82	30.53%	30.88%	0.30%
	B	262.46	31.08%		
	C	262.04	31.02%		
6	A	271.37	31.21%	31.23%	0.04%
	B	283.52	31.20%		
	C	287.64	31.27%		
7	A	286.38	31.22%	31.27%	0.09%
	B	301.44	31.21%		
	C	298.24	31.37%		
24	A	338.70	29.52%	29.13%	0.36%
	B	365.66	29.06%		
	C	384.84	28.82%		

Table 8.11: BL21 FCM raw forward scatter (mean FSC-A) and CV (% at peak mid-height) data for Chapter 3, Figure 3.25E histograms. Mean CV% and SD are provided.

BL21 harbouring the pET15b-P_{uti101}-*6xhis::gfp* construct was cultured in 100 mL TB + Amp and incubated at 37 °C, 150 rpm in triplicate. Samples were analysed by FCM at 1 h, 2 h, 3h, 4 h, 5 h, 6 h, 7 h and 26 h post-inoculation.

Time Post Inoculation (h)	Replicate	FSC-A	CV	Mean CV	SD
1	A	23744.27	23.81%	24.04%	0.20%
	B	23197.37	24.16%		
	C	22857.24	24.15%		
2	A	17461.51	25.02%	24.99%	0.22%
	B	17781.58	25.20%		
	C	18241.28	24.76%		
3	A	16409.89	26.79%	26.72%	0.13%
	B	16656.46	26.80%		
	C	16704.21	26.57%		
4	A	9694.15	27.11%	27.10%	0.06%
	B	9334.80	27.15%		
	C	9378.65	27.04%		
5	A	10457.44	26.52%	26.89%	0.34%
	B	10417.33	27.20%		
	C	10922.46	26.96%		
6	A	10689.76	25.99%	25.41%	0.53%
	B	10885.93	25.29%		
	C	11524.40	24.94%		
7	A	10401.27	26.19%	25.88%	0.41%
	B	10594.32	25.41%		
	C	10833.11	26.04%		
24	A	10574.63	25.90%	25.37%	1.11%
	B	10489.00	26.12%		
	C	12058.11	24.09%		

Table 8.12: BL21 FCM raw forward scatter (mean FSC-A) and CV (% at peak mid-height) data for Chapter 3, Figure 3.29, Exp 1 – top panel histograms. Mean CV% and SD are provided.

BL21 harbouring the pET15b-P_{uti101}-*6xhis::gfp* construct was cultured in 100 mL TB + Amp and incubated at 37 °C, 150 rpm. At OD_{600} 0.4-0.6, 6xHis::GFP expression was induced by adding urea to cultures in duplicate for each concentration (0 mM, 10 mM, 50 mM, 100 mM, 250 mM and 500 mM urea). Samples were analysed by FCM at 0 h, 2 h, 4 h and 24 h post-induction.

Time Post Induction (h)	Urea Concentration (mM)	Replicate	FSC-A	CV	Mean CV	SD
0	0	A	24133.24	22.36%	22.24%	0.12%
		B	23634.90	22.12%		
	10	A	21536.27	22.25%	22.32%	0.07%
		B	20923.04	22.38%		
	50	A	23495.40	22.32%	22.20%	0.11%
		B	22966.51	22.19%		
	100	A	23980.55	22.10%	22.27%	0.19%
		B	23564.79	22.47%		
	250	A	24031.46	22.25%	22.36%	0.18%
		B	23453.36	22.57%		
	500	A	23891.58	22.26%	22.84%	0.74%
		B	22921.11	22.58%		
2	0	A	12226.91	23.67%	23.64%	0.03%
		B	12261.03	23.62%		
	10	A	12368.70	23.64%	24.16%	1.08%
		B	11812.19	23.44%		
	50	A	18241.57	25.41%	26.16%	1.27%
		B	19038.49	25.44%		
	100	A	17769.08	27.62%	29.12%	2.43%
		B	17389.52	27.81%		
	250	A	23545.67	31.92%	30.97%	1.37%
		B	23560.57	31.59%		
	500	A	36663.11	29.40%	27.24%	3.76%
		B	37177.67	29.41%		
4	0	A	13229.91	22.90%	22.57%	0.31%
		B	13248.15	22.50%		
	10	A	13319.63	22.30%	25.88%	6.30%
		B	13097.55	22.18%		
	50	A	19824.69	33.16%	32.24%	1.46%
		B	21174.08	33.00%		
	100	A	22872.82	30.55%	32.09%	2.38%
		B	21382.05	30.89%		
	250	A	23529.81	34.83%	37.24%	4.95%
		B	24612.91	33.95%		
	500	A	39713.88	42.93%	38.13%	10.27%
		B	37405.87	45.12%		
24	0	A	11178.89	26.33%	25.58%	0.78%
		B	12160.41	24.78%		
	10	A	16493.93	25.63%	27.69%	3.49%
		B	16537.43	25.73%		
	50	A	23373.94	31.72%	31.63%	0.10%
		B	23442.35	31.64%		
	100	A	23559.38	31.53%	31.95%	1.42%
		B	23957.47	30.79%		
	250	A	27178.92	33.53%	36.40%	4.96%
		B	28681.85	33.54%		
	500	A	38515.28	42.12%	43.19%	1.51%
		B	37578.64	44.26%		

Table 8.13: BL21 FCM raw forward scatter (mean FSC-A) and CV (% at peak mid-height) data for Chapter 3, Figure 3.29, Exp 2 – bottom panel histograms. Mean CV% and SD are provided.

BL21 harbouring the pET15b-P_{uti101}-*6xhis::gfp* construct was cultured in 100 mL TB + Amp and incubated at 37 °C, 150 rpm. At OD_{600} 0.4-0.6, 6xHis::GFP expression was induced by adding urea to cultures in duplicate for each concentration (0 mM, 10 mM, 50 mM, 100 mM, 250 mM and 500 mM urea). Samples were analysed by FCM at 0 h, 2 h, 4 h and 24 h post-induction.

Time Post Induction (h)	Urea Concentration (mM)	Replicate	FSC-A	CV	Mean CV	SD
0	0	A	22052.58	21.20%	21.32%	0.12%
		B	22156.76	21.32%		
	10	A	22273.79	21.43%	21.28%	0.36%
		B	21691.44	21.54%		
	50	A	21751.73	20.87%	20.68%	0.34%
		B	21343.35	20.88%		
	100	A	21773.92	20.29%	20.48%	0.17%
		B	21764.83	20.52%		
	250	A	21456.65	20.63%	20.96%	0.29%
		B	21298.18	21.15%		
	500	A	21285.03	21.10%	21.16%	0.12%
		B	21338.92	21.08%		
2	0	A	12095.79	21.29%	20.93%	0.57%
		B	11645.42	21.23%		
	10	A	12212.50	20.28%	22.03%	2.89%
		B	12326.13	20.45%		
	50	A	14607.91	25.36%	28.56%	5.41%
		B	14778.79	25.51%		
	100	A	17363.29	34.81%	33.72%	1.17%
		B	16997.04	33.88%		
	250	A	21491.99	32.48%	32.64%	0.21%
		B	22215.17	32.88%		
	500	A	34009.45	32.56%	30.08%	4.83%
		B	33866.91	33.16%		
4	0	A	12446.94	24.51%	24.00%	0.60%
		B	12581.31	24.15%		
	10	A	14896.78	23.34%	26.48%	5.38%
		B	15654.43	23.41%		
	50	A	20897.28	32.69%	32.94%	0.77%
		B	21319.78	32.32%		
	100	A	24298.22	33.80%	34.33%	3.17%
		B	23975.10	31.46%		
	250	A	26485.04	37.73%	44.71%	11.38%
		B	26847.95	38.57%		
	500	A	34548.30	57.84%	45.40%	21.72%
		B	33717.13	58.04%		
24	0	A	13785.24	20.32%	20.79%	0.91%
		B	13303.90	20.21%		
	10	A	15631.59	21.83%	26.75%	8.68%
		B	17099.56	21.65%		
	50	A	25849.33	36.78%	43.88%	13.46%
		B	24958.28	35.46%		
	100	A	29602.33	59.41%	61.38%	4.01%
		B	34962.88	58.74%		
	250	A	34618.84	66.00%	73.83%	11.56%
		B	36199.01	68.37%		
	500	A	38272.48	87.11%	86.24%	1.24%
		B	37648.64	85.36%		

Table 8.14: BL21 FCM raw green fluorescence (mean FL1-A) and CV (% at peak mid-height) data for Chapter 3, Figure 3.30, Exp 1 – top panel histograms. Mean CV% and SD are provided.

BL21 harbouring the pET15b-P*uti101*-*6xhis::gfp* construct was cultured in 100 mL TB + Amp and incubated at 37 °C, 150 rpm. At OD_{600} 0.4-0.6, 6xHis::GFP expression was induced by adding urea to cultures in duplicate for each concentration (0 mM, 10 mM, 50 mM, 100 mM, 250 mM and 500 mM urea). Samples were analysed by FCM at 0 h, 2 h, 4 h and 24 h post-induction.

Time Post Induction (h)	Urea Concentration (mM)	Replicate	FL1-A	CV	Mean CV	SD
0	0	A	554.23	30.94%	31.12%	0.18%
		B	534.03	31.13%		
	10	A	567.92	31.29%	31.42%	0.25%
		B	562.19	31.71%		
	50	A	544.69	31.27%	31.19%	0.09%
		B	547.27	31.20%		
	100	A	568.95	31.10%	31.14%	0.06%
		B	543.90	31.21%		
	250	A	550.78	31.10%	31.23%	0.13%
		B	549.23	31.36%		
	500	A	549.88	31.24%	31.26%	0.22%
		B	547.34	31.49%		
2	0	A	475.07	31.05%	34.99%	6.50%
		B	480.07	31.43%		
	10	A	15133.31	42.50%	39.80%	6.92%
		B	14412.89	44.97%		
	50	A	35079.32	31.94%	31.49%	1.38%
		B	38999.21	32.59%		
	100	A	39496.95	29.95%	29.18%	1.55%
		B	41553.36	30.19%		
	250	A	43415.57	27.40%	28.25%	0.90%
		B	43461.72	28.15%		
	500	A	41857.84	29.19%	30.10%	1.98%
		B	41485.15	28.75%		
4	0	A	644.76	32.37%	33.23%	1.30%
		B	612.66	32.60%		
	10	A	27808.87	34.72%	32.70%	4.37%
		B	29774.77	35.69%		
	50	A	75798.52	27.69%	27.62%	0.08%
		B	81925.19	27.54%		
	100	A	74258.22	27.62%	28.65%	0.98%
		B	79167.90	28.74%		
	250	A	74054.05	29.58%	31.00%	2.11%
		B	71233.98	29.99%		
	500	A	75549.75	33.42%	32.76%	2.13%
		B	78208.35	34.48%		
24	0	A	1714.06	30.37%	29.46%	0.93%
		B	814.50	29.49%		
	10	A	82032.16	28.51%	28.84%	0.46%
		B	73574.32	28.64%		
	50	A	179568.88	29.36%	30.44%	0.95%
		B	143829.07	31.15%		
	100	A	180556.84	30.80%	30.44%	0.50%
		B	181172.56	29.87%		
	250	A	133119.63	30.64%	46.26%	27.51%
		B	158277.28	30.11%		
	500	A	125633.85	78.03%	79.00%	1.37%
		B	122170.63	79.97%		

Table 8.15: BL21 FCM raw green fluorescence (mean FL1-A) and CV (% at peak mid-height) data for Chapter 3, Figure 3.30, Exp 2 – bottom panel histograms. Mean CV% and SD are provided.

BL21 harbouring the pET15b-P$_{uti101}$-*6xhis::gfp* construct was cultured in 100 mL TB + Amp and incubated at 37 °C, 150 rpm. At OD_{600} 0.4-0.6, 6xHis::GFP expression was induced by adding urea to cultures in duplicate for each concentration (0 mM, 10 mM, 50 mM, 100 mM, 250 mM and 500 mM urea). Samples were analysed by FCM at 0 h, 2 h, 4 h and 24 h post-induction.

Time Post Induction (h)	Urea Concentration (mM)	Replicate	FL1-A	CV	Mean CV	SD
0	0	A	490.36	29.93%	30.01%	0.11%
		B	493.32	29.97%		
	10	A	505.16	30.13%	30.15%	0.04%
		B	480.01	30.19%		
	50	A	488.67	30.12%	30.14%	0.05%
		B	474.99	30.20%		
	100	A	487.46	30.10%	30.13%	0.13%
		B	481.07	30.27%		
	250	A	463.09	30.02%	30.21%	0.25%
		B	470.47	30.11%		
	500	A	473.23	30.49%	30.32%	0.25%
		B	467.34	30.44%		
2	0	A	456.42	30.04%	33.91%	6.47%
		B	474.83	30.32%		
	10	A	11758.78	41.38%	38.78%	6.55%
		B	10815.28	43.63%		
	50	A	29356.18	31.32%	30.95%	1.11%
		B	30589.05	31.83%		
	100	A	32955.64	29.71%	28.93%	1.39%
		B	32072.50	29.76%		
	250	A	40285.56	27.32%	28.15%	0.88%
		B	45202.24	28.06%		
	500	A	43724.94	29.08%	28.81%	0.24%
		B	43912.78	28.67%		
4	0	A	612.94	28.67%	30.35%	2.63%
		B	557.29	28.99%		
	10	A	25512.17	33.38%	31.44%	4.12%
		B	23060.28	34.23%		
	50	A	67771.94	26.71%	26.37%	0.41%
		B	67902.85	26.49%		
	100	A	64303.67	25.92%	27.19%	1.15%
		B	60558.46	27.49%		
	250	A	60454.48	28.16%	29.84%	2.42%
		B	63266.32	28.74%		
	500	A	67339.32	32.61%	32.68%	0.95%
		B	61170.79	33.67%		
24	0	A	864.36	31.77%	30.60%	1.78%
		B	810.45	31.47%		
	10	A	61213.83	28.55%	27.63%	1.91%
		B	52823.40	28.91%		
	50	A	177104.63	25.43%	73.27%	82.88%
		B	163486.17	25.42%		
	100	A	149929.17	168.97%	162.69%	19.70%
		B	124659.60	140.62%		
	250	A	125446.01	178.49%	182.62%	27.85%
		B	138144.79	157.07%		
	500	A	79359.39	212.31%	207.57%	6.71%
		B	74948.92	202.82%		

Table 8.16: BL21 FCM raw green fluorescence (mean FL2-A) and CV (% at peak mid-height) data for Chapter 3, Figure 3.35, Exp 1 – top panel histograms. Mean CV% and SD are provided.

BL21 carrying the pET-15b-P_{uti101}-*6xhis::gfp* construct was aerated in 100 mL TB + Amp in baffled Erlenmeyer flasks at 37 °C, 150 rpm. At OD_{600} = 0.5, 5 and 10, 6xHis::GFP expression was induced with urea in duplicate for each concentration. Samples were analysed by FCM at 0 h, 2 h, 4 h and 24 h post-induction.

Time Post Induction (h)	OD_{600} at Induction	Urea Concentration (mM)	Replicate	FL2-A	CV	Mean CV	SD
0	0.5	50	A	250.70	26.95%	27.03%	0.08%
			B	242.10	27.03%		
		100	A	251.27	27.10%	26.59%	0.54%
			B	248.00	26.66%		
	5	250	A	238.56	26.02%	26.04%	0.05%
			B	238.82	26.00%		
		500	A	238.01	26.09%	26.27%	0.24%
			B	240.13	26.19%		
	10	500	A	262.45	26.54%	26.61%	0.16%
			B	266.57	26.80%		
		1000	A	264.72	26.50%	25.84%	1.30%
			B	262.48	26.68%		
2	0.5	50	A	8568.78	24.35%	24.41%	0.07%
			B	8524.14	24.38%		
		100	A	9601.17	24.49%	24.71%	0.23%
			B	9260.09	24.70%		
	5	250	A	2276.61	24.95%	24.58%	0.63%
			B	2080.64	24.94%		
		500	A	1669.60	23.86%	23.20%	2.20%
			B	1707.58	24.99%		
	10	500	A	787.94	20.74%	18.19%	4.67%
			B	800.96	21.03%		
		1000	A	654.67	12.80%	16.53%	6.91%
			B	715.08	12.28%		
4	0.5	50	A	21662.78	24.50%	24.27%	0.72%
			B	19672.12	24.85%		
		100	A	19916.07	23.47%	23.04%	0.90%
			B	20061.18	23.65%		
	5	250	A	5223.33	22.01%	24.04%	2.33%
			B	3791.06	23.53%		
		500	A	2540.54	26.58%	24.92%	2.58%
			B	2716.87	26.24%		
	10	500	A	1578.90	21.95%	21.79%	1.25%
			B	1566.84	22.96%		
		1000	A	835.69	20.47%	20.82%	1.03%
			B	821.67	20.02%		
24	0.5	50	A	66752.64	21.98%	22.15%	0.27%
			B	68315.43	22.00%		
		100	A	64470.49	22.46%	22.79%	0.71%
			B	61881.70	22.31%		
	5	250	A	30699.38	23.60%	24.53%	1.07%
			B	28649.24	24.29%		
		500	A	20367.00	25.70%	25.98%	0.25%
			B	19720.58	26.16%		
	10	500	A	8565.20	26.09%	25.73%	0.43%
			B	10585.43	25.25%		
		1000	A	4875.22	25.86%	25.90%	0.05%
			B	4986.03	25.93%		

Table 8.17: BL21 FCM raw green fluorescence (mean FL2-A) and CV (% at peak mid-height) data for Chapter 3, Figure 3.35, Exp 2 – bottom panel histograms. Mean CV% and SD are provided.

BL21 carrying the pET-15b-P*uti101*-*6xhis::gfp* construct was aerated in 100 mL TB + Amp in baffled Erlenmeyer flasks at 37 °C, 150 rpm. At OD_{600} = 0.5, 5 and 10, 6xHis::GFP expression was induced with urea in duplicate for each concentration. Samples were analysed by FCM at 0 h, 2 h, 4 h and 24 h post-induction.

Time Post Induction (h)	OD_{600} at Induction	Urea Concentration (mM)	Replicate	FL2-A	CV	Mean CV	SD
0	0.5	50	A	239.48	25.22%	25.36%	0.13%
			B	240.53	25.45%		
		100	A	240.96	25.42%	25.21%	0.41%
			B	240.46	25.47%		
	5	250	A	228.43	24.74%	24.81%	0.06%
			B	226.94	24.85%		
		500	A	229.61	24.84%	24.75%	0.09%
			B	228.78	24.76%		
	10	500	A	270.23	24.66%	24.94%	0.29%
			B	263.96	24.92%		
		1000	A	252.50	25.24%	24.12%	1.66%
			B	264.14	24.92%		
2	0.5	50	A	10145.37	22.21%	22.00%	0.47%
			B	10219.38	22.32%		
		100	A	12310.96	21.46%	23.37%	2.57%
			B	11534.14	22.37%		
	5	250	A	2333.05	26.29%	26.03%	0.37%
			B	2130.56	26.20%		
		500	A	2154.01	25.61%	26.51%	1.38%
			B	2080.27	25.83%		
	10	500	A	1975.52	28.10%	28.10%	0.02%
			B	1289.54	28.09%		
		1000	A	1261.63	28.12%	26.27%	2.75%
			B	1392.37	27.59%		
4	0.5	50	A	21283.99	23.11%	22.68%	0.51%
			B	22917.18	22.81%		
		100	A	23672.56	22.12%	24.46%	3.78%
			B	22243.66	22.43%		
	5	250	A	5297.37	28.82%	27.70%	1.39%
			B	5107.70	28.14%		
		500	A	4892.58	26.15%	28.60%	3.83%
			B	4953.07	26.64%		
	10	500	A	2617.08	33.01%	32.93%	0.23%
			B	2486.42	33.10%		
		1000	A	2645.97	32.67%	42.76%	17.78%
			B	2708.44	32.31%		
24	0.5	50	A	60106.77	63.29%	68.17%	4.43%
			B	61833.50	69.27%		
		100	A	54564.37	71.95%	61.25%	24.46%
			B	49062.22	78.54%		
	5	250	A	16235.95	33.26%	31.25%	2.78%
			B	17580.25	32.41%		
		500	A	26675.47	28.07%	39.30%	18.93%
			B	26168.38	28.67%		
	10	500	A	7576.27	61.15%	52.22%	12.86%
			B	8664.01	58.02%		
		1000	A	14404.41	37.48%	38.27%	1.12%
			B	12163.11	39.06%		

Table 8.18: BL21 FCM raw forward scatter (mean FSC-A) and CV (% at peak mid-height) data for Chapter 3, Figure 3.36, Exp 1 – top panel histograms. Mean CV% and SD are provided.

BL21 carrying the pET-15b-P*uti101*-*6xhis::gfp* construct was aerated in 100 mL TB + Amp in baffled Erlenmeyer flasks at 37 °C, 150 rpm. At OD_{600} = 0.5, 5 and 10, 6xHis::GFP expression was induced with urea in duplicate for each concentration. Samples were analysed by FCM at 0 h, 2 h, 4 h and 24 h post-induction.

Time Post Induction (h)	OD_{600} at Induction	Urea Concentration (mM)	Replicate	FSC-A	CV	Mean CV	SD
0	0.5	50	A	19459.79	19.58%	19.77%	0.17%
			B	19147.39	19.91%		
		100	A	19139.45	19.81%	20.22%	0.75%
			B	19193.85	19.76%		
	5	250	A	9884.00	21.08%	21.01%	0.06%
			B	9708.46	20.98%		
		500	A	9879.42	20.98%	20.11%	1.56%
			B	9870.76	21.03%		
	10	500	A	12035.90	18.31%	17.73%	0.51%
			B	12628.56	17.35%		
		1000	A	12401.90	17.52%	19.69%	3.49%
			B	12222.14	17.83%		
2	0.5	50	A	11346.06	23.72%	23.36%	0.60%
			B	11073.96	23.70%		
		100	A	13046.98	22.67%	22.72%	0.33%
			B	13039.93	23.08%		
	5	250	A	13351.43	22.42%	21.97%	0.45%
			B	12947.46	21.95%		
		500	A	14812.09	21.53%	21.62%	0.19%
			B	14648.57	21.50%		
	10	500	A	12679.38	21.84%	21.14%	1.28%
			B	13554.66	21.92%		
		1000	A	13424.59	19.66%	21.16%	2.27%
			B	13807.15	20.04%		
4	0.5	50	A	15387.34	23.77%	23.35%	0.44%
			B	15749.73	23.38%		
		100	A	18279.26	22.89%	22.92%	0.23%
			B	18124.23	23.16%		
	5	250	A	16232.58	22.71%	22.04%	1.26%
			B	15307.77	22.83%		
		500	A	18331.15	20.59%	21.41%	1.06%
			B	18410.63	21.04%		
	10	500	A	15005.46	22.61%	22.78%	0.26%
			B	15813.74	22.64%		
		1000	A	15815.07	23.08%	23.69%	1.13%
			B	16097.09	23.00%		
24	0.5	50	A	21953.94	24.99%	25.32%	0.32%
			B	21947.54	25.33%		
		100	A	25690.26	25.63%	24.82%	1.06%
			B	25698.38	25.20%		
	5	250	A	22938.63	23.62%	21.90%	3.75%
			B	21167.84	24.47%		
		500	A	27328.76	17.60%	19.74%	2.27%
			B	24686.07	19.49%		
	10	500	A	18152.07	22.12%	22.16%	0.82%
			B	19794.22	21.37%		
		1000	A	17290.72	23.00%	23.13%	0.18%
			B	17532.83	23.25%		

Table 8.19: BL21 FCM raw forward scatter (mean FSC-A) and CV (% at peak mid-height) data for Chapter 3, Figure 3.36, Exp 2 – bottom panel histograms. Mean CV% and SD are provided.

BL21 carrying the pET-15b-P*uti101*-*6xhis::gfp* construct was aerated in 100 mL TB + Amp in baffled Erlenmeyer flasks at 37 °C, 150 rpm. At OD_{600} = 0.5, 5 and 10, 6xHis::GFP expression was induced with urea in duplicate for each concentration. Samples were analysed by FCM at 0 h, 2 h, 4 h and 24 h post-induction.

Time Post Induction (h)	OD_{600} at Induction	Urea Concentration (mM)	Replicate	FSC-A	CV	Mean CV	SD
0	0.5	50	A	17912.88	21.85%	21.75%	0.09%
			B	17928.45	21.69%		
		100	A	18092.61	21.71%	21.67%	0.11%
			B	18472.12	21.76%		
	5	250	A	9684.19	21.55%	21.66%	0.12%
			B	9578.12	21.78%		
		500	A	9507.36	21.64%	21.65%	0.05%
			B	9464.81	21.70%		
	10	500	A	10081.86	21.61%	22.20%	0.70%
			B	9897.70	22.02%		
		1000	A	9719.62	22.97%	23.33%	1.79%
			B	10250.16	21.75%		
2	0.5	50	A	12015.18	25.28%	24.76%	0.83%
			B	11987.61	25.20%		
		100	A	13736.05	23.81%	24.63%	0.87%
			B	13829.37	24.54%		
	5	250	A	11274.11	25.54%	25.41%	0.32%
			B	11623.42	25.64%		
		500	A	11662.65	25.05%	25.45%	0.60%
			B	11706.88	25.16%		
	10	500	A	10995.56	26.14%	25.88%	0.23%
			B	10703.51	25.77%		
		1000	A	11182.96	25.73%	26.82%	1.87%
			B	10900.69	25.75%		
4	0.5	50	A	15353.77	28.98%	28.10%	0.82%
			B	15673.05	27.98%		
		100	A	17254.22	27.35%	28.50%	1.36%
			B	17907.56	28.16%		
	5	250	A	11939.48	30.00%	29.69%	0.44%
			B	12093.64	29.89%		
		500	A	13056.93	29.19%	29.60%	0.73%
			B	12661.58	29.17%		
	10	500	A	11210.96	30.45%	30.57%	0.12%
			B	11287.88	30.58%		
		1000	A	11855.41	30.69%	28.33%	3.94%
			B	11494.80	30.51%		
24	0.5	50	A	20072.41	23.78%	23.68%	0.22%
			B	20412.66	23.83%		
		100	A	23392.22	23.43%	24.23%	0.80%
			B	22944.67	24.24%		
	5	250	A	12735.80	25.02%	23.84%	1.67%
			B	13254.74	24.58%		
		500	A	15795.88	21.93%	23.68%	2.72%
			B	14810.04	22.30%		
	10	500	A	10796.76	26.82%	26.36%	0.61%
			B	10949.28	26.60%		
		1000	A	12597.24	25.67%	26.06%	0.54%
			B	11468.63	26.44%		

Table 8.20: BL21 FCM raw green fluorescence (mean FL2-A) and CV (% at peak mid-height) data for Chapter 3, Figure 3.40, top panel histograms (P_{uti101}). Mean CV% and SD are provided.

BL21 carrying the pET-15b-P_{uti101}-*6xhis::gfp* construct was aerated in 50 mL TB + Amp in Erlenmeyer flasks at 37 °C, 200 rpm until OD_{600} 0.4-0.6 and induced with 0 mM, 50 mM or 500 mM urea. After 1 h, cells were spun down and resuspended in fresh TB to remove urea and growth resumed. Samples were analysed by FCM at 0 h, 2 h, 4 h and 24 h post-induction.

Time Post Induction (h)	Urea Concentration (mM)	Replicate	FL2-A	CV	Mean CV	SD
0	0	A	266.48	28.06%	28.11%	0.04%
		B	268.96	28.12%		
	50	A	256.21	28.14%	28.13%	0.10%
		B	255.60	28.02%		
	500	A	264.07	28.22%	25.94%	3.82%
		B	261.36	28.06%		
2	0	A	267.05	21.53%	26.36%	8.44%
		B	270.53	21.44%		
	50	A	6805.56	36.10%	33.53%	7.08%
		B	5926.25	38.97%		
	500	A	15654.23	25.52%	26.00%	0.57%
		B	14524.65	26.63%		
4	0	A	322.88	25.86%	33.87%	13.63%
		B	333.40	26.13%		
	50	A	5948.72	49.61%	40.28%	13.81%
		B	7199.45	46.82%		
	500	A	26536.68	24.42%	26.03%	2.61%
		B	25369.13	24.63%		
24	0	A	499.32	29.05%	34.81%	9.55%
		B	484.50	29.55%		
	50	A	6576.96	45.83%	42.02%	9.19%
		B	5240.75	48.69%		
	500	A	43577.40	31.53%	33.11%	2.23%
		B	41350.07	34.68%		

Table 8.21: BL21 FCM raw green fluorescence (mean FL2-A) and CV (% at peak mid-height) data for Chapter 3, Figure 3.40, top panel histograms (PAR4). Mean CV% and SD are provided.

BL21 carrying the pET-22b-PAR4-*6xhis::gfp* construct was aerated in 50 mL TB + Amp in Erlenmeyer flasks at 37 °C, 200 rpm until OD_{600} 0.4-0.6 and induced with 0 µM, 10 µM or 100 µM IPTG. After 1 h, cells were spun down and resuspended in fresh TB to remove IPTG and growth resumed. Samples were analysed by FCM at 0 h, 2 h, 4 h and 24 h post-induction.

Time Post Induction (h)	IPTG Concentration (µM)	Replicate	FL2-A	CV	Mean CV	SD
0	0	A	2411.13	31.24%	31.23%	0.04%
		B	2415.86	31.26%		
	10	A	2163.72	31.19%	31.17%	0.07%
		B	2201.31	31.09%		
	100	A	2035.46	31.22%	27.83%	5.97%
		B	2000.31	31.34%		
2	0	A	799.09	20.94%	24.98%	7.19%
		B	883.08	20.72%		
	10	A	2417.44	33.29%	30.30%	4.90%
		B	2671.63	32.96%		
	100	A	22512.86	24.65%	31.41%	11.65%
		B	22343.71	24.72%		
4	0	A	21632.80	44.87%	34.44%	10.30%
		B	9354.05	34.16%		
	10	A	10611.55	24.28%	24.39%	0.13%
		B	10202.62	24.37%		
	100	A	36646.72	24.53%	27.20%	4.79%
		B	34922.40	24.33%		
24	0	A	29951.56	32.73%	34.33%	2.01%
		B	31419.32	33.68%		
	10	A	28918.79	36.58%	35.28%	1.13%
		B	28825.02	34.69%		
	100	A	51449.00	34.57%	36.13%	2.20%
		B	45533.36	37.68%		